

*Physiologically based population
pharmacokinetic/pharmacodynamic modeling and
simulation approaches to support waivers of in vivo
clinical pharmacology studies*

Dissertation
zur Erlangung des Doktorgrades
der Naturwissenschaften

Vorgelegt beim Fachbereich 14
Biochemie, Chemie und Pharmazie
der Johann Wolfgang Goethe-Universität
in Frankfurt am Main

von

Ioannis Loios-Konstantinidis
aus Athen

Frankfurt (2021)
(D 30)

Vom Fachbereich für Biochemie, Chemie und Pharmazie der
Goethe-Universität als Dissertation angenommen.

Dekan: Prof. Dr. Clemens Glaubitz

1. Gutachter: Prof. Dr. Jennifer B. Dressman

2. Gutachter: Prof. Dr. Rodrigo Cristofolletti

Datum der Disputation:

To my younger and future self...

Acknowledgments

Even though it will not be enough to express my gratitude in words to all those people who played a role in this learning journey, I would still like to express my sincere thanks to some of these people who had a profound impact during that time.

First of all, I would like to express my sincere gratitude to my supervisor Prof. Dr. Jennifer Dressman for believing in me, shaping my scientific thinking and continuously supporting my personal and scientific development with her systematic guidance, knowledge and encouragement. She gave me the opportunity and freedom to pave my own research path and I have always very much enjoyed the scientific debate with her. I have learned so much from you Jenny and you have been a role model for me.

I would like to thank my family and beloved ones Tobias, Bergman, Christina Pentafragka, Katerina Komianou, Katerina Sifaki, Evi Gkioka, Elpida Konstiotti for their unconditional love and for brightening the days (and nights) of this journey.

I am grateful to Dr. Rafael Paraiso, Dr. Chara Litou, Dr. Maria Joao Gomes, Dommagoj Segregur, Dr. Kalpa Nagarsekar, Dr. Mukul Ashtikar and Omar Assaf for being “partners in crime” and for all the moments we shared. I am very thankful to Dr. Ana-Marija Grasic, David Busse, Ferdinand Weinelt and Luis Ilia for their friendship and all funny moments we had together. I would also like to thank Dr. Tom Fiolka and Dr. Martin Hofsaess for friendly discussions as well as Dr. Ed Kostewicz and Hannelore Berger for the constant support in the Institute of Pharmaceutical Technology.

During my PhD journey, I was lucky to have great mentors and collaborators. Therefore, I would like to especially thank Prof. Dr. Charlotte Kloft, Prof. Dr. Wilhelm Huisinga and Prof. Dr. Christos Reppas for inspiring my scientific curiosity, Dr. Anh-Thu Nguyen Trung, Dr. Stefania Beato and Dr. Tycho Heimbach for their excellent mentorship and immense support during my time at Novartis, Dr. Jobst Limberg for introducing me to the world of the regulatory health authorities and his mentorship during my secondment at BfArM, Dr. Nikoletta Fotaki, Dr. Masoud Jamei, Dr. David Turner, Dr. Mark McAllister, Dr. Bart Hens, Dr. Amitava Mitra for scientific discussions and fruitful collaborations. I am deeply thankful to Prof. Dr. Rodrigo Cristofolletti for invaluable scientific discussions, excellent collaborations and for accepting to review my thesis. It was a blast to work with him.

Special thanks to Simcyp (Certara UK Limited, Simcyp Division, Sheffield, UK) for providing academic licenses of the Simcyp Simulator® and the SIVA Toolkit® to Goethe University without charge. Also, I would like to thank Biorelevant.com (London, UK) for donating the FaSSIF V3 instant powder.

Last yet importantly, I would like to acknowledge the European Union’s Horizon 2020 Marie Skłodowska-Curie actions, which funded this work as part of the ETN-PEARRL (grant agreement No 674909). Special thanks to all fellow ESRs and partners of PEARRL and especially the program coordinator Dr. Brendan Griffin. I feel privileged for the excellent training, fruitful collaboration, thought sharing and interactions we had with all members of the project.

Table of Contents

1	Introduction	1
1.1	Modeling and simulation approaches for oral drug absorption	1
1.1.1	Quasi-equilibrium models.....	1
1.1.2	Steady-state models	2
1.1.3	Dynamic models.....	4
1.2	Physiologically based pharmacokinetic/pharmacodynamic (PBPK) models.....	10
1.2.1	Milestones in the development of PBPK models.....	10
1.2.2	Components of PBPK models.....	11
1.2.3	<i>In vitro in vivo</i> extrapolation in PBPK modeling.....	17
1.2.4	PBPK model building approaches	20
1.2.5	Structural identifiability	22
1.2.6	Statistical identifiability and sensitivity analyses.....	22
1.2.7	Physiological plausibility and correlation of physiological parameters	24
1.2.8	Parameter estimation approaches	24
1.2.9	Modeling physiological variability and uncertainty in PBPK models	26
1.2.10	Overparameterization and reduction of PBPK models.....	28
1.2.11	Qualification and credibility assessment of PBPK models.....	29
1.3	Combining physiologically based pharmacokinetic with pharmacodynamic models.....	32
1.4	Physiologically based pharmacokinetic analyses for biopharmaceutic applications in drug development and regulatory review	33
1.4.1	BCS-based biowaivers, clinically relevant drug product specifications and virtual bioequivalence.....	33
1.4.2	Food Effects and pH-dependent Drug-Drug interactions	35
2	Aims of the thesis and scientific issues addressed	38
3	Key results and discussion	40
3.1	Application of the relationship between pharmacokinetics and pharmacodynamics in drug development and therapeutic equivalence.....	40
3.1.1	Effect-compartment model	40
3.1.2	Irreversible target binding models.....	41
3.1.3	Indirect response models.....	41
3.2	The role of biopharmaceutic and pharmacokinetic properties to support waivers of <i>in vivo</i> bioequivalence.....	45
3.2.1	Rationale for compound selection.....	46
3.3	<i>In vitro</i> characterization of biopharmaceutic properties.....	48
3.3.1	<i>In vitro</i> aqueous and biorelevant solubility	48
3.3.2	<i>In vitro</i> dissolution testing.....	51

3.4	<i>In vitro in vivo</i> extrapolation in biopharmaceutics.....	56
3.4.1	Model-based analysis of <i>in vitro</i> solubility data.....	58
3.4.2	Model-based analysis of <i>in vitro</i> dissolution data.....	59
3.4.3	Case example: Naproxen	61
3.4.4	Case example: Ibuprofen	63
3.4.5	Case example: Flurbiprofen	64
3.5	PBPK/PD model development and validation.....	66
3.5.1	Case example: Naproxen	68
3.5.2	Case example: Ibuprofen	72
3.5.3	Case example: Flurbiprofen	73
3.6	PBPK-IVIVE linked modelling and simulation workflow to perform virtual bioequivalence.....	88
3.6.1	Case example: Naproxen	89
3.6.2	Case example: Ibuprofen	91
3.7	Population PBPK modelling to assess the Impact of genetic polymorphisms and co-medication on the pharmacokinetics of flurbiprofen.....	94
3.8	Population PBPK/PD modelling to dissect the effect of formulation and genetic polymorphisms on the exposure and response of flurbiprofen, a substrate of the polymorphic CYP2C9	101
3.9	Knowledge gaps, challenges, and limitations in PBPK modelling for oral biopharmaceutics...	102
3.10	Opportunities and future actions to increase confidence in and maximize the impact of PBPK models for oral drug absorption.....	104
4	Summary and Outlook	107
5	Deutsche Zusammenfassung (German Summary)	113
6	References	118
7	Supplementary material	146
7.1	Case example: Naproxen.....	146
7.2	Case example: Ibuprofen	149
7.3	Case example: Flurbiprofen	150
8	Appendix	156
<i>Appendix A1.</i>	List of publications.....	156
<i>Appendix A2.</i>	Personal contributions.....	157
<i>Appendix A3.</i>	Peer reviewed publications	159
<i>Appendix A4.</i>	Curriculum vitae	268
<i>Appendix A5.</i>	Eidesstattliche Erklärung	273

List of tables

Table 3-1: Mean (\pm SD) naproxen free acid and sodium salt equilibrium solubility in aqueous media at 37°C for 24h (Uniprep® method).	49
Table 3-2: Mean (\pm SD) equilibrium solubility of naproxen free acid and sodium salt in fasted and fed state biorelevant media at 37°C for 24h (Uniprep® method).	50
Table 3-3: Mean (\pm SD) equilibrium solubility of flurbiprofen in aqueous buffers and fasted state biorelevant media at 37°C for 24h (Uniprep® method).	51
Table 3-4: Parameter estimates (95% CI) resulting from the model-based analysis of naproxen in vitro solubility data in aqueous and biorelevant media. The pKa was estimated from the aqueous solubility values, whereas biorelevant solubilities were used to estimate the micelle-water partition coefficients ($\log K_{m:w}$ neutral, ion). The accuracy of the predictions was evaluated with the coefficient of determination (R^2).	61
Table 3-5: Estimated DLM scalar (S_{DLM}) values (95% CI) obtained from model-based analysis of in vitro dissolution data of naproxen free acid and sodium salt as both the pure drug powder and as commercially available IR tablets. For the commercial formulations, when dissolution without pre-treatment in a gastric medium was modelled, a first-order disintegration model was included. The goodness of fit between the predicted and observed dissolution profiles was evaluated with the coefficient of determination (R^2).	62
Table 3-6: Estimated product-specific particle size distributions (P-PSDs) of three ibuprofen suspensions (R, T-BE, T-NBE). A log-normal monodispersed distribution was assumed.	63
Table 3-7: Parameter estimates (95% CIs) resulting from the model-based analysis of in vitro solubility data for flurbiprofen in aqueous as well as biorelevant media. The pKa was estimated from the aqueous solubility values, whereas for the micelle-water partition coefficients ($\log K_{m:w}$ neutral, ion) estimation, biorelevant solubilities were used. The accuracy of the prediction was evaluated by calculating the coefficient of determination, R squared (R^2).	64
Table 3-8: Mean (95% CIs) DLM scalar (S_{DLM}) estimates obtained from model-based analysis of in vitro dissolution data in various media of flurbiprofen pure drug, 100 mg USP tablets® and 100 mg Antadys® formulations. The goodness of fit between predicted and observed dissolution profiles was evaluated with using the coefficient of determination, R squared (R^2).	65
Table 3-9: Mean (95% CIs) DLM scalar (S_{DLM}) estimates obtained from model-based analysis of Froben® in vitro dissolution data The in vitro data from single dissolution experiments were modelled assuming that disintegration is the rate limiting step to the flurbiprofen in vitro dissolution rate in intestinal media, whereas for the two-stage dissolution, the serial dilution model was used. The goodness of fit between predicted and observed dissolution profiles was evaluated with the coefficient of determination, R squared (R^2).	65
Table 3-10: Mean in silico population pharmacokinetic parameters of naproxen simulated plasma-concentration-time profiles under all tested in vivo dissolution inputs (S_{DLM} scalar values) as obtained from model-based analysis of the in vitro data.	69
Table 3-11: Mean (SD) reported pharmacokinetic parameters of naproxen in vivo studies used for the validation of the PBPK model	69
Table 3-12: Reported results of the two ibuprofen in vivo bioequivalence studies	72
Table 3-13: Simulated and observed PK parameters of the two bioequivalence studies used for validation of the refined ibuprofen PBPK model.	73
Table 3-14: Mean relative deviation (MRD) values of flurbiprofen plasma concentration predictions.....	81
Table 3-15: Comparison of mean predicted and observed AUC, C_{max} and apparent clearance (CL/F) values of flurbiprofen. Calculation of predicted to observed ratio ($R_{pred/obs}$) and geometric fold error (GMFE) values.	83

Table 3-16: Comparison of predicted and observed pharmacodynamic parameters (R_{max} , TR_{max} and AUCE) values of flurbiprofen and calculation of predicted to observed ratio ($R_{pred/obs}$).....	87
Table 3-17: Estimated 90% confidence interval (CI) around predicted C_{max} geometric mean (GeoMean) ratios after post hoc incorporation of bootstrapped IOV	93
Table 3-18: Comparison of mean predicted and observed DDI AUC, C_{max} and apparent clearance (CL/F) ratios of flurbiprofen-fluconazole/rifampicin interaction. Calculation of predicted to observed ratio ($R_{pred/obs}$) and geometric fold error (GMFE) values.....	99
Table 7-1: Mean (SD) demographic data of in vivo studies used for the development and verification of the PBPK model. (HV= healthy volunteers)	146
Table 7-2: Input parameters for naproxen PBPK model development and validation	147
Table 7-3: Input Parameters for Ibuprofen PBPK Model development and validation.....	149
Table 7-4: Mean (SD) demographic clinical study data used for the development and verification of flurbiprofen PBPK/PD model.....	150
Table 7-5: Mean (SD) demographic clinical study data used for the gene-drug-drug interaction (GDDI) modeling with flurbiprofen as victim drug.	152
Table 7-6: Summary of main CYP2C9 genotype-based metabolic differences in the default inputs of the Simcyp® North European Caucasian (NEurCaucasian) and Chinese healthy volunteer virtual populations (Simcyp v18.2; Certara, Sheffield, UK).	153
Table 7-7: Input parameters of flurbiprofen PBPK/PD model.....	154

List of Figures

Figure 1-1: Perfusion vs. permeability rate-limited tissue models. (a) Perfusion rate limited; (b) Permeability rate limited. K_p , tissue to plasma partition coefficient; RBC, red blood cell (Jones H, Rowland-Yeo K. *CPT Pharmacometrics Syst Pharmacol*. 2013 Aug 14;2(8): e63)..... 12

Figure 3-1: Four basic indirect response models characterized by either inhibition or stimulation or the response variable. The shapes of the responses are depicted on the right of each model (reproduced with permission by Dayneka NL, Garg V, Jusko WJ. *J Pharmacokinet Biopharm*. 1993 Aug;21(4):457-78). 43

Figure 3-2: Naproxen (circles) and naproxen sodium (diamonds) experimental mean aqueous equilibrium solubility values (24 h at 37°C) plotted against respective literature values (24 h at 25°C) in a pH-solubility profile. The *in vitro* solubility experiments were performed with the Uniprep® method in triplicate. The experimental results are in agreement with the literature values (24 h at 25°C) from Avdeef et al. and Chowhan et al. 49

Figure 3-3: *In vitro* dissolution (mean ± SD) of 500 mg naproxen free acid (A) and sodium salt (B) drug powder in Ph. Eur. phosphate buffer (pH=6.8), Level I and II FaSSIF V3. USP paddle apparatus at 75 rpm and 500 mL of dissolution medium at 37°C were used in all experiments. The experiments were performed in triplicate. Horizontal dashed red line represents 85% dissolved. Most standard deviation bars lie within the symbols. 53

Figure 3-4: *In vitro* dissolution (mean ± SD) of Naprosyn® 500 mg (A) and Anaprox® 550 mg (B) in FaSSIF V3 Levels I and II (solid lines, filled squares and circles respectively). The intestinal profiles in FaSSIF V3 Levels I and II (after the pre-treatment with FaSSGF Levels I and III respectively) during two-stage test are also depicted (dotted lines, empty squares, and circles, respectively). USP paddle apparatus at 75 rpm and 500 mL of dissolution medium at 37°C were used in all experiments. The experiments were performed in triplicate. Horizontal dashed red line represents the 85% dissolved. Most standard deviation bars lie within the symbols..... 54

Figure 3-5: (a), (b) *In vitro* dissolution (mean ± SD) of flurbiprofen API 100 mg (circles), USP tablets® 100 mg (triangles), Antadys® 100 mg (squares) and Froben® 100 mg (diamonds) in FaSSGF Levels I & III, respectively. USP paddle apparatus at 75 rpm and 250 mL of dissolution medium at 37°C were used in all experiments. All experiments were performed at least in triplicate ($n \geq 3$). Most standard deviation bars lie within the symbols. 55

Figure 3-6: *In vitro* dissolution (mean ± SD) of flurbiprofen API 100 mg (circles), USP tablets® 100 mg (triangles), Antadys® 100 mg (squares) and Froben® 100 mg (diamonds) in (a) FaSSIF V3 Level I (solid lines), (b) FaSSIF V3 Level II (dashed lines) and (c) Ph. Eur. Phosphate buffer (pH=6.8) (dashed dotted lines). (d) Two-stage test of Froben® 100 mg (diamonds) in FaSSGF Levels I (solid line) and III (dashed line) at the gastric and FaSSIF V3 Level I (solid line) and FaSSIF V3 Level II (dashed lines) at the intestinal compartments, respectively. USP II paddle apparatus at 75 rpm at 37±0.4°C was used in all experiments. The volume of dissolution medium at the gastric compartment was 250 mL, to which 250 mL of properly concentrated intestinal medium was added after 30 minutes. Horizontal dashed red line represents the 85% dissolved. All experiments were performed at least in triplicate ($n \geq 3$). Most standard deviation bars lie within the symbols. 56

Figure 3-7: Population mean simulated naproxen plasma concentration-time profiles and the 5th and 95th percentiles for the two extremes of the estimated S_{DLM} values: (a) $S_{DLM}=1$ (green and grey solid lines, respectively) and (b) $DLM=0.0022$ (blue and light grey dashed lines, respectively). In a worst/ best case virtual bioequivalence scenario of simulated healthy adult populations (a) was treated as the reference, whereas (b) as the test formulation. Observed clinical data from Charles & Mogg (circles), Zhout et al. (squares), Haberer et al. (a) (diamonds), Setiawati et al. (triangles), Rao et al. (crosses) and Haberer et al. (b) (asterisks) are overlaid for verification of the PBPK model performance and comparisons. Simulations run for 72 h, but to enable better comparison only the first 24 hours are plotted..... 70

Figure 3-8: Stepwise modeling workflow for the development and verification of the flurbiprofen PBPK/PD model. Training for the internal and test datasets for the external verification, obtained from clinical studies published in the open literature, are outlined with orange and green, respectively 76

Figure 3-9: Mean flurbiprofen plasma concentration-time profiles after oral administration of 100 mg tablet in healthy Caucasians. Population simulations ($n=100$) under four in vivo dissolution scenarios are shown as green and grey lines for the mean and the 5th & 95th percentiles, respectively. Each dissolution scenario is represented by the corresponding S_{DLM} value and is shown with different line style: $S_{DLM}=0.125$ (solid line), $S_{DLM}=0.071$ (dotted line), $S_{DLM}=0.0054$ (dashed-dotted line) and $S_{DLM}=0.0018$ (dashed line). Observed data with SD, if available, are depicted as (a) circles (Jamali et al.-Ansaïd) and squares (Jamali et al.-Froben); (b) triangles (Patel et al.); (c) diamonds (Suri et al.); (d) asterisks (Szpunar et al.). 77

Figure 3-10: Mean flurbiprofen plasma concentration-time profiles after intravenous and oral administration in healthy Chinese (a, d) and Caucasians (b, c, e, f). Population simulations ($n=100$) are shown as green and grey solid lines for the mean and the 5th & 95th percentiles, respectively. Observed data with SD, if available, are depicted as circles and squares. References link to a specific observed dataset described in study Table 1. Administration protocol: (a) 50 mg intravenously; (b) 67.9 mg oral solution; (c) 100 mg oral solution; (d) 150 mg oral tablet; (e) 200 mg oral tablet; (f) 300 mg oral tablet. 78

Figure 3-11: Mean flurbiprofen plasma concentration-time profiles after administration of 40 mg oral solution in CYP2C9 1*/1* and 1*/3* healthy Korean volunteers. Population simulations ($n=100$) are shown as green and grey lines for the mean and the 5th & 95th percentiles, respectively. Observed data with SD, if available, are depicted as circles. 79

Figure 3-12: Mean flurbiprofen plasma concentration-time profiles after administration of 50 mg oral tablet in CYP2C9 1*/1*, 1*/2* and 1*/3* healthy Caucasian volunteers. Population simulations ($n=100$) are shown as green and grey lines for the mean and the 5th & 95th percentiles, respectively. Observed data with SD, if available, are depicted as circles. 80

Figure 3-13: Mean flurbiprofen response-time profiles after administration of 100 mg oral tablet in healthy Caucasians. (a), (b) Genetic polymorphism: Population simulations ($n=100$) in CYP2C9 1*/1*, 1*/2* and 1*/3* are shown for the mean as green (solid), yellow (dash dotted) and orange (dashed) lines, respectively. Grey lines with the corresponding style represent the 5th & 95th percentiles (c), (d) Dissolution rate: Population simulations ($n=100$) under four in vivo dissolution scenarios are shown as green and grey lines for the mean and the 5th & 95th percentiles, respectively. Each dissolution scenario is represented by the corresponding S_{DLM} value and is shown with different line style: $S_{DLM}=0.125$ (solid line), $S_{DLM}=0.071$ (dotted line), $S_{DLM}=0.0054$ (dashed line) and $S_{DLM}=0.0018$ (dashed-dotted line). 86

Figure 3-14: Average virtual bioequivalence results (% Geometric mean T/R ratio) of 10 trials with 12 simulated individuals in each trial. Intra-subject variability of 30% was chosen and added through Simcyp® (V18.1; Certara, Sheffield, UK) VBE module (V1.0) to the mean GET, pH of fasted stomach, pH and bile salt concentration of fasted duodenum, jejunum I and II. The 80-125% bioequivalence limits (red dashed lines) and the area of acceptance (light green shaded area) are shown for each tested PK parameter: (A) C_{max} , (B) AUC_{tlast} (AUC calculated up to the last simulated time point), and (C) AUC_{inf} (AUC extrapolated to infinity). Error bars represent the 90% confidence intervals, which in subplots (B) and (C) lie within the symbols. 90

Figure 3-15: Dissolution “safe space”, within which bioequivalence is anticipated for naproxen products. The light green shaded area delimits the safe space area in which bioequivalence (with respect to C_{max} and AUC) was established between the very slow (red solid line & squares) and the fast (blue solid line & circles) dissolution profiles. Additional typical dissolution profiles are co-plotted ($n=3$). The horizontal red dashed line represents 85% dissolved. 91

Figure 3-16: Predicted plasma C_{max} ratios T-NBE/R (A) and T-BE/R (B) without adding IOV to any system parameter. Closed symbols represent geometric mean ratios for C_{max} , and horizontal bars represent the respective 90% CIs. 93

Figure 3-17: Power curve for the two one-sided test procedure with IOV of 20%. Horizontal gray line represents the a priori 80% power recommended in regulatory guidelines for sample size estimation in average BE studies. Shaded areas represent the predicted maximum and minimum values for C_{max} TBE/R (light gray) and TNBE/R (dark gray) in the ten virtual trials. 94

Figure 3-18: Mean plasma concentration-time profiles after administration of flurbiprofen alone and with the perpetrator drug in healthy volunteers. (a)-(e): Population simulations (n=100) without or with the CYP2C9 inhibitor, fluconazole (FCN), are shown for the mean as blue (FLU + 0 mg FCN), red (FLU + 200 mg FCN), light green (FLU + 400 mg FCN s.d.) and dark green (FLU + 400 mg FCN q.d.) solid lines and observed data with SD, if available, are depicted as circles, diamonds, squares, and triangles, respectively. (f): Population simulations (n=100) without or with the CYP2C9 inducer, rifampicin (RIF), are shown for the mean as blue (FLU + 0 mg RIF) and orange (FLU + 600 mg RIF) solid lines and observed data with SD, if available, are depicted as circles and asterisks, respectively. Shaded areas represent the 5th & 95th percentiles. 97

Figure 3-19: Mean plasma concentration-time profiles after administration of 50 mg flurbiprofen as oral tablet alone and with 200 mg or 400 mg fluconazole (FCN) in CYP2C9 1*/1*, 1*/3* and 3*/3* healthy Caucasian volunteers. Population simulations (n=100) are shown for the mean as blue (FLU + 0 mg FCN), red (FLU + 200 mg FCN) and light green (FLU + 400 mg FCN) solid lines and observed data with SD, if available, are depicted as circles, diamonds, and squares, respectively. Shaded areas represent the 5th & 95th percentiles..... 98

Figure 7-1: Sensitivity analysis of naproxen simulated plasma concentration-time profiles of population representative individual on (A) DLM scalar values ranging from 0.001 (blue solid line) to 0.1 (dashed line) and (B) mean gastric residence time (MGRT) with values ranging from 0.1 (blue solid line) to 2h (dashed dotted line) . The values of all other parameters were kept constant (GET=0.25 h). Observed clinical data from Charles & Mogg (circles), Zhout et al. (squares), Haberer et al. (a) (diamonds), Setiawati et al. (triangles), Rao et al. (crosses) and Haberer et al. (b) (asterisks) are overlaid for comparisons. Simulations were run for 72 h, but to enable better comparison only the first 24 hours are plotted..... 148

1 Introduction

1.1 Modeling and simulation approaches for oral drug absorption

In 1996, Yu et al. published a review article that comprehensively discussed the utilities and limitations of early quantitative absorption models.^{1,2} Details about these early absorption models can be found in the reference. In principle, the absorption rate can be mathematically described by the equation 1:

$$\text{Absorption rate} = \frac{dM}{dt} = \iint_A J_w dA = \iint_A P_w \cdot C_w dA \quad (1)$$

where $J_w(x, y, z, t)$ is the drug flux (mass/area/time) through the intestinal wall at any position and time, $P_w(x, y, z, t)$ is the effective permeability of intestinal membrane, $C_w(x, y, z, t)$ is the drug concentration at the intestinal membrane surface, and A is the entire gastrointestinal surface. The effective permeability (P_w) and local drug concentration (C_w) are time and location dependent. The underlying assumptions of Eq. (1) are first, that sink conditions exist for the drug inside the intestinal membrane; and second, that there is no luminal reaction. At that time the intestinal membrane was treated as a film and intracellular reactions had not been introduced. Nevertheless, Eq. (1) indicates two important properties of drug substance that affect oral absorption: solubility (i.e., the limit of C_w), and permeability (i.e., the ability of drug substance transport across the intestinal membrane).

Early absorption models were classified into three categories: quasi-equilibrium models, steady-state models, and dynamic models, based on their dependence on spatial and temporal variables.^{1,2}

Briefly, the quasi-equilibrium models are independent of the spatial and temporal variables, while the steady-state models are independent of the temporal variable, but dependent on the spatial variable. The dynamic models are dependent on both temporal and spatial variables.

1.1.1 Quasi-equilibrium models

1.1.1.1 Absorption potential (AP)

In 1985, Dressman et al.³ proposed a quasi-equilibrium model which employed the pH-partition theory to provide a rough estimation of the fraction of dose absorbed according to the following equation:

$$AP = \log\left(P \cdot F_{non} \cdot \frac{S_0 \cdot V_L}{X_0}\right) \quad (2)$$

where AP is the absorption potential as a predictor of the fraction absorbed, P is the 1-octanol–water partition coefficient that correlates with the permeability ratio (the permeability of gut wall to drug to the aqueous permeability of drug), F_{non} is the fraction of the non-ionized drug species at pH 6.5, S_0 is the intrinsic solubility (at 37 °C), V_L is the intraluminal volume, and X_0 is the dose administered.³ This model was validated using seven drugs against their observed oral bioavailability. An “S” shape relationship was observed between the absorption potential and oral bioavailability. Although the absorption potential does not account for all processes affecting oral drug absorption, two of the most important properties of drug substance, solubility, and permeability, were included in the model.

In addition, the model considered that solubility and permeability may change in different pH media due to ionization, and corrected the parameter values to pH 6.5, which is reflective of the pH in the small intestine. Nevertheless, this semi-mechanistic model is only relevant for drugs that are predominantly passively absorbed through the gut wall.

1.1.2 Steady-state models

Four main models, with differences in the convection and diffusion assumptions, have been used to describe the mass transfer in the gastrointestinal (GI) tract and the intestinal wall permeabilities.⁴ These models include the laminar flow, the plug flow, the complete radial mixing (also known as film model) models for convective mass transport in a tube and the perfect mixing tank model, which in contrast to the first three models belongs to the dynamic models. The transport of a solute in cylindrical coordinates can be in general defined as follows:

$$u_z \cdot \frac{\partial C}{\partial z} = D \cdot \frac{1}{R} \cdot \frac{\partial}{\partial r} \left(r \cdot \frac{\partial C}{\partial r} \right) \quad (3)$$

where u_z is the axial velocity, D is the solute diffusivity, C represents the concentration of A in B; r and z are the radial and axial coordinates, respectively.

Briefly, in the laminar flow model the velocity profile is assumed to follow the behavior of a Newtonian fluid in a tube, whereas in the plug flow model the velocity profile is considered to be independent of both r and z .

1.1.2.1 Complete radial mixing (CRM) model

In the complete radial mixing (CRM) model, as with the plug flow model, the velocity profile is assumed to be constant. In addition, the concentration is assumed to be constant radially, but not axially. Thus, there is complete radial, but not axial, mixing to give uniform radial velocity and concentration profiles. As is the case with all steady state models, the CRM is independent of temporal variables, but dependent on spatial variables and as a result it can only predict the extent, but not the rate of drug absorption.² Amidon et al. employed a simplified film model to correlate the extent of absorption with membrane permeability.⁴ The analytical solution for the estimation of the fraction absorbed was given by the ratio of the outlet *versus* the inlet concentration, as follows:

$$f_a = 1 - e^{(-4 \cdot P_{eff}^* \cdot G_z)} \quad (4)$$

where P_{eff}^* is the effective (dimensionless) intestinal permeability (a function of the dimensionless true wall permeability P_w^* and the aqueous permeability P_a^*) and G_z is the Graetz number, a dimensionless number that characterizes fluid flow in a tube as a function of solute diffusivity (D), perfusion flow rate (Q) and length of the tube (L):

$$P_{eff}^* = \frac{P_w^* \cdot P_a^*}{P_w^* + P_a^*} \quad (5)$$

$$P_w^* = P_w \cdot R/D \quad (6)$$

$$P_a^* = R/\delta \quad (7)$$

$$G_z = \pi \cdot D \cdot L/2 \cdot Q \quad (8)$$

where R is the radius of the tube and δ the film thickness. Since no aqueous resistance is included directly in the model, the wall resistance is usually augmented with a film or diffusion layer resistance. That is, it is assumed that complete radial mixing occurs up to a thin region or film adjacent to the membrane. The aqueous (luminal) resistance is confined, within this model, entirely to this region and lies in series with the membrane. Hence, the effective permeability includes an aqueous or luminal resistance term as shown in equation 5.

1.1.2.1.1 Macroscopic approach

Sinko et al.⁵ extended this simplified CRM model by including the effect of solubility as a concentration gradient and proposed a macroscopic mass balance approach. The small intestine is assumed to be a cylindrical tube with the surface area of $2\pi RL$, where R is the radius and L is the length of the tube. The stomach is assumed to be an infinite reservoir with constant output rate with respect to concentration and volume. Absorption is not considered dissolution-limited and mass disappearance is due to absorption or mass flow out of the tube (but not due to chemical degradation). In this context, the rate of mass absorbed as well as the fraction absorbed can be described by equations 9 and 10:

$$\frac{dM}{dt} = -Q \cdot (C_0 - C_m) = \iint_A J_w dA \quad (9)$$

$$f_a = 1 - \frac{C_m}{C_0} = \frac{2\pi RL}{Q} \cdot P_{eff} \cdot \int_0^1 C_b^* dz^* \quad (10)$$

where P_{eff} is the effective permeability, Q is the perfusion flow rate, C_0 and C_m are the inlet and outlet concentrations, respectively; $C_b^* = C_b/C_0$ is the dimensionless concentration, $z^* = z/L$ is the fractional length with C_b and z being the bulk drug concentration in the lumen and the length from the inlet to the absorption site, respectively.

Based on the steady state assumption, the authors also derived the dimensionless mass transfer coefficient, namely the absorption number (A_n), which is the ratio of key processes affecting drug disappearance from the lumen: absorption and convection and is equal to:

$$A_n = \frac{\pi R L P_{eff}}{Q} = \frac{P_{eff} \cdot t_{res}}{R} \quad (11)$$

where t_{res} is the mean residence time and the ratio R/P_{eff} is the absorption time. The observation that the A_n , and in particular the P_{eff} , controls the absorption of drugs across enterocyte membranes is one of the most relevant findings of the macroscopic approach. The macroscopic mass balance approach has been further extended to include facilitated drug absorption and degradation.⁶

Nevertheless, due to the inherent simplicity of macroscopic approaches, this mass balance model is mainly useful for highly soluble drugs, whereas in cases where the *in vivo* dissolution is critical for oral drug absorption, the more detailed microscopic approach is advantageous.

1.1.2.1.2 Microscopic mass balance approach

Microscopic mass balances in solid and solution phases in a volume element of the cylinder were used to derive a set of differential equations, and these were further combined with the hydrodynamic considerations of the CRM model to predict oral absorption for poorly soluble drugs showing dissolution rate-limited absorption by including a variable dissolution resistance as a function of particle size.⁷ The major limitations of this approach are that the model assumes that all particles are spheres of the same size and that the solubility is constant throughout the intestine. The microscopic approach considers the three fundamental dimensionless parameters to estimate the fraction of dose absorbed: i) the absorption number (A_n), ii) the dose number (D_0) and iii) the dissolution number (D_n) as shown in the Equations 11-13:

$$D_0 = \frac{M_0/V}{C_s} \quad (12)$$

$$D_n = \frac{3DC_s t_{res}}{\rho r_0^2} = \frac{t_{res}}{t_{dis}} \quad (13)$$

where C_s is the drug equilibrium solubility, M_0 is the dose, V is the volume (assumed to be 250 mL), r_0 is the initial particle radius, ρ is the particle density and t_{dis} is the time required for a solid drug particle to dissolve.

The microscopic mass balance approach using the A_n , D_0 and D_n was applied to investigate the effect of micronization on the absorption, and thus the relative bioavailability of digoxin and griseofulvin.^{8,9} This theoretical analysis of dissolution and absorption was one of the first attempts to provide quantitative assessments between delivery systems and/or dosage forms and to guide formulation development. Since then, the microscopic mass balance approach has been further extended to include intestinal transit rate variability and particle size distribution effects when predicting the expected variability in absorption of poorly water-soluble drugs.

1.1.3 Dynamic models

1.1.3.1 Dispersion model

The dispersion model approach was first proposed to simulate dynamic absorption processes [35]. The dispersion model assumes that the small intestine can be considered as a uniform tube with constant axial velocity, constant dispersion behavior and a constant concentration profile across the tube diameter. Then, the absorption of highly soluble drugs in the small intestine can be delineated by the following dispersion model equation:

$$\frac{\partial C}{\partial t} = a \cdot \frac{\partial^2 C}{\partial z^2} - v \cdot \frac{\partial C}{\partial z} - K_a \cdot C \quad (14)$$

where C is the concentration of a drug, z is the axial distance from the stomach, K_a , is the absorption rate constant, v is the velocity in the axial direction, and a is the longitudinal coefficient that accounts

for mixing by both molecular diffusion and physiological effects, such as membrane surface solute binding, peristaltic and villous activities, and the multi-S course of the small intestine. The dispersion model equation (Eq. 14) generally has to be solved numerically. Although in some boundary cases analytical solutions may be possible, they are still very complex and computationally intensive.^{2,9,10}

Despite providing a quantitative framework for oral drug absorption the dispersion model has not been widely used due to its complexity. On the other hand, a concept extracted from the dispersion model, namely the anatomical reserve length, has been used to explain absorption phenomena.^{11,12} The reserve length for absorption is defined as the length of the intestine remaining after absorption is complete. Assuming no or minor absorption from the stomach or colon, respectively, the maximum reserve length would then be the length of the small intestine. Thus, the reserve length is longer when absorption is fast and efficient in the upper small intestine. Mathematically, this can be represented by

$$RL = L - l = L - \frac{3Rv}{2P_{eff}} \quad (15)$$

where RL , L , l and are the anatomical reserve, the small intestinal and the intestinal length at which absorption is complete, respectively; R is the small intestinal radius and v the axial velocity.

1.1.3.2 Mixing tank model

This approach, originally proposed by Dressman et al. to investigate dissolution-controlled drug absorption, considers the GI tract as one or more serial mixing tanks with mass transfer following first-order transit kinetics.¹³ In terms of hydrodynamics, the mixing tank model assumes that both radial and axial mixing are complete, and thus the contents are assumed to be well-stirred with instantaneous dilution of the inputted dose, which leads to uniform distribution of dissolved and solid drug.^{13,14} For this reason, mixing tank models can also be considered as compartmental models, dependent on temporal and spatial variables. The rate of change of the drug amount in a single mixing tank is given by the following equations:

$$\frac{dM_i}{dt} = -\left(K_a + \frac{Q}{V_i}\right) \cdot M_i \quad (16)$$

$$\frac{dA}{dt} = K_a \cdot M_i \quad (17)$$

where M_i is the drug amount at a given mixing tank i and A is the amount of drug absorbed.

The mixing tank model implements a modified Noyes-Whitney equation to handle drug dissolution and the first-order absorption rate constant can be estimated from the effective permeability:

$$K_a = \frac{2P_{eff}}{R} \quad (18)$$

Several applications of the original model and its extensions, including double peak absorption phenomena and the effect of particle size distribution on dissolution, have been reported in the literature.¹⁴⁻¹⁷

1.1.3.3 Compartmental absorption and transit (CAT) model

The compartmental absorption and transit (CAT) model was originally developed in the 1990s by Yu et al.¹ After an extensive review of the available human intestinal transit flow data, the authors concluded that the transit time throughout the human small intestine is normally distributed around 199 ± 78 minutes and that seven compartments would be optimal in describing the small intestinal transit process using a compartmental approach. The model treated the stomach and colon each as one compartment. The mass transfer from one compartment to the next one follows first-order kinetics, and the model can be mathematically described by the following series of differential equations:

$$\frac{dM_s}{dt} = -K_s \cdot M_s \quad (19)$$

$$\frac{dM_n}{dt} = K_t \cdot M_{n-1} - K_t \cdot M_n, \quad n = 1, 2, \dots, 7 \quad (20)$$

$$\frac{dM_c}{dt} = K_c \cdot M_n, \quad n = 8 \quad (21)$$

$$\frac{dM_a}{dt} = K_a \cdot \sum_{n=1}^7 M_n \quad (22)$$

$$M_0 = M_s + \sum_{n=1}^7 M_n + M_c + M_a \quad (23)$$

Equations (19)– (21) describe the drug mass transfer from the stomach to the small intestine and colon, respectively. In equation (20), when $n=1$, the term $K_t \cdot M_{n-1}$ is replaced by $K_s \cdot M_s$. M_s , M_n , and M_c , which are the amounts of drug in the stomach, the n^{th} small intestinal compartment, and the colon, respectively. The rate of drug absorption to the systemic circulation is expressed by the equation (22) with M_a being the amount of drug absorbed. K_s , K_t , and K_c represent the first order gastric emptying, small intestinal and colon transit rate constants, respectively. Equation (23) closes the mass balance loop with M_0 corresponding to the administered oral dose.

The CAT model assumes no absorption from the stomach or colon, passive transport across the small intestinal membrane, instantaneous dissolution, and first-order drug transit from one compartment to the next. In the model, K_a is proportional to the effective permeability. The original model was able to describe the relationship between fraction absorbed and effective permeability for ten drugs covering a wide range of fraction absorbed.¹⁸ When coupled with a three compartment PK model, the CAT model was also able to predict the pharmacokinetic (PK) profiles of atenolol.¹⁸

The original CAT model did not include components such as *in vivo* dissolution, transporter mediated transport, and intestinal metabolism. Nevertheless, it served as the basic structure model for more complicated absorption models.

1.1.3.4 Advanced compartmental absorption and transit (ACAT) model

The advanced CAT (ACAT) model is an extended CAT-like model which incorporates gut wall metabolism, active drug uptake by or efflux from the enterocyte membrane, gastric emptying rate constants appropriate to the dosing situation, degradation rate constants where applicable and drug dissolution models.^{19,20} Besides gastric emptying rate and intestinal transit time, the ACAT model also includes pH, fluid volume, bile salt concentration, transporters, metabolic enzymes, and pore radius in each GI compartment. Unlike the original CAT model, where instant dissolution was assumed, the drug product is treated as a combination of unreleased, undissolved, and dissolved forms in the ACAT model. All three of these species can transit to the next luminal compartment. Therefore, for immediate release formulations, the ACAT model can simulate *in vivo* dissolution using formulation properties (such as particle size distribution, shape, and density) together with drug substance properties (such as solubility vs. pH profiles, and diffusivity). The model can also utilize the *in vitro* dissolution profile as a model input to predict absorption for modified release drug products.²¹

The ACAT has been continuously developed and commercialized over the past two decades under the trade name GastroPlus™.^{22,23}

1.1.3.5 Advanced dissolution, absorption, and metabolism (ADAM) and multi-layer (M-ADAM) models

The Advanced Dissolution, Absorption and Metabolism (ADAM) model enables simulation of the absorption of drugs from solution as well as from solid dosage forms, including suspensions, modified and controlled release formulations.²⁴ It is also possible to simulate metabolic and transporter drug-drug interactions as well as metabolite formation (enterocyte and gut lumen-mediated) and the relevant interactions in the small intestinal segments and colon. The ADAM model facilitates realistic simulation of gut absorption, transport, metabolism, and interactions. Further, it permits the investigation of the effect of formulations (e.g., controlled/modified release) on bioavailability when multiple drugs are administered. Also available is a standalone program, the Simcyp *In vitro* (Data) Analysis (SIVA) Toolkit. The main purpose of SIVA is to enable modelling of *in vitro* experimental results with a view to extracting parameters for input to *in vivo* simulations; this includes both solubility, including biorelevant media, and dissolution modules covering USP II, USP IV, media change, two-phase and transfer experiments.

The ADAM model has an optional extension, the multi-layer ADAM (M-ADAM) model, which incorporates the following features: (1) an unstirred boundary layer (UBL) for oral absorption from the luminal fluid into the enterocyte, (2) a permeability-limited basolateral membrane separating the enterocyte and the intestinal interstitial fluid (ISF) and (3) a lymphatic absorption route from the intestinal ISF to the systemic circulation. The M-ADAM model possesses full functionality for uptake and efflux transporters in the basolateral membrane of the enterocyte. The model is also capable of calculating drug concentrations within the UBL and enterocyte compartments, which can then be used as the driving force for drug permeation (passive and active), to describe transporter drug-drug interactions (DDI) at both the apical and basolateral membranes as well as disposition within the ISF, while retaining the capacity to predict enterocyte concentrations for metabolic and efflux transporter DDI.

The structure of ADAM and M-ADAM models within the Simcyp Simulator® is based upon the ACAT model.²² However, some important differences and additions make the ADAM and M-ADAM models significantly different from the original ACAT model. These differences include:

- Handling of luminal fluid volumes and fluid dynamics in a physiologically based manner.
- Handling of *in vitro* dissolution rate input and controlled release profiles, including separate profiles for the fed and fasted states for the stomach and small intestine.
- The use of the Wang and Flanagan diffusion layer dissolution model for spherical particles, which includes a fluid dynamics-based model for predicting diffusion layer thickness based on luminal fluid velocities.²⁵
- Inclusion of a supersaturation/precipitation, which can be parameterized by applying the SIVA toolkit modelling tools to *in vitro* transfer experiment results.
- The particle population balance (PPB) model, which permits handling of two solid states (polymorphs) of drug simultaneously – dual solid state in formulation and/or precipitation to a different solid state to that of the dosage form (or precipitation to two solid states simultaneously). The PPB model also has a nucleation model based upon classical nucleation theory (CNT).
- The incorporation of gradients and inter-individual variability in gut luminal pH and bile salt concentrations (in both the fasted and fed states).
- Handling the saturable kinetics of gut wall transporters and generic options covering apical uptake and efflux transporters, and basolateral uptake and efflux transporters which are not assigned to any specific transporter iso-form are available.
- The inclusion of a bile salt concentration-dependent model for predicting the impact on solubility and dissolution of the partitioning of drug into bile salt micelles. Luminal bile salt concentrations can be static or time-dependent using the Advanced Dynamic Bile Salt Model (ADBSM).²⁶
- The inclusion of a model for the calculation, or user input, of the pH (and thence concentration) at the dissolving particle surface ($\text{pH}_{\text{surface}}$) taking into account the buffering effect of luminal bicarbonate.
- The inclusion of a mechanistic model for handling the potential enterohepatic recirculation of drugs. This is linked to mechanistic transporter models for predicting biliary clearance including P-gp, MRP2 and BCRP and the ADBSM noted above.
- The facility to include luminal drug degradation (chemical instability and/or metabolism by luminal microflora). Metabolism of the substrate to the substrate primary metabolite in the gut lumen and back-conversion to the parent (substrate) via luminal contents such as gut microflora.
- The ability to account for luminal fluid viscosity in the fasted and fed states, which has particular impact on dissolution rate in the fed state.

Recent publications have described the use of the ADAM model and SIVA to establish an *in vitro in vivo* extrapolation (IVIVE) approach in biopharmaceutics and to predict the oral pharmacokinetics of several compounds.^{27–33}

1.1.3.6 PK-Sim absorption model

PK-Sim[®], as part of the Open Systems Pharmacology (OSP) suite, is a comprehensive open-source software tool for PBPK modeling and simulation. The original absorption model in PK-Sim[®] was a so-called “plug-flow-with dispersion” model, which incorporated the small intestine as single, continuous compartment with spatially varying properties.^{34–37} More recently, the absorption model in PK-Sim[®] was revised to include the large intestine, detailed mucosa for intestinal DDIs, active transport, and gut wall metabolism simulation as well as dissolution functions.^{38–40} Briefly, the absorption model includes 12 compartments representing the lumen of the GI tract: stomach, duodenum, upper and lower jejunum, upper and lower ileum, cecum, colon ascendens, colon transversum, colon descendens, sigmoid, and rectum, and 11 compartments representing the intestinal mucosa.³⁹ Each mucosa compartment contains four sub-compartments representing the intracellular (i.e., enterocytes), the interstitial, the red blood cells, and the plasma. The model was further revised to account for dosage form dependent GI transit, disintegration, and dissolution processes of various immediate release and modified release dosage forms.⁴⁰ Each segment contains physiological liquid volumes and drug in solution. The solid dosage forms are transported along the GI tract independently and, once released and dissolved according to the respective dissolution function, the drug is transferred from the solid to the dissolved species. Other model characteristics include representation of food including caloric content to account for food effects, enterohepatic cycling, mucosal blood flow provides and active transport processes.

1.2 Physiologically based pharmacokinetic/pharmacodynamic (PBPK) models

Modeling and simulation approaches have become an integral part of drug discovery and development. Appropriate models can provide a framework for predicting the exposure, response, and time course of a drug for different dosage forms, regimens in target populations. Physiologically based pharmacokinetic/pharmacodynamic (PBPK/PD) models can be used to predict the PK of a drug and, when combined with PD models, can predict the therapeutic and/or toxic effect of new molecular entities at the site of action. PBPK models are constructed using a series of differential equations that are parameterized with known physiological variables and represent a quantitative mechanistic framework by which the absorption, distribution, metabolism, and excretion (ADME) of drugs can be described. Due to the increasing availability of *in vitro* systems that serve as surrogates of *in vivo* reactions, *in vitro in vivo* extrapolation (IVIVE) is integral to this approach. Application of PBPK modeling used in conjunction with IVIVE of ADME data can provide a useful starting point to understand and extrapolate PK and dose across different species, populations, and disease states.^{41,42}

1.2.1 Milestones in the development of PBPK models

The origins of PBPK models can be traced back in 1937 to the work of the Swedish physiologist and biophysicist, Teorell. During summer of 1937, Teorell published two papers both with the same title: “Kinetics of distribution of substances administered to the body”, the first one dealing with extravascular modes of administration, while the second one with intravascular ones.^{43,44} Until then, physicians’ interests had been mainly focusing on finding the proper dosing schemes or routes of administration, however, Teorell’s aim was to mathematically derive relations describing the distribution kinetics of substances (i.e., time-course) in the body. In this pioneer work, the body was considered as a water pipeline throughout which blood flows and oxygenates the tissues. The latter have a certain volume, and the drug is transferred to them by diffusion, with the liver and kidneys being the only ones to have elimination capacity. Teorell derived and solved the system of differential equations by assigning biologically plausible values to the mass transfer rate constants and volumes and calculated the time-course of drug amount in the specified tissues (blood, drug depot, kidney, liver, tissues).⁴³ Although there were other PBPK studies⁴⁵ reported in the early 1960s,⁴⁵ it was not until Bischoff et al. published a series of papers in the late 1960s and early 1970s that the scientific community was provided with a more rigorous methodology for PBPK modeling.^{46–48} Through the 1980s and 1990s, PBPK modeling techniques gradually began to gain more acceptance. Typically, these models shared certain characteristics, for example, the models were drug-specific, the majority of compartments were well-stirred, the models were parameterized using *in vivo* observations, it was not possible to incorporate *in vitro* data as inputs, and variability was incorporated using Monte Carlo techniques.

Until the early 2000s, the application of PBPK models in the pharmaceutical industry had been limited due to the mathematical complexity of the models and the perceived demand for a large number of parameters required as inputs to the models. For example, in the past, large amounts of *in vivo* animal tissue concentration data were required to assess the distribution of a drug in tissues.^{7,8} The development of methods to predict tissue to plasma partition ratios² addressed a significant hurdle in the use of PBPK models. Advancement and integration of *in vitro in vivo* extrapolation (IVIVE)

techniques have significantly contributed to the recent resurgence of modern PBPK models. IVIVE-linked PBPK models allowed “bottom-up” simulations and predictions of plasma and tissue concentrations. Further, IVIVE techniques facilitated separation of the compound and species (system) parameters, which is a major paradigm shift enabling the development of generic PBPK models, as opposed to compound-specific models. The population based PBPK models are nowadays capable of predicting the inter-subject, and occasionally the intrasubject variability, using ‘correlated’ Monte Carlo methods.

Over the past two decades, the number of publications involving PBPK modeling has exponentially increased, demonstrating the widespread use of this approach across the scientific community.^{49,50} PBPK is now being used throughout the drug discovery and development process. Drug discovery is becoming increasingly “data rich” with high-throughput screening of numerous compounds for pharmacological and PK properties. In the development process, along with the prediction of drug PK at various doses and under various dosing conditions, particular interest has been generated in PBPK modeling applications supporting drug-drug interactions, biopharmaceutics, and pediatrics assessments in regulatory submissions with the aim to waive dedicated *in vivo* clinical pharmacology studies. Furthermore, in several regulatory guidance documents on PBPK modeling analyses (either of general interest or application-specific such as biopharmaceutics) and assessment of *in vivo* (clinical) and *in vitro* DDI potential of new drug candidates recently issued by both the U.S. Food and Drug Administration (FDA) and the European Medicines Agency (EMA), the use of PBPK modeling has been advocated.^{51–56} Therefore, it appears that PBPK modeling is “here to stay”.⁵⁷

Overall, PBPK models are composed of different types of information that are combined during model building and that can be used to generate simulations of different treatment scenarios. Such building blocks of information included in the model can be divided into system-related parameters, drug-specific parameters, and administration protocol properties (dosing regimen, formulation, etc.), respectively.

1.2.2 Components of PBPK models

1.2.2.1 Model structure and assumptions

PBPK models consist of compartments corresponding to the different tissues of the body, which are connected by the blood circulating system. A whole-body PBPK model contains an explicit representation of the organs that are most relevant to the absorption, distribution, metabolism, and excretion (ADME) of the drug due to their physiological function.⁵⁸ Each compartment is defined by the tissue volume (or weight) and the tissue-specific blood flow. Typically, these compartments represent the main tissues of the body, namely, adipose, bone, brain, gut, heart, liver, kidney, lung, muscle, pancreas, skin, and spleen. The tissues are linked by the arterial and venous blood compartments, and each one of them is characterized by an associated blood-flow rate, volume, tissue-partition coefficient, and permeability. However, reduced models that “lump” tissues with similar blood flow rate properties together to reduce the number of compartments and the overall model complexity have also been described.^{59–62} Each tissue is typically described as either perfusion rate limited or permeability rate limited.^{63–65} A schematic representation of these different types of tissue models is shown in Figure 1-1.

Perfusion rate-limited kinetics tends to occur for small lipophilic molecules where the blood flow to the tissue becomes the limiting process. This type of model assumes that at steady state, the total drug concentration in the tissue is in equilibrium with the total drug concentration in the circulation as determined by the drug-specific tissue partition coefficient (K_p) value, whereas free drug concentrations are equal. The time required to reach steady state is determined by the blood flow rate, tissue volume, and K_p value for the particular tissue. Typically, a highly perfused tissue will reach steady state faster than a poorly perfused tissue.

Permeability rate-limited kinetics typically occurs for larger, polar molecules where the permeability across the cell membrane becomes the limiting process. In this case, the tissue is divided into essentially two compartments, representing the intracellular space and the extracellular space, which are separated by a cell membrane that acts as a diffusional barrier (Figure 1-1). In principle, at steady state, this model will also reach an equilibrium at which free drug concentrations are generally equal. However, for this particular type of kinetics, the time to reach equilibrium is highly dependent on the drug-specific permeability rather than the blood flow. The permeability is used to estimate a rate constant that drives the equilibrium across the cell membrane between the intracellular and the extracellular concentrations. If active transport processes are involved, either into or out of the intracellular space, free concentrations in the intracellular space may be higher or lower than the extracellular space, respectively.⁴¹

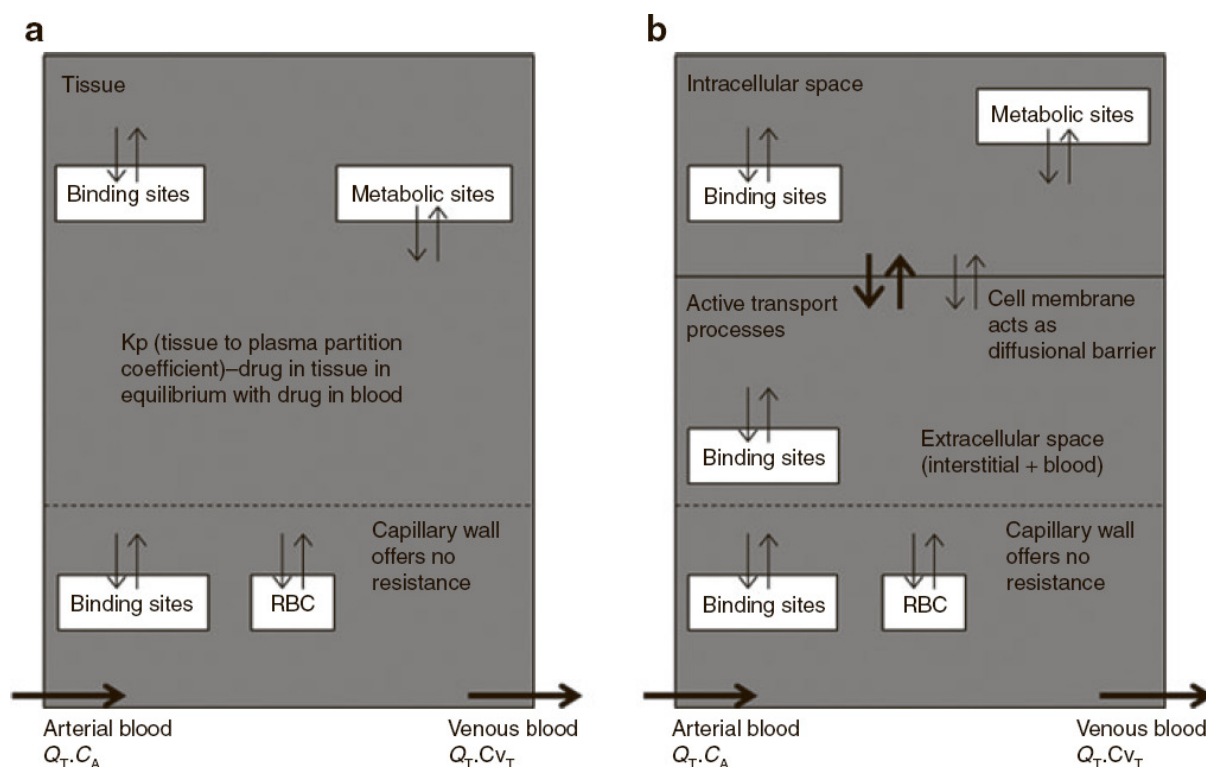


Figure 1-1: Perfusion vs. permeability rate-limited tissue models. (a) Perfusion rate limited; (b) Permeability rate limited. K_p , tissue to plasma partition coefficient; RBC, red blood cell (Jones H, Rowland-Yeo K. *CPT Pharmacometrics Syst Pharmacol*. 2013 Aug 14;2(8): e63).

In the majority of cases, PBPK models used in drug discovery assume perfusion rate-limited kinetics with the liver and kidney being the only elimination organs.^{41,64–67} The mass balance differential

equations used in these models have been described in detail elsewhere.^{41,64,65} Briefly, for non-eliminating tissues, the tissue concentration-time course is equal to the rate of the drug “in” minus the rate of the drug “out” of the tissue and can be described as follows:

$$V_T \cdot \frac{dC_T}{dt} = Q_T \cdot C_A - Q_T \cdot C_{v_T} \quad (24)$$

$$C_{v_T} = \frac{C_T}{K_p} \cdot (B:P) \quad (25)$$

where V_T , Q_T , C_T are the tissue (T) volume, blood flow rate and total drug concentration in the tissue, respectively; C_A and C_{v_T} are the arterial (“entering” the tissue) and venous (“entering” the tissue) drug concentrations with B:P being the blood to plasma concentration ratio.

For eliminating tissues, the free concentration in the venous blood leaving the tissue (which is assumed to be equal to the free concentration of drug at the enzyme/elimination site) is used to drive the elimination rate. In this case, the above equation is modified to account for clearance as follows:

$$V_T \cdot \frac{dC_T}{dt} = Q_T \cdot C_A - Q_T \cdot C_{v_T} - CL_{int} \cdot C_{v_{u,T}} \quad (26)$$

where CL_{int} is the intrinsic clearance of the drug and $C_{v_{u,T}}$ the unbound venous drug concentration. The CL_{int} refers to the intrinsic ability of the unbound drug to be metabolized by relevant enzymes in the absence of extrinsic factors such as protein binding and blood flow.

The model structure described so far can be used to simulate plasma and tissue plasma concentration–time profiles following intravascular administration. However, for extravascular administration, with the oral route being the most important, a number of absorption models have been described in the literature.^{24,39,40,68,69} Essentially, the gut is separated into two main compartments representing the lumen (unabsorbed drug) and the enterocyte (absorbed drug). Each compartment is further split into a number of sub-compartments corresponding to the different regions of the gastrointestinal tract, namely, the stomach, duodenum, jejunum, ileum, cecum, and colon. Despite differences in the number of sub-compartments between models, typically each sub-compartment is defined by a volume, transit time, pH, and bile salt concentration. The volume and transit times are used in a similar way to the perfused tissue equations to describe the movement of the drug through the gastrointestinal tract. Drug (e.g., pKa, solubility, logP) and formulation (e.g., excipients, drug particle size) specific parameters are used to define the fate of the drug in the gastrointestinal tract (i.e., liberation, dissolution, nucleation, precipitation) and its permeation through the gut wall. By default, these models assume passive absorption, however metabolic and active transport process can be incorporated if relevant. Details about oral absorption models and their evolution over the past decades can be found in section 1.1.

1.2.2.2 System-related input parameters

System-related input parameters refer to the anatomical and physiological characteristics of the species and/or populations considered by the respective PBPK platform. These include, for instance, organ volumes, composition, blood flows, surface areas, protein expression levels and metabolic

activity. Blood flow governs mass transfer within the body, and its rate is specific to each organ and species. PBPK system-parameters and platform qualification for the most common species such as mouse, rat, dog, monkey, and human are typically provided in all commercially available PBPK software. Nevertheless, depending on the source, analysis, and interpretation of the available data, significant differences in the species physiological and anatomical characteristics between the PBPK platforms may still exist.

An even more detailed and mechanistic description of a subset of organs can also be included in such models to obtain a more precise representation of drug disposition in the specific tissue such as the brain, the liver, the kidney, the lung, the skin and more importantly the intestine.^{24,38,39,70-76} Considering the mechanistic nature of these models, it is also possible to incorporate physiological and mechanistic features to predict the PK in specific prandial or disease states, ethnicities and/or population groups. In this context, for example, several authors have incorporated known changes in the hepatic and/or renal physiology as function of disease and/or age, to predict the exposure in different patient populations and age groups.⁷⁷⁻⁸⁰ Databases to support this modeling of exercise can be found in the literature or be available by the PBPK software provider and include, but are not limited to, elderly, pediatric, pregnancy, obese, hepatically or impaired, cancer, Japanese and Chinese populations.^{77,79,81-91}

The ability to include sources of physiological and biochemical variability in the system parameters and to simulate the expected PK in a population of individuals rather than for an average subject is an indispensable component of PBPK models. A virtual population can be generated from values and equations describing the demographic, anatomical, and physiological variables using a correlated Monte-Carlo approach.^{84,92} The distributions and co-variable effect of system parameters in PBPK models are derived from analysis of real-world population and patient data. This allows prediction of population variability prior to clinical studies in contrast to a statistical approach (e.g., population PK analysis), which requires prior clinical data to characterize the variability levels.⁹³⁻⁹⁵

1.2.2.3 Drug-specific input parameters

Parameterization of PBPK models require numerous drug-specific input parameters based on the understanding of the absorption, distribution, metabolism, and excretion (ADME) properties of a particular compound. *In vivo* intrinsic organ clearance (CL_{int}) together with tissue-plasma partition coefficients (K_p) are key parameters for the characterization and prediction success of drug distribution and elimination. For example, the drug clearance estimated from *in vitro* systems (e.g., recombinant enzymes, microsomes, and hepatocytes) can be scaled to hepatic intrinsic clearance using a number of physiological scaling factors, such as intersystem extrapolation factors, microsomal recovery and hepatocellularity. These values can then be either used directly (after relevant unit conversion) into PBPK models or can be further translated to whole organ hepatic clearance (CL_h) using drug blood-binding and liver blood flow data within well-defined liver models (e.g., well-stirred, parallel tube).⁹⁶ These *in vitro-in vivo* extrapolation (IVIVE) approaches for hepatic clearance prediction have been described in detail and extensively validated by a number of authors^{41,96-98}

For other clearance mechanisms, such as renal or biliary excretion, active uptake and transport, a number of other approaches have been implemented to predict the *in vivo* behavior. These mainly include single- or multi-species allometric scaling and *in vitro-in vivo* extrapolation (e.g., for biliary secretion and active transport).⁹⁹⁻¹⁰⁴

Another important set of compound-specific parameters are the K_p values which are used to characterize the distribution of the compound into different tissues in the body. K_p values are defined as the ratio of total concentration of compound in the tissue to total concentration of compound in the plasma at steady state. More mechanistically, these K_p values represent the degree of tissue accumulation attributed to processes such as protein binding, lysosomal trapping, and lipid dissolution. Several methodologies have been described in the literature for the prediction of K_p values. The development of mechanistic, tissue composition-based equations for the prediction of K_p values and hence distribution in rat, dog, and human have enabled the routine application of PBPK methods in early drug discovery. Such models estimate the extent of tissue distribution from the physicochemical and *in vitro* binding (to proteins and lipids) characteristics of the drug. Based on tissue composition, these coefficients can account for the distribution between drug-binding tissue constituents, such as proteins or lipids, on the one hand, and water on the other. Although all known partition coefficient models assume that tissue is composed of a limited number of components, and they all include partition coefficients for water/protein and lipid/water, their specific calculation methods deviate with respect to the kind of parameters used and result in different values of tissue concentration.

Initially, Poulin et al. calculate the lipo-hydrophilicity of tissue as a mixture of neutral lipids, phospholipids, and water. In addition to the volumetric tissue composition, fraction unbound (f_u), lipophilicity ($\log P$ and $\log D$), and pK_a are used as compound-specific input parameters.^{97,98,105–107} Here, as well as in all the following concepts for the calculation of organ/plasma partition coefficients, f_u quantifies specific reversible binding to proteins in plasma and tissue, whereas lipophilicity accounts for nonspecific binding to lipids. Rodgers et al. extended the concepts of Poulin et al. to electrostatic interactions at physiological pH.^{99,100} These include binding of ionized and unionized drugs to acidic phospholipids and neutral lipids, respectively. Electrostatic drug interactions with extracellular proteins are also taken into account. Subsequently, the partition coefficients are calculated considering the lipophilicity and pK_a value of the drug and the pH values of the tissues. Berezhkovskiy modified the calculation method by Poulin et al. by accounting for peripheral drug elimination, which results in a different volume of distribution.^{105,108} Other tissue distribution models have been described by Willmann et al. to provide the default K_p calculation method in PK-Sim software, as well as by Schmitt et al.^{34,109,110} Based on the above tissue-composition models, the volume of distribution at steady state (V_{ss}) can be easily calculated as follows:

$$V_{ss} = \sum_{T=1}^n V_T \cdot Kp_T + V_{plasma} \quad (27)$$

where V_T , Kp_T are the tissue-specific volumes and partition coefficients, respectively. A number of studies have been performed to investigate the ability of these different mechanistic approaches to predict K_p using a range of drug datasets and have reported varying degrees of accuracy.^{64,65,67,98,111,112}

An important component of any PK simulation after oral administration is the prediction of the rate and extent of absorption. The dynamic mechanistic oral absorption models (see section 1.1.3) rely on a variety of *in vitro* or *in silico* input data such as solubility, permeability, particle size, $\log P$, and pK_a to describe the dissolution, solubilization, precipitation, uptake from the enterocyte and absorption of drug as it transits through the different segments of the gastrointestinal tract.

Human effective permeability is one of the key parameters for oral drug absorption. At early stages of drug discovery, this can be predicted from *in silico* models or measured in high-throughput assays, such as the parallel artificial membrane permeability assay and Ralph Russ canine kidney cells. At more advanced stages, permeability measurements from Caco-2 and MDCK cell lines are often the first choice. To utilize such data in PBPK models it is necessary to scale these *in vitro* data to the *in vivo* situation (i.e., human effective permeability). The test compound is typically calibrated against a number of reference drugs for which human *in vivo* jejunal permeability data has been measured.¹¹³

Another key input parameter is the *in vitro* solubility. This value at a given pH can be used to approximate the *in vivo* solubility over a range of pH values in the gastrointestinal based on the pKa and pH-partition theory. However, and especially for poorly soluble drugs, aqueous solubility might not be representative of the *in vivo* situation due to micelle-mediated solubilization by the bile components which are present in the GIT. In this case, solubility in media simulating the contents of the gastrointestinal lumen, so called biorelevant media, offer a more pragmatic estimate of the *in vivo* solubility in the site of absorption.¹¹⁴

In addition, the fraction of unbound drug in the enterocyte ($f_{u, \text{gut}}$), gut wall metabolism and active transport process, such intestinal and hepatic uptake or efflux are also important drug-specific input parameters. In the case of the intestine, parameters describing the kinetics of drug efflux (V_{max} , K_m) can be obtained from Caco-2 or other cell line systems by incubating the test compound over a range of concentrations. These parameters can then be scaled to the *in vivo* situation by correcting for the surface area differences between *in vitro* and *in vivo* and can serve as input in PBPK models to simulate the effects of the P-glycoprotein (P-gp) and the breast cancer resistance protein (BCRP) on the absorption of the compound. However, such applications are currently limited by the lack of *in vitro*-*in vivo* correlation of P-gp and BCRP kinetic parameters.¹¹⁵⁻¹¹⁷

In the case of the liver, organic anion transport proteins (OATPs)-mediated uptake can also be incorporated into the generic PBPK model framework. This is achieved by modeling the liver as a permeability-limited tissue, incorporating active uptake and passive diffusion of unbound drug at the sinusoidal membrane and biliary secretion at the canalicular membrane. Compound-specific parameters to support these models can be estimated from *in vitro* sandwich-cultured hepatocyte data and scaled to the *in vivo* situation accounting for the hepatocellularity per gram of liver and liver weight.^{101,103} To determine accurately these transport parameters, particularly biliary efflux, the intracellular concentration of the drug must be estimated, hence *in vitro* models describing the dynamics of the hepatocyte system have been adopted to calculate precisely these *in vitro* uptake parameters.^{101,104} Integration of relevant scaled *in vitro* parameters into PBPK models have been used to simulate *in vivo* PK for OATP, however, in most cases successful predictions were only achieved when empirical scaling factors were incorporated.^{104,118,119}

The last category of drug-specific parameters to consider is the interaction properties of the investigational drug. These include the reversible (K_i) and time-dependent inhibition (K_I , k_{inact}) as well as the induction (E_{max} , EC_{50}) properties of the drug, which are critical for the prediction of drug-drug interaction potential of the drug as perpetrator. The relevant input parameters can be derived experimentally in a variety of *in vitro* systems (e.g., human hepatocytes). The inhibition parameters can be used directly as input into PBPK models, however the value maximum induction potential (E_{max}) should be calibrated against a positive control (e.g., rifampicin).¹²⁰⁻¹²⁵

1.2.2.4 Trial design

Population PBPK and virtual clinical trial simulations require specific information about the population of interest as well as the trial design. As population demographic characteristics affect the physiology and in turn the individual PK, appropriate trial design is usually critical for successful PBPK predictions. The age, sex, ethnicity, and disease state of the virtual population should closely match the demographics of the individuals which had been or intended to be enrolled in an actual clinical trial. In addition, the route of administration, dosing regimen and possible meal or liquid administration should be also precisely satisfied.¹²⁶

1.2.3 *In vitro in vivo* extrapolation in PBPK modeling

ADME properties of drugs can determine various features of their concentration–time profiles in the systemic circulation as well as in the organs of the body. However, these values are rarely reflective of the drug alone because they depend on the population of the individuals in whom the measurements have been carried out and the conditions under which the study was performed.⁴² In other words, the data reflect the properties of the system and the study conditions as much as they reflect those of the drug. The intrinsic and extrinsic factors determining the changes (variation) in the kinetics values are of particular interest to drug regulatory authorities when dealing with labeling requirements.¹²⁷ Some of these include effects of food/diet, age, gender, race, genetic polymorphism of drug metabolizing enzymes and transporters, concomitant medications, comorbid disease, and organ dysfunction.

This leads to the dilemma of having to conduct many studies to confirm or reject the significant influence of the parameters of interest. PBPK–IVIVE linked models provide an alternative that can be used to select the studies that would be most relevant to conduct and guide experimental and/or clinical design, especially when prospective clinical studies are not feasible. In principle, this works by redefining the kinetics parameters such that they become more reflective of the drug itself rather than of the system or the study conditions. In addition to facilitating recognition of covariates, using PBPK to separate the attributes of systems, drugs, and trial designs in the various models and databases²⁵ is not an easy task, given that many pieces of data on physiology, biology, and biochemistry are not defined in relation to demographics (e.g., genetics, age, and environment) or disease states.⁹² The building blocks of PBPK models, namely parameters defining ADME and their links to *in vitro* data—are described in detail in section 1.2.2. However, a brief overview of the elements that make up the PK of drugs and lead to interindividual variability in exposure in response to identical doses is provided here.

1.2.3.1 Oral drug absorption

The most common route for drug intake is the oral route. Bioavailability (F) of orally administered solid dosage forms involves release of the drug from the formulation, dissolution, passage through the gut wall, and then passage through the liver. Bioavailability is often considered as having three components: the fraction of the dose that enters the gut wall (f_a), the fraction that escapes metabolism in the gut wall and enters the portal vein (f_g), and the fraction that enters the liver and escapes metabolism (f_h). The total bioavailability is the product of these three components (i.e., $F = f_a \times f_g \times f_h$). Both absolute and relative values of F and each of its components can be assessed by means

of *in vitro* experiments and subsequent IVIVE.²⁴ However, the ability to extrapolate the data relating to solubility, dissolution, and permeability requires a full understanding of the environment in the gut lumen as well as a cell line that adequately reflects the permeability through the gut wall. For example, *in vitro* solubility and dissolution experiments, even using biorelevant media, are performed typically with phosphate buffer species, under non-sink conditions and with hydrodynamics deviating from the *in vivo* situation, which makes extrapolation to the *in vivo* situation challenging.^{30,32} Other elements, even those known to be present in the average population, might be missing in the specific population of interest. For example, the attributes of the gastrointestinal tract relating to motility, pH, volume of fluid (secretion and re-absorption rate), and composition (bile salt concentration) are not entirely known in pediatric patients, the elderly, those with hepatic impairment, during pregnancy, or after bariatric surgery. Although all these categories of patients still require pharmacotherapy, they are rarely investigated before the drugs are released into the market. For details about current knowledge gaps in oral drug absorption and IVIVE of absorption-related parameters, the reader is referred to the perspectives papers by Loiosio-Konstantinidis and Dressman as well as by Vinarov et al.^{128,129}

The bioavailability of orally administered drugs can also be influenced by first-pass gut wall metabolism and transport.^{130–133} Again, the data on abundance and location of enzymes and transporters in the gastrointestinal tract in relation to the routine *in vitro* test systems are sparse. Moreover, the formulation can affect the gut metabolism of the drug by releasing active ingredients in different regions,¹³⁴ since the abundance of enzymes and transporters in the gut wall varies regionally.^{130,135–144} Cytochrome P450 (CYP) 3A and multidrug resistance P-glycoprotein (P-gp; also known as MDR1, ABCB1) are present at high levels in the villous tips of enterocytes in the small intestine.¹⁴⁵ Nonetheless, other CYP-related and non-CYP related enzymes, such as the UDP-glucuronosyltransferases (UGTs), are also present in the small intestine and are involved in drug metabolism.^{146,147} Quantitative links (extrapolation factors) for all the intestinal metabolic routes are reported sporadically and are far from ideal.^{116,146,148,149}

Although the models describing the absorption of orally administered drugs can accommodate all the aforementioned elements, obtaining informative *in vitro* data for quantitative extrapolation remains a challenge, and some degree of validation using observed data (combining the *in vitro* and *in vivo* approaches) is usually carried out in order to increase confidence.¹⁵⁰ The lack of or limitations to available information makes drug use in specific patient populations (including those listed above) susceptible to off-label use, particularly when no alternative drugs are available.

1.2.3.2 Hepatic, biliary, and renal clearance

The traditional early screening methodologies for IVIVE of clearance were designed and used for assessing overall stability and residence time within the body rather than for identifying elimination by various routes.⁵⁴ The relative success of IVIVE in using data from *in vitro* systems to predict hepatic intrinsic clearance and associated variability in human populations has resulted from the increasing amount of available information on appropriate scaling factors.¹⁵¹ However, covariates of many scaling factors that have population attributes such as age, particularly in neonates and younger children, are not as refined as one might wish.¹⁵² There is a whole battery of *in vitro* systems for assessing metabolic clearance, including human liver subfractions (microsomes, cytosols, and hepatocytes) and recombinantly expressed enzymes.^{153–157} The use of expressed enzymes allows the clearance values to be expressed per unit of enzyme (e.g., CYP or UGT). Estimating the net intrinsic metabolic clearance in total liver ($CL_{hep, int, un}$) from data obtained with recombinantly expressed enzymes boils down to a summation of the clearances from each metabolic pathway and each enzyme

(considering the abundance of each enzyme in the target population), followed by multiplication to milligrams of microsomal protein per gram of liver and whole mass of liver.^{154,158} On some occasions, the activity of one unit of enzyme in the expressed system might be a few multiples higher or lower than one unit of enzyme in the human liver; these can be accommodated by intersystem extrapolation factors (ISEFs).^{159–161} It is obvious that these simple scaling methods do not automatically consider the effects of time- or concentration-related nonlinearity. However, once they are incorporated into sets of PBPK differential equations, they can be expressed as concentration- or time-variant parameters according to Michaelis-Menten kinetics by defining the clearance as the ratio of the maximum velocity of metabolism per unit of enzyme (V_{max}) and the Michaelis constant (K_m). In addition, a dynamic pool of time-variant enzymes that respond to any induction or suppression of enzyme synthesis and accelerated or stabilized enzyme degradation could be defined as sub-models.^{162–167} Combining all these aspects opens a great opportunity for quantitative handling of covariates related to metabolic clearance, including genetics, age (ontogeny), ethnicity, sex, pregnancy, obesity, co-morbid diseases such as cirrhosis⁴ and chronic kidney failure, effect of environmental factors such as smoking, complex drug–drug interactions involving metabolites and the nonlinearity of these with time.^{33,62,79,85,90,168–180} Recent advances in quantitative proteomics and liquid biopsy to measure the abundance and variability of each enzyme and transporter in various tissues may allow more informed extrapolation to diverse populations, although some coordination and global validation of the results using the same set of samples might be necessary to overcome some discrepancies in the reported values.^{144,181–186}

Renal excretion plays a major role in the elimination of many drugs. Although factors determining the extent of renal elimination have been known for many years (e.g., lipophilicity and ionization, plasma protein and erythrocyte binding), only a few *in vitro* systems for predicting renal clearance of xenobiotics are currently available.^{71,187–189} The IVIVE efforts to estimate biliary excretion have also been limited, although some success in using sandwich-cultured hepatocytes has been reported.^{101,190,191} In all clearance predictions, understanding the value of the unbound fraction of the drug in plasma in an individual, based on the concentration levels of albumin, α -acid-glyco-protein, and plasma lipids, is an integral part of the exercise.¹⁹² Although this can be measured *in vitro* for any target population, defining protein binding on the basis of binding affinities to various plasma proteins and partition to lipids also enables automatic extrapolation to other groups whose modified plasma protein levels are well characterized, such as the elderly, pregnant women, and neonates.^{193–195}

1.2.3.3 Tissue distribution

Tissue volumes and tissue blood flows are essential components of PBPK models. Correlations between tissue volumes and tissue blood flows should be considered when modeling interindividual variability in drug distribution using PBPK models. There are drug-related characteristics (such as the ability to cross membranes, bind to plasma proteins, and partition into red blood cells, tissues, or fat as well as specific affinity to influx or efflux transporter proteins) that can influence the dynamics of distribution to various tissues and thereby affect the concentration–time profile of drugs.⁴² Many of these can be measured *in vitro* and thus used for IVIVE purposes. As described earlier, current IVIVE approaches for assessing the distribution of the drugs to various tissues involves estimation of tissue-to-plasma partition coefficient based on affinity to lipids and binding to common proteins present in the tissue interstitial space, combined with *in vitro* measurements of protein binding in blood and plasma.^{106,108,196–198} By determining the partition to various tissues, the volume of distribution of drugs can be estimated. The proportion of the drug in different tissues changes over time. Consequently, the drug concentrations profiles in tissue are not necessarily evolved in parallel with those in plasma,

even in the commonly assumed case of a perfusion-limited entry to tissues. Many of the systems parameters defining the tissue compositions are not yet known in humans, and animal data are used instead.¹⁹⁹ In addition, in the membranes of various tissues (e.g., liver) there are numerous drug transporters. These transporters can influence drug distribution into the tissues, particularly for drugs with low passive permeability. Modeling the diffusion-limited transporter-related distribution of drugs into tissue requires separation of extracellular compartments from intracellular water.⁴¹

1.2.4 PBPK model building approaches

PBPK models may be initiated from an *in vitro* understanding of drug related ADME mechanisms. Alternatively, PBPK model development may be based solely or partly on observed clinical data. In this section, a brief overview of the various PBPK modeling strategy approaches is provided.

“Bottom-up” approach

A “bottom-up” approach involves extrapolation of *in vitro* data for modeling of the mechanisms that define LADME processes and the related concentration-time profiles. This approach relies on high-quality *in vitro* and preclinical data and may be verified later in drug development as clinical data become available. The application of “bottom-up” models depends heavily on the quality of the initial data, as well as the availability and predictive accuracy of verified *in vitro*–*in vivo* extrapolation (IVIVE) methods, factors, and scalars. Moreover, especially at early stages of drug development, a degree of uncertainty is associated with scalars for extrapolation of *in vitro* data to *in vivo* settings, especially where transporters are involved. As a result, early bottom-up models will require verification with *in vivo* clinical data, and when model performance is deemed to be insufficient an alternative approach including calibration of parameters might be required at later stages and for regulatory decision-making.

“Top-down” approach

A “top-down” approach mainly involves fitting of the model parameters to clinically observed plasma concentration–time profile and/ or urine data of a drug following administration of intravenous (i.v.) dose, single or multiple oral ascending doses, DDI scenarios, or exposure across multiple formulations. This approach is commonly used in population PK (PopPK) data analysis, where statistical approaches are applied. In top-down approaches the main objective is to fit a model so that it describes adequately the observed data, estimate mean population parameters and their associated variability (inter- or intra-individually), and to identify significant covariates of PK parameters. Usually, these types of models are capable of interpolating data, but extrapolation outside the data space used to fit the model is challenging.

“Middle-out” approach

The “middle-out” approach is a combination of “bottom-up” and “top-down” approaches. In this approach the initial model relies on a foundation of high-quality physicochemical, *in vitro*, preclinical, and mass-balance data in combination with other *in silico* or built-in PBPK prediction of drug distribution parameters. “Middle-out” PBPK models also rely significantly in IVIVE, however, calibration of key parameters with observed clinical data is allowed. For instance, the fraction metabolized (f_m) by a specific enzyme (e.g., CYP3A) can be refined/optimized to recover the observed DDI with a strong inhibitor.²⁰⁰ The refinement of model parameters using clinical data may be

performed by either visual inspection, sensitivity analysis or using more powerful parameter-estimation algorithms, including sparse data methods such as nonlinear mixed effects and Bayesian maximum-likelihood procedures (see also section 1.2.8). The refined parameters in a “middle-out” PBPK model are usually uncertain due to experimental challenges, measurement with low confidence, or lack of data (such as kinetic parameters, ontogeny profiles of transporters, etc.) and can sometimes be sourced from a semi-mechanistic PopPK model. The model predictive performance should be assessed using external verification datasets from independent clinical studies to confirm the model. After verification, the refined model can be used to address clinically relevant questions, such as requesting a waiver for dedicated DDI clinical trials, or to extrapolate PK and scale the dosing from adults to younger children and neonates or infants.^{82,201,202}

The recent guidance documents published by the European Medicines Agency (EMA) and the US Food and Drug administration (FDA) acknowledge the limitations in the use of a purely IVIVE-driven (“bottom-up”) approach while emphasizing the added benefits of PBPK-IVIVE models in “extrapolation” to conditions that have not yet been studied.^{51,52} These benefits are not commonly associated with the classical data analysis of clinical studies (top-down approach).

The “middle-out” models, which are also known as hybrid multilevel models, combine advantages and strengths of the two other approaches. Therefore, they are not just restricted to explaining the observed data, but they intend to go backwards (in explaining the clinical observations) in order to go forwards beyond the perimeters of the initial clinical study using the prior *in vitro* and system information.²⁰³ While both of “top-down” and “bottom-up” approaches have their advantages, it is becoming apparent that a verified bottom-up or an integrative “middle-out” approach may provide enhanced flexibility of PBPK models by applying the “predict, learn, confirm, apply” paradigm and allow *a priori* decision-making.²⁰⁴

It should be noted that the boundary between “bottom-up” and “middle-out” as well as the distinction between “top-down” and “middle-out” is often obscure. For instance, “top-down” models may also infer mechanistic meanings for the fitted parameters under investigating a clinical observation, however, the frequency of using “external” data/information is less frequent in these models as opposed to the “middle-out” approach. Similarly, it is common that a “bottom-up” model building leverages clinical data as soon as the latter is available.

Combining these models is not a seamless process and is fraught with issues, as reviewed by Tsamandouras *et al.*²⁰⁵ If viewed purely from a mathematical point of view, these “middle-out” approaches suffer from structural identifiability issues. The absence of a unique correspondence between parameter values and the observed output is concerning for the researcher who wants to quantify the physiological process. On the other hand, even structurally identifiable models may suffer from numerical non-identifiabilities. This occurs when clinical observations are made in a space that makes the model outcome insensitive to changes made to certain model parameter values (particularly in the face of noise and variations). Finally, estimating parameter values without considering the correlation between parameters can be an issue. The importance of such intercorrelations has been underlined to some extent by some recent research reports.^{203,206}

1.2.5 Structural identifiability

Warnings about the issue of parameter identifiability in biological mathematical modelling (including PBPK modelling) have been repeatedly raised in the literature.^{205,207–211} However, this issue seems to have been overlooked in many case studies using a “middle-out” approach. According to the definitions related to identifiability, a parameter is unidentifiable if an infinite number of solutions exist.²¹² Conversely, it is locally identifiable if there are only a finite number of solutions and globally identifiable if only one solution exists. Similarly, the model is unidentifiable if at least one of its parameters is unidentifiable and, locally or globally identifiable if all parameters are locally or globally identifiable, respectively.^{208,212} There are two types of parameter identifiability: statistical and structural. Statistical identifiability is related to the experimental error of the observed data. However, even with error-free data, a model parameter could be structurally non-identifiable. The concept of structural identifiability (also referred in the literature as “*a priori* identifiability”) is important to ensure that the unknown model parameters of interest are uniquely identifiable from a specified experiment, assuming noise-free data.²¹² A PBPK model consists of many parameters, some of which may have unknown values either due to technical difficulties in measurement techniques or because they have simply never been measured. The unknown parameters are usually estimated through fitting of the model to the observed data from well-defined study sets using a known specific dosing regimen.^{204,205,209} A controlled input specifies data with observations from confident well-defined study sets, e.g., at a known specific dose. However, estimation of model parameters through this approach can have limitations when the number of unknown parameters is large relative to the information contained in the available data or the available information is sufficient, yet inappropriate, for calibration of parameters of interest.²⁰⁴ Various sets of parameter values can result in an equally good fit to the data in a way that individual parameters cannot be uniquely identified. In this case, the model loses mechanistic meaning and applicability and is said to be “unidentifiable.” As a result, extrapolation to populations outside the studied conditions is unjustified or may lead to false conclusions.^{205,209} In practice indications for identifiability issues are failure of the optimization procedure to converge, parameter values that prove sensitive to the initial estimates used for optimization and the presence of highly correlated parameter estimates.²⁰⁹

Various mathematical identifiability analysis approaches have been previously described in the literature.^{210,213} Proposed approaches to deal with structural identifiability in PBPK modeling include measuring some of the unknown physiological parameter values (if possible), reduction in the number of parameters (by grouping several unidentifiable parameters into a single identifiable parameter), redefining parameters (re-parameterization), or generating data that could be used in calibration with a different *in vivo* dataset.^{209,210,214,215} Several statistical approaches can also be used to declare a PBPK model as identifiable.²¹⁶ Importantly, it should be noted that structural identifiability analysis is an element of the experimental design and is recommended to be performed at an early stage.

1.2.6 Statistical identifiability and sensitivity analyses

Even when the model is itself structurally identifiable, it may suffer from statistical or so-called practical non-identifiabilities.²¹⁷ Statistical identifiability problems are related to the scatter (noise) of the observations, which is reflected in the standard errors of the individual parameter estimates.

This issue arises mainly either due to insufficient number and quality of observations or due to lack of sensitivity of the model's output to differences in the values of the parameter or combination of both. These conditions particularly apply in PBPK modelling in which ethical and experimental considerations may affect the quantity and quality of the data, but the physiological-anatomical topology of the estimated parameter is remote from the model's observed output (usually plasma). Statistical non-identifiability is usually manifested with increased uncertainty (standard errors) in the parameter estimates and/or problems in the optimization routines to converge to a minimum, as the objective function related to an insensitive model parameter is relatively flat. In order to overcome these hurdles, experimental and sampling design can be optimized to improve the information content of the data.²¹⁸ In addition, before estimation of an unknown parameter, parameter sensitivity analysis might be useful to investigate if the output is sensitive to parameter perturbation.

Sensitivity analysis (SA) is a method that examines how the variation in the output of the model can be attributed, qualitatively or quantitatively, to different sources of variation.^{219,220} The various SA methods that exist for the analysis of complex deterministic models can be grouped into two categories: local (LSA) or one-at-a-time methods that consider sensitivities close to a specific set of input parameter values, and global methods, which calculate the contribution of a parameter over the set of all possible input parameters.²¹⁹ In most cases when SA has been conducted on PBPK models published in the peer-reviewed literature this has been a LSA. This involves the adjustment of individual model parameters, whilst all other parameters are held constant, and observation of the predicted changes in model output, either at a single time or throughout a time course. The results are usually expressed as normalized sensitivity coefficients (SCs), which are the percentage change in the output produced by a fixed and constant percentage (usually 1%) change in the parameter. When trying to establish the contribution of a parameter to model predictions, LSA techniques are fairly rapid and simple to implement but can give somewhat misleading results if there are substantial interactions among multiple parameters.^{220,221} For example, PBPK models usually describe non-linear processes such as saturation metabolism, and certainly contain interactions or inter-correlations between parameters (e.g., organ blood perfusion rates and cardiac output). LSA might be inappropriate for these types of parameters, especially if the plausible range of the parameter is much wider than this technique allows and in such cases the uncertainty in the parameter should be represented via a joint probability distribution. In short, LSA results may be unreliable unless the interactions between parameters are negligible, and the system behaves linearly over the dose range of interest. Thus LSA should be applied with caution, especially as the purpose of PBPK models is very often to extrapolate beyond the domain of "observation" used to construct and evaluate the model.^{151,222} When LSA is less appropriate and/or the input variables are known to be affected by uncertainties of different orders of magnitude, a global SA (GSA) that is independent from assumptions about the model structure is called for.^{220,223–225}

In contrast to LSA, GSA methods calculate the contribution of a parameter over the set of all possible input parameters. In a PBPK modeling context a global method would perturb all organ and tissue masses, blood perfusion rates, metabolic parameters, and partition coefficients within plausible ranges. The contribution to model output of any single parameter and/or interactions of multiple parameters is measured yielding useful quantitative information about the overall relative importance of all model parameters. The most commonly applied global method quantifies the importance of parameters as an exact percentage of the total output variance that each factor (or group of factors) is accounting for.²¹⁹ Recently, two types of GSA that differ in the aims and, thus, in the parameter

variability were proposed by Melillo et al.²²⁶: inter-compound and intra-compound GSA. The inter-compound GSA aims to understand which are the parameters that mostly influence the variability of the metrics of interest in the whole space of the drugs' properties, and thus, it is useful during the development of "global" PBPK models (i.e., compound-independent). On the other hand, the intra-compound GSA aims to highlight how much the uncertainty associated with the parameters of a given drug impacts the uncertainty in the model prediction and is thus useful during drug specific PBPK applications. The reader is referred to the work by Saltelli et al.^{220,221} for a comprehensive review of the different methods and technical issues related to sensitivity analysis and to Melillo et al. and Yau et al. and for applications in PBPK modelling.^{183,227,228}

1.2.7 Physiological plausibility and correlation of physiological parameters

Model fitting to plasma concentration profile by visual inspection or model diagnostics does not necessarily guarantee model performance and adequacy if the values of estimated parameter are outside the physiological plausible space. Therefore, it is highly recommended to routinely assess whether parameters' estimates are biologically plausible and have physical meaning. Furthermore, in this context, evaluation of the predictive performance of the model in instances where at least one of the system's pathways is perturbed has been considered to be beneficial (e.g., drug-drug interactions).^{205,207}

An additional issue when attempting to estimate parameters in a PBPK model arise from the fact that some of these parameters are intrinsically correlated, through the underlying physiology. In the event that this correlation between model parameters is neglected, biased, imprecise, and often physiologically un-realistic or non-sense parameter estimates may result. Therefore, in the case of two highly correlated parameters it is usually recommended either to use a fixed physiologically plausible value extracted from the literature for one of them, or to re-parameterize the model in terms of a composite variable.²⁰⁵ An example of the latter is to parameterize the model in terms of the intrinsic clearance of a compound per molar unit of enzyme, instead of separately estimating a different clearance in each eliminating tissue as a separate parameter. In general, even if indicated for example from GSA, optimization of system-related parameters is highly discouraged and a sound scientific rationale for parameter selection and optimization is paramount.²⁰⁴ For instance, changing tissue blood flow and organ sizes will change the PK profile of a drug, but it is not clear how such an analysis would be informative within the same intended population without scientific justification. Overall, the parameters and their ranges should be based on what is known about the biological system and the drug mechanisms and should not be chosen arbitrarily.

1.2.8 Parameter estimation approaches

As discussed in the previous sections, parameter estimation in PBPK models is challenging because of the large number of involved parameters and the relatively small amount of observed data usually available. Several approaches have been performed in the literature in order to fit PBPK models to observed data. "Parameter estimation" refers to statistically derived methods for calibration, such as maximum likelihood or Bayesian methods to estimate posterior distributions, although in practice

these methods typically rely on numerical optimization or sampling.^{229–231} More specifically, one of the proposed methods is to optimize all model parameters together, termed as ‘global optimization’, using Monte Carlo optimization or the simplex method.²³² However, It should be noted that this approach may provide unrealistic estimates for some of the well-defined physiological parameters (e.g. flows and volumes) possibly due to identifiability issues, and therefore it is recommended that these parameters should be constrained (see section 1.2.7). Alternatively, more modern methods such as genetic algorithms, which are based on the concept of natural selection, can be applied to optimize simultaneously many parameters in these complex models.^{233,234} Nevertheless, the most common approach is to fix the majority of model parameters (to values known from physiology or previous *in vitro* and *in vivo* experiments) and optimize only a few unknown, typically drug-specific, parameters.^{207,235} This is can be achieved either by a trial and error and visual calibration to the observed concentration profiles or by more formal statistical approaches, such as non-linear least squares and maximum likelihood methods. The latter is not without limitations, though, and caution should be taken when these parameter estimates are used for extrapolation. It should be recognized that with such an approach the parameter estimates are conditional on the values that have been assumed for the fixed parameters.²³² Nevertheless, many of these fixed parameters in complex PBPK models involving IVIVE may carry a certain degree of inaccuracy and/or imprecision as with every experimentally obtained result. In addition, as model parameters might be correlated through the underlying system physiology, fixing some of them while optimizing for others distorts the covariance structure of the parameters and may lead to biased estimates.²⁰⁵ Finally, it should be pointed out that as with any optimized parameter, the fitted estimate itself is always accompanied with a level of uncertainty which derives from imperfect data or any model misspecifications.²⁰⁷ It is striking that a large fraction of the recently published PBPK models (in the pharmaceutical arena) that performed parameter optimization estimation do not report any uncertainty on the fitted estimate, while only a few do. Reporting a single value for an estimated parameter does not provide any information on the reliability of the estimate. More importantly, when this parameter is related to a mechanistic hypothesis, which is a subject of extrapolation, any conclusions or predictions cannot be trusted. On such occasions, sensitivity analysis is a useful tool to examine different scenarios and support conclusions.

Model uncertainty is variation that derives from errors in the experimental procedure, measurement, modelling and assumptions of the studied system.²³⁶ As it is not itself a system property (in contrast to variability), it can be reduced through optimization of the experiment (see details in section 1.2.9). Although difficult, it is desirable to disentangle and separate uncertainty and variability in a parameter estimation process. Ideally, it is desirable to derive parameter estimates not only for the ‘average individual’, but also their distribution in the population.²⁰⁵ However, a part of the observed variability is *a priori related* to differences in key system related parameters mechanistically affected by well-established covariates (e.g. age, weight) and this information should not be neglected.⁹⁵ The majority of published studies using PBPK modelling focus on the structural model allowing only for “average” individual predictions. In practice, clinical data that are used for fitting are often extracted from published studies and therefore only average population and no individual concentration-time profiles are available. It should be noted that in this case, not only is inter-individual variability on model parameters unattainable, but also parameter estimates might be biased as averaging of data can produce a distorted picture of the individual model function. On the other hand, it is possible that even when individual PK data are available, these are treated as if they arise from the same unique

subject, in a so-called “naïve pooled” analysis approach.²³⁷ The limitations of such an approach have been repeatedly described and the use of hierarchical population modelling is in general strongly recommended.

1.2.9 Modeling physiological variability and uncertainty in PBPK models

As mentioned earlier, compound-specific parameters generated in assays have uncertainties associated with the measurements, while those that are predicted will likely be associated with prediction errors. By incorporating the uncertainties in every compound parameter used as input to a PBPK model, one can predict the overall uncertainty in the predicted concentration–time profile and consequently in the PK parameters calculated using the profile, such as volume of distribution and clearance. An uncertainty assessment aids robust predictions. Similarly, all physiological parameters are generally variable across any given population and by incorporating all known variability within a population for each of the physiological or anatomical parameters, as well as in enzyme and transporter levels, the resulting overall variability in the concentration–time profile that is expected in a population can be estimated. Several approaches for uncertainty and variability analysis are available including the Monte–Carlo (MC) method, fuzzy simulation, and the Bayesian Markov chain Monte Carlo (MCMC) simulation.^{236,238–246}

Uncertainty is different from variability, although their effects may be confounded and compounded. Uncertainty is essentially due to lack of knowledge and may have various sources. For example, measurements are made only with finite precision and as a result there is always some uncertainty (“noise”) around the estimated parameters’ values. Also, limited population samples (e.g., small sample size in a PK study) introduces an element of randomness when attempting to extrapolate the results to the whole population. Finally, our inability to describe or model precisely a system may arise from lack of understanding, oversimplifications or model misspecifications, which in turn translate into parametric uncertainty.²⁴³ While variability is by its nature irreducible and unavoidable, since it is an integral component of biological systems, uncertainty can be reduced by additional experiments, increased physiological understanding or applying more suitable models. Nevertheless, the fact that uncertainty is almost always present hampers a precise assessment of the inherent population variability.

Two major, complementary, modelling approaches have been developed to understand, evaluate and predict the population variability: *a priori* (“bottom-up”) and *a posteriori* (“top down”) modelling. Variability in the pharmacokinetics of a drug in a population can translate to differences in its efficacy and safety within that population. Population PK modeling aims to characterize the observed pharmacokinetic variability in a population in terms of patient demographic, pathophysiological or genetic factors so that clinically significant differences can be identified and addressed through appropriate dosage corrections in any population.^{247–249} Population variability can be modeled by an *a posteriori* (“top down”) approach in which empirical or semi-mechanistic compartmental PK models aim to explain observed variability in terms of plausible covariates.^{250,251} Alternatively, variability can be modeled by an *a priori* (“bottom-up”) approach, in which determinants of variability in each of the PK-determining parameters are used to estimate an overall variability in the concentration–time profile, which is then compared with the observed variability. *A priori* modeling enables early assessment of the impact of variability from different sources (e.g., ethnicity, age, gender, disease

states) on the pharmacokinetics and thereby on the efficacy or safety of the drug. Price et al. describe the modeling of interindividual variability using the physiological parameters for PBPK modeling.²⁵² The objective is the creation of a virtual population that is representative of a real population that is going to be included in a clinical study, so that the clinical study can become a confirmatory rather than an exploratory study. *A priori* modeling can be approached either through a deterministic description of the determinants of variability or through stochastic Monte Carlo simulations.⁹⁵ Each physiological parameter can be characterized by a probability distribution with a population mean and variance. For parameters such as clearances and rate constants, the logarithms of individual values are normally distributed and therefore, a log-normal distribution may be appropriate. For others, a normal (Gaussian) distribution may be assumed. Uniform distribution and Weibull distributions are other commonly used distributions. Once the statistical distribution is specified and defined quantitatively with appropriate values for each of the physiological parameters, the Monte Carlo (MC) approach involves multiple sampling from each distribution using a simple random or Latin hypercube method and computation of model outputs, resulting in a set of output values that can be statistically treated to obtain 90 or 95% confidence intervals for each of the PK parameters such as clearance and volume of distribution.^{95,250,252,253} Many physiological parameters vary in proportion to each other (i.e. they are correlated covariates). For example, cardiac output and breathing rate vary in proportion to one another. Similarly, the correlations, where they exist, in enzyme/transporter abundances should be captured. Blood flow rates to various organs are also correlated, as the total blood flow to all organs should always add up to the cardiac output. A variability analysis that neglects these nested and universal interdependencies and constraints will overestimate the expected variability in a subpopulation. Thus, when sampling different physiological and anatomical parameters with MC, the covariance/ interdependence of parameters should be addressed. One way to address interdependencies is to link physiological parameters to lean body mass or to other body parameters via fixed scaling coefficients.⁹⁴

Many of the shortcomings mentioned in section 1.2.8 could be avoided if a Bayesian approach is combined with population hierarchical modelling.²⁰⁵ As explained before, the information contained in the available data is usually insufficient to estimate the numerous parameters in a complex PBPK model. In addition, these parameters are often mechanistic in nature and thus prior information about their range can be extracted from physiology, *in vitro* experiments, and previous literature. Bayesian methods use a set of known prior distributions that may be specified independently of each other to arrive at a posterior probability distribution, using newly available data.^{93,246} When this approach is combined with a hierarchical population model, it yields posterior distributions not only at the individual but also at the population level.^{254,255} True determinants of variability from population data are obtained after removing the contributions from uncertainty. However, it is often difficult to obtain an analytical expression for the posterior probability distribution, which is needed for an MC simulation. Typically, in Bayesian analysis, these distributions are instead produced by Markov-chain Monte Carlo (MCMC) methods when the posterior distribution cannot be captured in an analytical expression.²⁵⁶

The advantages of an approach that uses prior information in PBPK modelling can be summarized as follows: prior beliefs are naturally updated in the light of new data, biologically plausible ranges for the physiological parameters can be set and the estimation procedure in terms of identifiability with regard to parameters that cannot be informed from the available data can be stabilized. However, it is often challenging to summarize prior knowledge in terms of appropriate statistical prior

distributions, particularly for IVIVE incorporated PBPK models, where most of the prior information with regard to drug-related parameters comes from *in silico* methods and *in vitro* experiments, which either produce point estimates (e.g. mechanistic predictions of partition coefficients) or estimates in which uncertainty and variability cannot be separated (e.g. intrinsic clearance predictions from pooled human liver microsomes).²⁰⁵ Moreover, if the analyzed data do not contain enough information with regard to the model parameters, the resulting parameter estimates will shrink back towards the prior information, which will not be updated. Finally, the Bayesian population approach is very computationally intensive and time-consuming, even nowadays.^{257,258}

The maximum *a posteriori* (MAP) estimation method also uses prior information, but unlike the Bayesian method, it does not assume a distribution governing randomness on the parameter estimate. Rather, as an output one obtains parameter estimates which are considered as unknown constants in the model. This method was introduced by Gislenskog et al., as a way to stabilize a sparse data population analysis with information from previous studies when the data from the sparsely sampled datasets are inaccessible or impractical to pool.²⁵⁹ Briefly, this is achieved by incorporating a penalty term on the objective function upon minimization, which reflects a representation of the available prior knowledge with regards to model parameters. This method has been successfully applied in PBPK modelling, providing parameter estimates which were in close agreement with those from a typical Bayesian analysis, but with a substantial improvement in computation times.^{258,260}

1.2.10 Overparameterization and reduction of PBPK models

In practice, from a typical single pharmacokinetic study it is usually challenging to fit more than three exponentials to a plasma concentration profile, even with reasonably noise free data sampled over a long period after the dose is administered, due to identifiability constraints.²¹³ In this context, complex PBPK models with numerous compartments and parameters can be considered *a priori* as overparameterized. The increased dimensionality of such models causes computational and numerical problems during estimation, and thus simpler (“lumped”), but still physiologically satisfactory models - depending also on the intended application - can be beneficial. This can be achieved with model order reduction techniques, which aim to reduce formally the dimensionality of a system of differential equations without losing the key dynamic information.²⁶¹ One of these methods, proper lumping of tissue compartments, has been applied in PBPK to derive simpler models with kinetic behavior similar to that of the original complex model and a formal methodology for this procedure has been proposed.⁶¹ Other lumping procedures have been also applied to PBPK models, with the latter methods being appealing in that they imposes fewer restrictions on lumping conditions and allow concentration predictions in the tissues of the original non-lumped model.^{60,262} However, it should be stated that lumping procedures are valid only locally in the parameter space i.e. for a particular set of parameter values.²⁶³ This is of high importance in the context of PBPK models where most of the model parameters are not precisely known and carry a certain degree of uncertainty and variability. In order to address this issue to some extent, a Bayesian automated lumping method has been proposed by Dokoumetzidis and Aarons which is more optimal on average as it makes compromises between the different parameter values.²⁶³ Finally, an appealing approach that avoids some of the parameter estimation difficulties in complex PBPK models is the use of minimal or semi-mechanistic models.²⁰⁵ These models offer great flexibility as they retain their physiological

mechanistic nature only in the parts of the model that are relevant to the desired modelling purpose.^{32,264} A generic minimal PBPK model was recently published that allows the estimation of physiologically relevant pharmacokinetic parameters and offers a reasonable alternative to full PBPK modelling when only limited plasma concentration data are available.²⁶⁵

1.2.11 Qualification and credibility assessment of PBPK models

In general, a software platform is an operating environment that is used to write (in the case of coding a model), compile (building a model in software or platform) and run applications. In the case of PBPK models, the platform includes three key components: a computational framework, a physiological framework of the system, and a set of drug properties. The computational component includes the program code, model structure, mathematical equations, as well as a runtime engine for executing applications. Furthermore, within the platform a selection of appropriate mechanistic models describing absorption, distribution, metabolism, and elimination can be applied to the drug model. The physiological framework comprises system-dependent parameters that describe the physiology of humans or the biology of a preclinical species. These system parameters are population-specific and account for population variability and correlation between parameters. A PBPK platform may also contain a database of virtual populations such as healthy volunteers of different ethnicities and/or ages, as well as patient populations. The drug model component of the PBPK platform comprises drug-dependent parameters and will vary depending on the question to be addressed by the PBPK modeling.²⁰⁴ Similar to virtual populations, a PBPK platform may also contain a library of already parametrized drug models. Hence, a PBPK platform is an integrated software environment that enables PBPK models to be built and used for simulations. The PBPK platform may or may not provide compound or population-specific databases. From a software perspective, a platform includes various components such as graphical user interface (GUI), data structures, collections of various models and a computational engine, as well as interfaces for presenting the simulation results. The PBPK models within a platform are developed to handle specific tasks based on certain assumptions.²⁶⁶ For example, the use of PBPK modeling and simulations to support regulatory submissions may cover a wide range of applications in the areas of drug–drug interactions (DDI), biopharmaceutics (e.g., food effect, clinically relevant dissolution specifications) and extrapolation across specific populations such as the different age groups in the pediatric population.

Recently, definitions of the various terminologies used in modeling practices, including “qualification”, “validation” and “verification” of models have been described.^{204,207,266} Verification is the first step in establishing the credibility of a model as it ensures the accuracy and reliability of the underlying mathematical code and calculations. For all software, code and numerical solutions should be evaluated for errors and algorithms should be checked for correct implementation and function. For example, if the model incorporates many stochastic differential equations, verification may include assessing the stability in the numerical integration. If user-developed software is employed, then it is the user’s responsibility to perform verification.

While verification (or qualification) generally refers to a set of prerequisites that ensure “permission” to handle the intended use, validation focuses on the predictive performance of the model. The documentation needed to support the qualification and verification of a PBPK platform should cover all three components of the platform. The software qualification is intended to ensure that the

software does what it is intended to do from a computational perspective.²⁶⁷ Verification of the system-dependent components involves documentation of the physiological framework, the equations used to describe the system, as well as the physiological parameters feeding it. The drug model validation assesses the correctness, accuracy and consistency between the input parameters and underlying mechanisms and assumptions within the related physiological system, as well as the ability of the model to successfully simulate sets of observed data, sometimes following several iterations of a “learn and confirm” cycle.²⁰⁴ Moreover, validation activities include assessment of model input, which can be subdivided into quantification of sensitivities and uncertainties. The verification and validation activities should be tailored to the context of use, and the rigor of the selected activities should be driven by the overall model impact and the associated risks, to ensure applicability and sufficient credibility.²⁶⁶

Regarding the qualification of virtual populations used in PBPK modeling and simulation, the recent guidelines from both the EMA and FDA primarily focus on the healthy volunteer population, with the EMA draft guideline providing additional guidance on model applications using a pediatric virtual population. However, pharmacokinetic alterations in other specific populations such as hepatic or renal impairment populations have been reported and PBPK-guided dosing recommendation strategy for such populations is becoming nowadays standard practice in regulatory submissions.¹⁷⁰ However, based on the limited experience in PK extrapolation for untested scenarios in organ impairment populations, the confidence in these PBPK models remains rather low.²⁶⁸

In general, virtual population qualification in PBPK platforms involves development of the system-dependent parameters, followed by prospective prediction of PK in the population of interest. The development of any virtual population involves evaluation of the ability of the platform to generate virtual individuals with anatomical, physiological, genetic, and biological values that are similar to the values in the actual population. When establishing a “healthy volunteer” population, population-related data are generally assembled from public health databases such as NHANES (USA), NISRA (UK), and the Statistics Bureau (Japan).²⁰⁴ Different ethnic populations (Caucasians, Chinese, Japanese, and African, etc.) may be developed either as completely new populations or by adapting a previously built population for relevant demographics, physiological parameters, and incorporation of genetic polymorphisms of metabolizing enzymes and transporters. Comparison of observed interethnic PK differences of the model drug with PK predicted by PBPK modeling may be considered an essential component of verification of an ethnic population.

For specific and patient populations, changes in system parameters of the healthy volunteer population that describe the population of interest, such as pediatric, pregnancy, renal/hepatic impairment, geriatric and obesity, are either based upon mechanistic evidence or by fitting the model parameters to observed clinical data.^{168,169,269–271} For example, to establish a pediatric population, ontogeny changes in enzymes and transporters need to be explored by both quantification of the enzyme amount and evaluation of observed *in vivo* clearance of probe substrates.¹⁷⁹ Another example is the establishment of a patient population such an “oncology” population, where modeling of observed data in cancer patients led to identification of “albumin binding” and “alpha-acid glycoprotein binding” as key descriptors of a cancer population.²⁷² Nevertheless, a “global” cancer population is rather unlikely to be able to address the complexity and heterogeneity of physiological alteration in most cancer types. Finally, also in these populations, successful recovery of observed PK data of a drug or group of drugs in the specific population model strengthens its verification. Upon

verification, the specific population might be applied in a prospective PK extrapolation for other drugs with the aim to identify appropriate dosing recommendations.

PBPK model development is an iterative process that may involve multiple cycles of “predict, learn, confirm.” Usually, a base model is first developed using experimentally determined or *in silico* predicted physicochemical and *in vitro* drug absorption, distribution, metabolism, and excretion (ADME) parameters. The predictions from the initial model are then compared against the observed clinical PK data (e.g., PK from single ascending dose (SAD) or multiple ascending dose (MAD) studies) where a selection of model parameters may be refined to improve the drug model predictive performance based on sound physiological and scientific evidence. The predictive performance of the refined model will then be confirmed by comparing the prediction with additional clinical PK data (external datasets), such as results from a dedicated DDI study, that have not been used before. Although the complexity of the model increases as additional mechanisms are identified from new *in vitro* or clinical data, at any given stage during the drug model development process, a compound model can be considered validated for a particular use or application if the predictive performance for that particular use or application is deemed to be satisfactory based on commonly accepted criteria.²⁰⁷ For example, a drug may initially have been only identified as an inhibitor of CYP3A, but later found to be an inhibitor of a drug transporter as well. As long as the compound PBPK model is able to satisfactorily demonstrate its predictive performance of a DDI with a sensitive CYP3A substrate, the model is considered verified for its predictive performance for a DDI via CYP3A inhibition, although its predictive performance may have not yet been verified for a drug transporter inhibition. An exception would be if multiple mechanisms affect the same enzyme or transporter, or in cases where there is enzyme-transporter interplay. For example, if a drug inhibits and induces CYP3A4, the model needs to be verified for both mechanisms prior to declaring that the model is verified for CYP3A-related applications.

It is crucial for model identifiability to distinguish between the studies used for initial model development and refinement (training dataset), from the datasets for model validation. The design of a clinical study and the use of data to support model validation should be based on the purpose of the application

Primary and secondary PK parameters may be used for comparison between predicted and observed values during model development and validation. Visual inspection of overlays of predicted and observed PK profiles is also performed. When evaluating the accuracy and acceptability of predictions, a commonly applied criteria is for values to be within 1.25-fold or 2-fold of the observed values.²⁷³ However, results from one controlled clinical study may not be representative of the larger population, especially for drugs that exhibit high variability in PK or if the sample size was small in such studies. As a result, the 2-fold criterion may be unreasonable for such drugs or studies. Instead, Abduljalil et al. proposed to evaluate the success of model predictions by factoring the study sample size and the observed variance of the parameter of interest.²⁷⁴ Separately, the predictive performance of DDI simulations is usually evaluated by comparing the geometric mean ratios of C_{max} and AUC, and their respective 90% confidence intervals, in the presence or absence of a perpetrator. When the observed interaction is weak (less than 2-fold for inhibition and between 0.5-0.8-fold for induction), the 2-fold rule is irrelevant. Thus, Guest et al. proposed that the predictive performance for DDI be based on the observed AUC and C_{max} ratios, considering the intra-subject variability as well.²⁷⁵ In general, it is highly encouraged to consider multiple diagnostics and metrics to assess the PBPK model

performance. However, depending on the intended use, therapeutic area, safety, and efficacy factors, the criteria for acceptable performance may be adjusted accordingly.

1.3 Combining physiologically based pharmacokinetic with pharmacodynamic models

PBPK models offer a mechanistic framework to quantify the pharmacodynamic (PD) effect of a drug through coupling to simulated on- and off-target tissue concentrations. Since different organs are explicitly represented in whole body PBPK models, on- and off-target tissue exposure can be directly quantified. This enables a consideration of therapeutic or toxic effects by coupling PD to the corresponding PBPK models. To this end, tissue concentration profiles simulated with PBPK models may be used as input for downstream PD models. Notably, this coupling of PK and PD results in a multiscale PBPK/PD model that simultaneously describes drug ADME at the whole-body level and the resulting drug effect at the cellular or tissue scale.

Examples of such detailed PBPK-based models include glucose-insulin regulation in diabetes,¹⁰ management of endometriosis,²⁰ acetaminophen intoxication,¹⁵ drug-induced liver injury²¹ or model-based design and analysis of antithrombotic therapies.²² Ultimately, such PBPK/PD models aim for a mechanistic and physiological representation of systems interactions within the body,²³ thereby providing an important toolbox for disease or toxicity modeling in quantitative systems pharmacology.

PBPK/PD modeling offers great flexibility, maximizing the scope for extrapolation and prediction as well as enabling a mechanistic understanding of PK and PD through hypothesis testing. Similar to classic PK/PD, PBPK/PD integration and parameter estimation is achievable in two ways. In one approach, the differential equations of a whole-body PBPK model are solved simultaneously along with the appropriate differential equations for PD to get a response versus time, which is then integrated with the concentration–time profile of the target organ to get the response versus concentration. A simultaneous solving of the differential equations of PBPK and PD models as opposed to sequential PK/PD modeling is essential when there is a bidirectional dependence of PK and PD as in the case of target-mediated drug disposition. Nevertheless, considering the complexity of PBPK models this approach might be more challenging in terms of parameter estimation and the need for more computational power resources. Another approach to PBPK/PD integration is to combine the time course of tissue concentrations obtained from PBPK with a PD model. Indeed, PBPK/PD integration facilitates the use of tissue concentrations rather than plasma concentrations. Also, pharmacological targets of drug action are often located within tissues rather than exposed directly to plasma, thus making target tissue concentrations much more relevant for PK/PD integration. Although the pharmacologically relevant unbound drug concentrations are expected to be the same in plasma and tissues, this is not true for targets behind transporter barriers in organs like the central nervous system, liver, and kidney. The increase or decrease in target site concentrations with respect to plasma concentrations in these organs are determined by the expression and functionality of specific transporters.^{276–278}

For drugs which exert their pharmacological action on receptors by allosteric modification of receptor configuration from within cells or which act on targets within the cells in a tissue, unbound intracellular concentrations are the most relevant. For instance, many statins, such as atorvastatin, rely on hepatic

uptake transporters to reach the target enzyme and tend to get accumulated within the hepatocytes, leading to a higher than expected effect. Tissues are not homogenous and the concentrations in the pharmacologically relevant compartments within a tissue can be different from the unbound tissue concentration, either because of transporters or because of differences in ionization.

PBPK/PD models are also particularly suited for pre-systemic targets located in the lung, gut, or skin and for which plasma concentrations are not relevant. The target organ could be the site of pharmacological action or a site where toxic effects are expected. Provided the estimates of tissue partition coefficients are derived from reliable sources, target tissue concentrations can be combined with PD data, eliminating the use of distributional delay models, unless these are mechanistically appropriate. Hypothesis testing with PBPK can also identify any distributional delay, in which case a permeability-limited tissue distribution model can be used in the place of the generally default perfusion-limited model. Examples of PBPK/PD in the literature⁴⁸ are still rare. Nonetheless, examples of detailed PBPK-based models include glucose-insulin regulation in diabetes, management of endometriosis,, drug-induced liver injury or model-based design and analysis of antithrombotic therapies.^{33,279–282}

In summary, the advantages of combining PBPK with PD models include i) the mechanistic derivation of quantitative variation in target tissue concentrations and, thus better correlation with the PD effect, ii) better extrapolation capability, iii) use of permeability-limited distribution to quantify distributional delay in effect (multi-scale modeling) iv) hypothesis testing for understanding mechanisms underlying an observed response, and v) examination of the sensitivity of a system to parameter variation. Ultimately, PBPK/PD models aim for a mechanistic and physiological representation of systems interactions within the body, thereby providing an important toolbox for disease or toxicity modeling in quantitative systems pharmacology.¹²⁶

1.4 Physiologically based pharmacokinetic analyses for biopharmaceutic applications in drug development and regulatory review

1.4.1 BCS-based biowaivers, clinically relevant drug product specifications and virtual bioequivalence

1.4.1.1 BCS-based biowaivers

The BCS (Biopharmaceutics Classification System)-based biowaiver approach is intended to reduce the need for *in vivo* bioequivalence studies by providing an appropriate surrogate for *in vivo* bioequivalence, whereby *in vivo* bioequivalence studies may be exempted if appropriate *in vitro* data can be generated. BCS-based biowaivers are applicable only to orally administered immediate release (IR) solid dosage forms or suspensions where the drug substance(s) is categorized as BCS class I or III and meets the predefined solubility, permeability and dissolution criteria.^{283,284} Additional considerations involve linear pharmacokinetics of the drug substance within the context of a permeability assessment, no expectation for inactive ingredient effects on the oral bioavailability of the drug substance, and the absence of a narrow therapeutic index on the part of the drug.^{283,284} Recently, the International Council for Harmonization of Technical Requirements for Pharmaceuticals

for Human Use (ICH) drafted a guidance on BCS-based biowaivers (M9), the final version of which has been adopted by the Committee of Human Medicinal Products (CHMP) of the European Medicines Agency (EMA) and came into effect at the end of July 2020.²⁸⁵ Although the current guidelines advocate that the BCS-based biowaiver principles may be applied to BE purposes other than those specified in their context provided there is a thorough scientific rationale, the potential use of PBPK modeling to support BCS-based biowaiver applications is not explicitly stated. The BCS (Biopharmaceutics Classification System)-based biowaiver approach is intended to reduce the need for *in vivo* bioequivalence studies by providing an appropriate surrogate for *in vivo* bioequivalence, whereby *in vivo* bioequivalence studies may be exempted if appropriate *in vitro* data can be generated.

The current BCS-biowaiver approach has been widely criticized for being over-discriminating and overly strict, excluding opportunities not only for scientifically justified extensions to certain BCS class II compounds, but also for drug substances which are in theory eligible for BCS-based biowaivers, but which failed to comply with criteria in the dissolution performance.^{28,32,286–290} Several publications have implemented PBBM/PBPK modeling approaches, including VBE, to investigate the variables limiting drug absorption, support possible BCS-based biowaiver extensions and recommend specifications based on the *in vivo* performance.^{27,32,288,291–295} On the other hand, it has been suggested that products containing compounds belonging to BCS class I and III might exhibit a high risk of bioequivalence failure due to their intrinsic pharmacokinetic properties (e.g., if they have a high first pass effect or short half-life) and that the eligibility of their products for biowaiver might need to be revised.²⁹⁶ Further concerns have been raised, especially for products including BCS class III compounds, on the potential interactions of different excipients with gut transporters, which in turn could lead to increased risk for bioequivalence.^{297–301} On the whole, it seems that regulatory confidence in the performance of PBPK models for justification of biowaivers is still rather tentative.

1.4.1.2 Clinically relevant specifications

Developing and justifying dissolution specifications for product release can be a challenge for industry and regulatory agencies during the review of new drug (NDA) and abbreviated new drug applications (ANDA) for new and generic drugs, respectively.³⁰² In the past, dissolution specifications were established mainly to prove batch to batch consistency, but over the last decade or so the emphasis has shifted towards linking *in vitro* dissolution specifications to *in vivo* performance. The traditional establishment of *in vitro-in vivo* correlations/relations (IVIVC/R) is slowly being replaced by a PBBM-IVIVC/R framework, with the aim of defining a dissolution space within which all drug product batches would be expected to be bioequivalent to each other and/or to a reference batch. Using this approach, a mechanistic IVIVC/R becomes possible, meaning that the processes of *in vivo* dissolution, permeation (passive, transporter-mediated influx/efflux) and gut wall metabolism can be isolated and distinguished, thus permitting the direct correlation of *in vitro* with *in vivo* dissolution.

From an industrial perspective, the use of PBPK to inform IVIVC/R and establish clinically relevant specifications is considered to be a routine tool with several successful examples already published in the literature.^{302–305} PBPK-IVIVC/R-specific challenges and opportunities have been discussed elsewhere.^{303,306,307} In the regulatory setting, PBPK modeling to define clinically relevant specifications has been successful in a wide range of applications including drug substance particle size distribution,

change of manufacturing site or process, post approval specifications related to drug product shelf life and polymorphic purities.^{291,302,308}

1.4.1.3 Virtual bioequivalence

Numerous publications have highlighted the importance of mechanistic understanding between *in vitro*, *in silico* and *in vivo* events, which should lead to confidence in prospective clinical trial simulation and waivers of *in vivo* relative BA/BE studies.^{28,32,293,295,309,310} In this context, the emerging field of VBE has been attracting the attention of stakeholders in academia, industry and regulatory agencies. Although there is not yet any formal regulatory framework, the FDA has been encouraging the use of VBE as a tool to justify dissolution specifications, product quality and to support prediction of food effects, pH dependent DDIs and other biopharmaceutical applications. Interestingly, VBE approaches have already been adopted by the Office of Generic Drugs (OGD) within the FDA to investigate the risk associated with salt-to-base conversion in prasugrel products and the impact of isopropyl alcohol and slow dissolution on the *in vivo* performance of warfarin sodium tablets.^{294,311} Furthermore, case examples from both academia and industry have showcased the opportunities that VBE offers towards better understanding of the critical attributes related to product *in vivo* performance and elimination of unnecessary clinical studies.^{28,32,288,295,312–318} Nevertheless, one should be mindful of the challenges and limitations related to this relatively recent concept and the need to gain further confidence in prospective model performance by verifying the results with BE studies in healthy and/or the relevant specific/ patient populations. It is noteworthy that all the previously mentioned applications that were accepted by regulatory authorities refer to interactions with the US FDA, whereas the EMA appears to be more reluctant in the implementation of *in silico* approaches for regulatory purposes.

1.4.2 Food Effects and pH-dependent Drug-Drug interactions

1.4.2.1 Food effects

Assessment of the food effect on the rate and extent of absorption is part of the development of an orally administered drug product. Often, meal effect studies are conducted early in drug development as part of the first-in-human studies and may be repeated later with the to-be-marketed formulation to inform the product label. According to U.S. FDA guidance for Industry, “*Food-Effect Bioavailability and Bioequivalence Studies*”, conducting a food effect bioavailability study is recommended for a new chemical entity (NCE) during the investigational new drug application (IND) period and for generic drug products as part of the ANDA. However, for ANDAs of immediate-release products a waiver of fed state bioequivalence study may be possible when the labeling of the reference listed drug states that the product should be taken only on an empty stomach.^{319,319} By contrast, a food effect study is recommended for all modified-release (MR) products regardless of the classification of the drug substance according to the BCS. In the regulatory setting, for an NDA, absence of food effect on bioavailability is not established if the 90% confidence interval (CI) for the ratio of population geometric means between fed and fasted treatments, based on log-transformed data, is not contained in the equivalence limits of 80-125% for either AUC_{0-inf} (AUC_{0-t} when appropriate) or C_{max} . When the 90% CI fails to meet the limits of 80-125%, the sponsor should provide specific recommendations on the clinical significance of the food effect based on what is known from the total

clinical database about dose-response (exposure-response) and/or PK/PD relationships of the drug under study. The clinical relevance of any difference in T_{max} and lag time should also be indicated by the sponsor.^{320 320} For generic drugs, a clinically meaningful food effect is concluded if the 90% confidence interval of the ratio of the population geometric mean between fed and fasted treatment for NDAs or between reference listed drug (RLD) and test product for ANDAs in the fed state is not contained in the equivalence limits of 80-125% for AUC and/or C_{max} (based on the log-transformed data).

In order to anticipate, characterize and/or mitigate a food effect, significant resources may need to be invested during clinical development. For that reason, PBPK models can be a useful tool to foster understanding of the underlying food-drug interaction mechanisms, predict the clinical impact, extrapolate to various scenarios (e.g., formulation changes) and thus potentially be applied to waive fed state BE studies. Recently, Tistaert et al. summarized the industry's perspective on the use of PBBM to predict food effects by presenting a sample of five successful case examples.³²¹ PBPK models for food effect predictions have been routinely implemented for internal (within industry) decision-making and risk assessment, during first-in-human (FIH) to inform formulation development, during multiple-ascending dosing (MAD) regimens, when formulation modifications are made during late-stage clinical development and in life cycle management.³²¹

In 2018 a review from FDA examined the predictive performance of PBPK models in 48 food effect cases, of which 39 were prospective predictions.⁵⁰ The examples were distributed among the BCS classes almost uniformly, with a slightly higher proportion of class I compounds (37%).⁵⁰ The examples were distributed among the BCS classes almost uniformly, with a slightly higher proportion of class I compounds (37%). Successful prospective predictions, within 1.25-fold, were achieved for the 59% and 49% of the predicted versus observed AUC and C_{max} food effect ratios (i.e., the ratio of AUC or C_{max} in fed state versus in fasted state), respectively. Nonetheless, due to our limited understanding of GI physiology under fed conditions, the variety of meals and possible food-drug interactions, and the commonly applied "top-down" optimization of critical parameters such as dissolution and precipitation rates, confidence in using PBPK modeling to prospectively predict food effects is still considered low.^{50,32250,322} Interestingly, only 3% of the presented cases described a negative food effect, highlighting the importance of increasing our understanding of the mechanisms behind this type of interaction, especially for poorly soluble compounds.^{50.50} Despite several successful examples and proposed workflows, it must be acknowledged that best practices in PBPK modelling for food effects have not yet been established and significant improvement not only on the currently available *in silico* (e.g., PBPK platforms), but also on the *in vivo* (e.g., aspiration, MRI studies) and *in vitro* (e.g., fed state transfer models, permeability assays) tools is needed. Additionally, the importance of interactions of food components with intestinal enzymes and transporters leading to clinically significant alterations of exposure should be more fully explored. At present, there is limited data regarding such interactions and it is thus difficult to quantify their impact on PK using PBPK models.³²³⁻³²⁶ For detailed literature review regarding the interactions of food components with drug metabolizing enzymes and influx or efflux transporters in the gut the reader is referred to Won et al.³²⁷

1.4.2.2 Drug-drug interactions on absorption

Similar to food effects, PBBM has been commonly applied to predict and describe pH dependent DDIs mediated from co-administration of the investigational drug and gastric acid reducing agents (ARAs). The three main ARA classes on the market include antacids, histamine H2 receptor antagonists

(H2RAs), and proton pump inhibitors (PPIs). Among patients across all fields of medicine, especially in oncology, ARAs are often used for the symptomatic relief of drug side effects and GI related diseases. As a result of their frequent use, there is substantial potential for DDIs. Clinical data for several weakly basic compounds has shown reduced exposure (C_{max} and AUC) and occasionally, prolonged T_{max} in subjects or patients with elevated gastric pH.³²⁸ Currently, no specific regulatory framework is available.³²⁸ To initiate work in this area, in 2018 the U.S. FDA posted a public docket titled *“Framework for Assessing pH- Dependent Drug-Drug Interactions”* to solicit information and encourage dialogue, with the aim of establishing guidelines for the assessment of pH-dependent DDIs.³²⁹ Mitra et al.³²⁹ Mitra et al. presented a cross-industry perspective with seven successful case examples of PBBM in the prediction of ARA effect on drug exposure.³³⁰ The discussion was focused on the impact of ARA on the exposure due to elevated gastric pH, especially for poorly soluble weakly basic drugs.³³⁰ The authors suggested that waiving dedicated ARA clinical studies on a case-by-case scenario, when appropriately supported by PBPK modeling, clinical data, and appropriate biopharmaceutics experiments, would be a way forward. Although predicting the interaction of ARAs might be in some ways less complicated than forecasting food effects, for some ARAs other mechanisms (e.g., chelation by antacids) might be involved along with the increase in gastric pH.³²⁸ At this point, it is critical to identify biopredictive biopharmaceutic tools and use these to gain confidence in model performance and predictive accuracy of PBPK models regarding all ARA mechanisms, in order to establish best practices which will allow for waivers of the respective clinical studies.³²⁸ In any case, similar to food effects and post-absorptive DDIs, the clinical relevance of such interactions should be assessed by considering the dose-response relationships for both efficacy and safety.

2 Aims of the thesis and scientific issues addressed

Intrinsic and extrinsic patient factors (IEFs) such as dosage form, co-medication and genetic polymorphism may significantly impact drug exposure and subsequently lead to changes in the efficacy or safety of a drug. The ability to quantify and extrapolate the impact of such factors on the exposure and pharmacologic action of a drug represents a milestone in determining required dose adjustments and implementation of risk management strategies in clinical pharmacology. Under the prism of model-informed drug discovery and development (MID3), dynamic mechanistic models such as whole body physiologically based pharmacokinetic/pharmacodynamic (PBPK/PD) models may be useful for forecasting the influence as well as the interaction of multiple factors on PK and PD, and as a result could be used to guide formulation selection and clinical dosing recommendations.

Although PBPK models are now being routinely applied within pharmaceutical industry for internal decision making and to support regulatory review, confidence in PBPK modeling analyses to support waivers of dedicated clinical pharmacology studies for biopharmaceutic applications remains rather low. On the other hand, virtual bioequivalence in the context of clinical trial simulation has emerged as a promising, yet underdeveloped, field in the help of expanding the scope of PBPK modeling in biopharmaceutics. For instance, BCS-based biowaivers for BCS class II and IV drug are not currently accepted by health authorities. However, in some cases PBPK modeling by coupling *in vitro* dissolution to the *in vivo* formulation performance has demonstrated that such an approach could be scientifically justified under circumstances.²⁷ Similarly, PBPK modeling and VBE can be used to set clinically relevant drug product dissolution specifications and define (or broaden) the dissolution „safe space“.^{291,302} Nonetheless, even in the case of drug products showing differences in the extent and rate of absorption outside of the bioequivalence limits, meaning that they cannot be considered bioequivalent and thus interchangeable, their therapeutic equivalence might be retained as long as this is appropriately justified by exposure-response and/or exposure-safety analysis using empirical, semi- or fully-mechanistic PK/PD models.

In this context, the primary goal of the present thesis was to support and justify expansion of model-evidenced waivers of dedicated *in vivo* clinical pharmacology studies focusing on oral biopharmaceutic applications. This purpose was realized by:

- Proposing PBPK modelling and simulation (M&S) workflows to perform virtual bioequivalence trials by leveraging biorelevant *in vitro* dissolution testing and by implementing a novel, stepwise IVIVE approach for biopharmaceutic parameters.
- Applying the developed workstreams in a number pre-selected of compounds and investigating the role of specific PK properties in the sensitivity of *in vitro* and *in vivo* drug product performance for demonstrating of bioequivalence. Three BCS class II weak acids (i.e., ibuprofen, flurbiprofen and naproxen) were studied as case examples.
- Exploring the relative contribution of factors other than formulation performance, such as co-medication, ethnic sensitivity and genetic polymorphisms in population PK variability and bioequivalence. Flurbiprofen as a probe substrate of the polymorphic CYP2C9 was used to study the combined effects of formulation, genetic polymorphisms, and co-medication (i.e., CYP2C9 perpetrators).

- Linking exposure to pharmacologic response and translating exposure differences in pharmacodynamic effect to assess their clinical relevance for the patients.

In addition, in support of these aims, the following scientific issues were investigated or addressed:

- Development of mathematical models to describe the pharmacologic response (PD) and their link to exposure (PK). In particular, these investigations focused on the disconnection between PK and PD, showcasing examples for which significant drug exposure differences, and thus bioequivalence, would likely have been irrelevant for the therapeutic (or toxic) effect over the intended dosage range.
- Identification of knowledge gaps, challenges, limitations, opportunities, and future actions for PBPK modelling in oral biopharmaceutics.

3 Key results and discussion

3.1 Application of the relationship between pharmacokinetics and pharmacodynamics in drug development and therapeutic equivalence

As mentioned earlier, PK/PD, and especially PBPK/PD, models provide a mechanistic framework linking the tissue concentrations in the site of drug action to the pharmacologic effect. Early attempts in the development of PK/PD models had focused on describing the shape of the concentration-effect and effect-time curve using empirical models and by directly correlating pharmacologic response to systemic exposure. Nonetheless, it was soon recognized that this scenario is only valid at steady-state or when the equilibrium between plasma and the site of action is instantaneous and assuming that the distribution of free drug is the same (or proportionally the same) in all tissues. A variety of these so-called steady-state empirical direct effect models have been reported in the literature: linear, power, hyperbolic, sigmoid (e.g., E_{\max} model), logarithmic and logistic. Even though these models have been applied in a number of situations,^{331,332,333} they have two important limitations. First and most important, they are time-independent (also referred to as static or fixed effect models). Second, they lack a mechanistic and/or physiological understanding of the underlying system dynamics.³³⁴ An overview of existing non-steady state PK/PD models and their mathematical implementation is presented as part of this work. In addition, drug-specific case examples with evident disconnection between PK and PD, for which exposure fluctuations become less critical, if not irrelevant, for the pharmacologic response are of particular interest (Publication 1).

3.1.1 Effect-compartment model

In many cases, the site of action of a drug is kinetically distinct from the plasma and the equilibration between the plasma and the effect site is often rather slow. In such cases, there will be a temporal delay between the drug plasma (C_p) and effect site concentrations (C_e), and the effect will be a function of C_e rather than of C_p . In this context, and as a result of the challenges in measuring drug concentrations at the site of action, the so-called effect compartment or biophase distribution model was introduced by Segre et al. in 1970.³³⁵ In this model, a hypothetical compartment, which is assumed to receive only a negligible amount of drug, is added to link systemic PK with PD. A hallmark of the effect compartment model is the hysteresis observed in the effect-concentration plot, due to the time delay between pharmacokinetics and pharmacodynamics. For a detailed mathematic representation of the model the reader is referred to Holford and Sheiner.^{336,337} Well-known examples of drugs exhibiting a biophase distribution related delay in response include neuromuscular blocking agents such as d-tubocurarine (see section 2.2) and pancuronium,³³⁸ the calcium channel blocker verapamil,³³⁹ and the bronchodilator theophylline.³⁴⁰ Further cases that have been reported in the literature include quinidine, disopyramide, opioids such as pethidine, morphine, fentanyl, diclofenac, organic nitrates, benzodiazepines and digoxin.^{341–348}

3.1.2 Irreversible target binding models

In general, PD effects are initiated by the interaction of drugs with targets such as receptors, enzymes, ion channels and cell membranes. Typically, such interactions are of reversible nature with the equilibrium between association and dissociation of the drug to the target being defined by the respective affinity. However, in many cases an irreversible interaction may occur when the drug binds covalently to the target or the dissociate rate is much slower than the target lifetime span. In such cases, it was identified that the duration of action (expressed as return to baseline response) is likely not dependent on the drug's elimination half-life, but rather on the rate of de novo synthesis of the target. Examples of drugs causing irreversible inactivation of endogenous enzymes or receptors include aspirin,^{349,350} 5 α -reductase,^{351,352} and proton pump inhibitors (PPI).^{353,354,355} Similar effects have been reported for apoptosis in human cells, the reduction of viral load by antivirals,³⁵⁶ the cell death processes induced by anticancer drugs³⁵⁷ and myelosuppression due to drug-induced cytotoxicity.³⁵⁸ Such irreversible phenomena in pharmacodynamics can usually be described by a turnover model which uses classical receptor theory equations and correlates the pharmacological response to the receptor-drug complex (for agonists) or the fraction of free receptors (for antagonists). In general, the turnover model can be effectively used to model pharmacodynamic effects arising not only from irreversible receptor binding, but also from irreversible interaction between a drug and other targets such as endogenous enzymes or ion channels. A detailed summary of irreversible effects in pharmacodynamics along with the mathematical descriptions of the respective models can be found elsewhere.³⁵⁹

3.1.3 Indirect response models

Nearly all mechanistic PD models are based on the concepts of turnover and homeostasis.³⁶⁰ Biological compounds (biomarkers), structures, and functions are continually being produced and degraded. Thus, the starting condition or baseline of most PD models is the steady state that exists in the organism. The turnover rate may determine which type of PK/PD model applies. For very rapid turnover processes, direct effect or biophase models are relevant as the PK of the drug will be rate-limiting to the observed responses. When the production (k_{in}) and loss (k_{out}) rates of the biological factors are slower and directly altered by drugs, indirect response models pertain. These models typically exhibit a delay between the drug concentration-time and response-time profiles. The amplitude of the response and the extent of the time delay are dependent on the turnover rates (synthesis and degradation) of the pharmacological target as well as the magnitude of the effect. In general, turnover is generalized to include any process where the response or control factor is affected by production and loss. However, this section will focus on indirect response and signal transduction and feedback control models.

3.1.3.1 Basic and extended indirect response models

Nagashima et al.³⁶¹ were the first to implement an indirect response model, which was used to explain the anticoagulant effect of warfarin on the activity of the prothrombin complex. In 1993, Dayneka et al.³⁶² introduced four basic mathematical models describing indirect pharmacological processes, according to which the production and loss of the response, R, are governed by zero- and first-order rate constants, k_{in} and k_{out} , respectively. These four basic models, which are illustrated in Figure 3-1, have been applied extensively and some examples have been summarized by Jusko and Ko.³⁶³

These basic turnover models can be modified and/or extended to account for more complex physiological processes such as time-dependent production ($k_{in}(t)$),³⁶⁴ the rate of loss of cells according to their lifespan^{365–367} and capacity limited processes such as nonlinear synthesis and degradation functions.³⁶⁸ Further, many physiological processes such as secretion of hormones, secretion of gastric acid, gene expression, cardiac output and blood pressure are known to be subject to circadian rhythms, which might influence the pharmacokinetics and pharmacodynamics of various drugs.^{369–371} Symmetric circadian rhythms have been described by trigonometric functions, such as the cosine model introduced by Lew et al.,³⁷² whereas asymmetric circadian rhythms have been modelled with the addition of exponential, dual cosine or harmonic functions.^{373,364} The detailed mathematical formalism around these functions has been summarized by Krzyzanski.³⁷⁴

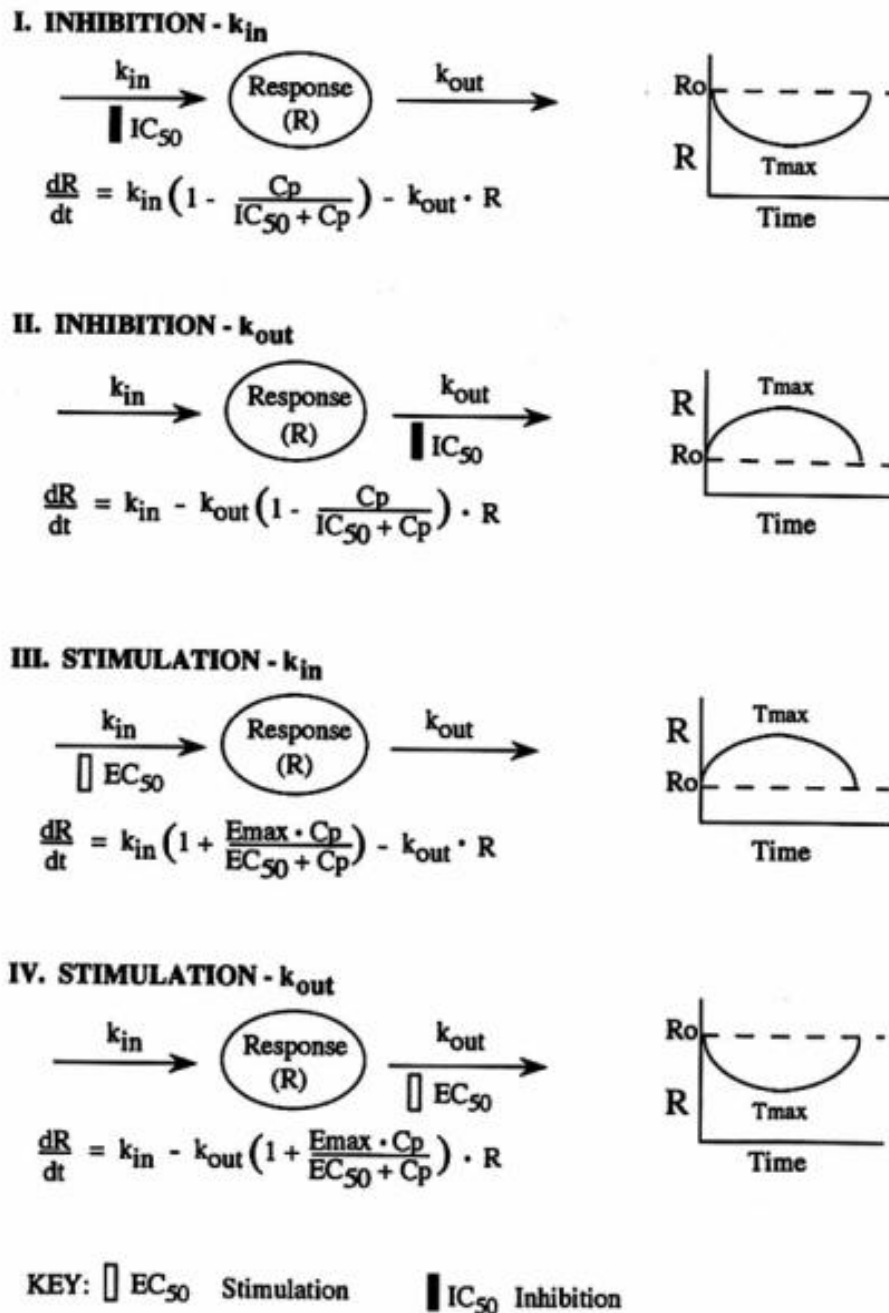


Figure 3-1: Four basic indirect response models characterized by either inhibition or stimulation or the response variable. The shapes of the responses are depicted on the right of each model (reproduced with permission by Dayneka NL, Garg V, Jusko WJ. *J Pharmacokinet Biopharm.* 1993 Aug;21(4):457-78).

3.1.3.2 Signal transduction and feedback control indirect response models

The sequence of events that takes place between receptor binding or activation and the observable effect is referred to as signal transduction and can involve signaling cascades, activation or inhibition of secondary messengers, gene up- or down-regulation and mRNA transcription to functional proteins. By definition, every transduction process has two inherent attributes: the transformation of the original signal and the introduction of a time-delay.^{375,376} Depending on the experimental time-scale, the time delay might or might not be discernable and in the latter case the response is described by a transduction model with no delay. For instance, this is true in the operational model of agonism

introduced by Black and Leff.³⁷⁷, which has been applied to describe the PK/PD of A₁ adenosine, μ -opioid and 5-HT_{1A} receptor agonists.^{378–382} However, in other cases the time delay produced by the transduction process is significant and the mathematical models need to be adjusted accordingly. The most common approach is the so-called transit compartment model, which has been applied to the modeling of the genomic effects of corticosteroids, in this case known as the 5th generation model for corticosteroids, as well as myelosuppression and hematologic toxicity in cancer chemotherapy.^{383–386}

Most physiological processes are subject to feedback control and belong to the so-called autoregulation systems. The PK/PD models that do not address these auto-regulatory mechanisms might fail to provide a complete insight of the drug-exposure relationship and it has been shown that this can lead to underestimation of the drug's potency.³⁷⁶ The feedback control indirect response (FC IDR) models usually incorporate terms proportional to the error signal itself, the integral and the derivative of the error signal in linear and, less commonly, in nonlinear combinations. There are also FC IDR models which include an additional state, the "moderator" state, which feeds back to alter the synthesis or turnover of the response.³⁸⁷ Numerous applications of PK/PD models incorporating feedback regulation mechanisms have been published in the literature.^{385,388,389}

Overall, PBPK/PD models incorporating a physiological understanding of the underlying mechanism(s) of action of the drug and progression of disease can serve as powerful tools for exploring and predicting clinical drug product performance. In the context of biopharmaceutics, bridging the gap between *in vitro*, *in vivo* and *in silico* methods by applying the Quality by Design (QbD) and the Biopharmaceutics Risk Assessment Roadmap (BioRAM),^{390,391} will allow pharmaceutical scientists to correctly assess the rationale for formulation selection and set targets for critical quality attributes based on clinical drug product performance. PBPK/PD modeling and simulation offers a framework not only to evaluate the degree of which formulation factors can steer the *in vivo* drug product performance, but also how differences in these will translate for the pharmacologic effect. For example, Cristofolletti and Dressman coupled a PBPK to an effect compartment and an E_{max} model to investigate the relevance of *in vitro* dissolution and single point PK metrics (i.e., bioequivalence criteria) of ibuprofen immediate release products on the produced dental pain relief.²⁷ The authors used an IVIVE-PBPK/PD model to simulate the effect of different dissolution rates from products containing ibuprofen free acid and salts and to assess whether these would a) reflect reported differences in pharmacokinetics as well as whether b) differences in pharmacokinetics would translate into difference in the ability of ibuprofen to relieve dental pain in adults.²⁷ It was shown that faster dissolution of the products containing salt forms of ibuprofen, led C_{max} to not meet the average bioequivalence (ABE) acceptance criteria. However, the simulated pain relief scores elicited by ibuprofen free acid and salts were identical. This indicates that the bioequivalence criteria for C_{max} might be over-discriminatory and not clinically relevant for assessing therapeutic equivalence of ibuprofen products. Confidence in the translatability and predictive capacity of PBPK/QSP and PK/PD models and IVIVE approaches is an essential element to integration of appropriate *in vitro* biorelevant tools with *in silico* models, which can then ensure prediction of the clinical outcome and thus guarantee therapeutic equivalence between products.

3.2 The role of biopharmaceutic and pharmacokinetic properties to support waivers of *in vivo* bioequivalence

According to the Code of Federal Regulation (21CFR320.1), bioavailability (BA) is defined as “the rate and extent to which the active ingredient or active moiety is absorbed from a drug product and becomes available at the site of action”, whereas BE is “the absence of a significant difference in the rate and extent to which the active ingredient or active moiety in pharmaceutical equivalents or pharmaceutical alternatives becomes available at the site of drug action when administered at the same molar dose under similar conditions in an appropriately designed study”. Interestingly, these definitions are in essence substantially different from the definition of bioavailability as the fraction of dose that becomes available in the systemic circulation and equals to the product of the dose fraction entering the enterocytes (f_a), escaping the first-pass metabolism in the gut (f_g) and the liver (f_h). The statutory definition of BE clearly indicates that the metrics used to assess BE should correlate with the efficacy and/or safety at the site of action. In the case where plasma or blood is the site of drug action, the “the rate and extent to which the active ingredient or active moiety in pharmaceutical equivalents or pharmaceutical alternatives becomes available” can be appropriately approximated by the rate of absorption, but even in this case absorption would correspond to the processes of *in vivo* disintegration, dissolution, permeation, and first pass metabolism in the gut or liver. On the other hand, it is obvious that when the site of action is other than the systemic circulation, the rate and extent of absorption rarely reflect the rate at which the drug becomes available at the site of pharmacologic action.

The current regulatory guidelines are based on the assumption of an instantaneous equilibrium between systemic exposure and drug concentration at the site of action.³⁹² In this context, C_{max} and AUC are by far the most commonly used metrics to assess BE in practice. The assessment of the “extent” of bioavailability is based upon measurement of AUC, which can be considered as a direct metric. In contrast, the assessment of the “rate” of bioavailability relies on the measurement of indirect indices (e.g., C_{max} , T_{max}), which are confounded by other kinetic processes. The indirect metrics incorporate post-absorptive variability e.g., first pass metabolism, which may increase the risk of false positive bioequivalent results.³⁹³ Furthermore, the absorption rate constant (k_a) obtained after conventional deconvolution of oral PK data using unit response data (either from intravenous or oral solution administration) is a mixture of all pre-systemic processes (i.e., absorption and first-pass metabolism). Despite criticism expressed for its relevance for *in vivo* absorption,^{290,394–400} C_{max} has become the gold standard surrogate for absorption rate.^{284,401} Coming from another point of view, some authors have advocated that the regulatory guidelines should concentrate on the clinical relevance of systemic exposure for safety and efficacy, and thus have argued for the usefulness of C_{max} as absorption rate metric.^{392,402} Indeed, the current updated BE guidelines have incorporated the exposure concept and redefined C_{max} as the peak of exposure, AUC_{0-t} as the total exposure and partial AUC as the early exposure, focusing on assuring comparable therapeutic effects between formulations.^{284,401}

From a biopharmaceutics perspective, BE studies benchmark the *in vivo* performance of a test formulation against a reference product, for which safety and efficacy have typically already been proven. The biopharmaceutics (BCS) and developability (DCS) classification systems provide a framework for an initial assessment of oral bioavailability and the biopharmaceutic risks associated with the development of a drug product.^{403–405} In general, both systems rely on the solubility (either

in aqueous or biorelevant media) and the fraction of dose absorbed, which is approximated by *in vitro* or *ex vivo* permeability measurements. From a regulatory perspective, the BCS-based biowaiver approach is intended to reduce the need for *in vivo* bioequivalence studies by providing an appropriate surrogate for *in vivo* bioequivalence, whereby *in vivo* bioequivalence studies may be exempted if appropriate *in vitro* data can be generated. BCS-based biowaivers are applicable only to orally administered immediate release (IR) solid dosage forms or suspensions where the drug substance(s) is categorized as BCS class I or III and meets the predefined solubility, permeability and dissolution criteria.^{283,284} Additionally, linear pharmacokinetics and a wide therapeutic index are required.^{283,284} The primary hypothesis of the BCS-based biowaiver approach is that drug products exhibiting similar drug release (with “similarity” defined by the regulatory guidelines) are expected to have similar *in vivo* dissolution, and thus to be bioequivalent. However, it is well established that the rate limiting step for absorption of BCS class I drugs is usually the gastric emptying time, whereas for BCS class III drugs, absorption is controlled by the intestinal permeability. Therefore, for these types of compounds the *in vitro* dissolution is not expected to correlate with the *in vivo* drug absorption and performance of the formulation.

On the other hand, within the BCS class II absorption is typically expected to be limited either by the dissolution rate or the drug solubility. Since BCS Class II is a quite complex group and contains a wide variety of drugs, some authors have proposed sub-classifications. For example, a BCS Class IIa would encompass acidic drugs, whilst a BCS Class IIb would contain weak bases.⁴⁰⁶ Some BCS Class II weak acids are expected to exhibit BCS Class I-like behavior *in vivo* because of high solubility and fast dissolution in the pH of the intestinal environment and despite very poor solubility in the gastric environment.^{28,287} In such cases, the absorption of those BCS class II weak acids will be controlled by the gastric emptying similar to BCS Class I compounds. Currently, waiving *in vivo* BE studies for BCS Class IIa drugs is not permitted by regulatory authorities. Interestingly, in the period from 2006 to 2015, the World Health Organization (WHO) recommended waivers of *in vivo* BE studies for some BCS class II weakly acidic compounds, that have a dose number of < 1 at pH 6.8 and were able to meet “rapid dissolution” criteria at pH 6.8 and attain similar dissolution to the comparator product at pH 1.2, 4.5, and 6.8. Nonetheless, this concept was not widely adopted by other regulatory authorities and the WHO has now pulled back from this position in its latest BE guidance (WHO 2015).

3.2.1 Rationale for compound selection

Considering the scientific and regulatory aspects analysed above, the main caveat of BCS is that, by its nature, ignores the impact of human physiology, the drug’s inherent PK properties and the between- and within-subject variability in drug product performance. For instance, similarity of *in vitro* dissolution between two products containing a BCS class I drug might be appropriate to ensure similar *in vivo* release, but this information is not necessarily relevant for the risk associated with showing bioequivalence between these two products. Similarly, for a BCS class II weak acid statistically significant differences in the *in vitro* dissolution at intestinal pH might not really translate to differences in C_{max} or AUC and, where this is the case, one could make a scientific argument that the drug could qualify for BCS-based biowaivers. In this ongoing scientific debate, PBPK/PD modeling and simulation can play a critical role to scientifically support a paradigm shift from “one size fits all” to a case-by-case bioequivalence risk assessment approach based on *in vitro* product performance, human

physiology, drug PK properties and their variability. Even more, it offers the unique opportunity to link *in vitro* product performance and *in vivo* exposure to drug efficacy and safety.

Since C_{max} is a composite of pre-systemic (absorption, first-pass metabolism) and systemic processes (distribution, elimination), the sensitivity of C_{max} to the *in vivo* absorption rate will also depend on the PK properties of the drug. Assuming a one-compartment disposition model with first order oral absorption, C_{max} is a function of dose (D), bioavailability (F), volume of distribution (V_d), the absorption rate (k_a), and elimination constant (k_e):

$$C_{max} = \frac{F \cdot D}{V_d} \cdot e^{-k_e \frac{\ln(k_a/k_e)}{(k_a - k_e)}} \quad (28)$$

In fact, several authors have emphasized that indirect metrics such as C_{max} are insensitive to changes in the absorption rate constant.^{397,402} Interestingly, Rostami-Hodjegan et al. had proposed that any comparison of indirect rate metrics should consider both the variability of the estimate and its sensitivity to change of the underlying absorption rate; the “goalposts” for comparison should move depending upon the metric, drug, and type of formulation.⁴⁰² The same authors argued that even though tight limits in drug release will ensure therapeutic equivalence, the latter may be possible with wider margins on drug release. Moreover, they proposed that removing the term “rate” from the definition of bioequivalence would put an end to the ambiguity associated with C_{max} . Nevertheless, from a clinical perspective, C_{max} is indeed relevant for both safety and efficacy.

Interestingly, the standard two-period two-treatment bioequivalence design does not consider the inter-occasion variability (IOV) of physiological and/or drug variables which might bias the outcome of bioequivalence assessments. For instance, 25% inter-occasion variability in PK could lead to bioinequivalence between two products despite identical *in vivo* release, even though the drug would not be classified as highly variable. To add more fuel to the scientific debate, granting BCS based biowaivers for Class I and III drugs based on *in vitro* dissolution similarity might be less appropriate as *in vivo* dissolution is not expected to be the rate-limiting step for absorption in either of those two classes. On the other hand, this argument might also be an oversimplification and it would generally be better to grant waivers of *in vivo* BE studies only after thorough scientific justification considering drug properties, formulation and biopharmaceutical attributes as well as the associated variability.

In this context, PBPK modeling and simulation offers a unique to investigate the scientific considerations discussed above, explore untested scenarios, and ultimately provide evidence based and drug specific recommendations for bioequivalence testing. Thus, the primary objective of the investigations was to develop, validate and apply PBPK/PD models and simulate virtual trials to assess the relative impact of *in vitro/in vivo* dissolution, PK characteristics (e.g., half-life) and intra-subject variability in *in vivo* drug product performance of BCS class II weakly acidic compounds and propose a PBPK-IVIVE integrated workflow for performing virtual bioequivalence trials. Three BCS class II weakly acidic model drugs (naproxen, flurbiprofen, ibuprofen) with similar disposition and metabolic properties were chosen for study. In general, all three drugs are highly bound to plasma proteins and thus have a low volume of distribution, have low pre-systemic (i.e., first-pass extraction) and systemic clearance, and exhibit almost complete bioavailability ($F > 0.9$). However, they significantly differ with regard to half-life: for naproxen the $t_{1/2}$ is 20-24 h, for flurbiprofen $t_{1/2} \approx 7$ h and for ibuprofen $t_{1/2} \approx 2$ h, reflecting moderate-to-long, moderate, and short half-lives, respectively.

For all three compounds, a systematic workflow was implemented including: i) *in vitro* characterization of biopharmaceutical properties (e.g., solubility, dissolution) followed by model-based analysis of the *in vitro* results, ii) development and comprehensive validation of PBPK/PD models and iii) simulation and risk assessment of bioequivalence trials. The case studies of naproxen (Publication 2) and ibuprofen (Publication 3) focused on best practices for IVIVE in biopharmaceutics, risk assessment and simulation of bioequivalence trials using PBPK modeling. The example of flurbiprofen (Publication 4) emphasized the importance of understanding the relative impact of intrinsic (e.g., genetic polymorphisms) and extrinsic (e.g., co-medications) factors on the drug's PK and PD when making recommendations for bioequivalence and therapeutic equivalence decisions. All three case examples provide mechanistic insights with respect to the dissolution limits critical for *in vivo* drug product performance, considering the PK properties of the drug and physiological variability, with the aim of challenging the status quo of the current BCS-based biowaiver approach and introducing an integrated *in vitro*, *in vivo*, and *in silico* risk assessment paradigm for waivers of *in vivo* bioequivalence studies.

3.3 *In vitro* characterization of biopharmaceutical properties

3.3.1 *In vitro* aqueous and biorelevant solubility

The equilibrium solubility was investigated in various aqueous and biorelevant dissolution media using the Uniprep™ system (Whatman®, Piscataway, NJ, USA). All aqueous buffers were prepared according to the European Pharmacopoeia, while the biorelevant media were prepared according to Markopoulos et al. and Fuchs et al.^{114,407} Briefly, an excess amount of the active pharmaceutical ingredient (API) was added to 3 mL of dissolution medium and the samples were incubated for 24 h at 37°C on an orbital mixer. The samples were then filtered through the 0.45 µm PTFE filter integrated in the Uniprep™ system. The filtrate was immediately diluted with mobile phase and analyzed by high-performance liquid chromatography (HPLC). Details on the development and validation of the HPLC method can be found in the original publications by Loisios-Konstantinidis et al.^{32,33} All measurements were performed at least in triplicate ($n \geq 3$) and the final pH was recorded. The *in vitro* solubility results for naproxen (NPX) and flurbiprofen (FLU) are presented in the following sections, while in the case of ibuprofen (IBU) the solubility values were available from Potthast et al. and Cristofolletti et al.^{408,409}

3.3.1.1 Case example: Naproxen

Table 3-1 and Table 3-2 summarize the equilibrium solubility values of naproxen in various aqueous and biorelevant media, respectively. In the case of the free acid, the final pH_{bulk} was significantly different from the initial pH values of the aqueous media due to the self-buffering effect. On the other hand, this behavior was not observed for the naproxen sodium salt, where the pH difference was equal or less to 0.1 pH unit. The higher solubility of the sodium salt compared to the free acid, especially in the intestinal pH media, is attributed to the difference in the final pH measured, keeping in mind that in this pH range the solubility increases exponentially with pH increase. Since naproxen is a weakly acidic compound, its pH-solubility profile is described by two regions: a) $\text{pH} < \text{pH}_{\text{max}}$, where the excess solid phase in equilibrium with the saturated solution consists of the unionized form and b) $\text{pH} > \text{pH}_{\text{max}}$, where the equilibrium species are exclusively in the ionized form.⁴¹⁰ Hence, unless self-association of solute molecules occurs, identical pH-solubility profiles at equilibrium are expected

regardless of the starting material (free acid or salt), as shown in the pH-solubility profile (Figure 3-2). In addition, the experimental values were compared to values reported in the literature, showing excellent agreement.⁴¹⁰⁻⁴¹²

Table 3-1: Mean (\pm SD) naproxen free acid and sodium salt equilibrium solubility in aqueous media at 37°C for 24h (Uniprep® method).

Aqueous medium	Naproxen		Naproxen Sodium	
	pH _{final}	Solubility (μ g/mL)	pH _{final}	Solubility (μ g/mL)
Water	4.5	70.4 (1.2)	6.7	358.4 (18.1)
HCl acid (pH=1.2)	1.3	29.4 (6.4)	1.2	28.4 (0.72)
Acetate buffer (pH=4.5)	4.5	84.8 (4.2)	4.6	103.1 (3.6)
Level I FeSSIF V1 (pH=5.0)	5.0	175.4 (0.0202)	5.1	241.6 (5.2)
Phosphate buffer (pH=6.5)	6.2	1627.6 (31.5)	6.6	2363.4 (31.5)
Phosphate buffer (pH=6.8)	6.5	3619.1 (112.6)	6.9	4957 (119)
Phosphate buffer (pH=7.4)	6.8	5981.6 (28.0)	7.5	10128 (674)

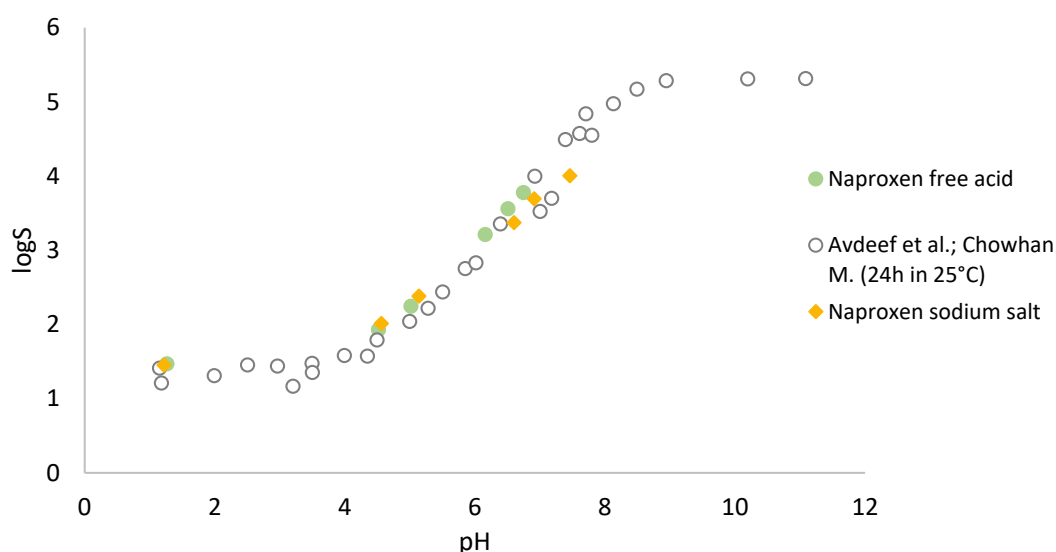


Figure 3-2: Naproxen (circles) and naproxen sodium (diamonds) experimental mean aqueous equilibrium solubility values (24 h at 37°C) plotted against respective literature values (24 h at 25°C) in a pH-solubility profile. The *in vitro* solubility experiments were performed with the Uniprep® method in triplicate. The experimental results are in agreement with the literature values (24 h at 25°C) from Avdeef *et al.* and Chowhan *et al.*

Similar to the solubility of naproxen free acid in phosphate buffers, a considerable decrease in the final pH_{bulk} was observed in fasted state biorelevant media. In fact, the reduction is even more pronounced in the fasted state biorelevant media due to their lower buffer capacity (5.6 mmol/L/ Δ pH in FaSSIF V3 *versus* 18.5 mmol/L/ Δ pH in European Pharmacopoeia phosphate buffers).⁴⁰⁷ Comparison of solubilities in compendial media with those in biorelevant media shows that micelle-mediated solubilization has a substantial impact on the overall solubility of naproxen. For instance, in FaSSIF V1 Level II, the solubility of both free acid and sodium salt was increased by 25.8% and 51.8%,

respectively, when compared to phosphate buffer (pH=6.5). Likewise, in media simulating the fed state, such as FeSSIF V1 Level II, a 2.4-fold increase in the solubility of the free acid and a 2.1-fold increase for the salt form were observed, in comparison to the respective medium without surfactants.

Table 3-2: Mean (\pm SD) equilibrium solubility of naproxen free acid and sodium salt in fasted and fed state biorelevant media at 37°C for 24h (Uniprep® method).

Biorelevant medium	Naproxen		Naproxen Sodium	
	pH _{final}	Solubility (μ g/mL)	pH _{final}	Solubility (μ g/mL)
<i>Fasted state</i>				
Level III FaSSGF (pH=1.6)	1.6	33.4 (1.1)	1.6	31.8 (0.92)
Level II FaSSIF V1 (pH=6.5)	5.9	2046 (150)	6.5	3587 (179)
Level II FaSSIF V3 (pH=6.7)	5.8	1624 (153)	6.7	3469 (187)
<i>Fed state</i>				
Level II FeSSGF _{middle} (pH=5.0)	4.9	352.6 (21.4)	5.1	575.2 (19.3)
Level II FeSSIF V1 (pH=5.0)	5.0	424.7 (26.6)	5.0	519.9 (18.9)
Level II FeSSIF V2 (pH=5.8)	5.8	890.0 (56.7)	5.8	799.5 (177)

3.3.1.2 Case example: Flurbiprofen

Table 3-3 summarizes the equilibrium solubility values of flurbiprofen in multiple aqueous and biorelevant media of different pH. Similar to naproxen, the final pH_{bulk} differed significantly from the initial pH values in phosphate buffers due to the self-buffering effect. The reduction is even more pronounced in the fasted state biorelevant media due to their lower buffer capacity (5.6 mmol/L/ Δ pH in FaSSIF V3 *versus* 18.5 mmol/L/ Δ pH in European Pharmacopoeia phosphate buffers) ⁴⁰⁷.

Micelle-mediated solubilization, at least for the ionized species, seems not to have a substantial impact on the overall solubility of flurbiprofen, which is instead strongly pH-dependent.

Table 3-3: Mean (\pm SD) equilibrium solubility of flurbiprofen in aqueous buffers and fasted state biorelevant media at 37°C for 24h (Uniprep® method).

Medium	Flurbiprofen	
	pH _{final}	Solubility ($\mu\text{g/mL}$)
<i>Aqueous buffers</i>		
FaSSGF Level I (pH=1.6)	1.6	18.1(0.17)
Acetate buffer (pH=4.5)	4.7	101.1(7.06)
FaSSIF V1 Level I (pH=5.0)	5.1	225.4(5.6)
Phosphate buffer (pH=6.5)	6.1	2024.4(128.2)
Phosphate buffer(pH=6.8)	6.3	3127.1(194.9)
<i>Fasted state biorelevant media</i>		
Level III FaSSGF (pH=1.6)	1.6	18.5(1.6)
Level II FaSSIF V1 (pH=6.5)	6.0	1954.9(3.9)
Level II FaSSIF V3 (pH=6.7)	5.9	1585.4(172.1)

3.3.2 *In vitro* dissolution testing

All *in vitro* dissolution tests were performed using a calibrated USP II (paddle) apparatus (Erweka DT 80, Heusenstamm, Germany) at $37\pm 0.4^\circ\text{C}$. Each vessel contained 500 mL of fresh, pre-warmed medium and the rotational speed was set at 75 rpm. Samples were typically withdrawn at 2.5, 5, 10, 15, 20, 30, 45, 60, 90 and 120 minutes via a 5 mL glass syringe connected to a stainless-steel cannula containing a 10 μm polyethylene cannula filter. Immediately thereafter, the sample was filtered through a 0.45 μm PTFE filter (ReZist™ 30, GE Healthcare UK Ltd., Buckinghamshire, UK), discarding the volume used to saturate the filter (~ 2 mL). The remaining filtrate was immediately diluted with mobile phase and analyzed by HPLC-UV. The removal of 5 mL at each sampling time was considered in the calculation of the percentage dissolved.

Since the conventional one-stage USP II dissolution test does not include a gastric compartment to account for disintegration of the dosage form in the stomach, differences in the disintegration time between simple, film-coated (i.e., with a non-functional coating), and sugar-coated formulations might bias the interpretation of the biorelevant *in vitro* dissolution behaviour, especially if drug is highly soluble in the particular medium, with respect to the *in vivo* performance. Hence, to investigate the disintegration effect on the *in vitro* performance, a two-stage dissolution test was performed per Loios-Konstantinidis et al.³²

The tested dosage forms were initially exposed to 250 mL of gastric medium (i.e., FaSSGF Levels I & III) and samples were removed at 5, 10, 15, 20, 30 minutes. After the withdrawal of the last sample, 6.8 mL of sodium hydroxide 1M and immediately thereafter 250 mL of FaSSIF V3 concentrate pH=6.7

(double concentration of all the constituents, apart from sodium hydroxide) were added to the vessel. Sodium hydroxide was added first, but almost simultaneously with FaSSIF V3. This was done to avoid using a very high pH in the FaSSIF V3 concentrate, which could cause deformation of the micellar structures. After the pH shift, further samples were removed at 32.5, 35, 40, 45, 50, 60 and 90 minutes. The two-stage dissolution tests were performed using calibrated USP II (paddle) apparatus (Erweka DT 80, Heusenstamm, Germany) at $37\pm 0.4^\circ\text{C}$ and the samples were analyzed by HPLC-UV (see section 2.5). Both single and two-stage dissolution experiments were performed at least in triplicate ($n\geq 3$) and the final pH in the vessel was recorded.

3.3.2.1 Case example: Naproxen

The *in vitro* dissolution behaviour of both the pure drug and formulations of naproxen free acid and its sodium salt was investigated. Naproxen is commercially available as immediate release tablets containing either 500 mg of the free acid (Naprosyn®) or 550 mg of the sodium salt form.

For the free acid (at 500 mg), dissolution in FaSSIF V3 Level II and in Ph. Eur. phosphate buffer pH=6.8 was very rapid (>85% within 5 minutes) and rapid (>85% within 30 minutes), respectively. On the other hand, the dissolution in FaSSIF V3 Level I (i.e., without bile salts) was much slower, with 85% dissolved reached only after 60 minutes. The observed differences in *in vitro* dissolution behavior are attributed to differences in buffer capacity (FaSSIF V3 Level I and II vs. phosphate buffer) and solubilization capacity (FaSSIF V3 Level II vs. Level I) of the tested media. Furthermore, as dissolution was under non-sink conditions in this series of experiments, the dissolution rate in FaSSIF V3 Level I was significantly slower, due to its low buffer capacity (5.6 mmol/L/ ΔpH), than in the compendial phosphate buffer (18.5 mmol/L/ ΔpH). At higher total phosphate buffer concentration, i.e., in the compendial medium, the bulk (pH_{bulk}) rather than the surface pH (pH_0) drives solubility and dissolution. By contrast, in the low buffer capacity FaSSIF V3 Level I medium the surface pH seems to control the dissolution rate and as a result the final pH is significantly altered (5.95 in FaSSIF V3 Level I vs. 6.62 in Ph. Eur. phosphate buffer). Nevertheless, the impact of buffer capacity on the overall dissolution behavior becomes much less prominent when bile salts are added to the medium, as shown in Figure 3-3. Moreover, it is also evident that the addition of the bile salt components in FaSSIF V3 Level II markedly enhances the dissolution rate. Although the main effect is likely through solubilization, improvements in wetting may have also contributed to the higher dissolution rate in the Level II medium.

On the contrary, none of these trends was observed for the sodium salt tablets and their dissolution was almost instantaneous (85% dissolved by the first sampling time at 2.5 min) in all tested media. This is mainly attributed to the higher solubility as well as the higher surface pH in the media invoked by the sodium salt of naproxen.

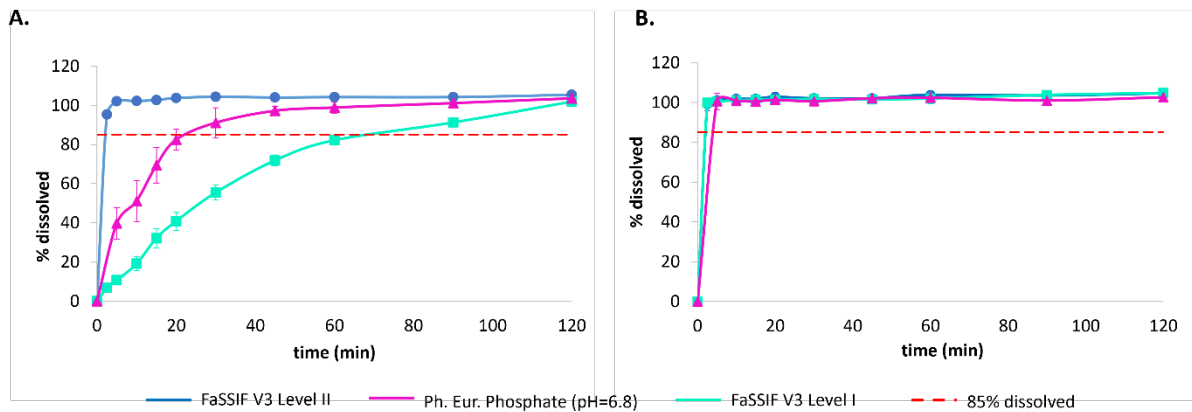


Figure 3-3: In vitro dissolution (mean \pm SD) of 500 mg naproxen free acid (A) and sodium salt (B) drug powder in Ph. Eur. phosphate buffer (pH=6.8), Level I and II FaSSIF V3. USP paddle apparatus at 75 rpm and 500 mL of dissolution medium at 37°C were used in all experiments. The experiments were performed in triplicate. Horizontal dashed red line represents 85% dissolved. Most standard deviation bars lie within the symbols.

The dissolution profiles in FaSSIF V3 Levels I and II along with the results for the “intestinal” part of the two-stage testing are presented for Naprosyn[®] and Anaprox[®] in Figure 3-4. In all cases, and for both formulations, dissolution was very rapid under conditions simulating the upper small intestine, with 85% dissolved in less than 15 min. Interestingly, a mismatch between the dissolution results of the APIs and dosage forms was observed. For instance, dissolution of naproxen free acid from the Naprosyn[®] tablet was much faster than the dissolution of the pure drug in FaSSIF V3 Level I. However, the dissolution rate of naproxen free acid from Naprosyn[®] in FaSSIF V3 Level II was slightly slower than the respective rate of the pure drug. Furthermore, although dissolution of sodium salt was virtually instantaneous in all media (85% dissolved within 2.5 min), the Anaprox[®] formulation of the salt form reached 85% dissolved only after 15 minutes. This indicates that the dissolution of the tablets under intestinal conditions was delayed due to disintegration, especially in the case of the sodium salt formulation. In order to account for disintegration in the stomach prior to exposure to the intestinal media, two-stage dissolution tests were subsequently performed. Since the amount dissolved under gastric conditions was less than 2% in all cases, only the “intestinal” part of the two-stage profiles is presented and compared with the conventional single-vessel dissolution profiles (Figure 3-4). Indeed, pre-treatment in gastric media accelerated the dissolution rate (85% dissolved reached 5 min earlier) from both Naprosyn[®] (naproxen free acid) and Anaprox[®] (naproxen sodium) tablets. Despite dissolution being very rapid in all cases, the disintegration effect was more prominent for Anaprox[®].

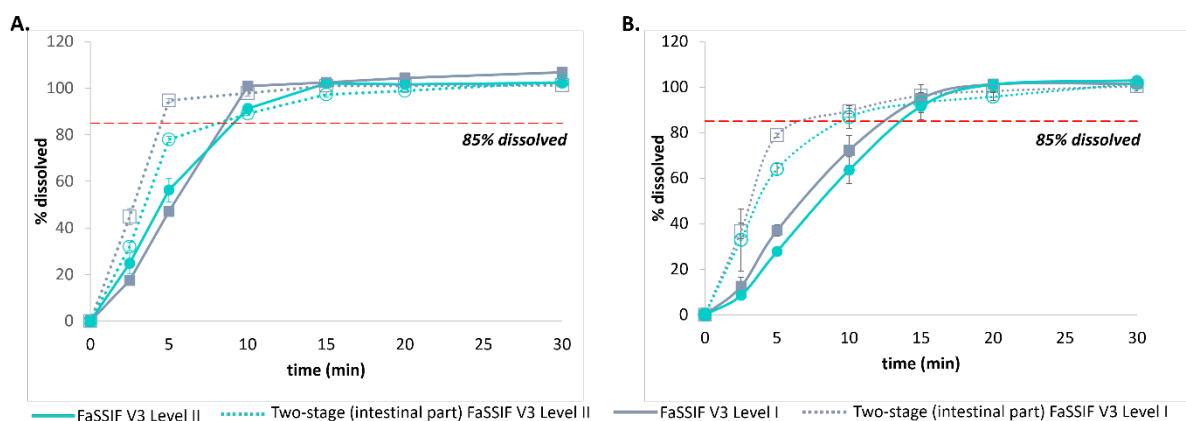


Figure 3-4: *In vitro* dissolution (mean \pm SD) of Naprosyn® 500 mg (A) and Anaprox® 550 mg (B) in FaSSIF V3 Levels I and II (solid lines, filled squares and circles respectively). The intestinal profiles in FaSSIF V3 Levels I and II (after the pre-treatment with FaSSGF Levels I and III respectively) during two-stage test are also depicted (dotted lines, empty squares, and circles, respectively). USP paddle apparatus at 75 rpm and 500 mL of dissolution medium at 37°C were used in all experiments. The experiments were performed in triplicate. Horizontal dashed red line represents the 85% dissolved. Most standard deviation bars lie within the symbols

3.3.2.2 Case example: Flurbiprofen

In this case example, the *in vitro* dissolution behaviour of the active pharmaceutical ingredient (API) powder and of three commercial immediate release (IR) dosage forms of flurbiprofen was investigated. The three IR flurbiprofen tablets were selected to have qualitatively and quantitatively different composition: a) 100 mg flurbiprofen USP (film-coated tablets, lot 3077637; Mylan Pharmaceuticals Inc., Morgantown, WV, USA), b) 100 mg Antadys® (film-coated tablets, lot 8M824; Teva Sante, Paris, France) and c) 100 mg Froben® (sugar-coated tablets, lot 31257J4; BGP Products GmbH, Baar, Switzerland). All dissolution results reported were performed at flurbiprofen's highest dose strength of 100 mg.

Figure 3-5 shows the mean percentage dissolved (\pm SD) of FLU in the tested formulations and as the pure drug over time in fasted state simulated gastric fluids (FaSSGF) of different simulation levels (I and III). As expected, the *in vitro* release of a poorly soluble weak acid under gastric conditions is incomplete, reaching a plateau at around 8.3% of the dose in both FaSSGF Levels I and III. The USP as well as the Antadys® tablets exhibit similar *in vitro* dissolution behaviour in both media. However, the unformulated drug reaches a maximum of only 5.5% in FaSSGF Level I. Since there is no difference in the solubility of FLU between the two media, this observation is attributed to the absence of surfactants and proteins (*i.e.*, pepsin) in FaSSGF Level I, leading to poor wetting of the drug powder.

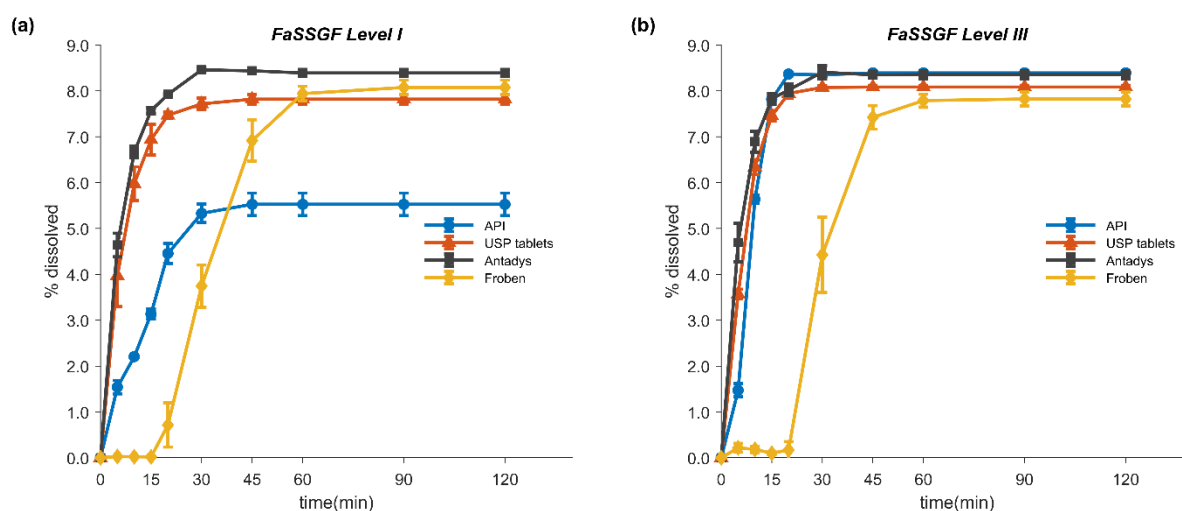


Figure 3-5: (a), (b) *In vitro* dissolution (mean \pm SD) of flurbiprofen API 100 mg (circles), USP tablets[®] 100 mg (triangles), Antadys[®] 100 mg (squares) and Froben[®] 100 mg (diamonds) in FaSSGF Levels I & III, respectively. USP paddle apparatus at 75 rpm and 250 mL of dissolution medium at 37°C were used in all experiments. All experiments were performed at least in triplicate ($n \geq 3$). Most standard deviation bars lie within the symbols.

Mean percentage dissolved (\pm SD) over time in compendial and fasted state simulated intestinal fluids (FaSSIF) for the unformulated API and the tested formulations are presented in Figure 3-6. For the pure drug, the dissolution in FaSSIF V3 Level II and in Ph. Eur. phosphate buffer pH 6.8 was very rapid (>85% within 2.5 and 15 minutes, respectively). On the other hand, dissolution in FaSSIF V3 Level I (i.e., without bile components) was much slower with 85% dissolved reached only after 60 minutes. Such behaviour can be assigned to differences in buffer capacity (FaSSIF V3 Level I and II vs. phosphate buffer), solubilization capacity (FaSSIF V3 Level II vs. Level I) and differences in wetting by the tested media. Interestingly, this behaviour is consistent with the observations in the case example of naproxen. In both cases, the difference of 0.1 pH units between the initial pH of Ph. Eur. phosphate buffer pH 6.8 and FaSSIF V3 (i.e., pH 6.7) is assumed to have a negligible effect.

Especially since dissolution was under non-sink conditions in this series of experiments, the dissolution rate of the pure drug in FaSSIF V3 Level I was significantly slower, due to its low buffer capacity (5.6 mmol/L/ Δ pH), than in the compendial phosphate buffer. At a higher total phosphate buffer concentration, as in the compendial medium, the bulk (pH_{bulk}) rather than the surface pH (pH₀) drives solubility and dissolution. By contrast, in the low buffer capacity medium FaSSIF V3 Level I the surface pH seems to control the dissolution rate. Indeed, the influence of the dissolving acid on the medium is so great that the bulk pH is significantly altered (final pH was 6.31 vs. 6.82 in Ph. Eur. phosphate buffer). The self-buffering effect on the overall dissolution behaviour was much less prominent when bile salts are added to the medium, as shown in Figure 3-6(b). Furthermore, it is evident that the addition of the bile salt components in FaSSIF V3 Level II markedly enhanced the dissolution rate of the unformulated flurbiprofen. Although the main effect is likely through solubilization, improvements in wetting seem to have also contributed to the higher dissolution rate in the Level II medium, given that a similar behaviour was observed in the gastric media.

For the USP tablets and Antadys[®], these trends were not observed, and dissolution was very fast (85% dissolved within 10 min.) in all tested “intestinal” media. Interestingly, Froben[®], the sugar-coated formulation, consistently showed long disintegration times, with no dissolution for up to 20 minutes in all cases, irrespective of the pH, buffer capacity or the inclusion of bile salt components in the

medium. These findings suggest that Froben[®] would be classified as not rapidly dissolving if the formulation is solely exposed to the intestinal media without considering the disintegration of the sugar coating since the percentage of dissolved drug barely reached 85% at 30 minutes. In order to account for disintegration in the stomach prior to exposure to the intestinal media, two-stage dissolution tests were performed according to Loiosos-Konstantinidis et al.³² The two-stage test results (Figure 3-6 (d)) confirmed that disintegration was limiting dissolution in the intestinal media and, as long as disintegration takes place in the gastric compartment, the dissolution in intestinal media is very fast, reaching 85% dissolved within the first 5 minutes.

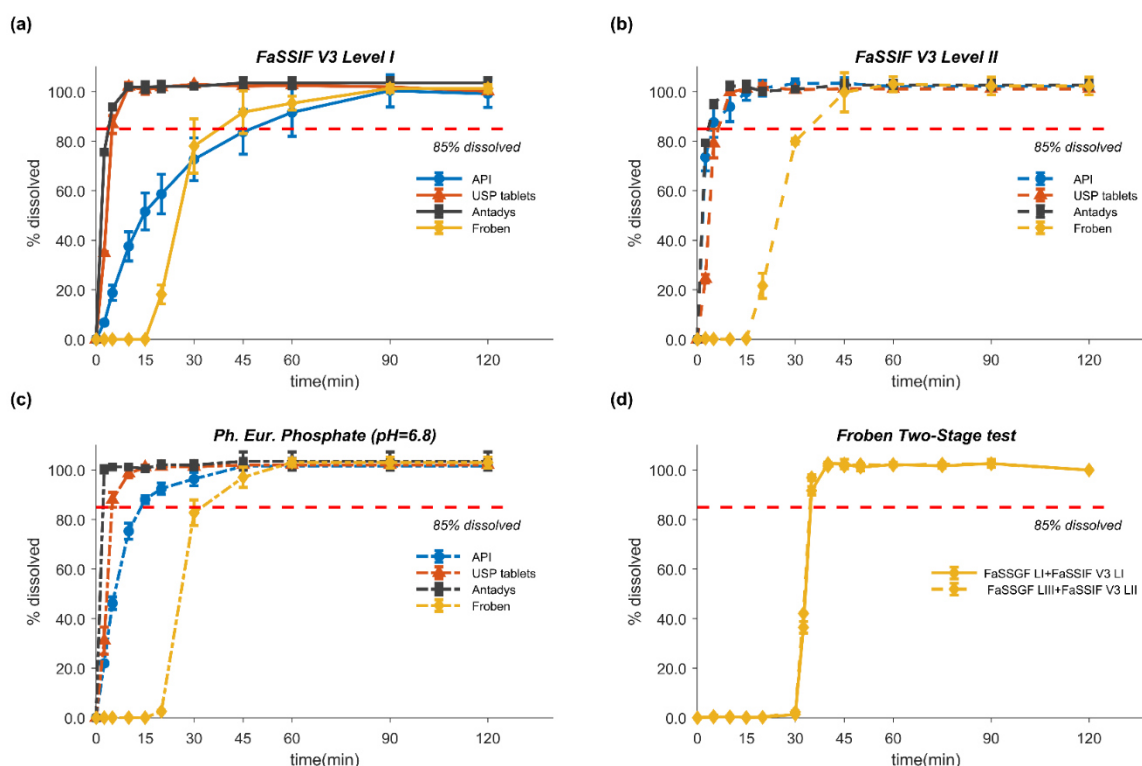


Figure 3-6: *In vitro* dissolution (mean \pm SD) of flurbiprofen API 100 mg (circles), USP tablets[®] 100 mg (triangles), Antadys[®] 100 mg (squares) and Froben[®] 100 mg (diamonds) in (a) FaSSIF V3 Level I (solid lines), (b) FaSSIF V3 Level II (dashed lines) and (c) Ph. Eur. Phosphate buffer (pH=6.8) (dashed dotted lines). (d) Two-stage test of Froben[®] 100 mg (diamonds) in FaSSGF Levels I (solid line) and III (dashed line) at the gastric and FaSSIF V3 Level I (solid line) and FaSSIF V3 Level II (dashed lines) at the intestinal compartments, respectively. USP II paddle apparatus at 75 rpm at $37\pm 0.4^{\circ}\text{C}$ was used in all experiments. The volume of dissolution medium at the gastric compartment was 250 mL, to which 250 mL of properly concentrated intestinal medium was added after 30 minutes. Horizontal dashed red line represents the 85% dissolved. All experiments were performed at least in triplicate ($n\geq 3$). Most standard deviation bars lie within the symbols.

3.4 *In vitro in vivo* extrapolation in biopharmaceutics

Solubility, disintegration, dissolution, supersaturation, precipitation, and permeation processes form an integral component of oral drug absorption kinetics. Over the past decades several *in vitro* biopharmaceutic tools of various degrees of biorelevance and complexity have been developed and utilized to simulate the nevertheless highly variable and heterogeneous *in vivo* environment of the gastrointestinal (GI) lumen. In research and drug development, the usefulness of such tools is mainly realized by their ability to predict and discriminate the *in vivo* performance of drug products. In this

context, integration of experimental results obtained from *in vitro* biopharmaceutical tools within PBPK models to simulate the *in vivo* oral drug absorption and thus the plasma concentration-time profile of a drug product is critical to success. IVIVE approaches with regard to key biopharmaceutical properties such as solubility, dissolution and precipitation can be applied to mechanistically analyze *in vitro* results from properly designed experiments and further link them to the *in vivo* situation. Despite the wide acceptance and routine application of IVIVE for the prediction of *in vivo* clearance, this concept has only recently gained attention in biopharmaceutics and has not been extensively applied using an integrated workflow.

As discussed earlier (section 1.1.3.5), the ADAM model is a population-based mechanistic absorption modelling framework available within the Simcyp® population-based simulator.²⁴ Also available is a stand-alone program, the Simcyp® *In vitro* (Data) Analysis (SIVA) Toolkit. The main purpose of SIVA is to enable modelling of *in vitro* experiments with a view to extracting and confirming parameters for input to *in vivo* simulations within ADAM in the main Simcyp® simulator.

In general, there are two fundamentally different ways to handle the *in vivo* dissolution of solid particles within ADAM. In the first one, the extent and rate of dissolution can be measured *in vitro*, preferably using biorelevant media, and the dissolution profile can be used directly within the PBPK platform. Obviously, this practice has several limitations, which arise from the disparity between *in vitro* and *in vivo* situation. For instance, *in vitro* dissolution experiments often employ different buffer species, hydrodynamics (i.e., agitation rates) and volumes than are extant *in vivo*, are performed under non-sink conditions and in contrast to the intraluminal environment they are rather static representations. Another major limitation with this approach is the lack of incorporation of inter-subject (and sometimes intra-subject) variability in physiological parameters affecting *in vivo* dissolution rate and oral drug absorption. As a result of the factors discussed above, the direct use of *in vitro* dissolution profiles to estimate *in vivo* dissolution rates in PBPK models may be not appropriate. Therefore, it is desirable to confirm and/or estimate the required parameters of the mechanistic equations through modelling of *in vitro* experiments and then apply these models and parameters to *in vivo* simulations where the system parameters differ in general to those of the *in vitro* system, an approach referred to as *in vitro-in vivo* extrapolation (IVIVE) of dissolution and solubility. Such biopharmaceutical IVIVE techniques rely on mechanistic understanding, appropriate experiments, and the modelling of *in vitro* dissolution profiles.

During luminal transit, the drug may undergo disintegration, dissolution, luminal degradation, supersaturation, precipitation, and re-dissolution. It is, however, not practical to mimic and therefore characterize all these complex processes in a single *in vitro* experiment. A way forward is to perform multiple, simpler independent experiments, each assessing relevant biopharmaceutical parameters of the drug product as required. Model based analysis of *in vitro* biopharmaceutical experiments includes both solubility (e.g., in aqueous and biorelevant media), and dissolution modules covering USP II, USP IV, two-stage, two-phase and transfer experiments. This IVIVE approach can be performed using a more mechanistic framework, including a theoretical dissolution model, the “diffusion layer model” (DLM). The DLM enables the incorporation of dynamic regional changes and between-subject differences in the physiological parameters related to pH, bile salts concentration, and fluid volume dynamics and facilitates the mechanistic translation of *in vitro* experiments to the *in vivo* situation. Overall, a stepwise modeling approach of *in vitro* biopharmaceutics experimental data is proposed in an attempt to mechanistically link *in vitro* with *in vivo* and disentangle the multiple factors affecting

oral drug absorption. For that purpose, *in vitro* aqueous and biorelevant solubility, dissolution and two-stage experiments were performed (Publications 2 and 4) and the results were mechanistically modelled (Publications 2, 3 and 4) to obtain estimates of relevant parameters for IVIVE and simulation of *in vivo* absorption of selected drugs and their drug products. A specific modeling workflow for the analysis of such *in vitro* data is recommended; starting from pH-dependent solubility, followed by the micelle-mediated solubilization (i.e., biorelevant solubility) and rounding out the investigations with single or two-stage dissolution and transfer (e.g., BioGIT) data analysis.

3.4.1 Model-based analysis of *in vitro* solubility data

Determination of the pH-solubility profile in various aqueous media comprises a cornerstone in the *in vitro* characterization of a drug's biopharmaceutical properties. The ionization and thus the extent of drug's solubilization at different pH levels, especially within the physiological range, is also critical for prediction of the *in vivo* absorption and drug product performance. Hence, full characterization of the pH-solubility profile, preferably experimentally, is important.

In SIVA, the aqueous phase solubility (S_i) as function of the intrinsic solubility (S_0) and the ionization constant (pK_a) are handled using the Henderson-Hasselbalch equation:

$$S_i = S_0 \cdot (10^{pH-pK_a}) \quad (29)$$

The intrinsic solubility can be determined experimentally as the lowest equilibrium solubility value observed in the pH-solubility profile and this is specific to the solid state of the drug (e.g., crystalline, or amorphous). Furthermore, the ionization constant is sensitive to the experimental method used for its determination, and thus calibration against the observed pH-solubility profile is recommended. At this point, the importance of the accuracy in the values used for S_0 and pK_a has to be stressed, since any error in these values will be further propagated and introduce bias in the determination of micelle-mediated solubilization and dissolution rate. The solubility factor, meaning the ratio between the solubility of unionized and ionized species at the plateau of the pH-solubility profile, which is dependent on the buffer species conjugate of the aqueous media, is another parameter to be considered.

It is essential to account for not only aqueous phase solubility but also the proportion, if any, of drug solubilized by bile components (e.g., bile salts, lecithin, or other surfactants) as this can be a significant contribution to the *in vivo* solubility. Evidence of the impact of this form of solubilization can be seen when comparing aqueous-only solubility at a stated pH with the solubility in a biorelevant medium at the same pH or, even more precisely, by comparing the drug solubility in Level I and II biorelevant media as described by Markopoulos et al.¹¹⁴ Particularly for lipophilic drugs, partitioning into micelles can increase the total solubility by several orders of magnitude. On the one hand, this solubilization effect can increase dissolution rate and thus the rate and/or extent of absorption, especially for drugs with solubility limited absorption. On the other hand, the dissolution rate increase may not be proportional to the solubility increase due to the lower diffusion rate of the relatively large, drug-loaded micelles compared to the drug monomers. In addition, there may also be a free fraction effect in relation to gut wall permeation, meaning that high partitioning into micellar structures might hamper permeation and absorption by reducing the fraction of free drug which is available for absorption. Overall, the effect of partitioning into micelles is a complex interplay of all the above-

mentioned factors, which can be quite difficult to anticipate without quantitative modelling. This requires separating, and thus mechanistically accounting for, the relative proportions of drug solubilized in the aqueous vs. the micelle phases. The total drug solubility can be described by the following equation:

$$S_{(BS)Tot} = \left([BS] \cdot \frac{S_0}{C_{H2O}} \cdot K_{m:w,unionized} + S_0 \right) + \left([BS] \cdot \frac{S_i}{C_{H2O}} \cdot K_{m:w,ionized} + S_i \right) \quad (30)$$

where $S_{(BS)Tot}$ is the total solubility of the drug in the presence of bile salts, [BS] is the concentration of bile salts in the presence of phospholipids and C_{H2O} is the water concentration (55.6 M). A key parameter for defining micelle-mediated solubility is the micelle: water partition coefficient ($K_{m:w}$), for which separate values must be defined for the neutral ($K_{m:w,unionized}$) and charged ($K_{m:w,ionized}$) drug species. Initial estimates of $K_{m:w,unionized}$ for taurocholate-lecithin (4:1 ratio) solutions can be obtained from a built-in linear regression equation based upon $\log P$ developed by Glommé et al.⁴¹³ By default, the predicted $K_{m:w,ionized}$ is assumed to be one or more orders of magnitude lower than the neutral species coefficient, depending upon the specific properties of the ionic species. The default value for cations is 10 (1 log unit), whereas for all other species it is 100 (2 log units) This assumes, as a generalization, that ionized species partition to a lesser extent than neutral species (which might not always be the case). Further, as these models were developed based on a limited number of drugs, estimation of $K_{m:w}$ from *in vitro* biorelevant solubility data at least with two surfactant concentrations, provided that confidence has been established in estimates of the aqueous solubility-related parameters, is typically the preferred method. Such a model facilitates the translation from micelle-mediated solubility parameters that are determined *in vitro* to the respective *in vivo* values, and thus enables the incorporation of the regional luminal pH values and bile salt concentrations in fasted and fed states and their inter-individual variability within the PBPK framework.

3.4.2 Model-based analysis of *in vitro* dissolution data

Once confidence in the estimation of solubility-related parameters has been established, further model-based analysis of the *in vitro* dissolution data obtained from both one and two-stage tests is performed within the serial dilution module of the SIVA Toolkit® (SIVA 3.0). The dissolution rate of spherical particles under sink and non-sink conditions within SIVA is described by an extension of the diffusion layer model (DLM) developed by Wang and Flanagan. (Eq. 31)^{25,414}

$$DR(t) = -N \cdot S_{DLM} \cdot \frac{D_{eff}}{h_{eff}(t)} \cdot 4\pi \cdot \alpha(t) \cdot \left(\alpha(t) + h_{eff}(t) \right) \cdot \left(S_{surface}(t) - C_{bulk}(t) \right) \quad (31)$$

where $DR(t)$ is the dissolution rate at time t ; N is the number of particles in each particle size bin; S_{DLM} is a lumped correction scalar applied without regard to the mechanistic origin of the required correction to the DLM. The S_{DLM} estimates obtained with SIVA can be applied to the Simcyp PBPK simulator to reflect differences between media or formulations by simulating the respective *in vivo* dissolution; D_{eff} is the effective diffusion coefficient; $h_{eff}(t)$ and $\alpha(t)$ represent the thickness of the hydrodynamic boundary layer and the particle radius at time t , respectively; $S_{surface}(t)$ corresponds to the saturation solubility at the particle surface (which may be different to the bulk fluid solubility, as discussed below); and $C_{bulk}(t)$ is the concentration of dissolved drug in the bulk solution at time t .

The $h_{eff}(t)$ value is calculated by the fluid dynamics sub-model, which enables the hydrodynamic conditions to be described according to local conditions and stirring rate. Fluid dynamics-based $h_{eff}(t)$ is the recommended option for describing the hydrodynamics, as it permits a more rational translation of estimated parameters, such as the S_{DLM} , to *in vivo* conditions, in which the hydrodynamics are usually quite different to those in *in vitro* experiments.

The local pH at the particle surface of ionisable drugs can significantly affect the $S_{surface}$ and consequently the dissolution rate^{415–420}. Since the *in vitro* dissolution media have a somewhat higher buffer capacity than the intestinal fluids, the self-buffering effect at the solid surface can be underestimated. For this reason, the surface pH should be calculated and directly input into SIVA. The calculation of the surface pH is based on the model first proposed by Mooney et al.⁴¹⁶, which assumes that dissolution is the result of both the chemical reaction between the conjugate base of the buffer species and the hydrogen cations released from the dissolving drug (in this case FLU) at the liquid-solid interface and the diffusion of the dissolved particles to the bulk. This model is very similar to the quasi-equilibrium model published by Ozturk et al.⁴¹⁸, a derivation of which is implemented in SIVA as the default option for surface pH calculations.

By fitting the DLM model to the observed dissolution data, S_{DLM} estimates for each dissolution and two-stage test are obtained. In the case of two-stage testing, different S_{DLM} values are obtained for the gastric and intestinal compartments, accounting for the changes in the respective *in vitro* conditions. Under fasted state intestinal conditions, all three model drugs discussed in this work are freely soluble and therefore *in vitro* dissolution is not expected to be solubility limited. When this is the case, disintegration of the solid dosage form in the intestinal dissolution medium might be the rate-limiting step for the *in vitro* dissolution rate, especially in single dissolution experiments where the dosage form is directly exposed to the intestinal medium without any pre-treatment with gastric medium to account for disintegration in the stomach. When disintegration is considerably slower than dissolution, and thus has an impact on the overall dissolution rate, the first-order disintegration option is activated in SIVA and used to obtain estimates of a first-order disintegration rate constant (k_d) for these experiments.

$$\%F_{release} = \%F_{max} \cdot (1 - e^{-k_d \cdot (t - t_{lag})}) \quad \text{for } t > t_{lag} \quad (32)$$

$$\%F_{release} = 0 \quad \text{for } t \leq t_{lag} \quad (33)$$

For the examples of flurbiprofen and naproxen, the option was kept deactivated when analysing the results of the two-stage experiments, since disintegration in the stomach is already addressed by the dissolution in the gastric medium. Both gastric and intestinal phases of the two-stage results were modelled simultaneously using the serial dilution model, which can account for more than one *in vitro* dissolution condition in the same experiment. Estimation of the relevant parameters for naproxen and flurbiprofen was performed using the Nelder-Mead algorithm and equal weighting was applied. The various estimated S_{DLM} and k_d values were implemented in the Simcyp® Simulator (V18.1; Certara, Sheffield, UK) to simulate various *in vivo* dissolution scenarios for the formulations under study and to generate *in vitro-in vivo* extrapolation relationships.

For the case of ibuprofen, an alternative IVIVE approach was implemented relating the *in vitro* dissolution rate to an estimated (i.e., not measured) product-specific particle size distribution (P-PSD). This method assumes that drug particle size controls the *in vivo* dissolution rate and has been used to justify clinically relevant drug product specifications (CRDPS).^{291,292,421} Apparently, this approach is only physiologically sound when *in vivo* dissolution is the rate-limiting step for oral drug absorption. Ibuprofen is a plastic–elastic material and thus subject to particle deformation during the drug product manufacturing processes¹⁵. Deformed particles bind or associate with one another, such that the effective surface area of the drug driving intraluminal dissolution might be smaller than the specific surface area measured for the drug substance¹⁵. Hence, product-specific monodispersed particle radii for the three different products: 1) a reference formulation (R), a bioequivalent to R product (TBE) and a non-bioequivalent to R product (TNBE) were fitted to the respective *in vitro* dissolution profiles available from the work by Cristofolletti and Dressman.⁴²²

Model-based analysis of the *in vitro* data in the SIVA[®] Toolkit was performed with either the Nelder Mead or the hybrid algorithm (i.e., with a genetic algorithm coupled to Nelder Mead) with a 5th order Runge-Kutta or Livermore solver. The appropriate weighting scheme was chosen according to the observed data ranges and their homogeneity, and the goodness of fit was assessed by the coefficient of determination (R squared) as well as visual predictive checks (e.g., residuals plots).

3.4.3 Case example: Naproxen

Table 3-4 summarizes the parameter estimates (95% CI) obtained by model-based analysis of the *in vitro* solubility data in compendial and biorelevant media. The pK_a was determined to be 4.43, which agrees with values reported in the literature (4.15-4.5).^{410,412,419,423,424} By estimating the micelle-water partition coefficients for both neutral and ionized species using the biorelevant solubilities, we were able to quantify the effect of physiologically relevant surfactants on the overall solubility of naproxen. As discussed in sections 3.4.1 and 3.4.2, these values were utilized within the Simcyp[®] Simulator to simulate the luminal conditions and the *in vivo* dissolution behavior, accounting at the same time for any inter-subject variability regarding bile salt-mediated solubilization in the virtual population. Using this approach, implementation of logK_{m:w} (of neutral and ionized species) in the PBPK model enabled mechanistic prediction of the *in vivo* luminal solubilization, which would have not been feasible if mean solubilities had been used as the intraluminal values.

Table 3-4: Parameter estimates (95% CI) resulting from the model-based analysis of naproxen *in vitro* solubility data in aqueous and biorelevant media. The pK_a was estimated from the aqueous solubility values, whereas biorelevant solubilities were used to estimate the micelle-water partition coefficients (logK_{m:w} neutral, ion). The accuracy of the predictions was evaluated with the coefficient of determination (R²).

Parameter	pK _a	logK _{m:w} neutral	logK _{m:w} ion
Estimate (95% CI)	4.43 (4.42-4.44)	5.37 (5.34-5.40)	4.00 (3.98-4.02)
R ²	0.9990	0.9999 ¹	

¹ logK_{m:w} neutral and ion were obtained by simultaneous fitting to the *in vitro* biorelevant solubility values

Table 3-5 presents the estimated DLM scalar (S_{DLM}) values (95% CI) obtained by model-based analysis of the intestinal *in vitro* dissolution profiles using the SIVA Toolkit®. Each naproxen form (i.e., pure drug vs. tablet formulations and free acid vs. sodium salt) was evaluated separately. The goodness of fit was visually inspected with residuals plots and assessed with the coefficient of determination (R^2). As shown in Table 3-5, the first-order disintegration model without a time-lag was applied only to those experiments where the formulations were not pre-exposed to gastric medium. Interestingly, S_{DLM} estimates obtained from the two-stage and single dissolution, combined with the disintegration model, matched. These results indicate that, in this case, the effect of disintegration can be properly accounted for using the methodology applied.

The slowest and fastest dissolution rate of naproxen free acid (as pure drug) observed in FaSSIF V3 Levels I and II, respectively, resulted in the lowest (0.0022) and highest (0.0810) estimated DLM values, respectively. Due to the virtually instantaneous dissolution of the sodium salt of naproxen in the pure drug form in all media, the default DLM value of one, without estimation, was utilized for the salt form (Table 3-5). Overall, the predicted dissolution profiles were in excellent agreement with the experimental profiles ($R^2 > 0.96$).

Table 3-5: Estimated DLM scalar (S_{DLM}) values (95% CI) obtained from model-based analysis of *in vitro* dissolution data of naproxen free acid and sodium salt as both the pure drug powder and as commercially available IR tablets. For the commercial formulations, when dissolution without pre-treatment in a gastric medium was modelled, a first-order disintegration model was included. The goodness of fit between the predicted and observed dissolution profiles was evaluated with the coefficient of determination (R^2).

Dissolution Medium	Pure drug		Formulation	
	Free acid	Sodium salt	Naprosyn®	Anaprox®
Level I FaSSIF V3				
S_{DLM} (95% CI)	0.0022 (0.0021-0.0023)	1*	0.0296 (0.0149-0.0443)	0.0212 (0.0131-0.0294)
k_d (95% CI)	n.a.	n.a.	0.305 (0.123-0.487)	0.288 (0.130-0.446)
R^2	0.997	n.a.	0.999	0.998
Level I FaSSIF V3 (two-stage)				
S_{DLM} (95% CI)	n.a.	n.a.	0.0305 (0.0191-0.0308)	0.0221 (0.0174-0.0267)
k_d (95% CI)	n.a.	n.a.	n.a.	n.a.
R^2	n.a.	n.a.	0.967	0.981
Level II FaSSIF V3				
S_{DLM} (95% CI)	0.0810 (0.0651-0.0970)	1*	0.0213 (0.0170-0.0255)	0.0168 (0.00996-0.0237)
k_d (95% CI)	n.a.	n.a.	0.702 (0.354-1.05)	0.228 (0.0975-0.358)
R^2	0.998	n.a.	0.999	0.999
Level II FaSSIF V3 (two-stage)				
S_{DLM} (95% CI)	n.a.	n.a.	0.0187 (0.0143-0.0230)	0.0158 (0.0138-0.0179)
k_d (95% CI)	n.a.	n.a.	n.a.	n.a.
R^2	n.a.	n.a.	0.975	0.991

Ph. Eur. Phosphate (pH=6.8)				
S_{DLM} (95% CI)	0.0136 (0.0121-0.0151)	1*	n.a.	n.a.
R^2	0.992	n.a.	n.a.	n.a.

n.a.: not available/applicable

* Default values of S_{DLM} due to very fast dissolution (>85% dissolved in 2.5 min)

3.4.4 Case example: Ibuprofen

In vitro dissolution and *in vivo* BE results used for this work have already been reported elsewhere.⁴²² Both BE studies were conducted by certified contract research organizations that were inspected by the Brazilian Health Regulatory Agency to assess compliance with the Good Clinical and Good Laboratory Practices guidance and the study protocols were approved by independent Ethics Committees. Briefly, samples from the same batches used in the two randomized, single-dose, two-way, open-label, crossover BE studies in healthy adults were kindly donated by the respective sponsors of the *in vivo* studies. The *in vitro* performances of three oral suspensions of ibuprofen, the Brazilian reference listed drug, a generic and a drug product that failed the BE test (hereinafter referred to as reference, R, test bioequivalent, TBE, and test non-bioequivalent, TNBE, respectively) were comprehensively assessed by Cristofolletti and Dressman, using a reverse translation approach in order to identify biopredictive dissolution conditions.⁴²²

Ibuprofen is a plastic-elastic material and thus subject to particle deformation during drug product manufacturing processes.⁴²⁵ Deformed particles bind or associate with one another, such that the effective surface area of the drug driving intraluminal dissolution might be smaller than the specific surface area measured for the drug substance.⁴²⁵ For that reason, product-specific monodispersed particle radii for the R, TBE and TNBE were fitted to the respective *in vitro* dissolution profiles using the built-in DLM within SIVA[®] (Version 3 Release 1; Certara UK Limited). A hybrid minimization algorithm combining the global search ability of the Genetic Algorithm with the local search strength of Hooke-Jeeves method was applied for parameter estimation. Several initial estimates were tested to ensure that the final estimates corresponded to the global minimum. The goodness-of-fit was assessed based on the coefficient of determination (R squared). In this example, the *in vitro* dissolution is linked to a hypothetical/estimated product specific particle size distribution (P-PSD), which then served as the model input to simulate differences in the *in vivo* dissolution and product performance. The estimated P-PSDs for each ibuprofen suspension are summarized in Table 3-6:

Table 3-6: Estimated product-specific particle size distributions (P-PSDs) of three ibuprofen suspensions (R, T-BE, T-NBE). A log-normal monodispersed distribution was assumed.

Formulation	Mean particle radius (min, max)	Distribution
R	195.3 (0.01, 214.8)	Log-normal
T-BE	174.3 (0.01, 191.7)	Log-normal
T-NBE	150.8 (0.01, 165.9)	Log-normal

3.4.5 Case example: Flurbiprofen

Table 3-7 presents the parameter estimates (95% CI) obtained by model-based analysis of the *in vitro* solubility data in compendial and biorelevant media. The pK_a was determined to be 4.05, a value which agrees with those reported in the literature^{287,411,426,427}. By estimating the micelle-water partition coefficients for both neutral and ionized species using the biorelevant solubilities, we were able to quantify the effect of physiologically relevant surfactants on the overall solubility of FLU. For the neutral species partitioning of the drug to micellar structures seemed to be about 1000-times more important ($\log K_{m:w \text{ neutral}}=5.36$) than for the ionized species ($\log K_{m:w \text{ neutral}}=2.56$), which is in agreement with the observations from the *in vitro* biorelevant solubility results. Similar to naproxen, these values were then used as inputs to the Simcyp® Simulator to simulate the intraluminal solubility and dissolution and the associated physiological population variability.

Table 3-7: Parameter estimates (95% Cis) resulting from the model-based analysis of *in vitro* solubility data for flurbiprofen in aqueous as well as biorelevant media. The pK_a was estimated from the aqueous solubility values, whereas for the micelle-water partition coefficients ($\log K_{m:w \text{ neutral}}$, ion) estimation, biorelevant solubilities were used. The accuracy of the prediction was evaluated by calculating the coefficient of determination, R squared (R^2)

Parameter	pK_a	$\log K_{m:w \text{ neutral}}$	$\log K_{m:w \text{ ion}}$
Estimate (95% Cis)	4.05 (4.42-4.44)	5.36 (4.61-6.11)	2.56 (1.38-5.02)
R^2	0.9990	0.9999 ¹	

¹ $\log K_{m:w \text{ neutral}}$ and ion were obtained by simultaneous fitting to the *in vitro* biorelevant solubility values

Table 3-8 and Table 3-9 summarize the estimated DLM scalar values (95% CIs) as obtained by model-based analysis of the gastric and intestinal *in vitro* dissolution profiles using the SIVA Toolkit®. The goodness of fit was visually inspected with residual plots and assessed with the coefficient of determination (R^2). As shown in Table 3-8, the slowest dissolution rate of the API, which was observed in FaSSIF V3 Level I, and the fastest rate, which was observed when dissolution from Antadys® in FaSSIF V3 Level II was tested, resulted in the lowest (0.00185) and highest (0.0125) estimated DLM scalar values (S_{DLM}), respectively. Differences in the S_{DLM} estimates for the gastric dissolution are not expected to have a major impact on the *in vivo* performance of flurbiprofen since the release in the stomach is very poor.

Since flurbiprofen is highly soluble in intestinal media, disintegration rather than drug solubility is expected to be the rate-limiting step for the dissolution rate of Froben®. In this context, all intestinal single-stage dissolution profiles of Froben® can be modelled by a universal first order-disintegration rate constant and a lag time. Alternatively, modelling of the profiles obtained from the two-stage tests as serial dilutions of different media should be a more physiological approximation of the GI lumen. The estimates from both approaches are presented in Table 3-9. All fitted dissolution profiles were in excellent agreement with the experimental results, with $R^2 > 0.94$ in every case.

In a dissolution-based *in vitro-in vivo* extrapolation (IVIVE) approach, the gastric and intestinal DLM scalar (S_{DLM}) estimates were transferred to the Simcyp® simulator to generate medium-customized and formulation-specific *in vivo* dissolution scenarios and simulate flurbiprofen *in vivo* performance.

Table 3-8: Mean (95% CIs) DLM scalar (S_{DLM}) estimates obtained from model-based analysis of in vitro dissolution data in various media of flurbiprofen pure drug, 100 mg USP tablets® and 100 mg Antadys® formulations. The goodness of fit between predicted and observed dissolution profiles was evaluated with using the coefficient of determination, R squared (R^2).

Dissolution Medium	Formulation		
	API powder	USP tablets	Antadys
FaSSGF Level III			
S_{DLM} (95% CIs)	0.0218 (0.0161-0.0274)	0.0929 (0.0731-0.113)	0.107 (0.087-0.127)
R^2	0.944	0.973	0.982
FaSSIF V3 Level I			
S_{DLM} (95% CIs)	0.00185 (0.001-0.00312)	0.0791 (0.0589-0.993)	0.120 (0.0979-0.142)
R^2	0.974	0.986	0.995
FaSSIF V3 Level II			
S_{DLM} (95% CIs)	0.0965 (0.0544-0.139)	0.0622 (0.0398-0.0847)	0.125 (0.106-0.143)
R^2	0.971	0.976	0.996
Ph. Eur. Phosphate Buffer			
S_{DLM} (95% CIs)	0.00542 (0.00468-0.00617)	0.0150 (0.0110-0.0189)	0.0449 (0.0448-0.0450)
R^2	0.986	0.983	0.999

Table 3-9: Mean (95% CIs) DLM scalar (S_{DLM}) estimates obtained from model-based analysis of Froben® in vitro dissolution data. The in vitro data from single dissolution experiments were modelled assuming that disintegration is the rate limiting step to the flurbiprofen in vitro dissolution rate in intestinal media, whereas for the two-stage dissolution, the serial dilution model was used. The goodness of fit between predicted and observed dissolution profiles was evaluated with the coefficient of determination, R squared (R^2).

Dissolution Model/Media	Formulation
	Froben
First order disintegration/ all intestinal media	
kd (h^{-1}) (95% CIs)	0.127(0.00844-0.0253)
T_{lag} (min) (95% CIs)	14.6 (8.91-20.1)
R^2	0.941
Serial Dilution / Two-stage (FaSSGF Level III + FaSSIF V3 Level II)	
$S_{DLM, Gastric}$ (95% CIs)	0.001 (0.001-0.0244)
$S_{DLM, Intestinal}$ (95% CIs)	0.0712 (0.0576-0.0849)
R^2	0.991

Overall, modelling of *in vitro* dissolution within the same mechanistic framework as that used for *in vivo* simulations provides three important benefits: 1) it allows assessment of the validity of the mechanistic dissolution model (the DLM in this case), and its assumptions, against a controlled and well-defined *in vitro* dissolution environment. This is otherwise difficult to assess in the complex *in vivo* luminal environment where dissolution is not directly measured; 2) it allows assessment of the quality and relevance of model input parameters such as solubility, particle size, disintegration rate etc.; and 3) it can help to identify incorrect parameters or assumptions of the model. In such circumstances the modeler may choose to re-measure and re-estimate certain parameters. A systematic IVIVE approach may therefore help to build confidence in the quality of the input parameters (and the associated assumptions) in mechanistic models and enable improvements in the predictive performance of *in vivo* absorption simulations using PBPK models.

3.5 PBPK/PD model development and validation

In all case examples, PBPK modeling and simulations were performed using the Simcyp® Population-based Simulator. The PBPK models were developed by implementing a “middle-out” stepwise sequential modeling strategy, in line with previously published literature and regulatory guidelines^{51,57,126,204,428,429}. Briefly, the initial model was developed by leveraging physicochemical parameters, *in vitro* data and/or *in silico* predictors for the absorption, distribution, metabolism, and excretion (ADME) processes. *In vitro* data generated for the purpose of this study or available in the literature were also incorporated after using an IVIVE approach. Depending on the case example, simulations were performed using either the Simcyp Healthy Volunteers, the North European Caucasian, or the Chinese healthy volunteer virtual populations. All input parameters for the naproxen and ibuprofen PBPK models, as well as for the flurbiprofen PBPK/PD model, can be found in Table 7-7.

The Advanced Dissolution Absorption and Metabolism (ADAM) model was used to mechanistically describe the absorption. The ADAM model has previously been described in detail by Jamei et al. and Darwich et al.^{24,29} The human effective permeability (P_{eff}) was calculated using either *in vitro* apparent permeability (P_{app}) data in Caco-2 cells for both the compound and positive (Verapamil) / negative (Atenolol) calibrators,²⁸⁷ or *ex vivo* measurements from the human intestine.⁴³⁰

The Diffusion Layer Model (DLM) with Advanced fluid Dynamics (Afd) and dynamic (time variant) pH were implemented to simulate the *in vivo* dissolution. Default settings of the software for luminal blood flow, fluid volume, bile salt content, segmental pH, metabolic activity, and small intestinal residence time were applied. The mean gastric emptying time (GET) in the fasted state was set to 0.25 h (matching the built-in ‘segregated transit time’ model value instead of the default value of 0.4 h used in the ‘global’ transit time model), as suggested by human clinical data and several authors^{431–434}. In all cases, the S_0 was set to the minimum experimentally measured equilibrium solubility value, while estimates for the neutral and ionised species $K_{m:w}$ were incorporated after modelling of the *in vitro* biorelevant solubility data. A dissolution-based IVIVE approach, using S_{DLM} estimates from *in vitro* data, was followed to account for formulation or media-related differences when simulating the respective *in vivo* dissolution scenarios. Further, to investigate the effect of *in vivo* dissolution of multiple formulations and under various conditions on the overall *in vivo* performance, selected S_{DLM} estimates were implemented to simulate the respective clinical studies used for the model validation in each case study. At dose levels other than the one with which the *in vitro* dissolution experiments

were performed, the highest gastric ($S_{DLM, stomach}$) and intestinal ($S_{DLM, SI}$) estimates corresponding to the fastest gastric and intestinal dissolution rates, respectively, were used to minimize the impact of formulation.

The PK disposition (i.e., distribution and elimination) of the PBPK models was described either with a “top down” approach by fitting a minimal PBPK model, meaning a “lumped” PBPK model in which the SAC represents all tissues excluding liver and portal vein, to available IV data, or by using a whole body PBPK model for the distribution of the drug coupled with enzyme kinetic parameters (from recombinant CYPs, UGTs, human liver microsomes or human hepatocytes). Genetic polymorphisms, when relevant, were also considered. Details of the PK disposition for each model drug are presented in the following sections.

The performance of the developed PBPK(/PD) models was evaluated by clinical trial simulations. In order to assess the distribution of population variability, at least 10 trials of 10 subjects ($n \geq 100$) each were simulated for each clinical study. Specifically, a two-step verification process was followed. The initial model was internally validated by comparing the predicted and observed plasma concentration profiles after IV and oral solution (67.9 mg) administration (training dataset). The model was further validated by comparing mean simulated and observed plasma concentration profiles and/or response parameters of external datasets including PK data from subjects with different genotypes (e.g., CYP2C9 1*/1*, 2*/2*, 3*/3*) and at various dose levels. In the case of flurbiprofen, a comprehensive validation of the model was performed by predicting several victim drug-drug interaction studies of flurbiprofen with CYP2C9 inhibitors at different dose levels. Virtual populations were selected to closely match the enrolled individuals in the respective *in vivo* clinical trials with regard to sample size, ethnicity, gender ratio, age, and weight range. Reported volumes of concomitant liquid intake, dosage form type and sampling schedule were also included in the study design.

The predictive performance of the PBPK models was assessed by multiple model diagnostics, including visual predictive checks (5th and 95th percentiles) as well as comparison of the predicted and observed plasma concentration values and PK parameters (C_{max} , AUC_{inf} , CL/F). For this purpose, the ratio ($R_{pred/obs}$) of model-predicted versus observed parameter values was determined ($R_{pred/obs}$ =model-predicted/clinically observed). The predictive accuracy was evaluated based on the “two-fold” rule ($-0.301 < \log R_{pred/obs} < 0.301$) as well as the more stringent deviation of 25% ($-0.097 < \log R_{pred/obs} < 0.097$).

As quantitative measures of model performance, mean relative deviations (MRDs) of the predicted plasma concentrations and geometric mean fold errors (GMFEs) of C_{max} , AUC_{inf} and CL/F were also calculated, as follows:

$$MRD = 10^{\frac{1}{N} \sqrt{\sum_i^N (\log_{10}(C_i) - \log_{10}(\hat{C}_i))^2}} \quad (34)$$

$$GMFE = 10^{\frac{1}{n} \sum_j^n \left| \log_{10} \left(\frac{\hat{a}_j}{a_j} \right) \right|} \quad (35)$$

Where C_i , \hat{C}_i are the i^{th} observed and predicted concentrations, respectively; a_j , \hat{a}_j correspond the observed and the respective predicted C_{max} , AUC_{inf} or CL/F values of the j^{th} clinical study; N and n

equal the number of observations and clinical studies, respectively. Overall MRD and GMFE values of ≤ 2 were considered as reasonable predictions.^{98,199,435}

In addition, the prediction accuracy of the simulated plasma profiles was also evaluated with the average fold error (AFE) and absolute average fold error (AAFE):

$$AFE = 10^{\frac{1}{n} \sum \log\left(\frac{pred_t}{obs_t}\right)} \quad (36)$$

$$AAFE = 10^{\frac{1}{n} \sum \left| \log\left(\frac{pred_t}{obs_t}\right) \right|} \quad (37)$$

where n is the number of time points at which the concentration was determined and $pred_t$, obs_t are the predicted and observed concentrations at a given time point t respectively. AFE deviation from unity is an indication of over- ($AFE > 1$) or under-prediction ($AFE < 1$) of the observed data, whereas $AAFE$ is a measure of the absolute error from the true value (or bias of the simulated profile). An $AAFE \leq 2$ is considered to be a successful prediction.^{98,199}

All PK profiles obtained from the literature were digitalized with the WebPlotDigitizer (version 4.1; PLOTCON; Oakland, USA). The parameter estimation within the PE module of the Simcyp® Simulator was performed with the Maximum Likelihood estimation method. Data post-processing and visualization were performed with MATLAB® 2019b (Mathworks Inc.; Natick, MA, USA) and R® version 3.5.3 (R Core Team (2019). R: A language and environment for statistical computing. R Foundation for Statistical Computing, Vienna, Austria (<https://www.R-project.org>)).

3.5.1 Case example: Naproxen

Seven clinical trials published in the open literature were used in support of the development and verification of the PBPK model for naproxen. Six studies were performed after oral administration of single dose of naproxen or its sodium salt at different dose levels in the fasted state. Data after intravenous administration were obtained from Runkel et al.^{436–438} The performance of the developed PBPK model was validated by simulation of several clinical studies after oral administration and by comparison with the mean observed pharmacokinetic profiles already available in the literature.^{439–443} A detailed summary of the trial design and demographics of the *in vivo* studies used for the development (training datasets) and validation (external datasets) of the naproxen PBPK model as well as all relevant input parameters can be found in Supplementary Material Table 7-1 and Table 7-2.

Table 3-10 summarizes all clinical trial simulations (10 trials by 10 individuals) performed for each *in vivo* dissolution scenario (see section 3.4.3) and the mean simulated population pharmacokinetic (popPBPK) parameters for the virtual healthy adult population. Regardless of the anticipated differences in *in vivo* dissolution, as reflected by the various S_{DLM} values, these results suggest that mean AUC remains almost constant, while slight, but more pronounced, variations in C_{max} and especially in T_{max} are observed. In all cases, the simulated PK parameters were within 1.25-fold of the observed data (Table 3-10 and Table 3-11) In addition, the average (AFE) and absolute average fold error (AAFE) ranged between 0.90-1.16 and 1.07-1.04, reflecting successful PBPK model performance.

Table 3-10: Mean *in silico* population pharmacokinetic parameters of naproxen simulated plasma-concentration-time profiles under all tested *in vivo* dissolution inputs (S_{DLM} scalar values) as obtained from model-based analysis of the *in vitro* data.

Formulation	Medium	S_{DLM}	Disintegration kd (h ⁻¹)/2-stage	<i>In silico</i> mean popPBPK parameters		
				T_{max} (h)	C_{max} (mg/L)	AUC (mg/L·h)
API						
Naproxen						
	Level I FaSSIF V3	0.0022	–	2.52	65.5	1302
	Ph. Eur. Phosphate	0.0136	–	1.80	69.0	1305
	Level II FaSSIF V3	0.0810	–	1.44	69.4	1306
Naproxen Na						
	all media	1	–	1.44	69.6	1306
Formulation						
Naprosyn®						
	Level I FaSSIF V3	0.0396	0.305	1.80	67.5	1277
		0.0305	2-stage	1.80	69.2	1306
	Level II FaSSIF V3	0.0213	0.702	1.80	67.8	1277
		0.0187	2-stage	1.80	69.1	1306
Anaprox®						
	Level I FaSSIF V3	0.0212	0.288	1.80	67.9	1277
		0.0221	2-stage	1.80	69.2	1306
	Level II FaSSIF V3	0.0168	0.228	1.80	67.7	1277
		0.0158	2-stage	1.80	69.1	1305

Table 3-11: Mean (SD) reported pharmacokinetic parameters of naproxen *in vivo* studies used for the validation of the PBPK model

Reference	Formulation & Dose	<i>In vivo</i> mean PK parameters (SD)		
		T_{max} (h)	C_{max} (mg/L)	AUC (mg/L·h)
Charles and Mogg ⁴³⁹	Naprosyn® 500 mg	1.50 ¹	71.4 ¹	1211 ¹
Zhou et al. ⁴⁴⁰	Naprosyn® 2 x 250 mg	2.6 (1.5)	87.3 (15.5)	1428 (193)
Haberer et al.(a) ⁴⁴¹	Anaprox® 550 mg	1.48	75.2	1294
Setiawati et al. ⁴⁴²	Anaprox® 550 mg	1.00 (0.5-2) ¹	72.0 (11.2)	1013 (186)
Rao et al. ⁴⁴³	IR Naproxen 500 mg	1.36 (0.81)	69.2 (20.9)	1435 (312)
Haberer et al. (b) ⁴⁴¹	IR Naproxen-Na 500 mg	1.53	74.9	1299

¹Median value

In Figure 3-7, the mean simulated naproxen plasma-concentration time profiles and the 5th and 95th percentiles of the virtual population for the two extreme DLM estimated values, i.e., $DLM_{min}=0.0022$ and $DLM_{max} = 1$ are illustrated. Note that these S_{DLM} values were extracted from the dissolution of the free acid and salt pure API forms, not the formulations, and were intentionally chosen as such in order to evaluate *in vivo* performance differences (if any) that could be detected under these extreme scenarios. As can be observed, the C_{max} of the simulated plasma profile corresponding to administration of the very slowly dissolving hypothetical formulation was only slightly lower than the one resulting from the very fast dissolving hypothetical formulation. On the other hand, T_{max} was significantly prolonged. Interestingly, regardless of whether the worst- or best-case scenario was applied, the dissolution profiles predicted the observed range of PK profiles reasonably well (see also AFE and AAFE values).

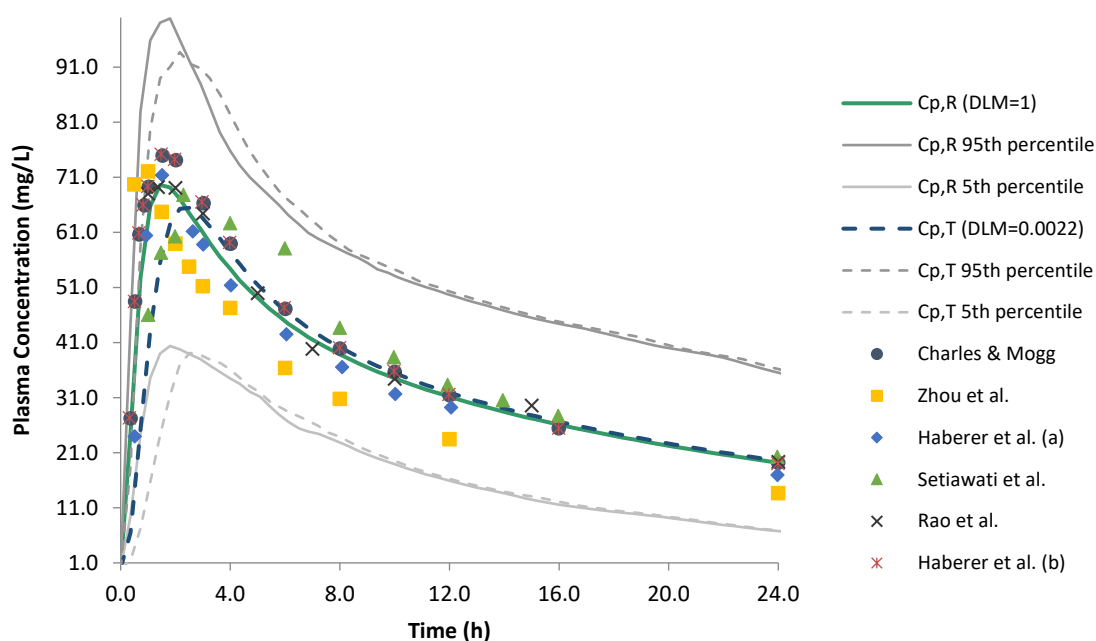


Figure 3-7: Population mean simulated naproxen plasma concentration-time profiles and the 5th and 95th percentiles for the two extremes of the estimated S_{DLM} values: (a) $S_{DLM}=1$ (green and grey solid lines, respectively) and (b) $DLM=0.0022$ (blue and light grey dashed lines, respectively). In a worst/ best case virtual bioequivalence scenario of simulated healthy adult populations (a) was treated as the reference, whereas (b) as the test formulation. Observed clinical data from Charles & Mogg (circles), Zhou et al. (squares), Haberer et al. (a) (diamonds), Setiawati et al. (triangles), Rao et al. (crosses) and Haberer et al. (b) (asterisks) are overlaid for verification of the PBPK model performance and comparisons. Simulations run for 72 h, but to enable better comparison only the first 24 hours are plotted.

In order to further explore the impact of key parameters on the simulated plasma profiles, one-at-a-time parameter sensitivity analysis (PSA) on the S_{DLM} and mean gastric residence time (MGRT) values in the fasted state was performed. MGRT and S_{DLM} were allowed to range from 0.1 to 2 hours and 0.001 to 0.1, respectively, while all other parameters in the model were kept constant. Supplementary Material Figure 7-1 shows the sensitivity of the mean simulated plasma profile of a population representative individual for various DLM and GET values, respectively. Despite a variation of S_{DLM} values of over a 100-fold, only slight or almost no differences in C_{max} (69.7-74.0 mg/L) or AUC (1175-1177 mg/L·h) are observed. T_{max} (1.40-2.65 h) seems to be more sensitive to *in vivo* dissolution changes than the other PK parameters indicating a shift of the regional absorption towards the lower GI. Nevertheless, this data clearly demonstrates that prolongation of MGRT is expected to reduce C_{max}

only up to 30% (52.2-75.5 mg/L) and T_{\max} (1.09-4.00 h), whereas AUC (1172-1180 mg/L·h) is not impacted.

3.5.2 Case example: Ibuprofen

The Simcyp® Simulator (Version 19, Release 1; Certara UK Limited) with its Advanced Dissolution, Absorption and Metabolism (ADAM) model coupled with a previously verified full-body PBPK model able to recapitulate observed inter-subject variability in ibuprofen exposure was used to simulate the absorption and systemic exposure of ibuprofen released from the R, TBE and TNBE oral suspensions.²⁷ Further details on the ibuprofen PBPK model, including development workflow and model verification, can be found elsewhere.²⁷ The established ibuprofen PBPK models was refined with the respective product-specific monodispersed particle radius distributions estimated in SIVA® for the R, T-BE and T-NBE batches. These were used as input for the mechanistic particle population balance model in Simcyp, which describes the particles' shrinkage as they dissolve and move to a different size bin.⁴⁴⁴ The default value of 50 log-distributed particle size bins was used in the simulations and the upper bound size was set at the respective product-specific monodispersed particle radius estimated in SIVA®. Table 7-3 lists the input parameters used for building the mechanistic absorption and disposition models of ibuprofen.

Verification of the updated PBPK model was carried out by simulating the two BE trials in which TBE and TNBE were administered as the test formulations. The virtual individuals were chosen to closely replicate the cohort enrolled in the respective *in vivo* BE trials (Table 3-12):

- a. T-BE *versus* R: oral single doses of ibuprofen 200 mg were administered to 23 healthy adults (12 men and 11 women; age range 21-41 years)
- b. T-NBE *versus* R: oral single doses of ibuprofen 400 mg were administered to 35 healthy adults (16 men and 19 women; age range 21-45 years)

Table 3-12: Reported results of the two ibuprofen *in vivo* bioequivalence studies

BE study	BE metric	Geometric mean point estimate (%)	90% Confidence interval	Within-subject variability (%)	Reference
T-BE vs. R	C _{max}	113.3	105.9-121.3	16.9	422
	AUC _{0-t}	105.9	102.0-109.9	9.2	422
T-NBE vs. R	C _{max}	126.5	118.4-135.2	13.1	422
	AUC _{0-t}	121.3	116.0-126.7	8.7	422

In order to capture the population variability at least 10 trials were simulated for each pairwise comparison. Predicted and observed ibuprofen pharmacokinetic profiles were compared to confirm the predictive capacity of this IVIVE-PBPK framework. Model adequacy was concluded if the prediction fold error for simulated mean AUC_{0-t} and C_{max} values were below 1.25-fold of mean observed values.

Mean simulated C_{max} and AUC_{0-t} values were within 1.2-fold of the respective mean observed BE metrics for R, TBE and TNBE formulations, indicating acceptable performance (Table 3-13). The refined PBPK-IVIVE model was then further applied in stepwise BE failure risk assessment (see details in section 3.6.2).

Table 3-13: Simulated and observed PK parameters of the two bioequivalence studies used for validation of the refined ibuprofen PBPK model.

Formulation	C_{max} (mg/L)			AUC_{0-t} (mg/L.h)		
	Pred	Obs	Pred/Obs	Pred	Obs	Pred/Obs
TBE 200 mg	14.5	16.6	0.87	59.1	66.4	0.89
R 200 mg	13.6	13.4	1.01	59.0	62.9	0.94
TNBE 400 mg	31.2	29.6	1.05	118.4	127.5	0.93
R 400 mg	26.6	22.9	1.16	118.0	107.8	1.09

Pred = predicted; Obs = observed

3.5.3 Case example: Flurbiprofen

For the development and verification of the PBPK model, seventeen plasma concentration-time profiles, including five for subjects with specific CYP2C9 genotypes, were used. *In vitro* dissolution data available for the 100 mg immediate release solid oral products were modelled and incorporated into the PBPK model to simulate various *in vivo* dissolution scenarios. At any other dose level, including the CYP2C9 polymorphism studies, the fastest dissolution rate ($S_{DLM}=0.125$) was used as input. When the administered form was an oral solution, the entire dose was considered by definition pre-dissolved. Data after intravenous administration were obtained from Mei et al.⁴⁴⁵. Nine studies were performed after oral administration of a single dose of flurbiprofen at different dose levels and dosage forms in the fasted state. Thirteen sets of plasma concentration-time profiles of flurbiprofen with or without co-administration of perpetrator from a total of six clinical studies available in the open literature were used to predict the effect of CYP2C9 inhibitors in the PK of flurbiprofen in CYP2C9 polymorphic healthy individuals. For a detailed summary of the trial design and demographics of the *in vivo* studies used for the development (training datasets) and validation (external datasets) of flurbiprofen PBPK/PD model, please refer to the Table 7-4 and Table 7-5.

The absorption component of flurbiprofen whole body PBPK model was set up using a stepwise IVIVE approach for estimation and confirmation of the biopharmaceutical parameters as described in section 3.5. The volume of distribution as function of the tissue plasma partition coefficients was initially predicted using the Rodgers-Rowland method and then further refined “top down” to match the IV data.¹⁹⁶ Flurbiprofen has been characterized as probe substrate of CYP2C9 and the contribution of CYP2C9 ($f_{mCYP2C9}=0.71$) on the overall metabolic clearance (CL) of FLU as well as the renal clearance ($CL_{renal}=0.066$ L/h) were obtained from Patel et al.⁴⁴⁶ In human recombinant (rhP450) CYP2C9 expressed in microsomes from the insect cell line Sf21, the mean V_{max} and K_m values for the 1*/1* (wild type), 2*/2* and 3*/3* were 15.79 and 8.756, 10.04 and 10.39, and 8.901 and 23.25, respectively⁴⁴⁷. These allele specific CYP2C9 *in vitro* kinetic parameters (V_{max} , K_m) were implemented to further inform the model. The metabolic clearance of heterozygotic subjects with CYP2C9 1*/2* and CYP2C9 1*/3* genotypes has been clinically observed to be 0.73 and 0.605 of the wild type (1*/1*) clearance, respectively⁴⁴⁸. For that reason, and in the absence of *in vitro* data, the V_{max} of CYP2C9 1*/1* was scaled down accordingly to account for the decrease in clearance in those genotypes. The K_m value was assumed to be the same as for CYP2C9 1*/1*. All presented V_{max} and K_m values were already normalized to account for microsomal incubation fraction unbound ($f_{u,mic}$). Since an inter-system extrapolation factor (ISEF) was not available for this particular rhP450 system, a literature ISEF value (equal to 0.38) from baculovirus-insect cell expressed CYP2C9 for another NSAID, diclofenac, was used

as an initial estimate¹⁶⁰. Using the retrograde model for healthy volunteers available within the reverse translational tools in Simcyp, the additional liver CL to match the reported $f_{mCYP2C9}$ and fraction excreted (f_e) was calculated. After oral administration of racemic flurbiprofen, 8.4 and 7.3% of the dose was excreted into the urine as the acyl glucuronide of (R)- and (S)-flurbiprofen, respectively⁴⁴⁶, indicating that glucuronidation is likely to play a minor role in the elimination pathways of flurbiprofen. The major UGT isoforms involved in glucuronidation of flurbiprofen is UGT2B7 and with minor contributions by UGT1A1, UGT1A3, UGT1A9 and UGT2B4^{449,450}. Even though genetic polymorphisms have been reported in UGT family members^{451,452}, the clinical and functional significance and genotype-phenotype correlation of UGT polymorphisms is an ongoing area of research. In the absence of data showing clinical relevance of UGT2B7 and UGT1A9 polymorphisms, these were not further considered for the development and verification of the present model.

Once the base model was established, a published inhibitory E_{max} model linked to an effect-compartment was coupled to the PBPK model of flurbiprofen⁴⁵³. In this PD model, the analgesic efficacy of flurbiprofen was assessed using two endpoints: a) subjective pain intensity ranking and b) tooth pulp evoked potentials (TPEP) amplitude. The percentage change of each endpoint after drug intake was considered as an indicator of pharmacodynamic activity, while the pre-dose value was defined as 100% (baseline).

The initial model was internally verified by comparing the predicted and observed plasma concentration profiles for the IV and the oral solution (67.9 mg) administrations. The model was further verified by comparing mean simulated and observed plasma concentration profiles, exposure and response parameters of external datasets including PK data from subjects with different CYP2C9 genotypes over the 40-300 mg dose range. Virtual populations were selected to closely match the enrolled individuals in the respective *in vivo* clinical trials regarding sample size, ethnicity, gender ratio, and age and weight range. Reported volumes of concomitant liquid intake, dosage form type and sampling schedule were also included in the study design. A schematic illustration of the modeling workflow is presented in Figure 3-8. The North European Caucasian (Sim-NEurCaucasian) and Chinese (Sim-Chinese) virtual populations of healthy volunteers were used for the population simulations of this study. The main differences in the inputs for the two populations related to CYP2C9 metabolism and genotype profile are summarized in Table 7-6. The intrinsic catalytic activity of CYP2C9 per unit amount of enzyme variant and tissue composition were assumed to be the same in both populations. The mean default intestinal and liver CYP2C9 abundances as well as the specific genotype frequencies of the Simcyp population libraries were used. As a Korean population is not yet available in the current Simcyp® version (v19.1), studies including Korean subjects were simulated using the Chinese virtual population, which is considered to be the population with the highest demographic and genetic proximity to the Korean population.⁴⁵⁴⁻⁴⁵⁶

The whole-body PBPK model of flurbiprofen accurately captures the plasma concentration-time profiles following intravenous and oral administration over a wide dose range (Figure 3-9, Figure 3-10, Figure 3-11 and Figure 3-12). The predictive performance of the PBPK model is comprehensively demonstrated via visual comparisons of predicted versus observed plasma concentration-time profiles as well as quantitative measures (MRDs, GMFEs). The simulated plasma concentration-time trajectories for all routes of administration, doses and drug products are in close agreement with the observed data. When a two-fold deviation was allowed, the predictive accuracy of the PBPK models was 100% for both AUC_{inf} , C_{max} and CL/F. When a more stringent acceptance criterion (i.e., 25% deviation) was applied, the predictive accuracy for AUC_{inf} , C_{max} and CL/F was 90%, 81% and 74%,

respectively. This predefined criterion is not meant to be equated to the bioequivalence acceptance limits (i.e., 80-125%), but rather is selected to be sufficiently conservative to prevent poor decision-making due to misclassified predictions. Moreover, the MRD values were in 94% of the studies within two-fold, with only about 20% less than 1.25-fold. Overall MRD for the FLU PBPK model was 1.54 (1.04-2.43), whereas the GMFE values for AUC_{inf} , C_{max} and CL/F were 1.54 (1.04-2.43), 1.14 (1.00-1.39), 1.15 (1.01-1.41) and 1.18 (1.06-1.39), respectively. Detailed results along with calculated MRD and GMFE values for all studies are presented in Table 3-14 and Table 3-15.

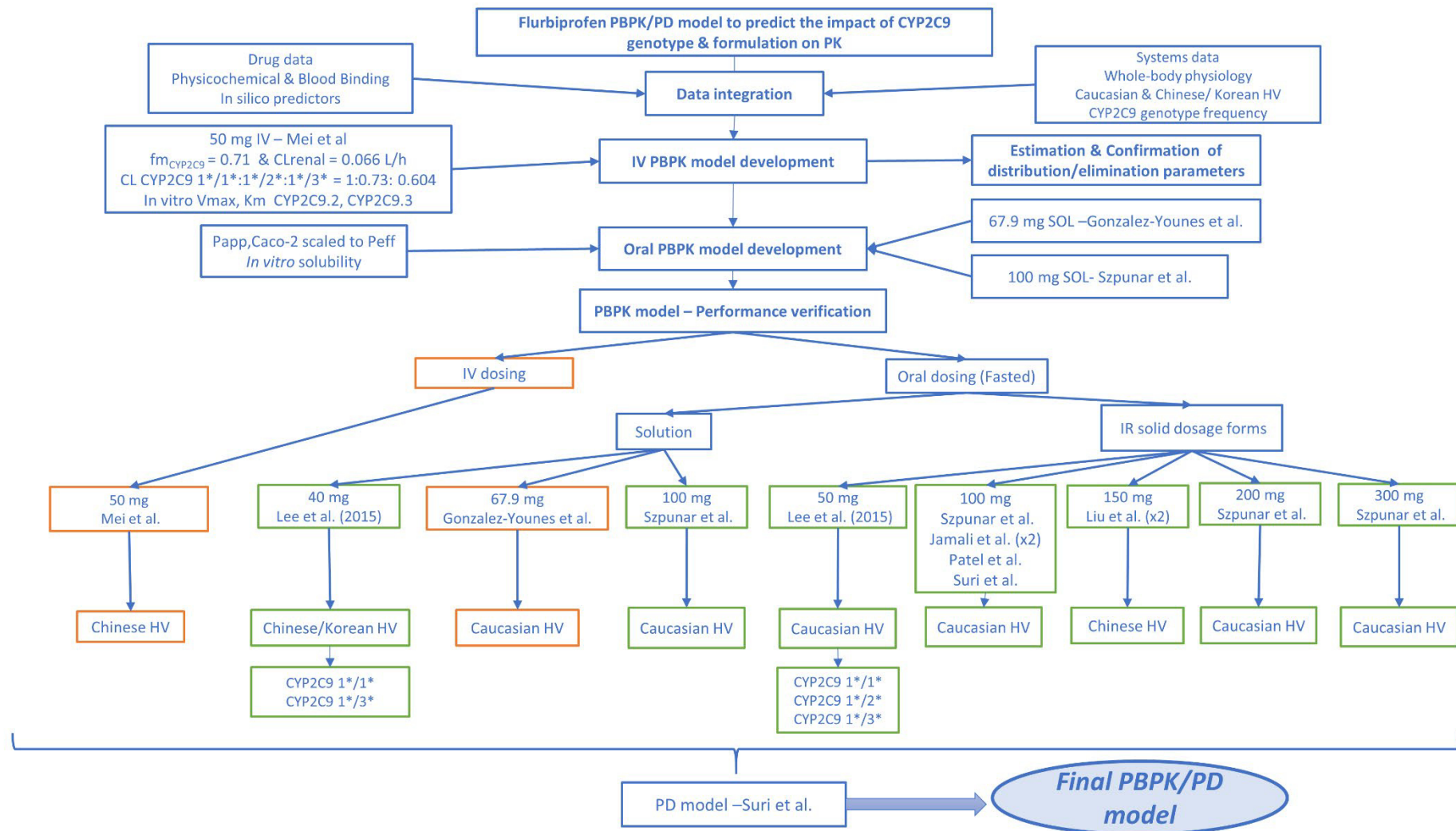


Figure 3-8: Stepwise modeling workflow for the development and verification of the flurbiprofen PBPK/PD model. Training for the internal and test datasets for the external verification, obtained from clinical studies published in the open literature, are outlined with orange and green, respectively

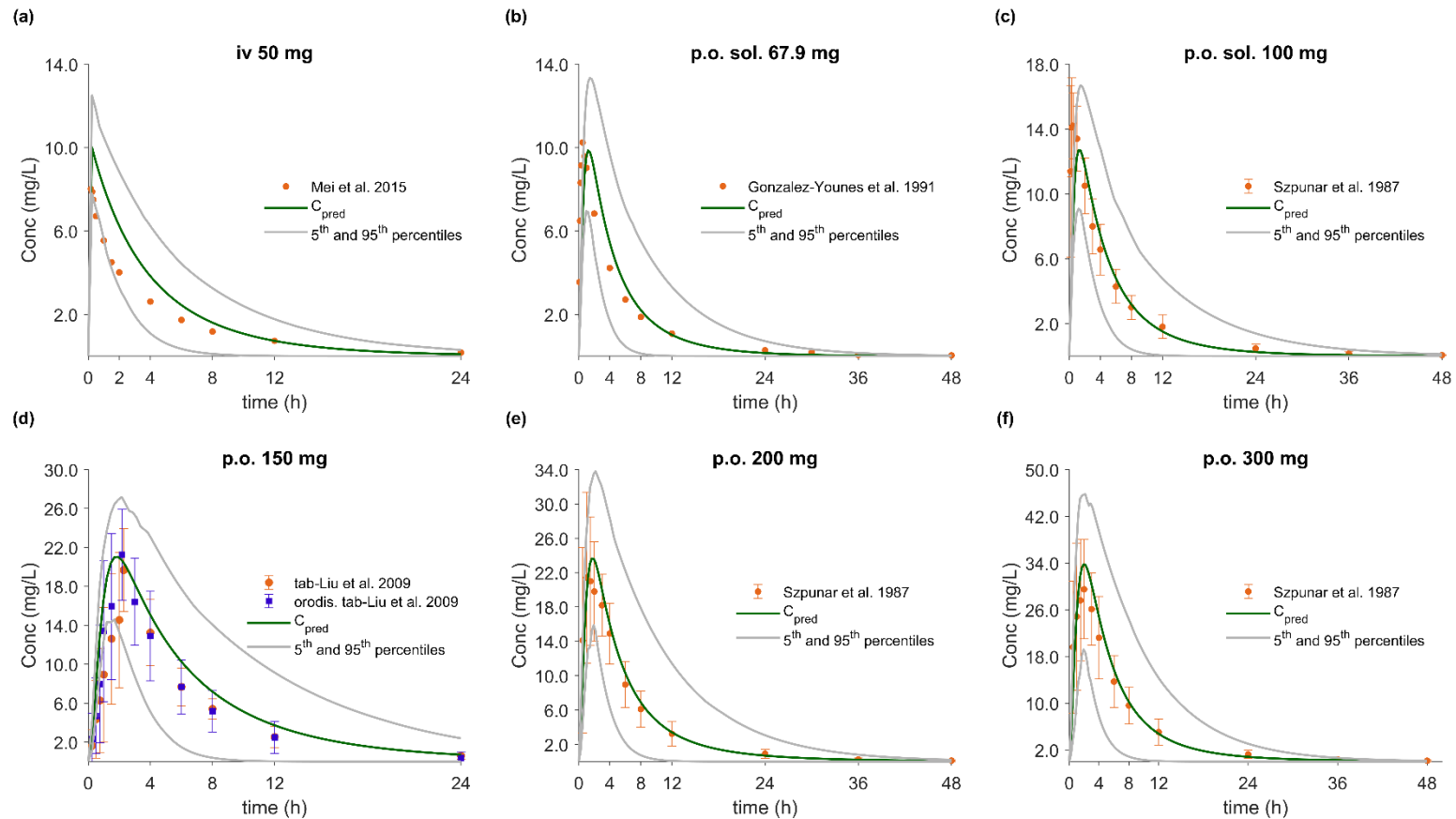


Figure 3-9: Mean flurbiprofen plasma concentration-time profiles after oral administration of 100 mg tablet in healthy Caucasians. Population simulations ($n=100$) under four in vivo dissolution scenarios are shown as green and grey lines for the mean and the 5th & 95th percentiles, respectively. Each dissolution scenario is represented by the corresponding S_{DLM} value and is shown with different line style: $S_{DLM}=0.125$ (solid line), $S_{DLM}=0.071$ (dotted line), $S_{DLM}=0.0054$ (dashed-dotted line) and $S_{DLM}=0.0018$ (dashed line). Observed data with SD, if available, are depicted as (a) circles (Jamali et al.-Ansaid) and squares (Jamali et al.-Froben); (b) triangles (Patel et al.); (c) diamonds (Suri et al.); (d) asterisks (Szpunar et al.).

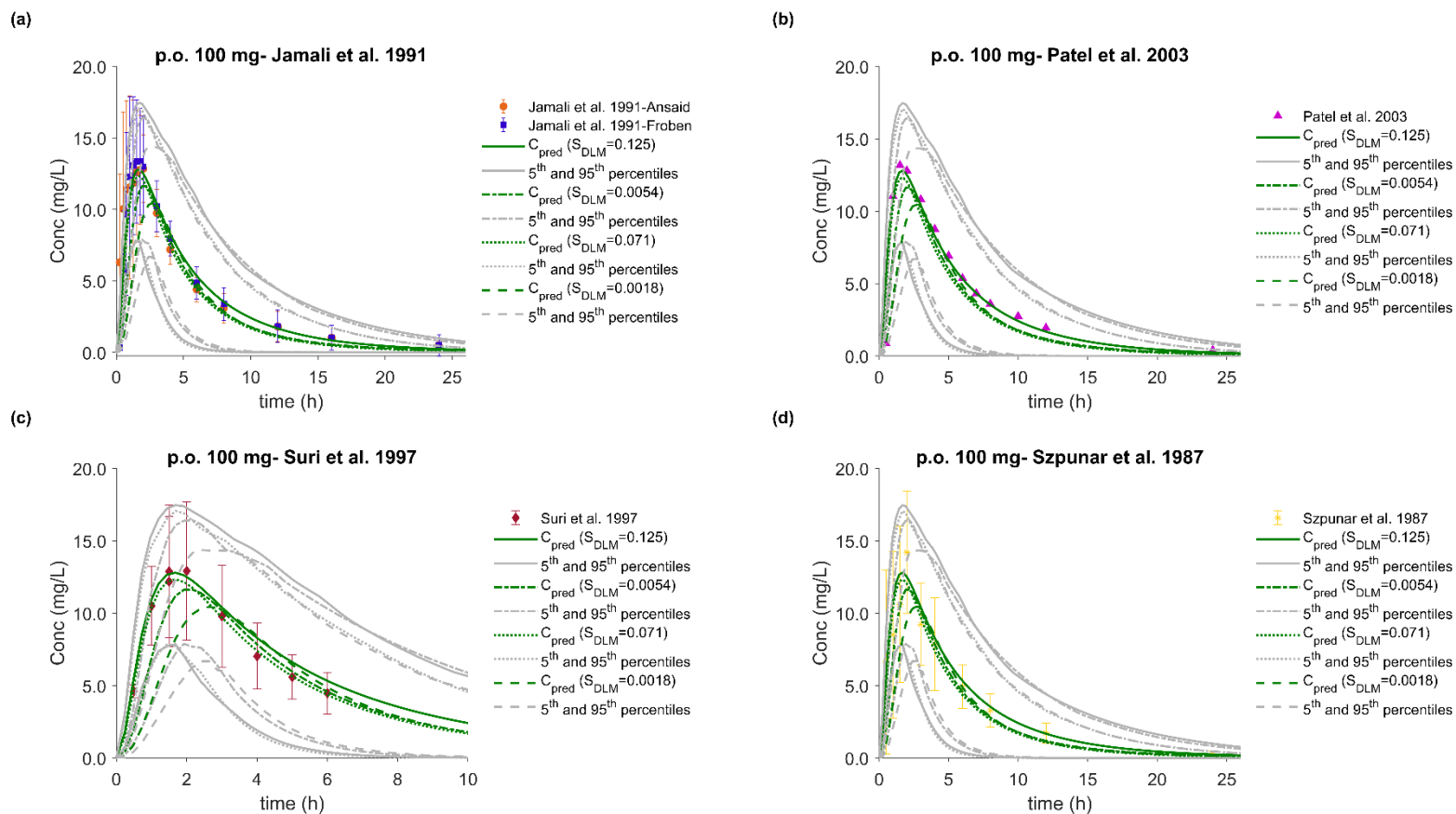


Figure 3-10: Mean flurbiprofen plasma concentration-time profiles after intravenous and oral administration in healthy Chinese (a, d) and Caucasians (b, c, e, f). Population simulations ($n=100$) are shown as green and grey solid lines for the mean and the 5th & 95th percentiles, respectively. Observed data with SD, if available, are depicted as circles and squares. References link to a specific observed dataset described in study Table 1. Administration protocol: (a) 50 mg intravenously; (b) 67.9 mg oral solution; (c) 100 mg oral solution; (d) 150 mg oral tablet; (e) 200 mg oral tablet; (f) 300 mg oral tablet.

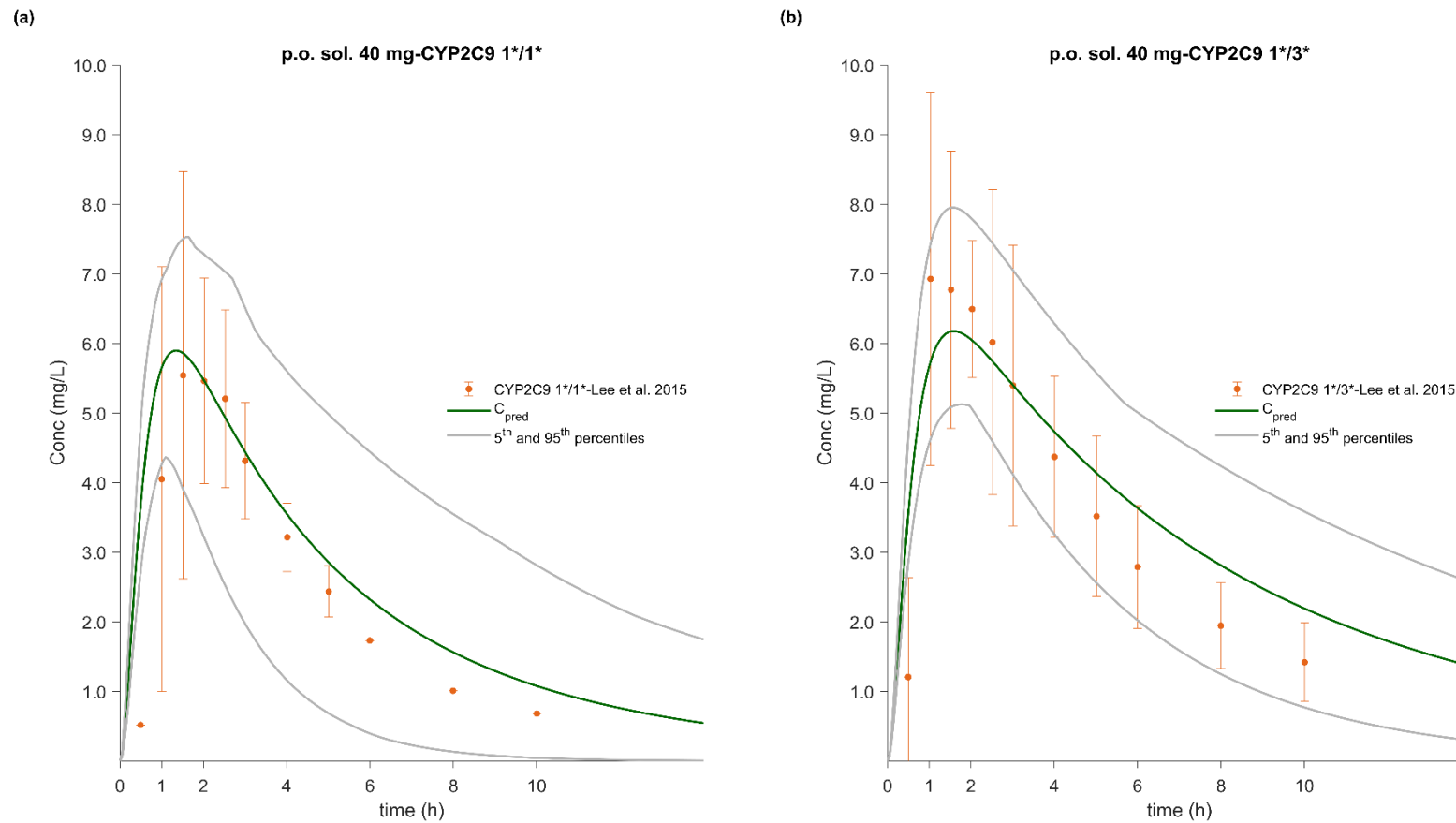


Figure 3-11: Mean flurbiprofen plasma concentration-time profiles after administration of 40 mg oral solution in CYP2C9 1*/1* and 1*/3* healthy Korean volunteers. Population simulations ($n=100$) are shown as green and grey lines for the mean and the 5th & 95th percentiles, respectively. Observed data with SD, if available, are depicted as circles.

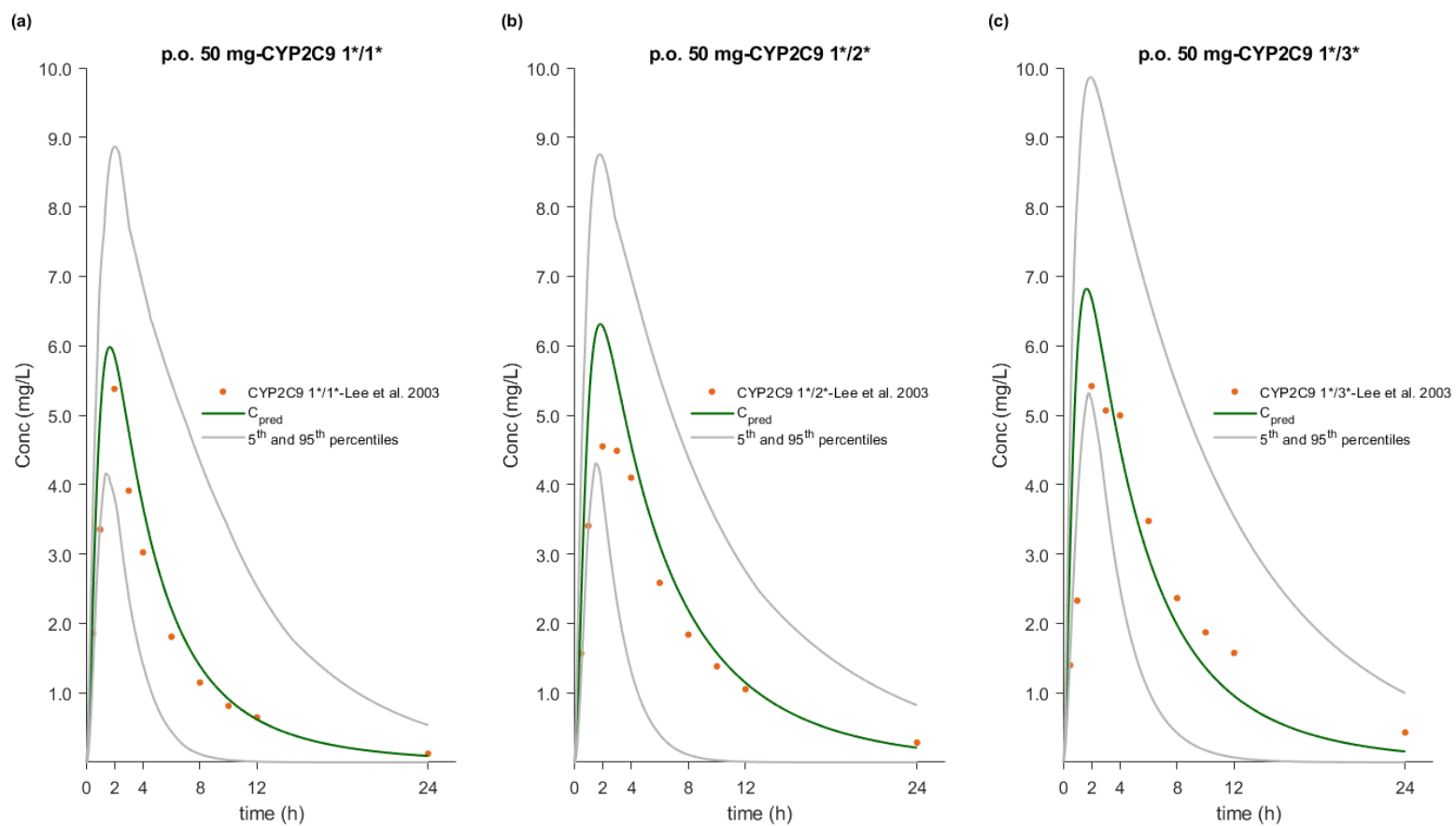


Figure 3-12: Mean flurbiprofen plasma concentration-time profiles after administration of 50 mg oral tablet in CYP2C9 1*/1*, 1*/2* and 1*/3* healthy Caucasian volunteers. Population simulations ($n=100$) are shown as green and grey lines for the mean and the 5th & 95th percentiles, respectively. Observed data with SD, if available, are depicted as circles.

The PBPK model successfully predicted (in 36 out of 38 studies) the observed concentration-time profiles and CYP2C9 genetic effects within a predefined two-fold deviation boundary (Table 3-14). In both cases where MRD fell outside the two-fold limit, the slowest dissolution rate, corresponding to 85% release only after 60 minutes, was used as the input profile and resulted in sub-optimal absorption and underprediction of C_{max} and AUC. The slight under prediction ($R_{pred/obs} = 0.76-0.78$) of C_{max} and AUC by Jamali et al. after oral administration of 100 mg was associated with the input of the slowest intestinal dissolution rate ($S_{DLM} = 0.0018$).⁴⁵⁷ By contrast, the C_{max} was overpredicted ($R_{pred/obs} = 1.36-1.39$) in CYP2C9 1*/3* individuals at 50 and 150 mg. Deviations from the 1.25-fold boundary in AUC ($R_{pred/obs} = 0.71-0.78$) and clearance ($R_{pred/obs} = 1.31-1.39$) were consistently predicted under all dissolution scenarios, except the slowest ($S_{DLM} = 0.0018$), when simulating the study by Patel et al.⁴⁴⁶ Nevertheless, it has to be noted that in most studies, the prediction errors fall within the observed inter-individual variability and that the participants were not subjected to prior genotype screening.

Table 3-14: Mean relative deviation (MRD) values of flurbiprofen plasma concentration predictions.

Route of administration ¹	Dose (mg)	Flurbiprofen MRD	Reference
iv (s.d.)	50	1.41	445
po (sol, s.d.)	67.9	1.85	458
po (sol, s.d.)	100	1.60	459
po (sol, s.d., CYP2C9 1*/1*)	40	1.52	460
po (sol, s.d., CYP2C9 1*/3*)	40	1.30	460
po (tab, s.d., CYP2C9 1*/1*)	50	1.24	448
po (tab, s.d., CYP2C9 1*/2*)	50	1.30	448
po (tab, s.d., CYP2C9 1*/3*)	50	1.62	448
po (tab, s.d., CYP2C9 1*/1*)	50	1.26	461
po (tab, s.d., CYP2C9 1*/1*)	50	1.25	461
po (tab, s.d., CYP2C9 1*/3*)	50	1.28	461
po (tab, s.d., CYP2C9 1*/3*)	50	1.25	461
po (tab, s.d., CYP2C9 3*/3*)	50	1.25	461
po (tab, s.d., CYP2C9 3*/3*)	50	1.20	461
po (tab (Ansaid®), s.d.)	100	1.31-2.38	457
$S_{DLM_SI} = 0.125$		1.31	
$S_{DLM_SI} = 0.0054$		1.72	
$k_d = 0.127 \text{ h}^{-1}$ & $T_{lag} = 14.6 \text{ min}$		1.64	
$S_{DLM_SI} = 0.0712$		1.65	
$S_{DLM_SI} = 0.0018$		2.38	
po (tab (Froben®), s.d.)	100	1.70-2.43	457
$S_{DLM_SI} = 0.125$		1.70	
$S_{DLM_SI} = 0.0054$		1.88	
$k_d = 0.127 \text{ h}^{-1}$ & $T_{lag} = 14.6 \text{ min}$		1.80	
$S_{DLM_SI} = 0.0712$		1.83	
$S_{DLM_SI} = 0.0018$		2.43	
po (tab (Froben®), s.d.)	100	1.69-1.92	446
$S_{DLM_SI} = 0.125$		1.69	
$S_{DLM_SI} = 0.0054$		1.78	
$k_d = 0.127 \text{ h}^{-1}$ & $T_{lag} = 14.6 \text{ min}$		1.92	
$S_{DLM_SI} = 0.0712$		1.90	
$S_{DLM_SI} = 0.0018$		1.79	
po (tab, s.d.)	100	1.04-1.74	453
$S_{DLM_SI} = 0.125$		1.11	
$S_{DLM_SI} = 0.0054$		1.20	

$k_d = 0.127 \text{ h}^{-1}$ & $T_{lag} = 14.6 \text{ min}$		1.12	
$S_{DLM_SI} = 0.0712$		1.04	
$S_{DLM_SI} = 0.0018$		1.74	
po (tab, s.d.)	150	1.51	462
po (orod, s.d.)	150	1.42	462
po (tab (Ansaid®), s.d.)	200	1.20	459
po (tab (Ansaid®), s.d.)	300	1.34	459
<hr/>			
MRD (range)		1.54 (1.04-2.43)	
MRD ≤ 1.25		9/38	
MRD ≤ 2		36/38	
<hr/>			

¹ iv: intravenous; po: per os; s.d.: single dose; sol: solution; tab: tablet; orod: orally dispersible

Table 3-15: Comparison of mean predicted and observed AUC, C_{max} and apparent clearance (CL/F) values of flurbiprofen. Calculation of predicted to observed ratio ($R_{pred/obs}$) and geometric fold error (GMFE) values.

Route of administration*	Dose (mg)	AUC _{inf} (mg/L·h)			C _{max} (mg/L)			CL/F (L/h)			Reference
		obs	pred	R _{pred/obs}	obs	pred	R _{pred/obs}	obs	pred	R _{pred/obs}	
iv (s.d.)	50	35.2	43.7	1.24	—	—	—	1.50	1.36	0.91	445
po (sol, s.d.)	67.9	55.1	56.1	1.01	10.8	9.99	0.92	—	—	—	458
po (sol, s.d.)	100	82.7	78.0	0.94	14.2	12.9	0.91	1.28	1.50	1.17	459
po (sol, s.d., CYP2C9 1*/1*)	40	29.3	29.1	0.99	5.54	5.86	1.06	1.39	1.16	0.83	460
po (sol, s.d., CYP2C9 1*/3*)	40	47.6	44.2	0.93	6.93	6.22	0.90	0.88	0.67	0.76	460
po (tab, s.d., CYP2C9 1*/1*)	50	29.4	28.6	0.97	5.38	5.84	1.09	1.77	1.67	0.83	448
po (tab, s.d., CYP2C9 1*/2*)	50	40.7	45.6	1.12	4.55	6.34	1.39	1.30	1.20	0.92	448
po (tab, s.d., CYP2C9 1*/3*)	50	51.1	46.4	0.91	5.42	6.68	1.23	1.00	1.03	1.03	448
po (tab, s.d., CYP2C9 1*/1*)	50	30.8 ^a	35.8 ^a	1.16	6.1 ^a	6.91 ^a	1.13	1.6 ^a	1.4 ^a	0.88	461
po (tab, s.d., CYP2C9 1*/1*)	50	30.8 ^a	36 ^a	1.17	6.1 ^a	6.8 ^a	1.11	1.6 ^a	1.43 ^a	0.89	461
po (tab, s.d., CYP2C9 1*/3*)	50	53.7 ^a	54.6 ^a	1.02	8.9 ^a	7.7 ^a	0.87	0.9 ^a	0.98 ^a	1.09	461
po (tab, s.d., CYP2C9 1*/3*)	50	53.7 ^a	53.1 ^a	0.99	8.9 ^a	7.44 ^a	0.84	0.9 ^a	0.96 ^a	1.07	461
po (tab, s.d., CYP2C9 3*/3*)	50	(85.8, 119) ^b	76.1	(0.89, 0.64)	(8, 9.4) ^b	6.99	(0.87, 0.74)	(0.6, 0.4) ^b	0.64	(1.07, 1.6)	461
po (tab, s.d., CYP2C9 3*/3*)	50	(85.8, 119) ^b	77.7	(0.91, 0.65)	(8, 9.4) ^b	7.1	(0.89, 0.76)	(0.6, 0.4) ^b	0.68	(1.13, 1.7)	461
po (tab (Ansaid®), s.d.)	100										457
S _{DLM,SI} = 0.125			81.1	1.01		12.8	1.00				
S _{DLM,SI} = 0.0054			66.5	0.83		11.6	0.90				
k _d = 0.127 h ⁻¹ & T _{lag} = 14.6 min		80.5	68.8	0.85	12.8	11.8	0.92	—	—	—	
S _{DLM,SI} = 0.0712			67.2	0.83		12.3	0.96				
S _{DLM,SI} = 0.0018			62.7	0.78		10.4	0.81				
po (tab (Froben®), s.d.)	100										457
S _{DLM,SI} = 0.125			81.1	0.99		12.8	0.96				
S _{DLM,SI} = 0.0054			66.5	0.81		11.6	0.87				
k _d = 0.127 h ⁻¹ & T _{lag} = 14.6 min		82.3	68.8	0.84	13.3	11.8	0.88	—	—	—	
S _{DLM,SI} = 0.0712			67.2	0.82		12.3	0.92				

$S_{DLM_SI} = 0.0018$		62.7	0.76		10.4	0.78					
po (tab (Froben®), s.d.)	100										446
$S_{DLM_SI} = 0.125$		81.1	0.92		12.7	0.96		1.42	1.12		
$S_{DLM_SI} = 0.0054$		66.5	0.76		11.6	0.88		1.68	1.32		
$k_d = 0.127 \text{ h}^{-1}$ & $T_{lag} = 14.6 \text{ min}$	87.8	68.8	0.78	13.2	11.8	0.89	1.27	1.66	1.31		
$S_{DLM_SI} = 0.0712$		67.2	0.77		12.2	0.92		1.66	1.31		
$S_{DLM_SI} = 0.0018$		62.7	0.71		11.0	0.84		1.77	1.39		
po (tab, s.d.)	100										453
$S_{DLM_SI} = 0.125$		81.1	1.20		12.7	0.98		1.42	0.93		
$S_{DLM_SI} = 0.0054$		66.5	0.98		11.6	0.90		1.68	1.11		
$k_d = 0.127 \text{ h}^{-1}$ & $T_{lag} = 14.6 \text{ min}$	67.7	68.8	1.02	12.9	11.8	0.91	1.52	1.66	1.09		
$S_{DLM_SI} = 0.0712$		67.2	0.99		12.2	0.95		1.66	1.09		
$S_{DLM_SI} = 0.0018$		62.7	0.93		11.0	0.86		1.77	1.16		
po (tab, s.d.)	150	124.3	154.4	1.24	15.2	20.7	1.36	—	—	—	462
po (orod, s.d.)	150	129.8	154.4	1.19	16.8	20.7	1.23	—	—	—	462
po (tab (Ansaid®), s.d.)	200	161.3	159.9	0.99	21.4	23.6	1.10	1.32	1.50	1.14	459
po (tab (Ansaid®), s.d.)	300	233.9	228.9	0.98	29.5	33.7	1.14	1.36	1.55	1.14	459
GMFE (range)		1.15 (1.01-1.56)			1.14 (1.00-1.39)			1.18 (1.03-1.7)			
GMFE ≤ 1.25		30/38			31/37			18/25			
GMFE ≤ 2		38/38			37/37			25/25			

*iv: intravenous; po: per os; s.d.: single dose; sol: solution; tab: tablet; orod: orally dispersible

^a: median value; ^b: individual values (n=2)

The established flurbiprofen PBPK model was then further coupled with a PD model for analgesic efficacy. The integrated PBPK/PD model was able to capture the pain-relieving response of S-FLU after oral administration of 100 mg racemic FLU. The predictive performance was assessed by comparing the predicted with the observed response-time profiles of the two PD endpoints, the TPEP amplitude and pain rating (see Figure 3-13). Regardless of the *in vivo* dissolution rate or the genotype of the virtual individuals, the predictive accuracy for the prediction of the PD metrics, maximum response (R_{\max}), time to maximum response (TR_{\max}) and area under the effect-time curve (AUCE), was in all in cases within 1.25-fold (see Table 3-16).

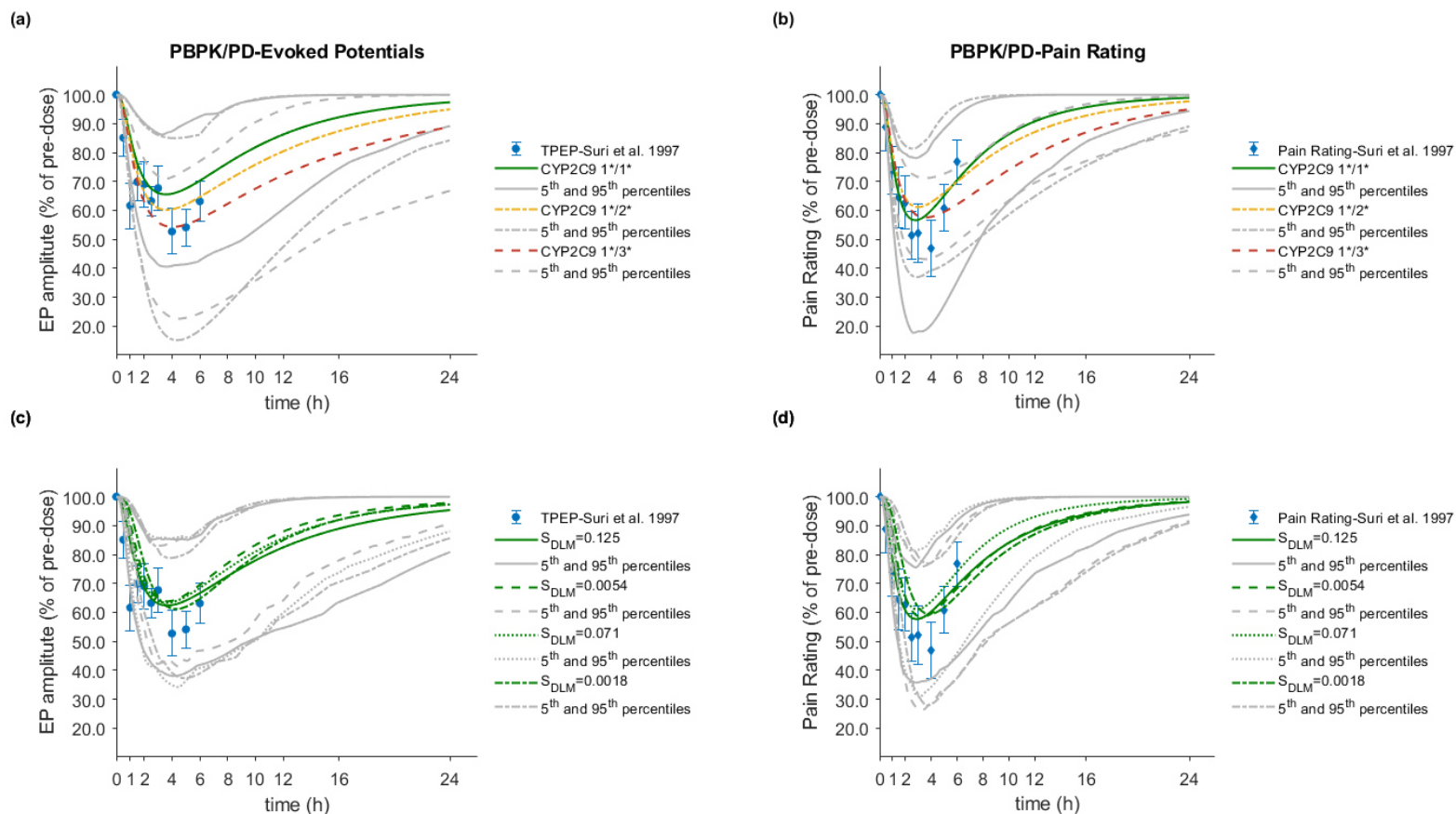


Figure 3-13: Mean flurbiprofen response-time profiles after administration of 100 mg oral tablet in healthy Caucasians. (a), (b) Genetic polymorphism: Population simulations ($n=100$) in CYP2C9 1*/1*, 1*/2* and 1*/3* are shown for the mean as green (solid), yellow (dash dotted) and orange (dashed) lines, respectively. Grey lines with the corresponding style represent the 5th & 95th percentiles (c), (d) Dissolution rate: Population simulations ($n=100$) under four in vivo dissolution scenarios are shown as green and grey lines for the mean and the 5th & 95th percentiles, respectively. Each dissolution scenario is represented by the corresponding S_{DLM} value and is shown with different line style: $S_{DLM}=0.125$ (solid line), $S_{DLM}=0.071$ (dotted line), $S_{DLM}=0.0054$ (dashed line) and $S_{DLM}=0.0018$ (dashed-dotted line).

Table 3-16: Comparison of predicted and observed pharmacodynamic parameters (R_{max} , TR_{max} and AUC) values of flurbiprofen and calculation of predicted to observed ratio ($R_{pred/obs}$).

PD effect ^a	R_{max} (%)			TR_{max} (h) ^b			AUC (%·h)			$T_{80\% \text{ baseline}}$ (h)
	obs	pred	$R_{pred/obs}$	obs	pred	$R_{pred/obs}$	obs	pred	$R_{pred/obs}$	Pred
TPEP amplitude reduction (%)										
CYP2C9 1*/1*		34.3	0.72		4.00	1.00		187.8	0.84	9.4
CYP2C9 1*/2*	47.3	39.7	0.84	4.00	4.00	1.00	224.2	218.6	0.98	11.9
CYP2C9 1*/3*		45.7	0.97		4.00	1.00		252.6	1.13	16.3
$S_{DLM_SI} = 0.125$		37.4	0.79		3.48	0.87		196.6	0.88	
$S_{DLM_SI} = 0.0054$	47.3	36.2	0.77	4.00	3.72	0.93	224.2	205.6	0.92	
$S_{DLM_SI} = 0.0712$		36.7	0.78		3.60	0.90		202.2	0.90	
$S_{DLM_SI} = 0.0018$		38.8	0.82		4.44	1.11		201.3	0.90	
Pain intensity reduction (%)										
CYP2C9 1*/1*		43.2	0.81		3.36	0.84		224.3	1.00	8.16
CYP2C9 1*/2*	53.1	38.9	0.73	4.00	3.36	0.84	224.2	210.3	0.94	9.12
CYP2C9 1*/3*		42.1	0.79		3.36	0.84		236.3	1.05	12.5
$S_{DLM_SI} = 0.125$		43.9	0.83		3.36	0.84		202.9	0.90	
$S_{DLM_SI} = 0.0054$	53.1	45.2	0.85	4.00	3.36	0.84	224.2	204.1	0.91	
$S_{DLM_SI} = 0.0712$		42.8	0.81		3.12	0.78		206.3	0.92	
$S_{DLM_SI} = 0.0018$		43.5	0.82		3.84	0.96		203.1	0.91	

^a: Population simulations using the healthy Caucasian virtual population^b: Median value

3.6 PBPK-IVIVE linked modelling and simulation workflow to perform virtual bioequivalence

Once confidence in the model validation and their predictive performance was established, the validated PBPK models were applied to simulate bioequivalence trials and perform risk assessment, providing a framework to guide project teams and enable model-informed decision-making during drug development and regulatory review. As part of this work, two complementary virtual bioequivalence approaches, differing in the implementation of inter-occasion variability, are presented.

Establishing bioequivalence has been a critical component of and remains a challenge during development of both new drug and generic products. The ability of PBPK model to account for both between-subject (BS), within-subject (WS) and inter-occasion variability (IOV) is crucial to the accuracy, success, and the applicability of VBE results. Although the current PBPK platforms can address the between-subject variability reasonably well, significant progress still needs to be made in estimating and integrating inter-occasion variability. Two independent modeling strategies to incorporate IOV in VBE studies have been reported in the literature: a) *a priori* estimated random error terms in replicate clinical study are added to the PK parameters, or, more mechanistically, b) the IOV is integrated into the system parameters and propagated in simulations.³¹⁷ Nevertheless, incorporation of IOV in virtual bioequivalence trials has been systematically neglected by both industry and regulatory partners.^{293,302} Inclusion of intra-subject variability becomes even more critical for drugs that have intra-subject variability <30% (i.e. are not “highly variable”), but still exhibit substantial intra-subject variability. To the best of our knowledge, the naproxen example represented the first time PBPK-IVIVE linked virtual bioequivalence examples incorporating IOV were presented in the literature.

In the case example of naproxen, the VBE trials were designed as fully replicated, two-sequence, two-treatment, two-period, crossover studies. In virtual BE studies between the hypothetical test and reference formulations, PK profiles for a total of 120 healthy adult volunteers (12 subjects in each of 10 trials) for each treatment were generated. In best-case and worst-case scenarios, the *in vivo* dissolution of the hypothetical reference and test formulations in the virtual individuals was simulated using the highest and lowest estimated DLM scalar value, respectively, as obtained by the model-based analysis of the *in vitro* dissolution data.

The existing default coefficients of variation (%CV) - i.e., between subject (BS) variability of the physiological parameters stored in the Simcyp® simulator (v18.1) database for the North European Caucasian healthy adult volunteers’ population were applied for each parameter. As an integral part of within-subject variability (WSV), IOV significantly contributes to the overall population variability and therefore it should be accounted for by the PBPK models. To model IOV, a CV of 30% was set, according to the literature and unpublished data from C. Reppas.^{463–466} IOV was added through the VBE module (V1.0) of Simcyp® simulator to the mean GET, pH of fasted stomach, pH and bile salt concentration in the fasted duodenum, jejunum I and II segments, and mechanistically propagated in the simulations. In each trial, a pre-specified number of randomly simulated individuals (n=12) were generated for each formulation (reference and test). The relevant PK metrics (C_{max} , AUC_{inf} , AUC_{0-t}) for each subject were calculated. The simulated average BE (ABE) trials were analyzed using the Phoenix® WinNonlin (v8.1; Certara; Princeton, NJ, USA) software for each relevant PK metric. As mentioned

earlier, the hypothetical reference and test formulations were assumed to have *in vivo* dissolution in the virtual individuals corresponding to the highest and lowest estimated S_{DLM} value, respectively.

On the other hand, for the case of ibuprofen products an alternative bioequivalence risk assessment approach was implemented, and virtual BE trials were run as one-sequence crossover studies. This is because, when a virtual trial is simulated in the Simcyp® simulator, the population is generated for the first period based on demographics, system and drug parameters and inter-subject variability for the selected population. Then for the second period, the same individuals are generated (provided that simulation seed is fixed), unless IOV is applied to selected parameters. Even though the magnitude of differences in pharmacokinetics between occasions can be quantified, the underlying mechanisms are generally not understood. Furthermore, very little is known about IOV of physiological parameters due to the complexity of such measurements. In this context, one-sequence crossover VBE trials were run for each pairwise comparison (*i.e.*, R vs TBE as well as R vs TNBE) without adding IOV to any system parameter. This approach focused on isolating the formulation impact on rate and extent of drug absorption and intra-subject variability was incorporated *post hoc*. In general, within-subject error in crossover BE studies can be divided into variation within one study occasion (*e.g.*, bioanalytical error) and IOV. Assuming negligible bioanalytical error for methods validated according to current regulatory guidelines, a bootstrap sampling method was applied with the purpose of approximating the sampling distribution of IOV for plasma C_{max} and AUC. Briefly, samples were taken with replacement from each sequence group in the original data sets for C_{max} and AUC observed after oral administrations of R and TNBE formulations, since this study reported the highest IOV for the exposure metrics. Subsequently, a multiplicative model for the analyses of BE was applied in order to obtain the IOV for each bootstrap sample and the bootstrap 95% CI for IOV in terms of plasma AUC and C_{max} were calculated. Afterwards, the exact power of the two-one-sided t-tests (TOST) procedure for various study designs was estimated based on the mean bootstrapped IOV, and power curves (showing the calculated power on the y-axis and the ratios between test and reference BE metrics on the x-axis) were generated to assess the probability of incurring a Type II error when considering different sample size scenarios.

3.6.1 Case example: Naproxen

In the case of naproxen, multiple non-replicated, two-sequence, two-treatment, two-period, crossover virtual bioequivalence trials ($n=10$) with 12 individuals per trial were conducted. In a worst-case / best-case scenario, two hypothetical naproxen formulations with extremely different *in vivo* dissolution rates were tested with the aim of designing a clinically relevant safe space. The reference (R) was assumed to have a DLM scalar value of one, corresponding to the instantaneous dissolution of naproxen sodium API powder, while the test (T) formulation was assigned the value of 0.0022, corresponding to the very slow dissolution of naproxen free acid API powder in FaSSIF V3 Level I.

Figure 3-14 presents the results of virtual bioequivalence trials for C_{max} , AUC calculated up to the last simulated time point (AUC_{last}) and extrapolated to infinity (AUC_{inf}). In all trials, C_{max} , AUC_{last} , AUC_{inf} met the average bioequivalence criteria (80-125%) with confidence intervals (CI) narrowly distributed around unity, especially for AUC. These findings suggest that naproxen formulations which reach 85% dissolved in media simulating the healthy human upper small intestine within 90 minutes or less are expected to be bioequivalent. Such wide limits can be justified by the high intestinal solubility and permeability as well as the long half-life of naproxen. The proposed dissolution “safe space” can be

further used to set clinically relevant dissolution specifications to minimize the risk of bioequivalence failure (Figure 3-15).

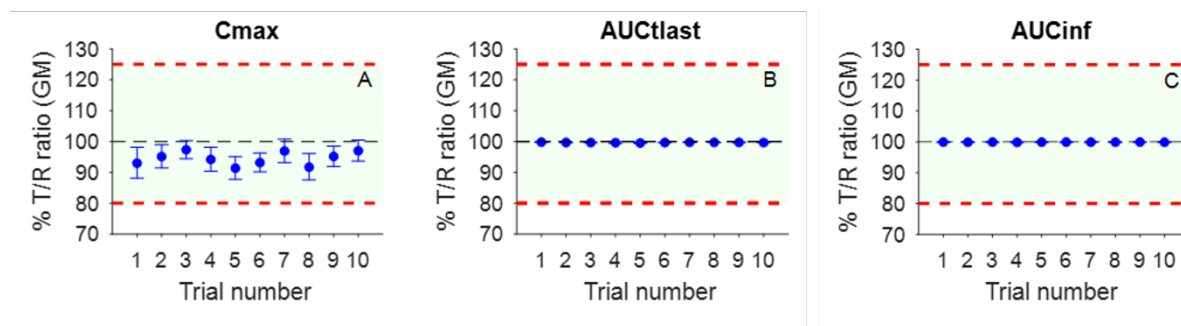


Figure 3-14: Average virtual bioequivalence results (% Geometric mean T/R ratio) of 10 trials with 12 simulated individuals in each trial. Intra-subject variability of 30% was chosen and added through Simcyp® (V18.1; Certara, Sheffield, UK) VBE module (V1.0) to the mean GET, pH of fasted stomach, pH and bile salt concentration of fasted duodenum, jejunum I and II. The 80-125% bioequivalence limits (red dashed lines) and the area of acceptance (light green shaded area) are shown for each tested PK parameter: (A) C_{max} , (B) AUC_{tlast} (AUC calculated up to the last simulated time point), and (C) AUC_{inf} (AUC extrapolated to infinity). Error bars represent the 90% confidence intervals, which in subplots (B) and (C) lie within the symbols

Overall, this example of naproxen highlights the usefulness of a PBPK-IVIVE linked VBE approach to mechanistically investigate the rate limiting steps for oral absorption and the impact of dissolution on the *in vivo* drug product performance. It is evident that the absorption and thus the *in vivo* performance of naproxen are governed primarily by gastric emptying and is not dissolution limited. This is also supported by the theoretical framework of the developability classification system (DCS/rDCS),^{404,405} according to which naproxen would more appropriately be classified as rDCS / DCS Class I. More importantly, this approach confirms the results from the relative bioavailability/bioequivalence study by Charles and Mogg, which concluded that two naproxen products (tablet and caplet) with very dissimilar *in vitro* dissolution behavior were bioequivalent.⁴³⁹ Despite the somewhat exaggerated value of IOV to 30%, a DLM scalar range from 0.0022 to 1 translated to minimal differences in C_{max} , with geometric mean point estimates between 0.9-1.00 and narrowly distributed 90% confidence intervals in all virtual BE studies (Figure 3-14). On the other hand, AUC remained practically unchanged with point estimate of ~1.00 in all VBE trials. In this case, the insensitivity of PK metrics to the dissolution rate was attributed one the one hand to the high intestinal permeability and solubility and on the other hand to the relatively long half-life of the drug. The risks from other potential factors contributing to the inter-occasion variability, such high first pass extraction, is also minimal in the case of naproxen due to its almost complete bioavailability ($F > 0.92$).

For naproxen, it was demonstrated 1) that bioequivalence failure due to dissolution is unlikely for naproxen products because of the wide safe space and 2) that the impact of formulation on the *in vivo* performance is not always correlated with the *in vitro* dissolution behavior. To the best of our knowledge, this is the first work which not only mechanistically incorporated inter-occasion variability in VBE assessment, but also propagated IOV in the simulations. Implementation of hierarchical levels of variability (inter-, intra-subject) in VBE trials is of critical importance to accurately describe the population variability and avoid biased bioequivalence results. Even though mixed effect modelling is rare in this context, this study highlights the importance of mechanistically assigning between-subject and inter-occasion variability values which are physiologically plausible and meaningful. Using %CV

values obtained from single observation in each individual within a specific population is not representative of the population between-subject (BSV) or inter-occasion variability since it comes solely from a single sample. In this case, the applied coefficient of variation is often conveniently misinterpreted as mixture of BSV and IOV. Likewise, implementation of arbitrary CV% values is inappropriate.

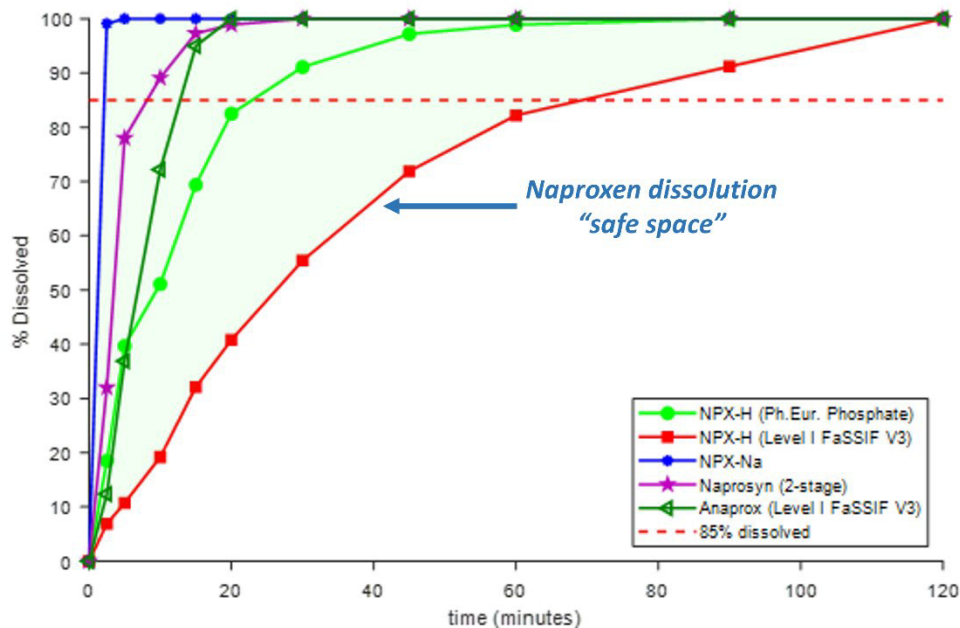


Figure 3-15: Dissolution “safe space”, within which bioequivalence is anticipated for naproxen products. The light green shaded area delimits the safe space area in which bioequivalence (with respect to C_{max} and AUC) was established between the very slow (red solid line & squares) and the fast (blue solid line & circles) dissolution profiles. Additional typical dissolution profiles are co-plotted ($n=3$). The horizontal red dashed line represents 85% dissolved.

3.6.2 Case example: Ibuprofen

The final ibuprofen IVIVE-PBPK model was used in a stepwise risk assessment of failing BE criteria for the T-BE and T-NBE formulations. At this juncture, all absorption- and disposition-related parameters were assumed not to change with time, i.e., IOV = 0, due to the limited data and therefore understanding about the underlying physiological processes. In this scenario, differences between the predicted pharmacokinetic profiles in periods 1 and 2 for the same virtual subject can only be attributed to the formulation effect. In other words, each virtual subject would have exactly the same physiology on the two occasions, representing the most optimistic scenario in terms of the amplitude of the estimated 90% CI for the geometric mean ratio of BE metrics. Predicted geometric mean ratios for plasma AUC in both comparisons, T-BE/R and T-NBE/R, were close to 1.0, resulting in bioequivalent conclusions for AUC in all VBE trials (*data not shown*). On the other hand, for C_{max} similar dissolution profiles reported for R and T-BE formulations (i.e., $f_2 \approx 53$) were translated into T-BE/R geometric mean ratios in the range of 1.04–1.06, whereas non-similar dissolution profiles reported for R and T-

NBE formulations (i.e., $f_2 \approx 38$) derived C_{\max} T-NBE/R geometric mean ratios of 1.10–1.15 (Figure 3-16).
422

To explore the hypothesis of drug product formulation contributing to the IOV of ibuprofen exposure metrics we compared the approximated distributions of IOV estimated for each pairwise comparison using a bootstrap resampling method. The bootstrap resampling was applied to explore how the estimated IOV might vary in the population. Founded on the law of large numbers, the empirical distribution calculated using the bootstrap principle is expected to approximate the density of the true distribution for the statistics in the population. The resulting bootstrap 95% CI for the IOV calculated for each pairwise comparison, namely R vs T-BE and R vs T-NBE, in terms of plasma AUC (i.e., 7.6–11.5% vs 6.2–13%) and C_{\max} (i.e., 13.8–20% vs 10.8–19%) overlapped. The overlapping between the bootstrapped 95% CIs for the IOV calculated for the studies comparing different formulations (i.e., TBE vs R and TNBE vs R) and the low variability observed in the discriminative *in vitro* dissolution test suggest that variability due to drug substance pharmacokinetics is the dominant element in the net IOV of ibuprofen C_{\max} and AUC. This is in line with the population pharmacokinetic analysis reported by Troconiz and co-workers, who showed that CL was the only pharmacokinetic parameter showing IOV (approximately 20%) for ibuprofen.⁴⁶⁷ Therefore, since ibuprofen does not seem to exhibit absorption-related IOV in exposure, a simple *post hoc* incorporation of IOV to the test and reference geometric mean ratios based on the reported *in vivo* intra-subject variability (see Table 3-12) was deemed acceptable to inform VBE trials. After *post hoc* incorporation of the bootstrapped IOV to the simulated C_{\max} T/R geometric mean ratios, the resulting 90% CIs overlapped with the *in vivo* observations for both pairwise comparisons (Table 3-12 and Table 3-17). All ten VBE trials comparing TBE vs R and TNBE vs R resulted bioequivalent and non-bioequivalent outcomes, respectively, confirming the predictive capacity of the model based VBE approach to anticipate the BE outcomes for drug products containing ibuprofen. On the other hand, simulated and observed AUC TNBE/R geometric mean ratios differed significantly, i.e., 1.01 vs 1.21, and the model was not able to recapitulate the non-bioequivalent result in terms of AUC observed in the *in vivo* BE study comparing TNBE vs R. Interestingly, ibuprofen C_{\max} , but not AUC, has been reported to be sensitive to drug product dissolution rate.^{468,469} A published meta-analysis revealed that 14 out of 25 adequately powered BE studies comparing immediate release formulations containing ibuprofen failed to meet BE criteria for C_{\max} , but resulted bioequivalent for AUC.⁴⁷⁰ Given the high permeability observed for ibuprofen throughout different small intestine segments and colon and the complete *in vitro* dissolution for TNBE and R formulations,⁴²² it is unlikely that the observed non-bioequivalent result for AUC is due to absorption-related variables. Furthermore, ibuprofen is rapidly absorbed after oral administration (oral absolute bioavailability is 96.5%) and is not subject to significant first-pass metabolism. Hence, differences in AUC when comparing TNBE vs R be due to IOV in first-pass effect for example if the compared products had delivered different intraluminal profiles is also less probable. Therefore, the mismatch between *in silico* and *in vivo* results for AUC has to be explained by the lack of propagating CL-related IOV to the simulations. However, this was out of the scope of this investigation, which was designed to explore absorption related factors affecting BE.

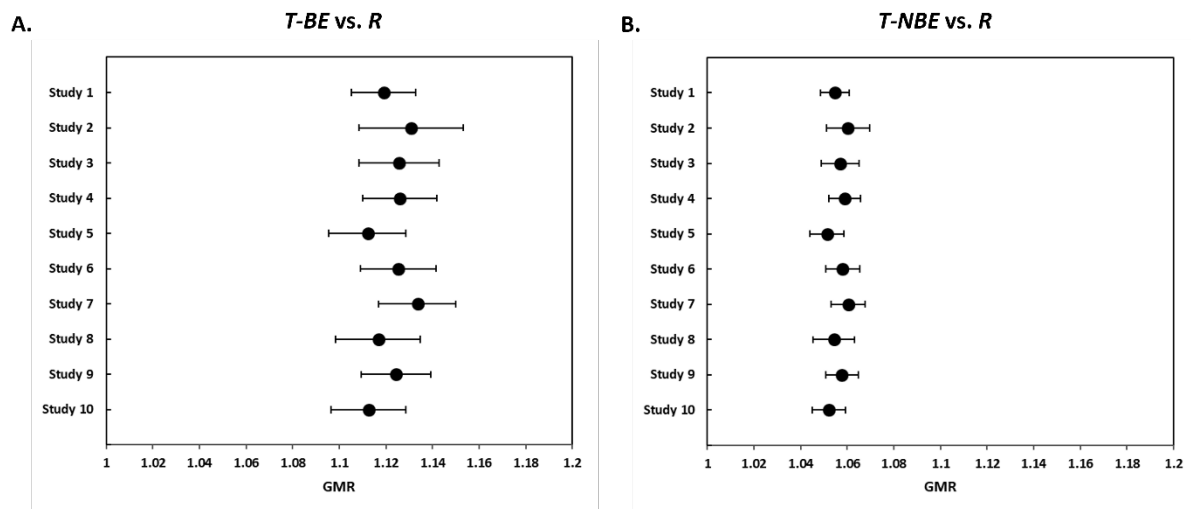


Figure 3-16: Predicted plasma C_{max} ratios T-NBE/R (A) and T-BE/R (B) without adding IOV to any system parameter. Closed symbols represent geometric mean ratios for C_{max} , and horizontal bars represent the respective 90% CIs

Table 3-17: Estimated 90% confidence interval (CI) around predicted C_{max} geometric mean (GeoMean) ratios after post hoc incorporation of bootstrapped IOV

	GeoMean C_{max} ratios	IOV updated 90% CI
Lowest predicted T-BE/R ratio	1.04	0.88-1.20
Highest predicted T-BE/R ratio	1.06	0.90-1.22
Lowest predicted T-NBE/R ratio	1.10	0.94-1.26
Highest predicted T-NBE/R ratio	1.15	0.99-1.31

The upper limit of the bootstrapped 95% CI for the IOV was used to generate power curves to assess the risks of failing to meet the BE criteria due to inflated Type II errors for different sample sizes and T/R ratios. Figure 3-17 presents power curves for sample sizes of 24, 36, and 120 subjects assuming the most critical IOV scenario (20%) resulting from the bootstrap 95% CI.

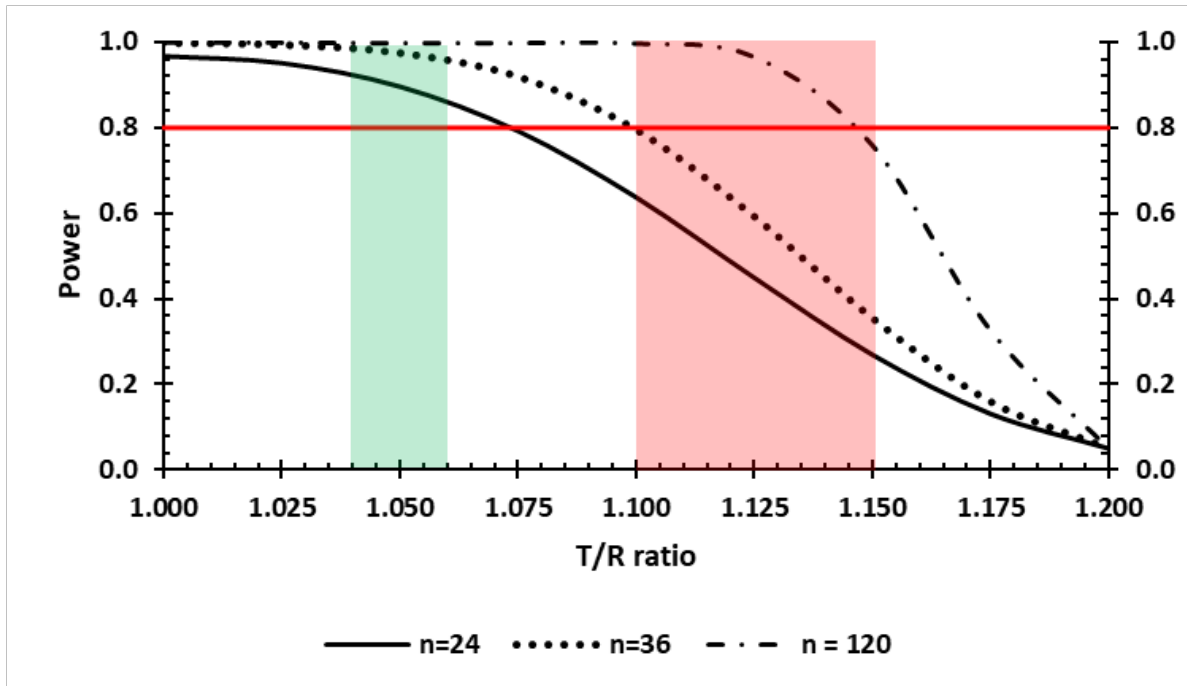


Figure 3-17: Power curve for the two one-sided test procedure with IOV of 20%. Horizontal gray line represents the a priori 80% power recommended in regulatory guidelines for sample size estimation in average BE studies. Shaded areas represent the predicted maximum and minimum values for C_{max} TBE/R (light gray) and TNBE/R (dark gray) in the ten virtual trials

For example, carrying out a 24-subject BE study to compare TBE and R formulations would result in an acceptable Type II error level (i.e., 20%), whereas the manufacturer's risk (i.e., probability of erroneously failing to reject the null hypothesis of inequivalence) would be significantly inflated when comparing TNBE vs R in the same experimental design (i.e., the probability of Type II error ranges from 40 to 80%; Type II error = 1 - power). In other words, up to four out of five 24-subject BE studies comparing TNBE vs R would fail just by chance. This is because the study is underpowered – there are not enough subjects to provide enough information (data) to distinguish between equivalence and non-equivalence scenarios. Underpowering of studies poses an ethical challenge to researchers carrying BE studies as an inconclusive result is a waste of human resources and subjects the volunteers unnecessarily to the drug. Implementing A virtual VBE risk assessment approach when carrying out VBE trials should be useful to support go/no-go decisions. For example, by taking the estimated market share for the generic candidate, as well as the ethical and economical costs required to carry out a BE study enrolling a certain number of subjects, decision-makers responsible for drug product development would be able to make better-informed decisions. This is in line with modern regulatory initiatives that advocate leveraging quantitative methods and modeling to modernize generic drug development and review.^{471–473}

3.7 Population PBPK modelling to assess the Impact of genetic polymorphisms and co-medication on the pharmacokinetics of flurbiprofen

CYP2C9 is a polymorphic enzyme, with more than fifty single nucleotide polymorphisms (SNPs) described in the regulatory and coding regions of the CYP2C9 gene. However, of those, only two coding SNPs, namely CYP2C9*2 and CYP2C9*3, have shown clinically relevant reductions in enzyme activity, while the CYP2C9*1 is the wild type variant⁴⁷⁴. These two SNPs result in six different genotypes that

confer three functionally different phenotypes: a) extensive metabolizers (EM; CYP2C9*1/*1), b) intermediate metabolizers (IM; CYP2C9*1/*2, CYP2C9*1/*3 and CYP2C9*2/*2) and poor metabolizers (PM; CYP2C9*2/*3 and CYP2C9*3/*3)⁴⁷⁴⁻⁴⁷⁶. Although the wild-type variant is the most common allele of the CYP2C9 polymorphic family, the frequency of CYP2C9 genetic polymorphisms varies significantly among different ethnic populations⁴⁷⁷⁻⁴⁷⁹. Flurbiprofen, as a probe substrate of CYP2C9, exhibits gene-dependent pharmacokinetics.^{480,481} Thus, it is critical not only to investigate the exposure of flurbiprofen with and without co-administration of CYP2C9 perpetrators in polymorphic subjects, but also explore ethnic sensitivity (e.g., Caucasian vs. Chinese) of such polymorphisms.

The PBPK model predicted accurately the impact of the three main CYP2C9 polymorphisms on the exposure of the drug in both Caucasian and Chinese healthy volunteers. Model predictions were within 1.25-fold for both AUC (0.91-1.12) and oral clearance (0.76-1.03), while C_{max} was only slightly over-predicted (up to 1.39-fold). These results further increase confidence on the validity of the allele-specific *in vitro* data and add to the overall model robustness. The observed decrease of about 27% and 40% in the clearance of CYP2C9 1*/2* and 1*/3* individuals, might need to be considered in terms of adjustments to the flurbiprofen recommended dose. These findings are in agreement with a large genotype-phenotype correlation clinical study in which the CYP2C9 genotype of 283 healthy subjects was correlated with the metabolic ratio of FLU, calculated from urine data, were used as the phenotypic metric.⁴⁸² In this study, the recommended dose for CYP2C9 1*/2* and 1*/3* subjects was found to be 84% and 60% of the dose administered to the wild type subjects, respectively.

The present PBPK analysis was extended to simultaneously investigate the effect of genetic polymorphism and perpetrator co-administration on FLU PK by predicting drug-drug and drug-gene interactions. It is well known that accurate prediction of the impact of a perpetrator on the pharmacokinetics of a victim drug ratifies the capacity of the victim drug PBPK model to correctly predict the amount of drug eliminated via the affected pathway and indicates that the perpetrator model describes properly the concentration of the inhibitor/inducer at the site(s) of interaction. Furthermore, accurately capturing not only drug-drug, but also drug-gene interactions reinforces confidence in the model to describe the effect of genotype on the pharmacokinetics of the substrate drug. A total of 13 sets of plasma concentration-time profiles were available in the literature for evaluation of model-predicted interactions. The $R_{pred/obs}$ of DDI AUC, C_{max} and CL/F ratios from eleven clinical studies with 200 and 400 mg fluconazole (inhibitor) and one with 600 mg rifampicin (inducer) co-administration ranged from 0.74 to 1.43 with GMFE values within 1.25-fold in eight, nine and ten out of twelve studies in total, respectively.

PBPK model simulations successfully predicted the FLU-fluconazole interaction under different dose levels and regimens in six clinical studies, in which no prior genotyping had been performed (Figure 3-18 (a)-(e)). All DDI AUC, C_{max} and CL/F ratios were within 1.25-fold. The rifampicin induction effect on the exposure of FLU was also accurately predicted from one study, with DDI ratios within 1.25-fold (Figure 3-18 (f)). The DDI predictive accuracy was further evaluated by calculation of the GMFE values for the DDI AUC, C_{max} and CL/F ratios, which ranged from 1.15 to 1.17. The corresponding $R_{pred/obs}$ values for DDI AUC, C_{max} and CL/F ratios of all modeled DDI studies together with the GMFEs are listed in Table 3-18.

Only one drug-drug-gene interaction study was available in the literature in which flurbiprofen alone or together with 200 and 400 mg fluconazole was administered to CYP2C9 1*/1*, 1*/3* and 3*/3* healthy volunteers.⁴⁶¹ In subjects with three CYP2C9 genotypes, the wild-type and both hetero- and

homozygotes for the CYP2C9*3 allele, the PBPK model successfully predicted the gene-dose-dependent interactions with the prototype moderate CYP2C9 inhibitor (fluconazole) at both dose levels. The AUC ratio was slightly underpredicted in 1*/1* and 1*/3* subjects at the 400 mg fluconazole dose level ($R_{\text{pred/obs}}=0.74-0.78$). Nevertheless, the concentration time course of the victim drug with and without coadministration at both inhibitor dose levels and for all genotypes was accurately captured (Figure 3-19).

Based on the *in silico* DDI studies, at a 400 mg dose of fluconazole the interaction in 1*/1* (or assuming 1*/1*) subjects would be classified as weak/moderate with AUC ratios between 1.53 and 2.87. Interactions at a 200 mg dose of fluconazole and a 600 mg dose of rifampicin would be considered as weak with AUC ratios 1.51-1.94 and 0.63, respectively. The interaction for 1*/3* and 3*/3* subjects at 200 mg with AUC ratios 1.58 and 1.09 and at 400 mg fluconazole with AUC ratios 1.84 and 1.16 with was predicted to be weak as well. All these simulated trials are in line with the results from the *in vivo* DDI studies. Interestingly, the flurbiprofen/fluconazole interaction is gene-dose-dependent. Virtually no change in the apparent oral clearance occurring in 3*/3* subjects due to the already reduced CYP2C9 activity was observed and despite the very limited number of subjects (n=2), this was also correctly predicted, indicating excellent model performance. From population simulations, a dose reduction of 34-38% in 1*/3* and 60-70% in 3*/3* subjects would be recommended. However, in the case of fluconazole administration, dose adjustments are required for 1*/1* and 1*/3*, but not for 3*/3* individuals.

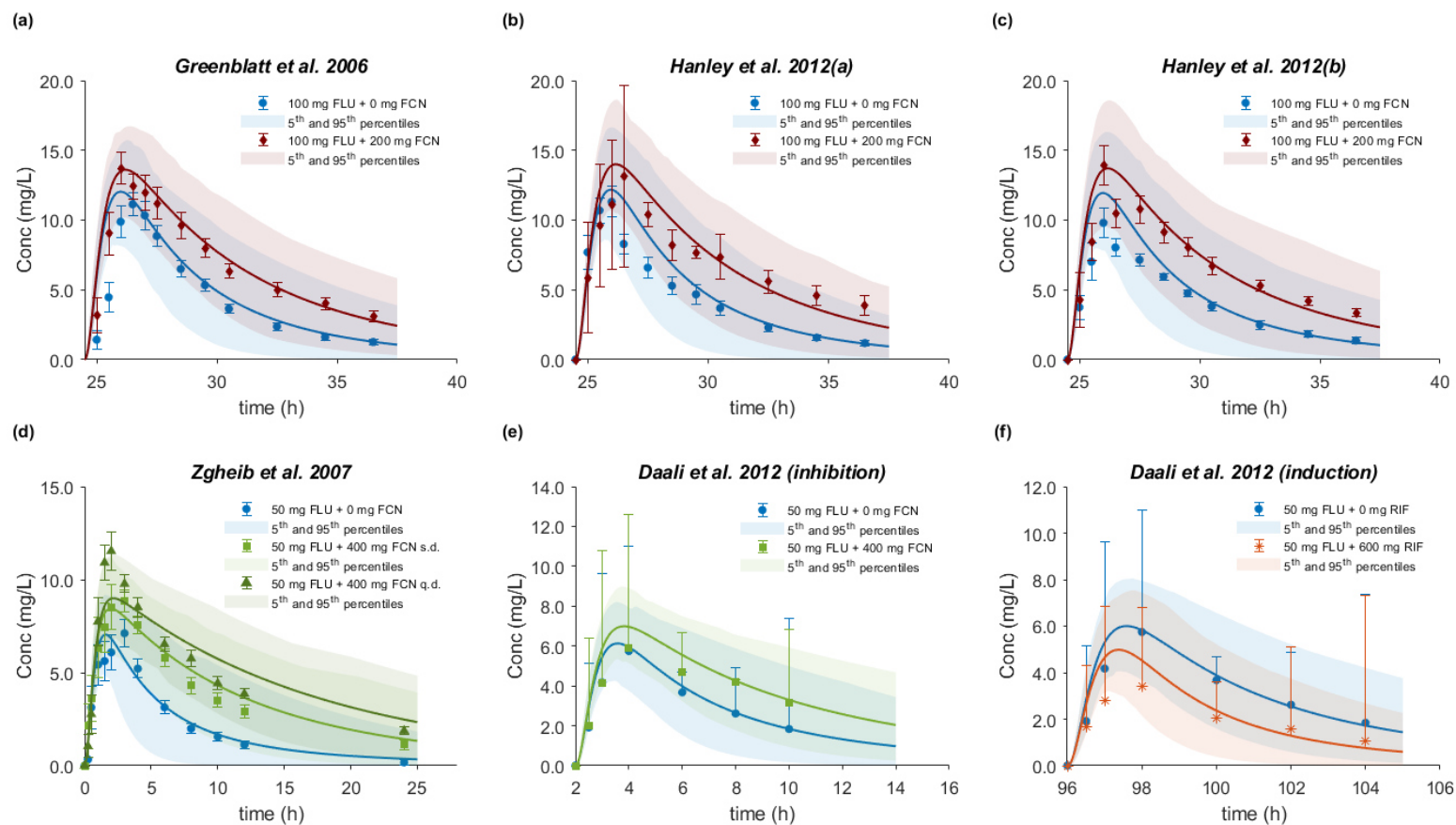


Figure 3-18: Mean plasma concentration-time profiles after administration of flurbiprofen alone and with the perpetrator drug in healthy volunteers. (a)-(e): Population simulations ($n=100$) without or with the CYP2C9 inhibitor, fluconazole (FCN), are shown for the mean as blue (FLU + 0 mg FCN), red (FLU + 200 mg FCN), light green (FLU + 400 mg FCN s.d.) and dark green (FLU + 400 mg FCN q.d.) solid lines and observed data with SD, if available, are depicted as circles, diamonds, squares, and triangles, respectively. (f): Population simulations ($n=100$) without or with the CYP2C9 inducer, rifampicin (RIF), are shown for the mean as blue (FLU + 0 mg RIF) and orange (FLU + 600 mg RIF) solid lines and observed data with SD, if available, are depicted as circles and asterisks, respectively. Shaded areas represent the 5th & 95th percentiles.

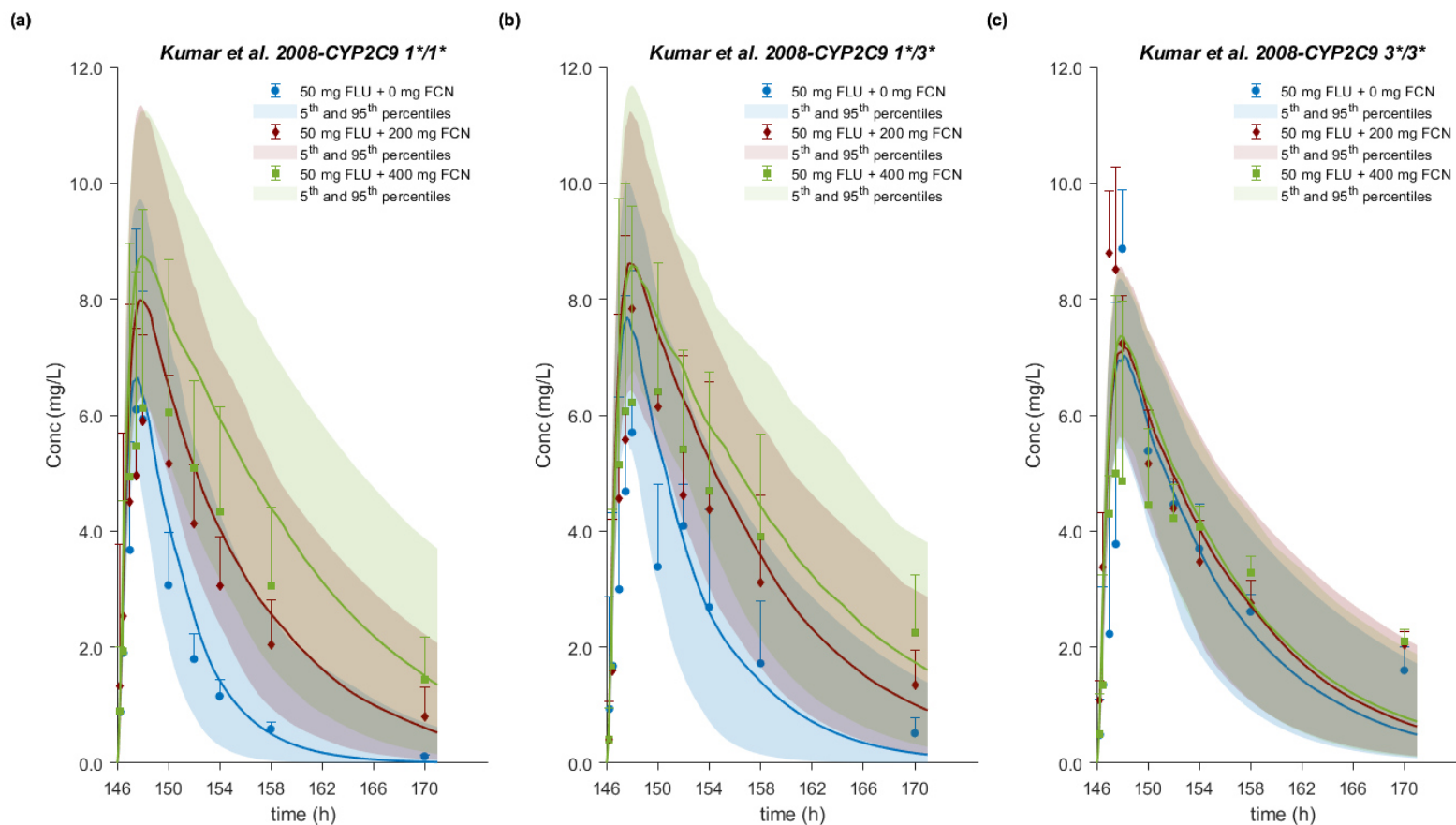


Figure 3-19: Mean plasma concentration-time profiles after administration of 50 mg flurbiprofen as oral tablet alone and with 200 mg or 400 mg fluconazole (FCN) in CYP2C9 1*/1*, 1*/3* and 3*/3* healthy Caucasian volunteers. Population simulations ($n=100$) are shown for the mean as blue (FLU + 0 mg FCN), red (FLU + 200 mg FCN) and light green (FLU + 400 mg FCN) solid lines and observed data with SD, if available, are depicted as circles, diamonds, and squares, respectively. Shaded areas represent the 5th & 95th percentiles

Table 3-18: Comparison of mean predicted and observed DDI AUC, C_{max} and apparent clearance (CL/F) ratios of flurbiprofen-fluconazole/rifampicin interaction. Calculation of predicted to observed ratio ($R_{pred/obs}$) and geometric fold error (GMFE) values.

Victim Drug Dosing	Perpetrator Drug Dosing	N° of Doses	Interval (h)	CYP2C9 genotype	DDI AUC ratio			DDI C_{max} ratio			DDI CL/F ratio			Reference
					obs	pred	$R_{pred/obs}$	obs	pred	$R_{pred/obs}$	obs	pred	$R_{pred/obs}$	
Flurbiprofen	Fluconazole													
po 50 mg s.d.	po 200 mg q.d.	7	2	1*/1*	2.02 ^a	1.94	0.96	1.03 ^a	1.18	1.15	0.5 ^a	0.51	1.02	461
po 50 mg s.d.	po 400 mg q.d.	7	2	1*/1*	3.03	2.36	0.78	0.99	1.23	1.24	0.31	0.42	1.35	461
po 50 mg s.d.	po 200 mg q.d.	7	2	1*/3*	1.8	1.58	0.88	0.87	1.11	1.28	0.56	0.63	1.13	461
po 50 mg s.d.	po 400 mg q.d.	7	2	1*/3*	2.48	1.84	0.74	0.94	1.14	1.21	0.44	0.54	1.23	461
po 50 mg s.d.	po 200 mg q.d.	7	2	3*/3*	(1.58, 1.28)	1.09	0.76	(1.08, 0.91)	1.02	1.02	(0.75, 0.66)	0.92	1.30	461
po 50 mg s.d.	po 400 mg q.d.	7	2	3*/3*	(1.39, 1.12)	1.16	0.92	(0.54, 0.90)	1.03	1.43	(1, 0.66)	0.86	1.04	461
po 100 mg s.d.	po 200 mg b.i.d.	2	0.5	n.a.	1.71 ^b	1.65	0.97	1.16 ^b	1.15	0.99	0.57	0.61	1.07	483
po 100 mg s.d.	po 200 mg b.i.d.	2	0.5	n.a.	1.81	1.51	0.83	1.23	1.13	0.92	0.55	0.68	1.24	484
po 100 mg s.d.	po 200 mg b.i.d.	2	0.5	n.a.	1.97 ^b	1.62	0.82	1.47 ^b	1.15	0.78	0.5	0.62	1.24	485
po 50 mg s.d.	po 400 mg s.d.	1	2	n.a.	2.16	2.23	1.03	1.24	1.2	0.97	0.46	0.48	1.04	481
po 50 mg s.d.	po 400 mg q.d.	7	2	n.a.	2.81	2.87	1.02	1.37	1.25	0.91	0.35	0.39	1.11	481
po 50 mg s.d.	po 400 mg s.d.	1	2	n.a.	1.21	1.53	1.26	1.14	1.14	1.00	0.67	0.67	1.00	486
	Rifampicin													
po 50 mg s.d.	po 600 mg q.d.	5	0	n.a.	0.56	0.63	1.13	0.71	0.83	1.17	1.85	1.73	0.94	Daali et al.
GMFE (range)					1.17 (1.02-1.35)			1.16 (1.00-1.43)			1.15 (1.00-1.35)			

GMFE \leq 1.25	8/12	9/12	10/12
GMFE \leq 2	12/12	12/12	12/12

n.a.= not available; s.d.= single dose; q.d.= once daily; b.i.d.=twice daily; ^a median; ^b geometric mean

3.8 Population PBPK/PD modelling to dissect the effect of formulation and genetic polymorphisms on the exposure and response of flurbiprofen, a substrate of the polymorphic CYP2C9

Several *in vitro* dissolution profiles from various marketed FLU immediate release oral products at the highest dose strength of 100 mg and under different *in vitro* conditions were generated. PBPK/PD population simulations, after translation of *in vitro* release into *in vivo* dissolution rates, provided insight into the impact of different *in vivo* dissolution rates on the PK/PD of flurbiprofen. Population simulations (n=100) were performed with the NEurCaucasian virtual population, and the enzymatic status of each virtual subject was tracked. The overall mean predicted plasma concentration-time profiles of each dissolution scenario were compared with observed PK profiles from five external datasets and among the data sets (Figure 3-10). Interestingly, it was shown that differences between the fastest (85% dissolved in 2.5 min) and the slowest (85% dissolved in 60 min) *in vitro* extrapolated *in vivo* dissolution rates ($S_{\text{DLM}} = 0.0018$ vs. $S_{\text{DLM}} = 0.125$) translated to a decrease in both C_{max} and AUC of only approximately 20% (Table 3-15), while T_{max} was prolonged by 30 minutes (*data not shown*). Nonetheless, in all cases, the predictive accuracy was acceptable with MRD between 1.04 and 2.43 and GMFE values ranging from 0.78 to 1.01 for C_{max} and 0.76 to 1.20 for AUC_{inf} .

Although flurbiprofen's AUC, and especially C_{max} , is more sensitive to *in vitro* dissolution compared to naproxen, these simulations indicate that *in vitro* dissolution rate still might not be the most critical attribute for the *in vivo* performance of flurbiprofen. For example, even though the predicted shift in the regional absorption peak from mid-jejunum at the fastest dissolution rate to the ileum at the slowest dissolution rate, the absorption of flurbiprofen was still predicted to be almost complete ($f_a > 0.93$) in all cases. Instead, these findings suggest that the interplay between absorption and distribution/metabolism plays a key role thus providing support for the hypothesis that "for compounds with similar biopharmaceutic properties, differences in post-absorptive PK properties will likely determine the relative sensitivity of C_{max} to dissolution rate". In the case at hand, flurbiprofen's half-life (5-7 h) is much shorter than naproxen's (20-24 h), but double than ibuprofen's (2-4 h).

To determine the extent to which changes in PK also result in changes in PD, simulations of the response-time profiles were compared with the actual clinical data for each dissolution rate and for both endpoints. The comparisons are shown in Figure 3-13 (c) and (d). Detailed results for the PD together with the calculated $R_{\text{pred/obs}}$ are also shown in Table 3-16. Differences in C_{max} and AUC_{inf} did not translate into changes of a similar degree in the R_{max} and AUC. In fact, they were mitigated to less than 7%, showing that *in vivo* dissolution rate has no or little or no effect on the degree and duration of analgesic effect. The only clinically relevant finding was that, at the slowest dissolution rate, the TR_{max} was prolonged to 1h. These findings suggest that very slow dissolution might be relevant to the onset of pain relief and time to maximum pain relief and therefore T_{max} may be a sensitive metric in single-dose bioequivalence studies of flurbiprofen to detect such differences. Although C_{max} is more sensitive to the dissolution rate of naproxen, the simulations suggest that the *in vitro* dissolution limits within which bioequivalence would be anticipated are quite wide.

In order to dissect and compare the relative effect of *in vitro* dissolution/formulation and CYP2C9 genetic polymorphisms on the PK/PD of flurbiprofen, PBPK population simulations using the NEurCaucasian and Chinese populations were performed to reproduce the clinical studies in CYP2C9 polymorphic subjects published by Lee et al. 2003 and Lee et al. 2015, respectively.^{448,460} The PBPK

model accurately captured the observed effect of three different CYP2C9 genotypes on FLU PK in Caucasian and Chinese populations. The range of GMFE values for C_{max} , AUC_{inf} and CL/F was 0.90-1.39, 0.91-1.12 and 0.76-1.03, respectively. An overall reduction of 42% and 38% in the clearance of CYP2C9 1*/3* individuals of both populations, which in turn led to a 1.52 and a 1.62-fold increase in AUC, respectively, was predicted. These findings are in close agreement with the observed data from Lee et al. 2003 and Lee et al. 2015 who reported a decrease in CYP2C9 1*/3* clearance of about 37% and 44%, resulting in a 1.62 and 1.74-fold increase in AUC, respectively (Table 3-15). Furthermore, the response-time curves of subjects with specific CYP2C9 genotypes (1*/1*, 1*/2* and 1*/3*) were simulated in order to explore potential PD differences. Population simulations showed no effect on R_{max} and TR_{max} , whereas a 1.35-fold increase in the AUC for the CYP2C9 1*/3* subjects was predicted when using the TPEP amplitude as the endpoint (Figure 3-13 (a), (b)). However, when the subjective pain rating score scale was used, no consistent increase in the AUC was observed. Interestingly, in comparison to the wild type (CYP2C9 1*/1*), the time post-administration to return to 80% of the initial value ($T_{80\% \text{ initial}}$) in 1*/3* subjects was delayed by about 7 and 4.5 hours for both TPEP and pain rating, respectively. A similar, but less pronounced, effect was also predicted for the 1*/2* subjects (Table 3-16). This might indicate a longer duration of action, especially in CYP2C9*3 heterozygotes. Nonetheless, any potential flurbiprofen dose optimization in CYP2C9 polymorphic subjects should be carefully evaluated under consideration of the exposure-safety as well as the exposure-response relationship.

3.9 Knowledge gaps, challenges, and limitations in PBPK modelling for oral biopharmaceutics

PBPK analyses for biopharmaceutics and oral drug absorption applications is often referred to using different terminology, including PBPK absorption modeling,³⁰⁶ physiologically based absorption modeling and physiologically based biopharmaceutics modeling (PBBM), to emphasize the mechanistic character of the absorption model component.^{53,309,487} The potential for using PBPK analyses for biopharmaceutics (or PBBM as its shorthand) to waive *in vivo* bioequivalence studies is well recognized by pharmaceutical industries, regulatory agencies and academic consortia alike.^{53,308,309} Within this framework, the emerging field of VBE and clinical trial simulation offers multiple opportunities to apply M&S approaches to inform, or even reduce, the number of clinical studies required and streamline drug development by bringing safe and efficacious drugs to patients faster. Of course, this is of great importance not only for generic, but also for new drug development, since a number of bioavailability/bioequivalence (BA/BE) studies are usually required in the process of bringing a new chemical entity (NCE) to market. Other applications of PBBM with the aim of a “waiver” include, but are not limited to, predicting the outcome of dedicated clinical pharmacology food effect studies, predicting interactions with acid reducing agents/proton pump inhibitors (ARA/PPI) that lead to alterations in drug absorption, and establishing clinically relevant drug product specifications (CRDPS). Furthermore, predictions of alterations in oral drug absorption due to physiological changes or disease in specific (e.g., pediatric, geriatric, achlorhydric) or patient (e.g., cancer, Crohn’s) populations are also of interest. However, the acceptance rate of PBPK modeling and simulation analyses in the context of biopharmaceutics and oral drug absorption applications for regulatory purposes currently remains rather low.^{204,488} Further progress towards understanding the

interplay between GI physiology, formulation and drug properties as well as the identifiability, parametrization and validation of PBPK models is required to increase confidence in their performance and thus their impact on regulatory decision-making.^{204,488}

Loisios-Konstantinidis and Dressman (Publication 5) discussed the challenges, knowledge gaps and opportunities of PBPK/PD modelling in support of waivers of *in vivo* clinical studies in the area of oral biopharmaceutics.¹²⁸ Improvements to the current PBPK platforms with regard to several physiological considerations are anticipated to increase confidence in the predictive performance. Some of the main topics of interest are intestinal permeability and regional differences therein (e.g., extent of colonic absorption), *in vivo* disintegration, especially in the fed state, active transport, gut wall metabolism and impact of functional excipients on oral uptake. For instance, best practices for the estimation of permeability from *in vitro*/*in situ* experiments have not been established. Even though mechanistic permeability, hydrodynamic and dynamic bile salt models are implemented in some platforms, further verification of their performance will underscore their utility.^{26,489,490} Furthermore, only very limited data, mostly from very small sample sizes and fasted healthy adults, are available on the intra-individual variability of physiological variables.^{463,491} As VBE is attracting more and more attention, it is crucial to better understand and implement both inter-subject and within-subject variability as well as their distributions.^{32,317} Inter- and intra- subject variability in the fed state, in specific or disease populations as well as subject-by-formulation variability must be considered as uncharted waters at the moment, while debate on best practices for clinical trials simulation, their sample size and the number of trials is ongoing.

Regarding predictions of food effects and ARA/PPI interactions, all physiological considerations should be taken into account. Currently, not all aspects of fed state physiology can be captured in the *in silico* models. These include interactions between food components (e.g., lipids, carbohydrates) and the drug substance/dosage form, interactions with enzymes and transporters, fed state precipitation models, intraluminal volumes and fluid compositions arising from different meals in different populations (e.g., elderly) and the effects of complex colloid structures. The ability to simulate ARA/PPI interactions using PBPK is more advanced, with the caveat that mechanisms other than elevated gastric pH, like chelation and ARA-induced metabolic or transporter DDIs, may also need to be considered and explicitly modelled.

Apart from physiological or translational challenges and limitations, the importance of ensuring structural and statistical identifiability in every PBPK modeling activity has to be stressed. Parameter estimation or optimization should be performed cautiously and needs to be well justified, as the risk of non-identifiability is higher in extensively parameterized models like quantitative systems pharmacology (QSP) and PBPK models, especially in absence of IV data or when the input data comes from various sources. Over-parametrization or optimization of systems parameters without solid justification constitute common malpractices as well. Last but not least, lack of transparency and publication bias towards positive results can be a limitation to confidence in PBPK model performance and learning from negative results will also be necessary to move the field forward. Clearly listed assumptions, identifiability assessment and a detailed modeling and simulation analysis plan constitute the way forward to best practices in PBPK modeling.

3.10 Opportunities and future actions to increase confidence in and maximize the impact of PBPK models for oral drug absorption

Considering the increasing number of drugs exhibiting unfavorable and complex absorption properties in development, it is likely that efficient oral drug delivery will become even more challenging in the future. Past successes hold no guarantee for the future, as the number of drugs with challenging physicochemical and biopharmaceutic properties, such as high molecular weight, low aqueous solubility, stability and/or permeability has increased dramatically. In 2019, the US-FDA granted a marketing authorization of the first oral glucagon-like peptide 1,⁴⁹² the first large molecule which has been approved by FDA for oral use.⁴⁹² This may signify a new era for oral absorption and offers plentiful opportunities for further *in vivo* research and computational tools. Increased effort and knowledge will be required to successfully respond to the contemporary challenges of oral drug development not only of small, but potentially also of large new molecules.

Multi-stakeholder, cross-continent research consortia such as the OrBiTo, PEARRL (www.pearrl.eu), UNGAP (www.cost.eu/actions/CA16206) and DDMore (www.ddmore.eu) projects,^{493,494} bringing together leading scientists in academia, industry and regulatory agencies have stimulated interdisciplinary dialogue, fostered inter-disciplinary collaboration and contributed to recent advances in oral biopharmaceutics and *in silico* tools. In order to best address the current knowledge gaps, exchange of knowledge and information is required to characterize and reduce uncertainty in physiological parameters as well as quantify and analyze the physiological variability. Increased interdisciplinary and intersectoral collaboration among biopharmaceutic, modeling and simulation and formulation scientists, statisticians and pharmacometricians as well as gastroenterologists, clinicians and engineers, who can all contribute in the refinement or development of mechanistic *in/ex vivo*, *in vitro* and *in silico* models, will create the path forward.^{493,494}

Major challenges in the characterization of GI tract result from the difficulties in accessing and visualizing its contents. Several advanced, preferably non-invasive, and real-time, imaging technologies have been adopted to overcome this hurdle, but further progress is still required. Magnetic resonance (MR), contrast-enhanced MR, computed tomography (CT) and nuclear imaging, capsule endoscopy, 3-D endoscope imaging, high-resolution electrical mapping and electrogastrogram have been used to visualize the gut lumen (patho)physiology and gain insight into the *in vivo* behavior of drug/formulation in preclinical species, healthy humans and patients.^{495–501} Furthermore, systematic exploration of the capabilities molecular dynamics (MD) simulations, synchrotron small angle X-ray scattering, coherent anti-Stokes Raman Spectroscopy and surface plasmon resonance would promote understanding of membrane transport, drug-colloidal structures interactions, lipid imaging at molecular level, drug or excipient release, disposition and intracellular concentrations.^{502–505} Thus, a plethora of opportunities, not only for GI imaging, but also for development of data analysis and *in silico* tools which will be interacting or even be integrated into PBPK models, is foreseen.⁵⁰⁶

Supporting these efforts, further integration of PBPK with pharmacometrics and pharmacogenomics is more than essential. Non-linear mixed effect (NLME) modeling would be helpful to analyze, defragment and reproduce the primary sources of variability observed in the GI tract. Common stochastic (e.g., Monte-Carlo simulation) or resampling (e.g., bootstrap) techniques and Bayesian approaches are considered beneficial to better understand the distribution of inter- and intra-subject

variability as well as for more accurate parameter estimation.^{59,93,246,507–511} As a result, this would accelerate advancements in the field of virtual bioequivalence and increase confidence by enabling more mechanistic and reliable simulations in which population variability is fully incorporated. At the same time, integration of pharmacometric and PBPK tools will improve clinical trial simulation and further optimize individualized and targeted treatment. Furthermore, the potential benefits from using GI biomarkers or tracers to understand the gut (patho)-physiology has been highlighted.^{512–515} Thus, biomarker modeling, especially for in-patient populations, is another point where the interaction of pharmacometricians with biopharmaceutical scientists would be advantageous for developing more mechanistic applications of PBPK models. Similar, further exploration of the as yet scarcely studied inter-correlations of GI physiological using covariate analysis is essential to accurately define individual GI physiologies within PBPK platforms.

A lack of *in vivo* human data about interactions of food components/nutrients and excipients with enzymes, transporters and in general with the intraluminal environment deserves extensive research in order to improve and enable incorporation of these aspects into *in silico* models. Limited information about GI physiology in specific (e.g., pediatric, elderly) and patient populations (e.g., cancer, cirrhotic) in different ethnic groups also represents a limitation to the confidence in current PBPK models/platforms. Effects of different type of meals or enzymes (e.g., lipases) on formulation performance and drug absorption, transporters and metabolizing enzymes abundance and activity levels in patient populations, potential mechanisms for oral administration of large molecules, impact of gut microbiome or mucosal integrity in inflammatory bowel diseases, ontogeny of GI and physiological alterations due to dietary habits or obesity are only some of the opportunities to be explored in the arena of oral drug absorption. In this context, there is a clear need for further analytical assays, aspiration and imaging studies providing improved characterization and in-depth profiling of the GI tract, which in turn would enable the development and verification of mechanistic *in vitro* and *in silico* models. Till now, most studies of this type have been focused on healthy adults, have studied just a few drugs and mainly “conventional” formulations, hindering extrapolation to other populations, compounds, and bio-enabling formulations. Standardization of methodologies and best practices in aspiration or imaging studies would foster these efforts.

At the same time, wherever possible, enhanced reproducibility, and comparability of *in vivo*, *in vitro* and *in silico* models is believed to be crucial. The clinical relevance of formulation and food effects as well as ARA/PPI interactions encompasses not only the capturing changes in pharmacokinetics caused by the interactions but also the ramifications for safety and efficacy. Therefore, further linking PBPK models with pharmacodynamic (PD) and toxicodynamic (TD) models is crucial to decision-making in clinical practice. A well-established exposure/response relationship is required to forecast the clinical outcome.

A major area of opportunity waiting to be exploited is the translation of CMC changes to clinical impact. Development of *in silico* tools to describe manufacturing processes and critical quality attributes (CQA) linked to *in vitro* tests, which would subsequently be connected with PBPK models, is of great interest. It is crucial to capture the effect of CQA changes on the *in vitro* and *in vivo* performance within the QbD and BioRAM paradigm so that confidence in PBPK predictions of drug quality and clinically relevant specifications can enable waivers of *in vivo* studies.³⁹⁰ In turn, another area of opportunity waiting to be exploited is the translation of CMC changes to clinical impact.

Last but not least, open-source tools, repositories (e.g., DDMore) and a common programming language/interface (e.g., Pharmacometric Markup Language) may improve transparency and interconnectivity on the application of current and future tools. A holistic approach, combining understanding of the rate-limiting processes and their interplay to predict *in vivo* performance is warranted. Regardless of the PBPK application, it will be up to pharmacometricians, M&S and biopharmaceutics scientists working together to establish a thorough understanding of all underlying assumptions/limitations and mechanisms critical to the clinical outcome.

4 Summary and Outlook

The work described in this thesis was part of the European Research and Innovation Program PEARRL, funded by the European Union's Horizon 2020 Marie Skłodowska-Curie actions, under grant agreement No 674909. This European Training Network (ETN) brought together partners from academia, regulatory sector, and pharmaceutical industry with the aim to advance the development of bio-enabling formulations, improve characterization of human GI tract, establish modeling and simulation practices to predict drug product *in vivo* performance, and ultimately provide future scientists with useful *in vivo*, *in vitro* and *in silico* biopharmaceutic tools.

Intrinsic and extrinsic patient factors (IEFs) such as dosage form, co-medication and genetic polymorphism may significantly impact drug exposure and subsequently lead to changes in the efficacy or safety of a drug. The ability to quantify and extrapolate the impact of such factors on the exposure and pharmacologic action of a drug represents a milestone in determining required dose adjustments and implementation of risk management strategies in clinical pharmacology. Under the prism of model-informed drug discovery and development (MID3), dynamic mechanistic models such as whole body physiologically based pharmacokinetic/pharmacodynamic (PBPK/PD) models may be useful for forecasting the influence as well as the interaction of multiple factors on PK and PD, and as a result could be used to guide formulation selection and clinical dosing recommendations.

Despite PBPK models being routinely applied within pharmaceutical industry for internal decision making and to support regulatory review, confidence in PBPK modeling analyses to support waivers of dedicated clinical pharmacology studies for biopharmaceutic applications remains rather low. On the other hand, virtual bioequivalence (VBE) in the context of clinical trial simulation has emerged as a promising, yet underdeveloped, field which will expand the scope of PBPK modeling in biopharmaceutics. For instance, BCS-based biowaivers for BCS class II and IV drug are not currently accepted by health authorities. However, in some cases PBPK modeling by coupling *in vitro* dissolution to the *in vivo* formulation performance has demonstrated that such an approach could be scientifically justified under certain circumstances.²⁷ Similarly, PBPK modeling and VBE can be used to set clinically relevant drug product dissolution specifications and define (or broaden) the dissolution „safe space“.^{291,302} Nonetheless, even in the case of drug products which show differences in the extent and rate of absorption outside of the bioequivalence limits, they may still be deemed therapeutically equivalent if this can be appropriately justified by exposure-response and/or exposure-safety analysis using empirical, semi- or fully-mechanistic PK/PD models. In this context, the primary goal of the present thesis was to support and justify expansion of model-evidenced waivers of dedicated *in vivo* clinical pharmacology studies focusing on oral biopharmaceutic applications.

Towards this goal we implemented the following steps:

- Conduct an extensive review of mathematical models to describe the pharmacologic response (PD) and their link to exposure (PK). In particular, this work focused on the disconnection between PK and PD, showcasing examples for which significant drug exposure differences, and thus bioequivalence, are likely irrelevant to the therapeutic (or toxic) effect.

- Propose PBPK modelling & simulation workflows to perform virtual bioequivalence trials by leveraging biorelevant *in vitro* dissolution testing and by implementing a novel, stepwise IVIVE approach for biopharmaceutical parameters.
- Apply the developed workstreams to a number of pre-selected compounds to investigate the role of specific PK properties in the sensitivity of *in vitro* and *in vivo* drug product performance for demonstrating of bioequivalence. Three BCS class II weak acids (i.e., ibuprofen, flurbiprofen and naproxen) that are widely used as pain relievers were studied as case examples.
- Evaluate the relative contribution of factors other than formulation performance, such as co-medication, ethnic sensitivity and genetic polymorphisms in population PK variability and bioequivalence. Flurbiprofen, which is a probe substrate of the polymorphic CYP2C9, was used to study the combined effects of formulation, genetic polymorphisms, and co-medication with CYP2C9 perpetrators.
- Create a link between exposure and pharmacologic response and translating exposure differences to pharmacodynamic effects in order to assess their clinical relevance.
- Summarize knowledge gaps, challenges, limitations and suggest opportunities and future actions for PBPK modelling in oral biopharmaceuticals.

At first, we reviewed a variety of PK/PD models, from empirical to fully mechanistic, and focused on drug-specific case examples with evident disconnection between PK and PD, for which exposure fluctuations (e.g., formulation driven) become less critical, if not irrelevant, for the pharmacologic response. According to the Code of Federal Regulation (21CFR320.1), bioavailability (BA) is defined as “the rate and extent to which the active ingredient or active moiety is absorbed from a drug product and becomes available at the site of action”, whereas BE is “the absence of a significant difference in the rate and extent to which the active ingredient or active moiety in pharmaceutical equivalents or pharmaceutical alternatives becomes available at the site of drug action when administered at the same molar dose under similar conditions in an appropriately designed study”. The statutory definition of BE clearly indicates that the metrics used to assess BE should correlate with the efficacy and/or safety at the site of action. Thus, identification of potential examples in which therapeutic equivalence might be ensured despite PK differences (or BE failure) were of particular interest for this work. At the same time, integration of appropriate *in vitro* biorelevant tools in *in silico* models to facilitate prediction of the clinical outcome and to guarantee therapeutic equivalence between products requires understanding of the underlying pharmacologic mechanisms and exposure-response/safety relationship.

From a biopharmaceutics perspective, BE studies benchmark the *in vivo* performance of a test formulation against a reference product, for which safety and efficacy have been typically already proven. The biopharmaceutics (BCS) and developability (DCS) classification systems provide a framework for an initial assessment of oral bioavailability and the biopharmaceutic risks associated with the development of a drug product.^{403–405} In general, both systems rely on the solubility (either in aqueous or biorelevant media) and the fraction of dose absorbed, which is approximated by *in vitro* or *ex vivo* permeability measurements. From a regulatory perspective, the BCS-based biowaiver approach is intended to reduce the need for *in vivo* bioequivalence studies by providing an appropriate surrogate for *in vivo* bioequivalence, whereby *in vivo* bioequivalence studies may be exempted if

appropriate *in vitro* data can be generated. BCS-based biowaivers are applicable only to orally administered immediate release (IR) solid dosage forms or suspensions where the drug substance(s) is categorized as BCS class I or III and meets the predefined solubility, permeability and dissolution criteria.^{283,284} Thus, waiving *in vivo* BE studies for BCS Class II or IV drugs is currently not permitted by regulatory authorities. For instance, similarity of *in vitro* dissolution between two products containing a BCS class I drug might be appropriate to ensure similar *in vivo* release, but this information is not necessarily relevant for the risks associated with showing bioequivalence between these two products. Similarly, for a BCS class II weak acid, significant differences in the *in vitro* dissolution at intestinal pH might not translate to differences in C_{max} or AUC and thus scientifically, such formulations could qualify for BCS-based biowaivers. Especially for C_{max} , which is an indirect metric of the absorption rate and as such dependent on pre- (e.g., absorption, first pass extraction) and systemic processes, several authors have expressed criticisms of its sensitivity to absorption rate and utility in general.^{397,402} Furthermore, none of the above approaches consider factors such as the inter-occasion variability (IOV) of physiological and/or drug variables, all of which can influence the outcome of bioequivalence assessments.

Considering the aforementioned scientific and regulatory aspects, in this work we challenge the status quo of the current bioequivalence assessment procedures and propose *in vitro in vivo* extrapolation (IVIVE) integrated PBPK/PD modelling and simulation workflows to scientifically support a paradigm shift from “one size fits all” to a case-by-case bioequivalence risk assessment approach based on *in vitro* product performance, human physiology, drug PK properties and the variability in these. In this context, we selected three BCS class II weakly acidic drugs (naproxen, flurbiprofen, ibuprofen) with similar disposition and metabolic properties as case examples. In general, all three drugs are highly bound to plasma proteins with low volume of distribution, have low pre-systemic (i.e., first-pass extraction) and systemic clearance, and exhibit almost complete bioavailability ($F > 0.9$). However, they differ significantly with regard to half-life, with naproxen ($t_{1/2} \approx 20-24$ h), flurbiprofen ($t_{1/2} \approx 7$ h) and ibuprofen ($t_{1/2} \approx 2$ h) exhibiting moderate-long, moderate, and short half-life, respectively. In all cases, we developed, validated, and applied PBPK/PD models and simulated virtual trials (e.g., VBE, DDI trials) to assess the relative impact of *in vitro/in vivo* dissolution, PK characteristics (e.g., half-life) and intra-subject variability in *in vivo* drug product performance. The modeling and simulation workflow which was implemented included i) *in vitro* characterization of biopharmaceutic properties (e.g., solubility, dissolution) followed by model-based analysis of the *in vitro* results, ii) development and comprehensive validation of PBPK/PD models and iii) simulation and risk assessment of bioequivalence trials.

In the case of naproxen, it was shown through VBE trials that failure of naproxen products to meet bioequivalence is unlikely to be due to dissolution issues, because of the wide “safe space” for dissolution. Additionally, the impact of formulation on the *in vivo* performance is not always correlated with the *in vitro* dissolution. For instance, it was shown that even naproxen products with very dissimilar *in vitro* dissolution (85% dissolved in 2.5 vs. 90 min) are expected to be bioequivalent *in vivo*. This outcome can be explained by both the biopharmaceutic properties (high intestinal solubility and permeability) and the long elimination half-life of naproxen.

In addition, to the best of our knowledge, this was the first report which mechanistically incorporated inter-occasion variability (IOV) in VBE assessment and propagated IOV in the simulations. Implementation of hierarchical levels of variability (inter-, intra-subject) in VBE trials is of critical

importance to accurately describe the population variability and avoid biased bioequivalence results. Even though mixed effect modelling is rare in this context, this study highlighted the importance of mechanistically assigning between-subject and inter-occasion variability values which are physiologically plausible and meaningful.

A different, but complementary, approach regarding VBE was adopted for ibuprofen and a risk assessment methodology for go/no-go BE decision-making was proposed. The ibuprofen PBPK model was initially refined and validated and then applied to compare the results of two *in vivo* BE studies, one with a bioequivalent and one with a non-bioequivalent product. At first, VBE was performed assuming no IOV, in which case any differences in the PK profiles between the two periods of the virtual study for the same individual can be only attributed to the formulation effect. In other words, each virtual subject would have exactly the same physiology on the two occasions, representing the most optimistic scenario in terms of the amplitude of the estimated 90% CI for the geometric mean ratio of BE metrics. However, neglecting IOV (as has been systematically done in the past), led to biased BE results: non-similar dissolution profiles reported for R and T-NBE formulations (with $f_2 \approx 38$) resulted in C_{max} T-NBE/R geometric mean ratios within the BE limits (1.10–1.15). To further explore the hypothesis of drug product formulation contributing to the IOV of ibuprofen exposure metrics we compared the approximated distributions of IOV estimated for each pairwise comparison using a bootstrap resampling method. After *post hoc* incorporation of the bootstrapped IOV to the simulated C_{max} T/R geometric mean ratios, the resulting 90% CIs overlapped with the *in vivo* observations for both pairwise comparisons. All ten VBE trials comparing TBE vs R and TNBE vs R resulted bioequivalent and non-bioequivalent results, respectively, confirming the predictive capacity of the model based VBE approach to anticipate the BE outcomes for drug products containing ibuprofen. Then, the upper limit of the bootstrapped 95% CI for the IOV was used to generate power curves to assess the risk of failing to meet the BE criteria due to inflated Type II errors for different sample sizes and T/R ratios. Based on the power curves it was shown that carrying out a 24-subject BE study to compare TBE and R formulations would result in an acceptable Type II error level (i.e., 20%), whereas the manufacturer's risk (i.e., probability of erroneously failing to reject the null hypothesis of inequivalence) would be significantly inflated when comparing TNBE vs R in the same experimental design (i.e., the probability of Type II error ranges from 40 to 80%; type II error = 1 - power).

In the last case example, a comprehensive PBPK/PD model for flurbiprofen was developed and validated to explore the relative impact of *in vitro* dissolution, co-medication and genetic polymorphisms on the exposure and response of this BCS class II weak acid. Flurbiprofen has a moderate half-life and is also a probe substrate of CYP2C9. In this study, a detailed biopharmaceutical analysis, including appropriately designed biorelevant *in vitro* experiments of various flurbiprofen formulations, was initially performed and was followed by *in vitro* data analysis and extrapolation to *in vivo* using a translational PBPK/PD framework.

Flurbiprofen, as a probe substrate of CYP2C9, exhibits gene-dependent pharmacokinetics.^{480,481} Thus, it is critical not only to investigate the exposure of flurbiprofen with and without co-administration of CYP2C9 perpetrators in polymorphic subjects, but also explore ethnic sensitivity (e.g., Caucasian vs. Chinese) of such polymorphisms. The established flurbiprofen PBPK model predicted accurately (within 1.25-fold) the impact of the three main CYP2C9 polymorphisms on the exposure of the drug in both Caucasian and Chinese healthy volunteers. The PBPK analysis was extended to further investigate

simultaneously the effect of genetic polymorphism and co-administration of the CYP2C9 perpetrators (fluconazole, rifampicin) on the PK of flurbiprofen. Based on the *in silico* DDI studies, at a 400 mg dose of fluconazole the interaction in 1*/1* (or assuming 1*/1*) subjects would be classified as weak/moderate with AUC ratio between 1.53 and 2.87. Interactions at a 200 mg dose of fluconazole and a 600 mg dose of rifampicin would be considered as weak with AUC ratios 1.51-1.94 and 0.63, respectively. The interaction for 1*/3* and 3*/3* subjects at 200 mg with AUC ratios 1.58 and 1.09 and at 400 mg fluconazole with AUC ratios 1.84 and 1.16 with was predicted to be weak as well. All these simulated trials are in line with the results from the *in vivo* DDI studies. Interestingly, the flurbiprofen/fluconazole interaction is gene-dose-dependent. Virtually no change in the apparent oral clearance occurring in 3*/3* subjects due to the already reduced CYP2C9 activity was observed and despite the very limited number of subjects (n=2), this was also correctly predicted, indicating excellent model performance. From population simulations, a dose reduction of 34-38% in 1*/3* and 60-70% in 3*/3* subjects would be recommended. However, in the case of fluconazole administration, dose adjustments are required for 1*/1* and 1*/3*, but not for 3*/3* individuals.

Several *in vitro* dissolution profiles from various marketed FLU immediate release oral products at the highest dose strength of 100 mg and under different *in vitro* conditions were generated. After translation of *in vitro* release into *in vivo* dissolution rates, the PBPK/PD population simulations provided insight into the impact of different *in vivo* dissolution rates on the PK/PD of flurbiprofen. Interestingly, it was shown that differences between the fastest (85% dissolved in 2.5 min) and the slowest (85% dissolved in 60 min) *in vitro* extrapolated to *in vivo* dissolution rates translated into a decrease in C_{max} and AUC of only approximately 20%. Exposure differences were mitigated to less than 7% with regard to response metrics, showing that *in vivo* dissolution rate has no or little effect on the degree and duration of analgesic effect. However, at the slowest dissolution rate the time to maximum response was prolonged to 1h. Despite flurbiprofen's AUC, and especially C_{max} , being more sensitive to *in vitro* dissolution comparing to naproxen, these simulations indicated that the *in vitro* dissolution rate might still not be the most critical attribute for the *in vivo* performance of flurbiprofen, thus enabling a wide dissolution "safe space". These findings suggest that the interplay between absorption and distribution/metabolism plays a key role in flurbiprofen performance *in vivo* and supports our hypothesis that, for compounds with similar biopharmaceutic properties, differences in PK properties will likely determine the relative sensitivity of C_{max} on dissolution rate, given also that flurbiprofen's half-life (5-7 h) is much shorter than naproxen's (20-24 h), but double than ibuprofen's (2-4 h).

In order to dissect and compare the relative effect of *in vitro* dissolution/formulation and CYP2C9 genetic polymorphisms on the PK/PD of flurbiprofen, PBPK population simulations using the NEurCaucasian, and Chinese populations were performed to reproduce the clinical studies in CYP2C9 polymorphic subjects. An overall reduction of 42% and 38% in the clearance of CYP2C9 1*/3* individuals of both populations, which in turn led to a 1.52 and a 1.62-fold increase in AUC, respectively, was predicted. Population simulations showed no effect on R_{max} and TR_{max} , whereas a 1.35-fold increase in the AUCE for the CYP2C9 1*/3* subjects was predicted. Interestingly, in comparison to the wild type (CYP2C9 1*/1*), the time to return to 80% of the initial value ($T_{80\% \text{ initial}}$) post-administration in 1*/3* subjects was delayed by about 7 and 4.5 hours for both TPEP and pain rating, respectively. A similar, but less pronounced, effect was also predicted for the 1*/2* subjects. This might indicate a longer duration of action, especially in CYP2C9*3 heterozygotes. Nonetheless, any potential flurbiprofen dose optimization in CYP2C9 polymorphic subjects should be carefully

evaluated under consideration of the exposure-safety as well as the exposure-response relationship. Overall, our comprehensive PBPK/PD analyses provided mechanistic insights on the impact of dissolution rate and genotype on the PK/PD of flurbiprofen.

The potential for using PBPK analyses for biopharmaceuticals to waive *in vivo* bioequivalence and other dedicated clinical pharmacology studies is well recognized by the pharmaceutical industry, regulatory agencies and academic consortia alike.^{53,308,309} However, further progress towards understanding of the interplay between GI physiology, formulation and drug properties as well as on the identifiability, parametrization and validation of PBPK models is required to increase confidence in their performance and thus their impact on regulatory decision-making.^{204,488} As a capstone of this thesis, we provided perspectives on current knowledge gaps, challenges, limitations as well as opportunities and future directions for the PBPK modelling and simulation analyses in biopharmaceutic applications.

In summary, this work highlighted the importance of considering inherent drug PK properties and inter-occasion variability for BE assessments and underlined the usefulness of integrated IVIVE-PBPK/PD modelling and simulation to dissect the relative impact of intrinsic and extrinsic factors such as *in vitro* dissolution, co-medication, and genetic polymorphisms. Novel virtual bioequivalence workstreams were established and proposed, which can support not only modelling and simulation, but also clinical decisions. Furthermore, it was the first time IOV was incorporated into virtual clinical trial simulations using PBPK and this was achieved using two complementary approaches. Finally, this work could be the basis for a new model-enabled and scientifically justified drug classification system based on bioequivalence risk/assessment and considering the totality of a drug's biopharmaceutic and PK properties along with the variability in these parameters.

5 Deutsche Zusammenfassung (German Summary)

Modellierungs- und Simulationskonzepte sind zu einem integralen Bestandteil von Arzneimittelforschung und -entwicklung geworden. Geeignete Modelle können Rahmenbedingungen bilden, um für verschiedene Darreichungsformen und verschiedene Therapien die Exposition, Wirkung und Zeitverlauf eines Wirkstoffes in Zielgruppen vorherzusagen. Physiologisch begründete pharmakokinetische/ pharmakodynamische (engl. Physiologically based pharmacokinetic/pharmacodynamic (PBPK/PD)) Modelle können verwendet werden, um die PK eines Wirkstoffes und, kombiniert mit PD Modellen, den therapeutischen und/oder toxischen Effekt von neuen molekularen Wirkstoffen am Wirkort vorherzusagen. PBPK-Modelle werden mithilfe einer Reihe von Differentialgleichungen erstellt, welche durch bekannte physiologische Variablen parametrisiert sind und ein quantitativ mechanistisches Framework repräsentieren, durch welche die Absorption, Distribution, Metabolismus und Exkretion (ADME) eines Wirkstoffes beschrieben werden kann. *In-vitro-in-vivo*-Extrapolation (IVIVE) ist aufgrund der Vielzahl von *In-vitro*-Systemen, die als Ersatz von *In-vivo*-Reaktionen dienen, ein wesentlicher Bestandteil dieses Ansatzes. Die Anwendung von PBPK-Modellierung in Verbindung mit IVIVE von ADME Daten kann ein hilfreicher Ansatzpunkt sein, um die PK und Dosierung über verschiedene Spezies, Populationen und Krankheiten zu verstehen und zu extrapolieren.^{41,42}

Intrinsische und extrinsische Faktoren wie die Darreichungsform, Komedikation und genetische Polymorphismen können einen signifikanten Einfluss auf die Exposition des Wirkstoffes haben und in der Folge zu Veränderungen in der Wirksamkeit oder Sicherheit eines Wirkstoffes führen. Die Fähigkeit die Auswirkungen solcher Faktoren auf die Exposition und die pharmakologische Aktivität eines Wirkstoffes zu quantifizieren und zu extrapolieren, repräsentiert einen Meilenstein bei der Bestimmung der erforderlichen Dosisanpassungen und der Umsetzung von Risikomanagementstrategien in der klinischen Pharmakologie. Unter dem Blickwinkel der modellbasierten Arzneimittelforschung und -entwicklung (engl. model-informed drug discovery and development (MID3)) können dynamisch mechanistische Modelle, wie z. B. whole-body PBPK/PD-Modelle, für die Vorhersage des Effekts sowie der Wechselwirkung mehrerer Faktoren auf PK und PD nützlich sein und könnten daher als Orientierung für die Wahl der Formulierung und für klinische Dosierungsempfehlungen dienen.

Obwohl PBPK-Modelle in der Pharmabranche inzwischen routinemäßig zur internen Entscheidungsfindung und zur Unterstützung der regulatorischen Bewertung eingesetzt werden, bleibt das Vertrauen Waiver von speziellen klinischen pharmakologischen Studien für biopharmazeutische Anwendungen durch PBPK- Modellanalysen zu stützen eher gering. Andererseits hat sich die virtuelle Bioäquivalenz im Zusammenhang mit der Simulation klinischer Studien als ein vielversprechendes, aber noch unterentwickeltes Feld erwiesen, mit dessen Hilfe der Anwendungsbereich der PBPK-Modellierung in der Biopharmazeutik erweitert werden kann. So werden beispielsweise BCS-basierte Biowaiver für Wirkstoffe der BCS-Klassen II und IV derzeit von den Gesundheitsbehörden nicht akzeptiert. In einigen Fällen hat die PBPK-Modellierung durch Verknüpfung der *In-vitro*-Freisetzung mit der *In-vivo*-Performance der Formulierung jedoch gezeigt, dass ein solcher Ansatz unter Umständen wissenschaftlich gerechtfertigt sein könnte.²⁷ Auf ähnliche Weise können PBPK-Modellierung und VBE verwendet werden, um klinisch relevante Spezifikationen

für die Wirkstofffreisetzung festzulegen und den "safe space" der Freisetzung zu definieren (oder zu erweitern).^{291,302} Doch selbst bei Wirkstoffen, die Unterschiede im Umfang und in der Rate der Absorption außerhalb der Bioäquivalenzgrenzen aufweisen, was bedeutet, dass sie nicht als bioäquivalent und damit austauschbar angesehen werden können, kann die therapeutische Äquivalenz beibehalten werden, sofern dies durch eine Expositions-Wirkungs-Analyse und/oder eine Expositions-Sicherheits-Analyse unter Verwendung empirischer, halb- oder vollmechanistischer PK/PD-Modelle angemessen begründet wird.

In diesem Zusammenhang bestand das Hauptziel der vorliegenden Dissertation darin, die Erweiterung modellgestützter Waiver von speziellen klinischen *In-vivo*-Pharmakologiestudien mit Schwerpunkt auf oralen biopharmazeutischen Anwendungen zu begründen und zu rechtfertigen. Dieses Ziel wurde erreicht durch:

- Entwurf von Workflows für PBPK-Modellierung und Simulationen (M&S) zur Durchführung virtueller Bioäquivalenzstudien unter der Nutzung von biorelevanten *In-vitro*-Freisetzungstests und durch die Implementierung eines neuartigen, schrittweisen IVIVE-Ansatzes für biopharmazeutische Parameter.
- Anwendung der entwickelten Arbeitsabläufe in einer Reihe von vorausgewählten Wirkstoffen und Analyse der Bedeutung spezifischer PK-Eigenschaften hinsichtlich der Sensitivität der *In-vitro*- und *In-vivo*-Performance des Wirkstoffes für den Nachweis der Bioäquivalenz. Drei schwach saure Wirkstoffe der BCS Klasse II (d.h. Ibuprofen, Flurbiprofen und Naproxen) wurden als Fallbeispiele untersucht.
- Untersuchung des relativen Beitrags von Faktoren zur Populationspharmakokinetik-Variabilität und Bioäquivalenz, abgesehen von der Performance der Formulierung, wie z.B. Komedikation, ethnische Sensitivität und genetische Polymorphismen. Als Untersuchungssubstrat des polymorphen CYP2C9 wurde hier Flurbiprofen genutzt, um die kombinierten Effekte von Formulierung, genetischen Polymorphismen und Komedikation (d.h. CYP2C9 Perpetratoren) zu betrachten.
- Verknüpfung der Exposition mit der pharmakologischen Antwort und Übertragung von Expositionsunterschieden in pharmakodynamische Effekte, um deren klinische Relevanz für die Patienten zu bewerten.

Darüber hinaus wurden zur Unterstützung dieser Ziele die folgenden wissenschaftlichen Fragen untersucht oder behandelt:

- Entwicklung von mathematischen Modellen zur Beschreibung der pharmakologischen Antwort (engl. pharmacologic response (PD)) und deren Verbindung zur Exposition (PK). Insbesondere konzentrierten sich diese Untersuchungen auf die Entkopplung von PK und PD und der Präsentation von Beispielen, für welche signifikante Unterschiede in der Exposition des Wirkstoffes und somit der Bioäquivalenz wahrscheinlich irrelevant für die therapeutische (oder toxische) Wirkung in dem vorgesehenen Dosierungsbereich gewesen wäre.
- Identifizierung von Kenntnislücken, Herausforderungen, Limitierungen, Möglichkeiten und künftige Maßnahmen für die PBPK-Modellierung in der oralen Biopharmazie.

Wie bereits erwähnt bieten PK/PD- und insbesondere PBPK/PD-Modelle einen mechanistischen Ansatz, der die Gewebekonzentrationen am Wirkort des Wirkstoffes mit der pharmakologischen Wirkung verknüpft. Im Rahmen dieser Arbeit wird zunächst ein Überblick über bestehende PK/PD-

Modelle und deren mathematischen Umsetzung vorgestellt. Darüber hinaus sind wirkstoffspezifische Fallbeispiele mit einer offensichtlichen Entkopplung von PK und PD von besonderem Interesse, bei denen Expositionsschwankungen weniger kritisch, wenn nicht gar irrelevant für die pharmakologische Reaktion sind (Publikation 1).

Laut dem *Code of Federal Regulations* (21CFR320.1) ist Bioverfügbarkeit definiert als “the rate and extent to which the active ingredient or active moiety is absorbed from a drug product and becomes available at the site of action”, wohingegen Bioäquivalenz definiert ist als “the absence of a significant difference in the rate and extent to which the active ingredient or active moiety in pharmaceutical equivalents or pharmaceutical alternatives becomes available at the site of drug action when administered at the same molar dose under similar conditions in an appropriately designed study”. Die Definition von Bioäquivalenz weist deutlich darauf hin, dass die Metriken, die genutzt werden um die Bioäquivalenz zu bewerten, mit der Wirksamkeit und/oder Sicherheit am Wirkort korrelieren sollten.

Von einer biopharmazeutischen Perspektive dienen Bioäquivalenz-Studien als Maßstab für die *In-vivo*-Performance einer Testformulierung gegenüber einem Referenzprodukt, für welches die Sicherheit und Wirksamkeit bereits auf gewöhnliche Weise nachgewiesen wurde. Das Biopharmazeutische Klassifizierungssystem (engl. Biopharmaceutics Classification System (BCS)) und das Developability Classification System (DCS) stellen den Rahmen für eine Ersteinschätzung der oralen Bioverfügbarkeit und der biopharmazeutischen Risiken, welche mit der Entwicklung eines Wirkstoffes verbunden sind, dar.^{402–404} Allgemein stützen sich beide Systeme auf die Löslichkeit (entweder in wässrigen oder biorelevanten Medien) und dem Anteil der absorbierten Dosis, welche durch *In-vitro*- oder *Ex-vivo*-Permeabilitätsmessungen angenähert werden. Aus regulatorischer Sicht sind BCS-basierte Biowaiveransätze darauf ausgerichtet, den Bedarf an *In-vivo*-Bioäquivalenzstudien durch angemessenen Ersatz für *In-vivo*-Bioäquivalenz zu reduzieren, wodurch *In-vivo*-Bioäquivalenzstudien erlassen werden können, sofern angemessene *In-vitro*-Daten generiert werden können. BCS-basierte Biowaiver können nur auf oral verabreichte feste Darreichungsformen mit sofortiger Freisetzung oder Suspensionen angewendet werden, bei denen der Medikamentenwirkstoff als BCS Klasse I oder III kategorisiert ist und die vordefinierte Löslichkeit, Permeabilität und Freisetzung erfüllt sind.^{283,284} Zusätzlich wird lineare Pharmakokinetik und ein breites therapeutisches Fenster benötigt.^{282,283}

Unter Berücksichtigung der bereits genannten wissenschaftlichen und regulatorischen Aspekte ist die größte Einschränkung von BCS, dass es aufgrund seiner Beschaffenheit den Einfluss der menschlichen Physiologie, inhärente PK-Eigenschaften des Wirkstoffes und die Variabilität des Arzneimittelwirkungsgrad zwischen und innerhalb von Personen ignoriert.

Beispielsweise führen statistisch signifikante Unterschiede in der *In-vitro*-Freisetzung unter dem intestinalen pH-Wert eines BCS Klasse II schwach sauren Wirkstoffen möglicherweise nicht zu Unterschieden in C_{max} oder AUC und, wo dies der Fall ist, könnte man das wissenschaftliche Argument anführen, dass der Wirkstoff für einen BCS-basierten Biowaiver qualifiziert sein könnte. In dieser laufenden Debatte kann PBPK Modellierung und Simulation eine entscheidende Rolle spielen, um wissenschaftlich einen Paradigmenwechsel von einem Pauschalansatz zu einem individuellen Risikoabschätzungsansatz basierend auf *In-vitro*-Daten, menschlicher Physiologie, PK-Eigenschaften und deren Variabilität zu voranzutreiben. Desweiteren bietet es die einzigartige Möglichkeit an, den *In-vitro*-Wirkstoffgrad und die *In-vivo*-Exposition mit Arzneimittelwirksamkeit und -sicherheit zu verknüpfen.

In diesem Zusammenhang bietet PBPK Modellierung und Simulation die Möglichkeit die oben genannten wissenschaftlichen Überlegungen zu untersuchen, ungetestete Szenarios zu erforschen und schließlich evidenzbasiert und arzneimittelspezifische Empfehlungen für Bioäquivalenzprüfungen zu erteilen. Daher bestand das Hauptziel darin PBPK/PD-Modelle zu entwickeln, zu validieren und anzuwenden sowie virtuelle Trials zu simulieren, um den relativen Effekt der *In-vitro/ In-vivo*-Freisetzung, PK-Charakteristiken (z.b. die Halbwertszeit) und die *intraindividuelle Variabilität* bei der *In-vivo*-Arzneimittelwirkung von BCS Klasse II schwach sauren Verbindungen zu beurteilen und einen PBPK-IVIVE integrierten Arbeitsablauf vorzuschlagen, um virtuelle Bioäquivalenzstudien durchzuführen.

Es wurden drei BCS Klasse II schwach saure Wirkstoffe (Naproxen, Flurbiprofen, Ibuprofen) mit ähnlicher Disposition und ähnlichen metabolischen Eigenschaften zur Untersuchung ausgewählt. Allgemein sind alle drei Wirkstoffe stark an Plasmaproteine gebunden und haben daher ein niedriges Verteilungsvolumen, niedrigen First-Pass-Effekt, niedrige systemische Clearance und eine nahezu vollständige Bioverfügbarkeit ($F > 0.9$). Allerdings unterscheiden sie sich signifikant in ihrer Halbwertszeit: Für Naproxen beträgt $t_{1/2} \approx 20-24$ h, für Flurbiprofen $t_{1/2} \approx 7$ h und für Ibuprofen $t_{1/2} \approx 2$ h, was moderate bis lange, moderate und kurze Halbwertszeiten widerspiegelt.

Für alle drei Wirkstoffe wurde ein systematischer Arbeitsablauf erstellt einschließlich: i) Charakterisierung von *in vitro* biopharmazeutischen Eigenschaften (z.b. Löslichkeit, Freisetzung) gefolgt von modellbasierten Analysen von *In-vitro*-Ergebnissen, ii) Entwicklung und umfassende Validierung von PBPK/PD-Modellen und iii) Simulierung und Risikoeinschätzung von Bioäquivalenzstudien. Die Fallstudien von Naproxen (Publikation 2) und Ibuprofen (Publikation 3) konzentrieren sich auf bewährte Verfahren der IVIVE für biopharmazeutische Parameter, Risikoabschätzung und Simulation von Bioäquivalenzstudien mit PBPK-Modellen, welche die inter-occasion Variabilität miteinbeziehen. Das Beispiel von Flurbiprofen (Publikation 4) hebt die Wichtigkeit des Verständnisses des relativen Einflusses von intrinsischen (z.b. genetische Polymorphismen) und extrinsischen (z.b. Komedikationen) Faktoren auf die PK und PD des Wirkstoffes hervor, wenn Empfehlungen für die Bioäquivalenz und die therapeutische Gleichwertigkeit gemacht werden. Alle drei Fallbeispiele liefern mechanistische Erkenntnisse über die Freisetzungsgrenzen, die für die *In-vivo*-Arzneimittelwirksamkeit kritisch ist, unter Berücksichtigung der PK-Eigenschaften des Wirkstoffes und der physiologischen Variabilität mit dem Ziel den Status quo des aktuellen BCS-basierten Biowaiveransatzes in Frage zu stellen und integrierte *In-vitro*-, *In-vivo*- und *In-silico*-Paradigma der Risikobewertung für Waiver von *In-vivo*-Bioäquivalenzstudien einzuführen.

In dem letzten Teil der Arbeit werden Herausforderungen, Kenntnislücken und Möglichkeiten von PBPK/PD-Modellierung zur Unterstützung von Waivern von *in vivo* klinischen Studien im Bereich von oralen Biopharmazeutika diskutiert (Publikation 5).¹²⁷ Es werden Verbesserungen erwartet zu den derzeitigen PBPK Plattformen im Bezug auf mehreren physiologischen Betrachtungen, um das Vertrauen in die Vorhersagekraft zu erhöhen. Einige der Schwerpunkte sind die regionalen Unterschiede von der intestinalen Permeabilität, der *In-vivo*-Disintegration, dem aktiven Transport, dem Metabolismus der Darmwand und dem Einfluss von Hilfsstoffen auf die orale Aufnahme. Ein weiterer Verbesserungspunkt ist, dass es nur sehr wenige Daten für die intra-individuelle Variabilität physiologischer Variablen gibt.^{463,491} Da VBE immer mehr Bedeutung gewinnt, ist es von entscheidender Bedeutung sowohl die Variabilität zwischen und innerhalb von Versuchspersonen sowie deren Verteilung besser zu verstehen und umzusetzen.^{32,316}

Im Großen und Ganzen schlägt diese Dissertation biorelevante *In-vitro*-Methoden für die Vorhersage von *In-vivo*-Formulierungsperformance und neue PBPK/PD-Methoden vor, um Daten von *in vitro* biopharmazeutischen Experimenten zu den *In-vivo*-Bedingungen zu extrapolieren. Außerdem ist dies das erste Mal nach unserem Kenntnisstand, dass PBPK/PD-Ansätze zur Durchführung virtueller Bioäquivalenzstudien vorgeschlagen werden, die auch die inter-occasion Variabilität der Pharmakokinetik berücksichtigen. Desweiteren hebt diese Arbeit die Bedeutung von pharmakokinetischen Eigenschaften auf Bioäquivalenz-Ergebnissen hervor und stellt ein neues Konzept zur Risikoeinschätzung von Bioäquivalenz vor, in welchem die Bewertung des Bedarfs eines Waivers von einer *In-vivo*-Bioäquivalenzstudie sowohl auf biopharmazeutischen als auch pharmakokinetischen Wirkstoffeigenschaften basiert und quantitativ mit PBPK/PD-Modellierung bewertet wird.

6 References

1. Yu, L. X., Crison, J. R. & Amidon, G. L. Compartmental transit and dispersion model analysis of small intestinal transit flow in humans. *Int J Pharm* **140**, 111–118 (1996).
2. Yu, L. X., Lipka, E., Crison, J. R. & Amidon, G. L. Transport approaches to the biopharmaceutical design of oral drug delivery systems: Prediction of intestinal absorption. *Adv. Drug Deliv. Rev.* **19**, 359–376 (1996).
3. Dressman, J. B., Amidon, G. L. & Fleisher, D. Absorption potential: Estimating the fraction absorbed for orally administered compounds. *J. Pharm. Sci.* **74**, 588–589 (1985).
4. Amidon, G. L., Kou, J., Elliott, R. L. & Lightfoot, E. N. Analysis of models for determining intestinal wall permeabilities. *J. Pharm. Sci.* **69**, 1369–1373 (1980).
5. Sinko, P. J., Leesman, G. D. & Amidon, G. L. Predicting Fraction Dose Absorbed in Humans Using a Macroscopic Mass Balance Approach. *Pharmaceutical Research: An Official Journal of the American Association of Pharmaceutical Scientists* **8**, 979–988 (1991).
6. Sinko, P., Leesman, G. & Amidon, G. Mass balance approaches for estimating the intestinal absorption and metabolism of peptides and analogues: theoretical development and applications. *Pharmaceutical research* **10**, 271–5 (1993).
7. Oh, D. M., Curl, R. L. & Amidon, G. L. Estimating the Fraction Dose Absorbed from Suspensions of Poorly Soluble Compounds in Humans: A Mathematical Model. *Pharmaceutical Research: An Official Journal of the American Association of Pharmaceutical Scientists* **10**, 264–270 (1993).
8. Kraml, M., Dubuc, J. & Gaudry, R. Gastrointestinal Absorption of Griseofulvin: II Influence of Particle Size in Man. *Antibiot. & Chemother.* **12**, 239–42 (1962).
9. Jounela, A. J., Pentikäinen, P. J. & Sothmann, A. Effect of particle size on the bioavailability of digoxin. *Eur. J. Clin. Pharmacol.* **8**, 365–370 (1975).
10. Ni, P. F., Ho, N. F. H., Fox, J. L., Leuenberger, H. & Higuchi, W. I. Theoretical model studies of intestinal drug absorption V. Non-steady-state fluid flow and absorption. *Int. J. Pharm.* **5**, 33–47 (1980).
11. Amidon, G. E., Ho, N. F. H., French, A. B. & Higuchi, W. I. Predicted absorption rates with simultaneous bulk fluid flow in the intestinal tract. *J. Theor. Biol.* **89**, 195–210 (1981).
12. Ho, F. ., Merkle, H. P. & Higuchi, W. I. Quantitative, mechanistic and physiologically realistic approach to the biopharmaceutical design of oral drug delivery systems. *Drug Dev. Ind. Pharm.* **9**, 1111–1184 (1983).
13. Dressman, J. B., Fleisher, D. & Amidon, G. L. Physicochemical model for dose dependent drug absorption. *J. Pharm. Sci.* **73**, 1274–1279 (1984).
14. Dressman, J. B. & Fleisher, D. Mixing-tank model for predicting dissolution rate control of oral absorption. *J Pharm Sci* **75**, 109–116 (1986).
15. Oberle, R. L. & Amidon, G. L. *The Influence of Variable Gastric Emptying and Intestinal Transit Rates on the Plasma Level Curve of Cimetidine; An Explanation for the Double Peak Phenomenon.* *Journal of Pharmacokinetics and Biopharmaceutics* **15**, (1987).
16. Hintz, R. J. & Johnson, K. C. The effect of particle size distribution on dissolution rate and oral absorption. *Int. J. Pharm.* **51**, 9–17 (1989).
17. Luner, P. E. & Amidon, G. L. Description and simulation of a multiple mixing tank model to predict the effect of bile sequestrants on bile salt excretion. *J. Pharm. Sci.* **82**, 311–318 (1993).
18. Yu, L. X. & Amidon, G. L. A compartmental absorption and transit model for estimating oral drug absorption. *Int. J. Pharm.* **186**, 119–125 (1999).
19. Yu, L. X. & Amidon, G. L. Characterization of small intestinal transit time distribution in humans. *Int. J. Pharm.* **171**, 157–163 (1998).

20. Yu, L. X. An integrated model for determining causes of poor oral drug absorption. *Pharmaceutical Research* **16**, 1883–1887 (1999).
21. Lukacova, V., Woltosz, W. S. & Bolger, M. B. Prediction of modified release pharmacokinetics and pharmacodynamics from in vitro, immediate release, and intravenous data. *AAPS J.* **11**, 323–334 (2009).
22. Agoram, B., Woltosz, W. S. & Bolger, M. B. Predicting the impact of physiological and biochemical processes on oral drug bioavailability. in *Advanced Drug Delivery Reviews* **50**, S41–S67 (2001).
23. Parrott, N. & Lave, T. Prediction of intestinal absorption: comparative assessment of GASTROPLUS (TM) and IDEA (TM). *Eur. J. Pharm. Sci.* **17**, 51–61 (2002).
24. Jamei, M. *et al.* Population-based mechanistic prediction of oral drug absorption. *AAPS J.* **11**, 225–237 (2009).
25. Wang, J. & Flanagan, D. R. General solution for diffusion-controlled dissolution of spherical particles. 1. Theory. *J. Pharm. Sci.* **88**, 731–738 (1999).
26. Stamatopoulos, K., Pathak, S. M., Marciani, L. & Turner, D. B. Population-Based PBPK Model for the Prediction of Time-Variant Bile Salt Disposition within GI Luminal Fluids. *Mol. Pharm.* **17**, 1310–1323 (2020).
27. Cristofolletti, R. & Dressman, J. B. Bridging the Gap Between In Vitro Dissolution and the Time Course of Ibuprofen-Mediating Pain Relief. *J. Pharm. Sci.* **105**, 3658–3667 (2016).
28. Cristofolletti, R. & Dressman, J. B. Use of Physiologically Based Pharmacokinetic Models Coupled with Pharmacodynamic Models to Assess the Clinical Relevance of Current Bioequivalence Criteria for Generic Drug Products Containing Ibuprofen. *J. Pharm. Sci.* **103**, 3263–3275 (2014).
29. S. Darwich, A., Neuhoff, S., Jamei, M. & Rostami-Hodjegan, A. Interplay of Metabolism and Transport in Determining Oral Drug Absorption and Gut Wall Metabolism: A Simulation Assessment Using the “Advanced Dissolution, Absorption, Metabolism (ADAM)” Model. *Curr. Drug Metab.* **11**, 716–729 (2010).
30. Pathak, S. M., Schaefer, K. J., Jamei, M. & Turner, D. B. Biopharmaceutic IVIVE—Mechanistic Modeling of Single- and Two-Phase In Vitro Experiments to Obtain Drug-Specific Parameters for Incorporation Into PBPK Models. *J. Pharm. Sci.* **108**, 1604–1618 (2019).
31. Pathak, S. M. *et al.* Model-Based Analysis of Biopharmaceutic Experiments to Improve Mechanistic Oral Absorption Modeling: An Integrated in Vitro in Vivo Extrapolation Perspective Using Ketoconazole as a Model Drug. *Mol. Pharm.* **14**, 4305–4320 (2017).
32. Loisios-Konstantinidis, I., Cristofolletti, R., Fotaki, N., Turner, D. B. & Dressman, J. Establishing virtual bioequivalence and clinically relevant specifications using in vitro biorelevant dissolution testing and physiologically-based population pharmacokinetic modeling. case example: Naproxen. *Eur. J. Pharm. Sci.* **143**, (2020).
33. Loisios-Konstantinidis, I., Cristofolletti, R., Jamei, M., Turner, D. & Dressman, J. Physiologically Based Pharmacokinetic/Pharmacodynamic Modeling to Predict the Impact of CYP2C9 Genetic Polymorphisms, Co-Medication and Formulation on the Pharmacokinetics and Pharmacodynamics of Flurbiprofen. *Pharmaceutics* **12**, 1049 (2020).
34. Willmann, S. *et al.* PK-Sim®: A physiologically based pharmacokinetic ‘whole-body’ model. *Drug Discovery Today: BIOSILICO* **1**, 121–124 (2003).
35. Willmann, S., Schmitt, W., Keldenich, J. & Dressman, J. B. A Physiologic Model for Simulating Gastrointestinal Flow and Drug Absorption in Rats. *Pharm. Res.* **20**, 1766–1771 (2003).
36. Willmann, S., Schmitt, W., Keldenich, J., Lippert, J. & Dressman, J. B. A physiological model for the estimation of the fraction dose absorbed in humans. *J. Med. Chem.* **47**, 4022–4031 (2004).
37. Willmann, S., Edginton, A. N. & Dressman, J. B. Development and Validation of a Physiology-based Model for the Prediction of Oral Absorption in Monkeys. *Pharm. Res.* **24**, 1275–1282 (2007).
38. Willmann, S., Thelen, K. & Lippert, J. Integration of dissolution into physiologically-based

- pharmacokinetic models III: PK-Sim[®]. doi:10.1111/j.2042-7158.2012.01534.x
39. Thelen, K. *et al.* Evolution of a detailed physiological model to simulate the gastrointestinal transit and absorption process in humans, Part 1: Oral solutions. *J. Pharm. Sci.* **100**, 5324–5345 (2011).
 40. Thelen, K., Coboeken, K., Willmann, S., Dressman, J. B. & Lippert, J. Evolution of a detailed physiological model to simulate the gastrointestinal transit and absorption process in humans, part II: Extension to describe performance of solid dosage forms. *J. Pharm. Sci.* **101**, 1267–1280 (2012).
 41. Jones, H. M. & Rowland-Yeo, K. Basic concepts in physiologically based pharmacokinetic modeling in drug discovery and development. *CPT Pharmacometrics Syst. Pharmacol.* **2**, e63 (2013).
 42. Rostami-Hodjegan, A. Physiologically based pharmacokinetics joined with in vitro-in vivo extrapolation of ADME: a marriage under the arch of systems pharmacology. *Clin. Pharmacol. Ther.* **92**, 50–61 (2012).
 43. Teorell, T. Kinetics of distribution of substances administered to the body, II : The intravascular modes of administration. *Arch. Int. Pharmacodyn. Ther.* **57**, 226–240 (1937).
 44. Paalzow, L. K. Torsten Teorell, the Father of Pharmacokinetics. *Ups. J. Med. Sci.* **100**, 41–46 (1995).
 45. MAPLESON, W. W. An electric analogue for uptake and exchange of inert gases and other. *J. Appl. Physiol.* **18**, 197–204 (1963).
 46. Bischoff, K. B. & Dedrick, R. L. Thiopental Pharmacokinetics. *J. Pharm. Sci.* **57**, 1346–1351 (1968).
 47. Bischoff, K. B., Dedrick, R. L. & Zaharko, D. S. Preliminary model for methotrexate pharmacokinetics. *J. Pharm. Sci.* **59**, 149–154 (1970).
 48. Bischoff, K. B., Dedrick, R. L., Zaharko, D. S. & Longstreth, J. A. Methotrexate pharmacokinetics. *J. Pharm. Sci.* **60**, 1128–1133 (1971).
 49. Rowland, M., Peck, C. & Tucker, G. Physiologically-based pharmacokinetics in drug development and regulatory science. *Annu. Rev. Pharmacol. Toxicol.* **51**, 45–73 (2011).
 50. Li, M., Zhao, P., Pan, Y. & Wagner, C. Predictive performance of physiologically based pharmacokinetic models for the effect of food on oral drug absorption: Current status. *CPT Pharmacometrics Syst. Pharmacol.* **7**, 82–89 (2018).
 51. U.S.FDA Center for Drug Evaluation and Research (CDER). *Physiologically Based Pharmacokinetic Analyses — Format and Content Guidance for Industry.* (2018).
 52. European Medicines Agency. Guideline on the reporting of physiologically based pharmacokinetic (PBPK) modelling and simulation. (2019). Available at: https://www.ema.europa.eu/en/documents/scientific-guideline/guideline-reporting-physiologically-based-pharmacokinetic-pbpb-modelling-simulation_en.pdf. (Accessed: 5th June 2021)
 53. U.S. Food and Drug Administration Center for Drug Evaluation and Research (CDER). Guidance for Industry The Use of Physiologically Based Pharmacokinetic Analyses — Biopharmaceutics Applications for Oral Drug Product Development , Manufacturing Changes , and Controls. (2020). Available at: <https://www.fda.gov/media/142500/download>. (Accessed: 11th October 2020)
 54. U.S.FDA Center for Drug Evaluation and Research (CDER). Clinical Drug Interaction Studies-Cytochrome P450 Enzyme-and Transporter-Mediated Drug Interactions Guidance for Industry. (2020). Available at: <https://www.fda.gov/Drugs/GuidanceComplianceRegulatoryInformation/Guidances/default.htm>. (Accessed: 25th April 2021)
 55. U.S.FDA Center for Drug Evaluation and Research (CDER). *In Vitro Drug Interaction Studies-Cytochrome P450 Enzyme-and Transporter-Mediated Drug Interactions Guidance for Industry.* (2020).
 56. Medicines Agency, E. Guideline on the investigation of drug interactions. (2012).
 57. Zhao, P., Rowland, M. & Huang, S.-M. Best practice in the use of physiologically based pharmacokinetic modeling and simulation to address clinical pharmacology regulatory questions. *Clin. Pharmacol. Ther.* **92**, 17–20 (2012).
 58. Peters, S. *Physiologically-Based Pharmacokinetic (PBPK) Modeling and Simulations: Principles,*

- Methods, and Applications in the Pharmaceutical Industry.* (John Wiley & Sons, Inc., 2012).
59. Wendling, T. *et al.* Reduction of a Whole-Body Physiologically Based Pharmacokinetic Model to Stabilise the Bayesian Analysis of Clinical Data. *AAPS J.* **18**, 196–209 (2016).
 60. Pilari, S. & Huisinga, W. Lumping of physiologically-based pharmacokinetic models and a mechanistic derivation of classical compartmental models. *J. Pharmacokinet. Pharmacodyn.* **37**, 365–405 (2010).
 61. Nestorov, I. A., Aarons, L. J., Arundel, P. A. & Rowland, M. Lumping of whole-body physiologically based pharmacokinetic models. *J. Pharmacokinet. Biopharm.* **26**, 21–46 (1998).
 62. Rowland Yeo, K., Jamei, M., Yang, J., Tucker, G. T. & Rostami-Hodjegan, A. Physiologically based mechanistic modelling to predict complex drug-drug interactions involving simultaneous competitive and time-dependent enzyme inhibition by parent compound and its metabolite in both liver and gut-The effect of diltiazem on the time-c. *Eur. J. Pharm. Sci.* **39**, 298–309 (2010).
 63. Nestorov, I. Whole-body physiologically based pharmacokinetic models. *Expert Opin. Drug Metab. Toxicol.* **3**, 235–249 (2007).
 64. Jones, H. M., Parrott, N., Jorga, K. & Lavé, T. A novel strategy for physiologically based predictions of human pharmacokinetics. *Clin. Pharmacokinet.* **45**, 511–542 (2006).
 65. Jones, H. M. *et al.* Simulation of human intravenous and oral pharmacokinetics of 21 diverse compounds using physiologically based pharmacokinetic modelling. *Clin. Pharmacokinet.* **50**, 331–347 (2011).
 66. Miller, N. A., Reddy, M. B., Heikkinen, A. T., Lukacova, V. & Parrott, N. Physiologically Based Pharmacokinetic Modelling for First-In-Human Predictions: An Updated Model Building Strategy Illustrated with Challenging Industry Case Studies. *Clin. Pharmacokinet.* **58**, 727–746 (2019).
 67. De Buck, S. S. *et al.* Prediction of human pharmacokinetics using physiologically based modeling: A retrospective analysis of 26 clinically tested drugs. *Drug Metab. Dispos.* **35**, 1766–1780 (2007).
 68. Sugano, K. A simulation of oral absorption using classical nucleation theory. *Int. J. Pharm.* **378**, 142–145 (2009).
 69. Kiyohiko Sugano. Introduction to computational oral absorption simulation. *Expert Opin. Drug Metab. Toxicol.* **5**, 259–293 (2009).
 70. Liu, X. *et al.* Use of a physiologically based pharmacokinetic model to study the time to reach brain equilibrium: An experimental analysis of the role of blood-brain barrier permeability, plasma protein binding, and brain tissue binding. *J. Pharmacol. Exp. Ther.* **313**, 1254–1262 (2005).
 71. Scotcher, D., Jones, C. R., Galetin, A. & Rostami-Hodjegan, A. Delineating the Role of Various Factors in Renal Disposition of Digoxin through Application of Physiologically Based Kidney Model to Renal Impairment Populations. *J. Pharmacol. Exp. Ther.* **360**, 484–495 (2017).
 72. Huang, W. & Isoherranen, N. Development of a Dynamic Physiologically Based Mechanistic Kidney Model to Predict Renal Clearance. *CPT Pharmacometrics Syst. Pharmacol.* **7**, 593–602 (2018).
 73. Neuhoff, S. *et al.* Application of permeability-limited physiologically-based pharmacokinetic models: Part I-digoxin pharmacokinetics incorporating P-glycoprotein-mediated efflux. *J. Pharm. Sci.* **102**, 3145–3160 (2013).
 74. Gaohua, L. *et al.* Development of a Multicompartment Permeability-Limited Lung PBPK Model and Its Application in Predicting Pulmonary Pharmacokinetics of Antituberculosis Drugs. *CPT Pharmacometrics Syst. Pharmacol.* **4**, 605–613 (2015).
 75. Polak, S. *et al.* Prediction of concentration-time profile and its inter-individual variability following the dermal drug absorption. *J. Pharm. Sci.* **101**, 2584–2595 (2012).
 76. Puttrevu, S. K., Arora, S., Polak, S. & Patel, N. K. Physiologically based pharmacokinetic modeling of transdermal selegiline and its metabolites for the evaluation of disposition differences between healthy and special populations. *Pharmaceutics* **12**, 1–28 (2020).
 77. Schlender, J. F. *et al.* Development of a Whole-Body Physiologically Based Pharmacokinetic Approach

- to Assess the Pharmacokinetics of Drugs in Elderly Individuals. *Clin. Pharmacokinet.* **55**, 1573–1589 (2016).
78. Salem, F., Johnson, T. N., Hodgkinson, A. B. J., Ogunbenro, K. & Rostami-Hodjegan, A. Does “Birth” as an Event Impact Maturation Trajectory of Renal Clearance via Glomerular Filtration? Reexamining Data in Preterm and Full-Term Neonates by Avoiding the Creatinine Bias. *J. Clin. Pharmacol.* **61**, 159–171 (2021).
79. Johnson, T. N., Bonner, J. J., Tucker, G. T., Turner, D. B. & Jamei, M. Development and applications of a physiologically-based model of paediatric oral drug absorption. *Eur. J. Pharm. Sci.* **115**, 57–67 (2018).
80. Edginton, A. N. & Willmann, S. Physiology-Based Simulations of a Pathological Condition. *Clin. Pharmacokinet.* **47**, 743–752 (2008).
81. Thompson, C. M. *et al.* Database for physiologically based pharmacokinetic (PBPK) modeling: Physiological data for healthy and health-impaired elderly. *J. Toxicol. Environ. Heal. - Part B Crit. Rev.* **12**, 1–24 (2009).
82. Marsousi, N., Desmeules, J. A., Rudaz, S. & Daali, Y. Usefulness of PBPK Modeling in Incorporation of Clinical Conditions in Personalized Medicine. *J. Pharm. Sci.* **106**, 2380–2391 (2017).
83. Kneller, L. A. & Hempel, G. Modelling Age-Related Changes in the Pharmacokinetics of Risperidone and 9-Hydroxyrisperidone in Different CYP2D6 Phenotypes Using a Physiologically Based Pharmacokinetic Approach. *Pharm. Res.* **37**, (2020).
84. Abduljalil, K., Jamei, M., Rostami-Hodjegan, A. & Johnson, T. N. Changes in individual drug-independent system parameters during virtual paediatric pharmacokinetic trials: Introducing time-varying physiology into a paediatric PBPK model. *AAPS J.* **16**, 568–576 (2014).
85. Pan, X. *et al.* Development and Application of a Physiologically-Based Pharmacokinetic Model to Predict the Pharmacokinetics of Therapeutic Proteins from Full-term Neonates to Adolescents. *AAPS J.* **22**, (2020).
86. Chen, J. *et al.* Relative contributions of the major human CYP450 to the metabolism of icotinib and its implication in prediction of drug-drug interaction between icotinib and CYP3A4 inhibitors/inducers using physiologically based pharmacokinetic modeling. *Expert Opin. Drug Metab. Toxicol.* **11**, 857–868 (2015).
87. Wang, H. Y., Chen, X., Jiang, J., Shi, J. & Hu, P. Evaluating a physiologically based pharmacokinetic model for predicting the pharmacokinetics of midazolam in Chinese after oral administration. *Acta Pharmacol. Sin.* **37**, 276–284 (2016).
88. Alqahtani, S. & Kaddoumi, A. Development of physiologically based pharmacokinetic/Pharmacodynamic model for Indomethacin disposition in pregnancy. *PLoS One* **10**, 1–18 (2015).
89. Conner, T. M. *et al.* Physiologically based pharmacokinetic modeling of disposition and drug-drug interactions for valproic acid and divalproex. *Eur. J. Pharm. Sci.* **111**, 465–481 (2018).
90. van Dyk, M. & Rowland, A. Physiologically-based pharmacokinetic modeling as an approach to evaluate the effect of covariates and drug-drug interactions on variability in epidermal growth factor receptor kinase inhibitor exposure. *Transl. Cancer Res.* **6**, S1600–S1612 (2017).
91. Perkins, E. J. *et al.* Physiologically Based Pharmacokinetic Modelling of Cytochrome P450 2C9-Related Tolbutamide Drug Interactions with Sulfaphenazole and Tasisulam. *Eur. J. Drug Metab. Pharmacokinet.* **43**, (2017).
92. Jamei, M. *et al.* The Simcyp Population Based Simulator: Architecture, Implementation, and Quality Assurance. *Silico Pharmacol.* **1**, 9 (2013).
93. Krauss, M., Tappe, K., Schuppert, A., Kuepfer, L. & Goerlitz, L. Bayesian population physiologically-based pharmacokinetic (PBPK) approach for a physiologically realistic characterization of interindividual variability in clinically relevant populations. *PLoS One* **10**, 1–22 (2015).
94. Huisinga, W., Solms, A., Fronton, L. & Pilari, S. Modeling interindividual variability in physiologically

- based pharmacokinetics and its link to mechanistic covariate modeling. *CPT pharmacometrics Syst. Pharmacol.* **1**, e4 (2012).
95. Bois, F. Y., Jamei, M. & Clewell, H. J. PBPK modelling of inter-individual variability in the pharmacokinetics of environmental chemicals. *Toxicology* **278**, 256–267 (2010).
 96. Poulin, P. & Haddad, S. Toward a new paradigm for the efficient in vitro–in vivo extrapolation of metabolic clearance in humans from hepatocyte data. *J. Pharm. Sci.* **102**, 3239–3251 (2013).
 97. Poulin, P., Kenny, J. R., Hop, C. E. C. A. & Haddad, S. In Vitro–In Vivo Extrapolation of Clearance: Modeling Hepatic Metabolic Clearance of Highly Bound Drugs and Comparative Assessment with Existing Calculation Methods. *J. Pharm. Sci.* **101**, 838–851 (2012).
 98. Poulin, P. & Theil, F.-P. Development of a novel method for predicting human volume of distribution at steady-state of basic drugs and comparative assessment with existing methods. *J. Pharm. Sci.* **98**, 4941–4961 (2009).
 99. Rodgers, T., Leahy, D. & Rowland, M. Physiologically based pharmacokinetic modeling 1: Predicting the tissue distribution of moderate-to-strong bases. *J. Pharm. Sci.* **94**, 1259–1276 (2005).
 100. Rodgers, T. & Rowland, M. Physiologically based pharmacokinetic modelling 2: Predicting the tissue distribution of acids, very weak bases, neutrals and zwitterions. *J. Pharm. Sci.* **95**, 1238–1257 (2006).
 101. Kimoto, E., Bi, Y.-A. A., Kosa, R. E., Tremaine, L. M. & Varma, M. V. S. Hepatobiliary Clearance Prediction: Species Scaling From Monkey, Dog, and Rat, and In Vitro–In Vivo Extrapolation of Sandwich-Cultured Human Hepatocytes Using 17 Drugs. *J. Pharm. Sci.* **106**, 2795–2804 (2017).
 102. Paine, S. W., Ménochet, K., Denton, R., McGinnity, D. F. & Riley, R. J. Prediction of human renal clearance from preclinical species for a diverse set of drugs that exhibit both active secretion and net reabsorption. *Drug Metab. Dispos.* **39**, 1008–1013 (2011).
 103. Bi, Y. A., Kazolias, D. & Duignan, D. B. Use of cryopreserved human hepatocytes in sandwich culture to measure hepatobiliary transport. *Drug Metab. Dispos.* **34**, 1658–1665 (2006).
 104. Jones, H. M. *et al.* Mechanistic pharmacokinetic modeling for the prediction of transporter-mediated disposition in humans from sandwich culture human hepatocyte data. *Drug Metab. Dispos.* **40**, 1007–1017 (2012).
 105. Poulin, P. & Theil, F. P. A priori prediction of tissue: Plasma partition coefficients of drugs to facilitate the use of physiologically-based pharmacokinetic models in drug discovery. *J. Pharm. Sci.* **89**, 16–35 (2000).
 106. Poulin, P., Schoenlein, K. & Theil, F. P. Prediction of adipose tissue: Plasma partition coefficients for structurally unrelated drugs. *J. Pharm. Sci.* **90**, 436–447 (2001).
 107. Poulin, P. Prediction of Total Hepatic Clearance by Combining Metabolism, Transport, and Permeability Data in the In Vitro–In Vivo Extrapolation Methods: Emphasis on an Apparent Fraction Unbound in Liver for Drugs. *J. Pharm. Sci.* **102**, 2085–2095 (2013).
 108. Berezhkovskiy, L. M. Volume of distribution at steady state for a linear pharmacokinetic system with peripheral elimination. *J. Pharm. Sci.* **93**, 1628–1640 (2004).
 109. Willmann, S., Lippert, J. & Schmitt, W. From physicochemistry to absorption and distribution: Predictive mechanistic modelling and computational tools. *Expert Opin. Drug Metab. Toxicol.* **1**, 159–168 (2005).
 110. Schmitt, W. General approach for the calculation of tissue to plasma partition coefficients. *Toxicol. Vitro.* **22**, 457–467 (2008).
 111. Murad, N. *et al.* Predicting volume of distribution in humans: Performance of in silico methods for a large set of structurally diverse clinical compounds. *Drug Metab. Dispos.* **49**, 169–178 (2021).
 112. Mathew, S. *et al.* Evaluation of Prediction Accuracy for Volume of Distribution in Rat and Human Using In Vitro, In Vivo, PBPK and QSAR Methods. *J. Pharm. Sci.* **110**, 1799–1823 (2021).
 113. LENNERNAS, H. Human Intestinal Permeability. *J. Pharm. Sci.* **87**, 403–410 (1998).

114. Markopoulos, C., Andreas, C. J., Vertzoni, M., Dressman, J. & Reppas, C. In-vitro simulation of luminal conditions for evaluation of performance of oral drug products: Choosing the appropriate test media. *Eur. J. Pharm. Biopharm.* **93**, 173–182 (2015).
115. Harwood, M. D. *et al.* In vitro-in vivo extrapolation scaling factors for intestinal p-glycoprotein and breast cancer resistance protein: Part i: A cross-laboratory comparison of transporter-protein abundances and relative expression factors in human intestine and caco-2 cells. *Drug Metab. Dispos.* **44**, 297–307 (2016).
116. Harwood, M. D. *et al.* In vitro-in vivo extrapolation scaling factors for intestinal p-glycoprotein and breast cancer resistance protein: Part II. the impact of cross-laboratory variations of intestinal transporter relative expression factors on predicted drug disposition. *Drug Metab. Dispos.* **44**, 476–480 (2016).
117. Meng, Z., Ellens, H. & Bentz, J. Extrapolation of Elementary Rate Constants of P-glycoprotein-Mediated Transport from MDCKII-hMDR1-NKI to Caco-2 Cells. *DRUG Metab. Dispos. Drug Metab Dispos* **45**, 190–197 (2017).
118. Watanabe, T., Kusuhara, H., Maeda, K., Shitara, Y. & Sugiyama, Y. Physiologically based pharmacokinetic modeling to predict transporter-mediated clearance and distribution of pravastatin in humans. *J. Pharmacol. Exp. Ther.* **328**, 652–662 (2009).
119. Vaidyanathan, J., Yoshida, K., Arya, V. & Zhang, L. Comparing Various In Vitro Prediction Criteria to Assess the Potential of a New Molecular Entity to Inhibit Organic Anion Transporting Polypeptide 1B1. *J. Clin. Pharmacol.* S59–S72 (2016). doi:10.1002/jcph.723
120. Einolf, H. J. *Comparison of different approaches to predict metabolic drug-drug interactions.* *Xenobiotica* **37**, (2007).
121. Einolf, H. J. *et al.* Evaluation of various static and dynamic modeling methods to predict clinical CYP3a induction using in vitro CYP3A4 mRNA induction data. *Clin. Pharmacol. Ther.* **95**, 179–188 (2014).
122. Grimm, S. W. *et al.* The conduct of in vitro studies to address time-dependent inhibition of drug-metabolizing enzymes: A perspective of the Pharmaceutical Research and Manufacturers of America. *Drug Metab. Dispos.* **37**, 1355–1370 (2009).
123. Obach, R. S. *et al.* The utility of in vitro cytochrome P450 inhibition data in the prediction of drug-drug interactions. *J. Pharmacol. Exp. Ther.* **316**, 336–348 (2006).
124. Mathialagan, S. *et al.* Quantitative prediction of human renal clearance and drug-drug interactions of organic anion transporter substrates using in vitro transport data: A relative activity factor approach. *Drug Metab. Dispos.* **45**, 409–417 (2017).
125. Mathialagan, S., Feng, B., Rodrigues, A. D. & Varma, M. V. S. Drug-Drug Interactions Involving Renal OCT2/MATE Transporters: Clinical Risk Assessment May Require Endogenous Biomarker-Informed Approach. *Clin. Pharmacol. Ther.* **0**, (2020).
126. Kuepfer, L. *et al.* Applied Concepts in PBPK Modeling: How to Build a PBPK/PD Model. *CPT pharmacometrics Syst. Pharmacol.* **5**, 516–531 (2016).
127. Zhao, P. *et al.* Applications of physiologically based pharmacokinetic (PBPK) modeling and simulation during regulatory review. *Clin. Pharmacol. Ther.* **89**, 259–267 (2011).
128. Loisios-Konstantinidis, I. & Dressman, J. Physiologically Based Pharmacokinetic/Pharmacodynamic Modeling to Support Waivers of in Vivo Clinical Studies: Current Status, Challenges, and Opportunities. *Molecular Pharmaceutics* **18**, 1–17 (2021).
129. Vinarov, Z. *et al.* Current challenges and future perspectives in oral absorption research: An opinion of the UNGAP network. *Adv. Drug Deliv. Rev.* **171**, 289–331 (2021).
130. Peters, S. A., Jones, C. R., Ungell, A. L. & Hatley, O. J. D. Predicting Drug Extraction in the Human Gut Wall: Assessing Contributions from Drug Metabolizing Enzymes and Transporter Proteins using Preclinical Models. *Clin. Pharmacokinet.* **55**, 673–696 (2016).
131. Jones, C. R. *et al.* Gut Wall Metabolism. Application of Pre-Clinical Models for the Prediction of Human

- Drug Absorption and First-Pass Elimination. *AAPS J.* **18**, 589–604 (2016).
132. Fagerholm, U. Prediction of human pharmacokinetics -gastrointestinal absorption. *J. Pharm. Pharmacol.* **59**, 905–916 (2007).
 133. Yang, J., Jamei, M., Yeo, K., Tucker, G. & Rostami-Hodjegan, A. Prediction of Intestinal First-Pass Drug Metabolism. *Curr. Drug Metab.* **8**, 676–684 (2007).
 134. Olivares-Morales, A., Kamiyama, Y., Darwich, A. S., Aarons, L. & Rostami-Hodjegan, A. Analysis of the impact of controlled release formulations on oral drug absorption, gut wall metabolism and relative bioavailability of CYP3A substrates using a physiologically-based pharmacokinetic model. *Eur. J. Pharm. Sci.* **67**, 32–44 (2015).
 135. Krishna, D. R. & Klotz, U. Extrahepatic Metabolism of Drugs in Humans. *Clin. Pharmacokinet.* **26**, 144–160 (1994).
 136. Erratum: Quantitative proteomics of clinically relevant drug-metabolizing enzymes and drug transporters and their intercorrelations in the human small intestine (*Drug Metab Dispos* (2020) 48:4 (245–254) DOI:10.1124/dmd.119.089656). *Drug Metabolism and Disposition* **48**, 407 (2020).
 137. Thummel, K. E., Kunze, K. L. & Shen, D. D. Enzyme-catalyzed processes of first-pass hepatic and intestinal drug extraction. *Adv. Drug Deliv. Rev.* **27**, 99–127 (1997).
 138. Van De Kerkhof, E. G. *et al.* Innovative methods to study human intestinal drug metabolism in vitro: Precision-cut slices compared with Ussing chamber preparations. *Drug Metab. Dispos.* **34**, 1893–1902 (2006).
 139. Tucker, T. G. H. A., Milne, A. M., Fournel-Gigleux, S., Fenner, K. S. & Coughtrie, M. W. H. Absolute immunoquantification of the expression of ABC transporters P-glycoprotein, breast cancer resistance protein and multidrug resistance-associated protein 2 in human liver and duodenum. *Biochem. Pharmacol.* **83**, 279–285 (2012).
 140. Martignoni, M., Groothuis, G. M. M. & de Kanter, R. Species differences between mouse, rat, dog, monkey and human CYP-mediated drug metabolism, inhibition and induction. *Expert Opin. Drug Metab. Toxicol.* **2**, 875–894 (2006).
 141. Seithel, A., Karlsson, J., Hilgendorf, C., Björquist, A. & Ungell, A. L. Variability in mRNA expression of ABC- and SLC-transporters in human intestinal cells: Comparison between human segments and Caco-2 cells. *Eur. J. Pharm. Sci.* **28**, 291–299 (2006).
 142. Gertz, M., Davis, J., Harrison, A., Houston, J. & Galetin, A. Grapefruit Juice-Drug Interaction Studies as a Method to Assess the Extent of Intestinal Availability: Utility and Limitations. *Curr. Drug Metab.* **9**, 785–795 (2008).
 143. Galetin, A., Gertz, M. & Houston, J. B. Contribution of intestinal cytochrome P450-mediated metabolism to drug-drug inhibition and induction interactions. *Drug Metab. Pharmacokinet.* **25**, 28–47 (2010).
 144. Couto, N. *et al.* Quantitative proteomics of clinically relevant drug-metabolizing enzymes and drug transporters and their intercorrelations in the human small intestine. *Drug Metab. Dispos.* **48**, 245–254 (2020).
 145. Thiebaut, F. *et al.* Cellular localization of the multidrug-resistance gene product P-glycoprotein in normal human tissues. *Proc. Natl. Acad. Sci. U. S. A.* **84**, 7735–7738 (1987).
 146. Naritomi, Y., Nakamori, F., Furukawa, T. & Tabata, K. Prediction of hepatic and intestinal glucuronidation using in vitro-in vivo extrapolation. (2015). doi:10.1016/j.dmpk.2014.10.001
 147. Paine, M. F. *et al.* The human intestinal cytochrome P450 ‘pie’. *Drug Metab. Dispos.* **34**, 880–886 (2006).
 148. Hatley, O. J. D., Jones, C. R., Galetin, A. & Rostami-Hodjegan, A. Quantifying gut wall metabolism: methodology matters. *Biopharm. Drug Dispos.* **38**, 155–160 (2017).
 149. Kadono, K. *et al.* Quantitative prediction of intestinal metabolism in humans from a simplified intestinal availability model and empirical scaling factor. *Drug Metab. Dispos.* **38**, 1230–1237 (2010).

150. Gibson, C. R. *et al.* Prediction of Phase I single-dose pharmacokinetics using recombinant cytochromes P450 and physiologically based modelling. *Xenobiotica* **39**, 637–648 (2009).
151. Barter, Z. *et al.* Scaling Factors for the Extrapolation of In Vivo Metabolic Drug Clearance From In Vitro Data: Reaching a Consensus on Values of Human Microsomal Protein and Hepatocellularity Per Gram of Liver. *Curr. Drug Metab.* **8**, 33–45 (2006).
152. Barter, Z. E., J. E., C., J. R., H., J. E., S. & J. C., L. Covariation of Human Microsomal Protein Per Gram of Liver with Age : Absence of Influence of Operator and Sample. *Drug Metab. Dispos.* **36**, 2405–2409 (2008).
153. Yamagata, T. *et al.* Comparison of methods for the prediction of human clearance from hepatocyte intrinsic clearance for a set of reference compounds and an external evaluation set. *Xenobiotica* **47**, 741–751 (2017).
154. Galetin, A., Brown, C., Halifax, D., Ito, K. & Houston, J. B. Utility of recombinant enzyme kinetics in prediction of human clearance: Impact of variability, CYP3A5, and CYP2C19 on CYP3A4 probe substrates. *Drug Metab. Dispos.* **32**, 1411–1420 (2004).
155. Stringer, R. A., Strain-Damerell, C., Nicklin, P. & Houston, J. B. Evaluation of recombinant cytochrome p450 enzymes as an in vitro system for metabolic clearance predictions. *Drug Metab. Dispos.* **37**, 1025–1034 (2009).
156. Karlsson, F. H., Bouchene, S., Hilgendorf, C., Dolgos, H. & Peters, S. A. Utility of in vitro systems and preclinical data for the prediction of human intestinal first-pass metabolism during drug discovery and preclinical development. *Drug Metab. Dispos.* **41**, 2033–2046 (2013).
157. Yau, E., Petersson, C., Dolgos, H. & Peters, S. A. A comparative evaluation of models to predict human intestinal metabolism from nonclinical data. *Biopharm. Drug Dispos.* **38**, 163–186 (2017).
158. Rostami-Hodjegan, A. & Tucker, G. T. Simulation and prediction of in vivo drug metabolism in human populations from in vitro data. *Nat. Rev. Drug Discov.* **6**, 140–148 (2007).
159. Chen, Y., Liu, L., Nguyen, K. & Fretland, A. J. Utility of Intersystem Extrapolation Factors in Early Reaction Phenotyping and the Quantitative Extrapolation of Human Liver Microsomal Intrinsic Clearance Using Recombinant Cytochromes P450. *Drug Metab. Dispos.* **39**, 373–382 (2011).
160. Crewe, H. K., Barter, Z. E., Rowland Yeo, K. & Rostami-Hodjegan, A. Are there differences in the catalytic activity per unit enzyme of recombinantly expressed and human liver microsomal cytochrome P450 2C9? A systematic investigation into inter-system extrapolation factors. *Biopharm. Drug Dispos.* **32**, 303–318 (2011).
161. Proctor, N. J., Tucker, G. T. & Rostami-Hodjegan, A. Predicting drug clearance from recombinantly expressed CYPs: Intersystem extrapolation factors. *Xenobiotica* **34**, 151–178 (2004).
162. Almond, L., Yang, J., Jamei, M., Tucker, G. & Rostami-Hodjegan, A. Towards a Quantitative Framework for the Prediction of DDIs Arising from Cytochrome P450 Induction. *Curr. Drug Metab.* **10**, 420–432 (2009).
163. Almond, L. M. *et al.* Correction to ‘Prediction of Drug-Drug Interactions Arising from CYP3A induction Using a Physiologically Based Dynamic Model’. *Drug Metab. Dispos.* **44**, 877–877 (2016).
164. Yang, J. *et al.* Determining Rates , and Implications for the Prediction of Drug Interactions. *Curr. Drug Metab.* **9**, 384–393 (2008).
165. Nagar, S., Jones, J. P. & Korzekwa, K. A numerical method for analysis of in vitro time-dependent inhibition data. Part 1. Theoretical considerations. *Drug Metab. Dispos.* **42**, 1575–1586 (2014).
166. Filppula, A. M., Parvizi, R., Mateus, A., Baranczewski, P. & Artursson, P. Improved predictions of time-dependent drug-drug interactions by determination of cytosolic drug concentrations. *Sci. Rep.* **9**, 1–14 (2019).
167. Chiba, M., Ishii, Y. & Sugiyama, Y. Prediction of Hepatic Clearance in Human From In Vitro Data for Successful Drug Development. *AAPS J.* **11**, 262–276 (2009).
168. Abduljalil, K., Furness, P., Johnson, T. N., Rostami-Hodjegan, A. & Soltani, H. Anatomical, physiological

- and metabolic changes with gestational age during normal pregnancy: A database for parameters required in physiologically based pharmacokinetic modelling. *Clin. Pharmacokinet.* **51**, 365–396 (2012).
169. Ghobadi, C. *et al.* Application of a systems approach to the bottom-up assessment of pharmacokinetics in obese patients: Expected variations in clearance. *Clin. Pharmacokinet.* **50**, 809–822 (2011).
 170. Heimbach, T. *et al.* Physiologically-Based Pharmacokinetic Modeling in Renal and Hepatic Impairment Populations: A Pharmaceutical Industry Perspective. *Clin. Pharmacol. Ther.* **0**, 1–14 (2020).
 171. Kovar, L. *et al.* Comprehensive Parent-Metabolite PBPK/PD Modeling Insights into Nicotine Replacement Therapy Strategies Key Points. (123AD). doi:10.1007/s40262-020-00880-4
 172. Zhao, P. *et al.* Evaluation of exposure change of nonrenally eliminated drugs in patients with chronic kidney disease using physiologically based pharmacokinetic modeling and simulation. *J. Clin. Pharmacol.* **52**, 91–108 (2012).
 173. Plowchalk, D. R. & Rowland Yeo, K. Prediction of drug clearance in a smoking population: Modeling the impact of variable cigarette consumption on the induction of CYP1A2. *Eur. J. Clin. Pharmacol.* **68**, 951–960 (2012).
 174. Otsuka, Y., Choules, M. P., Bonate, P. L. & Komatsu, K. Physiologically-Based Pharmacokinetic Modeling for the Prediction of a Drug–Drug Interaction of Combined Effects on P-glycoprotein and Cytochrome P450 3A. *CPT Pharmacometrics Syst. Pharmacol.* **9**, 659–669 (2020).
 175. Taskar, K. S. *et al.* Physiologically-Based Pharmacokinetic Models for Evaluating Membrane Transporter Mediated Drug–Drug Interactions: Current Capabilities, Case Studies, Future Opportunities, and Recommendations. *Clinical Pharmacology and Therapeutics* **107**, 1082–1115 (2020).
 176. Dickinson, G. L., Lennard, M. S., Tucker, G. T. & Rostami-Hodjegan, A. The use of mechanistic DM-PK-PD modelling to assess the power of pharmacogenetic studies – CYP2C9 and warfarin as an example. *Br. J. Clin. Pharmacol. Br J Clin Pharmacol* **641**, 14–26 (2007).
 177. Storelli, F., Desmeules, J. & Daali, Y. Physiologically-Based Pharmacokinetic Modeling for the Prediction of CYP2D6-Mediated Gene–Drug–Drug Interactions. *CPT Pharmacometrics Syst. Pharmacol.* **8**, 567–576 (2019).
 178. Türk, D. *et al.* Physiologically Based Pharmacokinetic Models for Prediction of Complex CYP2C8 and OATP1B1 (SLCO1B1) Drug-Drug-Gene Interactions: A Modeling Network of Gemfibrozil, Repaglinide, Pioglitazone, Rifampicin, Clarithromycin and Itraconazole. *Clin. Pharmacokinet.* **58**, 1595–1607 (123AD).
 179. Johnson, T. N., Rostami-Hodjegan, A. & Tucker, G. T. Prediction of the clearance of eleven drugs and associated variability in neonates, infants and children. *Clin. Pharmacokinet.* **45**, 931–956 (2006).
 180. Inoue, S. *et al.* Prediction of in vivo drug clearance from in vitro data. II: Potential inter-ethnic differences. *Xenobiotica* **36**, 499–513 (2006).
 181. Prasad, B. *et al.* Ontogeny of Hepatic Drug Transporters as Quantified by LC-MS/MS Proteomics. *Clin. Pharmacol. Ther.* 362–370 (2016). doi:10.1002/cpt.409
 182. Achour, B. *et al.* Liquid Biopsy Enables Quantification of the Abundance and Interindividual Variability of Hepatic Enzymes and Transporters. *Clin. Pharmacol. Ther.* **109**, 222–232 (2021).
 183. Melillo, N., Darwich, A. S., Magni, P. & Rostami-Hodjegan, A. Accounting for inter-correlation between enzyme abundance: a simulation study to assess implications on global sensitivity analysis within physiologically-based pharmacokinetics. *J. Pharmacokinet. Pharmacodyn.* **6**, (2019).
 184. Ohtsuki, S. *et al.* Simultaneous absolute protein quantification of transporters, cytochromes P450, and UDP-glucuronosyltransferases as a novel approach for the characterization of individual human liver: Comparison with mRNA levels and activities. *Drug Metab. Dispos.* **40**, 83–92 (2012).
 185. Drozdik, M. *et al.* Protein Abundance of Clinically Relevant Drug-Metabolizing Enzymes in the Human Liver and Intestine: A Comparative Analysis in Paired Tissue Specimens. *Clin. Pharmacol. Ther.* **104**, 515–524 (2018).
 186. Vildhede, A., Kimoto, E., Pelis, R. M., Rodrigues, A. D. & Varma, M. V. S. Quantitative Proteomics and

- Mechanistic Modeling of Transporter-Mediated Disposition in Nonalcoholic Fatty Liver Disease. *Clin. Pharmacol. Ther.* **107**, 1128–1137 (2020).
187. Kunze, A., Huwyler, J., Poller, B., Gutmann, H. & Camenisch, G. In vitro-in vivo extrapolation method to predict human renal clearance of drugs. *J. Pharm. Sci.* **103**, 994–1001 (2014).
 188. Scotcher, D., Jones, C., Posada, M., Galetin, A. & Rostami-Hodjegan, A. Key to Opening Kidney for In Vitro-In Vivo Extrapolation Entrance in Health and Disease: Part II: Mechanistic Models and In Vitro-In Vivo Extrapolation. *AAPS J.* **18**, 1082–1094 (2016).
 189. Scotcher, D. *et al.* Mechanistic Models as Framework for Understanding Biomarker Disposition: Prediction of Creatinine-Drug Interactions. *CPT Pharmacometrics Syst. Pharmacol.* **9**, 282–293 (2020).
 190. Jones, H. M. *et al.* Mechanistic Pharmacokinetic Modelling for the Prediction of Transporter-mediated Disposition in Human from Sandwich Culture Human Hepatocyte Data. *Drug Metab Dispos.* (2012). doi:10.1124/dmd.111.042994
 191. Nakakariya, M. *et al.* In vivo biliary clearance should be predicted by intrinsic biliary clearance in sandwich-cultured hepatocytes. *Drug Metab. Dispos.* **40**, 602–609 (2012).
 192. Francis, L. J., Houston, J. B. & Hallifax, D. Impact of plasma protein binding in drug clearance prediction: A database analysis of published studies and implications for in vitro-in vivo extrapolation. *Drug Metab. Dispos.* **49**, 188–201 (2021).
 193. McNamara, P. J. & Alcorn, J. Protein binding predictions in infants. *AAPS PharmSci* **4**, (2002).
 194. Poggesi, I. *et al.* Pharmacokinetics in special populations. *Drug Metabolism Reviews* **41**, 422–454 (2009).
 195. Celestin, M. N. & Musteata, F. M. Impact of Changes in Free Concentrations and Drug-Protein Binding on Drug Dosing Regimens in Special Populations and Disease States. *J. Pharm. Sci.* (2021). doi:10.1016/j.xphs.2021.05.018
 196. Rodgers, T. & Rowland, M. Mechanistic Approaches to Volume of Distribution Predictions: Understanding the Processes. *Pharm. Res.* **24**, 918–933 (2007).
 197. Poulin, P. & Theil, F. P. Prediction of pharmacokinetics prior to in vivo studies. 1. Mechanism-based prediction of volume of distribution. *J. Pharm. Sci.* **91**, 129–156 (2002).
 198. Poulin, P. & Theil, F. P. Prediction of pharmacokinetics prior to in vivo studies. II. Generic physiologically based pharmacokinetic models of drug disposition. *J. Pharm. Sci.* **91**, 1358–1370 (2002).
 199. Obach, R. S. *et al.* The prediction of human pharmacokinetic parameters from preclinical and in vitro metabolism data. *J. Pharmacol. Exp. Ther.* **283**, 46–58 (1997).
 200. Budha, N. R. *et al.* Evaluation of Cytochrome P450 3A4-Mediated Drug-Drug Interaction Potential for Cobimetinib Using Physiologically Based Pharmacokinetic Modeling and Simulation. *Clin. Pharmacokinet.* **55**, 1435–1445 (2016).
 201. Vaidhyanathan, S. *et al.* Bioequivalence Comparison of Pediatric Dasatinib Formulations and Elucidation of Absorption Mechanisms Through Integrated PBPK Modeling. *J. Pharm. Sci.* **108**, 741–749 (2019).
 202. Michelet, R., Van Bocxlaer, J., Allegaert, • Karel & Vermeulen, A. The use of PBPK modeling across the pediatric age range using propofol as a case. doi:10.1007/s10928-018-9607-8
 203. Rostami-Hodjegan, A. Reverse Translation in PBPK and QSP: Going Backwards in Order to Go Forward With Confidence. *Clin. Pharmacol. Ther.* **103**, 224–232 (2018).
 204. Shebley, M. *et al.* Physiologically Based Pharmacokinetic Model Qualification and Reporting Procedures for Regulatory Submissions: A Consortium Perspective. *Clin. Pharmacol. Ther.* **104**, 88–110 (2018).
 205. Tsamandouras, N., Rostami-Hodjegan, A. & Aarons, L. Combining the ‘bottom up’ and ‘top down’ approaches in pharmacokinetic modelling: Fitting PBPK models to observed clinical data. *Br. J. Clin. Pharmacol.* **79**, 48–55 (2015).

206. Doki, K. *et al.* Implications of intercorrelation between hepatic CYP3A4-CYP2C8 enzymes for the evaluation of drug–drug interactions: a case study with repaglinide. *Br. J. Clin. Pharmacol.* **84**, 972–986 (2018).
207. Peters, S. A. & Dolgos, H. Requirements to Establishing Confidence in Physiologically Based Pharmacokinetic (PBPK) Models and Overcoming Some of the Challenges to Meeting Them. *Clin. Pharmacokinet.* **58**, 1355–1371 (2019).
208. Iliadis, A. Structural identifiability and sensitivity. *J. Pharmacokinet. Pharmacodyn.* **9**, (2019).
209. Slob, W., Janssen, P. H. M. & Van Den Hof, J. M. Structural identifiability of PBPK models: Practical consequences for modeling strategies and study designs. *Crit. Rev. Toxicol.* **27**, 261–272 (1997).
210. Yates, J. W. T. Structural identifiability of physiologically based pharmacokinetic models. *J. Pharmacokinet. Pharmacodyn.* **33**, 421–439 (2006).
211. Muñoz-Tamayo, R. *et al.* Review: To be or not to be an identifiable model. Is this a relevant question in animal science modelling? *Animal* **12**, 701–712 (2018).
212. Bellman, R. & Åström, K. J. On structural identifiability. *Math. Biosci.* **7**, 329–339 (1970).
213. Godfrey, K. R., Jones, R. P. & Brown, R. F. Identifiable pharmacokinetic models: The role of extra inputs and measurements. *J. Pharmacokinet. Biopharm.* **8**, 633–648 (1980).
214. Cheung, S. Y. A., Majid, O., Yates, J. W. T. & Aarons, L. Structural identifiability analysis and reparameterisation (parameter reduction) of a cardiovascular feedback model. *Eur. J. Pharm. Sci.* **46**, 259–271 (2012).
215. Cheung, S. Y. A., Yates, J. W. T. & Aarons, L. The design and analysis of parallel experiments to produce structurally identifiable models. *J. Pharmacokinet. Pharmacodyn.* **40**, 93–100 (2013).
216. Garcia, R. I., Ibrahim, J. G., Wambaugh, J. F., Kenyon, E. M. & Setzer, R. W. Identifiability of PBPK models with applications to dimethylarsinic acid exposure. *J. Pharmacokinet. Pharmacodyn.* **42**, 591–609 (2015).
217. Hengl, S., Kreutz, C., Timmer, J. & Maiwald, T. Data-based identifiability analysis of non-linear dynamical models. *Bioinformatics* **23**, 2612–2618 (2007).
218. Gueorguieva, I. *et al.* Optimal design for multivariate response pharmacokinetic models. *J. Pharmacokinet. Pharmacodyn.* **33**, 97–124 (2006).
219. McNally, K., Cotton, R. & Loizou, G. D. A workflow for global sensitivity analysis of PBPK models. *Front. Pharmacol.* **JUN**, 1–22 (2011).
220. Saltelli, A., Tarantola, S., Campolongo, F. & Ratto, M. *Sensitivity analysis in practice: a guide to assessing scientific models (Google eBook)*. (2004).
221. Razavi, S. *et al.* The Future of Sensitivity Analysis: An essential discipline for systems modeling and policy support. *Environ. Model. Softw.* **137**, 104954 (2021).
222. Yeo, K. R., Kenny, J. R. & Rostami-Hodjegan, A. Application of in vitro-in vivo extrapolation (IVIVE) and physiologically based pharmacokinetic (PBPK) modelling to investigate the impact of the CYP2C8 polymorphism on rosiglitazone exposure. *Eur. J. Clin. Pharmacol.* **69**, 1311–1320 (2013).
223. Gueorguieva, I., Nestorov, I. A. & Rowland, M. Reducing whole body physiologically based pharmacokinetic models using global sensitivity analysis: Diazepam case study. *J. Pharmacokinet. Pharmacodyn.* **33**, 1–27 (2006).
224. Hsieh, N. H., Reisfeld, B., Bois, F. Y. & Chiu, W. A. Applying a global sensitivity analysis workflow to improve the computational efficiencies in physiologically-based pharmacokinetic modeling. *Front. Pharmacol.* **9**, 1–17 (2018).
225. Scherholz, M. L., Forder, J. & Androulakis, I. P. A framework for 2-stage global sensitivity analysis of GastroPlus™ compartmental models. *J. Pharmacokinet. Pharmacodyn.* **45**, 309–327 (2018).
226. Melillo, N. *et al.* Inter-compound and Intra-compound Global Sensitivity Analysis of a Physiological Model for Pulmonary Absorption of Inhaled Compounds. *AAPS J.* **22**, 1–11 (2020).

227. Melillo, N., Aarons, L., Magni, P. & Darwich, A. S. Variance based global sensitivity analysis of physiologically based pharmacokinetic absorption models for BCS I-IV drugs. doi:10.1007/s10928-018-9615-8
228. Yau, E. *et al.* Global Sensitivity Analysis of the Rodgers and Rowland Model for Prediction of Tissue: Plasma Partitioning Coefficients: Assessment of the Key Physiological and Physicochemical Factors That Determine Small-Molecule Tissue Distribution. *AAPS J.* **22**, (2020).
229. Barton, H. A. *et al.* Characterizing uncertainty and variability in physiologically based pharmacokinetic models: State of the science and needs for research and implementation. *Toxicol. Sci.* **99**, 395–402 (2007).
230. Gelman, A., Bois, F. & Jiang, J. Physiological Pharmacokinetic Analysis Using Population Modeling and Informative Prior Distributions. *J. Am. Stat. Assoc.* **91**, 1400–1412 (1996).
231. Kalbfleisch, J. G. *Probability and Statistical Inference - Volume 2: Statistical Inference.* (Springer Nature, 1985).
232. Woodruff, T. J. & Bois, F. Y. Optimization issues in physiological toxicokinetic modeling: a case study with benzene. *Toxicol. Lett.* **69**, 181–196 (1993).
233. Yang, J. *et al.* Implications of mechanism-based inhibition of CYP2D6 for the pharmacokinetics and toxicity of MDMA. *J. Psychopharmacol.* **20**, 842–849 (2006).
234. Goldberg, D. *Genetic Algorithms in Search, Optimization and Machine Learning.* (Addison-Wesley Publishing Co., Inc., 1989).
235. Peters, S. A. Identification of intestinal loss of a drug through physiologically based pharmacokinetic simulation of plasma concentration-time profiles. *Clin. Pharmacokinet.* **47**, 245–259 (2008).
236. Nestorov, I. Modelling and simulation of variability and uncertainty in toxicokinetics and pharmacokinetics. *Toxicol. Lett.* **120**, 411–420 (2001).
237. Bonate, P. *Pharmacokinetic pharmacodynamic modeling and simulation.*
238. Woodruff, T. J., Bois, F. Y., Auslander, D. & Spear, R. C. Structure and Parameterization of Pharmacokinetic Models: Their Impact on Model Predictions. *Risk Anal.* **12**, 189–201 (1992).
239. Farrar, D., Allen, B., Crump, K. & Shipp, A. Evaluation of uncertainty in input parameters to pharmacokinetic models and the resulting uncertainty in output. *Toxicol. Lett.* **49**, 371–385 (1989).
240. Krewski, D., Wang, Y., Bartlett, S. & Krishnan, K. Uncertainty, Variability, and Sensitivity Analysis in Physiological Pharmacokinetic Models. *J. Biopharm. Stat.* **5**, 235–243 (1995).
241. Seng, K. Y., Nestorov, I. & Vicini, P. Physiologically based pharmacokinetic modeling of drug disposition in rat and human: A fuzzy arithmetic approach. *Pharm. Res.* **25**, 1771–1781 (2008).
242. Seng, K. Y., Vicini, P. & Nestorov, I. A. A fuzzy physiologically based pharmacokinetic modeling framework to predict drug disposition in humans. *Annu. Int. Conf. IEEE Eng. Med. Biol. - Proc.* 6485–6488 (2006). doi:10.1109/IEMBS.2006.260879
243. Bois, F. Y. Applications of population approaches in toxicology. *Toxicol. Lett.* **120**, 385–394 (2001).
244. Bernillon, P. & Bois, F. Y. Statistical Issues in Toxicokinetic Modeling: A Bayesian Perspective. *Environ. Health Perspect.* **108**, 883–893 (2000).
245. Krauss, M., Tappe, K., Schuppert, A., Kuepfer, L. & Goerlitz, L. Bayesian Population Physiologically-Based Pharmacokinetic (PBPK) Approach for a Physiologically Realistic Characterization of Interindividual Variability in Clinically Relevant Populations Physiologically-Based Pharmacokinetic (PBPK) Approach for a Physiologically Realistic Characterization of Interindividual Variability in Clinically Relevant Populations. (2015). doi:10.1371/journal.pone.0139423
246. Krauss, M. *et al.* Using Bayesian-PBPK modeling for assessment of inter-individual variability and subgroup stratification. *Silico Pharmacol.* **11**, 1:6 (2013).
247. Ette, E. I. & Williams, P. J. Population pharmacokinetics I: Background, concepts, and models. *Ann. Pharmacother.* **38**, 1702–1706 (2004).

248. Ette, E. I. & Williams, P. J. Population pharmacokinetics II: Estimation methods. *Ann. Pharmacother.* **38**, 1907–1915 (2004).
249. Ette, E. I., Williams, P. J. & Lane, J. R. Population pharmacokinetics III: Design, analysis, and application of population pharmacokinetic studies. *Ann. Pharmacother.* **38**, 2136–2144 (2004).
250. Sheiner, L. B. & Ludden, T. M. Population pharmacokinetics/dynamics. *Annu. Rev. Pharmacol. Toxicol.* **32**, 185–209 (1992).
251. Sheiner, L. B. & Steimer, J.-L. Pharmacokinetic/pharmacodynamic modeling in drug development. *Annu. Rev. Pharmacol. Toxicol.* **40**, 67–95 (2000).
252. Price, P. S. *et al.* Modeling Interindividual Variation in Physiological Factors Used in PBPK Models of Humans. *Crit. Rev. Toxicol.* **33**, 469–503 (2003).
253. McKay, M. D., Beckman, R. J. & Conover, W. J. A Comparison of Three Methods for Selecting Values of Input Variables in the Analysis of Output from a Computer Code. *Technometrics* **21**, 239 (1979).
254. Wakefield, J. & Bennett, J. The Bayesian Modeling of Covariates for Population Pharmacokinetic Models. *J. Am. Stat. Assoc.* **91**, 917–927 (1996).
255. Wakefield, J. The bayesian analysis of population pharmacokinetic models. *J. Am. Stat. Assoc.* **91**, 62–75 (1996).
256. Gelman, A. & Rubin, D. B. Markov chain Monte Carlo methods in biostatistics. *Stat. Methods Med. Res.* **5**, 339–355 (1996).
257. Gibiansky, L., Gibiansky, E. & Bauer, R. Comparison of Nonmem 7.2 estimation methods and parallel processing efficiency on a target-mediated drug disposition model. *J. Pharmacokinet. Pharmacodyn.* **39**, 17–35 (2012).
258. Langdon, G., Gueorguieva, I., Aarons, L. & Karlsson, M. Linking preclinical and clinical whole-body physiologically based pharmacokinetic models with prior distributions in NONMEM. *Eur. J. Clin. Pharmacol.* **63**, 485–498 (2007).
259. Gisleskog, P. O., Karlsson, M. O. & Beal, S. L. Use of prior information to stabilize a population data analysis. *J. Pharmacokinet. Pharmacodyn.* **29**, 473–505 (2002).
260. Gueorguieva, I., Aarons, L. & Rowland, M. Diazepam pharmacokinetics from preclinical to phase I using a Bayesian population physiologically based pharmacokinetic model with informative prior distributions in Winbugs. *J. Pharmacokinet. Pharmacodyn.* **33**, 571–594 (2006).
261. Okino, M. S. & Mavrovouniotis, M. L. Simplification of mathematical models of chemical reaction systems. *Chem. Rev.* **98**, 391–408 (1998).
262. Brochot, C., Tóth, J. & Bois, F. Y. Lumping in pharmacokinetics. *J. Pharmacokinet. Pharmacodyn.* **32**, 719–736 (2005).
263. Dokoumetzidis, A. & Aarons, L. A method for robust model order reduction in pharmacokinetics. *J. Pharmacokinet. Pharmacodyn.* **36**, 613–628 (2009).
264. Itohara, K. *et al.* A Minimal Physiologically-Based Pharmacokinetic Model for Tacrolimus in Living-Donor Liver Transplantation: Perspectives Related to Liver Regeneration and the cytochrome P450 3A5 (CYP3A5) Genotype. *CPT Pharmacometrics Syst. Pharmacol.* **8**, 587–595 (2019).
265. Cao, Y. & Jusko, W. J. Applications of minimal physiologically-based pharmacokinetic models. *J. Pharmacokinet. Pharmacodyn.* **39**, 711–723 (2012).
266. Kuemmel, C. *et al.* Consideration of a Credibility Assessment Framework in Model-Informed Drug Development: Potential Application to Physiologically-Based Pharmacokinetic Modeling and Simulation. *CPT Pharmacometrics Syst. Pharmacol.* **9**, 21–28 (2020).
267. CM, F. A model qualification method for mechanistic physiological QSP models to support model-informed drug development. *CPT pharmacometrics Syst. Pharmacol.* **5**, 43–53 (2016).
268. Grimstein, M. *et al.* Physiologically Based Pharmacokinetic Modeling in Regulatory Science: An Update From the U.S. Food and Drug Administration’s Office of Clinical Pharmacology. *Journal of*

- Pharmaceutical Sciences* **108**, 21–25 (2019).
269. Johnson, T. N., Boussery, K., Rowland-Yeo, K., Tucker, G. T. & Rostami-Hodjegan, A. A semi-mechanistic model to predict the effects of liver cirrhosis on drug clearance. *Clin. Pharmacokinet.* **49**, 189–206 (2010).
270. W, Z. *et al.* Predictive Performance of Physiologically Based Pharmacokinetic and Population Pharmacokinetic Modeling of Renally Cleared Drugs in Children. *CPT pharmacometrics Syst. Pharmacol.* **5**, 475–483 (2016).
271. Sayama, H., H, T., H, K., M, K. & M, I. Application of a physiologically based pharmacokinetic model informed by a top-down approach for the prediction of pharmacokinetics in chronic kidney disease patients. *AAPS J.* **16**, 1018–1028 (2014).
272. Cheeti, S., Budha, N. R., Rajan, S., Dresser, M. J. & JY, J. A physiologically based pharmacokinetic (PBPK) approach to evaluate pharmacokinetics in patients with cancer. *Biopharm. Drug Dispos.* **34**, 141–154 (2013).
273. Vieira, M. D. L. T. *et al.* PBPK model describes the effects of comedication and genetic polymorphism on systemic exposure of drugs that undergo multiple clearance pathways. *Clin. Pharmacol. Ther.* **95**, 550–557 (2014).
274. Abduljalil, K., Cain, T., Humphries, H. & Rostami-Hodjegan, A. Deciding on Success Criteria for Predictability of Pharmacokinetic Parameters from In Vitro Studies: An Analysis Based on In Vivo Observations. *Drug Metab. Dispos.* **42**, 1478–1484 (2014).
275. Guest, E. J., Aarons, L., Houston, J. B., Rostami-Hodjegan, A. & Galetin, A. Critique of the two-fold measure of prediction success for ratios: Application for the assessment of drug-drug interactions. *Drug Metab. Dispos.* **39**, 170–173 (2011).
276. Giacomini, K. M. *et al.* Membrane transporters in drug development. *Nat. Rev. Drug Discov.* **2010** **9**, 215–236 (2010).
277. Chu, X. *et al.* Intracellular Drug Concentrations and Transporters: Measurement, Modeling, and Implications for the Liver. *Clin. Pharmacol. Ther.* **94**, 126 (2013).
278. Shugarts, S. & Benet, L. Z. The Role of Transporters in the Pharmacokinetics of Orally Administered Drugs. *Pharm. Res.* **26**, 2039 (2009).
279. Balazki, P., Schaller, S., Eissing, T. & Lehr, T. A Quantitative Systems Pharmacology Kidney Model of Diabetes Associated Renal Hyperfiltration and the Effects of SGLT Inhibitors. *CPT Pharmacometrics Syst. Pharmacol.* **7**, 788–797 (2018).
280. Burghaus, R. *et al.* Computational investigation of potential dosing schedules for a switch of medication from warfarin to rivaroxaban—an oral, direct Factor Xa inhibitor. *Front. Physiol.* **0**, 417 (2014).
281. C, T. *et al.* Model-based contextualization of in vitro toxicity data quantitatively predicts in vivo drug response in patients. *Arch. Toxicol.* **91**, 865–883 (2017).
282. Riggs, M. M., Bennetts, M., van der Graaf, P. H. & Martin, S. Integrated pharmacometrics and systems pharmacology model-based analyses to guide GnRH receptor modulator development for management of endometriosis. *CPT pharmacometrics Syst. Pharmacol.* **1**, (2012).
283. U.S. Food and Drug Administration Center for Drug Evaluation and Research (CDER). Guidance for Industry Waiver of In Vivo Bioavailability and Bioequivalence Studies for Immediate-Release Solid Oral Dosage Forms Based on a Biopharmaceutics Classification System. (2017). Available at: <https://www.fda.gov/media/70963/download>. (Accessed: 7th November 2020)
284. European Medicines Agency Committee for Medicinal Products for Human use (CHMP). Guideline on the investigation of bioequivalence (revision 1). (2010). Available at: https://www.ema.europa.eu/en/documents/scientific-guideline/guideline-investigation-bioequivalence-rev1_en.pdf. (Accessed: 7th November 2020)
285. Bransford, P. *et al.* ICH M9 Guideline in Development on Biopharmaceutics Classification System-Based

- Biowaivers: An Industrial Perspective from the IQ Consortium. *Molecular Pharmaceutics* **17**, 361–372 (2020).
286. Loiosio-Konstantinidis, I. *et al.* Application of the relationship between pharmacokinetics and pharmacodynamics in drug development and therapeutic equivalence: a PEARL review. *J. Pharm. Pharmacol.* **71**, 699–723 (2019).
287. Yazdaniyan, M., Briggs, K., Jankovsky, C. & Hawi, A. The 'High Solubility' Definition of the Current FDA Guidance on Biopharmaceutical Classification System May Be Too Strict for Acidic Drugs. *Pharm. Res.* **21**, 293–299 (2004).
288. Hofsäss, M. A. & Dressman, J. Evaluation of Differences in Dosage form Performance of Generics Using BCS-Based Biowavier Specifications and Biopharmaceutical Modeling – Case Examples Amoxicillin and Doxycycline. *J. Pharm. Sci.* (2020). doi:10.1016/j.xphs.2020.04.011
289. Kovačević, I., Parojčić, J., Homšek, I., Tubić-Grozdanis, M. & Langguth, P. Justification of biowaiver for carbamazepine, a low soluble high permeable compound, in solid dosage forms based on IVIVC and gastrointestinal simulation. *Mol. Pharm.* **6**, 40–47 (2009).
290. Cristofaletti, R. *et al.* Past, Present, and Future of Bioequivalence: Improving Assessment and Extrapolation of Therapeutic Equivalence for Oral Drug Products. *J. Pharm. Sci.* **107**, 2519–2530 (2018).
291. Pepin, X. J. H. *et al.* Justification of Drug Product Dissolution Rate and Drug Substance Particle Size Specifications Based on Absorption PBPK Modeling for Lesinurad Immediate Release Tablets. (2016). doi:10.1021/acs.molpharmaceut.6b00497
292. Pepin, X. J. H. *et al.* Bridging in vitro dissolution and in vivo exposure for acalabrutinib. Part I. Mechanistic modelling of drug product dissolution to derive a P-PSD for PBPK model input. *Eur. J. Pharm. Biopharm.* **142**, 421–434 (2019).
293. Babiskin, A. H. & Zhang, X. Application of Physiologically Based Absorption Modeling for Amphetamine Salts Drug Products in Generic Drug Evaluation. *J. Pharm. Sci.* **104**, 3170–3182 (2015).
294. Fan, J., Zhang, X. & Zhao, L. Utility of Physiologically Based Pharmacokinetic Absorption Modeling to Predict the Impact of Salt-to-Base Conversion on Prasugrel HCl Product Bioequivalence in the Presence of Proton Pump Inhibitors. *AAPS J.* **19**, 1479–1486 (2017).
295. Doki, K., Darwich, A. S., Patel, N. & Rostami-Hodjegan, A. Virtual bioequivalence for achlorhydric subjects: The use of PBPK modelling to assess the formulation-dependent effect of achlorhydria. *Eur. J. Pharm. Sci.* **109**, 111–120 (2017).
296. Colón-Useche, S. *et al.* Investigating the Discriminatory Power of BCS-Biowaiver in Vitro Methodology to Detect Bioavailability Differences between Immediate Release Products Containing a Class I Drug. *Mol. Pharm.* **12**, 3167–3174 (2015).
297. Ruiz-Picazo, A., Lozoya-Agullo, I., González-Álvarez, I., Bermejo, M. & González-Álvarez, M. Effect of excipients on oral absorption process according to the different gastrointestinal segments. *Expert Opin. Drug Deliv.* **0**, (2020).
298. Chen, M. L., Sadrieh, N. & Yu, L. Impact of osmotically active excipients on bioavailability and bioequivalence of BCS class III drugs. *AAPS J.* **15**, 1043–1050 (2013).
299. Al-Ali, A. A. A., Nielsen, R. B., Steffansen, B., Holm, R. & Nielsen, C. U. Nonionic surfactants modulate the transport activity of ATP-binding cassette (ABC) transporters and solute carriers (SLC): Relevance to oral drug absorption. *Int. J. Pharm.* **566**, 410–433 (2019).
300. Flanagan, T. Potential for pharmaceutical excipients to impact absorption: A mechanistic review for BCS Class 1 and 3 drugs. *Eur. J. Pharm. Biopharm.* **141**, 130–138 (2019).
301. García-Arieta, A. Interactions between active pharmaceutical ingredients and excipients affecting bioavailability: Impact on bioequivalence. *Eur. J. Pharm. Sci.* **65**, 89–97 (2014).
302. McAllister, M. *et al.* Developing Clinically Relevant Dissolution Specifications for Oral Drug Products—Industrial and Regulatory Perspectives. *Pharmaceutics* **12**, 19 (2019).
303. Stillhart, C. *et al.* PBPK Absorption Modeling: Establishing the In Vitro–In Vivo Link—Industry

- Perspective. *AAPS Journal* **21**, (2019).
304. Lennernäs, H. Regional intestinal drug permeation: Biopharmaceutics and drug development. *Eur. J. Pharm. Sci.* **57**, 333–341 (2014).
 305. Abend, A. *et al.* Dissolution and Translational Modeling Strategies Enabling Patient-Centric Drug Product Development: the M-CERSI Workshop Summary Report. *AAPS J.* **20**, (2018).
 306. Zhang, X. *et al.* Mechanistic Oral Absorption Modeling and Simulation for Formulation Development and Bioequivalence Evaluation: Report of an FDA Public Workshop. *CPT Pharmacometrics Syst. Pharmacol.* **6**, 492–495 (2017).
 307. Stillhart, C. *et al.* Characterising Drug Release from Immediate-Release Formulations of a Poorly Soluble Compound, Basmisanil, Through Absorption Modelling and Dissolution Testing. *AAPS J.* **19**, 827–836 (2017).
 308. Pepin, X. J. *et al.* Current State and Future Expectations of Translational Modeling Strategies to Support Drug Product Development, Manufacturing Changes and Controls: A Workshop Summary Report. *J. Pharm. Sci.* (2020). doi:10.1016/j.xphs.2020.04.021
 309. Heimbach, T. *et al.* Dissolution and Translational Modeling Strategies Toward Establishing an In Vitro-In Vivo Link—a Workshop Summary Report. *AAPS J.* **21**, 29 (2019).
 310. Al-Tabakha, M. M. & Alomar, M. J. In Vitro Dissolution and in Silico Modeling Shortcuts in Bioequivalence Testing. *Pharmaceutics* **12**, 45 (2020).
 311. Zhang, X. *et al.* Integrating *In Vitro*, Modeling, and *In Vivo* Approaches to Investigate Warfarin Bioequivalence. *CPT Pharmacometrics Syst. Pharmacol.* **6**, 523–531 (2017).
 312. Ibarra, M. *et al.* Integration of in vitro biorelevant dissolution and in silico PBPK model of carvedilol to predict bioequivalence of oral drug products. *Eur. J. Pharm. Sci.* **118**, 176–182 (2018).
 313. Mitra, A., Kesisoglou, F. & Dogterom, P. Application of Absorption Modeling to Predict Bioequivalence Outcome of Two Batches of Etoricoxib Tablets. *AAPS PharmSciTech* **16**, 76–84 (2015).
 314. Jereb, R., Opara, J., Legen, I., Petek, B. & Grabnar-Peklar, D. In vitro–In vivo Relationship and Bioequivalence Prediction for Modified-Release Capsules Based on a PBPK Absorption Model. *AAPS PharmSciTech* **21**, 1–11 (2020).
 315. Rebeka, J. *et al.* PBPK Absorption Modeling of Food Effect and Bioequivalence in Fed State for Two Formulations with Crystalline and Amorphous Forms of BCS 2 Class Drug in Generic Drug Development. *AAPS PharmSciTech* **20**, 1–10 (2019).
 316. Basu, S. *et al.* Physiologically Based Pharmacokinetic Modeling to Evaluate Formulation Factors Influencing Bioequivalence of Metoprolol Extended-Release Products. *J. Clin. Pharmacol.* **59**, 1252–1263 (2019).
 317. Wedagedera, J., Cain, T., Pathak, S. M. & Jamei, M. *Virtual Bioequivalence Assessment of Two Tramadol Formulations using the Advanced Dissolution Absorption and Metabolism (ADAM) Model via Simcyp R Package.* (2017).
 318. Pathak, S. M. *et al.* Establishment of Virtual Bioequivalence Using Population-Based PBPK Modelling: Application to the Setting of Dissolution Limits. *AAPS J* **11**, (1997).
 319. U.S. Food and Drug Administration Center for Drug Evaluation and Research (CDER). Guidance for Industry Bioequivalence Studies with Pharmacokinetic Endpoints for Drugs Submitted Under an ANDA. 24 (2013). Available at: <https://www.fda.gov/media/87219/download>. (Accessed: 7th November 2020)
 320. U.S. Food and Drug Administration Center for Drug Evaluation and Research (CDER). Guidance for Industry Food-Effect Bioavailability and Fed Bioequivalence Studies. (2002). Available at: <https://www.fda.gov/media/70945/download>. (Accessed: 7th November 2020)
 321. Tistaert, C. *et al.* Food Effect Projections via Physiologically Based Pharmacokinetic Modeling: Predictive Case Studies. *J. Pharm. Sci.* **108**, 592–602 (2019).
 322. Jones, H. M. *et al.* Physiologically based pharmacokinetic modeling in drug discovery and development:

- A pharmaceutical industry perspective. *Clinical Pharmacology and Therapeutics* **97**, 247–262 (2015).
323. Harris, R. Z., Jang, G. R. & Tsunoda, S. Dietary Effects on Drug Metabolism and Transport. *Clinical Pharmacokinetics* **42**, 1071–1088 (2003).
 324. Dresser, G. K., Kim, R. B. & Bailey, D. G. Effect of Grapefruit Juice Volume on the Reduction of Fexofenadine Bioavailability: Possible Role of Organic Anion Transporting Polypeptides*. *Clin. Pharmacol. Ther.* **77**, 170–177 (2005).
 325. Dresser, G. Fruit juices inhibit organic anion transporting polypeptide-mediated drug uptake to decrease the oral availability of fexofenadine. *Clin. Pharmacol. Ther.* **71**, 11–20 (2002).
 326. Misaka, S. *et al.* Green Tea Ingestion Greatly Reduces Plasma Concentrations of Nadolol in Healthy Subjects. *Clin. Pharmacol. Ther.* **95**, 432–438 (2014).
 327. Won, C. S., Oberlies, N. H. & Paine, M. F. Mechanisms underlying food-drug interactions: Inhibition of intestinal metabolism and transport. *Pharmacol. Ther.* **136**, 186–201 (2012).
 328. Lahner, E., Annibale, B. & Delle Fave, G. Systematic review: impaired drug absorption related to the co-administration of antisecretory therapy. *Aliment. Pharmacol. Ther.* **29**, 1219–1229 (2009).
 329. U.S Food and Drug Administration. [Docket No. FDA-2018-N-1820], Framework for Assessing pH-Dependent Drug-Drug Interactions: Establishment of a Public Docket; Request for Comments. Available at: <https://www.govinfo.gov/content/pkg/FR-2018-05-22/pdf/2018-10927.pdf>. (Accessed: 3rd August 2020)
 330. Mitra, A. *et al.* Prediction of pH-Dependent Drug-Drug Interactions for Basic Drugs Using Physiologically Based Biopharmaceutics Modeling: Industry Case Studies. *J. Pharm. Sci.* **109**, 1380–1394 (2020).
 331. Levy, G. Relationship between rate of elimination of tubocurarine and rate of decline of its pharmacological activity. *Br. J. Anaesth.* **36**, 694–695 (1964).
 332. Galeazzi, R. L., Benet, L. Z. & Sheiner, L. B. Relationship between the pharmacokinetics and pharmacodynamics of procainamide. *Clin. Pharmacol. Ther.* **20**, 278–89 (1976).
 333. Frazier, E. P., Schneider, T. & Michel, M. C. Effects of gender, age and hypertension on β -adrenergic receptor function in rat urinary bladder. *Naunyn. Schmiedeberg's. Arch. Pharmacol.* **373**, 300–309 (2006).
 334. Wright, D. F. B., Winter, H. R. & Duffull, S. B. Understanding the time course of pharmacological effect: A PKPD approach. *Br. J. Clin. Pharmacol.* **71**, 815–823 (2011).
 335. Segre, G. Kinetics of interaction between drugs and biological systems. *Farmaco. Sci.* **23**, 907–18 (1968).
 336. Holford, N. H. G. & Sheiner, L. B. Understanding the Dose-Effect Relationship: Clinical Application of Pharmacokinetic-Pharmacodynamic Models. *Clin. Pharmacokinet.* **6**, 429–453 (1981).
 337. Holford, N. H. G. & Sheiner, L. B. Kinetics of pharmacologic response. *Pharmacol. Ther.* **16**, 143–166 (1982).
 338. Evans, M. A., Shanks, C. A., Brown, K. F. & Triggs, E. J. Pharmacokinetic and pharmacodynamic modelling with pancuronium. *Eur. J. Clin. Pharmacol.* **26**, 243–50 (1984).
 339. Schwartz, J. B., Verotta, D. & Sheiner, L. B. Pharmacodynamic modeling of verapamil effects under steady-state and nonsteady-state conditions. *J. Pharmacol. Exp. Ther.* **251**, 1032–8 (1989).
 340. Whiting, B., Kelman, A. W., Barclay, J. & Addis, G. J. Modelling theophylline response in individual patients with chronic bronchitis. *Br. J. Clin. Pharmacol.* **12**, 481–7 (1981).
 341. Holford, N. H., Coates, P. E., Guentert, T. W., Riegelman, S. & Sheiner, L. B. The effect of quinidine and its metabolites on the electrocardiogram and systolic time intervals: concentration-effect relationships. *Br. J. Clin. Pharmacol.* **11**, 187–95 (1981).
 342. Gabrielsson, J. L., Johansson, P., Bondesson, U., Karlsson, M. & Paalzow, L. K. Analysis of pethidine disposition in the pregnant rat by means of a physiological flow model. *J. Pharmacokinetic. Biopharm.* **14**, 381–395 (1986).

343. Björkman, S., Wada, D. R., Stanski, D. R. & Ebling, W. F. Comparative physiological pharmacokinetics of fentanyl and alfentanil in rats and humans based on parametric single-tissue models. *J. Pharmacokinet. Biopharm.* **22**, 381–410 (1994).
344. Lemmens, H. J. M., Dyck, J. B., Shafer, S. L. & Stanski, D. R. Pharmacokinetic-pharmacodynamic modeling in drug development: Application to the investigational opioid trefentanil. *Clin. Pharmacol. Ther.* **56**, 261–271 (1994).
345. Torres-López, J. E., Lopez-Muñoz, F. J., Castañeda-Hernández, G., Flores-Murrieta, F. J. & Granados-Soto, V. Pharmacokinetic-pharmacodynamic modeling of the antinociceptive effect of diclofenac in the rat. *J. Pharmacol. Exp. Ther.* **282**, 685–90 (1997).
346. Morrison, R. A. *et al.* Isosorbide dinitrate kinetics and dynamics after intravenous, sublingual, and percutaneous dosing in angina. *Clin. Pharmacol. Ther.* **33**, 747–756 (1983).
347. Mould, D. R. *et al.* Simultaneous modeling of the pharmacokinetics and pharmacodynamics of midazolam and diazepam. *Clin. Pharmacol. Ther.* **58**, 35–43 (1995).
348. Kelman, A. W. & Whiting, B. Modeling of drug response in individual subjects. *J. Pharmacokinet. Biopharm.* **8**, 115–30 (1980).
349. Hong, Y., Gengo, F. M., Rainka, M. M., Bates, V. E. & Mager, D. E. Population pharmacodynamic modelling of aspirin- and ibuprofen-induced inhibition of platelet aggregation in healthy subjects. *Clin. Pharmacokinet.* **47**, 129–137 (2008).
350. Yamamoto, K. *et al.* Pharmacodynamics analysis of antiplatelet effect of aspirin in the literature - Modeling based on inhibition of cyclooxygenase in the platelet and the vessel wall endothelium. *Jpn J Hosp Pharm* **22**, 133–141 (1996).
351. Gisleskog, P. O., Hermann, D., Hammarlund-Udenaes, M. & Karlsson, M. O. A model for the turnover of dihydrotestosterone in the presence of the irreversible 5 alpha-reductase inhibitors G1198745 and finasteride. *Clin. Pharmacol. Ther.* **64**, 636–647 (1998).
352. Katashima, M. *et al.* Pharmacokinetic and pharmacodynamic study of a new nonsteroidal 5 alpha-reductase inhibitor, 4-[3-[3-[Bis(4-isobutylphenyl)methylamino]benzoyl]-1H-indol-1-yl]-butyric acid, in rats. *J. Pharmacol. Exp. Ther.* **284**, 914–920 (1998).
353. Abelo, A., Eriksson, U. G., Karlsson, M. O., Larsson, H. & Gabrielsson, J. A turnover model of irreversible inhibition of gastric acid secretion by omeprazole in the dog. *J. Pharmacol. Exp. Ther.* **295**, 662–669 (2000).
354. Katashima, M. *et al.* Comparative pharmacokinetic/pharmacodynamic analysis of proton pump inhibitors omeprazole, lansoprazole and pantoprazole, in humans. *Eur. J. Drug Metab. Pharmacokinet.* **23**, 19–26 (1998).
355. Puchalski, T. A., Krzyzanski, W., Blum, R. A. & Jusko, W. J. Pharmacodynamic modeling of lansoprazole using an indirect irreversible response model. *J. Clin. Pharmacol.* **41**, 251–258 (2001).
356. Snoeck, E. *et al.* A comprehensive hepatitis C viral kinetic model explaining cure. *Clin. Pharmacol. Ther.* **87**, 706–713 (2010).
357. Simeoni, M. *et al.* Predictive pharmacokinetic-pharmacodynamic modeling of tumor growth kinetics in xenograft models after administration of anticancer agents. *Cancer Res.* **64**, 1094–1101 (2004).
358. Friberg, L. E., Freijs, A., Sandstrom, M. & Karlsson, M. O. Semiphysiological model for the time course of leukocytes after varying schedules of 5-fluorouracil in rats. *J. Pharmacol. Exp. Ther.* **295**, 734–740 (2000).
359. Russu, A. & Poggesi, I. Turnover model with irreversible inactivation. in *Systems Pharmacology and Pharmacodynamics* (eds. Mager, D. E. & Kimko, H. H. C.) 217 (Springer Nature, 2016).
360. Jusko, W. J. Moving from Basic Toward Systems Pharmacodynamic Models. *J. Pharm. Sci.* **102**, 2930–2940 (2013).
361. Nagashima, R., O'Reilly, R. A. & Levy, G. Kinetics of pharmacologic effects in man: The anticoagulant action of warfarin. *Clin. Pharmacol. Ther.* **10**, 22–35 (1969).

362. Dayneka, N. L., Garg, V. & Jusko, W. J. Comparison of Four Basic Models of Indirect Pharmacodynamic Responses. *J. Pharmacokinet. Biopharm.* **21**, 457–78 (1993).
363. Jusko, W. J. & Ko, H. C. Physiologic indirect response models characterize diverse types of pharmacodynamic effects. *Clin. Pharmacol. Ther.* **56**, 406–419 (1994).
364. Chakraborty, A., Krzyzanski, W. & Jusko, W. J. Mathematical modeling of circadian cortisol concentrations using indirect response models: comparison of several methods. *J. Pharmacokinet. Biopharm.* **27**, 23–43 (1999).
365. Krzyzanski, W., Ramakrishnan, R. & Jusko, W. J. Basic Pharmacodynamic Models for Agents That Alter Production of Natural Cells. *J. Pharmacokinet. Pharmacodyn.* **27**, 467–489 (1999).
366. Budha, N. R., Kovar, A. & Meibohm, B. Comparative Performance of Cell Life Span and Cell Transit Models for Describing Erythropoietic Drug Effects. *AAPS J.* **13**, 650–661 (2011).
367. Samtani, M. N., Perez-Ruixo, J. J., Brown, K. H., Cerneus, D. & Molloy, C. J. Pharmacokinetic and Pharmacodynamic Modeling of Pegylated Thrombopoietin Mimetic Peptide (PEG-TPOm) After Single Intravenous Dose Administration in Healthy Subjects. *J. Clin. Pharmacol.* **49**, 336–350 (2009).
368. Yao, Z., Krzyzanski, W. & Jusko, W. J. Assessment of Basic Indirect Pharmacodynamic Response Models with Physiological Limits. *J. Pharmacokinet. Pharmacodyn.* **33**, 167–193 (2006).
369. Labrecque, G. & Bélanger, P. M. Biological rhythms in the absorption, distribution, metabolism and excretion of drugs. *Pharmacol. Ther.* **52**, 95–107 (1991).
370. Sällström, B. *et al.* A Pharmacodynamic Turnover Model Capturing Asymmetric Circadian Baselines of Body Temperature, Heart Rate and Blood Pressure in Rats: Challenges in Terms of Tolerance and Animal-handling Effects. *J. Pharmacokinet. Pharmacodyn.* **32**, 835–859 (2005).
371. Sukumaran, S., Almon, R. R., DuBois, D. C. & Jusko, W. J. Circadian rhythms in gene expression: Relationship to physiology, disease, drug disposition and drug action. *Adv. Drug Deliv. Rev.* **62**, 904–917 (2010).
372. Lew, K. H. *et al.* Gender-based effects on methylprednisolone pharmacokinetics and pharmacodynamics. *Clin. Pharmacol. Ther.* **54**, 402–414 (1993).
373. Rohatagi, S. *et al.* Dynamic modeling of cortisol reduction after inhaled administration of fluticasone propionate. *J. Clin. Pharmacol.* **36**, 938–41 (1996).
374. Krzyzanski, W. Direct, Indirect, and Signal Transduction Response Modeling. in *Systems Pharmacology and Pharmacodynamics* (eds. Mager, D. E. & Kimko, H. H. C.) 177–210 (Springer, 2016).
375. Mager, D. E. & Jusko, W. J. Pharmacodynamic modeling of time-dependent transduction systems. *Clin. Pharmacol. Ther.* **70**, 210–216 (2001).
376. Zhang, Y. & D’Argenio, D. Z. Feedback Control Indirect Response Models. in *Systems Pharmacology and Pharmacodynamics* (eds. Mager, D. E. & Kimko, H. H. C.) 229–254 (2016).
377. Black, J. W. & Leff, P. Operational models of pharmacological agonism. *Proc. R. Soc. London. Ser. B, Biol. Sci.* **220**, 141–62 (1983).
378. Van Der Graaf, P. H., Van Schaick, E. A., Mathot, R. A., Ijzerman, A. P. & Danhof, M. Mechanism-based pharmacokinetic-pharmacodynamic modeling of the effects of N6-cyclopentyladenosine analogs on heart rate in rat: estimation of in vivo operational affinity and efficacy at adenosine A1 receptors. *J. Pharmacol. Exp. Ther.* **283**, 809–16 (1997).
379. Greene, S. J. *et al.* Partial adenosine A1 receptor agonism: a potential new therapeutic strategy for heart failure. *Heart Fail. Rev.* **21**, 95–102 (2016).
380. Cox, E. H., Van Hemert, J. G., Tukker, E. J. & Danhof, M. Pharmacokinetic-pharmacodynamic modelling of the EEG effect of alfentanil in rats. *J. Pharmacol. Toxicol. Methods* **38**, 99–108 (1997).
381. Cox, E. H., Kerbusch, T., Van der Graaf, P. H. & Danhof, M. Pharmacokinetic-pharmacodynamic modeling of the electroencephalogram effect of synthetic opioids in the rat: correlation with the interaction at the mu-opioid receptor. *J. Pharmacol. Exp. Ther.* **284**, 1095–103 (1998).

382. Zuideveld, K. P., van Gestel, A., Peletier, L. A., Van der Graaf, P. H. & Danhof, M. Pharmacokinetic-pharmacodynamic modelling of the hypothermic and corticosterone effects of the 5-HT_{1A} receptor agonist flesinoxan. *Eur. J. Pharmacol.* **445**, 43–54 (2002).
383. Ramakrishnan, R., Dubois, D. C., Almon, R. R., Pyszczynski, N. A. & Jusko, W. J. Fifth-Generation Model for Corticosteroid Pharmacodynamics: Application to Steady-State Receptor Down-Regulation and Enzyme Induction Patterns during Seven-Day Continuous Infusion of Methylprednisolone in Rats. *J. Pharmacokinet Pharmacodyn* **29**, 1–24 (2002).
384. Sandström, M. *et al.* Model Describing the Relationship Between Pharmacokinetics and Hematologic Toxicity of the Epirubicin-Docetaxel Regimen in Breast Cancer Patients. *J. Clin. Oncol.* **23**, 413–421 (2005).
385. Friberg, L. E., Henningsson, A., Maas, H., Nguyen, L. & Karlsson, M. O. Model of Chemotherapy-Induced Myelosuppression With Parameter Consistency Across Drugs. *J. Clin. Oncol.* **20**, 4713–4721 (2002).
386. Friberg, L. E., Freijs, A., Sandst Om, M. & Karlsson, M. O. Semiphysiological Model for the Time Course of Leukocytes after Varying Schedules of 5-Fluorouracil in Rats. *J. Pharmacol. Exp. Ther.* **295**, 734–40 (2000).
387. Boje, K. M. K., Pollack, G. M., Gabrielsson, J. & Peletier, L. A. A Flexible Nonlinear Feedback System That Captures Diverse Patterns of Adaptation and Rebound. (2008). doi:10.1208/s12248-008-9007-x
388. Wakelkamp, M., Alván, G., Gabrielsson, J. & Paintaud, G. Pharmacodynamic modeling of furosemide tolerance after multiple intravenous administration. *Clin. Pharmacol. Ther.* **60**, 75–88 (1996).
389. Ahlström, C., Kroon, T., Peletier, L. A. & Gabrielsson, J. Feedback modeling of non-esterified fatty acids in obese Zucker rats after nicotinic acid infusions. *J. Pharmacokinet. Pharmacodyn.* **40**, 623–638 (2013).
390. Selen, A. *et al.* The biopharmaceutics risk assessment roadmap for optimizing clinical drug product performance. *J. Pharm. Sci.* **103**, 3377–3397 (2014).
391. Dickinson, P. A. *et al.* Clinical Relevance of Dissolution Testing in Quality by Design. *AAPS J.* **10**, 380–390 (2008).
392. Chen, M.-L., Lesko, L. & Williams, R. L. *Measures of Exposure versus Measures of Rate and Extent of Absorption.* *Clin Pharmacokinet* **40**, (2001).
393. Polli, J. E. In vitro studies are sometimes better than conventional human pharmacokinetic in vivo studies in assessing bioequivalence of immediate-release solid oral dosage forms. *AAPS J.* **10**, 289–99 (2008).
394. Karalis, V., Symillides, M. & MacHeras, P. On the leveling-off properties of the new bioequivalence limits for highly variable drugs of the EMA guideline. *Eur. J. Pharm. Sci.* **44**, 497–505 (2011).
395. Aarons, L. Assessment of rate of absorption in bioequivalence studies. *J. Pharm. Sci.* **76**, 853–855 (1987).
396. Chen, M. L. *et al.* Bioavailability and bioequivalence: An FDA regulatory overview. *Pharm. Res.* **18**, 1645–1650 (2001).
397. Endrenyi, L. & Al-Shaikh, P. Sensitive and Specific Determination of the Equivalence of Absorption Rates. *J. Pharm. Sc* **83**, 1554–1557 (1994).
398. Bois, F. Y. *et al.* Bioequivalence: Performance of Several Measures of Rate of Absorption. *Pharmaceutical Research: An Official Journal of the American Association of Pharmaceutical Scientists* **11**, 966–974 (1994).
399. Lacey, L. F., Keene, O. N., Duquesnoy, C. & Bye, A. Evaluation of different indirect measures of rate of drug absorption in comparative pharmacokinetic studies. *J. Pharm. Sci.* **83**, 212–215 (1994).
400. Reppas, C., Lacey, L. F., Keene, O. N., Macheras, P. & Bye, A. Evaluation of Different Metrics as Indirect Measures of Rate of Drug Absorption from Extended Release Dosage Forms at Steady-State. *Pharmaceutical Research: An Official Journal of the American Association of Pharmaceutical Scientists* **12**, 103–107 (1995).

401. U.S.FDA Center for Drug Evaluation and Research (CDER). *Guidance for Industry Bioavailability and Bioequivalence Studies Submitted in NDAs or INDs-General Considerations*. (2014).
402. Rostami-Hodjegan, A., Jackson, P. R. & Tucker, G. T. Sensitivity of Indirect Metrics for Assessing “Rate” in Bioequivalence Studies—Moving the “Goalposts” or Changing the “Game”. *J. Pharm. Sci.* **83**, 1554–1557 (1994).
403. Amidon, G. L., Lennernäs, H., Shah, V. P. & Crison, J. R. A Theoretical Basis for a Biopharmaceutic Drug Classification: The Correlation of in Vitro Drug Product Dissolution and in Vivo Bioavailability. *Pharmaceutical Research: An Official Journal of the American Association of Pharmaceutical Scientists* **12**, 413–420 (1995).
404. Butler, J. M. & Dressman, J. B. The Developability Classification System: Application of Biopharmaceutics Concepts to Formulation Development. *J. Pharm. Sci.* **99**, 4940–4954 (2010).
405. Rosenberger, J., Butler, J., Muenster, U. & Dressman, J. Application of a Refined Developability Classification System. *J. Pharm. Sci.* **108**, 1090–1100 (2019).
406. Tsume, Y., Mudie, D. M., Langguth, P., Amidon, G. E. & Amidon, G. L. The Biopharmaceutics Classification System: Subclasses for in vivo predictive dissolution (IPD) methodology and IVIVC. *Eur. J. Pharm. Sci.* **57**, 152–163 (2014).
407. Fuchs, A., Leigh, M., Kloefer, B. & Dressman, J. B. Advances in the design of fasted state simulating intestinal fluids: FaSSIF-V3. *Eur. J. Pharm. Biopharm.* **94**, 229–240 (2015).
408. Potthast, H. *et al.* Biowaiver monographs for immediate release solid oral dosage forms: Ibuprofen. *J. Pharm. Sci.* **94**, 2121–2131 (2005).
409. Cristofolletti, R. *et al.* Integrating Drug- and Formulation-Related Properties With Gastrointestinal Tract Variability Using a Product-Specific Particle Size Approach: Case Example Ibuprofen. *J. Pharm. Sci.* **108**, 3842–3847 (2019).
410. Avdeef, A. Solubility of sparingly-soluble ionizable drugs. *Adv. Drug Deliv. Rev.* **59**, 568–590 (2007).
411. Avdeef, A. & Berger, C. M. pH-Metric Solubility. 2: Correlation Between the Acid-Base Titration and formulations for use in early animal bioavailability and toxicity studies. Later in development, solubility takes on a broader. *Pharm. Res.* **17**, (2000).
412. Chowhan, Z. T. pH-Solubility Profiles of Organic Carboxylic Acids and Their Salts. *J. Pharm. Sci.* **67**, 1257–1260 (1978).
413. Glomme, A., März, J. & Dressman, J. B. Predicting the Intestinal Solubility of Poorly Soluble Drugs. in *Pharmacokinetic Profiling in Drug Research: Biological, Physicochemical, and Computational Strategies* (eds. Testa, B., Kraemer, S., Wunderli-Allensprach, H. & Folkers, G.) 259–280 (John Wiley & Sons, Ltd, 2007). doi:10.1002/9783906390468.CH16
414. Wang, J. & Flanagan, D. R. General solution for diffusion-controlled dissolution of spherical particles. 2. Evaluation of experimental data. *J. Pharm. Sci.* **91**, 534–542 (2002).
415. Mooney, K. G., Mintun, M. A., Himmelstein, K. J. & Stella, V. J. Dissolution kinetics of carboxylic acids I: Effect of pH under unbuffered conditions. *J. Pharm. Sci.* **70**, 13–22 (1981).
416. Mooney, K. G., Mintun, M. A., Himmelstein, K. J. & Stella, V. J. Dissolution Kinetics of Carboxylic Acids II: Effect of Buffers. *J. Pharm. Sci.* **70**, 22–32 (1981).
417. Mooney, K. G., Rodriguez-gaxiola, M., Mintun, M., Himmelstein, K. J. & Stella, V. J. Dissolution Kinetics of Phenylbutazone. *J. Pharm. Sci.* **70**, 1358–1365 (1981).
418. Ozturk, S. S., Palsson, B. O. & Dressman, J. B. Dissolution of Ionizable Drugs in Buffered and Unbuffered Solutions. *Pharm. Res.* **05**, 272–282 (1988).
419. Sheng, J. J., McNamara, D. P. & Amidon, G. L. Toward an In Vivo dissolution methodology: A comparison of phosphate and bicarbonate buffers. *Mol. Pharm.* **6**, 29–39 (2009).
420. Serajuddin, A. T. M. & Jarowski, C. Effect of diffusion layer pH and solubility on the dissolution rate of pharmaceutical bases and their hydrochloride salts. I: Phenazopyridine. *J. Pharm. Sci.* **74**, 142 (1985).

421. Pepin, X. J. H. *et al.* Bridging in vitro dissolution and in vivo exposure for acalabrutinib. Part II. A mechanistic PBPK model for IR formulation comparison, proton pump inhibitor drug interactions, and administration with acidic juices. *Eur. J. Pharm. Biopharm.* **142**, 435–448 (2019).
422. Cristofolletti, R. & Dressman, J. B. FaSSIF-V3, but not compendial media, appropriately detects differences in the peak and extent of exposure between reference and test formulations of ibuprofen. *Eur. J. Pharm. Biopharm.* **105**, 134–140 (2016).
423. McNamara, D. P. & Amidon, G. L. Dissolution of acidic and basic compounds from the rotating disk: Influence of convective diffusion and reaction. *J. Pharm. Sci.* **75**, 858–868 (1986).
424. Davies, N. M. & Anderson, K. E. Clinical pharmacokinetics of naproxen. *Clin. Pharmacokinet.* **32**, 268–293 (1997).
425. VNP, L., P, L., A, G. & MP, F. Influence of granulation and compaction on the particle size of ibuprofen--development of a size analysis method. *Int. J. Pharm.* **321**, 72–77 (2006).
426. Avdeef, A. pH-metric Solubility. 1. Solubility-pH Plots. Gibbs Buffer and pK, in Profiles from Bjerrum the Solid State. *Pharm. Pharmacol. Commun. Pharm. Pharmacol. Commun* **4**, 165–178 (1998).
427. Risdall, P. C., Adams, S. S., Crampton, E. L. & Marchant, B. The Disposition and Metabolism of Flurbiprofen in Several Species Including Man. *XENOBIOTICA* **8**, 691–704 (1978).
428. Ke, A., Barter, Z., Rowland-Yeo, K. & Almond, L. Towards a Best Practice Approach in PBPK Modeling: Case Example of Developing a Unified Efavirenz Model Accounting for Induction of CYPs 3A4 and 2B6. *CPT Pharmacometrics Syst. Pharmacol.* **5**, 367–376 (2016).
429. European Medicines Agency (EMA). *Committee for Medicinal Products for Human Use (CHMP) Guideline on the reporting of physiologically based pharmacokinetic (PBPK) modelling and simulation.* (2018).
430. Lennernas, H. *et al.* Human effective permeability data for furosemide, hydrochlorothiazide, ketoprofen and naproxen to be used in the proposed biopharmaceutical classification for IR-products. *Pharm. Res. (New York)* **12(9 SUPPL)** 396 (1995).
431. Hens, B. *et al.* Gastrointestinal transfer: In vivo evaluation and implementation in in vitro and in silico predictive tools. *Eur. J. Pharm. Sci.* **63**, 233–242 (2014).
432. Psachoulis, D. *et al.* Precipitation in and Supersaturation of Contents of the Upper Small Intestine After Administration of Two Weak Bases to Fasted Adults. *Pharm. Res.* **28**, 3145–3158 (2011).
433. Cristofolletti, R., Patel, N. & Dressman, J. B. Differences in Food Effects for 2 Weak Bases With Similar BCS Drug-Related Properties: What Is Happening in the Intestinal Lumen? *J. Pharm. Sci.* **105**, 2712–2722 (2016).
434. Paixão, P. *et al.* Gastric emptying and intestinal appearance of nonabsorbable drugs phenol red and paromomycin in human subjects: A multi-compartment stomach approach. *Eur. J. Pharm. Biopharm.* **129**, 162–174 (2018).
435. Edginton, A. N., Schmitt, W. & Willmann, S. Development and evaluation of a generic physiologically based pharmacokinetic model for children. *Clin. Pharmacokinet.* **45**, 1013–1034 (2006).
436. Runkel, R., Chaplin, M., Boost, G., Segre, E. & Forchielli, E. Absorption, Distribution, Metabolism, and Excretion of Naproxen in Various Laboratory Animals and Human Subjects. *J. Pharm. Sci.* **61**, 703–708 (1972).
437. Runkel, R. *et al.* Naproxen Oral Absorption Characteristics. *Chem. Pharm. Bull. (Tokyo)*. **20**, 1457–1466 (1972).
438. Runkel, R. *et al.* Naproxen-metabolism, excretion and comparative pharmaco kinetics. *Scand J Rheumatol.* **2**, 29–36 (1973).
439. Charles, B. G. & Mogg, G. A. G. Comparative in vitro and in vivo bioavailability of naproxen from tablet and caplet formulations. *Biopharm. Drug Dispos.* **15**, 121–128 (1994).
440. Zhou, D., Zhang, Q., Lu, W., Xia, Q. & Wei, S. Single- and multiple-dose pharmacokinetic comparison of

- a sustained-release tablet and conventional tablets of naproxen in healthy volunteers. *J. Clin. Pharmacol.* **38**, 625–629 (1998).
441. Haberer, L. J., Walls, C. M., Lener, S. E., Taylor, D. R. & McDonald, S. A. Distinct pharmacokinetic profile and safety of a fixed-dose tablet of sumatriptan and naproxen sodium for the acute treatment of migraine. *Headache* **50**, 357–373 (2010).
442. Setiawati, E. *et al.* Bioequivalence Study with Two Naproxen Sodium Tablet Formulations in Healthy Subjects. *J. Bioequivalence Bioavailab. -Open Access Res. Artic. JBB J Bioequiv Availab* **1**, 28–33 (2009).
443. Rao, B. R., Rambhau, D. & Rao, V. V. S. Pharmacokinetics of Single-Dose Administration of Naproxen at 10 : 00 and 22 : 00 Hours. *Int. Soc. Chronobiol.* **10**, 137–142 (1993).
444. ME, K., SC, R. & MA, H. A population balance equation model of aggregation dynamics in Taxus suspension cell cultures. *Biotechnol. Bioeng.* **109**, 472–482 (2012).
445. Mei, C. *et al.* Liquid chromatography-tandem mass spectrometry for the quantification of flurbiprofen in human plasma and its application in a study of bioequivalence. *J. Chromatogr. B Anal. Technol. Biomed. Life Sci.* **993–994**, 69–74 (2015).
446. Patel, B. K. *et al.* Disposition of flurbiprofen in man : influence of stereochemistry and age. *Xenobiotica* **33**, 1043–1057 (2003).
447. Wang, L. *et al.* Effect of CYP2C9 genetic polymorphism on the metabolism of flurbiprofen in vitro. *Drug Dev Ind Pharm* **41**, 1363–1367 (2015).
448. Lee, C. R. *et al.* Differences in flurbiprofen pharmacokinetics between CYP2C9*1/*1, *1/*2, and *1/*3 genotypes. *Eur. J. Clin. Pharmacol.* **58**, 791–794 (2003).
449. Kuehl, G. E., Lampe, J. W., Potter, J. D. & Bigler, J. Glucuronidation of nonsteroidal antiinflammatory drugs Identifying the enzymes in human liver microsomes.pdf. **33**, 1027–1035 (2005).
450. Mano, Y., Usui, T. & Kamimura, H. Predominant contribution of UDP-glucuronosyltransferase 2B7 in the glucuronidation of racemic flurbiprofen in the human liver. *Drug Metab. Dispos.* **35**, 1182–1187 (2007).
451. Nielsen, L. M. *et al.* Lack of genetic association between OCT1, ABCB1, and UGT2B7 variants and morphine pharmacokinetics. *Eur. J. Pharm. Sci.* **99**, 337–342 (2017).
452. Ayuso, P., Neary, M., Chiong, J. & Owen, A. Meta-analysis of the effect of CYP2B6, CYP2A6, UGT2B7 and CAR polymorphisms on efavirenz plasma concentrations. *J. Antimicrob. Chemother.* **74**, 3281–3290 (2019).
453. Suri, A., Grundy, B. L. & Derendorf, H. Pharmacokinetics and pharmacodynamics of enantiomers of ibuprofen and flurbiprofen after oral administration. *Int. J. Clin. Pharmacol. Ther.* **35**, 1–8 (1997).
454. Kim, Y. *et al.* Development of a Korean-specific virtual population for physiologically based pharmacokinetic modelling and simulation. *Biopharm. Drug Dispos.* **40**, 135–150 (2019).
455. Myrand, S. P. *et al.* Pharmacokinetics/genotype associations for major cytochrome P450 enzymes in native and first- and third-generation Japanese populations: Comparison with Korean, Chinese, and Caucasian populations. *Clin. Pharmacol. Ther.* **84**, 347–361 (2008).
456. Yoon, Y.-R. *et al.* Frequency of cytochrome P450 2C9 mutant alleles in a Korean population. *Br. J. Clin. Pharmacol.* **51**, 277–280 (2008).
457. Jamali, F. *et al.* Comparative bioavailability of two flurbiprofen products: Stereospecific versus conventional approach. *Biopharm. Drug Dispos.* **12**, 435–445 (1991).
458. Gonzalez-Younes, I., Wagner, J. G., Gaines, D. A., Ferry, J. J. & Hageman, J. M. Absorption of flurbiprofen through human buccal mucosa. *J. Pharm. Sci.* **80**, 820–3 (1991).
459. Szpunar, G. J. *et al.* Pharmacokinetics of flurbiprofen in man. I. Area/dose relationships. *Biopharm. Drug Dispos.* **8**, 273–283 (1987).
460. Lee, Y. J. *et al.* Effects of CYP2C9*1/*3 genotype on the pharmacokinetics of flurbiprofen in Korean subjects. *Arch. Pharm. Res.* **38**, 1232–1237 (2015).

461. Kumar, V., Brundage, R., Oetting, W. S., Leppik, I. E. & Tracy, T. S. Differential Genotype Dependent Inhibition of CYP2C9 in Humans. *Drug Metab. Dispos.* **36**, 1242–1248 (2008).
462. Liu, Y.-M. *et al.* Pharmacokinetic and bioequivalence comparison between orally disintegrating and conventional tablet formulations of flurbiprofen: A single-dose, randomized-sequence, open-label, two-period crossover study in healthy chinese male volunteers. (2009). doi:10.1016/j.clinthera.2009.08.008
463. Grimm, M., Koziolok, M., Kühn, J. P. & Weitschies, W. Interindividual and intraindividual variability of fasted state gastric fluid volume and gastric emptying of water. *Eur. J. Pharm. Biopharm.* **127**, 309–317 (2018).
464. fruehauf, h. *et al.* Intersubject and intrasubject variability of gastric volumes in response to isocaloric liquid meals in functional dyspepsia and health. *Neurogastroenterol. Motil.* **19**, 553–561 (2007).
465. Lartigue, S. *et al.* Inter- and intrasubject variability of solid and liquid gastric emptying parameters. A scintigraphic study in healthy subjects and diabetic patients. *Dig. Dis. Sci.* **39**, 109–115 (1994).
466. Petring, O. U. & Flachs, H. Inter- and intrasubject variability of gastric emptying in healthy volunteers measured by scintigraphy and paracetamol absorption. *Br. J. Clin. Pharmacol.* **29**, 703–8 (1990).
467. Trocóniz, I. F. *et al.* Pharmacokinetic-Pharmacodynamic Modelling of the Antipyretic Effect of Two Oral Formulations of Ibuprofen. *Clin. Pharmacokinet.* **38**, 505–518 (2000).
468. Sugano, K. & Terada, K. Rate- and Extent-Limiting Factors of Oral Drug Absorption: Theory and Applications. *J. Pharm. Sci.* **104**, 2777–2788 (2015).
469. Legg, T. J., Laurent, A. L., Leyva, R. & Kellstein, D. Ibuprofen Sodium Is Absorbed Faster than Standard Ibuprofen Tablets: Results of Two Open-Label, Randomized, Crossover Pharmacokinetic Studies. *Drugs R D* **14**, 283–290 (2014).
470. Blume H & Mutschler M. Bioäquivalenz, Qualitätsbewertung wirkstoffgleicher Fertigarzneimittel, Teil I/II, Isosorbiddinitrat 6. Ergänzungslieferung, Govi-Verlag Pharmazeutischer Verlag, Frankfurt/Main-Eschborn. (Govi-Verlag Pharmazeutischer Verlag, Frankfurt/Main-Eschborn., 1996).
471. Lionberger, R. A. Innovation for Generic Drugs: Science and Research Under the Generic Drug User Fee Amendments of 2012. *Clin. Pharmacol. Ther.* **105**, 878–885 (2019).
472. R, L. Decision Science for Generic Drug Development and Review. *J. Clin. Pharmacol.* **59**, 1249–1251 (2019).
473. E, M., FT, M. & KE, K. Regulatory Considerations for Building an In Silico Clinical Pharmacology Backbone by 2030. *Clin. Pharmacol. Ther.* **107**, 746–748 (2020).
474. Human Cytochrome P450 (CYP) Allele Nomenclature Committee. CYP2C9 allele nomenclature. (2016). Available at: <https://www.pharmvar.org/htdocs/archive/cyp2c9.htm>. (Accessed: 9th May 2020)
475. Yamazaki, H. *et al.* Comparative Studies on the Catalytic Roles of Cytochrome P450 2C9 and Its Cys- and Leu-Variants in the Oxidation of Warfarin, Flurbiprofen, and Diclofenac by Human Liver Microsomes. *Biochem. Pharmacol.* **56**, 243–251 (1998).
476. Van Booven, D. *et al.* Cytochrome P450 2C9-CYP2C9. *Pharmacogenetics and Genomics* **20**, 277–281 (2010).
477. Scott, S. A., Khasawneh, R., Peter, I., Kornreich, R. & Desnick, R. J. Combined CYP2C9, VKORC1 and CYP4F2 frequencies among racial and ethnic groups. *Pharmacogenomics* **11**, 781–791 (2010).
478. Kirchheiner, J. & Brockmöller, J. Clinical consequences of cytochrome P450 2C9 polymorphisms. *Clinical Pharmacology and Therapeutics* **77**, 1–16 (2005).
479. Lee, C. R., Goldstein, J. A. & Pieper, J. A. Cytochrome P450 2C9 polymorphisms: A comprehensive review of the in-vitro and human data. *Pharmacogenetics* **12**, 251–263 (2002).
480. Lee, C. B. *et al.* Tolbutamide, flurbiprofen, and losartan as probes of CYP2C9 activity in humans. *J. Clin. Pharmacol.* **43**, 84–91 (2003).
481. Zgheib, N. K., Frye, R. F., Tracy, T. S., Romkes, M. & Branch, R. A. Evaluation of flurbiprofen urinary

- ratios as in vivo indices for CYP2C9 activity. *Br. J. Clin. Pharmacol.* **63**, 477–487 (2007).
482. Vogl, S., Lutz, R. W., Schönfelder, G. & Lutz, W. K. CYP2C9 genotype vs. metabolic phenotype for individual drug dosing-A correlation analysis using flurbiprofen as probe drug. *PLoS One* **10**, (2015).
483. Hanley, M. J. *et al.* Effect of blueberry juice on clearance of buspirone and flurbiprofen in human volunteers. *Br. J. Clin. Pharmacol.* **75**, 1041–1052 (2013).
484. Greenblatt, D. J. *et al.* Interaction of flurbiprofen with cranberry juice , grape juice , tea , and fluconazole : In vitro and clinical studies. **450**, 125–133
485. Hanley, M. J., Masse, G., Harmatz, J. S., Court, M. H. & Greenblatt, D. J. Pomegranate juice and pomegranate extract do not impair oral clearance of flurbiprofen in human volunteers: Divergence from in vitro results. *Clin. Pharmacol. Ther.* **92**, 651–657 (2012).
486. Daali, Y. *et al.* Oral flurbiprofen metabolic ratio assessment using a single-point dried blood spot. *Clin. Pharmacol. Ther.* **91**, 489–496 (2012).
487. Kesisoglou, F., Chung, J., Van Asperen, J. & Heimbach, T. Physiologically Based Absorption Modeling to Impact Biopharmaceutics and Formulation Strategies in Drug Development-Industry Case Studies. *Pharmaceutics* (2016). doi:10.1016/j.xphs.2015.11.034
488. Sager, J. E., Yu, J., Ragueneau-Majlessi, I. & Isoherranen, N. Physiologically Based Pharmacokinetic (PBPK) Modeling and Simulation Approaches: A Systematic Review of Published Models, Applications, and Model Verification. *Drug Metab. Dispos.* **43**, 1823–37 (2015).
489. Schütt, M., Stamatopoulos, K., Simmons, M. J. H., Batchelor, H. K. & Alexiadis, A. Modelling and simulation of the hydrodynamics and mixing profiles in the human proximal colon using Discrete Multiphysics. *Comput. Biol. Med.* **121**, 103819 (2020).
490. Pade, D., Jamei, M., Rostami-Hodjegan, A. & Turner, D. B. Application of the MechPeff model to predict passive effective intestinal permeability in the different regions of the rodent small intestine and colon. *Biopharm. Drug Dispos.* **38**, 94–114 (2017).
491. Elvang, P. A. *et al.* Co-existing colloidal phases of human duodenal aspirates: Intraindividual fluctuations and interindividual variability in relation to molecular composition. *J. Pharm. Biomed. Anal.* **170**, 22–29 (2019).
492. Bucheit, J. D. *et al.* Oral Semaglutide: A Review of the First Oral Glucagon-Like Peptide 1 Receptor Agonist. *Diabetes Technology and Therapeutics* **22**, 10–18 (2020).
493. Swat, M. J. *et al.* Pharmacometrics Markup Language (PharmML): Opening new perspectives for model exchange in drug development. *CPT: Pharmacometrics and Systems Pharmacology* **4**, 316–319 (2015).
494. Abrahamsson, B. *et al.* Six years of progress in the oral biopharmaceutics area – A summary from the IMI OrBiTo project. *Eur. J. Pharm. Biopharm.* **152**, 236–247 (2020).
495. Saphier, S., Rosner, A., Brandeis, R. & Karton, Y. Gastro intestinal tracking and gastric emptying of solid dosage forms in rats using X-ray imagining. *Int. J. Pharm.* **388**, 190–195 (2010).
496. Gómez-Lado, N. *et al.* Gastrointestinal tracking and gastric emptying of coated capsules in rats with or without sedation using CT imaging. *Pharmaceutics* **12**, (2020).
497. Lu, K. H., Cao, J., Oleson, S. T., Powley, T. L. & Liu, Z. Contrast-Enhanced Magnetic Resonance Imaging of Gastric Emptying and Motility in Rats. *IEEE Trans. Biomed. Eng.* **64**, 2546–2554 (2017).
498. Blaabjerg, L. I., Fan, L., Chen, X. & Sassene, P. J. The use of capsule endoscopy to determine tablet disintegration in vivo. *Pharmaceutics* **12**, (2020).
499. Berry, R. *et al.* Functional physiology of the human terminal antrum defined by high-resolution electrical mapping and computational modeling. *Am. J. Physiol. - Gastrointest. Liver Physiol.* **311**, G895–G902 (2016).
500. Gharibans, A. A., Kim, S., Kunkel, D. C. & Coleman, T. P. High-Resolution Electrogastrogram: A Novel, Noninvasive Method for Determining Gastric Slow-Wave Direction and Speed. *IEEE Trans. Biomed. Eng.* **64**, 807–815 (2017).

501. Yoshimoto, K. *et al.* Gastric Contraction Imaging System Using a 3-D Endoscope. *IEEE J. Transl. Eng. Heal. Med.* **2**, (2014).
502. Potcoava, M. C., Futia, G. L., Aughenbaugh, J., Schlaepfer, I. R. & Gibson, E. A. Raman and coherent anti-Stokes Raman scattering microscopy studies of changes in lipid content and composition in hormone-treated breast and prostate cancer cells. *J. Biomed. Opt.* **19**, 111605 (2014).
503. Phan, S., Salentinig, S., Hawley, A. & Boyd, B. J. How relevant are assembled equilibrium samples in understanding structure formation during lipid digestion? *Eur. J. Pharm. Biopharm.* **96**, 117–124 (2015).
504. Viitala, T., Granqvist, N., Hallila, S., Raviña, M. & Yliperttula, M. Elucidating the Signal Responses of Multi-Parametric Surface Plasmon Resonance Living Cell Sensing: A Comparison between Optical Modeling and Drug–MDCKII Cell Interaction Measurements. *PLoS One* **8**, e72192 (2013).
505. Rezhdo, O. *et al.* Characterization of colloidal structures during intestinal lipolysis using small-angle neutron scattering. *J. Colloid Interface Sci.* **499**, 189–201 (2017).
506. Scotcher, D. *et al.* Physiologically Based Pharmacokinetic Modeling of Transporter-Mediated Hepatic Disposition of Imaging Biomarker Gadoxetate in Rats. *Mol. Pharm.* **18**, (2021).
507. Krauss, M. & Schuppert, A. Assessing interindividual variability by Bayesian-PBPK modeling. *Drug Discov. Today Dis. Model.* **22**, 15–19 (2016).
508. Lang, J., Vincent, L., Chenel, M., Ogungbenro, K. & Galetin, A. Simultaneous Ivabradine Parent-Metabolite PBPK/PD Modelling Using a Bayesian Estimation Method. *AAPS J.* **22**, 1–16 (2020).
509. Tsiros, P., Bois, F. Y., Dokoumetzidis, A., Tsiliki, G. & Sarimveis, H. Population pharmacokinetic reanalysis of a Diazepam PBPK model: a comparison of Stan and GNU MCSim. *J. Pharmacokinetic. Pharmacodyn.* **46**, 173–192 (2019).
510. Jamei, M. Recent Advances in Development and Application of Physiologically-Based Pharmacokinetic (PBPK) Models: a Transition from Academic Curiosity to Regulatory Acceptance. *Curr. Pharmacol. Reports* **2**, 161–169 (2016).
511. Jamei, M. Where Do PBPK Models Stand in Pharmacometrics and Systems Pharmacology? *CPT Pharmacometrics Syst. Pharmacol.* psp4.12493 (2020). doi:10.1002/psp4.12493
512. Sager, M. *et al.* Low dose caffeine as a salivary tracer for the determination of gastric water emptying in fed and fasted state: A MRI validation study. *Eur. J. Pharm. Biopharm.* **127**, 443–452 (2018).
513. Feldman, M., Smith, H. J. & Simon, T. R. Gastric emptying of solid radiopaque markers: Studies in healthy subjects and diabetic patients. *Gastroenterology* **87**, 895–902 (1984).
514. Parker, H. L. *et al.* Gastric and postgastric processing of ¹³C markers renders the ¹³C breath test an inappropriate measurement method for the gastric emptying of lipid emulsions in healthy adults. *J. Nutr.* **147**, 1258–1266 (2017).
515. Luo, L. *et al.* Assessment of serum bile acid profiles as biomarkers of liver injury and liver disease in humans. *PLoS One* **13**, (2018).
516. Zhao, Y. *et al.* Evaluation of human intestinal absorption data and subsequent derivation of a quantitative structure-activity relationship (QSAR) with Abraham descriptors. *J. Pharm. Sci.* **90**, 749–784 (2001).
517. Pérez, M. A. C. *et al.* A topological sub-structural approach for predicting human intestinal absorption of drugs. *Eur. J. Med. Chem.* **39**, 905–916 (2004).
518. Bergström, C. A. S., Andersson, S. B. E., Fagerberg, J. H., Ragnarsson, G. & Lindahl, A. Is the full potential of the biopharmaceutics classification system reached? *Eur. J. Pharm. Sci.* **57**, 224–231 (2014).
519. Brown, H. S., Griffin, M., Houston, J. B. & Li, A. P. Evaluation of cryopreserved human hepatocytes as an alternative in vitro system to microsomes for the prediction of metabolic clearance. *Drug Metab. Dispos.* **35**, 293–301 (2007).

520. Paixão, P., Gouveia, L. F. & Morais, J. A. G. Prediction of the human oral bioavailability by using in vitro and in silico drug related parameters in a physiologically based absorption model. *Int. J. Pharm.* **429**, 84–98 (2012).
521. Martin, W. *et al.* Pharmacokinetics and absolute bioavailability of ibuprofen after oral administration of ibuprofen lysine in man. *Biopharm. Drug Dispos.* **11**, 265–278 (1990).
522. Lee, H. I. *et al.* Simultaneous determination of flurbiprofen and its hydroxy metabolite in human plasma by liquid chromatography-tandem mass spectrometry for clinical application. *J. Chromatogr. B Anal. Technol. Biomed. Life Sci.* **971**, 58–63 (2014).
523. Czyski, A. Determination of the Lipophilicity of Ibuprofen, Naproxen, Ketoprofen, and Flurbiprofen with Thin-Layer Chromatography. *J. Chem.* **2019**, 1–6 (2019).
524. Kaiser, D. G., Brooks, C. D. & Lomen, P. L. *Pharmacokinetics of Flurbiprofen*.
525. Aarons, L., Khan, A. Z., Grennan, D. M. & Alam-Siddiqi, M. The binding of flurbiprofen to plasma proteins. *J. Pharm. Pharmacol.* **37**, 644–646 (1985).
526. Lin, J. H., Cocchetto, D. M. & Duggan, D. E. Protein-binding as a primary determinant of the clinical pharmacokinetic properties of nonsteroidal antiinflammatory drugs. *Clin Pharmacokinet* **12**, 402–432 (1987).
527. Szpunar, G. J., Albert, K. S. & Wagner, J. G. Pharmacokinetics of flurbiprofen in man. II. Plasma protein binding. *Res. Commun. Chem. Pathol. Pharmacol.* **64**, 17–30 (1989).
528. Wang, H., Yuan, L. & Zeng, S. Characterizing the effect of UDP-glucuronosyltransferase (UGT) 2B7 and UGT1A9 genetic polymorphisms on enantioselective glucuronidation of flurbiprofen. *Biochem. Pharmacol.* **82**, 1757–1763 (2011).

7 Supplementary material

7.1 Case example: Naproxen

Table 7-1: Mean (SD) demographic data of in vivo studies used for the development and verification of the PBPK model. (HV= healthy volunteers)

Formulation & Dose	N° of Subjects	Female Ratio	Ethnicity	Population	Age (y)	BW Range (kg)	BH Range (cm)	Reference
Intravenous								
93 mg with 30 μ C tritium label in 100 mL phosphate buffer	3	0.33	Caucasian	HV	–	49.9-86.3	–	436–438
Oral								
Naprosyn® 500 mg	16	0.125	Caucasian	HV	22.1 (4.4)	67.6 (8.3)	175.7 (9.0)	439
Naprosyn® 2 x 250 mg	10	0	Chinese	HV	19-38	51-74	–	440
Anaprox® 550 mg	8	0.63	Caucasian	HV	44.3 (8.5)	71.44 (12.3)	–	441
Anaprox® 550 mg	26	0.15	Caucasian	HV	19-46	–	–	442
IR Naproxen 500 mg	12	0	Indian	HV	18-22	46-62.5	160-182.5	443
IR Naproxen-Na 500 mg	16	0.63	Caucasian	HV	44.3 (8.5)	71.44 (12.3)	–	441

Table 7-2: Input parameters for naproxen PBPK model development and validation

Parameters	Value	Reference/ Comments
Physicochemical & Blood Binding		
MW (g/mol)	230.3	PubChem
logP _{o:w}	3.2	516–518
pKa	4.43	estimated from <i>in vitro</i> data (Table 3-4)
Blood/ Plasma ratio	0.55	519
Fraction unbound in plasma	0.01	424,520
Absorption		
Model	ADAM	
P _{eff, human} (x10 ⁻⁴ cm/s)	8.5	430
Formulation type	Immediate Release	
<i>In vivo</i> dissolution	see Table 3-5	estimated DLM scalars from <i>in vitro</i> dissolution data (see Figure 3-3 and Figure 3-4)
S ₀ (mg/mL)	0.0294	Measured <i>in vitro</i> (Table 3-1)
Particle density (g/mL)	1.20	Default value within ADAM
Particle size distribution	Monodispersed	Assumed as data not available
Particle radius (μm)	10	Default value within ADAM
logK _{m:w} neutral	5.37	estimated from <i>in vitro</i> data (see Table 3-4)
logK _{m:w} ion	4.00	estimated from <i>in vitro</i> data (see Table 3-4)
Distribution		
Model	Minimal PBPK with SAC	
V _{ss} (L/kg)	0.15	PE module
V _{sac} (L/kg)	0.075	PE module
Q _{sac} (L/h)	1.00	PE module
Elimination		
CL _{iv} (L/h)	0.40	PE module
CL _{renal} (L/h)	0.02	520

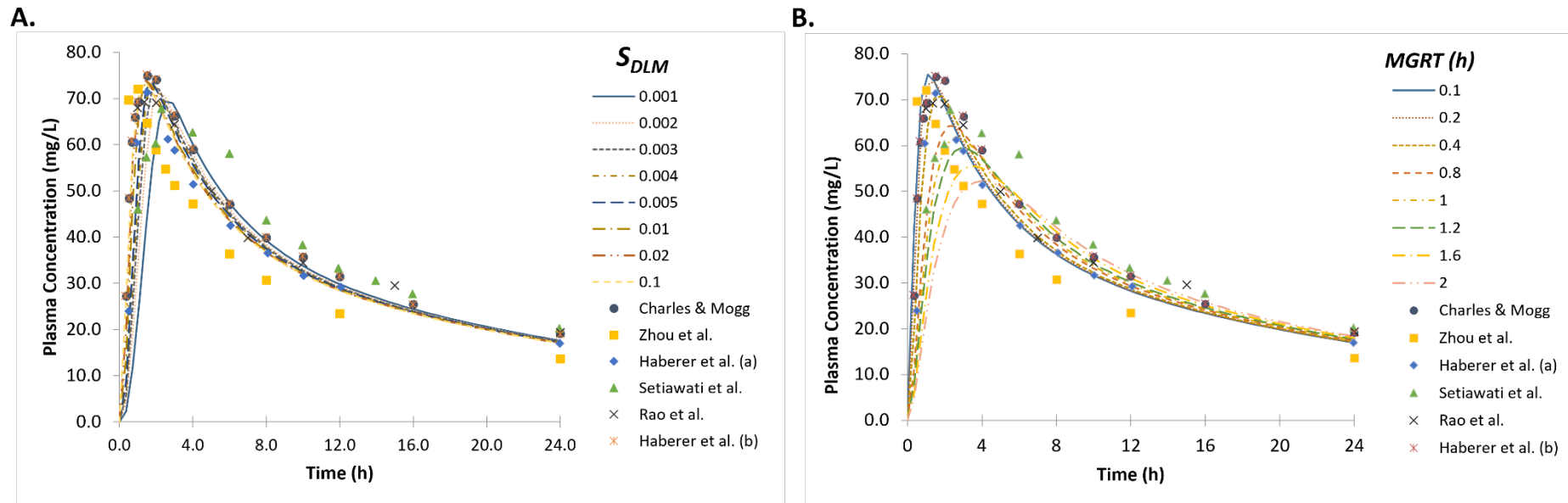


Figure 7-1: Sensitivity analysis of naproxen simulated plasma concentration-time profiles of population representative individual on (A) DLM scalar values ranging from 0.001 (blue solid line) to 0.1 (dashed line) and (B) mean gastric residence time (MGRT) with values ranging from 0.1 (blue solid line) to 2h (dashed dotted line). The values of all other parameters were kept constant (GET=0.25 h). Observed clinical data from Charles & Mogg (circles), Zhou et al. (squares), Haberer et al. (a) (diamonds), Setiawati et al. (triangles), Rao et al. (crosses) and Haberer et al. (b) (asterisks) are overlaid for comparisons. Simulations were run for 72 h, but to enable better comparison only the first 24 hours are plotted.

7.2 Case example: Ibuprofen

Table 7-3: Input Parameters for Ibuprofen PBPK Model development and validation

Parameters	Value	Reference/ Comments
Physicochemical & Blood Binding		
MW (g/mol)	206.27	27
logP _{o:w}	3.23	27
pKa	4.5	27
Blood/ Plasma ratio	0.55	Predicted by Simcyp Simulation Toolbox
Fraction unbound in plasma	0.01	Predicted by Simcyp Simulation Toolbox
Absorption		
Model	ADAM	
f _{u,gut}	1.0	Predicted by Simcyp Simulation Toolbox
P _{eff, human} (x10 ⁻⁴ cm/s)	17.0	27
S ₀ (mg/mL)	0.043	27
Solubility factor (SF)	79.0	27
Formulation type	IR Suspension	
DLM particle handling model	Particle Population Balance	
Surface solubility options	Mechanistic surface pH model	
h _{eff} method	Fluid Dynamics	
Type of Dispersion	Monodispersed	
Mean Particle Size (min, max, bins)		
R	195.3 (0, 214.8, 50)	Estimated using the SIVA toolkit from <i>in vitro</i> dissolution data by Cristofolletti and Dressman ⁴²²
T-BE	174.3 (0, 191.7, 50)	
T-NBE	150.8(0, 165.9, 50)	
Distribution		
Model	Full PBPK	
V _{ss} (L/kg)	0.093	predicted by Method 2
K _p scalar	1	default
Elimination		
Model	IV Clearance	
Cl _{IV} (L/h) (%CV)	3.5 (30.0)	521

7.3 Case example: Flurbiprofen

Table 7-4: Mean (SD) demographic clinical study data used for the development and verification of flurbiprofen PBPK/PD model.

Dosing information	CYP2C9 genotype	N° of Subjects	Female Ratio	Ethnicity	Age (y)	BW/ BW Range (kg)	BH/ BH Range (cm)	Reference
Intravenous								
50 mg as 10mg/mL solution (injection within 2 minutes)	n.a.	24	0	Chinese	–	–	–	Mei et al. ⁴⁴⁵
Oral								
25 mL of oral solution containing 67.9 mg FLU with 175 mL water	n.a.	12	0	Caucasian	25-31	–	–	Gonzalez-Younes et al. ⁴⁵⁸
40 mL oral solution containing 100 mg FLU with 180 mL water	n.a.	15	0	Caucasian	29 (18-40)	76.4 (62.3-109.1)	177 (168-188)	Szpunar ⁴⁵⁹
Froben® -solution 40 mg	1*/1*	12	0	Korean	23.1 (2.4)	65.1 (7.1)	174.8 (5.0)	Lee et al. ⁵²²
Froben® -solution 40 mg	1*/3*	8	0	Korean	22 (2.7)	64.6 (7.1)	172.8 (6.4)	Lee et al. ⁵²²
USP-tablets (Mylan Pharmaceuticals) 50 mg	1*/1*	5	0.533	Caucasian	24 (5)	79 (18)	–	Lee et al. ⁴⁴⁸
USP-tablets (Mylan Pharmaceuticals) 50 mg	1*/2*	5	0.533	Caucasian	24 (5)	79 (18)	–	Lee et al. ⁴⁴⁸
USP-tablets (Mylan Pharmaceuticals) 50 mg	1*/3*	5	0.533	Caucasian	24 (5)	79 (18)	–	Lee et al. ⁴⁴⁸
Froben® 100 mg with 100 mL water	n.a.	23	0	Caucasian	27.2 (18-35)	71.8 (52.5)	–	Jamali et al. ⁴⁵⁷
Ansaid® 100 mg with 100 mL water	n.a.	23	0	Caucasian	27.2 (18-35)	71.8 (52.5)	–	Jamali et al. ⁴⁵⁷
Froben® 100 mg with 150 mL water	n.a.	4	0.5	Caucasian	26.8 (2.2)	67.8 (4.1)	–	Patel et al. ⁴⁴⁶
100 mg tablet with 200 mL water	n.a.	6	-	Caucasian	–	–	–	Suri et al. ⁴⁵³
Ansaid® 100 mg with 180 mL water	n.a.	15	0	Caucasian	29 (18-40)	76.4 (62.3-109.1)	177 (168-188)	Szpunar ⁴⁵⁹
3 x 50 mg conventional tablets (reference)	n.a.	20	0	Chinese	21.4 (2.5)	63.2 (5.1)	174.4 (4.2)	Liu et al. ⁴⁶²
3 x 50 mg orally disintegrated tablets (test)	n.a.	20	0	Chinese	21.4 (2.5)	63.2 (5.1)	174.4 (4.2)	Liu et al. ⁴⁶²

2 x Ansaid® 100 mg with 180 mL water	n.a.	15	0	Caucasian	29 (18-40)	76.4 (62.3-109.1)	177 (168-188)	Szpunar ⁴⁵⁹
3 x Ansaid® 100 mg with 180 mL water	n.a.	15	0	Caucasian	29 (18-40)	76.4 (62.3-109.1)	177 (168-188)	Szpunar ⁴⁵⁹

n.a.: not available

Table 7-5: Mean (SD) demographic clinical study data used for the gene-drug-drug interaction (GDDI) modeling with flurbiprofen as victim drug.

Victim drug dosing	Perpetrator drug dosing	Perpetrator In vitro Ki (μM)	N° of Doses	Interval (h)	CYP2C9 genotype	N° of Subjects	Female Ratio	Ethnicity	Age (y)	BW/ BW Range (kg)	BH/ BH Range (cm)	Reference
Flurbiprofen	Fluconazole											
po 50 mg s.d.	po 200 mg q.d.	11	7	2	1*/1*	11	0.64	—	25 (19-36)	73.7 (51-108)	166 (154-193)	Kumar et al. ⁴⁶¹
po 50 mg s.d.	po 400 mg q.d.	11	7	2	1*/1*	11	0.64	—	25 (19-36)	73.7 (51-108)	166 (154-193)	Kumar et al. ⁴⁶¹
po 50 mg s.d.	po 200 mg q.d.	17	7	2	1*/3*	8	0.63	—	23 (19-28)	66.9 (49-84)	167 (160-189)	Kumar et al. ⁴⁶¹
po 50 mg s.d.	po 400 mg q.d.	17	7	2	1*/3*	8	0.63	—	23 (19-28)	66.9 (49-84)	167 (160-189)	Kumar et al. ⁴⁶¹
po 50 mg s.d.	po 200 mg q.d.	23	7	2	3*/3*	2	0.0	—	(25,29)	(77, 85)	(177, 179)	Kumar et al. ⁴⁶¹
po 50 mg s.d.	po 400 mg q.d.	23	7	2	3*/3*	2	0.0	—	(25,29)	(77, 85)	(177, 179)	Kumar et al. ⁴⁶¹
po 100 mg s.d.	po 200 mg b.i.d.	14.3/20.3	2	0.5	—	12	0.25	Caucasian (n=8), other(n=4) ^a	19-54	—	—	Hanley et al. ⁴⁸³
po 100 mg s.d.	po 200 mg b.i.d.	29.9	2	0.5	—	14	0.21	—	29 \pm 8	81 \pm 14	—	Greenblatt et al. ⁴⁸⁴
po 100 mg s.d.	po 200 mg b.i.d.	14.3/20.3	2	0.5	—	12	0.17	—	24-55	—	—	Hanley et al. 2012 ⁴⁸⁵

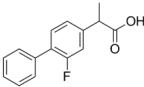
Victim Drug administration	Perpetrator Drug administration	Perpetrator In vitro Ki (μM)	N° of Doses	Interval (h)	CYP2C9 genotype	N° of Subjects	Female Ratio	Ethnicity	Age (y)	BW/ BW Range (kg)	BH/ BH Range (cm)	References
Flurbiprofen	Fluconazole											
po 50 mg s.d.	po 400 mg s.d	10	1	2	—	12	0.58	Caucasian (n=10), other (n=2) ^b	37 ± 3.1	—	—	Zgheib et al. ⁴⁸¹
po 50 mg s.d.	po 400 mg q.d	10	7	2	—	12	0.58	Caucasian (n=10), other (n=2) ^b	37 ± 3.1	—	—	Zgheib et al. ⁴⁸¹
po 50 mg s.d.	po 400 mg s.d	10	1	2	—	10	0.0	Caucasian (n=9), African (n=1)	27 (23-39)	—	—	Daali et al. ⁴⁸⁶
	Rifampicin											
po 50 mg s.d.	po 600 mg q.d.	n.a. ^c	5	0	—	10	0.0	Caucasian (n=9), African (n=1)	27 (23-39)	—	—	Daali et al. ⁴⁸⁶

n.a.= not available; ^a Hispanic(n=2), Asian(n=1), Afro-American (n=1); ^b Afro-American (n=2); ^c default value of Simcyp library compound

Table 7-6: Summary of main CYP2C9 genotype-based metabolic differences in the default inputs of the Simcyp® North European Caucasian (NEurCaucasian) and Chinese healthy volunteer virtual populations (Simcyp v18.2; Certara, Sheffield, UK).

Parameters	North European Caucasian						Chinese					
	1*/1*	1*/2*	1*/3*	2*/2*	2*/3*	3*/3*	1*/1*	1*/2*	1*/3*	2*/2*	2*/3*	3*/3*
Frequency	0.672	0.186	0.111	0.011	0.017	0.003	0.924	0.0024	0.0712	0	0	0.0024
CYP2C9 abundance in GI tract (pmol/mg)	12.5	11.4	11.4	11.4	11.4	3.4	10.3	9.3	9.3	9.3	9.3	2.8
CYP2C9 abundance in liver (pmol/mg)	83.4	75.8	75.8	75.8	75.8	23	68.5	62.3	62.3	62.3	62.3	18.9
Average liver volume (L)	1.65056						1.402976					

Table 7-7: Input parameters of flurbiprofen PBPK/PD model.

Parameters	Value	Reference/ Comments
Physicochemical & Blood Binding		
Chemical Structure		
MW (g/mol)	244.3	
logP _{o:w}	3.99	426,523
pKa	4.05	updated from <i>in vitro</i> solubility data (see section 3.2)
Blood/ Plasma ratio	0.55	524
Fraction unbound in plasma	0.01	427,524–527
Absorption		
Model	ADAM	
P _{app, Caco-2} (x10 ⁻⁶ cm/s)	20.1	measured value ²⁸⁷
P _{app, Caco-2, ref} (x10 ⁻⁶ cm/s)	1.57	negative calibrator (Atenolol) value ²⁸⁷
P _{app, Caco-2, ref} (x10 ⁻⁶ cm/s)	15.8	positive calibrator (Verapamil) value ²⁸⁷
P _{eff, human} (x10 ⁻⁴ cm/s)	4.83	predicted by Simcyp Permeability Calibrator-custom correlation
Formulation type	Immediate Release	
<i>In vivo</i> dissolution	see Tables 7 and 8	estimated DLM scalars from <i>in vitro</i> data (see section 2.7)
S ₀ (mg/mL)	0.018	<i>in vitro</i> data (see section 3.1)
logK _{m:w} neutral	5.37	estimated from <i>in vitro</i> data (see section 2.6, 3.2)
logK _{m:w} ion	2.46	estimated from <i>in vitro</i> data (see section 2.6, 3.2)
Distribution		
Model	Full PBPK	
V _{ss} (L/kg)	0.074	predicted by Method 2
K _p scalar	0.7	optimized based on IV data-PE module
Elimination		
F _{ox}	0.71	446
Model	Allelic-specific Enzyme Kinetics	
CYP2C9 1*/1*-V _{max} (pmol/min/pmol CYP)	15.79	Recombinant CYP (f _{u,mic} =1) ⁴⁴⁷
CYP2C9 1*/1*-K _m (μM)	8.756	Recombinant CYP (f _{u,mic} =1) ⁴⁴⁷
CYP2C9 1*/2*-V _{max} (pmol/min/pmol CYP)	11.53	Scaled for CL _{CYP2C9 1*/1*} / CL _{CYP2C9 1*/3*} =0.73 ⁴⁴⁸
CYP2C9 1*/2*-K _m (μM)	8.756	Recombinant CYP (f _{u,mic} =1) ⁴⁴⁷
CYP2C9 1*/3*-V _{max} (pmol/min/pmol CYP)	9.55	Scaled for CL _{CYP2C9 1*/1*} / CL _{CYP2C9 1*/3*} =0.605 ⁴⁴⁸
CYP2C9 1*/3*-K _m (μM)	8.756	Recombinant CYP (f _{u,mic} =1) ⁴⁴⁷

CYP2C9 2*/2*-V _{max} (pmol/min/pmol CYP)	10.04	Recombinant CYP (f _{u,mic} =1) ⁴⁴⁷
CYP2C9 2*/2*-K _m (μM)	10.39	Recombinant CYP (f _{u,mic} =1) ⁴⁴⁷
CYP2C9 3*/3*-V _{max} (pmol/min/pmol CYP)	8.901	Recombinant CYP (f _{u,mic} =1) ⁴⁴⁷
CYP2C9 3*/3*-K _m (μM)	23.25	Recombinant CYP (f _{u,mic} =1) ⁴⁴⁷
CYP2C9-ISEF	0.3	optimized based on IV data-PE module
UGT2B7-V _{max} (pmol/min/mg protein)	119.7	Recombinant UGT ⁵²⁸
UGT2B7-K _m (μM)	50.21	Recombinant UGT ⁵²⁸
UGT1A9-V _{max} (pmol/min/mg protein)	3.286	Recombinant UGT ⁵²⁸
UGT1A9-K _m (μM)	182.2	Recombinant UGT ⁵²⁸
Additional HLM liver	7.88	Retrograde model for a target f _{mCYP2C9} =0.71
CL _{int} (μL/min/mg protein)		
CL _{renal} (L/h)	0.066	446
Pharmacodynamics Model	Effect compartment linked to Inhibitory E _{max} model	453
k _{eo} (h ⁻¹) (%CV)	0.56 (43)	PD endpoint: <i>Evoked Potentials</i>
IC ₅₀ (mg/L)	25.8 (21)	
k _{eo} (h ⁻¹) (%CV)	0.89 (24)	PD endpoint: <i>Pain rating score</i>
IC ₅₀ (mg/L)	27.6 (10)	

8 Appendix

Appendix A1. List of publications

Publications in peer-reviewed journals:

Publication 1

Loisios-Konstantinidis J, Paraiso RLM, Fotaki N, McAllister M, Cristofolletti R, Dressman J. Application of the relationship between pharmacokinetics and pharmacodynamics in drug development and therapeutic equivalence: a PEARRL review. *J Pharm Pharmacol*. 2019 Apr;71(4):699-723. doi: 10.1111/jphp.13070. Epub 2019 Feb 22. PMID: 30793317

Publication 2

Loisios-Konstantinidis J, Cristofolletti R, Fotaki N, Turner DB, Dressman J. Establishing virtual bioequivalence and clinically relevant specifications using in vitro biorelevant dissolution testing and physiologically-based population pharmacokinetic modeling. case example: Naproxen. *Eur J Pharm Sci*. 2020 Feb 15;143:105170. doi: 10.1016/j.ejps.2019.105170. Epub 2019 Nov 27. PMID: 31783158.

Publication 3

Loisios-Konstantinidis J, Hens B, Mitra A, Kim S, Chiann C, Cristofolletti R. Using Physiologically Based Pharmacokinetic Modeling to Assess the Risks of Failing Bioequivalence Criteria: a Tale of Two Ibuprofen Products. *AAPS J*. 2020 Aug 23;22(5):113. doi: 10.1208/s12248-020-00495-4. PMID: 32830289. (*Equal first authorship*)

Publication 4

Loisios-Konstantinidis J, Cristofolletti R, Jamei M, Turner D, Dressman J. Physiologically Based Pharmacokinetic/Pharmacodynamic Modeling to Predict the Impact of CYP2C9 Genetic Polymorphisms, Co-Medication and Formulation on the Pharmacokinetics and Pharmacodynamics of Flurbiprofen. *Pharmaceutics*. 2020 Nov 2;12(11):1049. doi: 10.3390/pharmaceutics12111049. PMID: 33147873; PMCID: PMC7693160.

Publication 5

Loisios-Konstantinidis J, Dressman J. Physiologically Based Pharmacokinetic/Pharmacodynamic Modeling to Support Waivers of *In Vivo* Clinical Studies: Current Status, Challenges, and Opportunities. *Mol Pharm*. 2021 Jan 4;18(1):1-17. doi: 10.1021/acs.molpharmaceut.0c00903. Epub 2020 Dec 15. PMID: 33320002.

Appendix A2. Personal contributions

Publication 1: Application of the relationship between pharmacokinetics and pharmacodynamics in drug development and therapeutic equivalence: a PEARRL review.

My personal contributions to this work were: i) conceptualization, ii) design of the methodology and literature search iii) formal analysis and investigation of the content of the collected literature, iv) preparation of all equations and some visualizations (Figure 1), v) writing (preparation of original draft) of all sections in the manuscript except for the subsections “Proton pump inhibitors” and “Acetylsalicylic acid”, which were written by the second author Rafael Paraiso, v) review, editing and handling correspondence during the peer-review of the manuscript

Publication 2: Establishing virtual bioequivalence and clinically relevant specifications using in vitro bioequivalent dissolution testing and physiologically-based population pharmacokinetic modeling. case example: Naproxen.

My personal contributions to this work were: i) conceptualization of the research, ii) design of the methodology and literature search for the selection of the studied compound/drug, iii) design, development and validation of the analytical method (HPLC-UV), iv) design, planning and execution of all *in vitro* solubility and dissolution experiments, iv) design, planning and execution of all modeling and simulation activities (i.e., model-based analysis of *in vitro* data, development and validation of PBPK models, performance and statistical analysis of virtual bioequivalence trials), v) formal analysis and interpretation of the *in vitro* data and *in silico* simulations, vi) preparation of all visualizations (Figures and Tables), vii) writing the complete manuscript, viii) review, editing and handling correspondence during the peer-review of the manuscript

Publication 3: Using Physiologically Based Pharmacokinetic Modeling to Assess the Risks of Failing Bioequivalence Criteria: a Tale of Two Ibuprofen Products.

My personal contributions to this work were: i) planning and execution of the research and modeling and simulation activities (i.e., model-based analysis of *in vitro* data, development and validation of PBPK models, performance and statistical analysis of virtual bioequivalence trials) in collaboration with Bart Hens and Rodrigo Cristofolletti, ii) formal analysis and interpretation of the data in collaboration with Bart Hens, Rodrigo Cristofolletti, Sarah Kim and Chang Chiann, iii) writing of the sections “Methods” and “Results” and contribution to the section “Discussion” of the manuscript, iv) contribution to the review and editing of the manuscript

Publication 4: Physiologically Based Pharmacokinetic/Pharmacodynamic Modeling to Predict the Impact of CYP2C9 Genetic Polymorphisms, Co-Medication and Formulation on the Pharmacokinetics and Pharmacodynamics of Flurbiprofen.

My personal contributions to this work were: i) conceptualization of the research, ii) design of the methodology and literature search for the selection of the studied compound/drug, iii) design, development and validation of the analytical method (HPLC-UV), iv) design, planning and execution of all *in vitro* solubility and dissolution experiments, iv) design, planning and execution of all modeling and simulation activities (i.e., model-based analysis of *in vitro* data, development and validation of PBPK/PD models, extrapolation to different ethnic groups and genetic polymorphisms), v) formal analysis and interpretation of the *in vitro* data and *in silico* simulations, vi) preparation



of all visualizations (Figures and Tables), vii) writing the complete manuscript, viii) review, editing and handling correspondence during the peer-review of the manuscript

Publication 5: Physiologically Based Pharmacokinetic/ Pharmacodynamic Modeling to Support Waivers of *In Vivo* Clinical Studies: Current Status, Challenges, and Opportunities.

My personal contributions to this work were: i) conceptualization of the research, ii) design of the methodology and literature search v) formal analysis and interpretation of the in vitro data and in silico simulations, iii) formal analysis and investigation of the content of the collected literature, iv) preparation of all visualizations (Figures and Tables), v) writing the complete manuscript, vi) review, editing and handling correspondence during the peer-review of the manuscript

Appendix A3. Peer reviewed publications

Application of the relationship between pharmacokinetics and pharmacodynamics in drug development and therapeutic equivalence: a PEARL review

Ioannis Loisos-Konstantinidis^a , Rafael L. M. Paraiso^a, Nikoletta Fotaki^b , Mark McAllister^c, Rodrigo Cristofolletti^d and Jennifer Dressman^a

^aInstitute of Pharmaceutical Technology, Goethe University, Frankfurt am Main, Germany, ^bDepartment of Pharmacy and Pharmacology, Faculty of Science, University of Bath, Bath, ^cPfizer Drug Product Design, Sandwich, UK and ^dDivision of Therapeutic Equivalence, Brazilian Health Surveillance Agency (ANVISA), Brasilia, Brazil

Keywords

drug development; modelling and simulation; pharmacokinetics/pharmacodynamics; regulatory science; therapeutic equivalence

Correspondence

Jennifer Dressman, Biocenter, Institute of Pharmaceutical Technology, Johann Wolfgang Goethe University, Max-von-Laue-Str. 9, Frankfurt am Main 60438, Germany. E-mail: dressman@em.uni-frankfurt.de

Received November 15, 2018

Accepted January 19, 2019

doi: 10.1111/jphp.13070

Abstract

Objectives The objective of this review was to provide an overview of pharmacokinetic/pharmacodynamic (PK/PD) models, focusing on drug-specific PK/PD models and highlighting their value added in drug development and regulatory decision-making.

Key findings Many PK/PD models, with varying degrees of complexity and physiological understanding have been developed to evaluate the safety and efficacy of drug products. In special populations (e.g. paediatrics), in cases where there is genetic polymorphism and in other instances where therapeutic outcomes are not well described solely by PK metrics, the implementation of PK/PD models is crucial to assure the desired clinical outcome. Since dissociation between the pharmacokinetic and pharmacodynamic profiles is often observed, it is proposed that physiologically based pharmacokinetic and PK/PD models be given more weight by regulatory authorities when assessing the therapeutic equivalence of drug products.

Summary Modelling and simulation approaches already play an important role in drug development. While slowly moving away from 'one-size fits all' PK methodologies to assess therapeutic outcomes, further work is required to increase confidence in PK/PD models in translatability and prediction of various clinical scenarios to encourage more widespread implementation in regulatory decision-making.

Introduction

Over the last decades, pharmacokinetic/pharmacodynamic (PK/PD) models have been evolving rapidly, starting with the pioneering work in the 1960s, then moving from empirical descriptions to models based on mechanistic and physiological approaches and still evolving today in the form of state-of-the-art mathematical models describing the progression of diseases as well as entire biological systems, under the umbrella of systems pharmacology and computational biology.^[1–7]

At the beginning of the conjunction of pharmacokinetics with pharmacodynamics, empirical models which were based on the shape of the effect–concentration curve and which assumed that the pharmacologic response is directly related to the drug plasma concentration were

introduced. Soon, it was recognized that this scenario is only valid when the equilibrium between the plasma and the site of action is instantaneous, when the free drug concentration and its distribution to all tissues are the same (or remain proportionally the same) and when the system is at steady state. A variety of these so-called steady-state empirical direct effect models have been reported in the literature: linear, power, hyperbolic, sigmoid (E_{max} model), logarithmic and logistic. Even though these models have been applied in a number of situations,^[1,8,9] they have two important limitations. First and most important, they are time-independent (also referred to as static models). Second, they lack a mechanistic and/or physiological understanding of the underlying pharmacokinetics and pharmacodynamics.^[10] For these reasons, non-steady-state, mechanistic and physiologically based

modelling approaches were introduced and these are more widely used these days in drug development.

In parallel to the developments in modelling approaches, major regulatory authorities have been moving slowly but surely from ‘one-size fits all’ concepts to a more case-by-case, scientifically justified approach, in which the application of modelling and simulation (M&S) is playing a valuable supporting role. Physiologically based pharmacokinetic (PBPK) and PK/PD models have already been implemented in the assessment of drug–drug interactions (DDIs) and extrapolation of results from adults to paediatric populations.^[11–16] In addition, generic dermatologic and inhalation products have been approved based on pharmacodynamic or clinical endpoint bioequivalence studies (BE).^[17,18]

Most recently, pharmacokinetic metrics providing information about delivery of the drug to the body and exposure (i.e. onset and duration of action),^[19] such as partial areas under the concentration–time curve have been recommended by the US-FDA for the evaluation of several complex oral products combining immediate (IR) with extended release.^[20–22] However, there are still many cases, especially for systematically acting drugs, where the value of M&S methods has not yet been widely recognized by the regulatory authorities. Such cases include the virtual bioequivalence of oral drug products, the justification for potential extension of BCS-based biowaivers to some BCS class II compounds and reduction of the number of volunteers for bioequivalence studies of highly variable drugs. In view of the fact that single-point pharmacokinetic metrics (i.e. C_{max} , AUC) used to assess bioequivalence do not always comprise an appropriate surrogate for therapeutic equivalence (TE), which by definition is the ultimate goal of bioequivalence studies,^[23] it would seem appropriate to implement M&S approaches to assure therapeutic outcomes in this arena too.

The aim of this review was to provide an overview of existing non-steady-state PK/PD models, focusing on drug-specific case examples. These are intended to serve as examples of the importance of mechanistic PK/PD models in assuring desired therapeutic outcomes in clinical practice and to encourage wider implementation of PK/PD in support of regulatory decision-making.

The effect compartment model

Overview

In many cases, the site of action of a drug is kinetically distinct from plasma and the equilibration between the plasma and the effect site is often rather slow. In such cases, there will be a temporal delay between the drug plasma (C_p) and effect-site concentrations (C_e) and the effect will be a function of C_e rather than of C_p . Even though bioanalytical methods have improved greatly over the last decades, measuring the concentration at the effect site often remains a challenge, due to the lack of tissue accessibility.

In 1970, a hypothetical compartment serving as a link between the pharmacokinetic and pharmacodynamic models to address the equilibration kinetics was introduced by Segre *et al.*^[2] and was applied for the first time by Forester *et al.*^[24] to describe the time course of effect of various cardiac glycosides.^[25] This approach, using a so-called ‘effect compartment’ or ‘biophase distribution’ model (Figure 1), was further elaborated and described mathematically by Holford and Sheiner^[3,26] as follows:

$$\frac{dA_e}{dt} = k_{1e} \cdot A_p - k_{e0} \cdot A_e. \quad (1)$$

where A_p and A_e are the amounts of drug in the plasma (main compartment) and in the effect compartment,

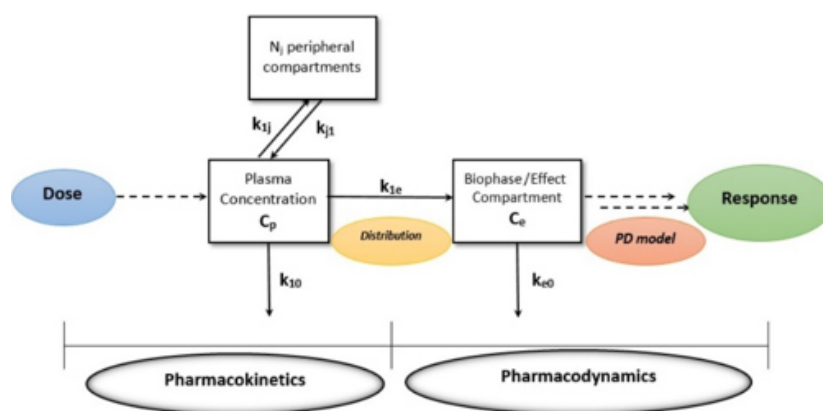


Figure 1 Schematic illustration of the biophase distribution model. The hypothetical effect compartment bridges the pharmacokinetic with the pharmacodynamic model. In most cases, the link is with the central (plasma) compartment, without excluding the possibility of linking the effect compartment with a peripheral compartment instead (adapted with permission from ref. [10]) [Colour figure can be viewed at wileyonlinelibrary.com]

respectively, and k_{1e} , k_{e0} are the first-order rate constants for distribution and elimination from the hypothetical compartment, respectively.

Assuming that the effect compartment receives a negligible amount of drug and that distribution to and clearance from the biophase compartment are equal, the model can be simplified and then coupled with a pharmacodynamic model, for example a sigmoid E_{\max} model:

$$k_{1e} \cdot V_p = k_{e0} \cdot V_e \quad (2)$$

$$\frac{dC_e}{dt} = k_{e0} \cdot (C_p - C_e) \quad (3)$$

$$E(C_e(t)) = \frac{E_{\max} \cdot C_e(t)^\gamma}{C_e(t)^\gamma + EC_{e50}^\gamma}, \quad (4)$$

where C_p , V_p , C_e and V_e are the concentration and the volume in the central and effect compartment respectively; E_{\max} , EC_{e50} and γ represent the maximum effect, the concentration in the effect site required to reach 50% of the maximum effect and the sigmoidicity factor, respectively. Alternatively, the hypothetical compartment could be coupled with a peripheral compartment instead of the central compartment. However, it is not very common to use samples obtained at the effect site (e.g. using microdialysis) or any other peripheral compartment as a pharmacokinetic surrogate.

A hallmark of the effect compartment model is the hysteresis observed in the effect–concentration plot due to the time delay between pharmacokinetics and pharmacodynamics. In fact, this is a common attribute of non-steady-state pharmacokinetic/pharmacodynamic (PK/PD) models.^[27] Well-known examples of drugs exhibiting a biophase distribution delay-related response include neuromuscular blocking agents such as d-tubocurarine (see Section ‘Applications and case examples’) and pancuronium,^[28] the calcium channel blocker verapamil,^[29] and the bronchodilator theophylline.^[30] Further cases that have been reported in the literature include quinidine, disopyramide, opioids such as pethidine, morphine and fentanyl, diclofenac, organic nitrates, benzodiazepines and digoxin.^[31–38] In the following section, the models for tubocurare, pancuronium, ibuprofen and morphine are used to illustrate application of the effect compartment model.

Applications and case examples

d-tubocurarine and pancuronium

The assumption of a direct relationship between pharmacokinetics and drug response has been questioned for more than half a century, as illustrated by the case of d-tubocurarine.

Already in the early 1960s, the first attempts to simultaneously model pharmacokinetics and pharmacodynamics, based on the available plasma concentration and effect data for d-tubocurarine, were made. In 1964, Levy implemented a log-linear model to describe the time course of d-tubocurarine response, assuming one-compartment pharmacokinetics following intravenous bolus administration, based on the results of Ryan *et al.*^[39] The log-linear model assumed that the effect of muscular relaxation is a linear function of the logarithm of the amount of d-tubocurarine present in the plasma, while elimination of the amount of d-tubocurarine in the body occurs exponentially with time.^[11] In 1972, an open three-compartment model for the pharmacological effect of d-tubocurarine was proposed by Gibaldi *et al.*^[40] The amount of drug in the central compartment at the time of recovery from neuromuscular block was deemed by these authors to be dose-independent. This observation, combined with the very rapid onset of action of d-tubocurarine, led the authors to the conclusion that the site of action is located in the central compartment,^[40] implying instantaneous equilibration between plasma concentration and response. However, the data on which this model was based had been collected during the terminal elimination phase, during which a pseudo-equilibrium between plasma and tissues concentration is reached and the distributional delay is minimized.

By contrast, Hull *et al.*^[41] showed that after administration of pancuronium, a similar to d-tubocurarine neuromuscular blocking agent, a linear relationship between the logarithm of concentration and the response is a poor predictor of the early phase response, in which a hysteresis between the concentration in any compartment and twitch depression is observed. By adding a biophase compartment, expressed similarly to equation (3), and assuming that the same degree of paralysis (i.e. during onset and offset of action) is associated with the same C_e , they were able to empirically relate the intensity of pharmacologic effect to the concentration at the site of action at every time point using a fixed effect pharmacodynamic model.^[41] In the case of d-tubocurarine, the effect compartment model, as described mathematically by Holford and Sheiner,^[3,26] was successfully applied as well. Plasma concentration and effect data after intravenous administration were analysed from healthy subjects and patients with renal failure. The model was able to fit data from both groups without statistically significant differences in the pharmacokinetic or pharmacodynamic parameters between the two groups.^[42] Interestingly, the equilibration half-life (4 min) for pancuronium estimated in a more empirical way by Hull *et al.*^[41] was very similar to the one for d-tubocurarine reported by Sheiner *et al.*^[42] using an explicit PK/PD model.

In parallel, Stanski *et al.*^[43] explored the influence of various anaesthetic agents on the muscle-relaxing effect of d-tubocurarine. Halothane-induced anaesthesia, in comparison to anaesthesia with morphine and nitrous oxide, prolonged the equilibration half-life. An open two-compartment pharmacokinetic model coupled with a hypothetical effect compartment was implemented to fit both plasma and muscle paralysis data. Interestingly, changes in pharmacodynamic (k_{e0} , $t_{1/2ke0}$, EC_{50}) but not in pharmacokinetic parameters were observed for patients under halothane anaesthesia. Furthermore, it was possible to distinguish between the effects of the agents on the EC_{50} for muscle paralysis showing that halothane sensitizes the neuromuscular junction to d-tubocurarine. Provided that the diffusion of tubocurarine into the extracellular fluid of the muscle and the receptor affinity is high, the rate-limiting step for the onset of action is the rate of muscle perfusion, which is inversely proportional to the equilibration half-life ($t_{1/2ke0}$).^[43] Although the onset and the magnitude of response are dependent on muscle blood flow, the recovery from neuromuscular blockage is perfusion-independent and solely related to the drug–receptor dissociation rate.^[44] The significant increase in $t_{1/2ke0}$ under halothane-induced anaesthesia is consistent with the decreased muscle blood flow, which would suggest a later onset of paralysis. However, halothane also decreases the EC_{50} , which compensates for the decrease in perfusion and results in a similar onset to that observed under morphine and nitrous oxide anaesthesia.

In summary, the evaluation of the pharmacokinetics in concert with the pharmacodynamics of these two muscle relaxants enabled a more mechanistic description of their dose–response characteristics and a better understanding of the drug interaction with the anaesthetic. These early successes triggered further interest in combining pharmacokinetics with pharmacodynamics to achieve a more mechanistic description of the relationship between dose, dosing regimen and clinical effects.

Ibuprofen: dental pain relief

Ibuprofen was selected as a model drug to investigate the clinical relevance of bioequivalence metrics to the therapeutic effect. An analysis of 25 bioequivalence studies of Ibuprofen immediate-release oral dosage forms over a dose range of 200–600 mg showed that 14 of the studies failed to prove bioequivalence in C_{max} , even though AUC fell within the bioequivalence limits.^[45] The authors reported that ibuprofen, a weakly acidic BCS class II compound, is at higher risk to fail bioequivalence because of C_{max} variations. However, in cases where the plasma concentration is related non-linearly and/or indirectly to the drug effect,^[3,46] the C_{max} and t_{max} values may not be accurate

metrics for the therapeutic response. For example, if the C_{max} is higher than anticipated, this will not necessarily translate to toxic effects. Likewise, if the C_{max} is lower, this will not necessarily result in lack of efficacy.^[47]

Dissociation between pharmacokinetics and pharmacodynamics is common for non-steroidal anti-inflammatory drugs (NSAIDs). This may be because of delayed distribution to the biophase or related to an indirect response mechanism, for example when the pharmacodynamic endpoint is the inhibition of inflammation mediators.^[48] Pain relief and antipyresis after administration of ibuprofen formulations have been extensively modelled in different populations. In this section, the main studies for pain relief after third molar extraction are presented, while studies investigating the antipyretic effect are addressed in Section ‘Ibuprofen: antipyretic response’.

Third molar extraction pain models describe the post-operative onset of inflammation, with maximum pain intensity occurring in 12 h or less. Relief from pain associated with tooth extraction exhibits high reproducibility and a low placebo effect, features that are important for differentiation among various doses and thus for the identification of dose–response curves.^[49–52] The most commonly evaluated endpoints in dental pain models are the *pain intensity difference* (PID) and *sum of pain intensity difference* (SPID), the *pain relief* (PAR) and *total pain relief* (TOTPAR), the *time to remedication* (REMD), the *time to first perceptible pain relief* (TFPR) and *time to first meaningful pain relief* (TFMP).^[53,54]

In a double-blind, randomized, single- and multi-dose study of 254 adult patients, who had undergone third molar surgery, Hersh *et al.*^[50] reported a positive dose–response relationship for sum pain intensity (SPID), TOTPAR, REMD and overall pain relief, after administration of 200 and 400 mg of ibuprofen as a single dose. During the multi-dose phase, no significant differences between the two dose levels were detected. The authors concluded that patients could benefit from higher doses for pain treatment immediately after the extraction, but that lower doses would be satisfactory thereafter. These results suggest that the single-dose approach adopted for bioequivalence testing might be over-discriminating for the assessment of ibuprofen formulations with regard to the maintenance of dental pain relief. Indeed, McQuay *et al.*^[55] observed no significant differences between 200 and 400 mg of ibuprofen in a double-blind, randomized, placebo-controlled, single-dose study comparing the analgesic effect of 200 and 400 mg of ibuprofen with placebo and with 200 mg ibuprofen plus 50, 100 or 200 mg caffeine in 161 adult patients after third molar removal. In a further study, a positive dose–response relationship of ibuprofen over the dose range 50–400 mg with regard to SPID and TOTPAR was reported by Schou *et al.*^[54] However, in terms of

TOTPAR, the doses of 200 and 400 mg did not differ significantly.

A meta-analysis of data from 13 trials with total of 994 patients reported an absolute increase of only 9% (from 59% to 68%) in the number of patients who achieved at least 50% pain relief when the dose of ibuprofen was doubled from 200 to 400 mg, meaning that 10 patients would need to be treated with the higher dose for just one of them to benefit.^[56] The analysis indicates that the dose–response relationship is rather flat in the dose range 200–400 mg with respect to dental pain relief by ibuprofen.

Li *et al.*^[53] applied a pharmacodynamic model to investigate the onset and offset of dental pain relief after administration of effervescent and standard tablets containing 400 mg ibuprofen. As an endpoint, a categorical pain relief score was applied and treated as a continuous variable, in agreement with Lemmens *et al.*^[57] The observed distributional delay of the response to ibuprofen was addressed by the addition of an effect compartment model and the overall effect as the sum of placebo and drug was described as following:

$$\frac{d(C_e[t])}{dt} = k_{e0} \cdot \{C_p[t] - C_e[t]\} \quad (5)$$

$$f_d(C_e) = \frac{E_{\max} \cdot C_e^\gamma}{C_e^\gamma + EC_{50}^\gamma} \quad (6)$$

$$f_p[t] = P_{\max} \cdot (1 - e^{-k_p \cdot t}) \quad (7)$$

$$PR(t) = f_p[t] + f_d(C_e) + \varepsilon, \quad (8)$$

where C_p and C_e are the drug concentrations in plasma and in the effect-site compartment, respectively; k_{e0} and k_p are the first-order rate constants for the placebo effect and equilibration, respectively; E_{\max} and P_{\max} are the maximum ibuprofen and placebo effect, $f_d(C_e)$ and $f_p[t]$ are the pain relief by ibuprofen and placebo, respectively; γ and EC_{50} are the sigmoidicity factor and the drug plasma concentration to achieve 50% of E_{\max} , respectively; $PR(t)$ represents the pain relief score at a given time t , and ε stands for the normally distributed residual variability.

The model was able to describe the pain relief score data adequately and the effect was directly related to the effect-site concentration, which increased much faster for the effervescent than the standard tablets, with the peak effect-site concentration occurring one hour earlier than for the standard tablet (1.0 h vs 2.0 h). The sigmoidicity factor was estimated to be 2.0 ± 0.43 , confirming the relatively flat dose–response curve of ibuprofen.

More recently, a PBPK/PD model for Ibuprofen was developed and validated by Cristofolletti and Dressman^[58] with the Simcyp Simulator version 12.2 (Certara, Sheffield,

UK.), fitting antipyretic and dental pain relief pharmacodynamic models to pharmacokinetic and pharmacodynamic data already published in the literature. The main goals of this study were a comprehensive evaluation of the clinical relevance of bioequivalence criteria for ibuprofen immediate-release oral dosage forms and a risk assessment of waiving *in vivo* bioequivalence studies of such products. To simulate the pharmacokinetic and pharmacodynamic profiles, virtual populations similar to those enrolled in the clinical studies by Walson *et al.*^[59] and Li *et al.*^[53] in terms of age and gender ratio were generated, such that virtual trials for the dental pain relief model included 100 adults per trial, aged between 18 and 40 years, and receiving tablets of 100, 200, 280 or 400 mg of ibuprofen. One-at-a-time sensitivity analysis for the gastric solubility, gastric emptying time, apparent permeability coefficient (P_{app}) and small intestine pH was conducted, and the effect of applying different dissolution rates in the simulations on the resulting pharmacokinetic and pharmacodynamic profiles was also investigated.^[58] The authors found that the dose–response curve for dental pain relief is shallow and, as a result, relatively insensitive to changes in plasma concentrations within the range 12–23 mg/l (applying an EC_{50} of 10.2 mg/l). Comparing the pharmacodynamic response after the simulated administration of 280 mg vs 400 mg Ibuprofen tablets to adults undergoing third molar extraction, no significant differences in the response occurred. Interestingly, although (under the assumption that the 400 mg tablet is the reference product and the 280 mg tablet is the test product in a virtual bioequivalence scenario) the test product would not be bioequivalent to the reference product in terms of pharmacokinetics (C_{\max} ratio ($C_{\max-T}/C_{\max-R}$) of 0.7), the 280 mg tablet would be still considered therapeutically equivalent to the 400 mg tablet for dental pain relief in adult patients.

Cristofolletti and Dressman also combined *in vitro in vivo* extrapolation with PBPK/PD modeling to simulate the effect of different dissolution rates from products containing ibuprofen-free acid (IBU-H) and salts (IBU salts) and to investigate whether these would (1) reflect reported differences in pharmacokinetics as well as whether (2) differences in pharmacokinetics would translate into difference in the ability of ibuprofen to relieve dental pain in adults.^[60] The model was able to adequately predict the observed pharmacokinetic profiles. The pain relief model by Li *et al.*^[53] was adopted to simulate ibuprofen response. As expected from the faster dissolution of the products containing salt forms of ibuprofen, the 90% confidence intervals for C_{\max} did not meet the average bioequivalence acceptance criteria. However, pain relief scores elicited by ibuprofen free acid and salts were identical. Interestingly, the simulated peak effect-site concentrations for both IBU-H and IBU salts 400 mg were found to be higher than the

estimated $EC_{80} \approx 20$ mg/l, indicating that the extent of pain relief would be insensitive to pharmacokinetic changes at this dose level. Importantly, the duration over which the effect-site concentrations are maintained above EC_{80} should be also taken into account. The authors concluded that the bioequivalence criteria for C_{max} might be over-discriminatory and not clinically relevant for assessing TE of ibuprofen products in terms of overall dental pain relief.

As illustrated by the example of ibuprofen, TE is not always captured appropriately by simple plasma concentration measurements due to the insensitivity of the pharmacodynamic response to the pharmacokinetics in the dose range typically applied. From this case example, it is evident that the interaction of the drug pharmacokinetics with the pharmacologic response should be taken into account to set clinically relevant specifications ('safe spaces') for drug products. M&S techniques would be a powerful tool in this direction, facilitating a regulatory transition from the current 'one-size fits all' bioequivalence paradigm to a scenario based on the clinically based, specific PK/PD characteristics of the drug product and thus able to provide a more accurate assessment of TE.

Anti-nociceptive effect of morphine

For drugs which exhibit high biological target affinity and/or reach their site of action by active transport mechanisms, distribution to the biophase may or may not impose a rate-limiting step. Over the past few years, several specific transporters that may influence the distribution of drugs to their site of action in the central nervous system (CNS) have been identified.^[61–64] However, the number of PK/PD studies exploring the functional role of these transporters in the distribution to the effect site is few. One interesting example is the anti-nociceptive effect of morphine, for which mechanism-based models of the biophase distribution within the CNS were established using intracerebral microdialysis.

Letrent *et al.*^[65] investigated the effect of GF120918, a potent and selective P-glycoprotein (P-gp) inhibitor, on the pharmacokinetics and pharmacodynamics of morphine in rats, which were randomized into GF120918 pretreated, vehicle and control groups. The concentrations of both morphine and its metabolite, morphine-3- β -glucuronide (M3G), in serum were quantified and the anti-nociception was expressed as the percentage of maximum possible response (% MPR). A two-compartment pharmacokinetic model, together with an effect compartment coupled to a sigmoidal E_{max} model, was employed to simultaneously fit the pharmacokinetic and pharmacodynamic data. Among the pharmacokinetic (AUC, Cl, MRT, V_{ss}) and pharmacodynamic (k_{e0} , EC_{50} , γ) parameters evaluated, only the equilibration rate constant (k_{e0})

and the %MPR were significantly altered by pretreatment with GF120918, indicating a faster onset and more intense action, respectively ($P = 0.0023$). The increased pharmacodynamic response could not be attributed to pharmacokinetic changes or to the elevated M3G concentrations. Since M3G does not possess any anti-nociceptive properties,^[66–68] the authors suggested that the inhibition of P-gp by GF120918 might diminish the efflux of morphine from brain capillary endothelial cells, leading to more rapid distribution and higher concentrations of morphine at its site of action. These data were supported by Xie *et al.*,^[69] who demonstrated, using trans-cortical microdialysis, that morphine concentrations in the brain were increased (1.7-fold) after administration to *mdr-1a* genetic deficient rats, whereas the metabolite M3G was unaffected.

Evaluation of the kinetics of biophase distribution within the CNS by intracerebral microdialysis, which has already been successfully applied to the characterization of the distributional behaviour in several cases,^[69–72] is a promising tool for the development of more sophisticated, mechanism-based models, enabling as yet unexplained aspects of the pharmacodynamics of CNS acting drugs to be illuminated.

Modelling of irreversible mechanisms of action

Overview

In this section, we describe some examples of drugs that act in the human body through irreversible inhibition at the site of action. In general, pharmacodynamic (PD) effects are initiated by the interaction of drugs with targets such as receptors, enzymes, ion channels, cell membranes etc. Such interactions may be reversible, with a balance between association and dissociation of the drug with the target, or irreversible when a drug bonds covalently to the target or the dissociation rate is extremely slow compared to the relevant time span. As a result of these interactions, a cascade of events is triggered, leading to the pharmacological effect, which can either stimulate (agonist) or inhibit (antagonist) a physiological process.^[73,74]

In many cases, drugs that irreversibly inhibit a physiological process are transformed, as a first step, into reactive metabolites, which then bind covalently to their target, resulting in its inactivation. In order for the pre-existing situation to be re-established, it is necessary to resynthesize the target. In such cases, the duration of action is likely to be independent of the pharmacokinetic half-life of elimination of the drug and instead depends essentially on the *de novo* synthesis of the target. The irreversible inactivation of endogenous enzymes or receptors caused by drugs, for

example, the antiplatelet effect of aspirin after binding cyclooxygenase-1,^[75,76] the 5α -reductase inhibitors^[77,78] and the proton pump inhibition by proton pump inhibitors (PPIs),^[79–81] is often described using such turnover models. Further examples are drugs that trigger apoptosis in human cells, bactericidal antibiotics,^[82] reduction of viral load due to the treatment with antivirals,^[83] cell death processes induced by anticancer drugs^[84] and cytotoxic drugs which cause myelosuppression.^[85]

In general, the turnover models that have been presented in the literature are based on the following differential equation:^[86]

$$\frac{dR}{dt} = k_{in} - k_{out} \cdot R - f(C) \cdot R \quad R(0) = R_0, \quad (9)$$

where R denotes the response produced by the drug, R_0 is its initial response value, k_{in} is a zero-order rate constant for the response, k_{out} is a first-order elimination rate constant and the function of the drug concentration $f(C)$ can be interpreted as a bimolecular interaction of the drug or its active metabolite with the target. This is the general equation representing the turnover rate of the response; however, more complex scenarios are also possible, requiring more mechanistic models to be developed as will be discussed later.

Figure 2 depicts a turnover model that can be applied to the interaction between the drugs with receptors, enzymes or ion channels. In the case of interaction with endogenous enzymes, the k_{in} and k_{out} parameters represent apparent rates of response formation and dissipation respectively and $f(C)$ represents the effect as a function of drug concentration.

Applications and case examples

Proton pump inhibitors

Proton pump inhibitors were chosen as the drug model for this topic since their inhibition of the proton pump (H^+ , K^+ -ATPase) enzyme present in the parietal cells of the stomach is irreversible. To understand the mechanism of

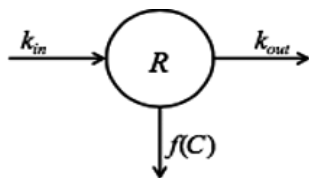


Figure 2 Schematic representation of the turnover model with irreversible inhibition of response (reproduced with permission from ref. [86]).

inhibition by the PPIs, models describing the turnover of H^+ , K^+ -ATPase have been described.

The PPIs are, in and of themselves, inactive drugs that require an acidic environment for their activation. These weakly basic substances reach the general circulation after absorption from the gastrointestinal tract and then become concentrated in the acid compartment of the parietal cells present in the gastric mucosa. Following their activation by conversion to the sulphonamide form in the acidic intracellular environment of the parietal cells, a covalent bond occurs between the activated PPI and cysteine residues present in H^+ , K^+ -ATPase. This enzyme is responsible for the final step in the secretory gastric acid process.^[80,87,88] As a consequence of the binding, the enzyme is inactivated and this results in suppression of acid secretion into the gastric lumen.^[79,89] PPIs inhibit both basal and stimulated gastric acid secretion, regardless of the nature of stimulation of the parietal cells. In order for the acid secretion to be re-established, *de novo* synthesis of H^+ , K^+ -ATPase is necessary.^[89–91]

Even though the elimination half-life of PPIs is only 1–2 h, the pharmacodynamic half-life of the inhibitory effect on H^+ , K^+ -ATPase is about 48 h, rendering a rapid elimination (PK) but long duration of response (PD) to members of this class.^[91–93] By comparison, the pharmacodynamics of drugs that reversibly bind to the proton pump to decrease acidic secretion in the stomach, such as cimetidine and other H_2 receptor antagonists, can be described with a direct response PD model.^[94]

To construct a mechanistic PK/PD model for PPIs, several factors have to be considered: the accumulation of PPI in the parietal cell, the amount of active enzymes present in the canaliculus of parietal cell, the rate of *de novo* synthesis of new proton pump enzymes, the metabolism and inactivation of PPIs, the extent of covalent PPI binding to the proton pump in the parietal cell and the stability of this binding.^[95] Because of this complexity, several different models have been proposed to describe the relationship between PK and PD for this class of drugs. There are empirical models that simply consider the turnover of the proton pump and those that are more mechanistic, taking into account the relevant physiology and PPI characteristics. In this section, we will focus on PK/PD models that have been used to describe the difference between the elimination half-life (PK) of PPIs and the temporal inhibition of acid secretion (PD) that results from binding of the PPI with H^+ , K^+ -ATPase.

Katashima *et al.*^[94] were the first to publish a mechanistic PK/PD model for PPIs. In the first study, a model relating the unbound plasma concentration (C_f) of lansoprazole and omeprazole to the inhibitory effect on stomach acid secretion was developed. This model,

illustrated in Figure 3, utilizes the apparent turnover process of H^+ , K^+ -ATPase to describe the relationship between plasma concentration and the inhibitory effect of the PPIs on gastric acid secretion.^[96]

According to this PK/PD model, the inactive form of the PPI is present in the plasma, and only after reaching the acidic environment of the parietal cells is it transformed into the active form. This form then reacts with active H^+ , K^+ -ATPase according to a second-order reaction with the rate constant, K , to establish a covalent bond between the activated PPI and H^+ , K^+ -ATPase, resulting in inactivation of the enzyme.

The total amount of proton pump (E_t) remains at a constant level (k_s/k_1) because H^+ , K^+ -ATPase is synthesized, on the one hand, at a rate described by the zero-order rate constant, K_s , but also eliminated, on the other hand, at a rate described by the first-order rate constant k_1 . The inactive proton pump recovers at a rate described by the first-order rate constant k_2 . Under these circumstances, the apparent turnover rate constant, k , is represented by $k_1 + k_2$. The time courses of variation in the amount of active H^+ , K^+ -ATPase (E) and the inactive fraction (E_c) are expressed by the following equations:

$$\frac{dE}{dt} = -K \cdot C_f \cdot E - k \cdot E + k_2 \cdot E_c + K_s \quad (10)$$

$$\frac{dE_c}{dt} = K \cdot C_f \cdot E - (k_1 - k_2) \cdot E_c \quad (11)$$

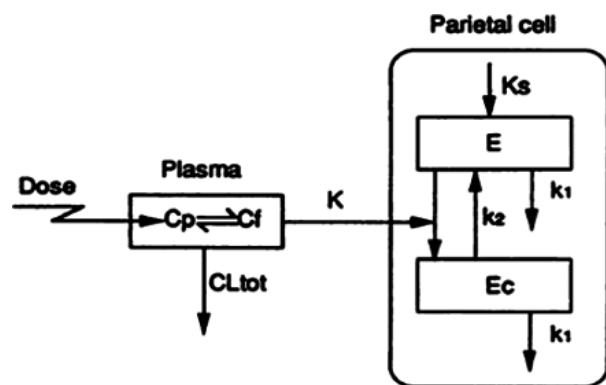


Figure 3 PK/PD model describing the relationship between PPI concentration in plasma and its inhibitory effect on gastric acid secretion. C_p is the plasma concentration of PPI, C_f is the unbound concentration of PPI in the plasma, CL_{tot} is the total clearance of PPI, K_s is the rate of biosynthesis of H^+ , K^+ -ATPase, E is the amount of active H^+ , K^+ -ATPase present, E_c is the amount of inactive H^+ , K^+ -ATPase and E_t is the total amount of H^+ , K^+ -ATPase, K is the apparent reaction rate constant of the PPI with H^+ , K^+ -ATPase, k_1 is the elimination rate constant of H^+ , K^+ -ATPase, k_2 is the recovery rate constant of inactive H^+ , K^+ -ATPase, and k is the apparent turnover rate constant of H^+ , K^+ -ATPase ($k_1 + k_2$) (adapted with permission from ref. [94]).

An *in vivo* pharmacokinetic and pharmacodynamic study in rats was conducted over a dose range of 0.006–3 mg/kg (IV) with omeprazole and lansoprazole. Using the data from intravenous administration in rats, the estimated half-life of the proton pump was 27 times longer than the elimination half-life for omeprazole and 66 times longer for lansoprazole. Using the PK/PD model described above, good agreement between predicted and observed data was achieved for both drugs.

After their success with the PK/PD model in describing the data from rats, Katashima *et al.*^[80] extended the model to human studies with pantoprazole (PPZ), lansoprazole (LPZ) and omeprazole (OPZ). The PK/PD analysis of these PPIs in humans was conducted using data obtained after oral administration of OPZ (40 mg), LPZ (30 mg) and PPZ (40 mg). Again, good agreement between the predicted and observed values for the parameters was achieved. The estimated half-life of elimination for omeprazole was 0.854 h, for lansoprazole 1.66 h and for pantoprazole 1.52 h, while the apparent recovery half-life of the inhibitory effect on gastric acid secretion was 27.5 h for omeprazole, 12.9 h for lansoprazole and 49.9 h for pantoprazole. These results confirmed the divergence between plasma concentration (PK) and the inhibitory effect on gastric acid secretion (PD) of these three PPIs.

The mechanistic PK/PD model was extended by Puchalski *et al.*^[81] for lansoprazole. Their model was set up to describe the intragastric pH time profile over a 24 h period, enabling the circadian rhythm of acid secretion and food effects on intragastric pH to be taken into account. Using this model, the estimated value for lansoprazole half-life of elimination was 3.2 h, somewhat longer than in the Katashima model (1.66 h), while in the clinical study, the pH had not returned to the baseline level after 24 h. As this proposed model took into account several factors that can interfere in the PPI absorption and activation, it should be particularly useful in the design of clinical studies, the prediction of the optimal dosing regimen and the investigation of PPI effects in different patient populations.^[81]

The inhibitory effect of PPIs on gastric acid secretion has also been described by Abelo *et al.*^[79] using a simpler, empirical turnover model type I, as introduced by Dayneka *et al.*^[97] (see Section “Basic” and “extended basic” indirect response models). In the basic turnover model shown in equation (12) and applied to omeprazole in Figure 4, it is assumed that the drug inhibits or stimulates the production of an effect, which can be characterized by the zero-order k_{in} turnover and the elimination first-order k_{out} rate constants as appropriate. The rate of change of the response (R) provoked in the absence of the drug is described with the following equation:

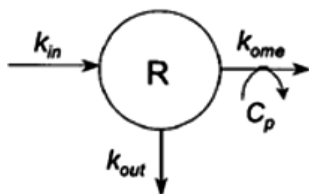


Figure 4 Basic turnover model for omeprazole. k_{in} represents the zero-order production rate, k_{out} the first-order elimination rate constant, C_p is the total plasma concentration of omeprazole and k_{ome} is the second-order rate constant for the irreversible binding of omeprazole to active H⁺, K⁺-ATPase (adapted with permission from ref. [79]).

$$\frac{dR}{dt} = k_{in} - k_{out} \cdot R \quad (12)$$

According to equation (12), the acid secretion (AS) is directly proportional to the concentration of the active proton pump enzyme (E). Equation (13) can be used to correct for the placebo effect on acid secretion:

$$R = \frac{AS(\text{Drug}, t)}{AS(\text{Placebo}, t)} = \frac{E(\text{Drug}, t)}{E(\text{Placebo}, t)} \quad (13)$$

Omeprazole irreversibly removes the enzyme from the system at a rate proportional to the amount of enzyme and the inhibitor concentration. Irreversible removal of the enzyme results in a decrease in the response according to equation (14):

$$\frac{dR}{dt} = k_{in} - (k_{out} + k_{ome} \cdot C_p) \cdot R \quad (14)$$

For a given concentration of omeprazole, the value for R at steady state (R_{ss}) will be:

$$R_{ss} = \frac{k_{in}}{k_{out} + k_{ome} \cdot C_{pss}} \quad (15)$$

This relationship states that with increasing omeprazole concentration, R_{ss} approaches zero.

Data from studies in dogs were used to predict the PK and PD parameters for omeprazole for this species, leading to a prediction for the half-life of elimination of 1.3 h and for the effective half-life for inhibition of acid secretion ($t_{1/2, K_{out}}$) of 51 h. Using allometric scaling, the predicted half-life for humans was 1.5 h and the effective half-life for inhibition of acid secretion ($t_{1/2, K_{out}}$) was 71.7 h. The discrepancy between predicted (71.7 h) and observed (48) $t_{1/2, K_{out}}$ in humans was attributed to differences in basal acid secretion between dogs and humans.^[98]

Ferron *et al.*^[99] also used the basic turnover irreversible PK/PD approach, in this case to describe the inhibition of

gastric acid secretion by pantoprazole in rats and humans. The model was able to adequately describe the time course of gastric acid secretion in rats at all doses studied. The next step was to apply it to gastric secretion data obtained after administration of pantoprazole in humans. The estimated half-life for pantoprazole was 0.5 h in rats and 0.8 h in humans, in agreement with the observed data in both species.

Both the mechanistic and empirical models described in this section were able to predict the discrepancy between the half-life elimination (PK) of PPIs and the time course of inhibition of acid secretion (PD). The models were also successful in describing further characteristics of PPIs, namely that the effect on acid secretion inhibition by PPIs is linked to the extent of exposure (AUC), and that the onset of action is governed by the maximum concentration (C_{max}). Thus, PK/PD modelling provides a powerful tool for analysing/predicting effects achieved with other dosing regimens. To circumvent the use of invasive methods in clinical studies for monitoring the gastric pH and inhibition of gastric acid secretion, it would be necessary to build PK/PD models that can also predict the extent of acid inhibition in terms of the pH value and the duration over which the pH is kept above a clinically relevant threshold value (usually pH 4) by the PPI.

In conclusion, M&S clearly shows why PPIs, despite having a short plasma half-life, are able to have a long duration of effect. Such models enable better decisions to be made about dosing intervals and also help to identify the time frames over which DDIs with PPIs may persist.

Acetylsalicylic acid

Similarly to the PPIs, aspirin (ASA) has a long duration of action, even though it has a short elimination half-life ($t_{1/2}$ 18–30 min).^[100,101] ASA inhibits platelet-derived thromboxane (TXB2), with approximately 60% inhibition still observed 4 days after discontinuation of ASA.^[100,101] This pronounced dissociation between the elimination half-life (PK) and the time-frame of drug action (PD) occurs because ASA binds covalently to COX-1, causing irreversible inhibition of this enzyme. The TXB2 activity can only be re-established by synthesis of new platelets, which is a process that occurs over a period of approximately 10–14 days.^[100] Because platelets are not nucleated, they are unable to synthesize new COX-1, and for this reason, platelet function will only normalize after the platelets that have been acetylated by ASA are removed from the systemic circulation and replaced by new platelets derived from megakaryocytes.^[102]

The first model describing cyclooxygenase activity in platelets and the blood vessel endothelium after oral administration of aspirin was developed by Yamamoto *et al.*^[76]

These authors used irreversible inhibition, with renewal by enzymatic turnover, to explain the long duration of the antiplatelet effect of aspirin in humans. In this study, thromboxane B₂ concentrations and the percentage of prostacyclin production in the blood vessels were used as biomarkers.^[76]

It has been suggested that non-selective COX-1 inhibitors, for example ibuprofen, could limit the cardio-protective effect of aspirin.^[103] For this reason, Hong *et al.*^[75] developed a PK/PD model that was based on the turnover of the COX-1 enzyme, in which the irreversible inhibition by aspirin and the reversible binding by ibuprofen were both incorporated. The rate changes of free enzyme concentration available for aspirin binding (*E*) and the ibuprofen-enzyme complex (EI) were described by the following equations:

$$\frac{dE}{dt} = k_{in} - k_{out} \cdot E - K \cdot C_{asa} \cdot E - k_{on} \cdot C_{ibu} \cdot E + k_{off} \cdot EI \quad (16)$$

$$\frac{dEI}{dt} = k_{on} \cdot C_{ibu} \cdot E - k_{off} \cdot EI - k_{out} \cdot EI \quad (17)$$

where k_{in} is the zero-order production effect rate constant, k_{out} is the first-order elimination rate constant, K is the second-order rate constant for the irreversible enzyme inactivation by aspirin, and k_{on} and k_{off} are the association and dissociation rate constants for binding of ibuprofen on the enzyme. C_{asa} and C_{ibu} represent the aspirin and ibuprofen concentrations in the plasma, assuming that both drugs follow a one-compartment PK model with first-order rate constants for absorption and elimination.

The mechanistic PK/PD model was able to reflect the antiplatelet effect of aspirin administered either alone or concomitantly with ibuprofen as well as simulating the PK and PD time courses. Significant inhibition of the antiplatelet effects of aspirin in the presence of a typical ibuprofen regimen was also demonstrated.

The most mechanistic PK/PD model describing the effects of aspirin on COX-1 activity to date was proposed by Giaretta *et al.*^[104] This model uses a population of megakaryocytes (MKs) and peripheral platelets present in the blood circulation to describe aspirin's antiplatelet activity, as shown in Figure 5.

For the construction of the PK/PD model for aspirin, the inactivation of COX-1 by low-dose aspirin and the recovery of COX-1 after stopping treatment were taken into consideration. Other physiological processes, for example the description of the megacariopoiesis process responsible for the maturation and generation of new platelets, were also accounted for. The basic characteristics of the megacariopoiesis process are shown in Figure 5. The schematic description of the resulting PK/PD model is shown in Figure 6. It consists of three linear compartments to describe the PK behaviour of aspirin and two non-linear compartments to describe the mechanism of inactivation of COX-1 (PD) in MK cells and in the platelets generated from them. A full mathematical description of the model has been published by Giaretta *et al.*^[104]

The PK and PD parameters of the model were inferred from the literature and calibrated by measurements of TXB₂, which represents the COX-1 activity in peripheral platelets, in 17 healthy subjects and 24 patients with essential thrombocythemia (ET).^[104] The model was able to reproduce both the mean TXB₂ inhibition time in healthy patients and the reduced inhibition of TXB₂ seen in patients with ET. Thus, this mechanistic PK/PD model may be helpful to customize aspirin regimens under conditions of altered megakaryopoiesis.

In addition to the dissociation between PK (short half-life of elimination) and PD (long response period) demonstrated by the models described above, the dose–response relationship for platelet inhibition by aspirin is flat. Feldman *et al.*^[100] demonstrated that even with a 10-fold increase in dose of aspirin, only a twofold increase in response (inhibition of TXB₂) was observed. Since doses of

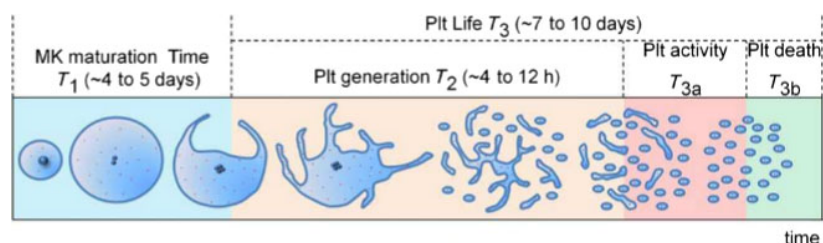


Figure 5 Mechanism of platelet formation derived from a single megakaryocytes (MK). The figure above shows the life cycle of an MK. During the maturation stage (T_1), the MK cell exhibits endomitosis, and as a result of this process, there is an accumulation of proteins, leading to an increase in the cytoplasmic volume. During platelet generation (T_2), cytoplasmic fragmentation takes place, leading to the formation of pseudopods that generate platelet precursors. These precursors divide into young platelets and access the peripheral blood with an average lifetime represented by T_{3a} and the average death rate by T_{3b} (adapted with permission from ref. [104]). [Colour figure can be viewed at wileyonlinelibrary.com]

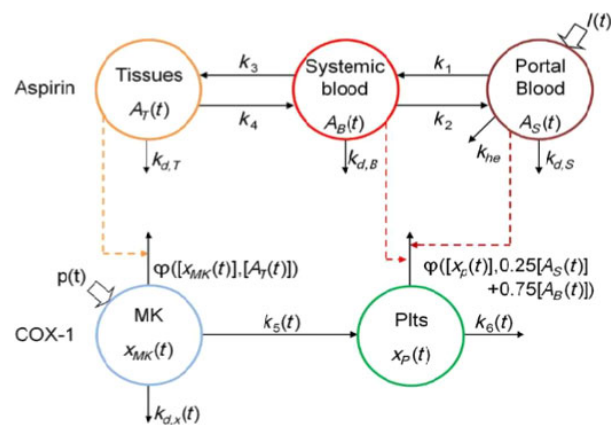


Figure 6 PK/PD model of aspirin interaction with megakaryocyte (MK) and platelets. PK is represented by a linear three-compartment PK model. $A_T(t)$ represents the amount of aspirin in the tissues, $A_B(t)$ the amount of aspirin in the systemic blood and $A_S(t)$ in the portal blood. $I(t)$ represents the dose of administered aspirin. The parameters k_1 , k_2 , k_3 and k_4 are constants that represent the transfer rate of aspirin between compartments, while $k_{d,T}$, $k_{d,B}$ and $k_{d,S}$ are the rate constants for hydrolysis from each compartment and k_{he} describes first-pass metabolism in the liver. The PD model consists of two compartments to describe the interaction of aspirin with COX-1 in MK and platelet units separately. $x_{MK}(t)$ and $x_P(t)$ represent the amount of COX-1 enzyme in the MK unit and in the platelet, respectively. $\rho(t)$ and $k_{d,x}(t)$ are the rate constants of the MK COX-1 pathway, $k_s(t)$ represents the production and rate of COX-1 degradation in the MK unit and $k_6(t)$ the disappearance of the enzyme due to peripheral destruction of platelets. The flow φ represents aspirin-mediated acetylation of COX-1 as a function of COX-1 and aspirin concentrations (adapted with permission from ref. [104]). [Colour figure can be viewed at wileyonlinelibrary.com]

81 and 325 mg of ASA are not significantly different with regard to this clinical response, applying a low dose of aspirin to prevent platelet aggregation is justified.^[100]

In summary, mechanistic models of the pharmacodynamic action of aspirin on platelets appear to be useful for customizing the prevention of thrombus formation and for designing clinical trials in special patient populations for example the elderly, pregnant women, children, obese patients, etc. Indeed, regulatory authorities are increasingly relying on and encouraging the use of M&S to forecast changes in PK and PD in rare diseases and in special populations of patients in whom it is challenging to perform clinical trials.

Exemestane

Exemestane, an irreversible aromatase type I (Ar type I) inhibitor for the treatment of advanced breast cancer of postmenopausal women, provides a further, interesting example of irreversible binding and biological target inactivation.

In an open, three-period, randomized, crossover study of 12 healthy postmenopausal women, Valle *et al.*^[105]

investigated the effects of formulation (suspension vs tablet) and administration of food (i.e. fasted vs fed) on the pharmacokinetics and pharmacodynamics of exemestane. As had already been demonstrated by previous clinical trials, oral administration of exemestane (25 mg/day) inactivates peripheral aromatase, leading to a 85–95% decrease in basal plasma estrone, estradiol and estrone sulphate (EIS) concentrations in postmenopausal women with advanced breast cancer.^[106–108] First, population pharmacokinetic models, consisting of a mono- or bi-exponential absorption and three-compartment distribution function, with empirical Bayesian estimates for each individual were developed. Absorption lag times were determined for both absorption models. An inhibitory (type I) indirect response pharmacodynamic model (see more details in Section ‘Basic’ and ‘extended basic’ indirect response model’), in which synthesis and elimination of EIS (which is indirectly related to aromatase activity) are governed by zero- and first-order rate constants, respectively, was implemented to describe the dissociation between plasma concentrations and the observed effect:

$$\frac{dC_{EIS}}{dt} = k_s - k_o \cdot C_{EIS} \quad (18)$$

$$\frac{dC_{EIS}}{dt} = k_s \cdot \left(\frac{C^\gamma}{C^\gamma + IC_{50}^\gamma} \right) - k_o \cdot C_{EIS} \quad C_{EIS}(0) = C_{EIS0} \quad (19)$$

where C_{EIS} is the plasma concentration of estrone sulphate, k_s is the zero-order rate constant for synthesis and k_o is the first-order rate constant for elimination, C^γ is the exemestane plasma concentration, IC_{50} represents the exemestane plasma concentration at which 50% of inhibition is achieved and γ is the Hill-coefficient. This semi-empirical, non-linear mixed-effect modelling approach fitted the data adequately.

A more mechanistic model, incorporating the irreversible aromatase inactivation by exemestane, was also applied. In this model, the aromatase concentration, Ar, is assumed to be the system variable controlling the rate of synthesis of EIS. The production and elimination rate of aromatase is in turn governed by a zero-order (k_{se}) and first-order (k_{oe}) rate constant, respectively. The irreversible inhibition of aromatase by exemestane is characterized by an increase in the elimination of aromatase and represented by a second-order rate constant k_i . Assuming that the concentration of EIS precursor is constant and the concentration of aromatase is known, the model is fully identifiable. The rate of concentration changes of EIS and Ar is defined by the equations:

$$\frac{dC_{EIS}}{dt} = k_s \cdot Ar - k_o \cdot C_{EIS} \quad C_{EIS}(0) = C_{EIS0} \quad (20)$$

$$\frac{dAr}{dt} = k_{se} - k_{oe} \cdot Ar - k_i \cdot C_{EIS} \cdot Ar \quad Ar(0) = Ar_0, \quad (21)$$

where Ar_0 is the baseline concentration of aromatase.

The adoption of a more physiologically relevant mechanism of action in the model was expected to provide better results. Nevertheless, the goodness of fit was not significantly improved over the type I indirect response model. Despite being semi-empirical, the type I indirect response model was able to predict the drug effect in different scenarios (i.e. doses, dosage regimens), providing an external validation. In a sense, the initial, indirect response type I model could be considered as a 'collapsed' form of the mechanism-based model, under the assumptions that Hill-coefficient is equal to one ($\gamma = 1$) and that the aromatase dynamics equation is solved at equilibrium and then substituted in the EIS equation. These assumptions appear to be justified in the case of exemestane, since the pharmacodynamic parameters do not change significantly in the data range studied and a value of Hill-coefficient 1.75 ($\gamma = 1.75$) has been reported. Hence, a relatively flat dose response is implied.

An almost fourfold increase in the absorption rate of exemestane when administered as a suspension as compared to a tablet was detected, while food intake decreased the absorption rate. Interestingly, these differences were mitigated in terms of pharmacodynamic response such that the maximum effect and time to maximum effect were not significantly different among treatment groups. The authors concluded that even large differences in pharmacokinetics arising from formulation or administration with food were not translated to a meaningful difference in pharmacodynamics.

The example of exemestane is interesting for two main reasons: (1) it illustrates that a mechanism-based model of irreversible pharmacodynamics can be transformed, depending on data availability or fast equilibration, to a simplified, 'collapsed' model, without influencing the outcome appreciably, and (2) observed differences in absorption patterns and food effects are not always clinically relevant, especially when there is a long delay between plasma levels and the elicited drug response. Again, these findings support the consideration of pharmacodynamics as well as pharmacokinetics when determining whether two drug products or two dosing scenarios are therapeutically equivalent.

Indirect response and feedback control models

Overview

Most pharmacological targets are subject to homeostatic mechanisms, characterized by continuous degradation on

the one hand and re-synthesis of one or more biomarkers (e.g. enzymes, antibodies, circulating proteins or inflammation factors) to compensate for elimination on the other hand, which balance each other to maintain a stable steady state. This is often referred to as the turnover process. Some drugs elicit their action by perturbing the steady state, resulting in a temporary or a more permanent change in the marker value. Such mechanisms of action, which do not affect the response itself but rather influence the turnover process, are inherently indirect and the models describing their effect-time course are usually referred to as turnover or indirect response models. These models typically exhibit a delay between the drug concentration-time and response-time profiles. The amplitude of the response and the extent of the time delay are dependent on the turnover rates (synthesis and degradation) of the pharmacological target as well as the magnitude of the effect.

'Basic' and 'extended basic' indirect response models

Nagashima *et al.*^[109] were the first to implement an indirect response model, which was used to explain the anticoagulant effect of warfarin on the activity of the prothrombin complex. In 1993, Dayneka *et al.*^[97] introduced four basic mathematical models describing the indirect pharmacological processes, according to which the production and loss of the response, R , are governed by zero- and first-order rate constants, k_{in} and k_{out} , respectively. The drug can inhibit or stimulate the synthesis and/or the elimination process as follows:

Model I (inhibition of k_{in}):

$$\frac{dR}{dt} = k_{in} \cdot \left(1 - \frac{I_{max} \cdot C}{C + IC_{50}}\right) - k_{out} \cdot R, \quad R(0) = R_0. \quad (22)$$

Model II (inhibition of k_{out}):

$$\frac{dR}{dt} = k_{in} - k_{out} \cdot \left(1 - \frac{I_{max} \cdot C}{C + IC_{50}}\right) \cdot R, \quad R(0) = R_0. \quad (23)$$

Model III (stimulation of k_{in}):

$$\frac{dR}{dt} = k_{in} \cdot \left(1 + \frac{E_{max} \cdot C}{C + EC_{50}}\right) - k_{out} \cdot R, \quad R(0) = R_0. \quad (24)$$

Model IV (stimulation of k_{out}):

$$\frac{dR}{dt} = k_{in} - k_{out} \cdot \left(1 + \frac{E_{max}C}{C + EC_{50}}\right) \cdot R, \quad R(0) = R_0 \quad (25)$$

where k_{in} and k_{out} are the zero-order production and first-order elimination rate constants, C is the drug

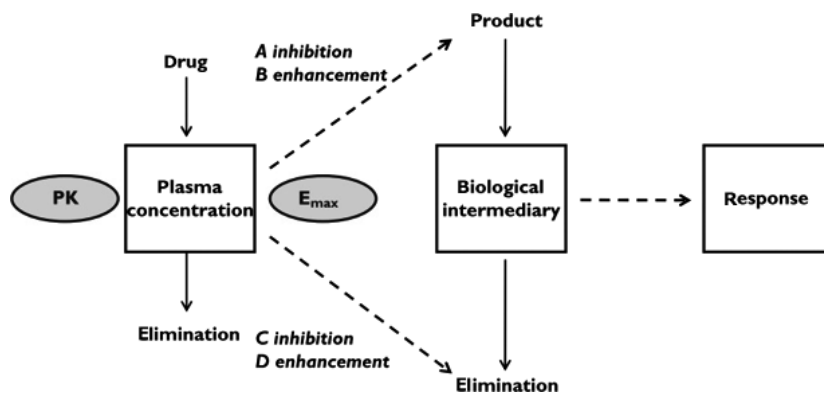


Figure 7 Conceptualization of the four basic turnover models. (a, b) inhibited and stimulated production of an intermediary/response function respectively, while (c, d) reduced and enhanced degradation of an intermediary/response function (adapted with permission from ref. [10]).

plasma concentration, and EC_{50} and IC_{50} represent the drug plasma concentrations achieving 50% of the maximum stimulating, E_{max} and inhibitory, I_{max} effects, respectively.

These four basic models, which are illustrated in Figure 7, have been applied extensively, and some examples have been summarized by Jusko and Ko.^[4] The inhibition of basophil trafficking by methylprednisolone and the furosemide-mediated inhibition of water reabsorption from the tubules and collecting duct were assessed by Model I and II, respectively, while the stimulation of the cyclic adenosine monophosphate (cAMP)-induced bronchodilation by the β -adrenergic receptor agonist terbutaline was described by Model III. In a further example, it was shown that the increase in cAMP by terbutaline activates the cellular membrane sodium–potassium pump, resulting in an increase of efflux of potassium ions from the plasma into cells, an effect that can be described with Model IV.

These basic turnover models can be modified and/or extended to account for more complex physiological processes such as time-dependent production ($k_{in}(t)$),^[110] the rate of loss of cells according to their lifespan^[111–113] and capacity limited processes such as non-linear synthesis and degradation functions.^[114] Further, many physiological processes such as secretion of hormones and gastric acid, gene expression, cardiac output and blood pressure are known to be subject to circadian rhythms, which might influence the pharmacokinetics and pharmacodynamics of various drugs.^[115–117] Symmetric circadian rhythms have been described by trigonometric functions, such as the cosine model introduced by Lew *et al.*,^[118] whereas asymmetric circadian rhythms have been modelled with the addition of exponential, dual cosine or harmonic functions.^[110,119] The detailed mathematical formalism around these functions has been summarized by Krzysanski.^[120]

Signal transduction and feedback control indirect response models

When a sequence of events takes place between receptor binding or activation and the observable effect, this is referred to as signal transduction and can involve signalling cascades, activation or inhibition of secondary messengers, gene up- or down-regulation and mRNA transcription to functional proteins. By definition, every transduction process has two inherent attributes: the transformation of the original signal and the introduction of a time delay.^[121,122] Depending on the experimental time scale, the time delay might or might not be discernable and in the latter case, the response is described by a transduction model with no delay, for example in the operational model of agonism introduced by Black and Leff.^[123] This model has been applied to describe the PK/PD relationships of A_1 adenosine, μ -opioid and 5-HT_{1A} receptor agonists.^[124–128] However, in other cases, the time delay produced by the transduction process is significant and the mathematical models need to be adjusted accordingly. The most common approach is the so-called transit compartment model (Figure 8), which has been applied to the modelling of the genomic effects of corticosteroids, in this case known as the fifth generation model for corticosteroids, as well as myelosuppression and haematologic toxicity in cancer chemotherapy.^[85,129–131]

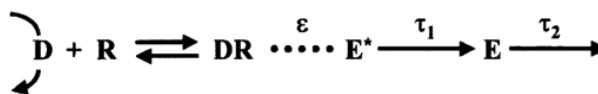


Figure 8 Model of time-dependent transduction. D represents the drug; R is the receptor; DR, the drug-receptor complex; ε is the intrinsic efficacy of drug; E^* stands for the biologic effect or signal; τ is the transit time and E is the effect (reproduced with permission from ref. [121]).

Most physiological processes are subject to feedback control and belong to the so-called autoregulation systems. The PK/PD models that do not address these auto-regulatory mechanisms fail to provide a complete insight of the drug-exposure relationship, and it has been shown that this can lead to underestimation of the drug's potency.^[122] The feedback control indirect response (FC IDR) models (see Figure 9) usually incorporate terms proportional to the error signal itself, the integral and the derivative of the error signal in linear and, less commonly, in non-linear combinations. There are also FC IDR models which include an additional state, the 'moderator' state, which feeds back to alter the synthesis or turnover of the response.^[132] Numerous applications of PK/PD models incorporating feedback regulation mechanisms have been published in the literature.^[131,133,134] The example of (S)-citalopram, a widely used selective serotonin reuptake inhibitor (SSRI), is presented in detail in the following section (see section 'Escitalopram').

Applications and case examples

Ibuprofen: antipyretic response

As mentioned in Section 'Ibuprofen: dental pain relief', the antipyretic effect of ibuprofen resulting from the inhibition of prostaglandin synthesis has been investigated in numerous clinical studies and an indirect response model has been applied to fit the reported pharmacodynamic data. In a single-dose, placebo-controlled, double-blind and parallel-group trial by Wilson *et al.*,^[59] the safety, efficacy, tolerability and dose-effect relationships of ibuprofen products, formulated as a suspension at doses of 5 and 10 mg/kg to treat febrile children, were compared to liquid formulations of acetaminophen. The patients ($N = 127$) were split into groups according to their initial temperature and on whether antibiotics were being administered concurrently. A positive dose-response relationship between ibuprofen suspension 5 and 10 mg/kg in the higher temperature (102.6–104°F), non-antibiotic group was demonstrated, whereas in the lower temperature group (101–102.5°F), both doses were equally effective. However, the

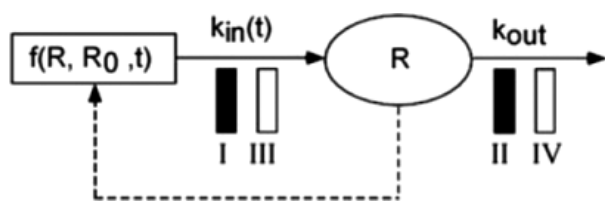


Figure 9 Schematic illustration of the four basic indirect response models including feedback control (FC IDR) (adapted with permission from ref. [122]).

authors pointed out that the plasma levels necessary for maximum effective antipyresis of ibuprofen (approximately 10 mg/l) are achievable even at doses <5 mg/kg, implying a ceiling effect in the antipyretic response at doses of 5 mg/kg or higher.

Similar results in 178 children were observed by Wilson *et al.*^[135] In a single-dose, placebo-controlled study, during which age and initial temperature were considered as covariates, both the 5 and 10 mg/kg doses were significantly superior to placebo, but not different from each other in terms of maximum reduction in temperature. However, it was concluded, based on the temperature at 6 h after administration, the change of temperature from the baseline value and the percentage of efficacy, that the 10 mg/kg dose was more effective. The effect of the age and the initial temperature value on the magnitude of the pharmacological action was also emphasized.

In a double-blind, randomized, single-dose study of 5 and 10 mg/kg ibuprofen to treat febrile children ($N = 153$), Brown *et al.*^[136] noted a dissociation between t_{max} and time of maximum temperature decrease and found no correlation between the extent of temperature change and plasma levels at $t_{R,max}$ or 6 h postadministration. Further, there was no evidence that pretreatment with antibiotics, race or gender influenced the antipyretic effect. By contrast, age and initial temperature were shown to be covariates. Interestingly, after compartmental pharmacokinetic analysis, only the pharmacodynamic, but not the pharmacokinetic parameters related to absorption (C_{max} , t_{max}) and elimination (k_{el} , $t_{1/2}$), were affected by the age of the child. In a subsequent paper, Brown *et al.*^[137] implemented an effect compartment model coupled with a sigmoid E_{max} pharmacodynamic model to describe the antipyretic effect of ibuprofen in children and further elaborated the model by adding a linear and/or sinusoidal cyclic function for the decrease in temperature as covariates to fit their own as well as previously reported data.^[135] Values of the estimated sigmoidicity factor (γ) were 3.97 ± 0.58 and 4.27 ± 0.63 for ibuprofen 5 and 10 mg/kg, respectively, implying that the dose-response relationship for antipyresis in children might be steeper than for dental pain relief in adults.

Troconiz *et al.*^[47] reported a temporal disconnection between t_{max} after administration to febrile children of 7 mg/kg ibuprofen as a suspension or as effervescent granules dosed at 200 or 400 mg (0.5 for the suspension and 1.9 h for the effervescent granules) and time of maximum decrease in body temperature (3 h in both cases), suggesting that the formulation and its pharmacokinetic behaviour have little impact on the antipyretic effect of ibuprofen. The antipyretic response of NSAIDs has been attributed to their ability to inhibit the synthetic pathway of prostaglandins, particularly of prostaglandin E_2 (PGE_2),

via an indirect mechanism.^[138] The following equation was derived to describe the pharmacodynamics of antipyresis by this mechanism:

$$\frac{dT}{dt} = k_{\text{syn}} \cdot \left(1 - E_{\text{max}} \cdot \frac{C^\gamma}{C^\gamma + EC_{50}^\gamma} \right) - k_{\text{out}} \cdot T, \quad (26)$$

where dT/dt represents the rate of body temperature change with time, k_{syn} and k_{out} are the zero-order and first-order rate constants for synthesis and degradation of the inflammation mediator (i.e. PGE₂), respectively, T is the body temperature, E_{max} is the maximum antipyretic effect, EC_{50} is the drug plasma concentration (C) required to achieve half of the maximum effect and γ is the sigmoidicity factor.

The proposed pharmacokinetic–pharmacodynamic model fitted the antipyretic profiles well. The estimated EC_{50} and k_{out} parameters were in agreement with those previously reported by Garg and Jusko^[139] (6.18 vs 10.2 mg/l for EC_{50} and 1.17 vs 0.89 h⁻¹ for k_{out}), who had also applied an indirect response model. The sigmoidicity factor was calculated to be 2.71 ± 0.18 , suggesting a relatively flat dose–response curve. In contrast to previous studies, however, age and initial temperature did not elicit covariate effects.^[135,140]

Based solely on the differences in C_{max} and t_{max} between the suspension and the effervescent granule formulations, a delayed onset of drug action would be expected for the effervescent granules. Nevertheless, the maximum antipyretic effect was similar and occurred at the same time for both formulations. Importantly, an almost identical mean effect-time course of 200 and 400 mg of ibuprofen effervescent granules in febrile children was observed, implying that at least for this formulation, there was no significant clinical benefit with a dose increase (Figure 10). Therefore, the authors concluded that the formulation-dependent pharmacokinetic differences are mitigated by the response mechanism, leading to similar pharmacodynamic responses for both formulations at both doses in febrile children.

Using a verified PBPK/PD model, Cristofolletti and Dressman^[58] simulated the antipyretic response with virtual trials of 2, 5, 7 or 10 mg/kg dosing of ibuprofen suspension to 100 febrile children per trial in the age range of 2–11 years. In terms of maximum decrease in temperature from the baseline value, the 5, 7 and 10 mg/kg doses were proven to be significantly superior to 2 mg/kg but not statistically different from one another. A rather flat dose–response curve (with $EC_{50} \approx 6.18$ mg/l) was confirmed for the antipyretic effect in children. Under the assumption that the 7 and 10 mg/kg dose represent the test and reference products, respectively, the test product would be bioequivalent to the reference in terms of C_{max} and AUC ratios ($C_{\text{max,T}}/C_{\text{max,R}}$ and $AUC_{\text{max,T}}/AUC_{\text{max,R}}$ around 0.7),

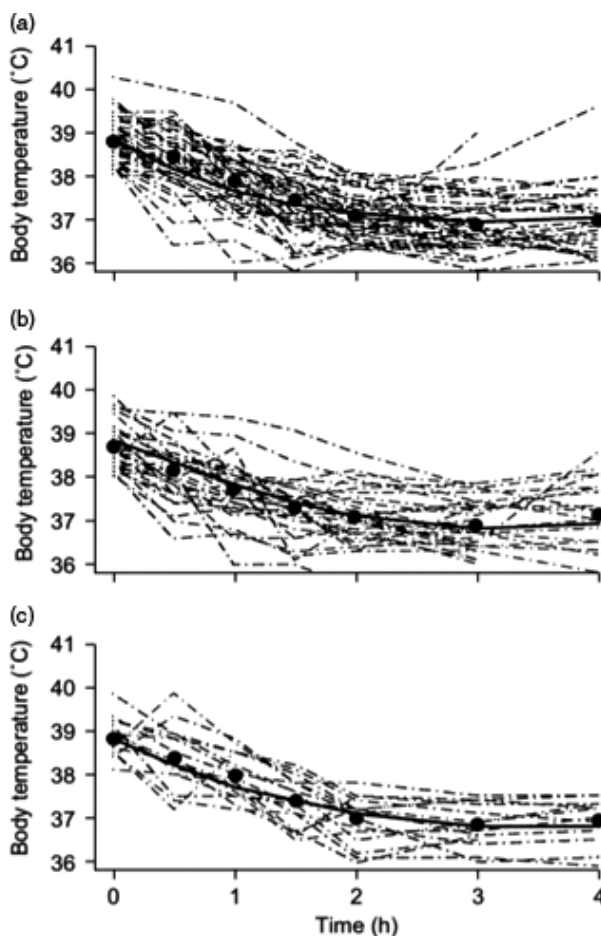


Figure 10 Individual (broken lines) and mean (circles) values observed antipyretic vs time profiles of ibuprofen after oral administration of 7 mg/kg in suspension (a) or 200 mg (b) or 400 mg (c) as effervescent granules to febrile children. Solid lines represent typical model predictions (reproduced with permission from ref. [47]).

but still therapeutically equivalent in children. This conclusion is supported by the data from Troconiz *et al.*,^[47] whose clinical trial demonstrated superimposable antipyretic profiles between ibuprofen suspension 7 mg/kg and effervescent granules 400 mg (normalized by children mean body weight as 11.8 mg/kg) after administration to febrile children.

Rosuvastatin

Of the currently available 3-hydroxy-3-methylglutaryl coenzyme A reductase (HMG-CoA reductase) inhibitors, rosuvastatin is one of the most effective at lowering the low density lipoprotein cholesterol. Mevalonic acid (MVA) synthesis, which takes place in the liver, is catalysed by HMG-CoA reductase and is the first irreversible stage of the cholesterol biosynthetic pathway.^[141–143]

A PK/PD model was developed to predict the response of rosuvastatin to different dosage regimens and identify differences in response between morning (at 07:00 a.m.) and evening (at 06:00 p.m.) administration. For this purpose, Aoyama *et al.*^[144] used a two-compartment pharmacokinetic model with first-order absorption and elimination from the central compartment, which was then linked to a modified inhibitory indirect response pharmacodynamic model describing the plasma concentrations of MVA. The model was further extended by incorporating a time-dependent periodic function in the zero-order synthesis rate constant of MVA to account for the circadian rhythm, as introduced by Krzyzanski *et al.*^[145,146] The model is presented in Figure 11 and described by the following equations:

$$\frac{dR}{dt} = k_{in} \cdot \left(1 - \frac{C_p^\gamma}{C_p^\gamma + IC_{p50}^\gamma} \right) - k_{out} \cdot R, \quad (27)$$

where R is the response, k_{in} is the time-dependent zero-order rate constant for the increase in plasma MVA concentration, k_{out} is the first-order rate constant for the decrease in plasma MVA concentration, C_p represents the plasma concentration of rosuvastatin, IC_{p50} is the plasma concentration at which k_{in} is reduced 50% and γ is the sigmoidicity factor. The time-dependent k_{in} to account for the circadian rhythm is defined as follows

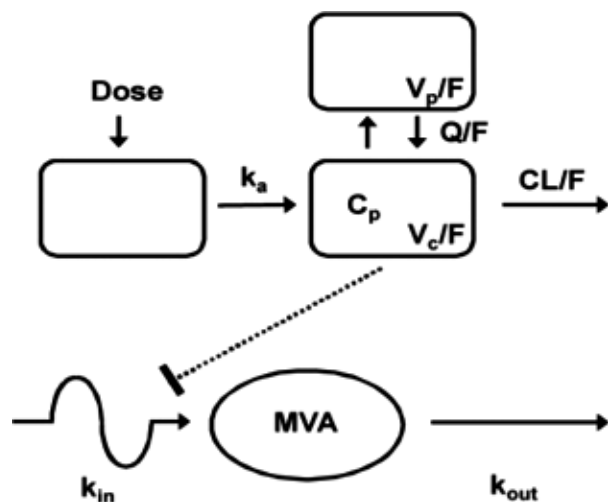


Figure 11 PK/PD model for Rosuvastatin: k_a is the absorption rate constant, V_c/F is the volume of distribution for the central compartment, CL/F is the clearance, V_p/F is the volume of distribution for the peripheral compartment, Q/F is the intercompartmental clearance, C_p is the plasma concentration of rosuvastatin, MVA is mevalonic acid, k_{in} represents the circadian production of mevalonic acid, and k_{out} is the first-order rate of mevalonic acid removal (reproduced with permission from ref. [144]).

$$k_{in} = k_m + k_{amp} \cdot \cos(2 \cdot \pi(t - tz)/24), \quad (28)$$

where k_m and k_{amp} represent the mean MVA synthesis and its amplitude rate constants, respectively, and tz is the acrophase time, during which MVA is synthesized at the maximum rate. The following function to describe the circadian rhythm of k_m was proposed by Krzyzanski *et al.*^[145]:

$$k_m = k_{out} \cdot IC - \frac{k_{amp} \cdot k_{out}^2}{k_{out}^2 + (2\pi/24)^2} \cdot \left[\cos\left(\frac{2 \cdot \pi \cdot (tz)}{24}\right) - \left(\frac{2 \cdot \pi}{24 \cdot k_{out}}\right) \cdot \sin\left(\frac{2 \cdot \pi \cdot (tz)}{24}\right) \right] \quad (29)$$

where IC is the initial plasma MVA concentration measured at 6 a.m., set to 4.32 ng/ml.

Application of the time course of rosuvastatin and MVA plasma concentration to the model enabled an adequate prediction of the clinical data reported by Martin *et al.*^[147] A higher reduction ratio of 7.7% in the area under the plasma MVA concentration–time curves over 24 h at steady state ($AUEC_{0-24}$) was observed after administration in the evening. Furthermore, sensitivity analysis on the pharmacokinetic parameters showed that changes in the pharmacokinetics have a greater effect on the $AUEC_{0-24}$ reduction ratio after morning than after evening administration. This was attributed to the circadian rhythm, with the acrophase time estimated to be 15.5 h. The authors concluded that evening administration of rosuvastatin might be useful in clinical practice.^[144] The main limitation of the model is that it is based only on the mean plasma pharmacokinetic and pharmacodynamic data. Therefore, it does not address the concentration at the effect site, which is the liver and not the plasma, or the intersubject variability. Most importantly, the use of only one mean PK/PD data set raises questions about the identifiability of the estimated parameters and caution should be exercised in drawing conclusions about the validity of this model.

Since the liver is the effect site for the statins, uptake into the liver is an important factor in their efficacy. Multiple transporters of the family of the organic anion transporting polypeptide (OATP) family are abundant in the liver, facilitating the active hepatic uptake of endogenous substances and xenobiotics, including statins, from sinusoidal blood.^[148–152] Rosuvastatin is a substrate of the OATP 1B1, 1B2, 1B3, 1A2 and the sodium-dependent taurocholate co-transporting polypeptide.^[148,153] The expression of OATP1B1 on the sinusoidal membrane of human hepatocytes is encoded by the gene *SLCO1B1*, which is subjected to single-nucleotide polymorphisms (SNPs). As already demonstrated for paravastatin, pitavastatin and simvastatin, such polymorphisms are associated with reduced

OATP1B1 *in vitro* activity and markedly increased plasma concentrations.^[154–158] Pasanen *et al.*^[155] investigated the effect of *SLCO1B1* polymorphism on the pharmacokinetics of atorvastatin and rosuvastatin, after oral administration in 32 healthy volunteers, with the following genotypes: *SLCO1B1* c.521CC ($n = 4$), *SLCO1B1* c.521CT ($n = 12$) and *SLCO1B1* c.521TT (wild type, $n = 16$). Significant increases in the $AUC_{0-48\text{ h}}$ and C_{max} (65% and 79%, respectively) in *SLCO1B1* c.521CC subjects compared to the reference genotype, *SLCO1B1* c.521TT, were observed. By contrast, increases in the $AUC_{0-48\text{ h}}$ (144% increase), but not the C_{max} , were reported after administration of atorvastatin. This study implies that the reduced OATP1B1-mediated hepatic uptake of rosuvastatin due to *SLCO1B1* polymorphism results in an increased risk of a reduced cholesterol-lowering effect as well as adverse effects such as myopathy and/or rhabdomyolysis.

Based on the model of Aoyama *et al.*,^[144] a full PBPK/PD model was built in the Simcyp Simulator by Rose *et al.*^[159] to investigate the impact of polymorphic hepatic uptake (OATP1A1, OATP1B4) and efflux transporters (BcRP, MRP2) on the disposition, pharmacologic and toxic effects of rosuvastatin. First, plasma concentrations were linked to the cholesterol-lowering effect of rosuvastatin, according to the plasma AUC of MVA. The simulations performed with the PBPK/PD model showed a large increase in the mean plasma AUC infinity (AUC_{∞}) of rosuvastatin by 63% and 111% for the *SLCO1B1* c.521CT and *SLCO1B1* c.521CC, respectively, compared to the wild type (*SLCO1B1* c.521TT). Similarly, a significant increase in MVA plasma AUC of 30% and 35% for the same genotypes was observed. However, the hepatic unbound intracellular water concentration (C_{uIW}) of rosuvastatin, which was predicted by a permeability limited liver model, was considered to be a more relevant driver of its pharmacodynamic effect. Interestingly, only a slight decrease in C_{uIW} -based AUC_{∞} of 5.7% and 9.6%, with a parallel decrease in MVA plasma AUC of 3.1% and 5.8% was reported for the heterozygote and homozygote, respectively. The latter findings are in agreement with a number of studies showing that OATP1B1 c.521T>C SNP has either no or only a slight effect on the cholesterol-lowering response to statins,^[160–162] and that when plasma concentrations were used as the input, the results were misleading.

With regard to toxic effects, the effect of genetic polymorphism on rosuvastatin-mediated myopathy was investigated by prediction of muscle concentrations using a perfusion-limited model. A strong correlation between plasma concentrations and the risk of muscle-related adverse effects was observed. Thus, in contrast to the results for the cholesterol-lowering effect of rosuvastatin, the plasma concentration appears to be a good surrogate for the concentration at the muscle when assessing the

risk of statin-induced muscle toxicity in individuals with polymorphic hepatic uptake transporter activity. This result was also in agreement with an already published study.^[163]

High interindividual variability among the different genotypes, limited availability of accurate *in vitro* data and/or published clinical studies at different dose levels as well as incomplete understanding of the impact of transporters on pharmacokinetics and/or pharmacodynamics, are some of the limitations which restrict the robustness of the models for rosuvastatin and their confidence in simulating different clinical scenarios. Despite these limitations, rosuvastatin serves as a useful case example to demonstrate the potential of linking PBPK with PD model to enhance physiological understanding and improve the ability to assess the impact of transporters on the pharmacologic and/or toxic response. Of particular importance was the finding that, in some instances, parameters other than the plasma concentration are appropriate indicators of the therapeutic and/or toxic effect. This example illustrates that implementation of (PB)PK/PD models (even on an exploratory basis) can provide valuable information during clinical drug development and significantly contribute to the clinical ramifications of genetic polymorphism, facilitating an optimal dosing regimen.

Escitalopram

Selective serotonin reuptake inhibitors, such as escitalopram, block the neuronal reuptake of serotonin (5-HT), resulting in increased neurotransmitter concentration at the terminal and somato-dendritic areas. However, the auto-receptors 5-HT_{1A} and 5-HT_{1B}, which regulate the 5-HT release from neurons by negative feedback control, are also situated at the terminal and somato-dendritic neuronal parts, respectively (Figure 12).^[164] Intracerebral microdialysis can be used to measure the extracellular concentration of 5-HT and thus its concentration at the site of action.^[165,166]

Bundgaard *et al.*^[167] developed an indirect response PK/PD model for escitalopram, including a moderator state (tolerance model) to account for the auto-inhibitory feedback. For this purpose, different doses of escitalopram were administered intravenously at a constant infusion rate over 60 min in four groups (vehicle, 2.5, 5 and 10 mg/kg) of six male Sprague–Dawley rats and the response was expressed as the change in extracellular 5-HT concentration. A two-compartment pharmacokinetic model with first-order elimination from the main compartment was used to fit the individual mean unbound plasma concentration–time profiles for each dose group, and the predicted profiles were used as the input to drive the pharmacodynamic model. A type II basic indirect response model was implemented to

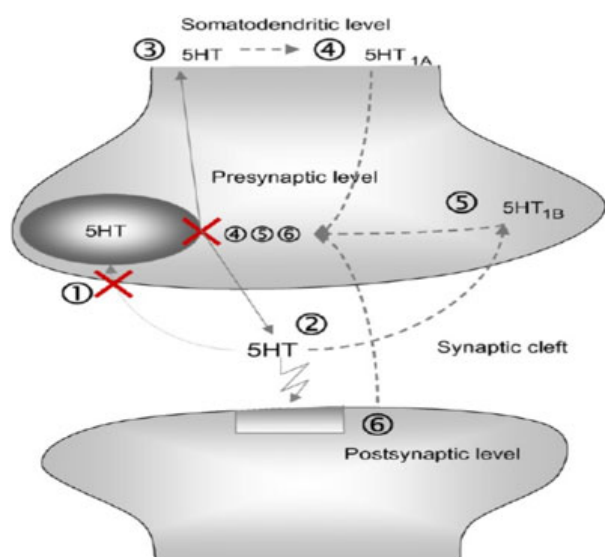


Figure 12 Schematic illustration of the auto-regulatory mechanisms of the 5-HT neurons following blockage of the 5-HT transporter (1) with selective serotonin reuptake inhibitors (SSRIs). By blocking the reuptake (1), the SSRIs increase the concentration of 5-HT at the synaptic (2) and somatodendritic level (3). The increased level of 5-HT then acts on somatodendritic and terminal 5-HT auto-receptors (4 and 5) as well as on postsynaptic 5-HT receptors (6), which exert negative feedback on the release of 5-HT into the synapse. In the proposed PK/PD model, the moderator M includes the sum of all negative feedback originating from (4) to (6) (see also Figure 13). Solid lines denote release/uptake pathways, and dashed lines denote control pathways (reproduced with permission from ref. [167]). [Colour figure can be viewed at wileyonlinelibrary.com]

describe the inhibition of 5-HT reuptake. In this model, the increase in the response, R , over the baseline value R_0 , feeds back to the moderator compartment and stimulates the production of the moderator, M . As a simplifying approximation, the rates in and out of M are described by a first-order rate constant k_{tol} . An increase in M induces a negative feedback on the generation of the response and thus enables the baseline value to be re-established. The model is illustrated in Figure 13 and described by the following equations:

$$\frac{dR}{dt} = \frac{k_{in}}{M} - k_{out} \cdot R \cdot I(C_p) \quad (30)$$

$$\frac{dM}{dt} = k_{tol} \cdot R - k_{tol} \cdot M \quad (31)$$

$$I(C_p) = 1 - \frac{I_{max} \cdot C_p^n}{IC_{50}^n + C_p^n} \quad (32)$$

where R , M and C_p represent the response, the moderator and the escitalopram unbound plasma concentration respectively, I_{max} , IC_{50} and n are the maximum inhibitory effect, the potency and sigmoidicity factor respectively,

and k_{in} , k_{out} and k_{tol} represent the turnover rate, fractional turnover rate and feedback rate constants, respectively (see Figure 13). By setting equations 30 and 31 equal to zero, the initial baseline conditions are obtained:

$$k_{in} = k_{out} \cdot R_0^2 \quad (33)$$

$$R_0 = M_0 = \sqrt{\frac{k_{in}}{k_{out}}} \quad (34)$$

The feedback control model fitted the response-time data well. Between unbound plasma concentration and 5-HT response, a distinct time delay was observed for all doses, leading to a counter-clockwise hysteresis loop. The development of tolerance was confirmed by the fact that the terminal phases of the hysteresis loops were not superimposable as a function of dose: the higher dose groups exhibited a lower response at the same concentration. Based on one-way analysis of variance (ANOVA) and post hoc analysis, maximal increases in 5-HT extracellular levels reached 337%, 424% and 456% of the baseline and the levels remained elevated for 135, 175 and 235 min at the 2.5, 5 and 10 mg/kg doses, respectively. Despite the significant differences in plasma concentrations, the basal response value was recovered within 360 min following the administration of all tested doses. In fact, neither the duration nor the magnitude of the response increased when the dose was increased from 5 to 10 mg/kg. These findings are in agreement with previous studies in rats, in which increasing the dose of escitalopram exhibited a ceiling effect in the extracellular levels of 5-HT in the frontal cortex, as measured by microdialysis.^[168,169]

The results from this study established the high potency ($IC_{50} = 4.4 \mu\text{g/l}$) of escitalopram, with almost complete ($I_{max} = 0.9$) inhibition of reuptake. A fast neuronal 5-HT reuptake with a half-life of <5 min ($t_{1/2k_{out}}$) was reported, whereas the half-life for the development of tolerance $t_{1/2k_{tol}}$ was estimated at 10 h. The importance of incorporating a moderator state to account for the physiological homeostatic autoregulation mechanisms was demonstrated by comparison of the pharmacodynamic parameters of this more mechanistic model with the conventional effect compartment model. The effect compartment model predicted higher EC_{50} values at increased doses, which was inconsistent with the physiological response. In addition, Zhang and D'Argenio^[122] used the same data sets to compare the performance of the basic model II inhibitory model with and without the addition of proportional and proportional-plus-integral feedback gain. When the feedback was omitted, the drug's potency was underestimated, while the model with the proportional-plus-integral feedback gain performed the best (lowest Akaike information criterion value).

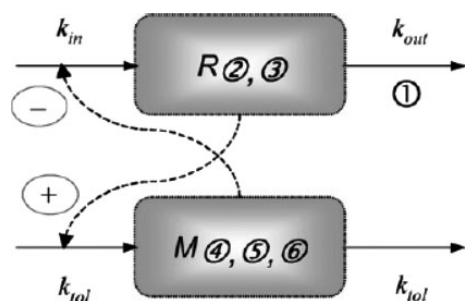


Figure 13 Schematic of the proposed negative feedback model of the acute action of selective serotonin reuptake inhibitors in rats. The response R acts linearly on the production of the moderator M , while M acts inversely on the production of R . Solid lines denote increase and loss of R and M , while dashed lines indicate how R and M influence each other. The numbers correspond to various sections of Figure 12 (reproduced with permission from ref. [167]).

These findings not only highlight the usefulness of implementing feedback control mechanisms in pharmacodynamic models but also the importance of assessing the PK/PD at multiple doses. It is evident that when the autoregulation of the pharmacodynamic response is not taken into account, the evaluation of *in vivo* potency can lead to an underestimation of drug's potency and application of unnecessarily high doses. Additionally, feedback control models may be useful for the comparison of the pharmacodynamic behaviour among SSRIs, to improve understanding of their antidepressant effects and as a guide to set effective plasma concentrations in clinical practice.

Outlook and concluding remarks

This review describes the large variety of PK/PD modelling approaches available to predict dose–concentration–effect relationships and to simulate various clinical scenarios. Models incorporating a physiological understanding of the underlying mechanism(s) of action of the drug and progression of disease can serve as powerful tools for exploring and predicting clinical drug product performance. Provided such models are adequately validated, they can also be implemented with confidence to drive model-informed decisions during drug development as well as at the regulatory level.

An even more complete understanding of a drug's therapeutic value would be possible if dose–concentration–adverse reactions relationships were to be simultaneously established through toxicokinetic/toxicodynamic models so that not only efficacy but also safety can be evaluated. This is important, since dose–response curves may differ significantly between the therapeutic and adverse effects in different patient populations as well as among different indications of the same drug.

A current limitation of mechanistic models is that their complexity often leads to issues of identifiability and

reproducibility of parameters. The commercially available PBPK models are often implemented with mostly (or only) literature data. In these models, the number of parameters is often far greater than would be required for application of classical compartmental models and it may be difficult to acquire reliable values for some parameters. The advent of more sophisticated analytical techniques such as microdialysis will promote a better understanding of the time profile of drug concentration at the effect site. In the meantime, to ensure maximum quality and to facilitate the interpretation of PK/PD models, transparency in the parameter values applied in the model, as well as in the underlying assumptions and the derived equations, together with harmonization based on good coding practice, is essential.

Once there is enough confidence in the translatability, estimation and prediction of preclinical and clinical PK/PD and systems pharmacology models, a move towards linking them with biorelevant *in vitro* tools to guarantee TE will be another key step forward in the drive to link the laboratory to the patient, which seems not only promising, but also imminent. Bridging the gap between *in vitro*, *in vivo* and *in silico* methods by applying the Quality by Design and the Biopharmaceutics Risk Assessment Roadmap^[170,171] will allow pharmaceutical scientists to correctly assess the relative impact of formulation, dose and dosing interval during the development of new drugs.

For the formulation scientist, M&S used in this way will assist in the selection of the most appropriate dosage form and to set formulation targets, knowing to what extent the formulation can be expected to steer the *in vivo* performance of the drug product. For the clinician, the approach helps to identify a dosing strategy which optimizes the efficacy/safety ratio.

For the analyst, M&S can provide guidance in setting clinically relevant dissolution specifications, taking into account not only which formulation factors steer the drug plasma concentration (critical quality attributes) but also how any differences in these will translate in the clinical outcome. In this context, robust PK/PD modelling approaches will play an essential role in model-informed drug development.

Finally, from a regulatory decision-making point of view, a seamless description of the relationship between the pharmacokinetic and pharmacodynamic characteristics of a drug together with a knowledge of how, and to what extent, formulation and formulation performance can influence the PK and PD provides an excellent, clinically relevant basis for an integrated approach to assessing applications for drug approval. Currently, pharmacodynamics considerations are taken into account in the approval of labelling of new drug products, for example, whether taking the drug before vs after a meal will influence efficacy. There is also a thrust towards virtual bioequivalence, for example, using

PBPK modelling to determine whether a change in the dissolution characteristics will impact the plasma profile significantly. A logical further step would be to combine these two approaches to optimize the approval process. Foreseen is a scenario in which the release testing in the laboratory reflects the release in the target patient population(s), the data are combined with verified PBPK models tailored to the target population(s) and then translated with PK/PD modelling into a prediction of the clinical outcome. This scenario would not only provide sponsors as well as the

regulatory authority with more flexibility in the approval procedure, without sacrificing efficacy or safety, but also be a way forward to move effectively towards a more personalized medicine concept.

Acknowledgements

This work was supported by the European Union's Horizon 2020 Research and Innovation Programme under grant agreement No 674909 (PEARRL).

References

- Levy G. Relationship between rate of elimination of tubocurarine and rate of decline of its pharmacological activity. *Br J Anaesth* 1964; 36: 694–695.
- Segre G. Kinetics of interaction between drugs and biological systems. *Farmaco Sci* 1968; 23: 907–918.
- Holford NHG, Sheiner LB. Understanding the dose-effect relationship: clinical application of pharmacokinetic-pharmacodynamic models. *Clin Pharmacokinet* 1981; 6: 429–453.
- Jusko WJ, Ko HC. Physiologic indirect response models characterize diverse types of pharmacodynamic effects. *Clin Pharmacol Ther* 1994; 56: 406–419.
- Rowland M *et al.* Physiologically based pharmacokinetics is impacting drug development and regulatory decision making. *CPT Pharmacometrics Syst Pharmacol* 2015; 4: 313–315.
- Jusko WJ. Moving from basic toward systems pharmacodynamic models. *J Pharm Sci* 2013; 102: 2930–2940.
- Androulakis IP. Systems engineering meets quantitative systems pharmacology: from low-level targets to engaging the host defenses. *Wiley Interdiscip Rev Syst Biol Med* 2015; 7: 101–112.
- Galeazzi RL *et al.* Relationship between the pharmacokinetics and pharmacodynamics of procainamide. *Clin Pharmacol Ther* 1976; 20: 278–289.
- Frazier EP *et al.* Effects of gender, age and hypertension on β -adrenergic receptor function in rat urinary bladder. *Naunyn Schmiedeberg's Arch Pharmacol* 2006; 373: 300–309.
- Wright DFB *et al.* Understanding the time course of pharmacological effect: a PKPD approach. *Br J Clin Pharmacol* 2011; 71: 815–823.
- U.S. Department of Health and Human Services *et al.* Physiologically Based Pharmacokinetic Analyses — Format and Content Guidance for Industry (Draft guidance), 2016. <http://www.fda.gov/Drugs/GuidanceComplianceRegulatoryInformation/Guidances/default.htm> (accessed 7 May 2018).
- European Medicines Agency. Guideline on the qualification and reporting of physiologically based pharmacokinetic (PBPK) modelling and simulation (Draft), 2016. http://www.ema.europa.eu/docs/en_GB/document_library/Scientific_guideline/2016/07/WC500211315.pdf (accessed 7 May 2018).
- U.S. Department of Health and Human Services *et al.* Clinical Drug Interaction Studies — Study Design, Data Analysis, and Clinical Implications Guidance for Industry (Draft Guidance), 2017. <http://www.fda.gov/Drugs/GuidanceComplianceRegulatoryInformation/Guidances/default.htm> (accessed 7 May 2018).
- European Medicines Agency. Guideline on the investigation of drug interactions, 2012. http://www.ema.europa.eu/docs/en_GB/document_library/Scientific_guideline/2012/07/WC500129606.pdf (accessed 7 May 2018).
- EMA. Committee for Medicinal Products for Human use (CHMP): Guideline on the role of pharmacokinetics in the development of medicinal products in the paediatric population DRAFT AGREED BY EFFICACY WORKING PARTY GUIDELINE ON THE ROLE OF PHARMACOKINE. In: EMEA/CHMP/EWP/147013/2004 C, 2006, eds., 2006. <http://www.emea.europa.eu> (accessed 7 May 2018).
- Center for Drug Evaluation and Research (CDER), Center for Biological Evaluation and Research (CBER), Food and Drug Administration. Guidance for Industry: General Clinical Pharmacology Considerations for Pediatric Studies for Drugs and Biological Products, 2014. <https://www.fda.gov/downloads/drugs/guidances/ucm425885.pdf> (accessed 7 May 2018).
- U.S. Department of Health and Human Services F and DAC for DE and R (CDER). Topical dermatological corticosteroids: in vivo bioequivalence. FDA, 1995. <https://www.fda.gov/downloads/Drugs/GuidanceComplianceRegulatoryInformation/Guidances/UCM070234.pdf> (accessed 7 May 2018).
- Lionberger RA. FDA critical path initiatives: opportunities for generic drug development. *AAPS J* 2008; 10: 103–109.
- Chen ML *et al.* Challenges and opportunities in establishing scientific and regulatory standards for determining therapeutic equivalence of modified-release products:

- workshop summary report. *Clin Ther* 2010; 32: 1704–1712.
20. U.S. Department of Health and Human Services, Food and Drug Administration, Center for Drug Evaluation and Research. Individual Product Bioequivalence Recommendation—Methylphenidate hydrochloride (Draft guidance). 2017. In: Guidance for Industry: Bioequivalence Recommendations for Specific Products. May 2007. <http://www.fda.gov/downloads/Drugs/GuidanceComplianceRegulatoryInformation/Guidances/ucm072872.pdf>. <https://www.fda.gov/downloads/Drugs/GuidanceComplianceRegulatoryInformation/Guidances/UCM581432.pdf> (accessed 7 May 2018).
 21. U.S. Department of Health and Human Services, Food and Drug Administration, Center for Drug Evaluation and Research. Individual Product Bioequivalence Recommendation—Budesonide (Draft guidance), 2014. In: Guidance for Industry: Bioequivalence Recommendations for Specific Products. May 2007. <http://www.fda.gov/downloads/Drugs/GuidanceComplianceRegulatoryInformation/Guidances/ucm072872.pdf>. <https://www.fda.gov/downloads/Drugs/GuidanceComplianceRegulatoryInformation/Guidances/UCM426317.pdf> (accessed 7 May 2018).
 22. U.S. Department of Health and Human Services, Food and Drug Administration, Center for Drug Evaluation and Research. Individual Product Bioequivalence Recommendation—Zolpidem (Final guidance), 2011. In: Guidance for Industry: Bioequivalence Recommendations for Specific Products. May 2007. <http://www.fda.gov/downloads/Drugs/GuidanceComplianceRegulatoryInformation/Guidances/ucm072872.pdf>. <https://www.fda.gov/downloads/Drugs/GuidanceComplianceRegulatoryInformation/Guidances/UCM175029.pdf> (accessed 7 May 2018).
 23. CFR - Code of Federal Regulations Title 21. <https://www.accessdata.fda.gov/scripts/cdrh/cfdocs/cfcfr/CFRSearch.cfm?fr=314.3> (accessed 16 August 2018).
 24. Forester W *et al.* The onset and magnitude of the contractile response to commonly used digitalis glycosides in normal subjects. *Circulation* 1974; 49: 517–521.
 25. Shapiro W *et al.* Relationship of plasma digitoxin and digoxin to cardiac response following intravenous digitalization in man. *Circulation* 1970; 42: 1065–1072.
 26. Holford NHG, Sheiner LB. Kinetics of pharmacologic response. *Pharmacol Ther* 1982; 16: 143–166.
 27. Louizos C *et al.* Understanding the hysteresis loop conundrum in pharmacokinetic/pharmacodynamic relationships. *J Pharm Pharm Sci* 2014; 17: 34–91.
 28. Evans MA *et al.* Pharmacokinetic and pharmacodynamic modelling with pancuronium. *Eur J Clin Pharmacol* 1984; 26: 243–250.
 29. Schwartz JB *et al.* Pharmacodynamic modeling of verapamil effects under steady-state and nonsteady-state conditions. *J Pharmacol Exp Ther* 1989; 251: 1032–1038.
 30. Whiting B *et al.* Modelling theophylline response in individual patients with chronic bronchitis. *Br J Clin Pharmacol* 1981; 12: 481–487.
 31. Holford NH *et al.* The effect of quinidine and its metabolites on the electrocardiogram and systolic time intervals: concentration–effect relationships. *Br J Clin Pharmacol* 1981; 11: 187–195.
 32. Gabrielson JL *et al.* Analysis of pethidine disposition in the pregnant rat by means of a physiological flow model. *J Pharmacokinetic Biopharm* 1986; 14: 381–395.
 33. Björkman S *et al.* Comparative physiological pharmacokinetics of fentanyl and alfentanil in rats and humans based on parametric single-tissue models. *J Pharmacokinetic Biopharm* 1994; 22: 381–410.
 34. Lemmens HJM *et al.* Pharmacokinetic-pharmacodynamic modeling in drug development: application to the investigational opioid trefentanyl. *Clin Pharmacol Ther* 1994; 56: 261–271.
 35. Torres-López JE *et al.* Pharmacokinetic-pharmacodynamic modeling of the antinociceptive effect of diclofenac in the rat. *J Pharmacol Exp Ther* 1997; 282: 685–690.
 36. Morrison RA *et al.* Isosorbide dinitrate kinetics and dynamics after intravenous, sublingual, and percutaneous dosing in angina. *Clin Pharmacol Ther* 1983; 33: 747–756.
 37. Mould DR *et al.* Simultaneous modeling of the pharmacokinetics and pharmacodynamics of midazolam and diazepam. *Clin Pharmacol Ther* 1995; 58: 35–43.
 38. Kelman AW, Whiting B. Modeling of drug response in individual subjects. *J Pharmacokinetic Biopharm* 1980; 8: 115–130.
 39. Ryan AR. Tubocurarine administration based upon its disappearance and accumulation curves in anaesthetized man. *Br J Anaesth* 1964; 36: 287–294.
 40. Gibaldi M *et al.* Kinetics of the elimination and neuromuscular blocking effect of d-tubocurarine in man. *Anesthesiology* 1972; 36: 213–218.
 41. Hull CJ *et al.* A pharmacodynamic model for pancuronium. *Br J Anaesth* 1978; 50: 1113–1123.
 42. Sheiner LB *et al.* Simultaneous modeling of pharmacokinetics and pharmacodynamics: application to d-tubocurarine. *Clin Pharmacol Ther* 1979; 25: 358–371.
 43. Stanski DR *et al.* Pharmacokinetics and pharmacodynamics of d-tubocurarine during nitrous oxide-narcotic and halothane anesthesia in man. *Anesthesiology* 1979; 51: 235–241.
 44. Goat VA *et al.* The effect of blood flow upon the activity of gallamine triethiodide. *Br J Anaesth* 1976; 48: 69–73.
 45. Blume H, Mutschler M. *Bioäquivalenz, Qualitätsbewertung wirkstoffgleicher Fertigarzneimittel, Teil I/II, Isosorbiddinitrat 6*. Ergänzungslieferung: Govi-Verlag Pharmazeutischer Verlag, Frankfurt/Main-Eschborn, 1996.
 46. Holford NH, Sheiner LB. Pharmacokinetic and pharmacodynamic

- modeling in vivo. *Crit Rev Bioeng* 1981; 5: 273–322.
47. Trocóniz IF *et al.* Pharmacokinetic-pharmacodynamic modelling of the antipyretic effect of two oral formulations of ibuprofen. *Clin Pharmacokinet* 2000; 38: 505–518.
 48. Lon H-K *et al.* Pharmacokinetic/pharmacodynamic modeling in inflammation. *Crit Rev Biomed Eng* 2012; 40: 295–312.
 49. Jain AK *et al.* Analgesic efficacy of low-dose ibuprofen in dental extraction pain. *Pharmacotherapy* 1986; 6: 318–322.
 50. Hersh EV *et al.* Single dose and multidose analgesic study of ibuprofen and meclizolam sodium after third molar surgery. *Oral Surg Oral Med Oral Pathol* 1993; 76: 680–687.
 51. Seymour RA *et al.* Post-operative dental pain and analgesic efficacy. Part II. Analgesic usage and efficacy after dental surgery. *Br J Oral Surg* 1983; 21: 298–303.
 52. Laska EM *et al.* The correlation between blood levels of ibuprofen and clinical analgesic response. *Clin Pharmacol Ther* 1986; 40: 1–7.
 53. Li H *et al.* Modeling the onset and offset of dental pain relief by ibuprofen. *J Clin Pharmacol* 2012; 52: 89–101.
 54. Schou S *et al.* Analgesic dose-response relationship of ibuprofen 50, 100, 200, and 400 mg after surgical removal of third molars: a single-dose, randomized, placebo-controlled, and double-blind study of 304 patients. *J Clin Pharmacol* 1998; 38: 447–454.
 55. McQuay HJ *et al.* Ibuprofen compared with ibuprofen plus caffeine after third molar surgery. *Pain* 1996; 66: 247–251.
 56. McQuay HJ, Moore RA. Dose-response in direct comparisons of different doses of aspirin, ibuprofen and paracetamol (acetaminophen) in analgesic studies. *Br J Clin Pharmacol* 2007; 63: 271–278.
 57. Lemmens H *et al.* Pharmacokinetics-pharmacodynamics (PK/PD) of ibuprofen in dental pain. *J Clin Pharmacol* 1996; 36: 856.
 58. Cristofolletti R, Dressman JB. Use of physiologically based pharmacokinetic models coupled with pharmacodynamic models to assess the clinical relevance of current bioequivalence criteria for generic drug products containing ibuprofen. *J Pharm Sci* 2014; 103: 3263–3275.
 59. Walson PD *et al.* Ibuprofen, acetaminophen and placebo treatment of febrile children. *Clin Pharmacol Ther* 1989; 46: 9–17.
 60. Cristofolletti R, Dressman JB. Bridging the gap between in vitro dissolution and the time course of ibuprofen-mediated pain relief. *J Pharm Sci* 2016; 105: 3658–3667.
 61. Jonker JW, Schinkel AH. Pharmacological and physiological functions of the polyspecific organic cation transporters: OCT1, 2, and 3 (SLC22A1–3). *J Pharmacol Exp Ther* 2003; 308: 2–9.
 62. de Lange ECM, Danhof M. Considerations in the use of cerebrospinal fluid pharmacokinetics to predict brain target concentrations in the clinical setting. *Clin Pharmacokinet* 2002; 41: 691–703.
 63. Lee G *et al.* Drug transporters in the central nervous system: brain barriers and brain parenchyma considerations. *Pharmacol Rev* 2001; 53: 569–596.
 64. De Boer AG *et al.* The role of drug transporters at the blood-brain barrier. *Annu Rev Pharmacol Toxicol* 2003; 43: 629–656.
 65. Letrent SP *et al.* Effect of GF120918, a potent P-glycoprotein inhibitor, on morphine pharmacokinetics and pharmacodynamics in the rat. *Pharm Res* 1998; 15: 599–605.
 66. Suzuki N *et al.* Intrathecal morphine-3-glucuronide does not antagonize spinal antinociception by morphine or morphine-6-glucuronide in rats. *Eur J Pharmacol* 1993; 249: 247–250.
 67. Ouellet DM, Pollack GM. Effect of prior morphine-3-glucuronide exposure on morphine disposition and antinociception. *Biochem Pharmacol* 1997; 53: 1451–1457.
 68. Hewett K *et al.* Lack of effect of morphine-3-glucuronide on the spinal antinociceptive actions of morphine in the rat: an electrophysiological study. *Pain* 1993; 53: 59–63.
 69. Xie R *et al.* The role of P-glycoprotein in blood-brain barrier transport of morphine: transcortical microdialysis studies in *mdr1a* (–/–) and *mdr1a* (+/+) mice. *Br J Pharmacol* 1999; 128: 563–568.
 70. de Lange EC *et al.* Methodological considerations of intracerebral microdialysis in pharmacokinetic studies on drug transport across the blood–brain barrier. *Brain Res Rev* 1997; 25: 27–49.
 71. Hammarlund-Udenaes M. The use of microdialysis in CNS drug delivery studies: pharmacokinetic perspectives and results with analgesics and antiepileptics. *Adv Drug Deliv Rev* 2000; 45: 283–294.
 72. Hammarlund-Udenaes M *et al.* Drug equilibration across the blood-brain barrier–pharmacokinetic considerations based on the microdialysis method. *Pharm Res* 1997; 14: 128–134.
 73. Mager DE *et al.* Diversity of mechanism-based pharmacodynamic models. *Drug Metab Dispos* 2003; 31: 510–518.
 74. Danhof M *et al.* Mechanism-based pharmacokinetic-pharmacodynamic modeling: biophase distribution, receptor theory, and dynamical systems analysis. *Annu Rev Pharmacol Toxicol* 2007; 47: 357–400.
 75. Hong Y *et al.* Population pharmacodynamic modelling of aspirin- and ibuprofen-induced inhibition of platelet aggregation in healthy subjects. *Clin Pharmacokinet* 2008; 47: 129–137.
 76. Yamamoto K *et al.* Pharmacodynamics analysis of antiplatelet effect of aspirin in the literature – modeling based on inhibition of cyclooxygenase in the platelet and the vessel wall endothelium. *Jpn J Hosp Pharm* 1996; 22: 133–141.
 77. Gisleskog PO *et al.* A model for the turnover of dihydrotestosterone in the presence of the irreversible 5 alpha-reductase inhibitors GI198745

- and finasteride. *Clin Pharmacol Ther* 1998; 64: 636–647.
78. Katashima M *et al.* Pharmacokinetic and pharmacodynamic study of a new nonsteroidal 5 alpha-reductase inhibitor, 4-[3-[3-[Bis(4-isobutylphenyl)methylamino]benzoyl]-1H-indol-1-yl]-butyric acid, in rats. *J Pharmacol Exp Ther* 1998; 284: 914–920.
 79. Abelo A *et al.* A turnover model of irreversible inhibition of gastric acid secretion by omeprazole in the dog. *J Pharmacol Exp Ther* 2000; 295: 662–669.
 80. Katashima M *et al.* Comparative pharmacokinetic/pharmacodynamic analysis of proton pump inhibitors omeprazole, lansoprazole and pantoprazole, in humans. *Eur J Drug Metab Pharmacokinet* 1998; 23: 19–26.
 81. Puchalski TA *et al.* Pharmacodynamic modeling of lansoprazole using an indirect irreversible response model. *J Clin Pharmacol* 2001; 41: 251–258.
 82. Nielsen EI *et al.* Pharmacokinetic/pharmacodynamic (PK/PD) indices of antibiotics predicted by a semimechanistic PKPD model: a step toward model-based dose optimization. *Antimicrob Agents Chemother* 2011; 55: 4619–4630.
 83. Snoeck E *et al.* A comprehensive hepatitis C viral kinetic model explaining cure. *Clin Pharmacol Ther* 2010; 87: 706–713.
 84. Simeoni M *et al.* Predictive pharmacokinetic-pharmacodynamic modeling of tumor growth kinetics in xenograft models after administration of anticancer agents. *Cancer Res* 2004; 64: 1094–1101.
 85. Friberg LE *et al.* Semiphysiological model for the time course of leukocytes after varying schedules of 5-fluorouracil in rats. *J Pharmacol Exp Ther* 2000; 295: 734–740.
 86. Russu A, Poggesi I. Turnover model with irreversible inactivation. In: Mager DE, Kimko HHC, eds. *Systems Pharmacology and Pharmacodynamics*. Cham, Switzerland: Springer Nature, 2016: 217.
 87. Nagaya H *et al.* Possible mechanism for the inhibition of gastric (H⁺ + K⁺)-adenosine triphosphatase by the proton pump inhibitor AG-1749. *J Pharmacol Exp Ther* 1989; 248: 799–805.
 88. Shin JM *et al.* The site of action of pantoprazole in the gastric H⁺/K⁺-ATPase. *Biochim Biophys Acta* 1993; 1148: 223–233.
 89. Fitton A, Wiseman L. Pantoprazole. A review of its pharmacological properties and therapeutic use in acid-related disorders. *Drugs* 1996; 51: 460–482.
 90. Im WB *et al.* Irreversible inactivation of rat gastric (H⁺ + K⁺)-ATPase in vivo by omeprazole. *Biochem Biophys Res Commun* 1985; 126: 78–82.
 91. Sachs G *et al.* Gastric acid secretion: activation and inhibition. *Yale J Biol Med* 1994; 67: 81–95.
 92. Gedda K *et al.* Turnover of the gastric H⁺, K⁺-adenosine triphosphatase alpha subunit and its effect on inhibition of rat gastric acid secretion. *Gastroenterology* 1995; 109: 1134–1141.
 93. Metz DC *et al.* Proton pump activation in stimulated parietal cells is regulated by gastric acid secretory capacity: a human study. *J Clin Pharmacol* 2002; 42: 512–519.
 94. Katashima M *et al.* Comparative pharmacokinetic/pharmacodynamic study of proton pump inhibitors, omeprazole and lansoprazole in rats. *Drug Metab Dispos* 1995; 23: 718–723.
 95. Shin JM, Sachs G. Differences in binding properties of two proton pump inhibitors on the gastric H⁺, K⁺-ATPase in vivo. *Biochem Pharmacol* 2004; 68: 2117–2127.
 96. Sugiura M *et al.* Prediction of therapeutic doses based on the pharmacokinetic/pharmacodynamic model of omeprazole, a proton pump inhibitor. *Drug Metab Pharmacokinet* 1992; 7: 813–820.
 97. Dayneka NL *et al.* Comparison of four basic models of indirect pharmacodynamic responses. *J Pharmacokinetic Biopharm* 1993; 21: 457–478.
 98. Polentarutti B *et al.* Modification of gastric pH in the fasted dog. *J Pharm Pharmacol* 2010; 62: 462–469.
 99. Ferron GM *et al.* Pharmacodynamic modeling of pantoprazole's irreversible effect on gastric acid secretion in humans and rats. *J Clin Pharmacol* 2001; 41: 149–156.
 100. Feldman M *et al.* A comparison of every-third-day versus daily low-dose aspirin therapy on serum thromboxane concentrations in healthy men and women. *Clin Appl Thromb Hemost* 2001; 7: 53–57.
 101. Nagelschmitz J *et al.* Pharmacokinetics and pharmacodynamics of acetylsalicylic acid after intravenous and oral administration to healthy volunteers. *Clin Pharmacol* 2014; 6: 51–59.
 102. Patrignani P *et al.* Selective cumulative inhibition of platelet thromboxane production by low-dose aspirin in healthy subjects. *J Clin Invest* 1982; 69: 1366–1372.
 103. Renda G *et al.* Celecoxib, ibuprofen, and the antiplatelet effect of aspirin in patients with osteoarthritis and ischemic heart disease. *Clin Pharmacol Ther* 2006; 80: 264–274.
 104. Giaretta A *et al.* In silico modeling of the antiplatelet pharmacodynamics of low-dose aspirin in health and disease. *Clin Pharmacol Ther* 2017; 102: 823–831.
 105. Valle M *et al.* A predictive model for exemestane pharmacokinetics/ pharmacodynamics incorporating the effect of food and formulation. *Br J Clin Pharmacol* 2005; 59: 355–364.
 106. Paridaens R *et al.* Safety, activity and estrogen inhibition by exemestane in postmenopausal women with advanced breast cancer: a phase I study. *Anticancer Drugs* 1998; 9: 675–683.
 107. Johannessen DC *et al.* Endocrine and clinical effects of exemestane (PNU 155971), a novel steroidal aromatase inhibitor, in postmenopausal breast cancer patients: a phase I study. *Clin Cancer Res* 1997; 3: 1101–1108.
 108. Geisler J *et al.* In vivo inhibition of aromatization by exemestane, a novel irreversible aromatase inhibitor, in postmenopausal breast cancer patients. *Clin Cancer Res* 1998; 4: 2089–2093.
 109. Nagashima R *et al.* Kinetics of pharmacologic effects in man: the

- anticoagulant action of warfarin. *Clin Pharmacol Ther* 1969; 10: 22–35.
110. Chakraborty A *et al.* Mathematical modeling of circadian cortisol concentrations using indirect response models: comparison of several methods. *J Pharmacokinetic Biopharm* 1999; 27: 23–43.
 111. Krzyzanski W *et al.* Basic pharmacodynamic models for agents that alter production of natural cells. *J Pharmacokinetic Biopharm* 1999; 27: 467–489.
 112. Budha NR *et al.* Comparative performance of cell life span and cell transit models for describing erythropoietic drug effects. *AAPS J* 2011; 13: 650–661.
 113. Samtani MN *et al.* Pharmacokinetic and pharmacodynamic modeling of pegylated thrombopoietin mimetic peptide (PEG-TPOm) after single intravenous dose administration in healthy subjects. *J Clin Pharmacol* 2009; 49: 336–350.
 114. Yao Z *et al.* Assessment of basic indirect pharmacodynamic response models with physiological limits. *J Pharmacokinetic Pharmacodyn* 2006; 33: 167–193.
 115. Labrecque G, Bélanger PM. Biological rhythms in the absorption, distribution, metabolism and excretion of drugs. *Pharmacol Ther* 1991; 52: 95–107.
 116. Sällström B *et al.* A pharmacodynamic turnover model capturing asymmetric circadian baselines of body temperature, heart rate and blood pressure in rats: challenges in terms of tolerance and animal-handling effects. *J Pharmacokinetic Pharmacodyn* 2005; 32: 835–859.
 117. Sukumaran S *et al.* Circadian rhythms in gene expression: relationship to physiology, disease, drug disposition and drug action. *Adv Drug Deliv Rev* 2010; 62: 904–917.
 118. Lew KH *et al.* Gender-based effects on methylprednisolone pharmacokinetics and pharmacodynamics. *Clin Pharmacol Ther* 1993; 54: 402–414.
 119. Rohatagi S *et al.* Dynamic modeling of cortisol reduction after inhaled administration of fluticasone propionate. *J Clin Pharmacol* 1996; 36: 938–941.
 120. Krzyzanski W. Direct, indirect, and signal transduction response modeling. In: Mager DE, Kimko HHC, eds. *Systems Pharmacology and Pharmacodynamics*. Cham, Switzerland: Springer, 2016: 177–210.
 121. Mager DE, Jusko WJ. Pharmacodynamic modeling of time-dependent transduction systems. *Clin Pharmacol Ther* 2001; 70: 210–216.
 122. Zhang Y, D'Argenio DZ. Feedback control indirect response models. In: Mager DE, Kimko HHC, eds. *Systems Pharmacology and Pharmacodynamics*. Cham, Switzerland: Springer Nature, 2016: 229–254.
 123. Black JW, Leff P. Operational models of pharmacological agonism. *Proc R Soc London B Biol Sci* 1983; 220: 141–162.
 124. Van Der Graaf PH *et al.* Mechanism-based pharmacokinetic-pharmacodynamic modeling of the effects of N6-cyclopentyladenosine analogs on heart rate in rat: estimation of in vivo operational affinity and efficacy at adenosine A1 receptors. *J Pharmacol Exp Ther* 1997; 283: 809–816.
 125. Greene SJ *et al.* Partial adenosine A1 receptor agonism: a potential new therapeutic strategy for heart failure. *Heart Fail Rev* 2016; 21: 95–102.
 126. Cox EH *et al.* Pharmacokinetic-pharmacodynamic modelling of the EEG effect of alfentanil in rats. *J Pharmacol Toxicol Methods* 1997; 38: 99–108.
 127. Cox EH *et al.* Pharmacokinetic-pharmacodynamic modeling of the electroencephalogram effect of synthetic opioids in the rat: correlation with the interaction at the mu-opioid receptor. *J Pharmacol Exp Ther* 1998; 284: 1095–1103.
 128. Zuideveld KP *et al.* Pharmacokinetic-pharmacodynamic modelling of the hypothermic and corticosterone effects of the 5-HT1A receptor agonist flesinoxan. *Eur J Pharmacol* 2002; 445: 43–54.
 129. Ramakrishnan R *et al.* Fifth-generation model for corticosteroid pharmacodynamics: application to steady-state receptor down-regulation and enzyme induction patterns during seven-day continuous infusion of methylprednisolone in rats. *J Pharmacokinetic Pharmacodyn* 2002; 29: 1–24.
 130. Sandström M *et al.* Model describing the relationship between pharmacokinetics and hematologic toxicity of the epirubicin-docetaxel regimen in breast cancer patients. *J Clin Oncol* 2005; 23: 413–421.
 131. Friberg LE *et al.* Model of chemotherapy-induced myelosuppression with parameter consistency across drugs. *J Clin Oncol* 2002; 20: 4713–4721.
 132. Gabrielsson J, Peletier LA. A flexible nonlinear feedback system that captures diverse patterns of adaptation and rebound. *AAPS J* 2008; 10: 70–83.
 133. Wakelkamp M *et al.* Pharmacodynamic modeling of furosemide tolerance after multiple intravenous administration. *Clin Pharmacol Ther* 1996; 60: 75–88.
 134. Ahlström C *et al.* Feedback modeling of non-esterified fatty acids in obese Zucker rats after nicotinic acid infusions. *J Pharmacokinetic Pharmacodyn* 2013; 40: 623–638.
 135. Wilson JT *et al.* Single-dose, placebo-controlled comparative study of ibuprofen and acetaminophen antipyresis in children. *J Pediatr* 1991; 119: 803–811.
 136. Brown RD *et al.* Single-dose pharmacokinetics of ibuprofen and acetaminophen in febrile children. *J Clin Pharmacol* 1992; 32: 231–241.
 137. Brown RD *et al.* Integrated pharmacokinetic-pharmacodynamic model for acetaminophen, ibuprofen, and placebo antipyresis in children. *J Pharmacokinetic Biopharm* 1998; 26: 559–579.
 138. Mackowiak PA. Concepts of fever. *Arch Intern Med* 1998; 158: 1870–1881.
 139. Garg V, Jusko WJ. Pharmacodynamic modeling of nonsteroidal anti-inflammatory drugs: antipyretic effect of ibuprofen. *Clin Pharmacol Ther* 1994; 55: 87–88.
 140. Kauffman RE, Nelson MV. Effect of age on ibuprofen pharmacokinetics and antipyretic response. *J Pediatr* 1992; 121: 969–973.

141. Olsson AG *et al.* Effect of rosuvastatin on low-density lipoprotein cholesterol in patients with hypercholesterolemia. *Am J Cardiol* 2001; 88: 504–508.
142. Davidson MH. Rosuvastatin: a highly efficacious statin for the treatment of dyslipidaemia. *Expert Opin Investig Drugs* 2002; 11: 125–141.
143. Schachter M. Chemical, pharmacokinetic and pharmacodynamic properties of statins: an update. *Fundam Clin Pharmacol* 2005; 19: 117–125.
144. Aoyama T *et al.* Pharmacokinetic/pharmacodynamic modeling and simulation of rosuvastatin using an extension of the indirect response model by incorporating a circadian rhythm. *Biol Pharm Bull* 2010; 33: 1082–1087.
145. Krzyzanski W *et al.* Algorithm for application of Fourier analysis for biorhythmic baselines of pharmacodynamic indirect response models. *Chronobiol Int* 2000; 17: 77–93.
146. Krzyzanski W, Jusko WJ. Indirect pharmacodynamic models for responses with multicompartmental distribution or polyexponential disposition. *J Pharmacokinet Pharmacodyn* 2001; 28: 57–78.
147. Martin PD *et al.* Pharmacodynamic effects and pharmacokinetics of a new HMG-CoA reductase inhibitor, rosuvastatin, after morning or evening administration in healthy volunteers. *Br J Clin Pharmacol* 2002; 54: 472–477.
148. Ho R, Kim R. Transporters and drug therapy: implications for drug disposition and disease. *Clin Pharmacol Ther* 2005; 78: 260–277.
149. Ho RH *et al.* Drug and bile acid transporters in rosuvastatin hepatic uptake: function, expression, and pharmacogenetics. *Gastroenterology* 2006; 130: 1793–1806.
150. Hirano M *et al.* Contribution of OATP2 (OATP1B1) and OATP8 (OATP1B3) to the hepatic uptake of pitavastatin in humans. *J Pharmacol Exp Ther* 2004; 311: 139–146.
151. Kameyama Y *et al.* Functional characterization of SLCO1B1 (OATP-C) variants, SLCO1B1*5, SLCO1B1*15 and SLCO1B1*15 + C1007G, by using transient expression systems of HeLa and HEK293 cells. *Pharmacogenet Genomics* 2005; 15: 513–522.
152. Hsiang B *et al.* A novel human hepatic organic anion transporting polypeptide (OATP2). Identification of a liver-specific human organic anion transporting polypeptide and identification of rat and human hydroxymethylglutaryl-CoA reductase inhibitor transporters. *J Biol Chem* 1999; 274: 37161–37168.
153. Kitamura S *et al.* Involvement of multiple transporters in the hepatobiliary transport of rosuvastatin. *Drug Metab Dispos* 2008; 36: 2014–2023.
154. Nishizato Y *et al.* Polymorphisms of OATP-C (SLC21A6) and OAT3 (SLC22A8) genes: consequences for pravastatin pharmacokinetics. *Clin Pharmacol Ther* 2003; 73: 554–565.
155. Pasanen MK *et al.* Different effects of SLCO1B1 polymorphism on the pharmacokinetics of atorvastatin and rosuvastatin. *Clin Pharmacol Ther* 2007; 82: 726–733.
156. Pasanen MK *et al.* SLCO1B1 polymorphism markedly affects the pharmacokinetics of simvastatin acid. *Pharmacogenet Genomics* 2006; 16: 873–879.
157. Niemi M *et al.* SLCO1B1 polymorphism and sex affect the pharmacokinetics of pravastatin but not fluvastatin. *Clin Pharmacol Ther* 2006; 80: 356–366.
158. Niemi M *et al.* High plasma pravastatin concentrations are associated with single nucleotide polymorphisms and haplotypes of organic anion transporting polypeptide-C (OATP-C, SLCO1B1). *Pharmacogenetics* 2004; 14: 429–440.
159. Rose RH *et al.* Application of a physiologically based pharmacokinetic model to predict OATP1B1-related variability in pharmacodynamics of rosuvastatin. *CPT Pharmacometrics Syst Pharmacol* 2014; 3: e124.
160. Tachibana-Iimori R *et al.* Effect of genetic polymorphism of OATP-C (SLCO1B1) on lipid-lowering response to HMG-CoA reductase inhibitors. *Drug Metab Pharmacokinet* 2004; 19: 375–380.
161. Pasanen MK *et al.* Polymorphism of the hepatic influx transporter organic anion transporting polypeptide 1B1 is associated with increased cholesterol synthesis rate. *Pharmacogenet Genomics* 2008; 18: 921–926.
162. Niemi M *et al.* Organic anion transporting polypeptide 1B1: a genetically polymorphic transporter of major importance for hepatic drug uptake. *Pharmacol Rev* 2011; 63: 157–181.
163. Niemi M. Transporter pharmacogenetics and statin toxicity. *Clin Pharmacol Ther* 2010; 87: 130–133.
164. Piñeyro G, Blier P. Autoregulation of serotonin neurons: role in antidepressant drug action. *Pharmacol Rev* 1999; 51: 533–591.
165. Bourne JA. Intracerebral microdialysis: 30 years as a tool for the neuroscientist. *Clin Exp Pharmacol Physiol* 2003; 30: 16–24.
166. Westerink BH, Timmerman W. Do neurotransmitters sampled by brain microdialysis reflect functional release? *Anal Chim Acta* 1999; 379: 263–274.
167. Bundgaard C *et al.* Mechanistic model of acute autoinhibitory feedback action after administration of SSRIs in rats: application to escitalopram-induced effects on brain serotonin levels. *Eur J Pharm Sci* 2006; 29: 394–404.
168. Ceglia I *et al.* Effects of chronic treatment with escitalopram or citalopram on extracellular 5-HT in the prefrontal cortex of rats: role of 5-HT1A receptors. *Br J Pharmacol* 2004; 142: 469–478.
169. Mørk A *et al.* The R-enantiomer of citalopram counteracts escitalopram-induced increase in extracellular 5-HT in the frontal cortex of freely moving rats. *Neuropharmacology* 2003; 45: 167–173.
170. Selen A *et al.* The biopharmaceutics risk assessment roadmap for optimizing clinical drug product performance. *J Pharm Sci* 2014; 103: 3377–3397.
171. Dickinson PA *et al.* Clinical relevance of dissolution testing in quality by design. *AAPS J* 2008; 10: 380–390.



Establishing virtual bioequivalence and clinically relevant specifications using *in vitro* biorelevant dissolution testing and physiologically-based population pharmacokinetic modeling. case example: Naproxen



Ioannis Loisios-Konstantinidis^a, Rodrigo Cristofolletti^b, Nikoletta Fotaki^c, David B. Turner^e, Jennifer Dressman^{a,d,*}

^a Institute of Pharmaceutical Technology, Goethe University, Frankfurt am Main, Germany

^b Center for Pharmacometrics and Systems Pharmacology, Department of Pharmaceutics, College of Pharmacy, University of Florida, Orlando, FL, United States

^c Department of Pharmacy and Pharmacology, Faculty of Science, University of Bath, Bath, United Kingdom

^d Fraunhofer IME - Translational Pharmacology and Medicine, Carl-von-Noorden Platz 9, Frankfurt am Main, Germany

^e Certara UK Limited, Simcyp Division, 1 Concourse Way, Sheffield S1 2BJ, United Kingdom

ARTICLE INFO

Keywords:

PBPK
Modeling & simulation
Virtual bioequivalence
IVIVE
Clinically relevant specifications
Dissolution safe-space
Biorelevant dissolution

ABSTRACT

Background: Physiologically-based population pharmacokinetic modeling (popPBPK) coupled with *in vitro* biopharmaceutics tools such as biorelevant dissolution testing can serve as a powerful tool to establish virtual bioequivalence and set clinically relevant specifications. One of several applications of popPBPK modeling is in the emerging field of virtual bioequivalence (VBE), where it can be used to streamline drug development by implementing model-informed formulation design and to inform regulatory decision-making e.g., with respect to evaluating the possibility of extending BCS-based biowaivers beyond BCS Class I and III compounds in certain cases.

Methods: In this study, Naproxen, a BCS class II weak acid was chosen as the model compound. *In vitro* biorelevant solubility and dissolution experiments were performed and the resulting data were used as an input to the PBPK model, following a stepwise workflow for the confirmation of the biopharmaceutical parameters. The naproxen PBPK model was developed by implementing a middle-out approach and verified against clinical data obtained from the literature. Once confidence in the performance of the model was achieved, several *in vivo* dissolution scenarios, based on model-based analysis of the *in vitro* data, were used to simulate clinical trials in healthy adults. Inter-occasion variability (IOV) was also added to critical *physiological* parameters and mechanistically propagated through the simulations. The various trials were simulated on a “worst/best case” dissolution scenario and average bioequivalence was assessed according to C_{max} , AUC and T_{max} .

Results: VBE results demonstrated that naproxen products with *in vitro* dissolution reaching 85% dissolved within 90 min would lie comfortably within the bioequivalence limits for C_{max} and AUC. Based on the establishment of VBE, a dissolution “safe space” was designed and a clinically relevant specification for naproxen products was proposed. The interplay between formulation-related and drug-specific PK parameters (e.g., $t_{1/2}$) to predict the *in vivo* performance was also investigated.

Conclusion: Over a wide range of values, the *in vitro* dissolution rate is not critical for the clinical performance of naproxen products and therefore naproxen could be eligible for BCS-based biowaivers based on *in vitro* dissolution under intestinal conditions. This approach may also be applicable to other poorly soluble acidic compounds with long half-lives, providing an opportunity to streamline drug development and regulatory decision-making without putting the patient at a risk.

1. Introduction

Physiologically-based population pharmacokinetic (popPBPK)

modeling has been implemented successfully to support and inform drug product development and regulatory decision-making. (Babiskin and Zhang, 2015; Doki et al., 2017; Heimbach et al., 2017;

* Correspondence author: Biocenter, Institute of Pharmaceutical Technology, Johann Wolfgang Goethe University, Max-von-Laue-Str. 9, Frankfurt am Main 60438, Germany.

E-mail address: dressman@em.uni-frankfurt.de (J. Dressman).

<https://doi.org/10.1016/j.ejps.2019.105170>

Received 4 September 2019; Received in revised form 25 November 2019; Accepted 26 November 2019

Available online 27 November 2019

0928-0987/ © 2019 Elsevier B.V. All rights reserved.

Mitra, 2019; Olivares-Morales et al., 2016; Parrott et al., 2014; Pepin et al., 2016; Stillhart et al., 2017; Suarez-Sharp et al., 2018; Zhang et al., 2017) Patient-centric, model-informed drug product development necessitates an *in vitro-in vivo-in silico* link to establish clinically relevant specifications and thus guarantee the quality of the drug product with respect to safety and efficacy. By encompassing model-informed formulation selection and prediction of clinical performance, modeling and simulation (M & S) provides a way forward to the design of “safe spaces”, and thus offer regulatory relief. Some examples include guiding development of biorelevant and/or biopredictive dissolution methods to support biowaiver extensions and enabling extrapolation to special populations (e.g., paediatrics). Although the current PBPK regulatory guidelines still mainly focus on the prediction of drug-drug interactions (DDIs), (European Medicines Agency (EMA), 2018a; U.S-FDA Center for Drug Evaluation and Research CDER, 2018a) the integration of translational biopharmaceutical modeling and dissolution testing has been attracting increased attention from leading pharmaceutical industries as well as regulatory bodies and over the last few years, the regulatory impact of mechanistic absorption modeling has significantly increased. (Babiskin and Zhang, 2015; Heimbach et al., 2019; Pepin et al., 2016; Zhang et al., 2017)

Establishing bioequivalence (BE) has been a critical component of and remains a challenge during development of both new drug and generic products. In the context of quality by design (QbD) and the biopharmaceutics risk assessment roadmap (BioRAM) (Selen et al., 2014; Dickinson et al., 2008), the importance of linking *in vitro* with *in vivo* data bi-directionally has received greater emphasis. Accordingly, virtual bioequivalence (VBE) can serve as a powerful tool to set clinically relevant specifications and predict anticipated clinical outcomes in healthy, patient and special-patient (e.g., paediatrics and/or co-administration of PPIs) populations. To accurately predict the *in vivo* performance of a drug product through clinical trial simulation, a certain set of conditions needs to be met. This includes integration of biorelevant *in vitro* data into the simulation model as well as mechanistic absorption modeling, disposition/elimination components and consideration of physiological and physicochemical interactions with the formulation. After developing the mechanistic absorption PBPK model, it must be verified via learn/confirm cycles which rely on evaluation against observed clinical data. Such models can then be used to predict the population pharmacokinetic variability of the test drug/formulation and therefore enable assessment of bioequivalence risks via virtual trials simulations. (Pathak et al., 1997)

The ability of PBPK to account for between-subject (BS), within-subject (WS) and inter-occasion variability (IOV) is crucial to the accuracy and the applicability of VBE results. Although the current techniques can address the between-subject variability reasonably well, progress still needs to be made in the area of estimating inter-occasion variability. Two independent modeling strategies to incorporate IOV in VBE studies have been implemented in the literature: a) *a priori* estimated random error terms in replicate clinical study are added to the PK parameters, or, more mechanistically, b) the IOV is integrated into the system parameters and propagated in simulations. (Wedagedera et al., 2017)

In this study, an *in vitro-in vivo-in silico* workflow to establish VBE and clinically relevant dissolution specifications is proposed. Naproxen and its sodium salt were chosen as the case example. Naproxen is a weakly acidic ($pK_a \approx 4.4$) non-steroid anti-inflammatory (NSAID) agent. It is a biopharmaceutical classification system (BCS) class II weak acid with poor solubility in the fasted stomach but freely soluble in the intestinal environment and has a high permeability, similar to ibuprofen and diclofenac. (Cristofolletti et al., 2013; Cristofolletti and Dressman, 2016; Kambayashi et al., 2013) Since the absorption of such compounds is usually complete, they have been identified as offering opportunities for a potential BCS-based biowaiver extension. (Cristofolletti and Dressman, 2016; Tubic-Grozdanis et al., 2008; Yazdani et al., 2004) The free acid (Naprosyn®) and the sodium salt

(Anaprox®) forms are administered orally as immediate release (IR) tablets. The purpose of this article is to characterize the *in vitro* dissolution behavior of naproxen pure API and formulations, integrate mechanistic absorption modeling with population-based PBPK, design a safe space and, last but not least, set clinically relevant dissolution specifications through VBE trials. The possibility/risk of granting BCS-biowaiver for naproxen products is also investigated.

2. Material and methods

2.1. Chemicals and reagents

Naproxen (lot #SLBV2253) and naproxen sodium (lot #MKCD6021) pure active pharmaceutical ingredient (API) were purchased commercially from Sigma-Aldrich Co., LLC. (St. Louis, MO). Naproxen tablets (500 mg Naprosyn®, lot 70,662; Minerva Pharmaceutical Inc., Athens, Greece) and naproxen sodium tablets (550 mg Anaprox®, lot 70,466; Minerva Pharmaceutical Inc., Athens, Greece) were commercially purchased from the Greek market. Fasted state simulated gastric fluid (FaSSGF)/fasted state simulated intestinal fluid (FaSSIF V1)/fed state simulated intestinal fluid (FeSSIF V1) powder (lot 01–1512–05NP), FeSSIF V2 powder (lot 03–1610–02) and FaSSIF V3 powder (lot PHA S 1,306,023) were kindly donated from Biorelevant.com Ltd., (Surrey, UK). Acetonitrile (lot 18A101551) and water (lot 17B174006) of HPLC-grade were from VWR Chemicals (Leuven, Belgium). Sodium hydroxide pellets (lot 14A100027), sodium chloride (lot 171074122), sodium acetate (lot 14B240013), hydrochloric acid 37% (lot 10L060526), orthophosphoric acid 85% (lot 12K210017) and glacial acetic acid 100% (lot 12B220508) were commercially obtained from VWR Chemicals (Leuven, Belgium). Sodium dihydrogen phosphate dehydrate (lot K93701642712), maleic acid (lot 57,118,880,544) and citric acid (lot K91221207425) were commercially purchased from Merck KGaA (Darmstadt, Germany). Pepsin from porcine gastric mucosa 19.6% and Lipofundin® MCT/LCT 20% were from Sigma-Aldrich Co., LLC. (St. Louis, MO) and B. Braun Melsungen AG (Melsungen, Germany), respectively.

2.2. *In vitro* solubility experiments

The solubility of naproxen and its sodium salt was investigated in various selected aqueous and biorelevant dissolution media using the Uniprep™ system (Whatman®, Piscataway, NJ, USA). All aqueous buffers were prepared according to the European Pharmacopoeia, while the biorelevant media were prepared according to Markopoulos et al. and Fuchs et al. (Fuchs et al., 2015; Markopoulos et al., 2015) The composition and physicochemical characteristics of the fasted and fed state biorelevant media used in this study are summarized in Table 1. An excess amount of API was added to 3 mL of dissolution medium and the samples were incubated for 24 h at 37 °C on an orbital mixer. The samples were then filtered through the 0.45 µm PTFE filter integrated in the Uniprep™ system. The filtrate was immediately diluted with mobile phase and analyzed by high-performance liquid chromatography (HPLC) (see Section 2.5). All measurements were performed at least in triplicate ($n \geq 3$).

2.3. *In vitro* dissolution tests

All dissolution tests were performed using calibrated USP II (paddle) apparatus (Erweka DT 80, Heusenstamm, Germany) at 37 ± 0.5 °C. Each vessel contained 500 mL of fresh, pre-warmed medium and the rotational speed was set at 75 rpm. Samples were withdrawn at 2.5, 5, 10, 15, 20, 30, 45, 60, 90 and 120 min via a 5 mL glass syringe connected to a stainless-steel cannula containing a 10 µm polyethylene cannula filter. Immediately thereafter, the sample was filtered through a 0.45 µm PTFE filter (ReZist™ 30, GE Healthcare UK Ltd., Buckinghamshire, UK), discarding the first 2 mL. The filtrate was

Table 1
Composition and physicochemical characteristics of biorelevant media in the fasted and fed states.

	Fasted state					Fed state			
	FaSSGF Level I	FaSSGF Level III	FaSSIF Level II	FaSSIF V3 Level I	FaSSIF V3 Level II	FeSSGF _{middle} Level II	FeSSIF Level I	FeSSIF Level II	FeSSIF V2 Level II
Sodium Taurocholate (mM)	—	0.08	3.0	—	1.4	—	—	15	10
Sodium Glycocholate (mM)	—	—	—	—	1.4	—	—	—	—
Glyceryl monooleate (mM)	—	—	—	—	—	—	—	—	5
Sodium Oleate (mM)	—	—	—	—	0.315	—	—	—	0.8
Lecithin (mM)	—	0.02	0.75	—	0.035	—	—	3.75	2
Lysolecithin (mM)	—	—	—	—	0.315	—	—	—	—
Cholesterol (mM)	—	—	—	—	0.2	—	—	—	—
Pepsin (mg/mL)	—	0.1	—	—	—	—	—	—	—
Sodium dihydrogen phosphate (mM)	—	—	28.7	13.51	13.51	—	—	—	—
NaOH (mM)	—	—	13.8	3.19	3.19	—	101	101	102.4
Acetic acid (mM)	—	—	—	—	—	18.31	144	144	—
Maleic acid (mM)	—	—	—	—	—	—	—	—	71.9
Sodium acetate (mM)	—	—	—	—	—	32.98	—	—	—
Lipofundin®: buffer	—	—	—	—	—	8.75: 91.25	—	—	—
Hydrochloric acid	q.s. pH 1.6	q.s. pH 1.6	—	—	—	q.s. pH 5	—	—	—
Sodium chloride (mM)	—	34.2	106	—	91.62	181.7	—	204	125.5
Osmolality (mOsm/kg)	—	121	270	—	215	400	—	635	390
Buffer capacity (HCl) ((mmol/L)/ΔpH)	n.a.	n.a.	12	5.6	5.6	25	76	76	25
pH	1.6	1.6	6.5	6.7	6.7	5.0	5.0	5.0	5.8

q.s.- quantum satis; n.a.- not applicable.

immediately diluted with mobile phase and analyzed by HPLC-UV (see Section 2.5). The removal of 5 mL at each sampling time was taken into account in the calculation of the percentage dissolved. All experiments were performed at least in triplicate ($n \geq 3$) and the final pH in the vessel was recorded.

2.4. Two-stage dissolution tests

Since the conventional one-stage USP II dissolution test does not include a gastric compartment to account for disintegration of the dosage form in the stomach, differences in the disintegration time between non-coated (i.e. 500 mg Naprosyn®) and simple coated formulation (i.e. 550 mg Anaprox®) might bias the interpretation of the biorelevant *in vitro* dissolution behavior with respect to the *in vivo* performance. Therefore, to investigate the disintegration effect on the *in vitro* performance of naproxen/ naproxen sodium formulations, a two-stage dissolution test for FaSSIF V3 was developed based on the publication by Mann et al. (Mann et al., 2017)

The dosage form was initially exposed to 250 mL of FaSSGF Level III and samples were removed at 5, 10, 15, 20, 30 min and treated as described in Section 2.3. After the withdrawal of the last sample, 6.8 mL of sodium hydroxide 1 M and immediately thereafter 250 mL of FaSSIF V3 concentrate pH=6.7 (double concentration of all the constituents, apart from sodium hydroxide) were added to the vessel. Instead of increasing the pH of the intestinal medium concentrate to counterbalance the acidic pH of the stomach medium as described in the original study, (Mann et al., 2017) sodium hydroxide was added first, but almost simultaneously, with the FaSSIF V3 concentrate. This was done to avoid using a very high pH in the FaSSIF V3 concentrate. After addition of sodium hydroxide and concentrated FaSSIF V3, further samples were removed at 32.5, 35, 40, 45, 50, 60 and 90 min. The two-stage experiments were performed using calibrated USP II (paddle) apparatus (Erweka DT 80, Heusenstamm, Germany) at 37 ± 0.5 °C and the samples were analyzed by HPLC-UV (see Section 2.5). All experiments were performed at least in triplicate ($n \geq 3$) and the final pH in the vessel was recorded.

2.5. Quantitative analysis of samples

Samples obtained from solubility and dissolution experiments were

first filtered through a 0.45 μm PTFE filter (ReZist™ 30 syringe filter or Uniprep™; Whatman®, Piscataway, NJ, USA) and subsequently, after appropriate dilution with mobile phase, they were analyzed by HPLC-UV (Hitachi Chromaster; Hitachi Ltd., Tokyo, Japan or Spectra System HPLC, ThermoQuest Inc., San Jose, USA). A BDS Hypersil C18, 5 μm, 150 x 4.6 mm (Thermo Scientific) analytical column combined with a pre-column (BDS Hypersil C-18, 3 μm, 10 x 4 mm) was used. The mobile phase consisted of 20 mM NaH₂PO₄ buffer adjusted to pH=3.0 and acetonitrile (60:40% v/v). The detection wavelength was set at 273 nm, the flow rate at 1.2 mL/min and the injection volume at 20 μL. Using this method, the retention time was approximately 7.3 min. The limit of detection (LOD) and quantification (LOQ) were 0.03 and 0.1 μg/mL, respectively.

2.6. Model-based analysis of *in vitro* solubility data

An experimental estimate of the naproxen pK_a was obtained by fitting the Henderson-Hasselbalch equation (Eq. (1)) to the mean aqueous equilibrium solubility (S_i) values using the SIVA Toolkit® ($n = 6$; all aqueous buffers). As intrinsic solubility (S_0), the lowest reported value in buffers was used. The pK_a was then compared with values available in the literature to confirm the validity of the aqueous solubility parameter estimates.

$$S_i = S_0 \cdot (10^{pH-pK_a}) \quad (1)$$

The impact of bile salt concentration ([BS]) and subsequent formation of micelles on the solubility of naproxen was investigated. This was done by mechanistically modeling the mean solubility values in fasted state biorelevant media ($n = 3$), accounting also for the relative proportions of naproxen solubilized in the aqueous *versus* the micelle phases, using the total solubility ($S_{(BS)Tot}$) equation (Eq. (2)) in SIVA Toolkit® version 3.0 (SIVA; Certara, Simcyp Division; Sheffield, UK). Estimates of the logarithm of the micelle-water partition coefficient for the neutral ($K_{m:w, unionized}$) and ionized drug ($K_{m:w, ionized}$) were obtained to quantify the micelle-mediated solubility.

$$S_{(BS)Tot} = \left([BS] \cdot \frac{S_0}{C_{H2O}} \cdot K_{m:w, unionized} + S_0 \right) + \left([BS] \cdot \frac{S_i}{C_{H2O}} \cdot K_{m:w, ionized} + S_i \right) \quad (2)$$

Where C_{H_2O} stands for the concentration of water.

Estimation of the relevant parameters was performed using the Nelder-Mead algorithm and weighting by the reciprocal of the predicted values was chosen. After model verification, all obtained estimates were used as input parameters for the development of the physiologically-based pharmacokinetic model (PBPK) model (see Section 2.9)

2.7. Model-based analysis of *in vitro* dissolution data

Once confidence in the estimation of solubility-related parameters was established, further model-based analysis of the *in vitro* dissolution data obtained from both the one and two-stage tests was performed within the serial dilution module of the SIVA Toolkit® (SIVA 3.0). The dissolution rate of spherical particles under sink and non-sink conditions within SIVA is described by an extension of the diffusion layer model (DLM) developed by Wang and Flanagan. (Eq. (3)) (Wang and Flanagan, 2002, 1999)

$$DR(t) = -N \cdot S_{DLM} \frac{D_{eff}}{h_{eff}(t)} \cdot 4\pi \cdot \alpha(t) \cdot (\alpha(t) + h_{eff}(t)) \cdot (S_{surface}(t) - C_{bulk}(t)) \quad (3)$$

where $DR(t)$ is the dissolution rate at time t ; N is the number of particles in a given particle size bin; S_{DLM} is a lumped, empirical, correction scalar without regard to the mechanistic origin of the required correction to the DLM. The estimated S_{DLM} values obtained with SIVA can be applied to the Simcyp PBPK simulator to reflect differences between media or formulations; D_{eff} is the effective diffusion coefficient; $h_{eff}(t)$ and $\alpha(t)$ represent the thickness of the hydrodynamic boundary layer and the particle radius at time t respectively; $S_{surface}(t)$ corresponds to the saturation solubility at the particle surface (which may be different to the bulk fluid solubility as discussed below); and $C_{bulk}(t)$ is the concentration of dissolved drug in bulk solution at time t .

The $h_{eff}(t)$ was calculated by the fluid dynamics sub-model, which enables the hydrodynamic conditions to be described according to local conditions and stirring rate. Fluid dynamics-based $h_{eff}(t)$ is the recommended option for describing the hydrodynamics, as it permits a more rational translation of estimated parameters such as the S_{DLM} to *in vivo* conditions, in which the hydrodynamics are usually quite different to *in vitro* experiments.

The local pH at the particle surface of ionisable drugs can significantly affect the $S_{surface}$ and consequently the dissolution rate (Mooney et al., 1981; Mooney et al., 1981a, 1981b; Ozturk et al., 1988; Serajuddin and Jarowski, 1985; Sheng et al., 2009). Since in the *in vitro* dissolution media have a somewhat higher buffer capacity than the intestinal fluids, the self-buffering effect at the solid surface can be underestimated. For this reason, the surface pH was calculated and directly input into SIVA. The calculation of the surface pH was based on the model proposed by Mooney et al. (K.G. Mooney et al., 1981a), which assumes that dissolution is the result of both chemical reaction between the conjugate base of the buffer species and the hydrogen cations released from the dissolving drug (in this case naproxen free acid (NPX-H)) the liquid-solid interface and the diffusion of the dissolved particles to the bulk. This model is very similar to the quasi-equilibrium model published by Ozturk et al. (Ozturk et al., 1988), a derivation of which is implemented in SIVA as the default option for surface pH calculations.

By fitting the DLM model to the observed dissolution data, accurate S_{DLM} estimates for each dissolution and two-stage test were obtained. In the case of two-stage testing, the gastric and intestinal profiles were treated separately. Under fasted state intestinal conditions, naproxen is freely soluble and therefore *in vitro* dissolution is not expected to be solubility limited. In that case, disintegration of the solid dosage form in the intestinal dissolution medium might be the rate-limiting step for the *in vitro* dissolution rate, especially in single dissolution experiments where the dosage form is directly exposed to the intestinal medium

without any pre-treatment with gastric medium to account for disintegration in the stomach. In order to distinguish and model the relative impact of disintegration on the overall dissolution, the first-order disintegration option was activated in SIVA and used to obtain estimates of the first-order disintegration rate constant (k_d) for these experiments. In the case of intestinal dissolution profiles generated after two-stage testing, the first-order disintegration option was deactivated since disintegration in the stomach had been already accounted for by the dissolution in the gastric medium. For dissolution experiments of the pure drug, the disintegration time was assumed to be negligible.

Estimation of the relevant parameters was performed using the Nelder-Mead algorithm and equal weighting was applied. The various estimated S_{DLM} and k_d values were implemented in the Simcyp® Simulator (V18.1; Certara, Sheffield, UK) to simulate various *in vivo* dissolution scenarios for the formulations under study and to generate *in vitro-in vivo* extrapolation relationships. These are necessary to predict the formulation or pure drug *in vivo* performance using PBPK modeling.

2.8. *In vivo* studies

Seven clinical trials published in the open literature were used in support of the development and verification of the PBPK model for naproxen. Six studies were performed after oral administration of single-dose of naproxen or its sodium salt at different dose levels in the fasted state. Data after intravenous administration were obtained from Runkel et al. (Runkel et al., 1973, 1972a, 1972b)

The results of bioavailability studies for the Naprosyn® formulation were published by Charles and Mogg (Charles and Mogg, 1994) and by Zhou et al. (Zhou et al., 1998) In the study by Charles and Mogg, sixteen Caucasian (12.5% females) healthy subjects with mean (SD) age of 22.1 (4.4) years old received one 500 mg Naprosyn® tablet with 100 mL water at 8:00 a.m. after an overnight fast. All individuals were within 20% of their ideal body weight for height and gender with a mean (SD) weight and height of 67.6 (8.3) kg and 175.7 (9.0) cm, respectively. In the study by Zhou et al., ten Chinese healthy male volunteers (with age and body weight ranging from 19–38 years and 51–74 kg respectively) received two 250 mg Naprosyn® tablets with 200 mL water at 8 a.m. after an overnight fast.

Regarding the Anaprox® formulation, a bioavailability study by Haberer et al. (Haberer et al., 2010) and a bioequivalence (BE) study by Setiawati et al. (Setiawati et al., 2009) have been reported in the literature. Using the same study design (two-treatments protocol), Haberer et al. tested the bioavailability of a tablet of 550 mg Anaprox® as well as of 500 mg of naproxen sodium, with the intention of incorporating this dose in a fixed dose combination tablet with sumatriptan. A tablet of 550 mg Anaprox® (treatment A) and of 500 mg of naproxen sodium (treatment B) were administered after an overnight fast to 8 and 16 healthy non-smoker volunteers, respectively. The proportion of females in the study was 63% and subjects had a mean (SD) age of 44.3 (8.5) years and a mean body weight of 71.44 (12.3) kg. In the study by Setiawati et al., twenty-six healthy volunteers (15% females), aged 19 to 46 years and with body mass index (BMI) 18–23, were administered a tablet containing 550 mg naproxen sodium with 200 mL of water in a sitting position at 07:00 a.m. after an overnight fast.

To investigate the bioavailability of naproxen free acid, Rao et al. administered 500 mg of pure drug powder filled in hard capsules together with a glass of water to twelve Indian healthy male volunteers, aged between 18 and 22 years, who had fasted overnight. (Rao et al., 1993) In all studies, no concomitant administration of any other drugs was permitted for at least 1 week before the study and food was withheld until 3 h post-dose.

All available demographic data from the aforementioned clinical studies were used to simulate the clinical trials and are summarized in Table 2. Since no pharmacokinetic differences due to race have been

Table 2Mean (SD) demographic data of *in vivo* studies used for the development and verification of the PBPK model. (HV = healthy volunteers).

Reference	Formulation & Dose	N° of Subjects	Female Ratio	Ethnicity	Population	Age (y)	BW Range (kg)	BH Range (cm)
Intravenous								
(Runkel et al., 1973, 1972a, 1972b)	93 mg with 30 μ C tritium label in 100 mL phosphate buffer	3	0.33	Caucasian	HV	–	49.9–86.3	–
Oral								
(Charles and Mogg, 1994)	Naprosyn® 500 mg	16	0.125	Caucasian	HV	22.1 (4.4)	67.6 (8.3)	175.7 (9.0)
(Zhou et al., 1998)	Naprosyn® 2 x 250 mg	10	0	Chinese	HV	19–38	51–74	–
Haberer et al. (a)(Haberer et al., 2010)	Anaprox® 550 mg	8	0.63	Caucasian	HV	44.3 (8.5)	71.44 (12.3)	–
(Setiawati et al., 2009)	Anaprox® 550 mg	26	0.15	Caucasian	HV	19–46	–	–
(Rao et al., 1993)	IR Naproxen 500 mg	12	0	Indian	HV	18–22	46–62.5	160–182.5
Haberer et al. (b)(Haberer et al., 2010)	IR Naproxen-Na 500 mg	16	0.63	Caucasian	HV	44.3 (8.5)	71.44 (12.3)	–

identified to date, all individuals were treated the same in terms of ethnicity for modeling purposes.

2.9. Development of the middle-out PBPK model and selection of *in silico* input parameters

PBPK modeling and simulations were performed using the Simcyp® Simulator (V18.1; Certara, Sheffield, UK). The naproxen PBPK model was developed by implementing a stepwise sequential modeling strategy, in line with previously published literature and the regulatory guidelines. (European Medicines Agency (EMA), 2018b; Ke et al., 2016; Kuepfer et al., 2016; Shebley et al., 2018; U.S-FDA Center for Drug Evaluation and Research CDER, 2018b; Zhao et al., 2012) Initially, an intravenous (IV) model was set up and, after optimizing the distribution/elimination parameters, it was adapted to mechanistically describe oral absorption. The compound file was also informed with physicochemical parameters including molecular weight (MW), octanol:water partition coefficient ($\log P_{o:w}$), fraction unbound in plasma (f_u) and blood to plasma ratio (B:P) obtained from the literature. (Bergström et al., 2014; Brown et al., 2007; Davies and Anderson, 1997; Lin et al., 1987; Paixão et al., 2012; Pérez et al., 2004; Zhao et al., 2001)

2.9.1. Intravenous (IV) model

Since the volume of distribution reported in the literature for naproxen usually lies between 0.05–0.2 L/kg (similar to the plasma water volume), (Awni et al., 1995; Franssen et al., 1986; Gøtzsche et al., 1988; Niazi et al., 1996; Upton et al., 1984; Van den Ouweland et al., 1988; Vree et al., 1993) the minimal PBPK (mPBPK) with a single adjusting compartment (SAC) was chosen as the distribution model. The mPBPK is a “lumped” PBPK model in which the SAC represents all tissues excluding liver and portal vein. Use of the SAC requires prior fitting to observed clinical data using the Simcyp® parameter estimation (PE) module. Implementing a “middle-out” strategy, the post-absorptive variables, *i.e.* the parameter values for volume of distribution at steady-state (V_{ss}), apparent SAC volume (V_{sac}), inter-compartmental (Q_{sac}) and *in vivo* IV clearance (CL_{IV}) were estimated using the PE module after simultaneous fitting of the mPBPK model to the observed intravenous data. (Runkel et al., 1973, 1972a, 1972b) The estimation was weighted by the number of individuals in the reported study and the resulting parameters were then compared with values reported in the literature.

2.9.2. P.O. (oral) model

For mechanistic absorption modeling the advanced dissolution absorption and metabolism (ADAM) model, (Jamei et al., 2009; S. Darwich et al., 2010) in which the gastrointestinal tract (GIT) is divided into 9 anatomically distinct segments starting from the stomach, through small the intestine to the colon, was used. It was assumed that no drug absorption occurred in the stomach. The effective permeability ($P_{eff,man}$) value in humans was obtained from the literature,

(Lennernas et al., 1995) whereas for S_0 , $\log K_{m:w, unionized}$, $\log K_{m:w, ionized}$ the estimates from model-based analysis of the *in vitro* solubility data were implemented (see Section 2.7). Default settings of the software for luminal blood flow, fluid volume, bile salt content, segmental pH, metabolic activity and small intestinal residence time were used. The mean gastric emptying time (GET) in the fasted state was set to 0.25 h (matching the built-in ‘segregated transit time’ model value instead of the default value of 0.4 h used in the ‘global’ transit time model), as suggested by human clinical data and several authors. (Cristofolletti et al., 2016; Hens et al., 2014; Paixão et al., 2018; Psachoulis et al., 2011) All relevant input parameters for the development of the PBPK models and simulations are summarized in Table 3.

2.10. Verification of PBPK model and clinical trial simulations

The performance of the developed PBPK model was verified by

Table 3

Input parameters for naproxen PBPK model development and simulations.

Parameters	Value	Reference/ Comments
Physicochemical & Blood Binding		
MW (g/mol)	230.3	PubChem
$\log P_{o:w}$	3.2	(Bergström et al., 2014; Pérez et al., 2004; Zhao et al., 2001)
pKa	4.43	estimated from <i>in vitro</i> data (see Section 3.2)
Blood/ Plasma ratio	0.55	(Brown et al., 2007)
Fraction unbound in plasma	0.01	(Davies and Anderson, 1997; Paixão et al., 2012)
Absorption		
Model	ADAM	
$P_{eff, human}$ ($\times 10^{-4}$ cm/s)	8.5	(Lennernas et al., 1995)
Formulation type	Immediate Release	
<i>In vivo</i> dissolution	see Table 7, Table 8	estimated DLM scalars from <i>in vitro</i> data (see Section 3.3.2) <i>in vitro</i> data (see Section 3.1)
S_0 (mg/mL)	0.0294	Default value within ADAM
Particle density (g/mL)	1.20	Assumed as data not available
Particle size distribution	Monodispersed	Default value within ADAM
Particle radius (μ m)	10	estimated from <i>in vitro</i> data (see Section 3.2)
$\log K_{m:w}$ neutral	5.37	estimated from <i>in vitro</i> data (see Section 3.2)
$\log K_{m:w}$ ion	4.00	estimated from <i>in vitro</i> data (see Section 3.2)
Distribution		
Model	Minimal PBPK with SAC	
V_{ss} (L/kg)	0.15	PE module
V_{sac} (L/kg)	0.075	PE module
Q_{sac} (L/h)	1.00	PE module
Elimination		
CL_{iv} (L/h)	0.40	PE module
CL_{renal} (L/h)	0.02	(Paixão et al., 2012)

simulation of several clinical studies after oral administration and by comparison with the mean observed pharmacokinetic profiles already available in the literature. (Charles and Mogg, 1994; Haberer et al., 2010; Rao et al., 1993; Setiawati et al., 2009; Zhou et al., 1998) Virtual populations were selected to closely match the enrolled individuals in the respective *in vivo* clinical trials with respect to sample size, ethnicity, gender ratio, and age and weight range. Reported volumes of concomitant liquid intake, dosage form type and sampling schedule were also included in the study design.

Using an *in vitro-in vivo* extrapolation (IVIVE) approach, the various DLM scalar estimates, (see Sections 2.7, 3.5) obtained by model-based analysis of the *in vitro* dissolution data with the diffusion layer model were input to best capture different *in vivo* dissolution scenarios. Further, to investigate the effect of *in vivo* dissolution of multiple formulations and under various conditions on the overall *in vivo* performance, the same DLM scalar estimates from *in vitro* dissolution data for each case were implemented to simulate the aforementioned clinical studies. Every *in vivo* dissolution scenario was evaluated by simulation of 10 trials, each with 10 subjects ($\Sigma = 100$). All virtual clinical trials were matched in terms of demographic data (e.g. gender ratio, age & weight range) as closely as possible to the reported studies.

2.11. Parameter sensitivity analysis (PSA)

Once confidence in the PBPK model performance was established, parameter sensitivity analysis (PSA) was conducted to identify the absorption rate limiting steps and their impact on *in vivo* performance (e.g., C_{max} , T_{max} , AUC). Variation of one or two parameters at a time over a physiologically realistic range of values was applied for gastric emptying time (GET) and the DLM scalar.

2.12. Virtual bioequivalence (VBE) trials

The virtual bioequivalence (VBE) trials were designed as fully replicated, two-sequence, two-treatment, two-period, crossover studies. In virtual BE studies between the hypothetical test and reference formulations, PK profiles for a total of 120 healthy adult volunteers (12 subjects in each of 10 trials) for each treatment were generated. The existing default coefficients of variation (%CV) - i.e., between subject (BS) variability of the physiological parameters stored in the Simcyp® simulator database for the North European Caucasian healthy adult volunteers' population were applied for each parameter. As an integral part of within-subject (WS) variability, inter-occasion variability (IOV) significantly contributes to the overall population variability and therefore it should be accounted for by the PBPK models. To model IOV, a CV of 30% was set, according to the literature and unpublished data from C. Reppas. (Fruehauf et al., 2007; Grimm et al., 2018; Lartigue et al., 1994; Petring and Flachs, 1990) IOV was added through the VBE module (V1.0) of Simcyp® simulator to the mean GET, pH of fasted stomach, pH and bile salts concentration of fasted duodenum, jejunum I and II segments and mechanistically propagated in the simulations. The IOV was intentionally set to the somewhat exaggerated value of 30% for all the relevant parameters to further challenge the establishment of bioequivalence. In each trial, a pre-specified number of randomly simulated individuals ($n = 12$) were generated for each formulation (reference and test). The relevant PK metrics (C_{max} , T_{max} , AUC) for each subject were calculated. The VBE trials were interpreted as crossover studies and average BE (ABE) was assessed using Phoenix® WinNonlin (v8.1; Certara; Princeton, NJ, USA) for each relevant PK metric. In a best-and worst-case scenario the hypothetical reference and test formulations were assumed to have *in vivo* dissolution in the virtual individuals corresponding to the highest and lowest estimated DLM scalar value, respectively, resulting from the model-based analysis of the *in vitro* dissolution data.

2.13. Data analysis and model diagnostics

The solubility and dissolution data are presented as the arithmetic mean with standard deviations. Model-based analysis of the *in vitro* data in SIVA® Toolkit was performed with either the Nelder Mead or the hybrid algorithm (genetic algorithm coupled to Nelder Mead) with a 5th order Runge-Kutta or Livermore solver. Different weighting schemes were tested and the goodness of fit was assessed by the Akaike (AIC, AICc) and Bayesian (BIC) information criteria as well as the coefficient of determination (R squared). All PK profiles obtained from the literature were digitalized with the WebPlotDigitizer (version 4.1; PLOTCON; Oakland, USA). The estimation of the post-absorptive parameters within the PE module of the Simcyp® Simulator was performed with the Maximum Likelihood estimation method. The prediction accuracy of the simulated plasma profiles was evaluated with the average fold error (AFE) and absolute average fold error (AAFE) (see Eqs. (4),5).

$$AFE = 10^{\frac{1}{n} \sum \log \left(\frac{pred_t}{obs_t} \right)} \quad (4)$$

$$AAFE = 10^{\frac{1}{n} \sum \left| \log \left(\frac{pred_t}{obs_t} \right) \right|} \quad (5)$$

where n is the number of time points at which the concentration was determined and $pred_t$, obs_t are the predicted and observed concentrations at a given time point t respectively. *AFE* deviation from unity is an indication of over- ($AFE > 1$) or under-prediction ($AFE < 1$) of the observed data, whereas *AAFE* is a measure of the absolute error from the true value (or bias of the simulated profile). An $AAFE \leq 2$ is considered to be a successful prediction. (Obach et al., 1997; Poulin and Theil, 2009)

Statistical analysis (including 95% CI) and VBE trials were performed with Simcyp® (V18.1; Certara, Sheffield, UK) and Phoenix® WinNonlin (v8.1; Certara; Princeton, NJ, USA). Data post-processing and plotting were performed with MATLAB® 2018a (Mathworks Inc.; Natick, MA, USA) and R® (version 3.5.1).

3. Results

3.1. *In vitro* solubility

3.1.1. Aqueous buffers

Table 4 summarizes the equilibrium solubility values in various aqueous media of different pH. In the case of the free acid, the final pH_{bulk} differed significantly from the initial pH values due to the self-buffering effect. This behavior was not observed for the sodium salt, where the pH difference was equal or less to 0.1 pH unit. The higher solubility of the sodium salt compared to the free acid, especially in the intestinal pH media, is attributed to the difference in the final pH measured, keeping in mind that in this pH range the solubility increases exponentially with pH increase. Since naproxen is a weakly acidic compound, its pH-solubility profile is described by two regions: a) pH

Table 4

Mean (\pm SD) equilibrium solubility in aqueous media at 37 °C for 24 h (Uniprep® method).

Aqueous medium	Naproxen		Naproxen Sodium	
	pH _{final}	Solubility (µg/mL)	pH _{final}	Solubility (µg/mL)
Water	4.5	70.4 (1.2)	6.7	358.4 (18.1)
HCl acid (pH=1.2)	1.3	29.4 (6.4)	1.2	28.4 (0.72)
Acetate buffer (pH=4.5)	4.5	84.8 (4.2)	4.6	103.1 (3.6)
Level I FeSSIF V1 (pH=5.0)	5.0	175.4 (0.0202)	5.1	241.6 (5.2)
Phosphate buffer (pH=6.5)	6.2	1627.6 (31.5)	6.6	2363.4 (31.5)
Phosphate buffer (pH=6.8)	6.5	3619.1 (112.6)	6.9	4957 (119)
Phosphate buffer (pH=7.4)	6.8	5981.6 (28.0)	7.5	10,128 (674)

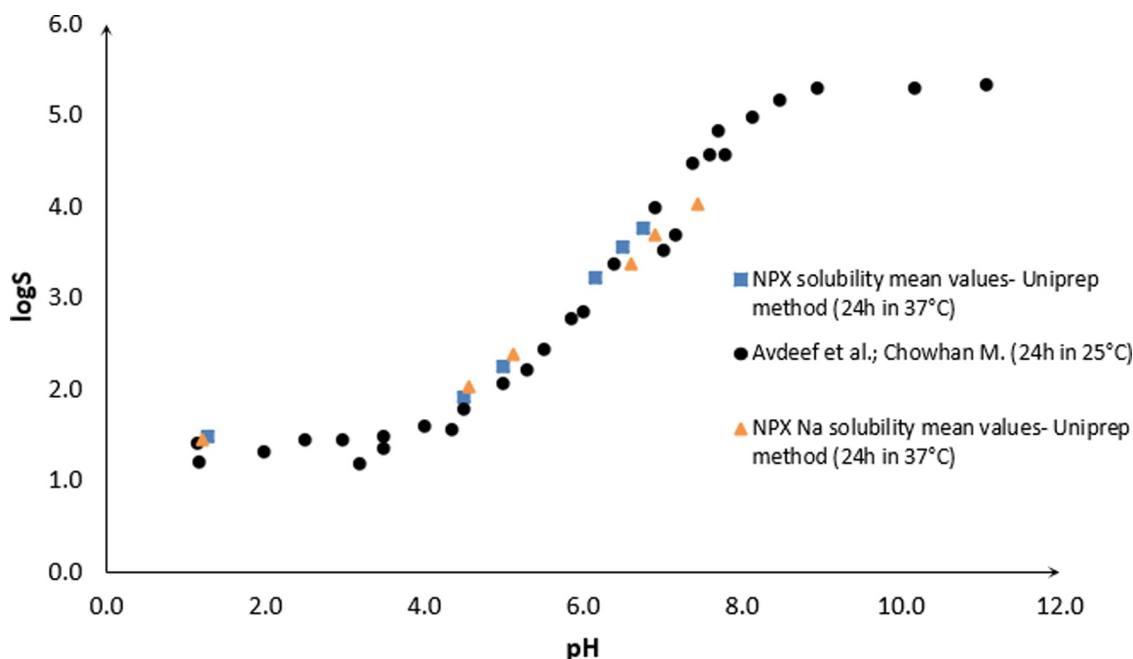


Fig. 1. Naproxen (squares) and naproxen sodium (triangles) experimental mean equilibrium solubility values (24 h at 37 °C) plotted against respective literature values (24 h at 25 °C) in a pH-solubility profile. The *in vitro* solubility experiments were performed with the Uniprep® method described in Section 2.2. The experimental results are in agreement with the literature values (24 h at 25 °C). The literature values were obtained from Avdeef et al. (Ref. 75); Chowhan et al. (Ref. 77).

< pH_{max} , where the excess solid phase in equilibrium with the saturated solution consists of the unionized form and b) $pH > pH_{max}$, where the equilibrium species are exclusively in the ionized form. (Avdeef, 2007) Hence, unless self-association of solute molecules occurs, identical pH-solubility profiles at equilibrium are expected regardless of the starting material (free acid or salt), as shown in Fig. 1. The experimental values were plotted as a pH-solubility profile and compared to values reported in the literature, showing excellent agreement (Fig. 1). (Avdeef, 2007; Avdeef and Berger, 2000; Chowhan, 1978)

3.1.2. Biorelevant media

The solubility was additionally investigated in selected Level II fasted and fed state biorelevant media (see Table 5). (Markopoulos et al., 2015) Similar to the solubility of the free acid in phosphate buffers, a considerable decrease in the final pH_{bulk} was observed in fasted state biorelevant media. In fact, the reduction is even more pronounced in the fasted state biorelevant media due to their lower buffer capacity (5.6 mmol/L/ ΔpH in FaSSIF V3 versus 18.5 mmol/L/ ΔpH in European Pharmacopoeia phosphate buffers). (Fuchs et al., 2015) Comparison of solubilities in compendial with those in biorelevant media shows that micelle-mediated solubilization has a substantial impact on the overall solubility of naproxen. Particularly in FaSSIF V1 Level II, the solubility of both free acid and sodium salt was

increased by 25.8% and 51.8%, respectively, when compared to phosphate buffer ($pH=6.5$). Likewise, in media simulating the fed state, such as FeSSIF V1 Level II, a 2.4-fold increase in the solubility of the free acid and a 2.1-fold increase for the salt form were observed, in comparison to the respective medium without surfactants.

3.2. Modeling of *in vitro* solubility

Table 6 summarizes the parameter estimates (95% CI) obtained by model-based analysis of the *in vitro* solubility data in compendial and biorelevant media, as described in Section 2.6. The pK_a was determined to be 4.43, which agrees with values reported in the literature (4.15–4.5). (Avdeef, 2007; Chowhan, 1978; Davies and Anderson, 1997; McNamara and Amidon, 1986; Sheng et al., 2009) By estimating the micelle-water partition coefficients for both neutral and ionized species using the biorelevant solubilities, we were able to quantify the effect of physiologically relevant surfactants on the overall solubility of naproxen. These values were utilized within the Simcyp® Simulator to simulate the luminal conditions and the *in vivo* dissolution behavior, accounting at the same time for any inter-subject variability regarding bile salt-mediated solubilization in the virtual population. Therefore, implementation of $\log K_{m:w}$ neutral and ion in the PBPK model allowed for mechanistic prediction of the *in vivo* luminal dissolution, which would not be possible if only mean solubility values had

Table 5

Mean (\pm SD) equilibrium solubility in fasted and fed state biorelevant media at 37 °C for 24 h (Uniprep® method).

Biorelevant medium	Naproxen pH_{final}	Solubility ($\mu g/mL$)	Naproxen Sodium pH_{final}	Solubility ($\mu g/mL$)
<i>Fasted state</i>				
Level III FaSSGF ($pH=1.6$)	1.6	33.4 (1.1)	1.6	31.8 (0.92)
Level II FaSSIF V1 ($pH=6.5$)	5.9	2046 (150)	6.5	3587 (179)
Level II FaSSIF V3 ($pH=6.7$)	5.8	1624 (153)	6.7	3469 (187)
<i>Fed state</i>				
Level II FeSSGF _{middle} ($pH=5.0$)	4.9	352.6 (21.4)	5.1	575.2 (19.3)
Level II FeSSIF V1 ($pH=5.0$)	5.0	424.7 (26.6)	5.0	519.9 (18.9)
Level II FeSSIF V2 ($pH=5.8$)	5.8	890.0 (56.7)	5.8	799.5 (177)

Table 6

Parameter estimates (95% CI) resulting from the model-based analysis of *in vitro* solubility data in aqueous as well as biorelevant media. The pKa was estimated from the aqueous solubility values, whereas for the micelle-water partition coefficients ($\log K_{m:w}$ neutral, ion) estimation, biorelevant solubilities were used. The accuracy of the predictions was evaluated with the R squared.

	pKa	$\log K_{m:w}$ neutral	$\log K_{m:w}$ ion
Estimate (95% CI)	4.43 (4.42–4.44)	5.37 (5.34–5.40)	4.00 (3.98–4.02)
R ²	0.9990	0.9999	

been used.

3.3. *In vitro* dissolution tests

3.3.1. Active pharmaceutical ingredient (API) powder

Mean percentage dissolved (\pm SD) over time in compendial and fasted state biorelevant media for the pure API of naproxen and its sodium salt are presented in Fig. 2 and Fig. 3, respectively. All dissolution experiments were performed as described in Section 2.3.

For the free acid, dissolution in FaSSIF V3 Level II and in Ph. Eur. phosphate buffer pH=6.8 was very rapid (>85% within 5 min in FaSSIF V3) and rapid (>85% within 30 min in phosphate buffer). On the other hand, the dissolution in FaSSIF V3 Level I (*i.e.* without bile components) was much slower with 85% dissolved reached only after 60 min. The observed difference in *in vitro* dissolution behavior is attributed to differences in buffer capacity (FaSSIF V3 Level I and II vs. phosphate buffer) and solubilization capacity (FaSSIF V3 Level II vs. Level I) of the tested media, whereas the difference of 0.1 pH units between the initial pH of Ph. Eur. phosphate buffer pH=6.8 and FaSSIF V3 is assumed to have a negligible effect.

Especially since dissolution was under non-sink conditions in this series of experiments, the dissolution rate in FaSSIF V3 Level I was significantly slower, due to its low buffer capacity (5.6 mmol/L/ Δ pH), than in the compendial phosphate buffer (13.5 vs. 50 mM phosphate buffer). At higher total phosphate buffer concentration, *i.e.* in the compendial medium, the bulk (pH_{bulk}) rather than the surface pH (pH_0) drives solubility and dissolution. By contrast, in the low buffer capacity FaSSIF V3 Level I medium the surface pH seems to control the dissolution rate and as a result the final pH is significantly altered (5.95 in FaSSIF V3 Level I vs. 6.62 in Ph. Eur. phosphate buffer). The effect of buffer capacity on the overall dissolution behavior becomes much less

prominent when bile salts are added to the medium, as shown in Fig. 2. Furthermore, it is evident that the addition of the bile salt components in FaSSIF V3 Level II markedly enhances the dissolution rate. Although the main effect is likely through solubilization, improvements in wetting may have also contributed to the higher dissolution rate in the Level II medium.

For the sodium salt, these trends were not observed and dissolution was almost instantaneous (85% dissolved by the first sampling time at 2.5 min) in all tested media. This is attributed to the higher solubility as well as higher surface pH generated by the sodium salt of naproxen.

3.3.2. Formulations

The dissolution profiles in FaSSIF V3 Levels I and II along with the results for the “intestinal” part of the two-stage testing are presented for Naprosyn® and Anaprox® in Fig. 4 and Fig. 5, respectively. In all cases, and for both formulations, dissolution was very rapid under conditions simulating the upper small intestine, with 85% dissolved in less than 15 min. Interestingly, a mismatch between the dissolution results of the APIs and dosage forms was observed. For instance, dissolution of the free acid form of the API was much faster from the dosage form (Naprosyn®) than from the pure API in FaSSIF V3 Level I. However, the dissolution of naproxen free acid from Naprosyn® in FaSSIF V3 Level II was slightly slower than from the pure API. Furthermore, although dissolution of sodium salt API was virtually instantaneous in all media (85% dissolved within 2.5 min), 85% dissolution was reached only after 15 min during release from Anaprox®.

These findings suggested that the dissolution of the tablets under intestinal conditions was delayed due to slow disintegration, especially in the case of the sodium salt formulation. In order to account for disintegration in the stomach prior to exposure to the intestinal media, two-stage dissolution tests were subsequently performed, as described in Section 2.4. Since the amount dissolved under gastric conditions was less than 2% in all cases (see Fig. 6), only the “intestinal” profiles of the 2-stage tests are plotted and directly compared with the conventional dissolution profiles (Fig. 4 and Fig. 5). Pre-treatment in gastric media accelerated the dissolution rate (85% dissolved reached 5 min earlier) of the API from both the Naprosyn® formulation of the free acid (Fig. 4) and the Anaprox® formulation of the sodium salt form (Fig. 5). Although in all cases dissolution would be considered very rapid, the disintegration effect was more prominent for Anaprox®, as shown also in Fig. 6. A model-based analysis of the anticipated *in vitro* dissolution differences is presented in Section 3.4.

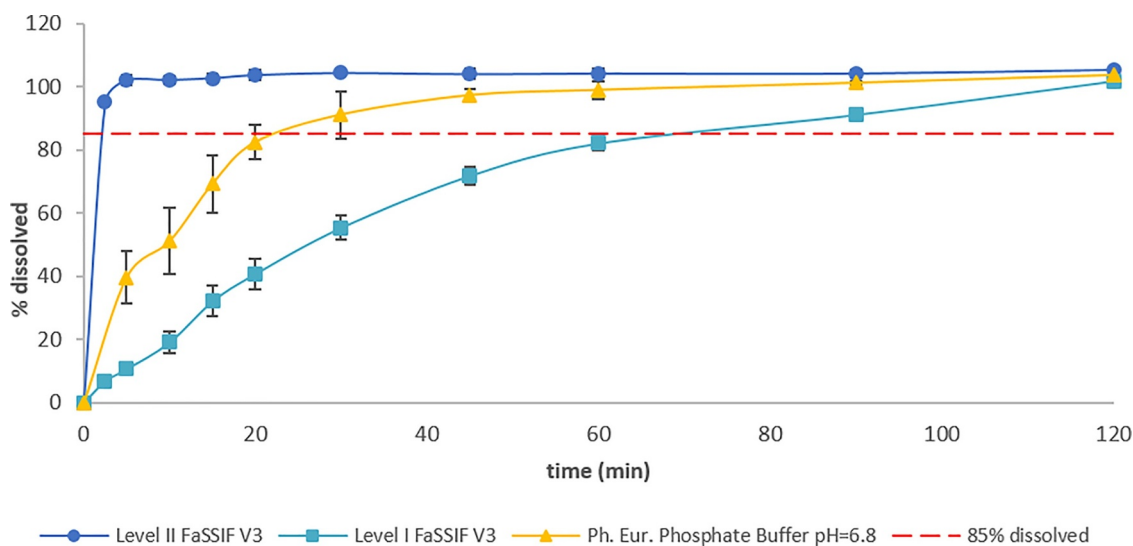


Fig. 2. *In vitro* dissolution (mean \pm SD) of 500 mg naproxen free acid API powder in Ph. Eur. phosphate buffer (pH=6.8), Level I and II FaSSIF V3. USP paddle apparatus at 75 rpm and 500 mL of dissolution medium at 37 °C were used in all experiments. The experiments were performed in triplicate. Horizontal dashed red line represents 85% dissolved. Most standard deviation bars lie within the symbols.

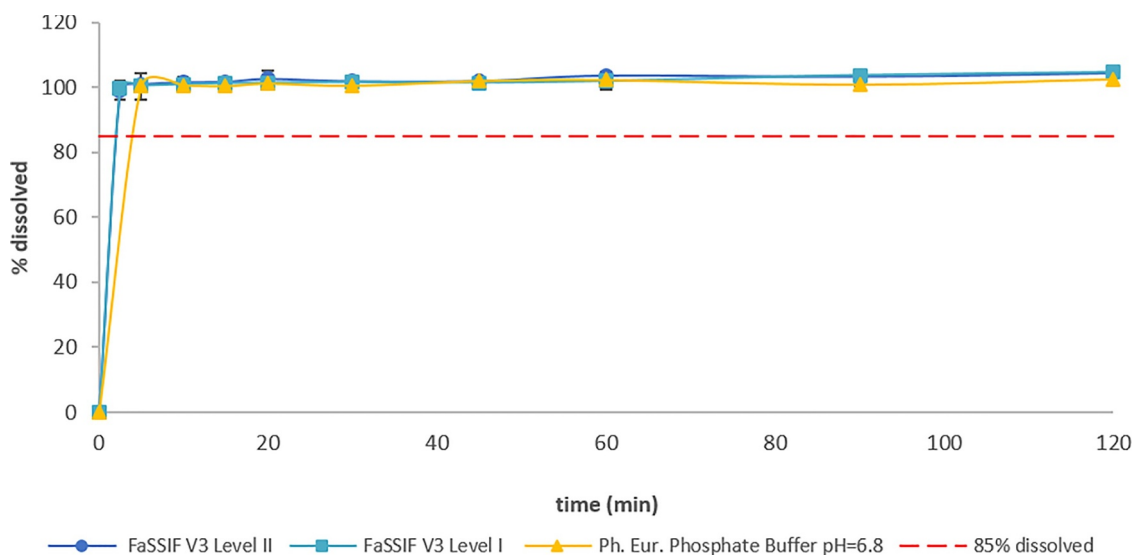


Fig. 3. *In vitro* dissolution (mean \pm SD) of 550 mg naproxen sodium API powder in Ph. Eur. phosphate buffer (pH=6.8), FaSSIF V3 Levels I and II. USP paddle apparatus at 75 rpm and 500 mL of dissolution medium at 37 °C were used in all experiments. The experiments were performed in triplicate. Horizontal dashed red line represents 85% dissolved. Most standard deviation bars lie within the symbols.

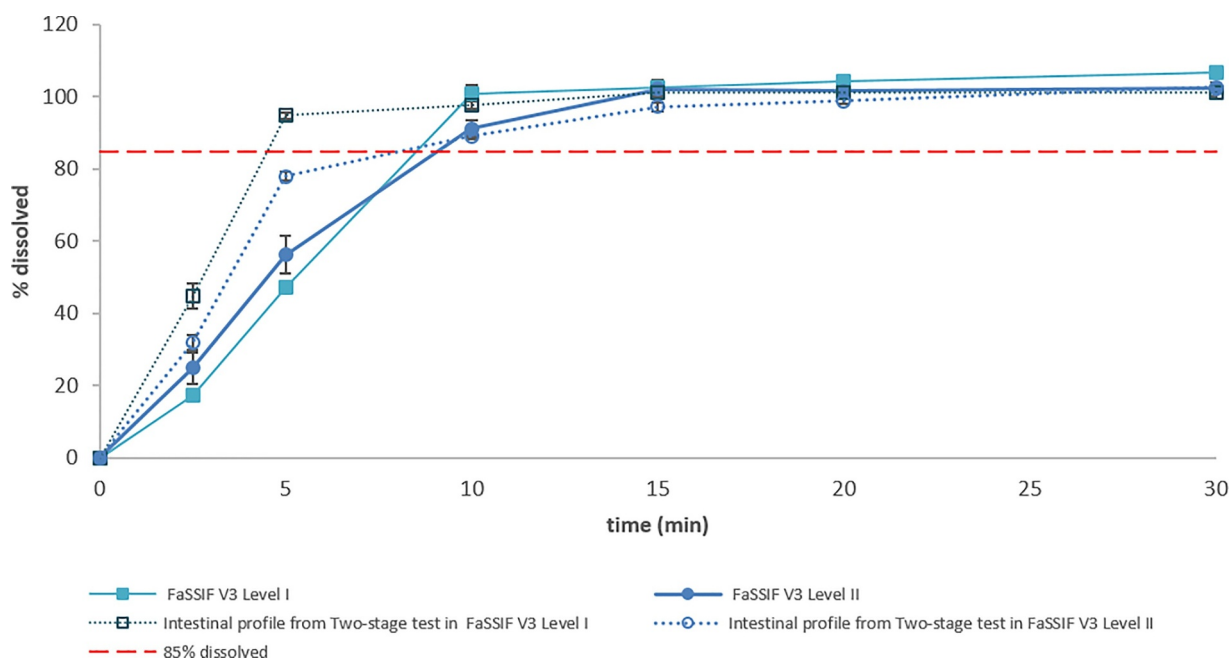


Fig. 4. *In vitro* dissolution (mean \pm SD) of Naprosyn® 500 mg in FaSSIF V3 Levels I and II (solid lines, filled squares and circles respectively). The intestinal profiles in FaSSIF V3 Levels I and II (after the pre-treatment with FaSSGF Levels I and III respectively) during two-stage test are also depicted (dotted lines, empty squares and circles, respectively). USP paddle apparatus at 75 rpm and 500 mL of dissolution medium at 37 °C were used in all experiments. The experiments were performed in triplicate. Horizontal dashed red line represents the 85% dissolved. Most standard deviation bars lie within the symbols.

3.4. Modeling of *in vitro* dissolution

Table 7 and Table 8 summarize the estimated DLM scalar values (95% CI) obtained by model-based analysis of the intestinal *in vitro* dissolution profiles using the SIVA Toolkit®. Each naproxen form (*i.e.* pure API and formulations of each of the free acid and sodium salt) was evaluated separately. The goodness of fit was visually inspected with residuals plots and assessed with the coefficient of determination (R^2). As shown in Table 8, the first-order disintegration model without time-lag was applied only to those experiments where the formulations were not pre-exposed to gastric medium. Matching between two-stage and single dissolution, combined with the disintegration model, DLM estimates were obtained. These results indicate that the effect of

disintegration can be properly accounted for using the methodology applied.

The slowest and fastest dissolution rate of the acid form of the API observed in FaSSIF V3 Levels I and II, respectively, resulted in the lowest (0.0022) and highest (0.0810) estimated DLM values. Due to the virtually instantaneous dissolution of the sodium salt API in all media, the default DLM value of 1, without estimation, was utilized for the salt form (Table 7). The predicted dissolution profiles were in excellent agreement with the experimental profiles ($R^2 > 0.96$).

3.5. PBPK model verification & clinical trial simulations

The PBPK model of naproxen was developed and verified as

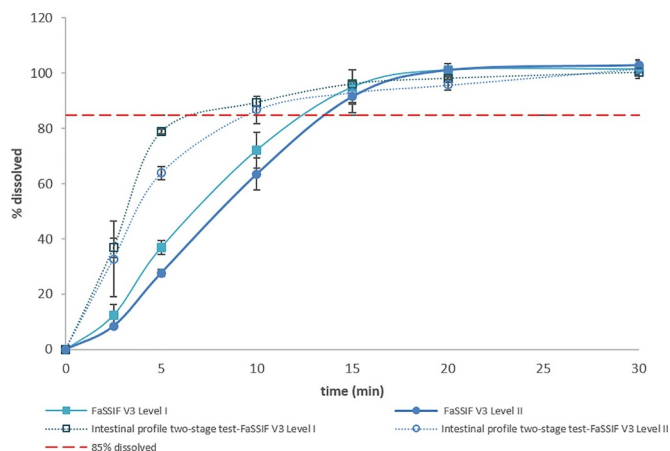


Fig. 5. *In vitro* dissolution (mean \pm SD) of Anaprox[®] 550 mg in FaSSIF V3 Levels I and II (solid lines, filled squares and circles respectively). The intestinal profiles in FaSSIF V3 Levels I and II (after the pre-treatment with FaSSGF Levels I and III respectively) during two-stage test are also depicted (dotted lines, empty squares and circles, respectively). USP paddle apparatus at 75 rpm and 500 mL of dissolution medium at 37 °C were used in all experiments. The experiments were performed in triplicate. Horizontal dashed red line represents the 85% dissolved. Most standard deviation bars lie within the symbols.

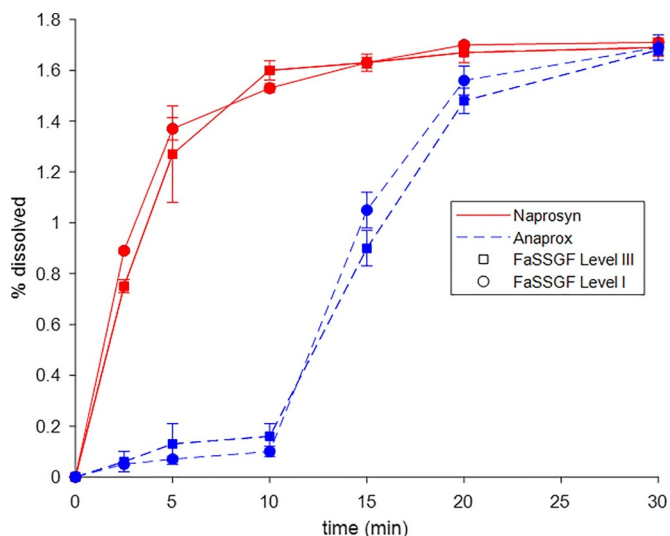


Fig. 6. *In vitro* dissolution (mean \pm SD) of Naprosyn[®] 500 mg (solid lines) and Anaprox[®] 550 mg (dashed lines) in FaSSGF Levels I and III (filled circles and squares, respectively). USP paddle apparatus at 75 rpm and 250 mL of dissolution medium at 37 °C were used in all experiments. The experiments were performed in triplicate. Horizontal dashed red line represents the 85% dissolved. Most standard deviation bars lie within the symbols.

described in Sections 2.9 and 2.10, respectively. Post-absorptive parameters (CL , V_{ss} , V_{sac} , Q_{sac}) were estimated from intravenous data, whereas for dissolution-absorption the Diffusion layer model-ADAM was used. Different *in vivo* dissolution scenarios were simulated according to the DLM scalar values obtained by model-based analysis of *in vitro* biorelevant dissolution profiles of the tested naproxen forms. The simulated profiles were compared against observed data from human *in vivo* PK studies (see Section 2.8). The generated virtual population closely matched the individuals enrolled in the respective *in vivo* studies in terms of ethnicity, gender ratio, and age and weight range. Volumes of concomitant liquid intake, dosage form type and sampling schedule were also taken into account for the virtual study design wherever available (see details in Section 2.10).

Table 9 summarizes all the simulations (10 trials x 10 individuals)

Table 7

Estimated DLM scalar values (95% CI) obtained from model-based analysis of *in vitro* dissolution in various media of naproxen free acid and sodium salt pure API powder. The goodness of fit between predicted and observed dissolution profiles was evaluated with the R squared (R^2).

Dissolution Medium	API Powder NPX	NPX Na
Level I FaSSIF V3		
DLM (95% CI)	0.0022 (0.0021–0.0023)	1*
R^2	0.997	–
Eur. Phar. Phosphate Buffer (pH = 6.8)		
DLM (95% CI)	0.0136 (0.0121–0.0151)	1*
R^2	0.992	–
Level II FaSSIF V3		
DLM (95% CI)	0.0810 (0.0651–0.0970)	1*
R^2	0.998	–

* default values of DLM scalar due to very fast dissolution (>85% dissolved in 2.5 min).

Table 8

Estimated DLM scalar and first-order disintegration rate constant (k_d) values (95% CI) obtained from model-based analysis of *in vitro* dissolution in various media of naproxen free acid (Naprosyn[®]) and sodium salt (Anaprox[®]) formulation. In the case of dissolution without pre-treatment in a gastric medium, a first-order disintegration model was included. The goodness of fit between predicted and observed dissolution profiles was evaluated with the R squared (R^2).

Dissolution Medium	Formulation Naprosyn	Anaprox
Level I FaSSIF V3		
DLM (95% CI)	0.0296 (0.0149–0.0443)	0.0212 (0.0131–0.0294)
k_d (95% CI)	0.305 (0.123–0.487)	0.288 (0.130–0.446)
R^2	0.999	0.998
Level I FaSSIF V3 (two-stage)		
DLM (95% CI)	0.0305 (0.0191–0.0308)	0.0221 (0.0174–0.0267)
k_d (95% CI)	–	–
R^2	0.967	0.981
Level II FaSSIF V3		
DLM (95% CI)	0.0213 (0.0170–0.0255)	0.0168 (0.00996–0.0237)
k_d (95% CI)	0.702 (0.354–1.05)	0.228 (0.0975–0.358)
R^2	0.999	0.999
Level II FaSSIF V3 (two-stage)		
DLM (95% CI)	0.0187 (0.0143–0.0230)	0.0158 (0.0138–0.0179)
k_d (95% CI)	–	–
R^2	0.975	0.991

performed for each *in vivo* dissolution scenario and the resulting mean *in silico* population pharmacokinetic (popPBPK) parameters for the virtual healthy adult population. Regardless of the anticipated differences *in vivo* dissolution, as reflected by the various estimated DLM values, these results suggest that mean AUC remains almost constant, while more pronounced variations in C_{max} and especially in T_{max} are observed. Direct comparisons of the mean *in silico* and *in vivo* pharmacokinetic parameters show very good agreement between simulated and observed data (Table 9 and Table 10). In all cases, the average (AFE) and absolute average fold error (AAFE) lay between 0.90–1.16 and 1.07–1.04, reflecting successful PBPK model performance and excellent predictions of the observed plasma profiles.

Fig. 7 illustrates the mean simulated naproxen plasma-concentration time profiles and the 5th and 95th percentiles of the virtual population for the two extreme DLM estimated values; i.e., $DLM_{min} = 0.0022$ and $DLM_{max} = 1$. Note that these DLM values were extracted from the dissolution of the free acid and salt pure API forms, not the formulations, and were intentionally chosen as such in order to evaluate *in vivo* performance differences (if any) that could be detected under these extreme scenarios. As can be observed, the C_{max} of the

Table 9

Mean *in silico* population pharmacokinetic (popPBPK) parameters of naproxen simulated plasma-concentration-time profiles under all tested *in vivo* dissolution inputs (DLM scalar values) obtained from model-based analysis of the *in vitro* data (see formulation and dissolution medium).

Formulation	Medium	S_{DLM}	Disintegration kd (h ⁻¹)/2-stage	<i>In silico</i> mean popPBPK parameters		
				T_{max} (h)	C_{max} (mg/L)	AUC (mg/L·h)
API						
Naproxen	Level I FaSSiF V3	0.0022	—	2.52	65.5	1302
	Ph. Eur. Phosphate	0.0136	—	1.80	69.0	1305
	Level II FaSSiF V3	0.0810	—	1.44	69.4	1306
Naproxen Na	all media	1	—	1.44	69.6	1306
Formulation						
Naprosyn	Level I FaSSiF V3	0.0396	0.305	1.80	67.5	1277
		0.0305	2-stage	1.80	69.2	1306
	Level II FaSSiF V3	0.0213	0.702	1.80	67.8	1277
		0.0187	2-stage	1.80	69.1	1306
Anaprox	Level I FaSSiF V3	0.0212	0.288	1.80	67.9	1277
		0.0221	2-stage	1.80	69.2	1306
	Level II FaSSiF V3	0.0168	0.228	1.80	67.7	1277
		0.0158	2-stage	1.80	69.1	1305

simulated plasma profile corresponding to administration of the very slowly dissolving hypothetical formulation was only slightly lower than the one resulting from the very fast dissolving hypothetical formulation. On the other hand, T_{max} was significantly prolonged. Interestingly, regardless of whether the worst or best case scenario was applied, the dissolution profiles predicted the observed range of PK profiles reasonably well (see also AFE and AAFE values).

In order to further explore the impact of key parameters on the simulated plasma profiles, one-at-a-time parameter sensitivity analysis (PSA) on the DLM scalar and GET in the fasted state was performed. GET and DLM were allowed to range from 0.1 to 2 h and 0.001 to 0.1, respectively, while all other parameters in the model were kept constant. Fig. 8 and Fig. 9 show the mean simulated plasma profiles of a representative individual of the virtual population for various DLM and GET values, respectively. Fig. 8 shows that over a 100-fold range of DLM values only slight or almost no differences in C_{max} (69.7–74.0 mg/L) or AUC (1175–1177 mg/L·h) are observed. T_{max} (1.40–2.65 h) seems to be more sensitive to *in vivo* dissolution changes (as reflected in the S_{DLM} values) than the other PK parameters. Fig. 9 clearly demonstrates that variation in GET markedly affects C_{max} (52.2–75.5 mg/L) and T_{max} (1.09–4.00 h), whereas AUC (1172–1180 mg/L·h) is not impacted.

As one would anticipate, PSA on dissolution rate in the stomach revealed no changes in the simulated C_{max} , T_{max} and AUC (data not shown), since poorly soluble weakly acidic compounds like naproxen barely dissolve in the fasted state gastric environment (see also Fig. 6).

3.6. Virtual bioequivalence

Multiple non-replicated, two-sequence, two-treatment, two-period,

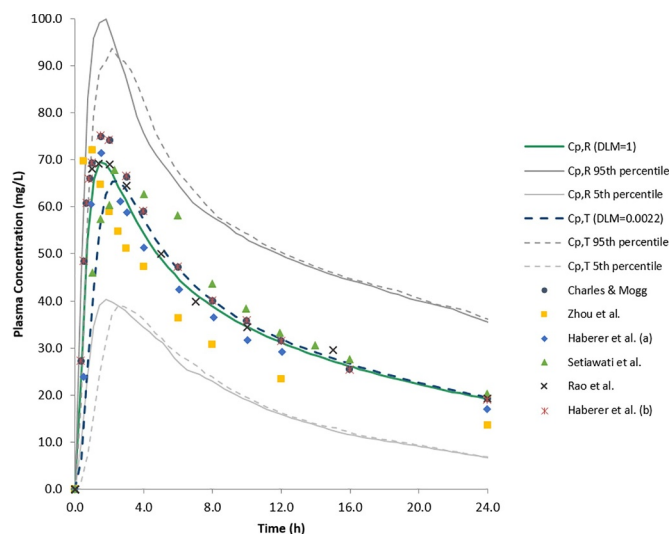


Fig. 7. Population mean simulated naproxen plasma concentration-time profiles and the 5th and 95th percentiles for the two extremes of the estimated S_{DLM} values: (a) $S_{DLM}=1$ (green and gray solid lines, respectively) and (b) $DLM=0.0022$ (blue and light gray dashed lines, respectively). In a worst/best case virtual bioequivalence scenario of simulated healthy adult populations (a) was treated as the reference, whereas (b) was the test formulation. Observed clinical data from Charles & Mogg (circles), Zhou et al. (squares), Haberer et al. (a) (diamonds), Setiawati et al. (triangles), Rao et al. (crosses) and Haberer et al. (b) (asterisks) are overlaid for verification of the PBPK model performance and comparisons. Simulations run for 72 h, but to enable better comparison only the first 24 h are plotted.

Table 10

Mean (SD) pharmacokinetic parameters of naproxen *in vivo* studies (^a Median value).

Reference	Formulation & Dose	<i>In vivo</i> mean PK parameters (SD)		
		T_{max} (h)	C_{max} (mg/L)	AUC (mg/L·h)
(Charles and Mogg, 1994)	Naprosyn® 500 mg	1.50 ^a	71.4 ^a	1211 ^a
(Zhou et al., 1998)	Naprosyn® 2 x 250 mg	2.6 (1.5)	87.3 (15.5)	1428 (193)
(Haberer et al., 2010)	Anaprox® 550 mg	1.48	75.2	1294
(Setiawati et al., 2009)	Anaprox® 550 mg	1.00 (0.5–2)	72.0 (11.2)	1013 (186)
(Rao et al., 1993)	IR Naproxen 500 mg	1.36 (0.81)	69.2 (20.9)	1435 (312)
Haberer et al. (b)(Haberer et al., 2010)	IR Naproxen-Na 500 mg	1.53	74.9	1299

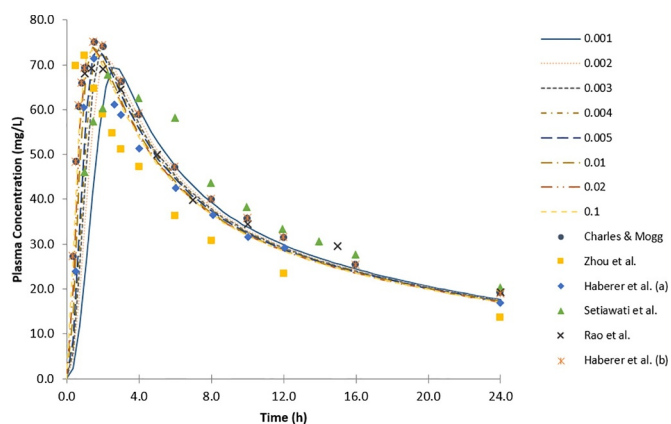


Fig. 8. Sensitivity analysis of naproxen simulated plasma concentration-time profiles of population representative individual on DLM scalar values ranging from 0.001 (blue solid line) to 0.1 (dashed line). The values of all other parameters were kept constant (GET = 0.25 h). Observed clinical data from Charles & Mogg (circles), Zhou et al. (squares), Haberer et al. (a) (diamonds), Setiawati et al. (triangles), Rao et al. (crosses) and Haberer et al. (b) (asterisks) are overlaid for comparison. Simulations run for 72 h, but to enable better comparison only the first 24 h are plotted.

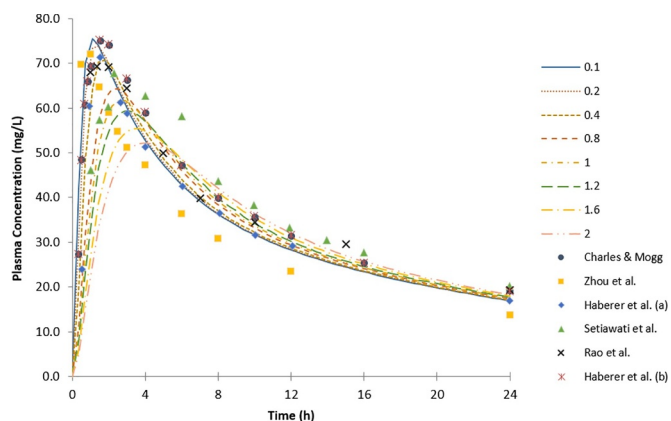


Fig. 9. Sensitivity analysis of naproxen simulated plasma concentration-time profiles of population representative individual on GET values in fasted state ranging from 0.1 (blue solid line) to 2 h (dash double dotted line). The values of all other parameters were kept constant (DLM = 1). Observed clinical data from Charles & Mogg (circles), Zhou et al. (squares), Haberer et al. (a) (diamonds), Setiawati et al. (triangles), Rao et al. (crosses) and Haberer et al. (b) (asterisks) are overlaid for comparison. Simulations run for 72 h, but to enable better comparison only the first 24 h are plotted.

Table 11

Mean *in silico* population pharmacokinetic (popPBPK) parameters of naproxen virtual clinical trials for the hypothetical reference and test formulations prior to bioequivalence assessment.

Trial N ^o	<i>In silico</i> mean popPBPK parameters Reference			Test		
	T _{max} (h)	C _{max} (mg/L)	AUC (mg/L·h)	T _{max} (h)	C _{max} (mg/L)	AUC (mg/L·h)
1	1.66	62.01	1249	2.26	57.66	1248
2	1.51	65.79	1275	2.31	62.58	1273
3	1.96	61.30	1624	2.59	59.67	1623
4	1.58	74.97	1659	2.41	70.61	1657
5	1.75	60.35	1785	2.84	55.14	1783
6	1.55	72.27	1404	2.56	67.34	1403
7	1.45	64.14	1426	2.02	62.17	1425
8	1.39	71.03	1473	2.47	65.14	1472
9	1.58	61.87	1340	2.26	58.88	1339
10	1.64	62.32	1348	2.39	60.46	1347

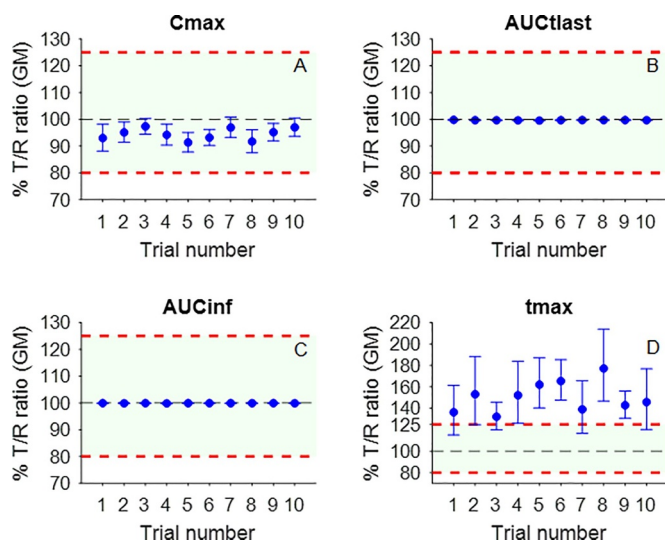


Fig. 10. Average virtual bioequivalence results (% Geometric mean T/R ratio) of 10 trials with 12 simulated individuals in each trial. Intra-subject variability of 30% was arbitrarily chosen and added through Simcyp® (V18.1; Certara, Sheffield, UK) VBE module (V1.0) to the mean GET, pH of fasted stomach, pH and bile salts concentration of fasted duodenum, jejunum I and II. The 80–125% bioequivalence limits (red dashed lines) and the area of acceptance (light green shaded area) are shown for each tested PK parameter: (A) C_{max}, (B) AUC_{last} (AUC calculated up to the last simulated time point), (C) AUC_{inf} (AUC extrapolated to infinity) and (D) T_{max}. Error bars represent the 90% confidence intervals, which in subplots (B) and (C) lie within the symbols.

cross-over virtual bioequivalence trials (n = 10) with 12 individuals per trial were conducted. In a worst/best case scenario, two hypothetical naproxen formulations with extremely different *in vivo* dissolution rates were tested with the aim of designing a clinically relevant safe space. The reference (R) was assumed to have a DLM scalar value of 1, corresponding to the instantaneous dissolution of naproxen sodium API powder, while the test (T) formulation was assigned the value of 0.0022, corresponding to the very slow dissolution of naproxen free acid API powder in FaSSiF V3 Level I (Table 11).

Fig. 10 presents the results of virtual bioequivalence trials for C_{max}, AUC calculated up to the last simulated time point (AUC_{last}) and extrapolated to infinity (AUC_{inf}). Bioequivalence with regard to T_{max} was also investigated. In all trials, C_{max}, AUC_{last}, AUC_{inf} met the average

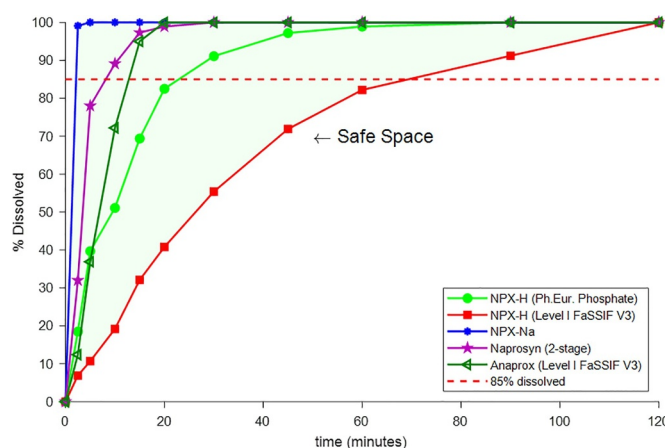


Fig. 11. Dissolution safe space for anticipated bioequivalence to naproxen products. The light green shaded area delimits the safe space area in which bioequivalence (with respect to C_{max} and AUC) was established between the very slow (red solid line & squares) and the fast (blue solid line & circles) dissolution profiles. Additional typical dissolution profiles are co-plotted (n = 3). The horizontal red dashed line represents 85% dissolved.

bioequivalence criteria (80–125%) with confidence intervals (CI) narrowly distributed around unity, especially for AUC. However, in terms of T_{max} bioequivalence failed in all 10 trials and most CI were far beyond the bioequivalence limits. These findings suggest that naproxen formulations which reach 85% dissolved in media simulating the healthy human upper small intestine within 90 min or less are expected to be bioequivalent. These borders correspond to the dissolution “safe space” and can be used to set clinically relevant dissolution specifications to minimize the risk of bioequivalence failure.

4. Discussion

The present study proposes a workflow and highlights the key role of mechanistic absorption and population-based PBPK modeling to establish virtual bioequivalence and set clinically relevant dissolution specifications by combining *in vitro*, *in vivo* and *in silico* methods.

In the naproxen case example, starting from *in vitro* solubility and dissolution data, an approach of stepwise sequential estimation/confirmation of biopharmaceutical parameters was followed, (Pathak et al., 2019) before applying them to the PBPK model. *In vitro* dissolution profiles in conventional and biorelevant media were translated to different *in vivo* dissolution scenarios by implementing an *in vitro-in vivo*-extrapolation (IVIVE) strategy. The healthy adult PBPK model for naproxen was developed by optimizing post-absorptive parameters from intravenous *in vivo* data which was then coupled with the ADAM model for mechanistic oral absorption modeling. The verification of the PBPK model was based on its ability to predict the observed plasma PK profiles after oral administration of naproxen in several *in vivo* studies and its performance under multiple *in vivo* dissolution scenarios was assessed.

Simulations of the clinical studies in conjunction with sensitivity analysis on the DLM scalar and gastric emptying time revealed that C_{max} and AUC are rather insensitive to dissolution changes, but that C_{max} is considerably affected by variations in gastric emptying time. However, changes in either the S_{DLM} or gastric emptying markedly altered T_{max} . These results indicate that the absorption and thus the *in vivo* performance of naproxen formulations seems to be governed by gastric emptying, but is not dissolution-limited. This is supported by the (refined) developability classification system (DCS/rDCS), (Butler and Dressman, 2010; Rosenberger et al., 2019) according to which naproxen would more appropriately be classified as rDCS/DCS I, and is in excellent agreement with the study of Charles and Mogg (Charles and Mogg, 1994), which concluded that two naproxen products (tablet and caplet) with very dissimilar *in vitro* dissolution behavior were bioequivalent. Furthermore, a DLM scalar range from 0.0022 to 1 translated to an increase in C_{max} only by 1.06 and 1.75 times earlier T_{max} , assuming the default value in Simcyp for the particle radius of 10 μ m. The AUC remained unchanged. In this case, the insensitivity of PK metrics to the dissolution rate was attributed both to the absence of saturable first pass extraction and the relatively long half-life ($t_{1/2} \approx 20$ h) of the drug.

Once enough confidence with the performance of the PBPK model was achieved, several VBE trials simulating a worst/best case scenario were performed. A safe space and a clinically relevant dissolution specification for naproxen products was proposed based on the outcome of these virtual trials. It was demonstrated that 85% dissolved reached within 90 min lies comfortably within a region of dissolution performance where bioequivalence is anticipated and is not anywhere near the edge of failure for either C_{max} or AUC. On the other hand, bioequivalence in T_{max} failed in all cases. In this study, *in vitro* dissolution of unformulated free acid and sodium salt forms of naproxen were used to simulate the worst/best case BE scenario. Although this constitutes an extreme limitation, it was done intentionally to challenge the VBE result, since if the VBE were to be based solely on the dissolution of the formulations, the safe space would be biased towards an already (partly) optimized formulation range.

Virtual bioequivalence studies have been already published in the recent past. (Babiskin and Zhang, 2015; Doki et al., 2017; Pathak et al., 1997; Pepin et al., 2016; Wedagedera et al., 2017; Zhang et al., 2017) However, in most of those studies the intra-subject (IIV) and inter-occasion (IOV) variability is either ignored or added directly to the PK metrics (*i.e.* C_{max} and AUC) as random error terms. By contrast, in the current study the intra-subject variability was added via the Simcyp® v18.1 VBE module 1.0 in several key absorption parameters, such as gastric emptying time, pH of fasted stomach, pH and bile salts concentration of fasted duodenum, jejunum I and II, and mechanistically propagated in simulations. In the context of challenging the establishment of bioequivalence, IOV was set to a somewhat exaggerated value of 30% for all parameters.

5. Conclusion

Mechanism-based absorption PBPK modeling can be considered as a promising and powerful bioequivalence risk assessment tool. This work highlights the importance of linking translational absorption modeling with population PBPK to examine VBE and set clinically relevant specifications. For naproxen, it was demonstrated that bioequivalence failure due to dissolution is unlikely for naproxen products because of the wide safe space. The example of naproxen illustrates that the impact of formulation on the *in vivo* performance is not always correlated with the *in vitro* dissolution behavior.

To the best of our knowledge, this is the first work which not only mechanistically incorporates inter-occasion variability in VBE assessment, but also propagates IOV in the simulations. Implementation of hierarchical levels of variability (BS, WS, IOV) in VBE trials is of critical importance in order to accurately describe the population variability and avoid biased, overoptimistic bioequivalence results due to underestimation of the overall variability. Even though mixed effect modeling is rare in this context, this study highlights the importance of mechanistically assigning between-subject and inter-occasion variability values which are physiologically plausible and meaningful. Using %CV values obtained from single observation in each individual within a specific population is not representative of the population BS or IOV since it comes solely from a single sample. In this case, the applied coefficient of variation is often conveniently misinterpreted as mixture of BS and IO variability. Likewise, implementation of arbitrary CV% values is inappropriate.

Moving a step further towards linking the lab to the patient, mechanistic extrapolation of *in vitro* data (*e.g.* dissolution) to the *in vivo* situation, as explicitly demonstrated for naproxen, is critical for the validity and interpretation of VBE results. In the context of bioequivalence trial simulation, which is of great interest for both regulatory agencies and the pharmaceutical industry, a mechanistic IVIVE approach will be essential to enable extrapolation to specific or disease populations, given that differences in factors like GI physiology need to be taken into account. The acquisition of further clinical data (*e.g.*, intraluminal and plasma concentrations) as well as advancement of the current biopharmaceutical tools are expected to significantly increase the reliability of virtual bioequivalence results in a variety of diseases, dosing conditions such as PPI co-administration and specific populations such as pediatric patients.

Consideration of drug-related pharmacokinetic characteristics (*e.g.*, half-life, first pass effect, protein binding) along with PBPK modeling will assist not only to select the most appropriate dosage form and to set formulation targets, but more importantly to understand to what extent the formulation can be expected to steer the *in vivo* performance of the drug product. Further validation of the proposed approach with a range of drugs and formulations is needed to increase confidence and spread awareness of the power of mechanistic absorption modeling and PBPK in formulation design and regulation.

Bridging the gap between *in vitro*, *in vivo* and *in silico* by applying mechanistic absorption coupled with population PBPK modeling can

guide model-informed formulation selection, allow for robust clinical outcome predictions, inform regulatory decision-making, permit regulatory flexibility (e.g. granting bioequivalency for some BCS class II weak acids like naproxen) and potentially reduce the cost/time of product development by replacing unnecessary clinical trials.

Future work could investigate the impact of bioequivalence in T_{max} on the onset of action and therefore the therapeutic equivalence of naproxen products. As has already been highlighted, (Cristofolletti et al., 2018; Loiosio-Konstantinidis et al., 2019) a scenario is foreseen in which by combining verified PBPK with pharmacodynamic (PD) models tailored to the target population(s), release testing in the laboratory will be linked to the therapeutic outcome.

Acknowledgments

This work was supported by the European Union's Horizon 2020 Research and Innovation Programme under grant agreement No 674909 (PEARL).

References

- Avdeef, A., 2007. Solubility of sparingly-soluble ionizable drugs. *Adv. Drug Deliv. Rev.* 59, 568–590.
- Avdeef, A., Berger, C.M., 2000. pH-Metric solubility. 2: correlation between the acid-base titration and formulations for use in early animal bioavailability and toxicity studies. later in development, solubility takes on a broader. *Pharm. Res.* 17.
- Awni, W.M., Braeckman, R.A., Cavanaugh, J.H., Locke, C.S., Linnen, P.J., Granneman, G.R., Dubé, L.M., 1995. The pharmacokinetic and pharmacodynamic interactions between the 5-Lipoxygenase inhibitor zileuton and the cyclo-oxygenase inhibitor naproxen in human volunteers. *Clin. Pharmacokinet.* 29, 112–124.
- Babiskin, A.H., Zhang, X., 2015. Application of physiologically based absorption modeling for amphetamine salts drug products in generic drug evaluation. *J. Pharm. Sci.* 104, 3170–3182.
- Bergström, C.A.S., Andersson, S.B.E., Fagerberg, J.H., Ragnarsson, G., Lindahl, A., 2014. Is the full potential of the biopharmaceutics classification system reached? *Eur. J. Pharm. Sci.* 57, 224–231.
- Brown, H.S., Griffin, M., Houston, J.B., Li, A.P., 2007. Evaluation of cryopreserved human hepatocytes as an alternative *in vitro* system to microsomes for the prediction of metabolic clearance. *Drug Metab. Dispos.* 35, 293–301.
- Butler, J.M., Dressman, J.B., 2010. The developability classification system: application of biopharmaceutics concepts to formulation development. *J. Pharm. Sci.* 99, 4940–4954.
- Charles, B.G., Mogg, G.A.G., 1994. Comparative *in vitro* and *in vivo* bioavailability of naproxen from tablet and caplet formulations. *Biopharm. Drug Dispos.* 15, 121–128.
- Chowhan, Z.T., 1978. pH-Solubility profiles of organic carboxylic acids and their salts. *J. Pharm. Sci.* 67, 1257–1260.
- Cristofolletti, R., Chiann, C., Dressman, J.B., Storpirtis, S., 2013. A comparative analysis of biopharmaceutics classification system and biopharmaceutics drug disposition classification system: a cross-sectional survey with 500 bioequivalence studies. *J. Pharm. Sci.* 102, 3136–3144.
- Cristofolletti, R., Dressman, J.B., 2016. Bridging the gap between *in vitro* dissolution and the time course of ibuprofen-mediated pain relief. *J. Pharm. Sci.* 105, 3658–3667.
- Cristofolletti, R., Patel, N., Dressman, J.B., 2016. Differences in food effects for 2 weak bases with similar bcs drug-related properties: what is happening in the intestinal lumen? *J. Pharm. Sci.* 105, 2712–2722.
- Cristofolletti, R., Rowland, M., Lesko, L.J., Blume, H., Rostami-Hodjegan, A., Dressman, J.B., 2018. Past, present, and future of pbpk modelling: improving assessment and extrapolation of therapeutic equivalence for oral drug products. *J. Pharm. Sci.* 107, 2519–2530.
- Davies, N.M., Anderson, K.E., 1997. Clinical pharmacokinetics of naproxen. *Clin. Pharmacokinet.* 32, 268–293.
- Dickinson, P.A., Lee, W.W., Stott, P.W., Townsend, A.I., Smart, J.P., Ghahramani, P., Hammett, T., Billett, L., Behn, S., Gibb, R.C., Abrahamsson, B., 2008. Clinical relevance of dissolution testing in quality by design. *AAPS J.* 10, 380–390.
- Doki, K., Darwich, A.S., Patel, N., Rostami-Hodjegan, A., 2017. Virtual bioequivalence for achlorhydric subjects: the use of pbpk modelling to assess the formulation-dependent effect of achlorhydria. *Eur. J. Pharm. Sci.* 109, 111–120.
- European Medicines Agency (EMA), 2018a. Committee for medicinal products for human use (CHMP) guideline on the reporting of physiologically based pharmacokinetic (PBPK) modelling and simulation.
- European Medicines Agency (EMA), 2018b. Committee for medicinal products for human use (CHMP) guideline on the reporting of physiologically based pharmacokinetic (PBPK) modelling and simulation.
- Franssen, M.J., Tan, Y., van de Putte, L.B., van Ginneken, C.A., Gribnau, F.W., 1986. Pharmacokinetics of naproxen at two dosage regimens in healthy volunteers. *Int. J. Clin. Pharmacol. Ther. Toxicol.* 24, 139–142.
- Fruehauf, H., Goetze, O., Steingöetter, A., Kwiatek, M., Boesiger, P., Thumshirn, M., Schwizer, W., Fried, M., 2007. Intersubject and intrasubject variability of gastric volumes in response to isocaloric liquid meals in functional dyspepsia and health. *Neurogastroenterol. Motil.* 19, 553–561.
- Fuchs, A., Leigh, M., Klofer, B., Dressman, J.B., 2015. Advances in the design of fasted state simulating intestinal fluids: FaSSIF-V3. *Eur. J. Pharm. Biopharm.* 94, 229–240.
- Götzsche, P.C., Andreasen, F., Egsmose, C., Lund, B., 1988. Steady state pharmacokinetics of naproxen in elderly rheumatics compared with young volunteers. *Scand. J. Rheumatol.* 17, 11–16.
- Grimm, M., Kozioliek, M., Kühn, J.P., Weitschies, W., 2018. Interindividual and intraindividual variability of fasted state gastric fluid volume and gastric emptying of water. *Eur. J. Pharm. Biopharm.* 127, 309–317.
- Haberer, L.J., Walls, C.M., Lener, S.E., Taylor, D.R., McDonald, S.A., 2010. Distinct pharmacokinetic profile and safety of a fixed-dose tablet of sumatriptan and naproxen sodium for the acute treatment of migraine. *Headache* 50, 357–373.
- Heimbach, T., Laisney, M., Samant, T., Elmeliyeg, M., Wu, F., Hanna, I., Lin, W., Zhang, J., Dodd, S., Nguyen-Trung, A.-T., Tian, H., Vogg, B., Beato, S., Garad, S., Choudhury, S., Ren, X., Mueller-Zsigmondy, M., Einolf, H., Umehara, K., Hourcade-Potelleret, F., He, H., PBPK modeling and simulations of oral drug absorption/food effect/ppi /PBIVVC: Opportunities and challenges dissolution and translational modeling strategies enabling patient-centric product development. 2017.
- Heimbach, T., Suarez-Sharp, S., Kakhi, M., Holmstock, N., Olivares-Morales, A., Pepin, X., Sjögren, E., Tsakalozou, E., Seo, P., Li, M., Zhang, X., Lin, H.-P., Montague, T., Mitra, A., Morris, D., Patel, N., Kesiosoglou, F., 2019. Dissolution and translational modeling strategies toward establishing an *in vitro-in vivo* link—a workshop summary report. *AAPS J.* 21, 29.
- Hens, B., Brouwers, J., Anneveld, B., Corsetti, M., Symillides, M., Vertzoni, M., Reppas, C., Turner, D.B., Augustijns, P., 2014. Gastrointestinal transfer: *in vivo* evaluation and implementation in *in vitro* and *in silico* predictive tools. *Eur. J. Pharm. Sci.* 63, 233–242.
- Jamei, M., Turner, D., Yang, J., Neuhooff, S., Polak, S., Rostami-Hodjegan, A., Tucker, G., 2009. Population-based mechanistic prediction of oral drug absorption. *AAPS J.* 11, 225–237.
- Kambayashi, A., Blume, H., Dressman, J., 2013. Understanding the *in vivo* performance of enteric coated tablets using an *in vitro-in silico-in vivo* approach: case example diclofenac. *Eur. J. Pharm. Biopharm.* 85, 1337–1347.
- Ke, A., Barter, Z., Rowland-Yeo, K., Almond, L., 2016. Towards a best practice approach in pbpk modeling: case example of developing a unified efavirenz model accounting for induction of CYPs 3A4 and 2B6. *CPT Pharmacometrics Syst. Pharmacol.* 5, 367–376.
- Kuepfer, L., Niederalt, C., Wendt, T., Schlender, J.-F., Willmann, S., Lippert, J., Block, M., Eissing, T., Teutonico, D., 2016. Applied concepts in pbpk modeling: how to build a pbpk/pd model. *CPT pharmacometrics Syst. Pharmacol.* 5, 516–531.
- Lartigue, S., Bizais, Y., Des Varannes, S.B., Murat, A., Pouliquen, B., Galmiche, J.P., 1994. Inter- and intraindividual variability of solid and liquid gastric emptying parameters. a scintigraphic study in healthy subjects and diabetic patients. *Dig. Dis. Sci.* 39, 109–115.
- Lennernas, H., Knutson, L., Knutson, T., Lesko, L., Salmonson, T., Amidon, G.L., 1995. Human effective permeability data for furosemide, hydrochlorothiazide, ketoprofen and naproxen to be used in the proposed biopharmaceutics classification for IR-products. *Pharm. Res. (New York)* 12 (9 SUPPL), 396.
- Lin, J.H., Cocchetto, D.M., Duggan, D.E., 1987. Protein binding as a primary determinant of the clinical pharmacokinetic properties of non-steroidal anti-inflammatory drugs. *Clin. Pharmacokinet.* 12, 402–432.
- Loiosio-Konstantinidis, I., Paraiso, R.L.M., Fotaki, N., McAllister, M., Cristofolletti, R., Dressman, J., 2019. Application of the relationship between pharmacokinetics and pharmacodynamics in drug development and therapeutic equivalence: a pearl review. *J. Pharm. Pharmacol.* 71, 699–723.
- Mann, J., Dressman, J., Rosenblatt, K., Ashworth, L., Muenster, U., Frank, K., Hutchins, P., Williams, J., Klumpp, L., Wielockx, K., Berben, P., Augustijns, P., Holm, R., Hofmann, M., Patel, S., Beato, S., Ojala, K., Tomaszewska, I., Bruel, J.-L., Butler, J., 2017. Validation of dissolution testing with biorelevant media: an orbito study. *Mol. Pharm.* 14, 4192–4201.
- Markopoulos, C., Andreas, C.J., Vertzoni, M., Dressman, J., Reppas, C., 2015. *In vitro* simulation of luminal conditions for evaluation of performance of oral drug products: choosing the appropriate test media. *Eur. J. Pharm. Biopharm.* 93, 173–182.
- McNamara, D.P., Amidon, G.L., 1986. Dissolution of acidic and basic compounds from the rotating disk: influence of convective diffusion and reaction. *J. Pharm. Sci.* 75, 858–868.
- Mitra, A., 2019. Maximizing the role of physiologically based oral absorption modeling in generic drug development. *Clin. Pharmacol. Ther.* 105, 307–309.
- Mooney, K.G., Mintun, M.A., Himmelstein, K.J., Stella, V.J., 1981. Dissolution kinetics of carboxylic acids I: effect of pH under unbuffered conditions. *J. Pharm. Sci.* 70, 13–22.
- Mooney, K.G., Mintun, M.A., Himmelstein, K.J., Stella, V.J., 1981a. Dissolution kinetics of carboxylic acids II: effect of buffers. *J. Pharm. Sci.* 70, 22–32.
- Mooney, K.G., Rodriguez-gaxiola, M., Mintun, M., Himmelstein, K.J., Stella, V.J., 1981b. Dissolution kinetics of phenylbutazone. *J. Pharm. Sci.* 70, 1358–1365.
- Niaz, S.K., Mahmood Alam, S., Ahmad, S.I., 1996. Dose dependent pharmacokinetics of naproxen in man. *Biopharm. Drug Dispos.* 17, 355–361.
- Obach, R.S., Baxter, J.G., Liston, T.E., Silber, B.M., Jones, B.C., MacIntyre, F., Rance, D.J., Wastall, P., 1997. The prediction of human pharmacokinetic parameters from preclinical and *in vitro* metabolism data. *J. Pharmacol. Exp. Ther.* 283, 46–58.
- Olivares-Morales, A., Ghosh, A., Aarons, L., Rostami-Hodjegan, A., 2016. Development of a novel simplified pbpk absorption model to explain the higher relative bioavailability of the OROS® formulation of oxybutynin. *AAPS J.* 18, 1532–1549.
- Ozturk, S.S., Palsson, B.O., Dressman, J.B., 1988. Dissolution of ionizable drugs in buffered and unbuffered solutions. *Pharm. Res.* 05, 272–282.
- Paixão, P., Bermejo, M., Hens, B., Tsume, Y., Dickens, J., Shedden, K., Salehi, N., Koenigsnecht, M.J., Baker, J.R., Hasler, W.L., Lionberger, R., Fan, J., Wysocki, J.,

- Wen, B., Lee, A., Frances, A., Amidon, G.E., Yu, A., Benninghoff, G., Löbenberg, R., Talatoff, A., Sun, D., Amidon, G.L., 2018. Gastric emptying and intestinal appearance of nonabsorbable drugs phenol red and paromomycin in human subjects: a multi-compartment stomach approach. *Eur. J. Pharm. Biopharm.* 129, 162–174.
- Paixão, P., Gouveia, L.F., Morais, J.A.G., 2012. Prediction of the human oral bioavailability by using *in vitro* and *in silico* drug related parameters in a physiologically based absorption model. *Int. J. Pharm.* 429, 84–98.
- Parrott, N., Hainzl, D., Scheubel, E., Krimmer, S., Boetsch, C., Guerini, E., Martin-Facklam, M., 2014. Physiologically based absorption modelling to predict the impact of drug properties on pharmacokinetics of bitopertin. *AAPS J* 16, 1077–1084.
- Pathak, S.M., Patel, N., Wedagedera, J., Turner, D.B., Jamei, M., Rostami-Hodjegan, A., Limited, S., 1997. Establishment of virtual bioequivalence using population-based pbpk modelling: application to the setting of dissolution limits. *AAPS J.*
- Pathak, S.M., Schaefer, K.J., Jamei, M., Turner, D.B., 2019. Biopharmaceutic IVIVE—Mechanistic modeling of Single- and Two-Phase *in vitro* experiments to obtain drug-specific parameters for incorporation into PBPK models. *J. Pharm. Sci.* 108, 1604–1618.
- Pepin, X.J.H., Flanagan, T.R., Holt, D.J., Eidelman, A., Treacy, D., Rowlings, C.E., 2016. Justification of drug product dissolution rate and drug substance particle size specifications based on absorption pbpk modeling for lesinurad immediate release tablets.
- Pérez, M.A.C., Sanz, M.B., Torres, L.R., Évalos, R.G., González, M.P., Díaz, H.G., 2004. A topological sub-structural approach for predicting human intestinal absorption of drugs. *Eur. J. Med. Chem.* 39, 905–916.
- Petring, O.U., Flachs, H., 1990. Inter- and intrasubject variability of gastric emptying in healthy volunteers measured by scintigraphy and paracetamol absorption. *Br. J. Clin. Pharmacol.* 29, 703–708.
- Poulin, P., Theil, F.-P., 2009. Development of a novel method for predicting human volume of distribution at steady-state of basic drugs and comparative assessment with existing methods. *J. Pharm. Sci.* 98, 4941–4961.
- Psachoulas, D., Vertzoni, M., Goumas, K., Kalioras, V., Beato, S., Butler, J., Reppas, C., 2011. Precipitation in and supersaturation of contents of the upper small intestine after administration of two weak bases to fasted adults. *Pharm. Res.* 28, 3145–3158.
- Rao, B.R., Rambhau, D., Rao, V.V.S., 1993. Pharmacokinetics of single-dose administration of naproxen at 10 : 00 and 22 : 00 hours. *Int. Soc. Chronobiol.* 10, 137–142.
- Rosenberger, J., Butler, J., Muenster, U., Dressman, J., 2019. Application of a refined developability classification system. *J. Pharm. Sci.* 108, 1090–1100.
- Runkel, R., Chaplin, M., Boost, G., Segre, E., Forchielli, E., 1972a. Absorption, distribution, metabolism, and excretion of naproxen in various laboratory animals and human subjects. *J. Pharm. Sci.* 61, 703–708.
- Runkel, R., Forchielli, E., Boost, G., Chaplin, M., Hill, R., Sevelius, H., Thompson, G., Segre, E., 1973. Naproxen-metabolism, excretion and comparative pharmacokinetics. *Scand J Rheumatol* 2, 29–36.
- Runkel, R., Karl, K., Boost, G., Sevelius, H., Forchielli, E., Hill, R., Magoun, R., Szakacs, J.B., Segre, E., 1972b. Naproxen oral absorption characteristics. *Chem. Pharm. Bull. (Tokyo)* 20, 1457–1466.
- Darwich, A.S., Neuhoﬀ, S., Jamei, M., Rostami-Hodjegan, A., 2010. Interplay of metabolism and transport in determining oral drug absorption and gut wall metabolism: a simulation assessment using the “Advanced dissolution, absorption, metabolism (ADAM)” model. *Curr. Drug Metab.* 11, 716–729.
- Selen, A., Dickinson, P.A., Müllertz, A., Crison, J.R., Mistry, H.B., Cruaños, M.T., Martínez, M.N., Lennernäs, H., Wigal, T.L., Swinney, D.C., Polli, J.E., Serajuddin, A.T.M., Cook, J.A., Dressman, J.B., 2014. The biopharmaceutics risk assessment roadmap for optimizing clinical drug product performance. *J. Pharm. Sci.* 103, 3377–3397.
- Serajuddin, A.T.M., Jarowski, C., 1985. Effect of diffusion layer pH and solubility on the dissolution rate of pharmaceutical bases and their hydrochloride salts. I: Phenazopyridine. *J. Pharm. Sci.* 74, 142.
- Setiawati, E., Deniati, S., Yunaidi, D., Handayani, L., Harinanto, G., Santoso, I., Sari, P.A., Rimainar, A., 2009. Bioequivalence study with two naproxen sodium tablet formulations in healthy subjects. *J. Bioequivalence Bioavailab. -Open Access Res. Artic.* *JBB J Bioequiv Availab* 1, 28–33.
- Shebley, M., Sandhu, P., Emami Riedmaier, A., Jamei, M., Narayanan, R., Patel, A., Peters, S.A., Reddy, V.P., Zheng, M., de Zwart, L., Beneton, M., Bouzom, F., Chen, J., Chen, Y., Cleary, Y., Collins, C., Dickinson, G.L., Djebli, N., Einolf, H.J., Gardner, I., Huth, F., Kazmi, F., Khalil, F., Lin, J., Odinecs, A., Patel, C., Rong, H., Schuck, E., Sharma, P., Wu, S.-P., Xu, Y., Yamazaki, S., Yoshida, K., Rowland, M., 2018. Physiologically based pharmacokinetic model qualification and reporting procedures for regulatory submissions: a consortium perspective. *Clin. Pharmacol. Ther.* 104, 88–110.
- Sheng, J.J., McNamara, D.P., Amidon, G.L., 2009. Toward an *in vivo* dissolution methodology: a comparison of phosphate and bicarbonate buffers. *Mol. Pharm.* 6, 29–39.
- Stillhart, C., Parrott, N.J., Lindenberg, M., Chalus, P., Bentley, D., Szepes, A., 2017. Characterising drug release from immediate-release formulations of a poorly soluble compound, bismisanil, through absorption modelling and dissolution testing. *AAPS J.* 19, 827–836.
- Suarez-Sharp, S., Cohen, M., Kesisoglou, F., Abend, A., Marroum, P., Delvadia, P., Kotzagiorgis, E., Li, M., Nordmark, A., Bandi, N., Sjögren, E., Babiskin, A., Heimbach, T., Kijima, S., Mandula, H., Raines, K., Seo, P., Zhang, X., 2018. Applications of clinically relevant dissolution testing: workshop summary report. *AAPS J* 20, 93.
- Tubic-Grozdanic, M., Bolger, M.B., Langguth, P., 2008. Application of gastrointestinal simulation for extensions for biowaivers of highly permeable compounds. *AAPS J* 10, 213–226.
- Upton, R., Williams, R., Kelly, J., Jones, R., 1984. Naproxen pharmacokinetics in the elderly. *Br. J. Clin. Pharmacol.* 18, 207–214.
- Van den Ouweland, F.A., Jansen, P.A., Tan, Y., Van de Putte, L.B., Van Ginneken, C.A., Gribnau, F.W., 1988. Pharmacokinetics of high-dosage naproxen in elderly patients. *Int. J. Clin. Pharmacol. Ther. Toxicol.* 26, 143–147.
- Vree, T.B., Van Den Biggelaar-Marteau, M., Verwey-Van Wissen, C.P.W.G.M., Vree, J.B., Guelen, P.J.M., 1993. Pharmacokinetics of naproxen, its metabolite O-desmethylnaproxen, and their acyl glucuronides in humans. *Biopharm. Drug Dispos.* 14, 491–502.
- Wang, J., Flanagan, D.R., 2002. General solution for diffusion-controlled dissolution of spherical particles. 2. evaluation of experimental data. *J. Pharm. Sci.* 91, 534–542.
- Wang, J., Flanagan, D.R., 1999. General solution for diffusion-controlled dissolution of spherical particles. 1. theory. *J. Pharm. Sci.* 88, 731–738.
- U.S-FDA Center for Drug Evaluation and Research (CDER), 2018b. Physiologically based pharmacokinetic analyses — format and content guidance for industry.
- U.S-FDA Center for Drug Evaluation and Research (CDER), 2018a. Physiologically based pharmacokinetic analyses — format and content guidance for industry.
- Wedagedera, J., Cain, T., Pathak, S.M., Jamei, M., 2017. Virtual bioequivalence assessment of two tramadol formulations using the advanced dissolution absorption and metabolism (ADAM) model via simcyp R package.
- Yazdani, M., Briggs, K., Jankovsky, C., Hawi, A., 2004. The “High solubility” definition of the current fda guidance on biopharmaceutical classification system may be too strict for acidic drugs. *Pharm. Res.* 21, 293–299.
- Zhang, X., Wen, H., Fan, J., Vince, B., Li, T., Gao, W., Kinjo, M., Brown, J., Sun, W., Jiang, W., Lionberger, R., 2017. Integrating *in vitro*, modeling, and *in vivo* approaches to investigate warfarin bioequivalence. *cpt pharmacometrics syst. Pharmacol* 6, 523–531.
- Zhao, P., Rowland, M., Huang, S.-M., 2012. Best practice in the use of physiologically based pharmacokinetic modeling and simulation to address clinical pharmacology regulatory questions. *Clin. Pharmacol. Ther.* 92, 17–20.
- Zhao, Y., Le, J., Abraham, M., Hersey, A., Eddershaw, P., Luscombe, C., Butina, D., Beck, G., Sherborne, B., Cooper, I., Platts, J., 2001. Evaluation of human intestinal absorption data and subsequent derivation of a quantitative structure-activity relationship (QSAR) with Abraham descriptors. *J. Pharm. Sci.* 90, 749–784.
- Zhou, D., Zhang, Q., Lu, W., Xia, Q., Wei, S., 1998. Single- and multiple-dose pharmacokinetic comparison of a sustained-release tablet and conventional tablets of naproxen in healthy volunteers. *J. Clin. Pharmacol.* 38, 625–629.



Research Article

Using Physiologically Based Pharmacokinetic Modeling to Assess the Risks of Failing Bioequivalence Criteria: a Tale of Two Ibuprofen Products

Ioannis Loisos-Konstantinidis,¹ Bart Hens,² Amitava Mitra,³ Sarah Kim,⁴
Chang Chiann,⁵ and Rodrigo Cristofolletti^{4,6}

Received 20 May 2020; accepted 31 July 2020

Abstract. The aims of the proposed study were to develop and verify a quantitative model-based framework to anticipate the *in vivo* bioequivalence of ibuprofen immediate release formulations. This stepwise approach integrated virtual bioequivalence trials to simulate the test to reference (T/R) ratio for positive (*i.e.*, bioequivalent) and negative (*i.e.*, non-bioequivalent) control formulations containing ibuprofen, approximated distribution of interoccasion variability (IOV) on ibuprofen peak (C_{\max}) and extent of exposure (AUC) by bootstrapping resampling methods, *post hoc* incorporation of IOV to simulated T/R ratios, and power curve analysis. After *post hoc* incorporation of the bootstrapped IOV to the simulated C_{\max} T/R geometric mean ratios, the resulting 90% confidence intervals overlapped with the *in vivo* observations for both pairwise comparisons. On the other hand, simulated and observed AUC TNBE/R geometric mean ratios differed, likely due to the lack of propagating clearance-related IOV to the simulations. This approach is in line with modern regulatory initiatives that advocate leveraging quantitative methods and modeling to modernize generic drug development and review.

KEY WORDS: bioequivalence; *in vitro-in vivo* extrapolation; physiology-based pharmacokinetics; quantitative methods; regulatory sciences.

INTRODUCTION

Most of the new chemical entities that populate the development pipeline are characterized by a low aqueous solubility (categorized as a Biopharmaceutics Classification System (BCS) class 2 or 4 drugs) which leads to challenges towards their intestinal absorption (1,2). Absorption-related parameters of poorly water-soluble drugs may change randomly between subjects (*i.e.*, interindividual variability; IIV) and study occasions (*i.e.*, interoccasion

variability; IOV) due to the highly variable conditions within the human gastrointestinal (GI) tract (3). Consequently, demonstrating bioequivalence (BE) between formulations containing these drugs may be challenging. BE studies are an integral part of biopharmaceutics and clinical pharmacology strategy for drug product development programs among generic and innovator companies (4–6). In the generic pharmaceutical industry, BE studies account for a significant share of the overall development costs.

Traditionally, the sample size of BE studies is based on a power calculation based on the within-subject variability and the test (T)/reference (R) ratio of the BE metrics. Since the exact value of the T/R ratio is generally not known prior to the pivotal BE trial, it is often assumed that the difference between the treatments does not exceed 5% (7). The greater the difference between T and R formulations is, the higher the sample size will be required (7) and, obviously, the higher will be the associated costs and the risks of failing the bioequivalence criteria. Preliminary small-scale, relative bioavailability studies are currently the gold standard to prospect the *in vivo* behavior of new formulations. However, pilot BE studies are costly and translatability issues are not uncommon. For example, Moreno and co-workers reported that approximately 50% of the simulated T/R ratio for C_{\max} in

Ioannis Loisos-Konstantinidis and Bart Hens are equal first authors

¹ Institute of Pharmaceutical Technology, Goethe University, Frankfurt am Main, Germany.

² Department of Pharmaceutical and Pharmacological Sciences, KU Leuven, Leuven, Belgium.

³ Clinical Pharmacology and Pharmacometrics, Janssen Pharmaceutical Companies of Johnson & Johnson, Horsham, Pennsylvania, USA.

⁴ Center for Pharmacometrics and Systems Pharmacology, Department of Pharmaceutics, College of Pharmacy, University of Florida, 6550 Sanger Road, Office 146, Orlando, Florida 32827, USA.

⁵ Institute of Mathematics and Statistics, University of Sao Paulo, Sao Paulo, Brazil.

⁶ To whom correspondence should be addressed. (e-mail: rcristofolletti@cop.ufl.edu)

small-resampled cohorts differed by more than 10% from T/R ratio observed in the respective pivotal trial (8).

In recent years, the emergence of physiologically based pharmacokinetics (PBPK) modeling platforms and biorelevant biopharmaceutics tools have shifted the regulatory paradigm, and consequently the drug product development workflow, towards quantitative modeling approaches (9). *In vitro-in vivo* extrapolation (IVIVE) of drug product performance via PBPK modeling has been advocated by academics, regulators and industry scientists (9). In this context, the virtual BE (VBE) concept gained traction and evolved from an academic nicety to a regulatory necessity, being listed among the research priorities of the Generic Drug User Fee Amendments to modernize generic drug development and review under the umbrella of model-informed drug development (10). Significant efforts on characterizing GI tract IIV (e.g., in terms of fluid volume and composition, intraluminal pH, transit time, etc.) have been carried out by different groups (11); however, IOV in GI parameters is much less understood. If IOV is simply omitted, as it has systematically happened in the past, and/or the selected system parameters are not indeed responsible for the major portion of variation in drug absorption between different occasions, predicted 90% confidence intervals (CIs) for BE metrics will be narrower than the observed ones, which may bias VBE-based decision-making (12). For example, VBE trials may predict positive BE outcomes that might be misleading due to not considering IOV (false positive).

In this context, the aim of this work was to develop and verify a quantitative BE risk assessment approach to inform the development of multi-source ibuprofen formulations. This stepwise approach integrated VBE trials to simulate the T/R ratio for positive and negative control formulations containing ibuprofen, approximated distribution of IOV on ibuprofen C_{\max} and AUC by bootstrapping resampling methods, *post hoc* incorporation of IOV to simulated T/R ratios and power curve analysis.

METHODS

Global Sensitivity Analysis

Global sensitivity analysis (GSA) techniques investigate the effects of simultaneous parameter variations over large (but finite) ranges and can account for the effects of interactions between parameters (13). Interactions in sensitivity analysis mean that the sensitivity of an output to a parameter may change according to the value of another parameter. The most relevant drug and system-related parameters namely intrinsic solubility, particle size, salt solubility, intestinal permeability, mean gastric residence time, initial gastric fluid volume, duodenum, jejunum and ileum microenvironments (pH and bicarbonate concentration) were chosen to understand their combined influence on ibuprofen rate of absorption simulated using a previously verified PBPK model (14). The GSA was carried out using the Morris method in the Simcyp® Simulator (Version 19, Release 1; Certara UK Limited). Briefly, the Morris method is a one-at-a-time method that starts by sampling a set of values within defined ranges for all input parameters and calculates the

corresponding model outcome. The second step changes the value of one parameter and calculates the resulting change in model outcome compared with the first run, which is repeated multiple times. A high μ^* (absolute mean) indicates a factor with an important overall influence on the model outputs whereas a high σ (standard deviation of μ^*) indicates either that the input parameter considered interacts with the others or that its effect is non-linear (15).

In Vitro Dissolution and *In Vivo* BE Data

In vitro dissolution and *in vivo* BE results used for this work have already been reported elsewhere (16). Both BE studies were conducted by certified contract research organizations that were inspected by the Brazilian Health Regulatory Agency to assess compliance with the Good Clinical and Good Laboratory Practices and the study protocols were approved by Independent Ethics Committees. Briefly, samples from two different generic ibuprofen suspension biobatches, a generic product (hereinafter referred to as test bioequivalent; TBE) and a drug product that failed the BE test (hereinafter referred to as test non-bioequivalent; TNBE), were kindly donated by the respective Brazilian generic manufacturers together with samples from the reference listed drug (R) used in the respective two-way, crossover BE studies in healthy adults under fasting conditions. The *in vitro* performance of the three ibuprofen 50 mg/mL oral suspensions was assessed using the USP 2 dissolution apparatus at 50 rpm with 500 mL of the revised fasted state simulated intestinal fluid (FaSSIF-V3) (17) with reduced phosphate buffer concentration (5 mM) at pH 6.7. This *in vitro* experimental condition was able to discriminate dissolution profiles of TBE, TNBE, and R (16). Table 1 shows the reported results of the two *in vivo* BE studies (point estimates and 90% confidence intervals) and the within-subject variability of the BE metrics (16).

PBPK Modeling

A stepwise modeling approach of the *in vitro* data, similar to Pathak and co-workers (18), was followed to mitigate identifiability issues when estimating solubility factor, intrinsic solubility, and particle size from *in vitro* experiments (19). This approach allows the combination of drug- and formulation-specific properties with GI variability, generating individualized intraluminal dissolution profiles, which is essential to inform virtual BE trials. Ibuprofen is a plastic-elastic material and thus subject to particle deformation during drug product manufacturing processes (20). Therefore, the particle size that will control dissolution rate *in vivo* is not necessarily the particle size measured in the raw material. Deformed particles (e.g., due to compression forces) bind or associate with one another, such that the effective surface area of the drug driving intraluminal dissolution might be smaller than the specific surface area measured for the drug substance (20). Hence, product-specific monodispersed particle radii for the R, TBE and TNBE were fitted to the respective *in vitro* dissolution profiles using the built-in semi-mechanistic diffusion layer model in the Simcyp® *In Vitro* data Analysis toolkit (SIVA® Version 3 Release 1; Certara UK Limited) (19). A hybrid minimization algorithm

Table I. Reported Results of the Two *In Vivo* BE Studies

Comparison	BE metrics	Geometric mean ratios (%)	90% Confidence intervals	Within-subject variability (%)	Reference
TBE <i>vs</i> R	C_{\max}	113.3	105.9–121.3	16.9	16
	AUC	105.9	102.0–109.9	9.2	16
TNBE <i>vs</i> R	C_{\max}	126.5	118.4–135.2	13.1	16
	AUC	121.3	116.0–126.7	8.7	16

combining the global search ability of the Genetic Algorithm with the local search strength of Hooke-Jeeves method was applied to ensure that the final estimates corresponded to the global minimum.

The Simcyp® Simulator (Version 19, Release 1; Certara UK Limited) with its Advanced Dissolution, Absorption and Metabolism (ADAM) model coupled with a previously verified full-body PBPK model able to recapitulate observed IIV in ibuprofen exposure was used to simulate the absorption and systemic exposure of ibuprofen released from the R, TBE and TNBE oral suspensions (14). Further details of the ibuprofen PBPK model, including development workflow and model verification, can be found elsewhere (21). The respective product-specific monodispersed particle radius estimated in SIVA® were used as inputs (*i.e.*, upper bound size) for the mechanistic particle population balance approach in Simcyp, which is derived from the population balance equations by Kolewe and co-workers (22), to describe particles' shrinkage as they dissolve and move to a different size bin. Table II lists the input parameters used for building the mechanistic absorption and disposition models of ibuprofen.

Verification of the updated PBPK model was carried out by comparing the simulated and observed mean extent and peak of exposure after oral administrations of R, TBE and TNBE formulations. Model adequacy was concluded if the prediction fold error for simulated mean AUC_{0-t} and C_{\max} values were below 1.25-fold of mean observed values. This criterion is more stringent than the previously proposed 1.5- and 2-fold error in drug pharmacokinetic parameters (24,25).

BE Risk Assessment

Virtual Bioequivalence Trials

When a crossover virtual bioequivalence (VBE) study is run in the Simcyp® simulator, the population is generated for the first period based on demographics, system and drug parameters and IIV for the selected population. Then, for the second period, the same generated individuals are used, unless IOV is applied to selected parameters. Even though the magnitude of differences in pharmacokinetics between occasions can be measured, the underlying mechanisms are generally not understood. In this context, we applied a stepwise risk assessment approach to inform VBE-based go/no go decision-making. First, we focused on isolating the formulation impact on rate and extent of drug absorption. IOV was not added to any system parameter, following the underlying assumption in BE studies, *i.e.*, clearance (CL) is assumed to be unchanged within the same individuals for a crossover design:

$$\frac{F_T}{F_R} = \frac{\frac{AUC_T \times Cl_T}{dose_T}}{\frac{AUC_R \times Cl_R}{dose_R}} = \frac{AUC_T \times Cl_T}{AUC_R \times Cl_R} = \frac{AUC_T}{AUC_R}$$

where F_T and F_R are the systemic fractions for the test (T) and reference (R) formulations, respectively, and AUC is the area under the systemic concentration-time curve.

The virtual individuals were chosen to closely replicate the cohort enrolled in the respective *in vivo* BE trials:

- TBE *versus* R: oral single doses of ibuprofen 200 mg were administered to 35 healthy adults under fasting conditions (18 men and 17 women; age range 18–50 years). Sampling schedule mimicked the respective *in vivo* BE study protocol, *i.e.*, 0, 0.17, 0.33, 0.5, 0.67, 0.83, 1, 1.25, 1.50, 1.75, 2, 2.33, 2.67, 3, 3.5, 4, 5, 6, 8, 10, and 12 h).
- TNBE *versus* R: oral single doses of ibuprofen 400 mg were administered to 23 healthy adults under fasting conditions (12 men and 11 women; age range 18–50 years). Sampling schedule mimicked the respective *in vivo* BE study protocol, *i.e.*, 0, 0.25, 0.5, 0.75, 1, 1.25, 1.50, 1.75, 2, 2.5, 3, 3.5, 4, 5, 6, 8, 12, and 14 h).

In order to capture the population variability, at least 10 trials were simulated for each pairwise comparison. The resulting T/R geometric mean ratios were compared to the observed ones and used in the subsequent steps of this BE risk assessment approach.

Bootstrap Distribution of IOV

Pragmatically, the within-subject variability from a two-way, crossover, oral BE study is composed of bioanalytical error, IOV due to drug product performance and IOV due to drug substance pharmacokinetics (*e.g.*, GI variability). Assuming negligible bioanalytical error for methods validated according to current regulatory guidelines, the within-subject variability would be a composite term lumping IOV due to drug substance pharmacokinetics and product performance, which will be hereinafter referred to as IOV. In fact, an apparent dissimilar IOV was observed between both available BE studies (*e.g.*, 17 *vs* 13% for C_{\max}) (16), suggesting a formulation effect on IOV. The influence of formulation on IOV magnitude was further investigated by applying a bootstrap resampling method with the purpose of approximating the sampling distribution of IOV for plasma C_{\max} and AUC. First, the sample function in R (version 3.6.0) (26) was used to generate 50 bootstrap samples per *in vivo* BE study.

Table II. Input Parameters for Ibuprofen PBPK Model Development and Verification

Parameters	Value	Reference/comments
Physicochemical & Blood Binding		
MW (g/mol)	206.27	(19)
$\log P_{o:w}$	3.23	(19)
pKa	4.5	(19)
Blood/plasma ratio	0.55	Predicted by Simcyp simulation toolbox
Fraction unbound in plasma	0.01	Predicted by Simcyp simulation toolbox
Absorption		
Model	ADAM	
$f_{u, gut}$	1.0	Predicted by Simcyp simulation toolbox
$P_{eff, human}$ ($\times 10^{-4}$ cm/s)	17.0	(19)
S_0 (mg/mL)	0.043	(14)
Solubility factor (SF)	79.0	(14)
Formulation type	IR suspension	
DLM particle handling model	Particle population balance	
Surface solubility options	Mechanistic surface pH model	
h_{eff} method	Fluid dynamics	
Type of dispersion	Monodispersed	
Mean particle size (min, max, bins)		
R	195.3 (0, 214.8, 50)	Estimated using the SIVA toolkit from (16)
T-BE	174.3 (0, 191.7, 50)	
T-NBE	150.8(0, 165.9, 50)	
Distribution		
Model	Full PBPK	
V_{ss} (L/kg)	0.093	Predicted by Method 2
K_p scalar	1	Default
Elimination		
Model	IV clearance	
Cl_{IV} (L/h) (%CV)	3.5 (30.0)	(23)

Briefly, for each BE study, samples were taken with replacement from each sequence group in the original data sets for C_{max} and AUC, generating 50 bootstrapped BE studies for each pairwise comparison, namely R vs TBE and R vs TNBE. Subsequently, a multiplicative model for the analyses of each of the 100 bootstrapped BE studies was applied in order to obtain the IOV for each bootstrap resample. The bootstrap 95% CI for IOV in terms of plasma AUC and C_{max} were calculated for both pairwise comparisons.

Power Curves

The power.TOST package in R (version 3.6.0) (26) was used to estimate the exact power of the two-one-sided t test (TOST) procedure for various study designs considering the bootstrapped IOV mean. Power curves showing the calculated power on the y -axis and the T/R ratios for BE metrics on the x -axis were built to assess the probability of incurring in type II error when considering the bootstrapped IOV and predicted C_{max} TBE/R and TNBE/R ratios.

RESULTS

Figure 1 highlights the qualitative ranking of the selected system-, drug- and formulation-dependent parameters according to their influence on ibuprofen C_{max} predicted by the verified PBPK model. Intrinsic solubility, solubility factor and

product-specific monodispersed particle size are drug- and formulation-dependent parameters, respectively, with an important overall influence on simulated ibuprofen C_{max} as well as seem to have high potential to interact with other inputs (high σ). For the system components, gastric emptying time and small intestine pH were the most influential input parameters.

Figure 2 shows the simulated cumulative *in vivo* dissolution profiles for the three studied formulations and regional distribution of the fraction of dose absorbed. Mean simulated C_{max} and AUC_{0-t} values were within 1.2-fold of the respective mean observed BE metrics for R, TBE and TNBE formulations (Table III). The final IVIVE-PBPK model was used in a stepwise risk assessment of failing BE criteria for the TBE and TNBE formulations. At this juncture, all absorption- and disposition-related parameters were assumed not to change with time, *i.e.*, IOV = 0, due to the limited understanding and data about the underlying physiological processes. In this scenario, differences between the predicted pharmacokinetic profiles in periods 1 and 2 for the same virtual subject can only be attributed to the formulation effect. In other words, each virtual subject would have exactly the same physiology on the two occasions, representing the most optimistic scenario in terms of the amplitude of the estimated 90% CI for the geometric mean ratio of BE metrics. Predicted geometric mean ratios for plasma AUC in both comparisons, TBE/R and TNBE/R, were close to 1.0, resulting in bioequivalent conclusions for AUC in all VBE trials (data not shown).

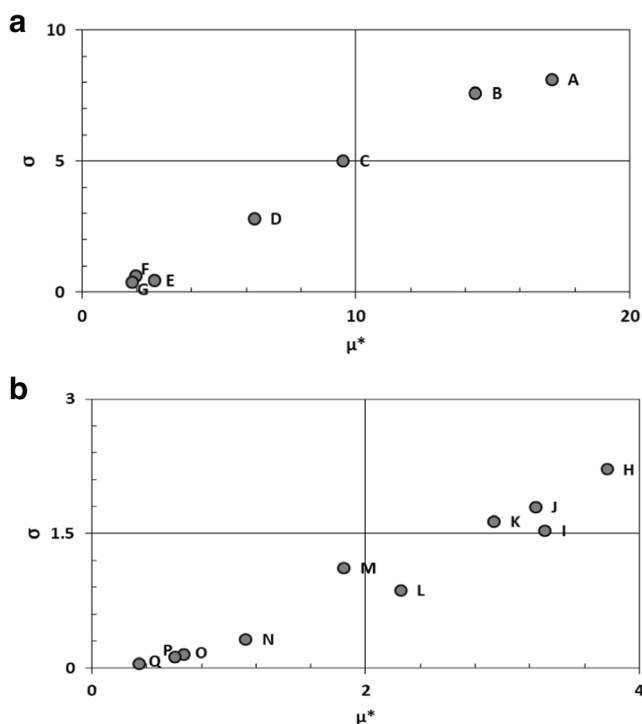


Fig. 1. GSA of drug (a) and system-dependent (b) parameters of the PBPK model on plasma C_{max} following oral administration of 400 mg ibuprofen to healthy adults under fasting conditions. A = particle radius; B = intrinsic solubility; C = solubility factor; D = CL_{iv} ; E = precipitation rate; F = ibuprofen pK_a ; G = supersaturation ratio; H = gastric emptying time; I = pH jejunum 1; J = pH duodenum; K = pH jejunum 2; L = bicarbonate pK_a ; M = pH ileum 1; N = bicarbonate concentration in jejunum 1; O = initial fluid volume in stomach; P = bicarbonate concentration in duodenum and Q = bicarbonate concentration in jejunum 2

On the other hand, predicted ratios of geometric means for C_{max} ranged from 1.04 to 1.06 for TBE vs R whereas it ranged from 1.10 to 1.15 for TNBE vs R (Fig. 3). *Post hoc* incorporation of observed within-subject error to the predicted geometric mean ratios for C_{max} resulted in bioequivalent and non-bioequivalent conclusions for the comparisons TBE vs R and TNBE vs R, respectively (Table IV).

The bootstrap resampling was applied to explore how the estimated IOV might vary in the population. Founded on the law of large numbers, the empirical distribution calculated using the bootstrap principle is expected to approximate the density of the true distribution for the statistics in the population. The resulting bootstrap 95% CI for the IOV calculated for each pairwise comparison, namely R vs TBE and R vs TNBE, in terms of plasma AUC (*i.e.*, 7.6–11.5% vs 6.2–13%) and C_{max} (*i.e.*, 13.8 vs 20% vs 10.8–19%) overlapped. This suggests that variability due to drug substance pharmacokinetics may be the dominant element in the net IOV for ibuprofen C_{max} and AUC. Figure 4 shows power curves for sample sizes of 24, 36, and 120 subjects assuming the most critical IOV scenario (20%) resulting from the bootstrap 95% CI. The power of any test of statistical significance is defined as the probability that it will reject a false null hypothesis (H_0) correctly and is the complementary probability of making a type II error (*i.e.*, not rejecting H_0 when it is false). As per the power curve, an acceptable type

II error level for the TNBE vs R comparison would be safely achieved only at the expenses of enrolling at least 120 healthy subjects in the *in vivo* study (Fig. 4).

DISCUSSION

A GSA was carried out to study how the uncertainty in the predicted rate of ibuprofen absorption, using C_{max} as a surrogate, can be apportioned to different sources of uncertainty in the model input. The Morris method was used to identify system-, drug-, and formulation-related inputs having large non-linear and/or interaction effect on ibuprofen C_{max} (*i.e.*, high μ^* and high σ values). Given the sensitivity of ibuprofen C_{max} to particle size, intrinsic solubility and solubility factor, we applied a mechanistic, stepwise modeling framework to leverage available experimental data, reduce uncertainty and estimate unknown parameters (*i.e.*, product-specific particle size). Furthermore, the impact of gastric emptying time and small intestine pH on ibuprofen C_{max} highlight the necessity of capturing the interplay between drug properties and GI variability to describe individual intraluminal dissolution profiles. Therefore, modeling *in vitro* dissolution profiles, rather than directly inputting experimental dissolution data (tabulated % dissolved vs time), is needed to inform population-based VBE trials.

An integrated IVIVE-PBPK model was used to translate the discriminative *in vitro* dissolution profiles reported for TBE (positive control), TNBE (negative control) and R formulations (16) into the respective plasma concentration-time profiles. The prediction fold errors for simulated AUC_{0-t} and C_{max} were less than 1.2-fold of the respective mean observed values (Table III). The simulated IIV of ibuprofen AUC (*i.e.*, 30–33%) can be traced back to ibuprofen CL variability. In the model, CL variability was set at 30% as reported by Martin and co-workers after intravascular administration of ibuprofen solution (23). Furthermore, simulated IIV of ibuprofen C_{max} did not differ among the three studied formulations (*i.e.*, 20–22%), being also rather similar to the reported IIV *in vivo* after oral administration of different immediate release formulations containing ibuprofen under fasting conditions (27). Therefore, IIV of ibuprofen exposure metrics seem to be mainly due to drug substance characteristics influencing variability in drug product rate and/or extent of absorption.

To explore the hypothesis of drug product formulation contributing to the IOV of ibuprofen exposure metrics we compared the approximated distributions of IOV estimated for each pairwise comparison using a bootstrap resampling method. The overlapping between the bootstrapped 95% CIs for the IOV calculated for the studies comparing different formulations (*i.e.*, TBE vs R and TNBE vs R) and the low variability observed in the discriminative *in vitro* dissolution test (16) suggest that variability due to drug substance pharmacokinetics also seems to be the dominant element in the net IOV of ibuprofen C_{max} and AUC. This is in line with the population pharmacokinetic analysis reported by Troconiz and co-workers, who showed that CL was the only pharmacokinetic parameter showing IOV (approximately 20%) (28). Therefore, since ibuprofen does not seem to exhibit absorption-related IOV in exposure, a simple *post hoc*

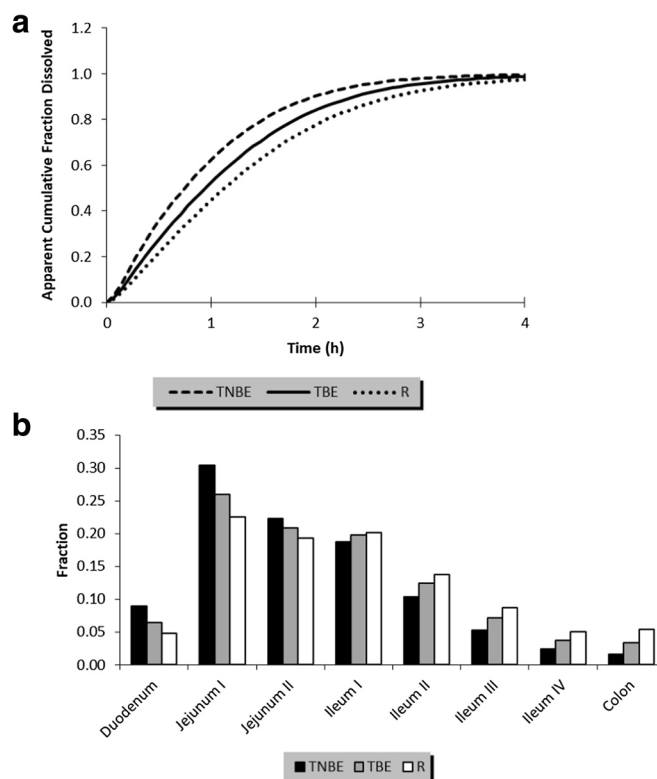


Fig. 2. Simulated ibuprofen cumulative *in vivo* dissolution profiles (a) and regional distribution of the fraction of dose absorbed (b)

incorporation of IOV to the T/R geometric mean ratios was deemed acceptable to inform VBE trials.

The verified IVIVE-PBPK model was utilized to inform ten crossover VBE trials, assuming no IOV, for each pairwise comparison. This approach aimed to estimate the respective T/R geometric mean ratios isolating the formulation impact on rate and extent of ibuprofen absorption. Similar dissolution profiles reported for R and TBE formulations (*i.e.*, $f_2 \approx 53$) (16) were translated into C_{\max} TBE/R geometric mean ratios in the range of 1.04–1.06 whereas non-similar dissolution profiles reported for R and TNBE formulations (*i.e.*, $f_2 \approx 38$) (16) derived C_{\max} TNBE/R geometric mean ratios of 1.10–1.15. After *post hoc* incorporation of the bootstrapped IOV to the simulated C_{\max} T/R geometric mean ratios, the resulting 90% CIs overlapped with the *in vivo* observations for both pairwise comparisons (Tables I and IV). All ten VBE trials comparing TBE vs R and TNBE vs R resulted

bioequivalent and non-bioequivalent, respectively, confirming the predictive capacity of the model-based VBE approach to anticipate the BE outcomes for drug products containing ibuprofen. On the other hand, simulated and observed AUC TNBE/R geometric mean ratios differed significantly, *i.e.*, 1.01 vs 1.21, and the model was not able to recapitulate the non-bioequivalent result in terms of AUC observed in the *in vivo* BE study comparing TNBE vs R. Interestingly, ibuprofen C_{\max} , but not AUC, has been reported to be sensitive to drug product dissolution rate (27,29). A published meta-analysis revealed that 14 out of 25 adequately powered BE studies comparing immediate release formulations containing ibuprofen failed to meet BE criteria for C_{\max} , but resulted bioequivalent for AUC (30). Given the high permeability observed for ibuprofen throughout different small intestine segments and colon and the complete *in vitro* dissolution for TNBE and R formulations (16,31), it is highly unlikely that the observed non-bioequivalent result for AUC be due to absorption-related issues. Furthermore, ibuprofen is rapidly absorbed after oral administration (oral absolute bioavailability was 96.5%) and is not subject to significant first-pass metabolism (32). Consequently, it is highly unlikely that observed differences in AUC when comparing TNBE vs R be due to differences in first-pass effect for example if the compared products had delivered different intraluminal profiles. Therefore, the mismatch between *in silico* and *in vivo* results for AUC may be explained by the lack of propagating CL-related IOV to the simulations (28). This was out of the scope of this manuscript, which was designed to explore absorption-related factors affecting BE.

Table III. Model Verification-mean Predicted and Observed BE Metrics

Formulation	C_{\max} (mg/L)			AUC (mg/L/h)		
	Pred	Obs	Pred/Obs	Pred	Obs	Pred/Obs
TBE 200 mg	14.5	16.6	0.87	59.1	66.4	0.89
R 200 mg	13.6	13.4	1.01	59.0	62.9	0.94
TNBE 400 mg	31.2	29.6	1.05	118.4	127.5	0.93
R 400 mg	26.6	22.9	1.16	118.0	107.8	1.09

Pred predicted, *Obs* observed

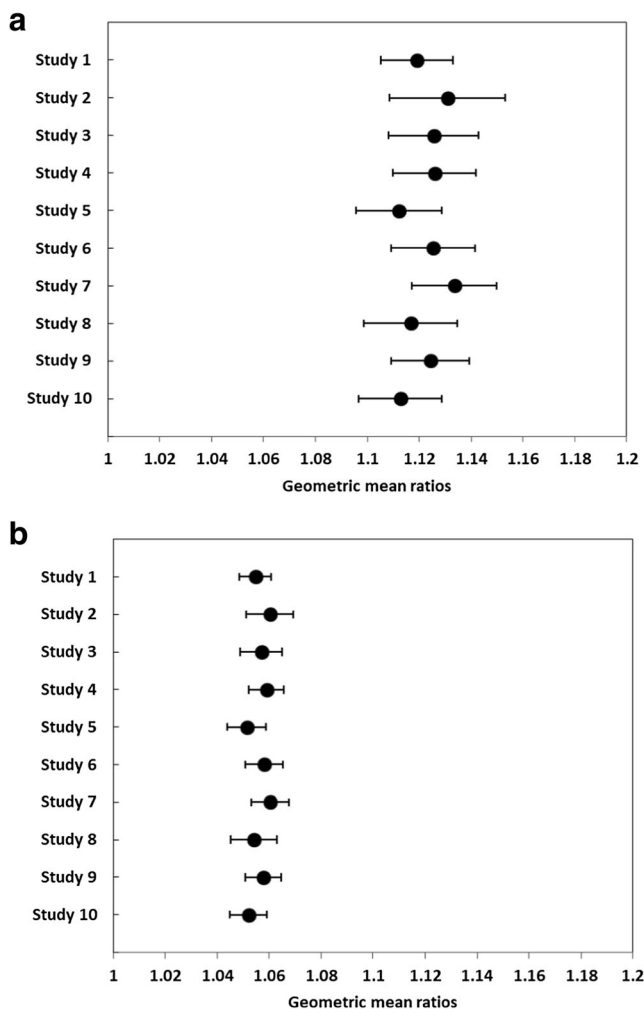


Fig. 3. Predicted plasma C_{max} TNBE/R (a) and TBE/R (b) without adding IOV to any system parameter. Closed symbols represent geometric mean ratios for the BE metrics and horizontal bars represent the respective 90% CIs

The upper limit of the bootstrapped 95% CI for the IOV (approximately 20%), which is similar to the reported IOV for ibuprofen CL, was used to generate power curves to assess the risks of failing to meet the BE criteria due to inflated type II error for different sample sizes and T/R ratios. For example, carrying out a 24-subject BE study to compare TBE and R formulations would result in an acceptable type II error level whereas

the producer’s risk (*i.e.*, probability of erroneously failing to reject the null hypothesis of inequivalence) would be significantly inflated when comparing TNBE vs R in the same experimental design (*i.e.*, the probability of type II error ranges from 40 to 80%; type II error = 1 - power). In other words, up to four out of five 24-subject BE studies comparing TNBE vs R would fail just by chance since the study becomes inconclusive due to insufficient information in the data to distinguish between equivalence and nonequivalence scenarios, which poses ethical challenges to researchers carrying out such a project. In fact, only 2% of the approved generics within the US jurisdiction showed the ratios of geometric means for BE metrics falling outside the range from 0.9 to 1.1 (33). Carrying out VBE trials might be useful to support project go/no-go decisions. For example, by taking the estimated market share for the generic candidate, ethical and economical costs required to carry out a BE study enrolling a certain number of subjects, decision-makers responsible for drug product development would be able to make better-informed decisions. This is in line with modern regulatory initiatives that advocate leveraging quantitative methods and modeling to modernize generic drug development and review (34–37).

CONCLUSION

The design and the application of VBE studies as performed in this manuscript can create a scientific framework of a roadmap to streamline drug products development. Translating *in vitro* results obtained under biorelevant conditions into systemic exposure via IVIVE-PBPK modeling has the potential to guide quantitative BE risk assessments and better inform decision-makers in charge of drug product development. Also, accurate estimation of T/R ratios for BE metrics in lieu of assuming a fixed 5% difference between treatments may avoid *in vivo* BE studies fated to fail, which is in line with important principles stated in ethical guidelines (*i.e.*, social and clinical value as well as scientific validity).

Future studies combining qualitative and quantitative GSA methods to map out major sources of variability in systemic drug exposure, and top-down analysis of replicate BE studies for different drugs are necessary to decompose IOV among the contributing system parameters. This will add an extra layer of confidence in VBE trials and foster its application to modernize drug product development and regulatory decisions.

ACKNOWLEDGMENTS

The authors thank Simcyp® Limited for providing an academic license of the Simcyp® Simulator v18.2 and 19.1 as well as the license of the SIVA® toolkit v3 to the Center for Pharmacometrics and Systems Pharmacology, University of Florida without charge. Bart Hens acknowledges the Flemish Research Council (FWO: applicant number 12R2119N). Ioannis Loiosos-Konstantinidis would like to thank the European Union’s Horizon 2020 Research and Innovation Program under grant agreement No 674909 (PEARLL).

Table IV. Estimated 90% CI Around Predicted C_{max} Geometric Mean Ratios After *Post Hoc* Incorporation of Bootstrapped IOV

Comparisons	Geometric mean ratios	90% CI
Lowest predicted TBE/R C _{max}	1.04	0.88–1.20
Highest predicted TBE/R C _{max}	1.06	0.90–1.22
Lowest predicted TNBE/R C _{max}	1.10	0.94–1.26
Highest predicted TNBE/R C _{max}	1.15	0.99–1.31

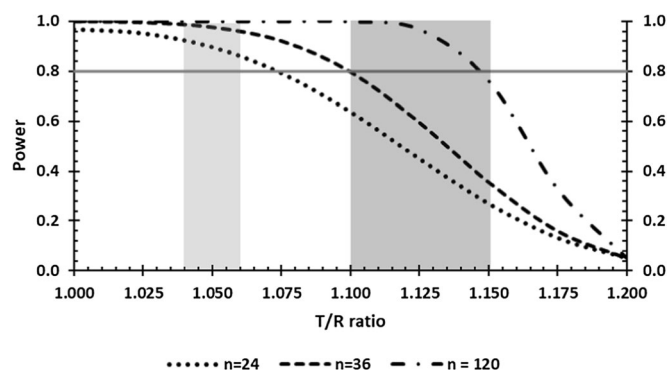


Fig. 4. Power curve for the two one-sided test procedure with IOV of 20%. Horizontal gray line represents the a priori 80% power recommended in regulatory guidelines for sample size estimation in average BE studies. Shaded areas represent the predicted maximum and minimum values for C_{\max} TBE/R (light gray) and TNBE/R (dark gray) in the ten virtual trials

AUTHORS' CONTRIBUTIONS

I.L.K., B.H., A.M., S.K., C.C., and R.C. wrote the manuscript; R.C. designed the research; I.L.K., B.H. and R.C. performed the research; I.L.K., B.H., S.K., C.C., and R.C. analyzed the data.

FUNDING INFORMATION

No funding was received for this research.

COMPLIANCE WITH ETHICAL STANDARDS

Conflict of Interest The authors declare that they have no conflict of interest.

REFERENCES

- Amidon GL, Lennernäs H, Shah VP, Crison JR. Theoretical basis for a biopharmaceutical drug classification: the correlation of in vitro drug product dissolution and in vivo bioavailability. *Pharm Res.* 1995;12:413–20.
- Loftsson T, Brewster ME. Pharmaceutical applications of cyclodextrins: basic science and product development. *J Pharm Pharmacol.* 2010;62:1607–21.
- Grimm M, Koziolok M, Kühn JP, Weitschies W. Interindividual and intraindividual variability of fasted state gastric fluid volume and gastric emptying of water. *Eur J Pharm Biopharm.* 2018;127:309–17.
- U.S. Food & Drug Administration (FDA). Bioequivalence studies with pharmacokinetic endpoints for drugs submitted under an ANDA — Guidance for Industry. 2013. <https://www.fda.gov/files/drugs/published/Bioequivalence-Studies-With-Pharmacokinetic-Endpoints-for-Drugs-Submitted-Under-an-Abbreviated-New-Drug-Application.pdf>. Accessed 03 March 2020.
- U.S. Food & Drug Administration (FDA). Guidance for Industry SUPAC-MR: modified release solid oral dosage forms scale-up and postapproval changes: Chemistry, Manufacturing, and Controls; In Vitro Dissolution Testing and In Vivo Bioequivalence Documentation. 1997. <https://www.fda.gov/regulatory-information/search-fda-guidance-documents/supac-mr-modified-release-solid-oral-dosage-forms-scale-and-postapproval-changes-chemistry>. Accessed 03 March 2020.
- European Medicines Agency (EMA). Guideline On The Investigation of Bioequivalence. 2010. https://www.ema.europa.eu/en/documents/scientific-guideline/guideline-investigation-bioequivalence-rev1_en.pdf. Accessed 03 March 2020.
- U.S. Food & Drug Administration (FDA). Statistical approaches to establishing bioequivalence. 2001. <https://www.fda.gov/media/70958/download>. Accessed 19 June 2020.
- Moreno I, Ochoa D, Román M, Cabaleiro T, Abad-Santos F. Utility of pilot studies for predicting ratios and intrasubject variability in high-variability drugs. *Basic Clin Pharmacol Toxicol.* 2016;119:215–21.
- Heimbach T, Suarez-Sharp S, Kakhi M, Holmstock N, Olivares-Morales A, Pepin X, *et al.* Dissolution and translational modeling strategies toward establishing an in vitro-in vivo link-a workshop summary report. *AAPS J.* 2019;21(2):29.
- Fang L, Kim MJ, Li Z, Wang Y, DiLiberti CE, Au J, *et al.* Model-informed drug development and review for generic products: summary of FDA public workshop. *Clin Pharmacol Ther.* 2018;104:27–30.
- Butler J, Hens B, Vertzoni M, Brouwers J, Berben P, Dressman J, *et al.* In vitro models for the prediction of in vivo performance of oral dosage forms: recent progress from partnership through the IMI OrBiTo collaboration. *Eur J Pharm Biopharm.* 2019;136:70–83.
- Loisios-Konstantinidis I, Cristofolletti R, Fotaki N, Turner DB, Dressman J. Establishing virtual bioequivalence and clinically relevant specifications using in vitro biorelevant dissolution testing and physiologically-based population pharmacokinetic modeling. case example: Naproxen. *Eur J Pharm Sci.* 2020. <https://doi.org/10.1016/j.ejps.2019.105170>.
- Sumner T, *et al.* Methodology for global-sensitivity analysis of time-dependent outputs in systems biology modelling. *J R Soc Interface.* 2012;9:2156–66.
- Cristofolletti R, Dressman JB. Bridging the gap between in vitro dissolution and the time course of ibuprofen-mediating pain relief. *J Pharm Sci.* 2016;105(12):3658–67.
- Morris MD. Factorial sampling plans for preliminary computational experiments. *Technometrics.* 1999;33(2):161–74.
- Cristofolletti R, Dressman JB. FaSSIF-V3, but not compendial media, appropriately detects differences in the peak and extent of exposure between reference and test formulations of ibuprofen. *Eur J Pharm Biopharm.* 2016;105:134–40.

17. Fuchs A, Leigh M, Kloefer B, Dressman JB. Advances in the design of fasted state simulating intestinal fluids: FaSSIF-V3. *Eur J Pharm Biopharm.* 2015;94:229–40.
18. Pathak SM, Ruff A, Kostewicz ES, Patel N, Turner DB, Jamei M. Model-based analysis of biopharmaceutical experiments to improve mechanistic oral absorption modeling: an integrated in vitro in vivo extrapolation perspective using ketoconazole as a model drug. *Mol Pharm.* 2017;14:4305–20.
19. Cristofolletti R, Hens B, Patel N, Esteban VV, Schmidt S, Dressman J. Integrating drug- and formulation-related properties with gastrointestinal tract variability using a product-specific particle size approach: case example ibuprofen. *J Pharm Sci.* 2019;108:3842–7.
20. Le VNP, *et al.* Influence of granulation and compaction on the particle size of ibuprofen—development of a size analysis method. *Int J Pharm.* 2006;321:72–7.
21. Jamei M, Marciniak S, Feng K, Barnett A, Tucker G, Rostami-Hodjegan A. The Simcyp population-based ADME simulator. *Expert Opin Drug Metab Toxicol.* 2009;5:211–23.
22. Kolewe ME, Roberts SC, Henson MA. A population balance equation model of aggregation dynamics in *Taxus* suspension cell cultures. *Biotechnol Bioeng.* 2012;109:472–82.
23. Martin W, Koselowske G, Töberich H, Kerkmann T, Mangold B, Augustin J. Pharmacokinetics and absolute bioavailability of ibuprofen after oral administration of ibuprofen lysine in man. *Biopharm Drug Dispos.* 1990;11(3):265–78.
24. Abduljalil K, Cain T, Humphries H, Rostami-Hodjegan A. Deciding on success criteria for predictability of pharmacokinetic parameters from in vitro studies: an analysis based on in vivo observations. *Drug Metab Dispos.* 2014;42(9):1478–84.
25. Guest EJ, Aarons L, Houston JB, Rostami-Hodjegan A, Galetin A. Critique of the two-fold measure of prediction success for ratios: application for the assessment of drug-drug interactions. *Drug Metab Dispos.* 2011;39(2):170–3.
26. R Core Team. R: A language and environment for statistical computing. 2019. <https://www.R-project.org/>. Accessed 03 March 2020.
27. Legg TJ, Laurent AL, Leyva R, Kellstein D. Ibuprofen sodium is absorbed faster than standard ibuprofen tablets: results of two open-label, randomized, crossover pharmacokinetic studies. *Drugs R D.* 2014;14(4):283–90.
28. Troconiz IF, Armenteros S, Planelles MV, Benitez J, Calvos R, Dominguez R. Pharmacokinetic-pharmacodynamic modelling of the antipyretic effect of two oral formulations of ibuprofen. *Clin Pharmacokinet.* 2001;38(6):505–18.
29. Sugano K, Terada K. Rate- and extent-limiting factors of oral drug absorption: theory and applications. *J Pharm Sci.* 2015;104(9):2777–88.
30. Blume H, Mutschler E. Bioäquivalenz, Qualitätsbewertung wirkstoffgleicher Fertigarzneimittel, Teil I/II, Isosorbiddinitrat 6. Ergänzungslieferung, Govi-Verlag Pharmazeutischer Verlag, Frankfurt/Main-Eschborn; 1996.
31. Lozoya-Agullo I, Araújo F, González-Álvarez I, Merino-Sanjuán M, González-Álvarez M, Bermejo M, *et al.* PLGA nanoparticles are effective to control the colonic release and absorption on ibuprofen. *Eur J Pharm Sci.* 2018;115:119–25.
32. Atkinson HC, Stanescu I, Frampton C, Salem II, Beasley CPH, Robson R. Pharmacokinetics and bioavailability of a fixed-dose combination of ibuprofen and paracetamol after intravenous and Oral administration. *Clin Drug Investig.* 2015;35:625–32.
33. Davit BM, Nwakama PE, Buehler GJ, Conner DP, Haidar SH, Patel DT, *et al.* Comparing generic and innovator drugs: a review of 12 years of bioequivalence data from the United States Food and Drug Administration. *Ann Pharmacother.* 2009;43:1583–97.
34. Mitra A. Maximizing the role of physiologically based Oral absorption modeling in generic drug development. *Clin Pharmacol Ther.* 2019;105:307–9.
35. Lionberger RA. Innovation for generic drugs: science and research under the generic drug user fee amendments of 2012. *Clin Pharmacol Ther.* 2019;105:878–85.
36. Lionberger RA. Decision science for generic drug development and review. *J Clin Pharmacol.* 2019;59:1249–51.
37. Manolis E, Musuamba FT, Karlsson KE. Regulatory considerations for building an in silico clinical pharmacology backbone by 2030. *Clin Pharmacol Ther.* 2020;107:746–8. <https://doi.org/10.1002/cpt.1772>.

Publisher's Note Springer Nature remains neutral with regard to jurisdictional claims in published maps and institutional affiliations.

Article

Physiologically Based Pharmacokinetic/Pharmacodynamic Modeling to Predict the Impact of CYP2C9 Genetic Polymorphisms, Co-Medication and Formulation on the Pharmacokinetics and Pharmacodynamics of Flurbiprofen

Ioannis Loisios-Konstantinidis ¹, Rodrigo Cristofolletti ², Masoud Jamei ³, David Turner ³ and Jennifer Dressman ^{1,4,*}

¹ Institute of Pharmaceutical Technology, Goethe University, Max-von-Laue str. 9, 60438 Frankfurt am Main, Germany; loisios-konstantinidis@em.uni-frankfurt.de

² Center for Pharmacometrics and Systems Pharmacology, Department of Pharmaceutics, College of Pharmacy, University of Florida, Orlando, FL 32827, USA; rcristofolletti@cop.ufl.edu

³ Certara UK Limited, Simcyp Division, 1 Concourse Way, Sheffield S1 2BJ, UK; masoud.jamei@certara.com (M.J.); david.turner@certara.com (D.T.)

⁴ Fraunhofer Institute of Translational Pharmacology and Medicine (ITMP), Carl-von-Noorden Platz 9, 60596 Frankfurt am Main, Germany

* Correspondence: dressman@em.uni-frankfurt.de

Received: 12 October 2020; Accepted: 26 October 2020; Published: 2 November 2020



Abstract: Physiologically based pharmacokinetic/pharmacodynamic (PBPK/PD) models can serve as a powerful framework for predicting the influence as well as the interaction of formulation, genetic polymorphism and co-medication on the pharmacokinetics and pharmacodynamics of drug substances. In this study, flurbiprofen, a potent non-steroid anti-inflammatory drug, was chosen as a model drug. Flurbiprofen has absolute bioavailability of ~95% and linear pharmacokinetics in the dose range of 50–300 mg. Its absorption is considered variable and complex, often associated with double peak phenomena, and its pharmacokinetics are characterized by high inter-subject variability, mainly due to its metabolism by the polymorphic CYP2C9 ($f_m\text{CYP2C9} \geq 0.71$). In this study, by leveraging *in vitro*, *in silico* and *in vivo* data, an integrated PBPK/PD model with mechanistic absorption was developed and evaluated against clinical data from PK, PD, drug-drug and gene-drug interaction studies. The PBPK model successfully predicted (within 2-fold) 36 out of 38 observed concentration-time profiles of flurbiprofen as well as the CYP2C9 genetic effects after administration of different intravenous and oral dosage forms over a dose range of 40–300 mg in both Caucasian and Chinese healthy volunteers. All model predictions for C_{\max} , AUC_{inf} and CL/F were within two-fold of their respective mean or geometric mean values, while 90% of the predictions of C_{\max} , 81% of the predictions of AUC_{inf} and 74% of the predictions of CL/F were within 1.25 fold. In addition, the drug-drug and drug-gene interactions were predicted within 1.5-fold of the observed interaction ratios (AUC , C_{\max} ratios). The validated PBPK model was further expanded by linking it to an inhibitory E_{\max} model describing the analgesic efficacy of flurbiprofen and applying it to explore the effect of formulation and genetic polymorphisms on the onset and duration of pain relief. This comprehensive PBPK/PD analysis, along with a detailed translational biopharmaceutic framework including appropriately designed biorelevant *in vitro* experiments and *in vitro-in vivo* extrapolation, provided mechanistic insight on the impact of formulation and genetic variations, two major determinants of the population variability, on the PK/PD of flurbiprofen. Clinically relevant specifications and potential dose adjustments were also proposed. Overall, the present work highlights the value of a translational PBPK/PD approach, tailored to target populations and genotypes, as an approach towards achieving personalized medicine.

Keywords: physiologically based pharmacokinetic (PBPK) modeling; pharmacokinetics/pharmacodynamics (PK/PD); *in vitro in vivo* extrapolation (IVIVE); mechanistic oral absorption modeling; drug–drug interaction (DDI); pharmacogenetics

1. Introduction

Intrinsic and extrinsic patient factors (IEFs) such as dosage form, co-medication, and genetic polymorphism may significantly impact drug exposure and subsequently lead to changes in the efficacy or safety of a drug. The ability to quantify such factors on the exposure and pharmacologic action of a drug would represent a milestone in determining required dose adjustments and implementation of risk management strategies. Under the prism of model-informed drug discovery and development (MID3), dynamic mechanistic models such as whole body physiologically based pharmacokinetic/pharmacodynamic (PBPK/PD) models may be useful for forecasting the influence as well as the interaction of multiple factors on pharmacokinetics (PK) and pharmacodynamics (PD), and as a result could be used to guide formulation selection and clinical dosing recommendations.

Flurbiprofen (FLU) is a potent non-steroid anti-inflammatory drug (NSAID) that has been used as the racemate for the symptomatic treatment of rheumatoid arthritis and osteoarthritis. FLU is a typical acidic representative of class II of the Biopharmaceutics Classification System (BCS), exhibiting very poor solubility in gastric conditions, but high solubility and permeability in the small intestine. FLU is entirely absorbed from the small intestine with a fraction absorbed (f_a) typically greater than 95%, while its absolute bioavailability ranges between 92% and 96% [1]. Even though it is almost completely absorbed, the intestinal absorption of FLU is considered complex and variable, since it is often associated with double peak phenomena and high inter-individual variability in plasma concentrations (up to 80–100%) [1–3]. The clinical PK of FLU is stereo-selective, with only the S-enantiomer being pharmacological active, and is linear in the dose range of 50–300 mg. Similar to most NSAIDs, it is highly bound (>99%) to plasma proteins, with a steady-state volume of distribution (V_{ss}) of around 0.1 L/kg [1,4,5]. FLU is mainly eliminated by oxidative metabolism in the liver by the cytochrome P450 (CYP) 2C9 to its major metabolite, 4-hydroxy flurbiprofen (4-OH FLU). CYP2C9 metabolic contribution is at least 71% and FLU has been identified as a probe drug for CYP2C9 activity. Further type II biotransformation reactions, such as glucuronidation, are mediated through UGT2B7 and UGT1A9.

CYP2C9 is a polymorphic enzyme, with more than 50 single nucleotide polymorphisms (SNPs) described in the regulatory and coding regions of the CYP2C9 gene. However, of those, only two coding SNPs, namely, CYP2C9*2 and CYP2C9*3, have shown to result in clinically relevant reductions in enzyme activity, while the CYP2C9*1 is the wild type variant [6]. The two afore-mentioned SNPs result in six different genotypes that confer three functionally different phenotypes: (a) extensive metabolizers (EM; CYP2C9*1/*1), (b) intermediate metabolizers (IM; CYP2C9*1/*2, CYP2C9*1/*3, and CYP2C9*2/*2), and poor metabolizers (PM; CYP2C9*2/*3 and CYP2C9*3/*3) [6–8]. Although the wild type variant is the most common allele of the CYP2C9 polymorphic family, the frequency of CYP2C9 genetic polymorphisms varies significantly among different ethnic populations [9–11]. Thus, increased FLU plasma exposure might be observed in subjects with different genotypes as well as after co-administration of CYP2C9 inhibitors.

PBPK modeling has been increasingly used in recent years for predictions of formulation effects, drug–drug interactions, and pharmacogenetics in drug development and to support regulatory decision-making [12–22]. A translational absorption PBPK/PD modeling approach is required in order to gain mechanistic insight into the effect of multiple intrinsic and extrinsic patient factors on the exposure and therapeutic response of a drug. For that purpose, we generated biorelevant *in vitro* data from multiple FLU formulations, and the biopharmaceutical parameters were then translated to *in vivo* dissolution and absorption scenarios. Leveraging *in vitro*, *in silico*, and *in vivo* data, we developed a comprehensive integrated PBPK/PD model and evaluated it against clinical PK/PD, pharmacogenetic

(PG), and drug–drug interaction studies. In summary, the aim of the present study was to evaluate the impact of formulation, genetic polymorphism, and co-medication on the pharmacokinetics and pharmacodynamics of FLU.

2. Materials and Methods

2.1. Chemicals and Reagents

FLU (lot #LRAA9230) pure active pharmaceutical ingredient (API) was purchased commercially from Sigma-Aldrich Co., LLC. (St. Louis, MO, USA). Three immediate release (IR) tablet formulations of FLU with qualitatively different compositions were selected for study: (a) 100 mg FLU United States Pharmacopoeia (USP film-coated tablets, lot 3077637; Mylan Pharmaceuticals Inc., Morgantown, WV, USA), (b) 100 mg Antadys (film-coated tablets, lot 8M824; Teva Sante, Paris, France), and (c) 100 mg Froben (sugar-coated tablets, lot 31257J4; BGP Products GmbH, Baar, Switzerland), purchased from the American, French, and Swiss markets, respectively. Fasted state-simulated gastric fluid (FaSSGF), fasted state-simulated intestinal fluid (FaSSIF V1), fed state-simulated intestinal fluid (FeSSIF V1) powder (lot 01-1512-05NP), and FaSSIF V3 powder (lot PHA S 1306023) were kindly donated from Biorelevant.com Ltd. (Surrey, United Kingdom). Acetonitrile (lot 18D181599) and water (lot 17B174006) of HPLC-grade were purchased from VWR Chemicals (Leuven, Belgium). Sodium hydroxide pellets (lot 14A100027), sodium chloride (lot 17I074122), sodium acetate (lot 14B240013), hydrochloric acid 37% (lot 10L060526), orthophosphoric acid 85% (lot 12K210017), and glacial acetic acid 100% (lot 12B220508) were obtained commercially from VWR Chemicals (Leuven, Belgium). Sodium dihydrogen phosphate dehydrate (lot K93701642712) and citric acid (lot K91221207425) were purchased from Merck KGaA (Darmstadt, Germany). Pepsin from porcine gastric mucosa 19.6% was obtained from Sigma-Aldrich Co., LLC.

2.2. In Vitro Solubility Experiments

The solubility of FLU was investigated in various aqueous and biorelevant dissolution media using the Uniprep system (Whatman, Piscataway, NJ, USA). All aqueous buffers were prepared according to the European Pharmacopoeia, while the biorelevant media were prepared according to Markopoulos et al. and Fuchs et al. [23,24]. An excess amount of API was added to 3 mL of dissolution medium and the samples were incubated for 24 h at 37 °C on an orbital mixer. The samples were then filtered through the 0.45 µm polytetrafluoroethylene (PTFE) filter integrated in the Uniprep system. The filtrate was immediately diluted with mobile phase and analyzed by high-performance liquid chromatography (HPLC) (see Section 2.5). All measurements were performed at least in triplicate ($n \geq 3$) and the final pH was recorded.

2.3. In Vitro Dissolution Tests

All dissolution tests were performed using a calibrated USP II (paddle) apparatus (Erweka DT 80, Heusenstamm, Germany) at 37 ± 0.4 °C. Each vessel contained 500 mL of fresh, pre-warmed medium and the rotational speed was set at 75 rpm. Samples were withdrawn at 2.5, 5, 10, 15, 20, 30, 45, 60, 90, and 120 min via a 5 mL glass syringe connected to a stainless-steel cannula containing a 10 µm polyethylene cannula filter. Immediately thereafter, the sample was filtered through a 0.45 µm PTFE filter (ReZist 30, GE Healthcare UK Ltd., Buckinghamshire, United Kingdom), discarding the first 2 mL. The filtrate was immediately diluted with mobile phase and analyzed by HPLC-UV (see Section 2.5). The removal of 5 mL at each sampling time was considered in the calculation of the percentage dissolved. All experiments were performed at least in triplicate ($n \geq 3$) and the final pH in the vessel was recorded.

2.4. Two-Stage Dissolution Test

Since the conventional one-stage USP II dissolution test does not include a gastric compartment to account for disintegration of the dosage form in the stomach, differences in the disintegration time between simple film-coated (i.e., 100 mg FLU USP and 100 mg Antadys) and sugar-coated formulations (i.e., 100 mg Froben) might bias the interpretation of the biorelevant *in vitro* dissolution behavior with respect to the *in vivo* performance. Hence, to investigate the disintegration effect on the *in vitro* performance of FLU formulations, we performed a two-stage dissolution test with FaSSIF V3 as the intestinal medium according to Loisos-Konstantinidis et al. [25]

The tested dosage forms were initially exposed to 250 mL of gastric medium (i.e., FaSSGF Levels I and III) and samples were removed at 5, 10, 15, 20, and 30 min and treated as described in Section 2.3. After the withdrawal of the last sample, we added 6.8 mL of sodium hydroxide 1M and immediately thereafter 250 mL of FaSSIF V3 concentrate pH = 6.7 (double concentration of all the constituents, apart from sodium hydroxide) to the vessel. Sodium hydroxide was added first, but almost simultaneously with FaSSIF V3. This was done to avoid using a very high pH in the FaSSIF V3 concentrate. After the pH shift, further samples were removed at 32.5, 35, 40, 45, 50, 60, and 90 min. The two-stage dissolution tests were performed using calibrated USP II (paddle) apparatus (Erweka DT 80, Heusenstamm, Germany) at 37 ± 0.4 °C and the samples were analyzed by HPLC-UV (see Section 2.5). All experiments were performed at least in triplicate ($n \geq 3$) and the final pH in the vessel was recorded.

2.5. Quantitative Analysis of Samples

Samples obtained from solubility and dissolution experiments were first filtered through a 0.45 µm PTFE filter (ReZist 30 syringe filter or Uniprep; Whatman, Piscataway, NJ, USA) and subsequently, after appropriate dilution with mobile phase, analyzed by HPLC-UV (Hitachi Chromaster; Hitachi Ltd., Tokyo, Japan or Spectra System HPLC, ThermoQuest Inc., San Jose, CA, USA). A BDS Hypersil C18, 5 µm, 150 × 4.6 mm (Thermo Scientific, Waltham, MA, United States) analytical column combined with a pre-column (BDS Hypersil C-18, 3µm, 10 × 4mm) was used. The mobile phase consisted of water adjusted to pH = 3.0 with trifluoroacetic acid (TFA) and acetonitrile (49.5:0.5:50% v/v). The detection wavelength was set at 247 nm, the flow rate at 1.0 mL/min, and the injection volume at 20 µL. Using this method, the retention time was approximately 6.8 min. The limit of detection (LOD) and quantification (LOQ) were 0.03 and 0.05 µg/mL, respectively.

2.6. Model-Based Analysis of In Vitro Solubility Data

An experimental estimate of FLU pK_a was obtained by fitting the Henderson–Hasselbalch equation (Equation (1)) to the mean aqueous equilibrium solubility (S_i) values using the SIVA Toolkit version 3.0 (SIVA 3; Certara, Simcyp Division; Sheffield, UK). The lowest reported value in buffers was assumed to represent the intrinsic solubility (S_0). The pK_a was then compared with values available in the literature to confirm the validity of the aqueous solubility parameter estimates.

$$S_i = S_0 \cdot (10^{pH - pK_a}) \quad (1)$$

The impact of bile salt concentration ($[BS]$) and subsequent formation of micelles on the solubility of FLU was investigated. This was achieved by mechanistically modelling the mean solubility values in fasted state biorelevant media ($n = 3$), accounting also for the relative proportions of FLU solubilized in the aqueous versus the micellar phases, using the total solubility ($S_{(BS)Tot}$) equation (Equation (2)) in SIVA 3.0. Estimates of the logarithm of the micelle-water partition coefficient for the neutral ($K_{m:w,unionized}$) and ionized drug ($K_{m:w,ionized}$) were obtained to quantify the micelle-mediated solubility.

$$S_{(BS)Tot} = \left([BS] \cdot \frac{S_0}{C_{H_2O}} \cdot K_{m:w,unionized} + S_0 \right) + \left([BS] \cdot \frac{S_i}{C_{H_2O}} \cdot K_{m:w,ionized} + S_i \right) \quad (2)$$

Estimation of the relevant parameters was performed using the Nelder–Mead algorithm with weighting by the reciprocal of the predicted values. All estimates based on the *in vitro* solubility data were used as *in silico* input parameters for the development of the physiologically based pharmacokinetic (PBPK) model.

2.7. Model-Based Analysis of In Vitro Dissolution Data

Once confidence in the estimation of solubility-related parameters was established, we performed further model-based analysis of the *in vitro* dissolution data obtained from both one and two-stage tests within the serial dilution module of the SIVA Toolkit (SIVA 3.0). The dissolution rate of spherical particles under sink and non-sink conditions within SIVA is described by an extension of the diffusion layer model (DLM) developed by Wang and Flanagan (Equation (3)) [26,27].

$$DR(t) = -N \cdot S_{DLM} \cdot \frac{D_{eff}}{h_{eff}(t)} \cdot 4\pi \cdot \alpha(t) \cdot (\alpha(t) + h_{eff}(t)) \cdot (S_{surface}(t) - C_{bulk}(t)) \quad (3)$$

where $DR(t)$ is the dissolution rate at time t , N is the number of particles in a given particle size bin, and S_{DLM} is a lumped correction scalar without regard to the mechanistic origin of the correction to the DLM. The S_{DLM} estimates obtained with SIVA can be applied to the Simcyp PBPK simulator to reflect differences between media or formulations by simulating the respective *in vivo* dissolution; D_{eff} is the effective diffusion coefficient; $h_{eff}(t)$ and $\alpha(t)$ represent the thickness of the hydrodynamic boundary layer and the particle radius at time t , respectively; $S_{surface}(t)$ corresponds to the saturation solubility at the particle surface (which may be different to the bulk fluid solubility, as discussed below); and $C_{bulk}(t)$ is the concentration of dissolved drug in bulk solution at time t .

The $h_{eff}(t)$ was calculated by the fluid dynamics sub-model, which enables the hydrodynamic conditions to be described according to local conditions and stirring rate. Fluid dynamics-based $h_{eff}(t)$ is the recommended option for describing the hydrodynamics, as it permits a more rational translation of estimated parameters such as the S_{DLM} to *in vivo* conditions, in which the hydrodynamics are usually quite different to *in vitro* experiments.

The local pH at the particle surface of ionizable drugs can significantly affect the $S_{surface}$ and consequently the dissolution rate [28–33]. Since the *in vitro* dissolution media have a somewhat higher buffer capacity than the intestinal fluids, the self-buffering effect at the solid surface can be underestimated. For this reason, the surface pH was calculated and directly input into SIVA. The calculation of the surface pH is based on the model first proposed by Mooney et al. [29], which assumes that dissolution is the result of both chemical reaction between the conjugate base of the buffer species and the hydrogen cations released from the dissolving drug (in this case FLU) at the liquid–solid interface and the diffusion of the dissolved particles to the bulk. This model is very similar to the quasi-equilibrium model published by Ozturk et al. [31], a derivative of which is implemented in SIVA as the default option for surface pH calculations.

By fitting the DLM model to the observed dissolution data, we obtained S_{DLM} estimates for each dissolution and two-stage test. In the case of two-stage testing, different S_{DLM} values were obtained for the gastric and intestinal compartments, accounting for the changes in the respective *in vitro* conditions. Under fasted state intestinal conditions, FLU is freely soluble and therefore dissolution is not expected to be solubility limited. In that case, disintegration of the solid dosage form in the intestinal dissolution medium might be the rate-limiting step for the *in vitro* dissolution rate, especially in single dissolution experiments where the dosage form is directly exposed to the intestinal medium without any pre-treatment in a gastric medium. When disintegration was considerably slower than dissolution, and thus had an impact on the overall dissolution rate, the first-order disintegration option was activated in SIVA and used to obtain estimates of a first-order disintegration rate constant (k_d) for those experiments. For the two-stage test experiments, the option was kept deactivated since disintegration in the stomach is already accounted for by the dissolution in the gastric medium. Both gastric and

intestinal phases of the two-stage results were modelled simultaneously using the serial dilution model, which can account for more than one *in vitro* dissolution condition in the same experiment.

Estimation of the relevant parameters was performed using the Nelder–Mead algorithm and equal weighting was applied. The various estimated S_{DLM} and k_d values were implemented in the Simcyp Simulator (V18.1; Certara, Sheffield, UK) to simulate various *in vivo* dissolution scenarios for the formulations under study and to generate *in vitro*–*in vivo* extrapolation relationships. These are necessary to predict the *in vivo* performance of the pure drug or formulation using PBPK modelling.

2.8. Clinical Studies

2.8.1. PBPK Development and Evaluation Studies

A total of 17 plasma concentration–time profiles from 10 clinical trials published in the open literature were used in support of the development and validation of the FLU physiologically based PBPK/PD model. Data after intravenous administration were obtained from Mei et al. [34]. In this crossover bioequivalence study, 24 healthy male Chinese subjects were administered a single dose (s.d.) of FLU axetil intravenously after an overnight fast.

Nine studies were performed after oral administration of a single dose of FLU at different dose levels and dosage forms in the fasted state. In the study by Gonzalez-Younes et al. [35], 12 Caucasian healthy, non-smoker males, aged between 25 and 31 years and weighing within 10% of their ideal body weight (BW) for height (BH), were administered 25 mL of oral solution containing 67.9 mg FLU in the fasted state. In a three-way three-treatment randomized crossover study, Szpunar et al. investigated the linearity of the pharmacokinetics of FLU [36]. In this study, 15 healthy subjects with mean (range) age of 29 (18–40) years old, and weight (range) and height (range) of 76.4 (62.3–109) and 177 (168–188) cm, respectively, were administered single oral doses of 100, 200, and 300 mg as immediate release (IR) tablets. Additionally, in a separate treatment, all participants received 40 mL of oral solution containing 100 mg FLU (2.5 mg/mL). In all treatments, all individuals received the medication at 7:00 a.m. with 180 mL water, after an overnight fast. In a pharmacokinetic study by Lee et al., 13 Korean male healthy volunteers, who had fasted overnight, received an oral solution of 40 mg from pre-dissolved Froben tablets [37]. The latter study also explored the effect CYP2C9-specific genotypes, CYP2C9 1*/1* (wild type) and 1*/3*, on the pharmacokinetics of FLU. Similarly, in the study by Lee et al., the differences in metabolism and pharmacokinetics among individuals with the CYP2C9 1*/1*, 1*/2*, and 1*/3* genotypes were investigated. A total of 15 (5 for each genotype), 8 female and 7 male, healthy Caucasian (one Hispanic) volunteers aged between 24 ± 5 years and weighing 79 ± 18 kg were administered a 50 mg FLU tablet after an overnight fast. As well as taking plasma samples, the researchers also collected pooled urine.

Several clinical studies after oral administration of FLU at its highest strength (100 mg) are available in the open literature [4,36,38,39]. In a relative bioavailability study with a crossover design by Jamali et al., 23 healthy Caucasian male subjects with a mean (range) age of 27.2 (18–35) years old received 100 mg Froben or 100 mg Ansaid with 100 mL water after an overnight fast. The mean (range) body weight was 71.8 (52.5–88.5) kg and all individuals were within 20% of their ideal body weight for their height [38]. In the study by Patel et al., 4 Caucasian (50% females) healthy volunteers with mean (SD) age and weight of 26.8 (2.2) years old and 67.8 (4.1) kg, respectively, took part [4]. All subjects had fasted overnight and on the next morning were administered a 100 mg Froben tablet with approximately 150 mL water. In a randomized, double blind, placebo-controlled, crossover study, Suri et al. investigated the pharmacokinetics (PK) and pharmacodynamics (PD) of FLU after oral administration. In this study, 6 healthy subjects were given 100 mg FLU orally as a single tablet with 200 mL water after an overnight fast, on 2 separate occasions [39]. No further demographic and background characteristics were described. The analgesic efficacy was evaluated by 2 independent pharmacodynamic endpoints, including a subjective pain intensity rating and tooth pulp-evoked potentials (TPEP) amplitude, which is more objective.

To investigate the bioequivalence between orally disintegrating and conventional FLU tablets in a randomized-sequence, open-label, 2-period crossover study, Liu et al. administered a single dose of 150 mg (as 3 tablets of 50 mg) FLU of either the orodispersible (test) or the conventional (reference) formulation to 20 healthy, non-smoking Chinese male volunteers [40]. After a 12 h fast, the subjects received the test product without any water intake, whereas 250 mL water were given with the reference product. The enrolled individuals had a mean (SD) age, weight, height, and body mass index (BMI) of 21.4 (2.5) years, 63.2 (5.1) kg, 174.4 (4.2) cm, and 20.8 (1.4) kg/m², respectively.

In all studies, concomitant administration of any other drugs was not permitted for at least 1 week before the study and food was withheld until 2 h post-dose.

All available demographic data from the aforementioned clinical studies were used in simulations of the clinical trials and they are summarized in Table 1.

Table 1. Mean (SD) demographic clinical study data used for the development and validation of the physiologically based pharmacokinetic/pharmacodynamic (PBPK/PD) model.

Drug Administration and Formulation	CYP2C9 Genotype	No. of Subjects	Female Ratio	Ethnicity	Age (years)	BW/BW Range (kg)	BH/BH Range (cm)	Reference
Intravenous								
50 mg as 10 mg/mL solution (injection within 2 min)	n.a.	24	0	Chinese	-	-	-	Mei et al. [34]
Oral								
25 mL of oral solution containing 67.9 mg FLU with 175 mL water;	n.a.	12	0	Caucasian	25–31	-	-	Gonzalez-Younes et al. [35]
40 mL oral solution containing 100 mg FLU with 180 mL water;	n.a.	15	0	Caucasian	29 (18–40)	76.4 (62.3–109.1)	177 (168–188)	Szpunar et al. [36]
Froben solution 40 mg;	1*/1*	12	0	Korean	23.1 (2.4)	65.1 (7.1)	174.8 (5.0)	Lee et al. [41]
Froben solution 40 mg;	1*/3*	8	0	Korean	22 (2.7)	64.6 (7.1)	172.8 (6.4)	Lee et al. [41]
USP tablets (Mylan Pharmaceuticals) 50 mg;	1*/1*	5	0.533	Caucasian	24 (5)	79 (18)	-	Lee et al. [42]
USP tablets (Mylan Pharmaceuticals) 50 mg;	1*/2*	5	0.533	Caucasian	24 (5)	79 (18)	-	Lee et al. [42]
USP tablets (Mylan Pharmaceuticals) 50 mg;	1*/3*	5	0.533	Caucasian	24 (5)	79 (18)	-	Lee et al. [42]
Froben 100 mg with 100 mL water;	n.a.	23	0	Caucasian	27.2 (18–35)	71.8 (52.5)	-	Jamali et al. [38]
Ansaid 100 mg with 100 mL water;	n.a.	23	0	Caucasian	27.2 (18–35)	71.8 (52.5)	-	Jamali et al. [38]
Froben 100 mg with 150 mL water;	n.a.	4	0.5	Caucasian	26.8 (2.2)	67.8 (4.1)	-	Patel et al. [4]
100 mg tablet with 200 mL water;	n.a.	6	-	Caucasian	-	-	-	Suri et al. [39]
Ansaid 100 mg with 180 mL water;	n.a.	15	0	Caucasian	29 (18–40)	76.4 (62.3–109.1)	177 (168–188)	Szpunar et al. [36]
3 × 50 mg conventional tablets (reference);	n.a.	20	0	Chinese	21.4 (2.5)	63.2 (5.1)	174.4 (4.2)	Liu et al. [40]
3 × 50 mg orally disintegrated tablets (test);	n.a.	20	0	Chinese	21.4 (2.5)	63.2 (5.1)	174.4 (4.2)	Liu et al. [40]
2 × Ansaid 100 mg with 180 mL water;	n.a.	15	0	Caucasian	29 (18–40)	76.4 (62.3–109.1)	177 (168–188)	Szpunar et al. [36]
3 × Ansaid 100 mg with 180 mL water;	n.a.	15	0	Caucasian	29 (18–40)	76.4 (62.3–109.1)	177 (168–188)	Szpunar et al. [36]

n.a.: not available.

2.8.2. Drug–Drug Interaction (DDI) Studies

A total of 13 sets of plasma concentration–time profiles of FLU with or without perpetrator co-administration from a total of 6 clinical studies available in the open literature were used for CYP2C9 drug–drug–gene predictions. In an open randomized crossover study, Kumar et al. investigated the impact of CYP2C9 genotype- and dose-dependent inhibition interactions of FLU *in vivo* [43]. From a total of 189 genotyped subjects, 11 CYP2C9 1*/1*, 8 CYP2C9 1*/3*, and 2 CYP2C9 3*/3* healthy subjects received either 50 mg FLU (Mylan Pharmaceuticals Inc., Maharashtra, India) as a tablet alone or 200 mg or 400 mg fluconazole as tablet once daily (q.d.) for 7 days, followed by 50 mg FLU on the 7th day. Subjects were required to fast overnight prior to the study day and FLU was administered 2 h after administration of the last fluconazole dose. In a total of 3 clinical studies investigating the potential of *in vivo* CYP2C9 inhibition by pomegranate, blueberry, cranberry or grape juice, the researchers used FLU as the index substrate and fluconazole as the inhibitor [44–46]. Following the same design and administration protocol, the researchers administered fluconazole to healthy volunteers as a 200 mg tablet twice on the afternoon before the day of study and 30 min prior to the administration of a 100 mg

FLU tablet on the study day. After FLU administration, venous blood samples were drawn over 12 h. In addition, Zgheib et al. evaluated the effect of study design, i.e., after administration of either a single or 7 once daily doses of 400 mg fluconazole, on the *in vivo* metabolism and pharmacokinetics of FLU [47]. A total of 12 healthy volunteers completed the study. After overnight fast, 50 mg of FLU was administered as a tablet (Ansaid) 2 hours after the last dose of fluconazole. Daali et al. assessed the usefulness of dried blood spots (DBS) to determine the FLU metabolic ratio by comparing plasma concentration with DBS profiles after 3 treatments: (a) administration of a 50 mg FLU tablet alone, (b) 50 mg of FLU together with a single 400 mg dose of fluconazole as the CYP2C9 inhibitor, and (c) 50 mg of FLU with 5 doses (once daily) of 600 mg rifampicin as the CYP2C9 inducer [48]. FLU administration to 10 healthy male subjects took place 2 hours after fluconazole and concomitantly with the last dose of rifampicin; between treatments there was at least a 2-week washout period.

In all studies, no concomitant administration of any other drugs was permitted for at least 1 week before the start of the study; food was withheld until 2 h post-dose and a washout period of at least 1 week was applied.

All available demographic and study design data of the DDI studies are presented in Table 2.

Table 2. Mean (SD) demographic clinical study data used for the gene–drug–drug interaction (GDDI) modeling.

Victim Drug Administration	Perpetrator Drug Administration	Perpetrator <i>in vitro</i> Ki (μM)	No. of Doses	Interval (h)	CYP2C9 genotype	No. of Subjects	Female Ratio	Ethnicity	Age (years)	BW/BW Range (kg)	BH/BH Range (cm)	References
Flurbiprofen	Fluconazole											
po 50 mg s.d.	po 200 mg q.d.	11	7	2	1*/1*	11	0.64	-	25 (19–36)	73.7 (51–108)	166 (154–193)	Kumar et al. [43]
po 50 mg s.d.	po 400 mg q.d.	11	7	2	1*/1*	11	0.64	-	25 (19–36)	73.7 (51–108)	166 (154–193)	Kumar et al. [43]
po 50 mg s.d.	po 200 mg q.d.	17	7	2	1*/3*	8	0.63	-	23 (19–28)	66.9 (49–84)	167 (160–189)	Kumar et al. [43]
po 50 mg s.d.	po 400 mg q.d.	17	7	2	1*/3*	8	0.63	-	23 (19–28)	66.9 (49–84)	167 (160–189)	Kumar et al. [43]
po 50 mg s.d.	po 200 mg q.d.	23	7	2	3*/3*	2	0.0	-	(25, 29)	(77, 85)	(177, 179)	Kumar et al. [43]
po 50 mg s.d.	po 400 mg q.d.	23	7	2	3*/3*	2	0.0	-	(25, 29)	(77, 85)	(177, 179)	Kumar et al. [43]
po 100 mg s.d.	po 200 mg b.i.d.	14.3/20.3	2	0.5	-	12	0.25	Caucasian (n = 8), other (n = 4) ^a	19–54	-	-	Hanley et al. [45]
po 100 mg s.d.	po 200 mg b.i.d.	29.9	2	0.5	-	14	0.21	-	29 ± 8	81 ± 14	-	Greenblatt et al. [46]
po 100 mg s.d.	po 200 mg b.i.d.	14.3/20.3	2	0.5	-	12	0.17	-	24–55	-	-	Hanley et al. [44]
Victim Drug Administration	Perpetrator Drug Administration	Perpetrator <i>in vitro</i> Ki (μM)	No. of Doses	Interval (h)	CYP2C9 genotype	No. of Subjects	Female Ratio	Ethnicity	Age (years)	BW/BW Range (kg)	BH/BH Range (cm)	References
Flurbiprofen	Fluconazole											
po 50 mg s.d.	po 400 mg s.d.	10	1	2	-	12	0.58	Caucasian (n = 10), other (n = 2) ^b	37 ± 3.1	-	-	Zgheib et al. [47]
po 50 mg s.d.	po 400 mg q.d.	10	7	2	-	12	0.58	Caucasian (n = 10), other (n = 2) ^b	37 ± 3.1	-	-	Zgheib et al. [47]
po 50 mg s.d.	po 400 mg s.d.	10	1	2	-	10	0.0	Caucasian (n = 9), African (n = 1)	27 (23–39)	-	-	Daali et al. [48]
	Rifampicin											
po 50 mg s.d.	po 600 mg q.d.	n.a. ^c	5	0	-	10	0.0	Caucasian (n = 9), African (n = 1)	27 (23–39)	-	-	Daali et al. [48]

n.a. = not available; ^a Hispanic (n = 2), Asian (n = 1), Afro-American (n = 1); ^b Afro-American (n = 2); ^c default value of Simcyp library compound.

2.9. PBPK Model Development and Verification

2.9.1. Software

PBPK modeling and simulations were performed using the Simcyp Population-based Simulator (V18.2; Certara, Sheffield, United Kingdom). The FLU PBPK model was developed by implementing a “middle-out” stepwise sequential modeling strategy, in line with previously published literature and regulatory guidelines [16,49–53]. Briefly, the initial model was developed through integration of physicochemical parameters, *in vitro* data, and/or *in silico* predictors for the absorption, distribution, metabolism, and excretion (ADME) processes. *In vitro* data generated for the purpose of this study were also incorporated after using an *in vitro*–*in vivo* extrapolation (IVIVE) approach. All input parameters for the FLU PBPK/PD model are summarized in Table 3. Simulations were performed using the virtual North European Caucasian and Chinese healthy volunteer populations of the software.

Table 3. Input parameters of flurbiprofen PBPK/PD model.

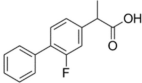
Parameters	Value	Reference/Comments
Physicochemical and Blood Binding		
		
Chemical Structure		
MW (g/mol)	244.3	
logP _{o/w}	3.99	[54,55]
pKa	4.05	Updated from <i>in vitro</i> solubility data (see Table 4 and Section 3.2)
Blood/plasma ratio	0.55	[56]
Fraction unbound in plasma	0.01	[5,56–59]
Absorption		
Model	ADAM	
P _{app, Caco-2} (×10 ^{−6} cm/s)	20.1	Measured value [60]
P _{app, Caco-2, ref} (×10 ^{−6} cm/s)	1.57	Negative calibrator (Atenolol) value [60]
P _{app, Caco-2, ref} (×10 ^{−6} cm/s)	15.8	Positive calibrator (Verapamil) value [60]
P _{eff, human} (×10 ^{−4} cm/s)	4.83	Predicted by Simcyp Permeability Calibrator–custom correlation
Formulation type	Immediate Release	
S ₀ (mg/mL)	0.018	<i>In vitro</i> data (see Table 4 and Section 3.1)
logK _{m:w} neutral	5.37	Estimated from <i>in vitro</i> data (see Table 5 and Sections 2.6 and 3.2)
logK _{m:w} ion	2.46	Estimated from <i>in vitro</i> data (see Table 5 and Sections 2.6 and 3.2)
<i>In vivo</i> dissolution	see Tables 6 and 7	Estimated DLM scalars from <i>in vitro</i> data (see Section 2.7)
Distribution		
Model	Full PBPK	
V _{ss} (L/kg)	0.074	Predicted by Method 2
K _p scalar	0.7	Optimized on the basis of IV data–PE module
Elimination		
F _{ox}	0.71	[4]
Model	Allelic-specific enzyme kinetics	
CYP2C9 1*/1*-V _{max} (pmol/min/pmol CYP)	15.79	Recombinant CYP (f _{u,mic} = 1) [61]
CYP2C9 1*/1*-K _m (μM)	8.756	Recombinant CYP (f _{u,mic} = 1) [61]
CYP2C9 1*/2*-V _{max} (pmol/min/pmol CYP)	11.53	Scaled for CL _{CYP2C9 1*/1*} /CL _{CYP2C9 1*/3*} = 0.73 [42]
CYP2C9 1*/2*-K _m (μM)	8.756	Recombinant CYP (f _{u,mic} = 1) [61]
CYP2C9 1*/3*-V _{max} (pmol/min/pmol CYP)	9.55	Scaled for CL _{CYP2C9 1*/1*} /CL _{CYP2C9 1*/3*} = 0.605 [42]
CYP2C9 1*/3*-K _m (μM)	8.756	Recombinant CYP (f _{u,mic} = 1) [61]
CYP2C9 2*/2*-V _{max} (pmol/min/pmol CYP)	10.04	Recombinant CYP (f _{u,mic} = 1) [61]
CYP2C9 2*/2*-K _m (μM)	10.39	Recombinant CYP (f _{u,mic} = 1) [61]
CYP2C9 3*/3*-V _{max} (pmol/min/pmol CYP)	8.901	Recombinant CYP (f _{u,mic} = 1) [61]
CYP2C9 3*/3*-K _m (μM)	23.25	Recombinant CYP (f _{u,mic} = 1) [61]
CYP2C9-ISEF	0.3	Optimized on the basis of IV data–PE module

Table 3. Cont.

Parameters	Value	Reference/Comments
UGT2B7- V_{max} (pmol/min/mg protein)	119.7	Recombinant UGT [62]
UGT2B7- K_m (μ M)	50.21	Recombinant UGT [62]
UGT1A9- V_{max} (pmol/min/mg protein)	3.286	Recombinant UGT [62]
UGT1A9- K_m (μ M)	182.2	Recombinant UGT [62]
Additional HLM liver CL_{int} (μ L/min/mg proein)	7.88	Retrograde model for a target $f_{mCYP2C9} = 0.71$
CL_{renal} (L/h)	0.066	[4]
Pharmacodynamics		
Model	Effect compartment linked to inhibitory E_{max} model	[39]
k_{eo} (h^{-1}) (%CV)	0.56 (43)	PD endpoint: <i>Evoked Potentials</i>
IC_{50} (mg/L)	25.8 (21)	
k_{eo} (h^{-1}) (%CV)	0.89 (24)	PD endpoint: <i>Pain rating score</i>
IC_{50} (mg/L)	27.6 (10)	

2.9.2. PBPK/PD Model Development

Physicochemical Characteristics and Blood Binding

FLU has a molecular weight (MW) of 244.3 g/mol and is a poorly soluble (BCS II) monoprotic acid with a pKa of 4.05. The logarithm of the octanol–water partition coefficient is 3.99 [55,60], while the values for the blood/plasma concentration ratio (B:P) and the fraction unbound (f_u) are 0.55 and 0.01, respectively [5,56–59].

Absorption

The Advanced Dissolution Absorption and Metabolism (ADAM) model was used to mechanistically describe the absorption of FLU. The ADAM model has previously been described in detail by Jamei et al. and Darwich et al. [63,64]. The human effective permeability (P_{eff}) was calculated using *in vitro* apparent permeability (P_{app}) data in Caco-2 cells for both the compound and positive (Verapamil)/ negative (Atenolol) calibrators [60]. The P_{eff} was predicted to be 4.83×10^{-4} cm/s through using a pH of 6.5 on the apical side of the Caco-2 cells and assuming only passive permeation. The diffusion layer model (DLM) with advanced fluid dynamics (AfD) and dynamic (time variant) pH were implemented to simulate the *in vivo* dissolution. Default settings of the software for luminal blood flow, fluid volume, bile salt content, segmental pH, metabolic activity, and small intestinal residence time were applied. The mean gastric emptying time (GET) in the fasted state was set to 0.25 h (matching the built-in “segregated transit time” model value rather than the default value of 0.4 h used in the “global” transit time model), as suggested by human clinical data and several authors [65–68]. The S_0 was set to the minimum experimentally measured value, while estimates for the neutral and ionized species $K_{m:w}$ (Equation (2)) were incorporated after modelling of the *in vitro* biorelevant solubility data (Section 2.6). A dissolution-based IVIVE approach, using S_{DLM} estimates from *in vitro* data, was followed to account for formulation or media-related differences when simulating the respective *in vivo* dissolution scenarios (Section 2.7). Further, to investigate the effect of *in vivo* dissolution of multiple formulations and under various conditions on the overall *in vivo* performance, we implemented selected S_{DLM} estimates to simulate the aforementioned clinical studies at the 100 mg dose level. At other dose levels, the highest gastric ($S_{DLM, stomach}$) and intestinal ($S_{DLM, SI}$) estimates corresponding to the fastest gastric and intestinal dissolution rates, respectively, were used to minimize the impact of formulation.

Distribution

A full PBPK distribution model was used and distribution parameters including organ/tissue partition coefficients (K_p) and volume of distribution at the steady state (V_{ss}) were predicted by the built-in Method 2 (the Rodgers–Rowland method) [69].

Metabolism and Excretion

The contributions of CYP2C9 ($f_{mCYP2C9} = 0.71$) on the overall metabolic clearance (CL) of FLU as well as the renal clearance ($CL_{renal} = 0.66$) were obtained from Patel et al. [4]. Using the retrograde model for healthy volunteers available within the PBPK software, we calculated additional liver CL to match the reported $f_{mCYP2C9}$. Using human recombinant (rhP450) CYP2C9 expressed in microsomes from the insect cell line Sf21, we found the mean V_{max} and K_m values for the 1*/1* (wild type), 2*/2*, and 3*/3* to be 15.79 and 8.756, 10.04 and 10.39, and 8.901 and 23.25, respectively [61]. These allele-specific CYP2C9 *in vitro* kinetic parameters (V_{max} , K_m) were implemented to further inform the model. The metabolic clearance of heterozygotic subjects with CYP2C9 1*/2* and CYP2C9 1*/3* genotypes has been clinically observed to be 0.73 and 0.605 of the wild type (1*/1*) clearance, respectively [42]. For that reason, and in the absence of *in vitro* data, the V_{max} of CYP2C9 1*/1* was scaled down accordingly to account for the decrease in clearance in those genotypes. The K_m value was assumed to be the same as for CYP2C9 1*/1*. All presented V_{max} and K_m values were already normalized to account for microsomal incubation fraction unbound ($f_{u,mic}$). Since an inter-system extrapolation factor (ISEF) was not available for this particular rhP450 system, we used a literature ISEF value (equal to 0.38) from baculovirus insect cell-expressed CYP2C9 for another NSAID, diclofenac, as an initial estimate [70]. After oral administration of racemic FLU, 8.4 and 7.3% of the dose was excreted into the urine as the acyl glucuronide of (R)- and (S)-FLU, respectively [4], indicating that glucuronidation made some contribution to the metabolic pathway of FLU. The major UGT isoform involved in FLU glucuronidation is UGT2B7, with minor contributions by UGT1A1, UGT1A3, UGT1A9, and UGT2B4 [71,72]. Even though genetic polymorphisms have been reported in UGT family members [73,74], the clinical and functional significance and genotype–phenotype correlation of UGT polymorphisms is an ongoing area of research. In absence of data showing clinical relevance of UGT2B7 and UGT1A9 polymorphisms, these were not considered for the development and validation of the present model.

Pharmacodynamics

A published inhibitory E_{max} model linked to an effect-compartment was coupled to the PBPK model for FLU [39]. The analgesic efficacy was assessed using 2 endpoints: (a) subjective pain intensity ranking and (b) tooth pulp-evoked potentials (TPEP) amplitude. The percentage change of each endpoint after drug intake was considered as an indicator of pharmacodynamic activity, while the pre-dose value was defined as 100% (initial value).

Model Optimization

The volume of distribution and clearance were further optimized by estimating the K_p scalar and the ISEF value, respectively, with simultaneous fitting of the model to PK data after 50 mg intravenous and 67.9 mg oral solution administrations (internal datasets).

2.9.3. PBPK/PD Model Validation and Evaluation of Predictive Performance

The performance of the developed PBPK/PD model was evaluated by clinical trial simulations. In order to assess the distribution of population variability, we simulated at least 10 trials of 10 subjects ($n \geq 100$) each for each clinical study. Specifically, a two-step validation process for the FLU PBPK/PD model was followed. The initial model was internally verified by comparing the predicted and observed plasma concentration profiles for the IV and the oral solution (67.9 mg) administrations. The model was then validated by comparing mean simulated and observed plasma concentration profiles, and exposure and response parameters of external datasets including PK data from subjects with different CYP2C9 genotypes in a 40–300 mg dose range. Virtual populations were selected to closely match the enrolled individuals in the respective *in vivo* clinical trials with regard to sample size, ethnicity, gender ratio, and age and weight range. Reported volumes of concomitant liquid intake,

dosage form type, and sampling schedule were also included in the study design. A schematic of the modeling workflow is presented in Figure 1.

The predictive performance of the model was assessed by visual predictive checks (5th and 95th percentiles), as well as by comparing predicted and observed plasma concentration values and PK parameters: maximum plasma concentration (C_{max}), area under the curve extrapolated to infinity (AUC_{inf}) and apparent clearance (CL/F). For this purpose, the ratio ($R_{pred/obs}$) of model-predicted versus observed parameter values was determined ($R_{pred/obs}$ = model-predicted/clinically observed). The predictive accuracy was evaluated on the basis of the “two-fold” rule ($-0.301 < \log R_{pred/obs} < 0.301$), as well as the more stringent deviation of 25% ($-0.097 < \log R_{pred/obs} < 0.097$).

As quantitative measures of model performance, mean relative deviations (MRDs) of the predicted plasma concentrations and geometric mean fold errors (GMFEs) of C_{max} , AUC_{inf} , and CL/F were also calculated, as follows:

$$MRD = 10^{\frac{1}{N}} \sqrt{\sum_i^N (\log_{10}(C_i) - \log_{10}(\hat{C}_i))^2} \quad (4)$$

$$GMFE = 10^{\frac{1}{n} \sum_j^n \left| \log_{10}\left(\frac{\hat{a}_j}{a_j}\right) \right|} \quad (5)$$

where C_i and \hat{C}_i are the i^{th} observed and predicted concentrations, respectively; a_j and \hat{a}_j correspond the observed and the respective predicted C_{max} , AUC_{inf} , or CL/F values of the j^{th} clinical study; and N and n are the number of observations and clinical studies, respectively. Overall MRD and GMFE values of ≤ 2 were considered as reasonable predictions [75–77].

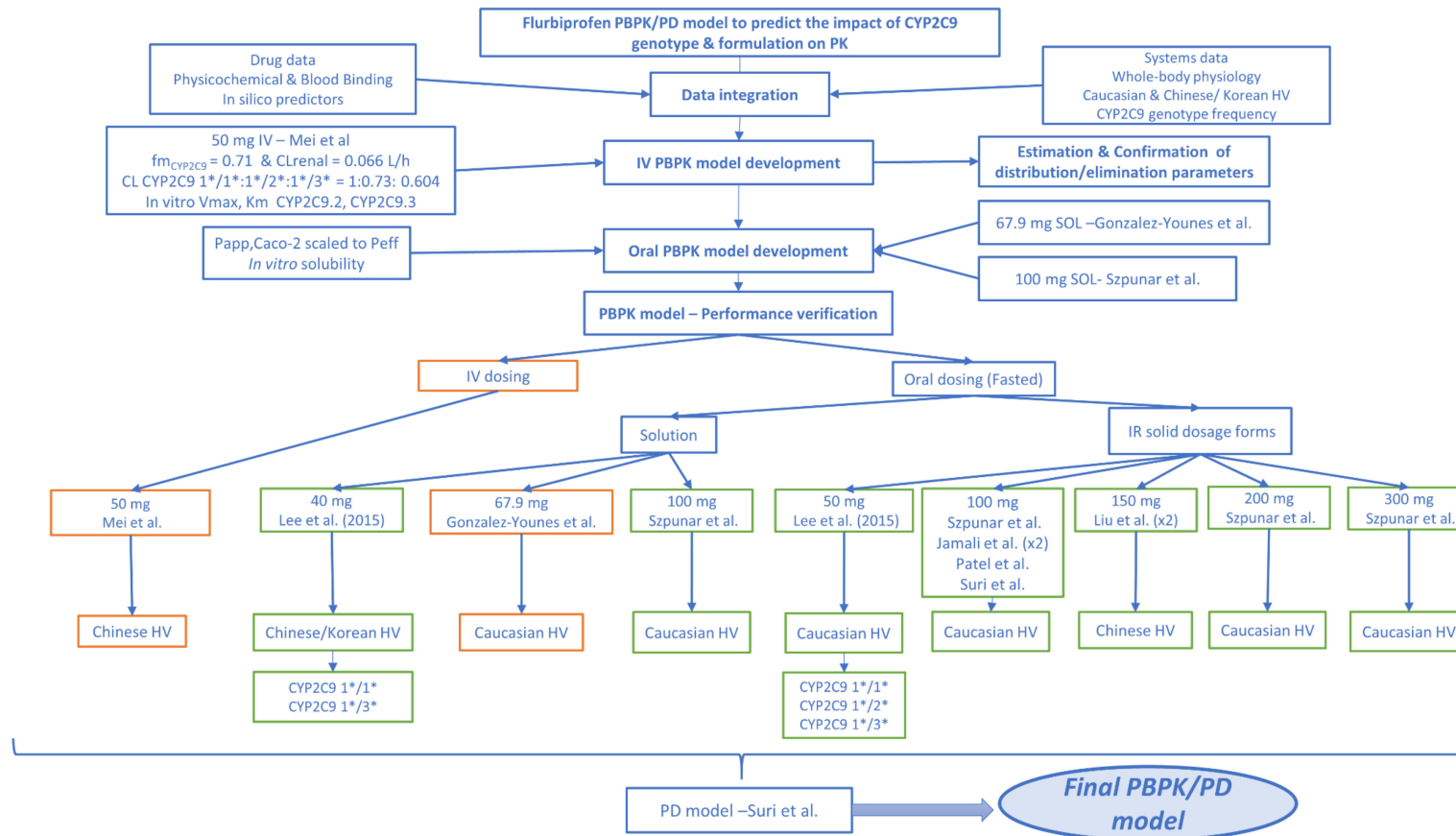


Figure 1. Stepwise modeling workflow for the development and verification of flurbiprofen PBPK/PD model. Training for the internal and test datasets for the external verification, obtained from clinical studies published in the open literature, are outlined with orange and green, respectively.

2.9.4. PBPK DDI Modeling

In addition to the evaluation methods described in Section 2.9.3, we simulated CYP2C9 drug–drug–gene interactions to evaluate the DDI performance of the developed PBPK/PD model. A total of 12 plasma concentration–time profiles after co-administration of flurbiprofen with the strong CYP2C9 inhibitor fluconazole and 1 with the CYP2C9 inducer rifampicin were used to predict the drug–drug–gene interactions of flurbiprofen.

PBPK Models of Perpetrator Drugs

The compound files for fluconazole (inhibitor) and rifampicin MD (inducer) are available in the Simcyp (v18.2) drug library, and the verified built-in values for the inhibition and induction parameters were used for these perpetrator drugs. For the clinical trial simulation, the administration protocol and the virtual subjects closely matched the ones from the actual studies.

PBPK DDI Modeling Evaluation

The model performance in predicting the DDIs was evaluated by comparison of the predicted to observed victim drug plasma concentration–time trajectories, when administered alone and during co-administration. The ratios of AUC from time zero to the time of the last measured concentration (AUC_{last}) and of C_{max} , with and without administration of the perpetrator drug, were calculated as follows:

$$DDI\ ratio = \frac{AUC_{last\ or\ C_{max}}\ victim\ drug\ during\ perpetrator\ coadministration}{AUC_{last\ or\ C_{max}}\ victim\ drug\ (control)} \quad (6)$$

To assess the DDI modeling, the GMFEs of the predicted DDI were calculated for AUC_{last} and C_{max} ratios according to Equation (5).

2.9.5. Virtual Populations

North European Caucasian (NEurCaucasian) and Chinese virtual populations of healthy volunteers were used for the population simulations of this study. The main differences in the inputs for the two populations related to CYP2C9 metabolism and genotype profile are summarized in Table S1. The intrinsic catalytic activity of CYP2C9 per unit amount of enzyme variant and tissue composition were assumed the same in both populations. The mean default intestinal and liver CYP2C9 abundances as well as the specific genotype frequencies of the Simcyp population libraries were used. As the Korean population is not available in the current Simcyp version (v19.1), we simulated studies including Korean subjects by using the Chinese virtual population, which is considered to be the population with the highest demographic and genetic proximity to the Korean population [78–80].

2.10. Data Analysis and Model Diagnostics

The solubility and dissolution data are presented as the arithmetic mean (standard deviation). Model-based analysis of the *in vitro* data in the SIVA Toolkit was performed with either Nelder–Mead or a hybrid algorithm with a 5th order Runge–Kutta solver. The appropriate weighting scheme was chosen on the basis of the observed data ranges and their homogeneity, and the goodness of fit was assessed by the coefficient of determination (R^2) as well as visual predictive checks (e.g., residuals plots). All PK profiles obtained from the literature were digitalized with the WebPlotDigitizer (version 4.1; PLOTCON; Oakland, USA). The parameter estimation within the PE module of the Simcyp Simulator was performed with the maximum likelihood estimation method.

Data post-processing and visualization were performed with MATLAB 2019b (Mathworks Inc.; Natick, MA, USA) and R version 3.5.3 (R Core Team (2019). R: A language and environment for statistical computing. R Foundation for Statistical Computing, Vienna, Austria. URL <https://www.R-project.org/>).

3. Results

3.1. In Vitro Solubility

Table 4 summarizes the equilibrium solubility values in multiple aqueous buffers and biorelevant media with different pH values. The final pH_{bulk} differed significantly from the initial pH values in phosphate buffers of different pH values due to the self-buffering effect. In fact, the reduction is even more pronounced in the fasted state biorelevant media due to their lower buffer capacity (5.6 mmol/L/ ΔpH in FaSSIF V3 versus 18.5 mmol/L/ ΔpH in European Pharmacopoeia phosphate buffers) [24]. Such a behavior was not observed for the FaSSGF Level I and III, the acetate buffer, and the FeSSIF Level I, where the respective pH change was limited to 0.1 pH unit.

Table 4. Mean (\pm SD) equilibrium solubility in aqueous buffers and fasted state biorelevant media at 37 °C for 24 h (Uniprep method).

Medium	Flurbiprofen	
	pH_{final}	Solubility ($\mu g/mL$)
Aqueous buffers		
FaSSGF Level I (pH = 1.6)	1.6	18.1 (0.17)
Acetate buffer (pH = 4.5)	4.7	101.1 (7.06)
FeSSIF V1 Level I (pH = 5.0)	5.1	225.4 (5.6)
Phosphate buffer (pH = 6.5)	6.1	2024.4 (128.2)
Phosphate buffer (pH = 6.8)	6.3	3127.1 (194.9)
Fasted state biorelevant media		
Level III FaSSGF (pH = 1.6)	1.6	18.5 (1.6)
Level II FaSSIF V1 (pH = 6.5)	6.0	1954.9 (3.9)
Level II FaSSIF V3 (pH = 6.7)	5.9	1585.4 (172.1)

Micelle-mediated solubilization seemed not to have a substantial impact on the overall solubility of FLU, which is instead highly dependent on pH.

3.2. Model-Based Analysis of In Vitro Solubility Data

Table 5 summarizes the parameter estimates (95% CI) obtained by model-based analysis of the *in vitro* solubility data in compendial and biorelevant media, as described in Section 2.6. The pK_a was determined to be 4.05, a value which agrees with values reported in the literature [54,57,60,81]. By estimating the micelle-water partition coefficients for both neutral and ionized species using the biorelevant solubilities, we were able to quantify the effect of physiologically relevant surfactants on the overall solubility of FLU. These values were used as inputs to the Simcyp Simulator (Table 3) to simulate luminal conditions and the *in vivo* dissolution behavior, accounting at the same time for inter-subject variability regarding bile salt-mediated solubilization in the virtual population. Therefore, implementation of $\log K_{m:w}$ values for the nonionised (“neutral”) and ionised forms of FLU in the PBPK model enabled mechanistic prediction of the *in vivo* luminal dissolution population variability, which would not be possible if only mean solubility values had been used.

Table 5. Parameter estimates (95% CI) resulting from the model-based analysis of *in vitro* solubility data in aqueous as well as biorelevant media. The pK_a was estimated from the aqueous buffer solubility values, whereas for the micelle-water partition coefficients ($\log K_{m:w}$ neutral, ion) estimation, we used biorelevant solubilities. The accuracy of the prediction was evaluated with the R^2 .

	pK_a	$\log K_{m:w}$ Neutral	$\log K_{m:w}$ Ion
Estimate (95% CI)	4.05 (4.42–4.44)	5.36 (4.61–6.11)	2.56 (1.38–5.02)
R^2	0.9990		0.9999

3.3. In Vitro Dissolution Tests

Figure 2 shows the mean percentage dissolved (\pm SD) of FLU in the tested formulations and as pure drug over time in fasted state simulated gastric fluids (FaSSGF) of different simulation levels (I and III). As expected, the *in vitro* release of this poorly soluble weak acid under gastric conditions was incomplete, reaching a plateau at around 8.3% of the dose in both FaSSGF Levels I and III. The USP as well as the Antadys tablets exhibited similar *in vitro* dissolution behavior in both media. However, the unformulated drug reached a maximum of only 5.5% in FaSSGF Level I. Since there was no difference in the solubility of FLU between the two media, this observation was attributed to the absence of surfactants and proteins (i.e., pepsin) in FaSSGF Level I, leading to poor wetting of the drug powder.

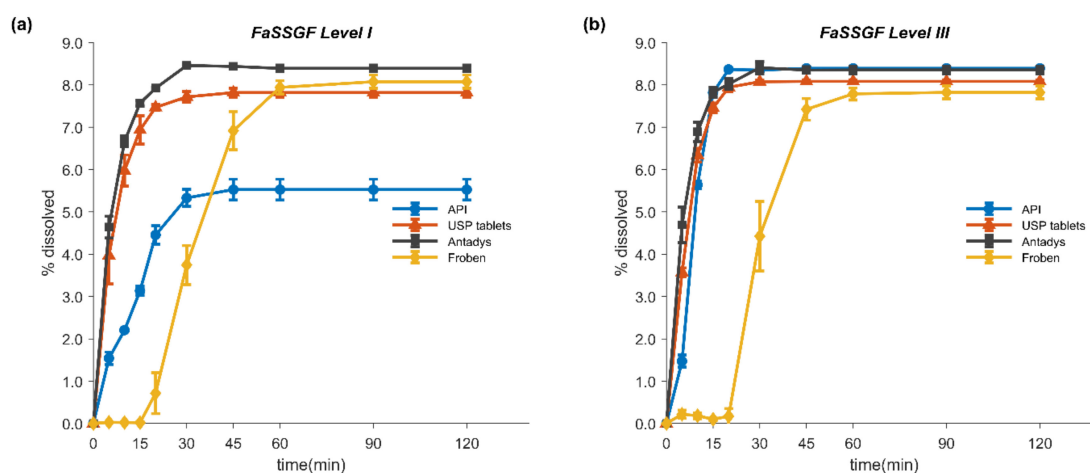


Figure 2. *In vitro* dissolution (mean \pm SD) of flurbiprofen active pharmaceutical ingredient (API) 100 mg (circles), FLU USP tablets 100 mg (triangles), Antadys 100 mg (squares), and Froben 100 mg (diamonds) in fasted state-simulated gastric fluid (FaSSGF) Levels I (a) and III (b), respectively. USP paddle apparatus at 75 rpm and 250 mL of dissolution medium at 37°C were used in all experiments. All experiments were performed at least in triplicate ($n \geq 3$). Most standard deviation bars lie within the symbols.

Mean percentage dissolved (\pm SD) over time in compendial and fasted state-simulated intestinal fluids (FaSSIF) for the unformulated API and the tested formulations are presented in Figure 3a–c. For the pure drug, the dissolution in FaSSIF V3 Level II and in Ph. Eur. phosphate buffer (pH 6.8) was very rapid (>85% within 2.5 and 15 min, respectively). On the other hand, dissolution in FaSSIF V3 Level I (i.e., without bile components) was much slower, with 85% dissolved reached only after 60 min. Such behavior can be assigned to differences in buffer capacity (FaSSIF V3 Level I and II vs. phosphate buffer), solubilization capacity (FaSSIF V3 Level II vs. Level I), and wettability of the tested media. The difference of 0.1 pH units between the initial pH of Ph. Eur. phosphate buffer (pH 6.8) and FaSSIF V3 is assumed to have had a negligible effect.

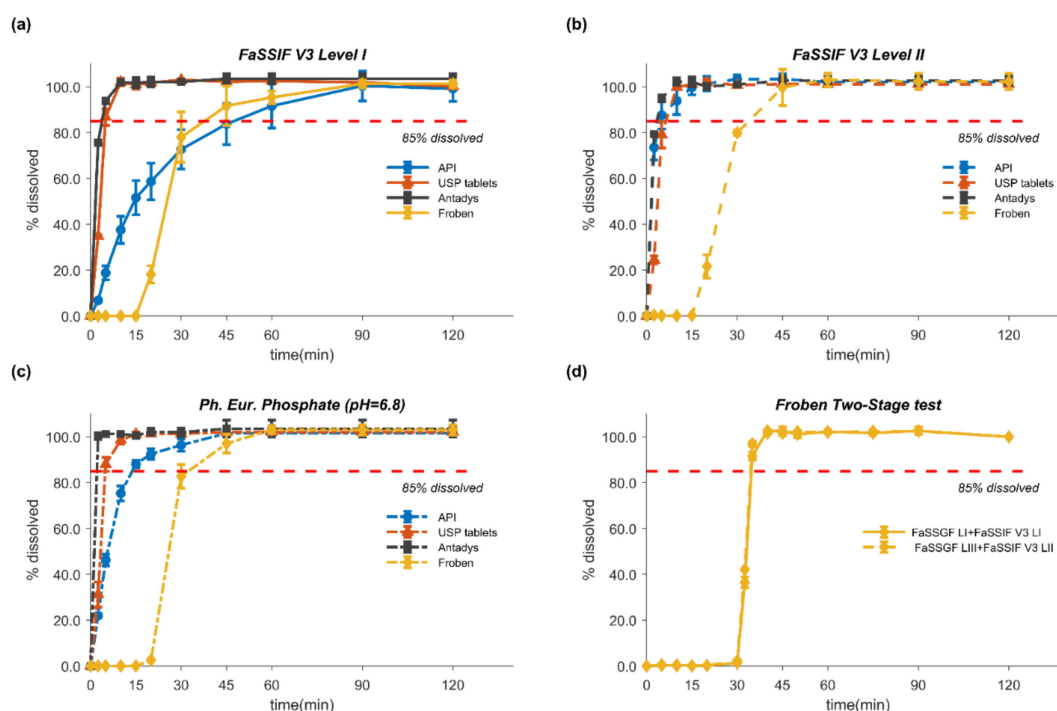


Figure 3. *In vitro* dissolution (mean \pm SD) of flurbiprofen API 100 mg (circles), FLU USP tablets 100 mg (triangles), Antadys 100 mg (squares), and Froben 100 mg (diamonds) in (a) FaSSIF V3 Level I (solid lines), (b) FaSSIF V3 Level II (dashed lines), and (c) Ph. Eur. phosphate buffer (pH = 6.8) (dashed dotted lines). (d) Two-stage test of Froben 100 mg (diamonds) in FaSSGF Levels I (solid line) and III (dashed line) at the gastric and FaSSIF V3 Level I (solid line) and FaSSIF V3 Level II (dashed lines) at the intestinal compartments, respectively. USP paddle apparatus at 75 rpm at 37 ± 0.4 °C was used in all experiments. The volume of dissolution medium in the gastric compartment was 250 mL, to which 250 mL of appropriately concentrated intestinal medium was added after 30 min. Horizontal dashed red lines represent the 85% dissolved. All experiments were performed at least in triplicate ($n \geq 3$). Most standard deviation bars lie within the symbols.

Especially since dissolution was performed under non-sink conditions in this series of experiments, the dissolution rate of the pure drug in FaSSIF V3 Level I was significantly slower, due to its low buffer capacity (5.6 mEq/L/ Δ pH), than in the compendial 50 mM phosphate buffer (25 mEq/L/ Δ pH) [82]. At the higher total phosphate buffer concentration of the compendial medium (50 mM), the bulk (pH_{bulk}) rather than the surface pH (pH_0) drove solubility and dissolution. By contrast, in the low buffer capacity FaSSIF V3 Level I medium, the surface pH seemed to control the dissolution rate. Indeed, the influence of the dissolving acid on the medium was so great that even the bulk pH was significantly altered (final pH was 6.31 vs. 6.82 in Ph. Eur. phosphate buffer). The self-buffering effect on the overall dissolution behavior was much less prominent when bile salts were added to the medium, as shown in Figure 3b. Furthermore, it was evident that the addition of the bile salt components in FaSSIF V3 Level II markedly enhanced the dissolution rate of the unformulated FLU. Although the main effect was likely through solubilization, improvements in wetting seemed to have also contributed to the higher dissolution rate in the Level II medium, given that a similar behavior was observed in the gastric media.

For the USP tablets and Antadys, these trends were not observed, and dissolution was very fast (85% dissolved within 10 min) in all tested “intestinal” media. Interestingly, Froben, the sugarcoated formulation, consistently showed long disintegration times, with no dissolution for up to 20 min. irrespective of the pH, buffer capacity, or the inclusion of bile salt components in the medium. These findings suggest that Froben would be classified as slowly dissolving if the formulation was

solely exposed to the intestinal media without considering the disintegration of the sugar coating in the stomach. In order to account for disintegration in the stomach prior to exposure to the intestinal media, we performed two-stage dissolution tests (Section 2.4). The results from the two-stage tests (Figure 3d) revealed that as long as disintegration takes place in the gastric compartment, the dissolution from Froben tablets in the intestinal medium is very fast, reaching 85% dissolved within 5 min.

3.4. Modeling of In Vitro Dissolution

Tables 6 and 7 summarize the estimated DLM scalar values (95% CIs) obtained by model-based analysis of the gastric and intestinal *in vitro* dissolution profiles using the SIVA Toolkit. The goodness of fit was visually inspected with residual plots and assessed with the coefficient of determination (R^2). As shown in Table 6, the slowest dissolution rate of the API observed in FaSSIF V3 Levels I and the fastest of Antadys in FaSSIF V3 Level II resulted in the lowest (0.00185) and highest (0.0125) estimated DLM scalar values (S_{DLM}), respectively. Differences in the S_{DLM} estimates of the gastric dissolution were not expected to have a major impact on the *in vivo* performance of FLU since the release in the stomach is very poor.

Table 6. Mean (95% CI) diffusion layer model (DLM) scalar (S_{DLM}) estimates obtained from model-based analysis of *in vitro* dissolution data in various media for flurbiprofen pure drug, 100 mg USP tablets, and 100 mg Antadys formulations. The goodness of fit between predicted and observed dissolution profiles was evaluated with the R^2 .

Dissolution Medium	API Powder	Formulation USP Tablets	Antadys
FaSSGF Level III			
S_{DLM} (95% CI)	0.0218 (0.0161–0.0274)	0.0929 (0.0731–0.113)	0.107 (0.087–0.127)
R^2	0.944	0.973	0.982
FaSSIF V3 Level I			
S_{DLM} (95% CI)	0.00185 (0.001–0.00312)	0.0791 (0.0589–0.993)	0.120 (0.0979–0.142)
R^2	0.974	0.986	0.995
FaSSIF V3 Level II			
S_{DLM} (95% CI)	0.0965 (0.0544–0.139)	0.0622 (0.0398–0.0847)	0.125 (0.106–0.143)
R^2	0.971	0.976	0.996
Ph. Eur. Phosphate Buffer			
S_{DLM} (95% CI)	0.00542 (0.00468–0.00617)	0.0150 (0.0110–0.0189)	0.0449 (0.0448–0.0450)
R^2	0.986	0.983	0.999

Given the high solubility of FLU in intestinal media, we expected disintegration rather than API solubility to be the rate-limiting step for the dissolution rate of Froben. In this context, all intestinal single-stage dissolution profiles of Froben can be modelled by a universal first-order disintegration rate constant and a lag time in dissolution. Alternatively, modeling of the profiles obtained from the two-stage tests as serial dilutions of different media should be a more physiological approximation of the gastrointestinal (GI) luminal conditions. The estimates from both approaches are presented in Table 7.

In a dissolution-based *in vitro–in vivo* extrapolation (IVIVE) approach, the gastric and intestinal DLM scalar (S_{DLM}) estimates were transferred to the Simcyp simulator to generate medium-customized and formulation-specific *in vivo* dissolution scenarios and to simulate FLU *in vivo* performance.

All fitted dissolution profiles were in excellent agreement with the experimental ones with $R^2 > 0.94$.

Table 7. Mean (95% CI) DLM scalar (S_{DLM}) estimates obtained from model-based analysis of Froben *in vitro* dissolution data. The *in vitro* data from single dissolution experiments were modelled under the assumption that disintegration is the rate-limiting step to flurbiprofen dissolution in intestinal media, whereas for the two-stage dissolution, the serial dilution model was used. The goodness of fit between predicted and observed dissolution profiles was evaluated with the R^2 .

Dissolution Model/Media	Formulation
	Froben
First order disintegration/all intestinal media	
kd (h^{-1}) (95% CI)	0.127 (0.00844–0.0253)
Tlag (min) (95% CI)	14.6 (8.91–20.1)
R^2	0.941
Serial Dilution/Two-stage (FaSSGF Level III + FaSSIF V3 Level II)	
$S_{DLM, \text{Gastric}}$ (95% CI)	0.001 (0.001–0.0244)
$S_{DLM, \text{Intestinal}}$ (95% CI)	0.0712 (0.0576–0.0849)
R^2	0.991

3.5. PBPK/PD Model Development and Evaluation

The whole-body PBPK model of FLU accurately described and predicted plasma concentration–time profiles following intravenous and oral administration over a wide dose range (Figures 4–7). For the development and validation of the PBPK model, we used 17 plasma concentration–time profiles, including 5 for subjects with specific CYP2C9 genotypes. *In vitro* dissolution data available for the 100 mg immediate release solid oral products were modelled and incorporated into the PBPK model to simulate various *in vivo* dissolution scenarios. At any other dose level, including the CYP2C9 polymorphism studies, we used the fastest dissolution rate ($S_{DLM} = 0.125$) as input. When the administered form was an oral solution, we considered the entire dose to be pre-dissolved.

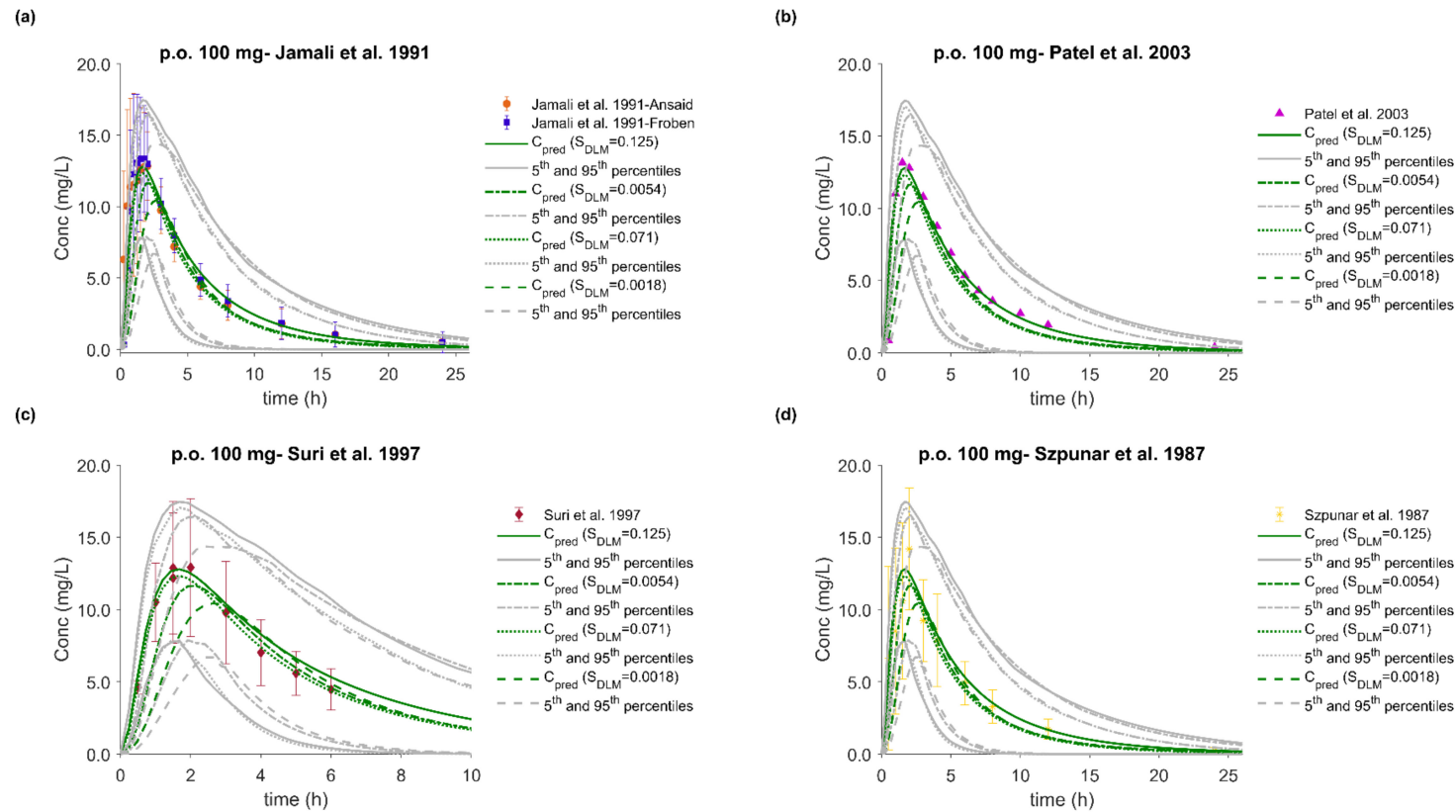


Figure 4. Mean flurbiprofen plasma concentration–time profiles after oral administration of 100 mg tablet in healthy Caucasians. Population simulations ($n = 100$) under four *in vivo* dissolution scenarios are shown as green and grey lines for the mean and the 5th and 95th percentiles, respectively. Each dissolution scenario is represented by the corresponding S_{DLM} value and is shown with different line style: $S_{DLM} = 0.125$ (solid line), $S_{DLM} = 0.071$ (dotted line), $S_{DLM} = 0.0054$ (dashed-dotted line), and $S_{DLM} = 0.0018$ (dashed line). Observed data with SD, if available, are depicted as (a) circles (Jamali et al., Ansaid) and squares (Jamali et al., Froben); (b) triangles (Patel et al.); (c) diamonds (Suri et al.); (d) asterisks (Szpunar et al.). References link to a specific observed dataset described in Table 1.

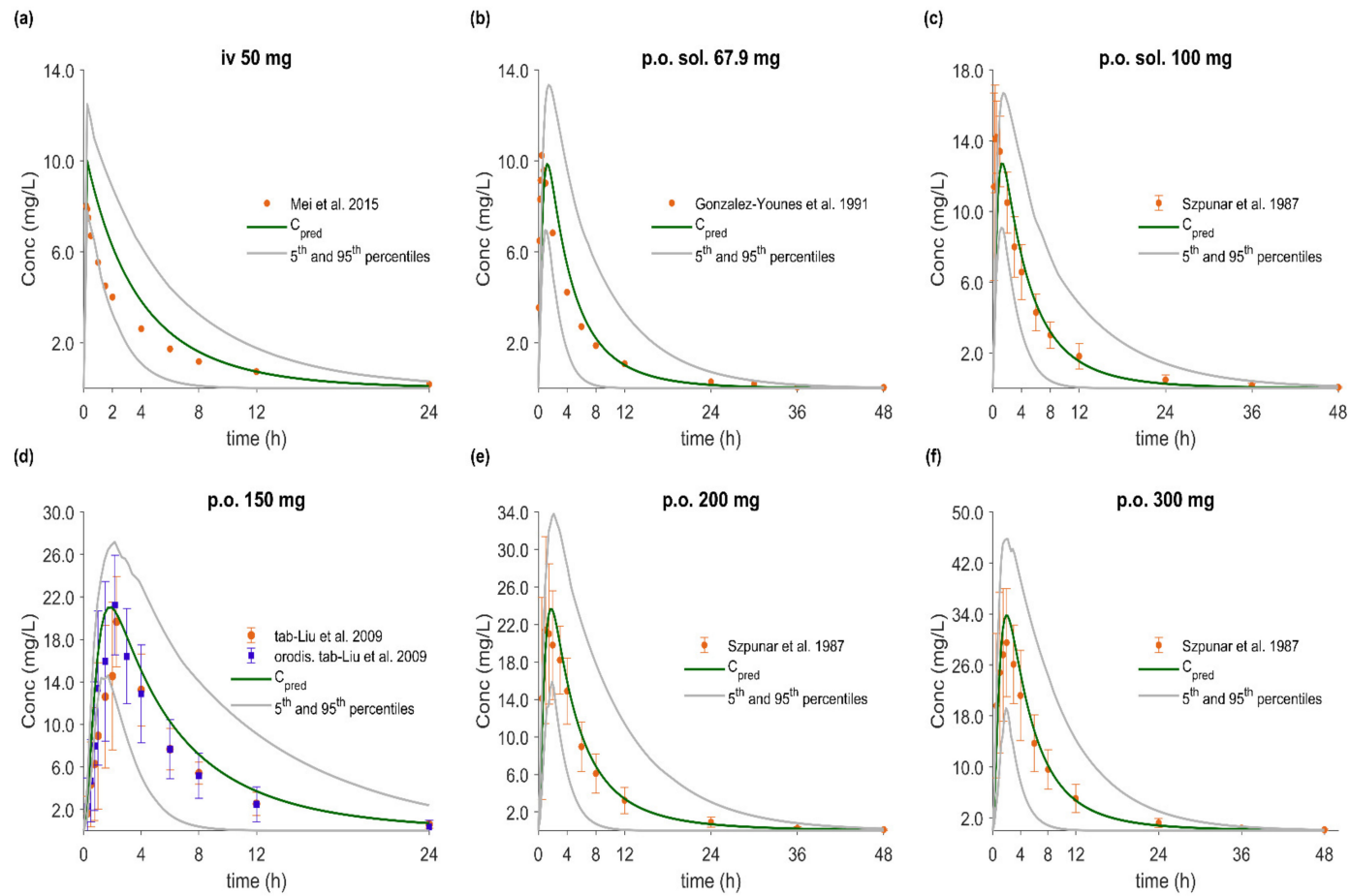


Figure 5. Mean flurbiprofen plasma concentration–time profiles after intravenous and oral administration in healthy Chinese (a,d) and Caucasian (b,c,e,f) individuals. Population simulations ($n = 100$) are shown as green and grey solid lines for the mean and the 5th and 95th percentiles, respectively. Observed data with SD, if available, are depicted as circles and squares. References link to a specific observed dataset described in Table 1. Administration protocol: (a) 50 mg intravenously; (b) 67.9 mg oral solution; (c) 100 mg oral solution; (d) 150 mg oral tablet; (e) 200 mg oral tablet; (f) 300 mg oral tablet.

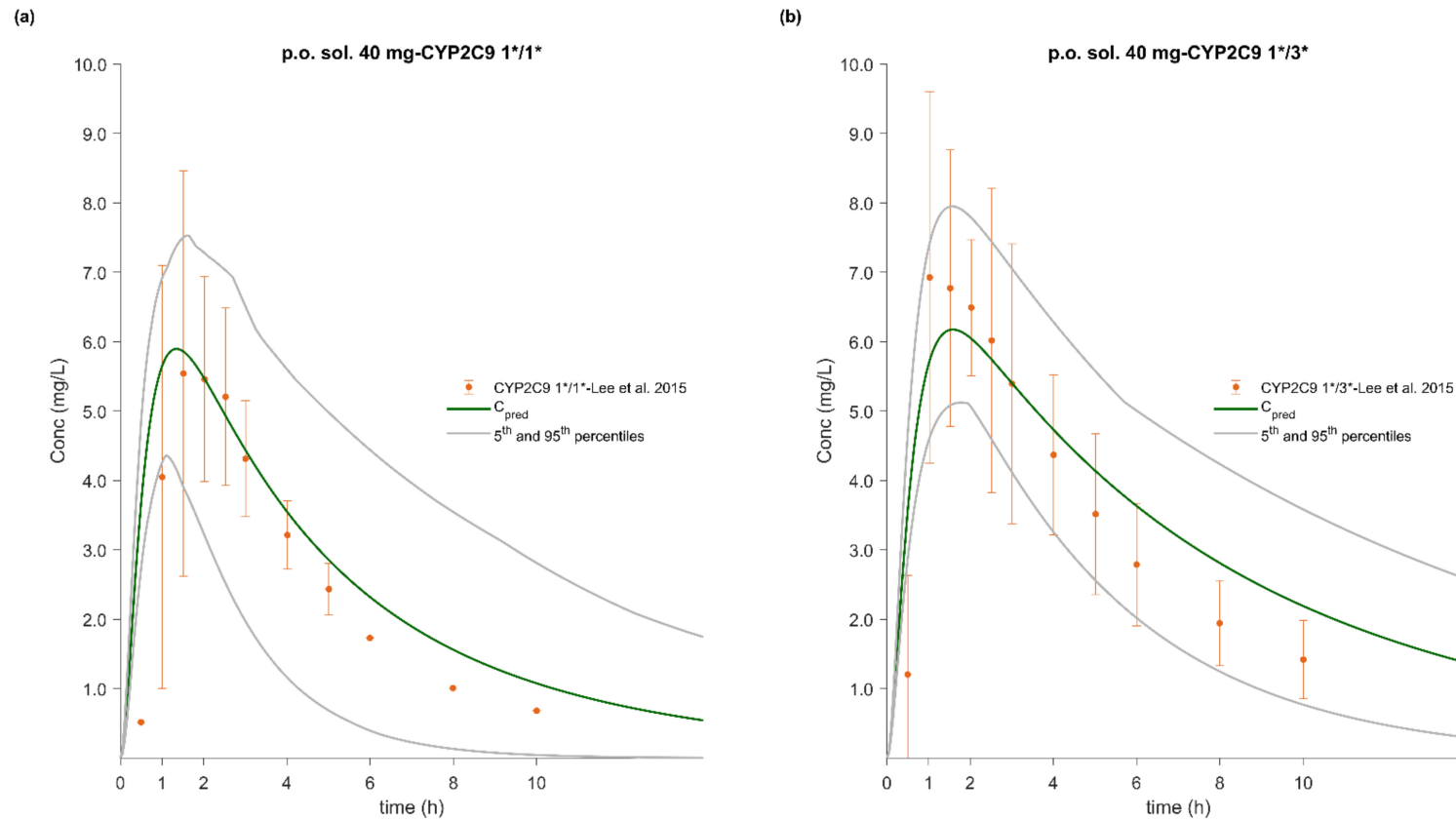


Figure 6. (a,b) Mean flurbiprofen plasma concentration–time profiles after administration of 40 mg oral solution in CYP2C9 1*/1* and 1*/3* healthy Korean volunteers, respectively. Population simulations ($n = 100$) are shown as green and grey lines for the mean and the 5th and 95th percentiles, respectively. Observed data, with SD, are depicted as circles. References link to a specific observed dataset described in Table 1.

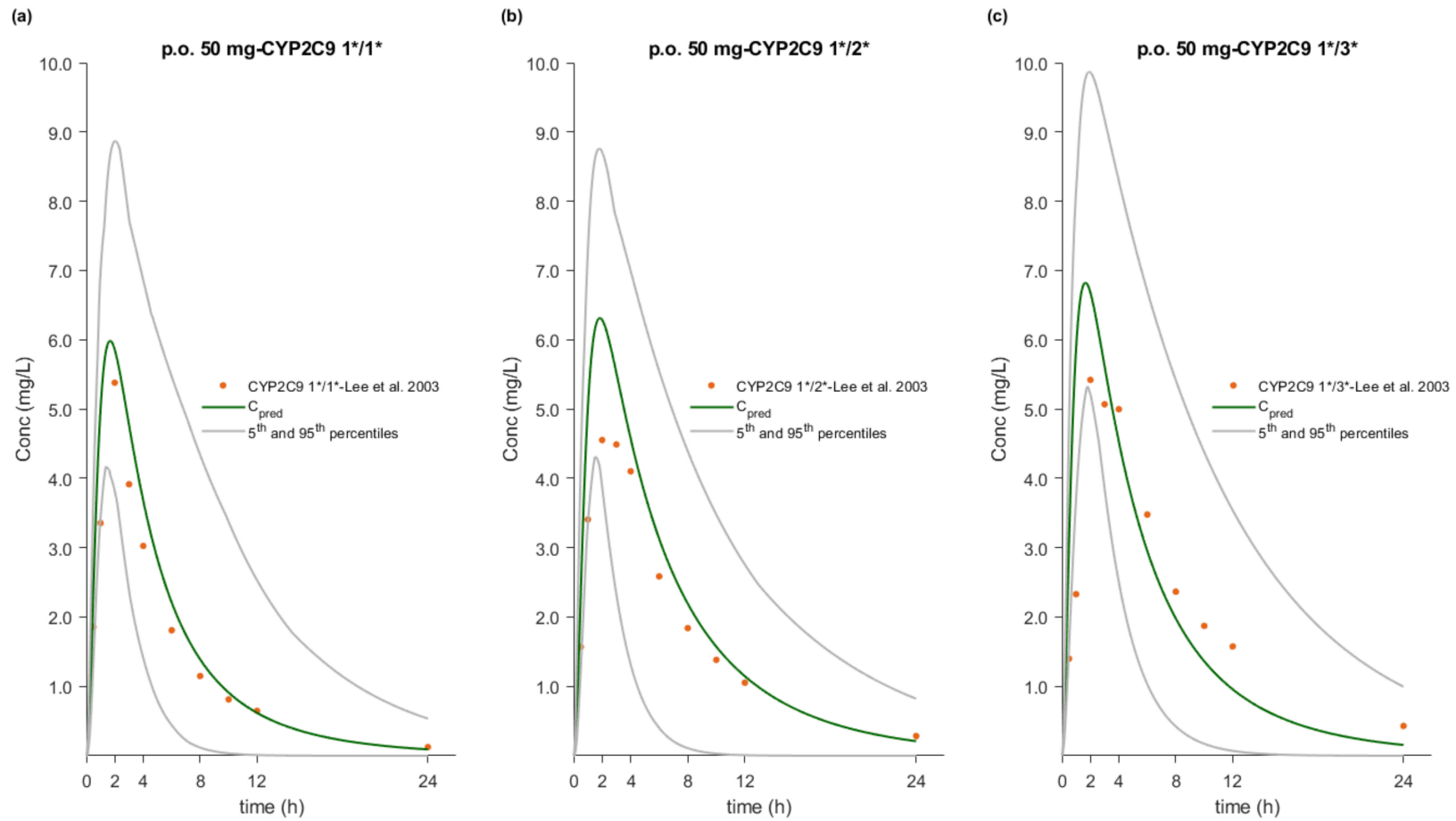


Figure 7. (a–c) Mean flurbiprofen plasma concentration–time profiles after administration of 50 mg oral tablet in CYP2C9 1*/1*, 1*/2*, and 1*/3* healthy Caucasian volunteers, respectively. Population simulations ($n = 100$) are shown as green and grey lines for the mean and the 5th and 95th percentiles, respectively. Observed mean data are depicted as circles. References link to a specific observed dataset described in Table 1.

The predictive performance of the PBPK model is demonstrated via visual comparisons of predicted versus observed plasma concentration–time profiles as well as quantitative measures such as MRDs and GMFEs. The predictions of plasma concentration–time trajectories for all routes of administration, doses, and drug products are in close agreement with the observed data. Applying a twofold deviation as the upper limit for an adequate prediction, the PBPK models achieved 100% ability to predict AUC_{inf} , C_{max} , and CL/F adequately. When a more stringent acceptance criterion (i.e., 25% deviation) was applied, the predictions of AUC_{inf} , C_{max} , and CL/F were adequate in 90%, 81%, and 74% of the cases, respectively. Moreover, the MRD values were within twofold in 94% of the studies, with only about 20% less than 1.25-fold. The overall MRD values for the FLU PBPK model and GMFE values for AUC_{inf} , C_{max} , and CL/F were 1.59 (1.04–2.43), 1.14 (1.00–1.39), 1.15 (1.01–1.41) and 1.18 (1.06–1.39), respectively. Detailed results along with calculated MRD and GMFE values for all studies are presented in Tables 8 and 9.

Table 8. Mean relative deviation (MRD) values of flurbiprofen plasma concentration predictions.

Route of Administration	Dose (mg)	Flurbiprofen MRD	Reference
<i>iv (s.d.)</i>	50	1.41	[34]
<i>po (sol, s.d.)</i>	67.9	1.85	[35]
<i>po (sol, s.d.)</i>	100	1.60	[36]
<i>po (sol, s.d., CYP2C9 1*/1*)</i>	40	1.52	[37]
<i>po (sol, s.d., CYP2C9 1*/3*)</i>	40	1.30	[37]
<i>po (tab, s.d., CYP2C9 1*/1*)</i>	50	1.24	[42]
<i>po (tab, s.d., CYP2C9 1*/2*)</i>	50	1.30	[42]
<i>po (tab, s.d., CYP2C9 1*/3*)</i>	50	1.62	[42]
<i>po (tab, s.d., CYP2C9 1*/1*)</i>	50	1.26	[43]
<i>po (tab, s.d., CYP2C9 1*/1*)</i>	50	1.25	[43]
<i>po (tab, s.d., CYP2C9 1*/3*)</i>	50	1.28	[43]
<i>po (tab, s.d., CYP2C9 1*/3*)</i>	50	1.25	[43]
<i>po (tab, s.d., CYP2C9 3*/3*)</i>	50	1.25	[43]
<i>po (tab, s.d., CYP2C9 3*/3*)</i>	50	1.20	[43]
<i>po (tab (Ansaid), s.d.)</i>	100	1.31–2.38	[38]
$S_{DLM_SI} = 0.125$		1.31	
$S_{DLM_SI} = 0.0054$		1.72	
$k_d = 0.127 h^{-1}$ and $T_{lag} = 14.6 min$		1.64	
$S_{DLM_SI} = 0.0712$		1.65	
$S_{DLM_SI} = 0.0018$		2.38	
<i>po (tab (Froben), s.d.)</i>	100	1.70–2.43	[38]
$S_{DLM_SI} = 0.125$		1.70	
$S_{DLM_SI} = 0.0054$		1.88	
$k_d = 0.127 h^{-1}$ and $T_{lag} = 14.6 min$		1.80	
$S_{DLM_SI} = 0.0712$		1.83	
$S_{DLM_SI} = 0.0018$		2.43	
<i>po (tab (Froben), s.d.)</i>	100	1.69–1.92	[4]
$S_{DLM_SI} = 0.125$		1.69	
$S_{DLM_SI} = 0.0054$		1.78	
$k_d = 0.127 h^{-1}$ and $T_{lag} = 14.6 min$		1.92	
$S_{DLM_SI} = 0.0712$		1.90	
$S_{DLM_SI} = 0.0018$		1.79	
<i>po (tab, s.d.)</i>	100	1.04–1.74	[39]
$S_{DLM_SI} = 0.125$		1.11	
$S_{DLM_SI} = 0.0054$		1.20	
$k_d = 0.127 h^{-1}$ and $T_{lag} = 14.6 min$		1.12	
$S_{DLM_SI} = 0.0712$		1.04	
$S_{DLM_SI} = 0.0018$		1.74	
<i>po (tab, s.d.)</i>	150	1.51	[40]
<i>po (orod, s.d.)</i>	150	1.42	[40]
<i>po (tab (Ansaid), s.d.)</i>	200	1.20	[36]
<i>po (tab (Ansaid), s.d.)</i>	300	1.34	[36]
MRD (range)		1.54 (1.04–2.43)	
MRD ≤ 1.25		9/38	
MRD ≤ 2		36/38	

Table 9. Comparison of mean predicted and observed AUC, C_{max} , and apparent clearance (CL/F) values of flurbiprofen. Calculation of predicted to observed ratio ($R_{pred/obs}$) and geometric fold error (GMFE) values.

Route of Administration	Dose (mg)	AUC _{inf} (mg/L·h)			C _{max} (mg/L)			CL/F (L/h)			Reference
		obs	pred	R _{pred/obs}	obs	pred	R _{pred/obs}	obs	pred	R _{pred/obs}	
iv (s.d.)	50	35.2	43.7	1.24	-	-	-	1.50	1.36	0.91	[34]
po (sol, s.d.)	67.9	55.1	56.1	1.01	10.8	9.99	0.92	-	-	-	[35]
po (sol, s.d.)	100	82.7	78.0	0.94	14.2	12.9	0.91	1.28	1.50	1.17	[36]
po (sol, s.d., CYP2C9 1*/1*)	40	29.3	29.1	0.99	5.54	5.86	1.06	1.39	1.16	0.83	[37]
po (sol, s.d., CYP2C9 1*/3*)	40	47.6	44.2	0.93	6.93	6.22	0.90	0.88	0.67	0.76	[37]
po (tab, s.d., CYP2C9 1*/1*)	50	29.4	28.6	0.97	5.38	5.84	1.09	1.77	1.67	0.83	[42]
po (tab, s.d., CYP2C9 1*/2*)	50	40.7	45.6	1.12	4.55	6.34	1.39	1.30	1.20	0.92	[42]
po (tab, s.d., CYP2C9 1*/3*)	50	51.1	46.4	0.91	5.42	6.68	1.23	1.00	1.03	1.03	[42]
po (tab, s.d., CYP2C9 1*/1*)	50	30.8 ^a	35.8 ^a	1.16	6.1 ^a	6.91 ^a	1.13	1.6 ^a	1.4 ^a	0.88	[43]
po (tab, s.d., CYP2C9 1*/1*)	50	30.8 ^a	36 ^a	1.17	6.1 ^a	6.8 ^a	1.11	1.6 ^a	1.43 ^a	0.89	[43]
po (tab, s.d., CYP2C9 1*/3*)	50	53.7 ^a	54.6 ^a	1.02	8.9 ^a	7.7 ^a	0.87	0.9 ^a	0.98 ^a	1.09	[43]
po (tab, s.d., CYP2C9 1*/3*)	50	53.7 ^a	53.1 ^a	0.99	8.9 ^a	7.44 ^a	0.84	0.9 ^a	0.96 ^a	1.07	[43]
po (tab, s.d., CYP2C9 3*/3*)	50	(85.8, 119) ^b	76.1	(0.89, 0.64)	(8, 9.4) ^b	6.99	(0.87, 0.74)	(0.6, 0.4) ^b	0.64	(1.07, 1.6)	[43]
po (tab, s.d., CYP2C9 3*/3*)	50	(85.8, 119) ^b	77.7	(0.91, 0.65)	(8, 9.4) ^b	7.1	(0.89, 0.76)	(0.6, 0.4) ^b	0.68	(1.13, 1.7)	[43]
po (tab (Ansaid), s.d.)	100										[38]
			81.1	1.01		12.8	1.00				
			66.5	0.83		11.6	0.90				
k _d = 0.127 h ⁻¹ and T _{lag} = 14.6 min		80.5	68.8	0.85	12.8	11.8	0.92	-	-	-	
			67.2	0.83		12.3	0.96				
			62.7	0.78		10.4	0.81				
po (tab (Froben), s.d.)	100										[38]
			81.1	0.99		12.8	0.96				
			66.5	0.81		11.6	0.87				
k _d = 0.127 h ⁻¹ and T _{lag} = 14.6 min		82.3	68.8	0.84	13.3	11.8	0.88	-	-	-	
			67.2	0.82		12.3	0.92				
			62.7	0.76		10.4	0.78				

Table 9. Cont.

Route of Administration	Dose (mg)	AUC _{inf} (mg/L·h)			C _{max} (mg/L)			CL/F (L/h)			Reference	
		obs	pred	R _{pred/obs}	obs	pred	R _{pred/obs}	obs	pred	R _{pred/obs}		
po (tab (Froben), s.d.)	100										[4]	
<i>S_{DLM_SI} = 0.125</i>			81.1	0.92		12.7	0.96		1.42	1.12		
<i>S_{DLM_SI} = 0.0054</i>			66.5	0.76	13.2	11.6	0.88	1.27	1.68	1.32		
<i>k_d = 0.127 h⁻¹ and T_{lag} = 14.6 min</i>		87.8	68.8	0.78		11.8	0.89		1.66	1.31		
<i>S_{DLM_SI} = 0.0712</i>			67.2	0.77		12.2	0.92		1.66	1.31		
<i>S_{DLM_SI} = 0.0018</i>			62.7	0.71		11.0	0.84		1.77	1.39		
<i>po (tab, s.d.)</i>	100										[39]	
<i>S_{DLM_SI} = 0.125</i>			81.1	1.20		12.7	0.98		1.42	0.93		
<i>S_{DLM_SI} = 0.0054</i>			66.5	0.98		11.6	0.90		1.68	1.11		
<i>k_d = 0.127 h⁻¹ and T_{lag} = 14.6 min</i>		67.7	68.8	1.02	12.9	11.8	0.91	1.52	1.66	1.09		
<i>S_{DLM_SI} = 0.0712</i>			67.2	0.99		12.2	0.95		1.66	1.09		
<i>S_{DLM_SI} = 0.0018</i>			62.7	0.93		11.0	0.86		1.77	1.16		
<i>po (tab, s.d.)</i>	150	124.3	154.4	1.24	15.2	20.7	1.36	-	-	-	[40]	
<i>po (orod, s.d.)</i>	150	129.8	154.4	1.19	16.8	20.7	1.23	-	-	-	[40]	
<i>po (tab (Ansaid), s.d.)</i>	200	161.3	159.9	0.99	21.4	23.6	1.10	1.32	1.50	1.14	[36]	
<i>po (tab (Ansaid), s.d.)</i>	300	233.9	228.9	0.98	29.5	33.7	1.14	1.36	1.55	1.14	[36]	
GMFE (range)			1.15 (1.01–1.56)			1.14 (1.00–1.39)			1.18 (1.03–1.7)			
GMFE ≤ 1.25			30/38			31/37			18/25			
GMFE ≤ 2			38/38			37/37			25/25			

^a: median value; ^b: individual values (*n* = 2).

The final PBPK model was further coupled with a PD FLU analgesic efficacy model. The integrated PBPK/PD model was able to capture the pain-relieving response of S-FLU after oral administration of 100 mg racemic FLU. The predictive performance was assessed by comparing the predicted with the observed response time profiles for two PD endpoints, the TPEP amplitude and pain rating (see Figure 8). Regardless of the *in vivo* dissolution rate or the genotype of the virtual individuals, the predictive accuracy for the prediction of the PD metrics, maximum response (R_{max}), time to maximum response (TR_{max}), and area under the effect-time curve (AUCE), was in all in cases within 1.25-fold (see Table S2).

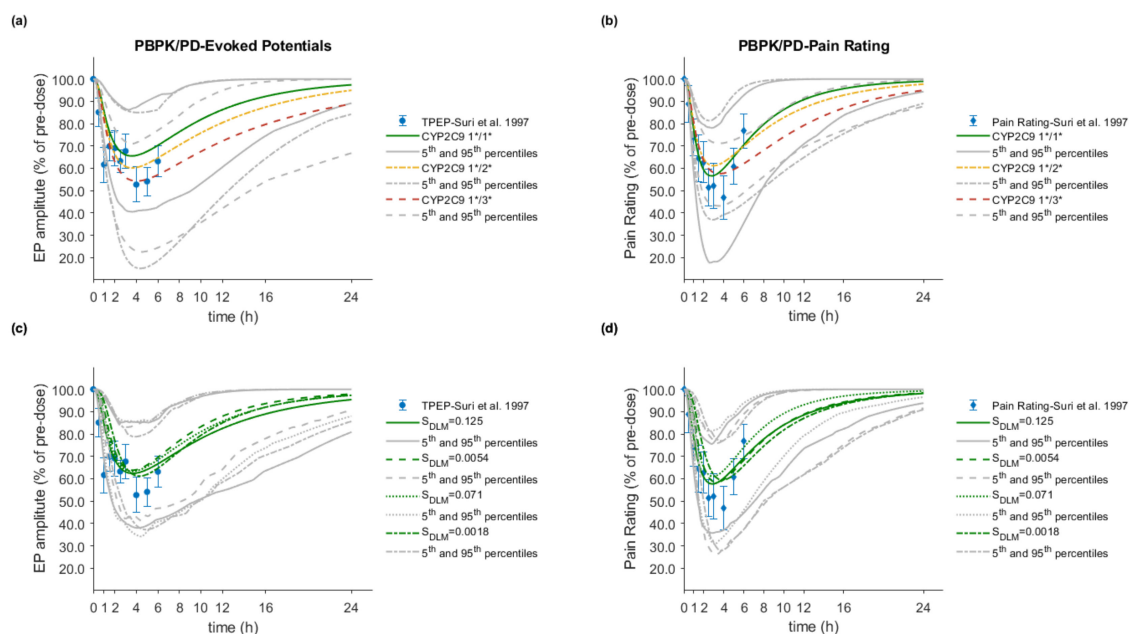


Figure 8. Mean flurbiprofen response time profiles after administration of 100 mg oral tablet in healthy Caucasians. (a,b) Genetic polymorphism: population simulations ($n = 100$) in CYP2C9 1*/1*, 1*/2* and 1*/3* are shown for the mean as green (solid), yellow (dash dotted), and orange (dashed) lines, respectively. Grey lines with the corresponding style represent the 5th and 95th percentiles. (c,d) Dissolution rate: Population simulations ($n = 100$) under four *in vivo* dissolution scenarios are shown as green and grey lines for the mean and the 5th and 95th percentiles, respectively. Each dissolution scenario is represented by the corresponding S_{DLM} value and is shown with different line style: $S_{DLM} = 0.125$ (solid line), $S_{DLM} = 0.071$ (dotted line), $S_{DLM} = 0.0054$ (dashed line), and $S_{DLM} = 0.0018$ (dashed-dotted line). Observed data with SD, if available, are depicted as circles. References link to a specific observed dataset described in Table 1.

3.6. Effect of Dissolution Rate

Several *in vitro* dissolution profiles from various marketed FLU immediate release oral products at the highest dose strength of 100 mg and under different *in vitro* conditions were generated. In a dissolution-based IVIVE approach, and after modeling of the *in vitro* data using the diffusion layer model, the obtained S_{DLM} values (for stomach and small intestine) were integrated into the PBPK/PD model to investigate the impact of different *in vivo* dissolution rates on the PK/PD of FLU. Population simulations ($n = 100$) were performed with the NEurCaucasian virtual population and the enzymatic status of each virtual subject was tracked. The overall mean predicted plasma concentration–time profiles of each dissolution scenario were compared with observed PK profiles from five external datasets and among the datasets (Figure 5). Between the results of the fastest ($S_{DLM} = 0.125$) and slowest ($S_{DLM} = 0.0018$) dissolution rates (corresponding to 85% dissolved under intestinal conditions in 2.5 and 60 min, respectively) a decrease of only about 20% in both C_{max} and AUC_{inf} was observed (Table 9). On the other hand, t_{max} was prolonged by 30 min (data not shown). Despite these differences,

in all cases, the predictive accuracy was acceptable with MRD between 1.04 and 2.43 and GMFE values ranging from 0.78 to 1.01 for C_{\max} and 0.76 to 1.20 for AUC_{inf} .

The PD metrics, R_{\max} , and AUCE of any of the two endpoints were not noticeably affected by the *in vivo* dissolution rates. Any previous discrepancies in the PK parameters (C_{\max} and AUC_{inf}) did not translate to differences in R_{\max} and AUCE, rather, they were mitigated to less than 5.5% and 7%, respectively. However, the TR_{\max} was prolonged by up to 1h when the slowest dissolution rate was applied, indicating a potential clinical relevance of slow dissolution on the onset and the time to maximum analgesic action. Simulations of the response time profiles and comparison with the actual clinical data for each dissolution rate and for both endpoints are depicted in Figure 8c,d. Detailed results for the PD together with the calculated $R_{\text{pred/obs}}$ are shown in Table S2.

3.7. Effect of CYP2C9 Genetic Polymorphism

PBPK simulations accurately captured the observed effect of three different CYP2C9 genotypes on FLU PK in Caucasian and Chinese populations. Population simulations ($n = 300$) were performed using the NEurCaucasian and Chinese virtual populations to reproduce the clinical studies published by Lee et al. (2003) and Lee et al. (2015), respectively [37,42]. The sample size in these population simulations was increased to 300 (30 trials of 10 subjects each) to ensure adequate representation of each genotype. The enzymatic status of each virtual subject was tracked, and the individual plasma concentration–time profiles were stratified on the basis of the CYP2C9 genotype. The range of GMFE values for C_{\max} , AUC_{inf} , and CL/F was 0.90–1.39, 0.91–1.12, and 0.76–1.03, respectively. An overall reduction of 42% and 38% in the clearance of CYP2C9 1*/3* individuals of both populations, which in turn led to a 1.52- and a 1.62-fold increase in AUC, respectively, was predicted. These findings are in close agreement with the observed data from Lee et al. (2003) and Lee et al. (2015), who reported a decrease in CYP2C9 1*/3* clearance of about 37% and 44%, resulting in a 1.62- and 1.74-fold increase in AUC, respectively. The genotypes and study specific MRDs and GMFEs are summarized in Tables 8 and 9.

The model was used to simulate the response time curves of subjects with specific CYP2C9 genotypes (1*/1*, 1*/2*, and 1*/3*) in order to explore potential PD differences. Population simulations showed no effect on R_{\max} and TR_{\max} , whereas a 1.35-fold increase in the AUCE for the CYP2C9 1*/3* subjects was predicted using the TPEP amplitude as the endpoint (Figure 8a,b). However, when the subjective pain rating score scale was used, no consistent increase in the AUCE was observed. Interestingly, in comparison to the wild type (CYP2C9 1*/1*), the time post-administration to return to 80% of the initial value ($T_{80\% \text{ initial}}$) in 1*/3* subjects was delayed by about 7 and 4.5 h for both TPEP and pain rating, respectively. A similar but less pronounced effect was also predicted for the 1*/2* subjects. Details of the simulation results together with the R_{\max} , TR_{\max} , AUCE, and $T_{80\% \text{ initial}}$ exact values are summarized in Table S2.

3.8. Drug–Drug–Gene Interactions

A total of 13 sets of plasma concentration–time profiles were available in the literature for evaluation of model-predicted interactions. Accurate prediction of the impact of a perpetrator on the pharmacokinetics of a victim drug ratifies the capacity of the victim drug PBPK model to correctly predict the amount of drug eliminated via the affected pathway and indicates that the perpetrator model properly describes the concentration of the inhibitor/induced at the site(s) of interaction. Furthermore, accurately capturing not only drug–drug but also drug–gene interactions reinforces the model confidence in describing the effect of genotype on the pharmacokinetics of the substrate drug.

In subjects with three CYP2C9 genotypes, the wild type and both hetero- and homozygotes for the CYP2C9*3 allele, the PBPK model successfully predicted the gene dose-dependent interactions with the prototype moderate inhibitor (fluconazole). The AUC ratio was slightly underpredicted in 1*/1* and 1*/3* subjects at the 400 mg fluconazole dose level ($R_{\text{pred/obs}} = 0.74\text{--}0.78$). Nevertheless,

the concentration time course of the victim drug with and without coadministration at both inhibitor dose levels and for all genotypes was accurately captured (Figure 9).

PBPK model simulations successfully predicted the FLU–fluconazole interaction under different dose levels and regimens in six clinical studies, in which no prior genotyping had been performed (Figure 10a–e). All DDI AUC, C_{\max} , and CL/F ratios were within 1.25-fold. The rifampicin inductive effect on the exposure of FLU was also accurately predicted from one study, with DDI ratios within 1.25-fold (Figure 10f).

The DDI predictive accuracy was further evaluated by calculation of the GMFE values for the DDI AUC, C_{\max} , and CL/F ratios, which ranged from 1.15 to 1.17. The corresponding $R_{\text{pred/obs}}$ values for DDI AUC, C_{\max} , and CL/F ratios of all modeled DDI studies together with the GMFEs are listed in Table 10.

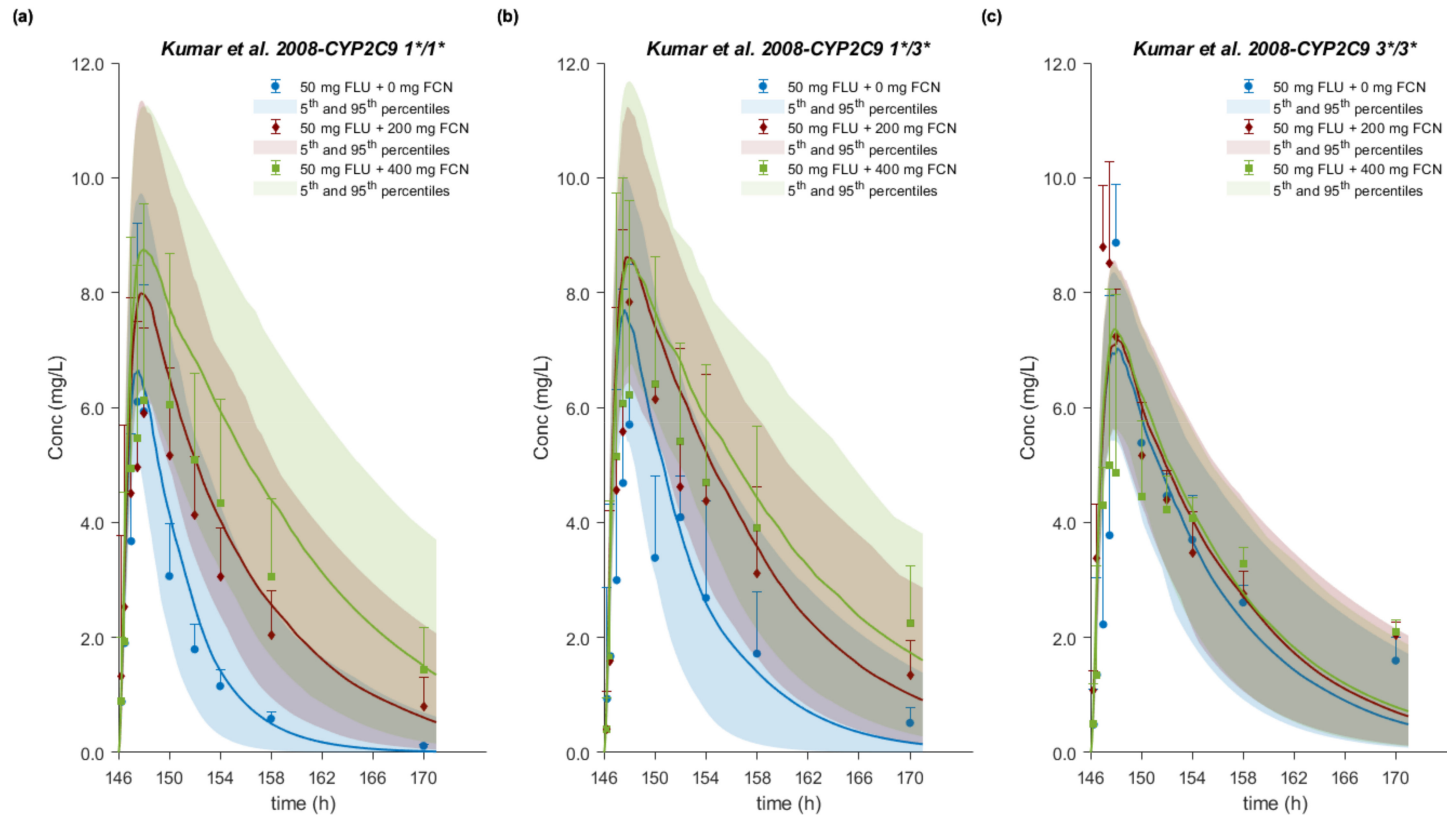


Figure 9. (a–c) Mean plasma concentration–time profiles after administration of 50 mg flurbiprofen as oral tablet alone and with 200 mg or 400 mg fluconazole (FCN) in CYP2C9 1*/1*, 1*/3*, and 3*/3* healthy Caucasian volunteers, respectively. Population simulations ($n = 100$) are shown for the mean as blue (FLU + 0 mg FCN), red (FLU + 200 mg FCN), and light green (FLU + 400 mg FCN) solid lines, and observed data with SD, if available, are depicted as circles, diamonds, and squares, respectively. Shaded areas represent the 5th and 95th percentiles. References link to a specific observed dataset described in Table 2.

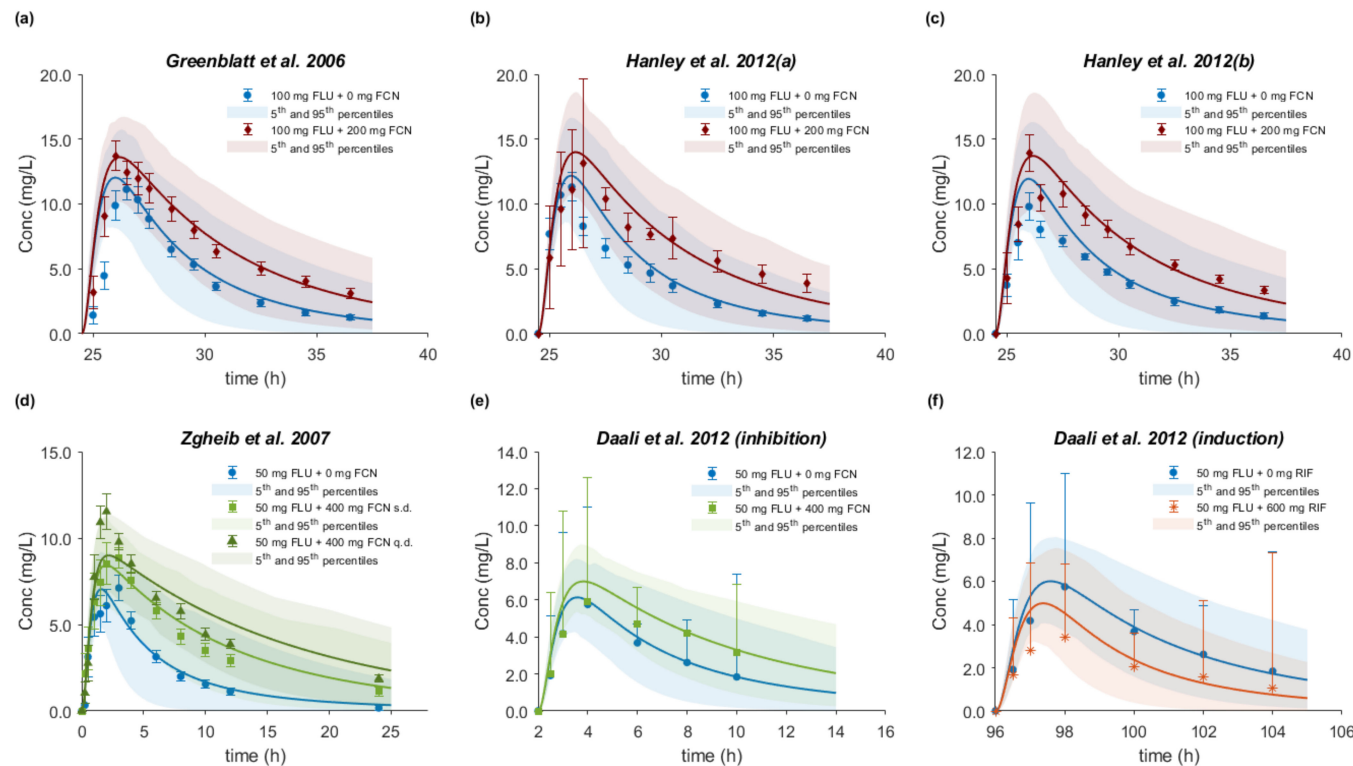


Figure 10. Mean plasma concentration–time profiles after administration of flurbiprofen alone and with the perpetrator drug in healthy volunteers. (a–e) Population simulations ($n = 100$) without or with the CYP2C9 inhibitor fluconazole (FCN) are shown for the mean as blue (FLU + 0 mg FCN), red (FLU + 200 mg FCN), light green (FLU + 400 mg FCN s.d.), and dark green (FLU + 400 mg FCN q.d.) solid lines, and observed data with SD, if available, are depicted as circles, diamonds, squares, and triangles, respectively. (f) Population simulations ($n = 100$) without or with the CYP2C9 inducer rifampicin (RIF) are shown for the mean as blue (FLU + 0 mg RIF) and orange (FLU + 600 mg RIF) solid lines, and observed data with SD, if available, are depicted as circles and asterisks, respectively. Shaded areas represent the 5th and 95th percentiles. References link to a specific observed dataset described in Table 2.

Table 10. Comparison of mean predicted and observed drug–drug interaction (DDI) AUC, C_{max} , and apparent clearance (CL/F) ratios of flurbiprofen–fluconazole/rifampicin interaction. Calculation of predicted to observed ratio ($R_{pred/obs}$) and geometric fold error (GMFE) values.

Victim Drug Administration	Perpetrator Drug Administration	No. of Doses	Interval (h)	CYP2C9 Genotype	DDI AUC Ratio			DDI C_{max} Ratio			DDI CL/F Ratio			Reference	
					obs	pred	$R_{pred/obs}$	obs	pred	$R_{pred/obs}$	obs	pred	$R_{pred/obs}$		
Flurbiprofen	Fluconazole														
po 50 mg s.d.	po 200 mg q.d.	7	2	1*/1*	2.02 ^a	1.94	0.96	1.03 ^a	1.18	1.15	0.5 ^a	0.51	1.02	[43]	
po 50 mg s.d.	po 400 mg q.d.	7	2	1*/1*	3.03	2.36	0.78	0.99	1.23	1.24	0.31	0.42	1.35	[43]	
po 50 mg s.d.	po 200 mg q.d.	7	2	1*/3*	1.8	1.58	0.88	0.87	1.11	1.28	0.56	0.63	1.13	[43]	
po 50 mg s.d.	po 400 mg q.d.	7	2	1*/3*	2.48	1.84	0.74	0.94	1.14	1.21	0.44	0.54	1.23	[43]	
po 50 mg s.d.	po 200 mg q.d.	7	2	3*/3*	(1.58, 1.28) [#]	1.09	0.76	(1.08, 0.91) [#]	1.02	1.02	(0.75, 0.66) [#]	0.92	1.30	[43]	
po 50 mg s.d.	po 400 mg q.d.	7	2	3*/3*	(1.39, 1.12) [#]	1.16	0.92	(0.54, 0.90) [#]	1.03	1.43	(1.00, 0.66) [#]	0.86	1.04	[43]	
po 100 mg s.d.	po 200 mg b.i.d.	2	0.5	n.a.	1.71 ^b	1.65	0.97	1.16 ^b	1.15	0.99	0.57	0.61	1.07	[45]	
po 100 mg s.d.	po 200 mg b.i.d.	2	0.5	n.a.	1.81	1.51	0.83	1.23	1.13	0.92	0.55	0.68	1.24	[46]	
po 100 mg s.d.	po 200 mg b.i.d.	2	0.5	n.a.	1.97 ^b	1.62	0.82	1.47 ^b	1.15	0.78	0.5	0.62	1.24	[44]	
po 50 mg s.d.	po 400 mg s.d.	1	2	n.a.	2.16	2.23	1.03	1.24	1.2	0.97	0.46	0.48	1.04	[47]	
po 50 mg s.d.	po 400 mg q.d.	7	2	n.a.	2.81	2.87	1.02	1.37	1.25	0.91	0.35	0.39	1.11	[47]	
po 50 mg s.d.	po 400 mg s.d.	1	2	n.a.	1.21	1.53	1.26	1.14	1.14	1.00	0.67	0.67	1.00	[48]	
po 50 mg s.d.	Rifampicin po 600 mg q.d.	5	0	n.a.	0.56	0.63	1.13	0.71	0.83	1.17	1.85	1.73	0.94	Daali et al.	
GMFE (range)					1.17 (1.02–1.35)			1.16 (1.00–1.43)			1.15 (1.00–1.35)				
GMFE ≤ 1.25					8/12			9/12			10/12				
GMFE ≤ 2					12/12			12/12			12/12				

n.a.= not available; ^a median; ^b geometric mean. [#] individual values (n=2)

4. Discussion

In the present study, we developed a comprehensive PBPK/PD model of FLU, which allows for consistent and accurate representation of the dose–exposure relationship after intravenous and oral administration of different dosage forms in Caucasian and Chinese healthy populations over a wide dose range (40–300 mg). The model mechanistically describes the absorption and precisely predicts the impact of formulation and dissolution rate on the PK of FLU. By integrating *in vitro* metabolism with demographic and *in vivo* data, the model is able to quantify the contribution of the CYP2C9 polymorphic alleles on the elimination pathways, providing gainful insight into the magnitude of genetic polymorphism on the pharmacokinetic behavior of FLU. By linking the verified PBPK model with an inhibitory E_{max} model describing the analgesic efficacy of the drug, we used the final PBPK/PD model to explore the effect of system or extrinsic factors on the onset and duration of pain-relieving action as well as to suggest dose adjustments for specific genetic sub-populations. Furthermore, the PBPK model successfully predicted gene dose-dependent DDIs, allowing for dose optimization recommendations, increasing confidence in the predictive accuracy and robustness of the model.

High inter-individual variability in PK studies of FLU has been associated with complex and variable oral absorption, including double peak phenomena [2]. This variability, often reaching up to 100%, is consistent among studies with respect to both C_{max} and AUC. As a typical BCS class II weak acid, flurbiprofen absorption from the small intestine is expected to be dissolution-limited and therefore the formulation and its dissolution rate will be critical to the *in vivo* performance. At the same time, FLU is mainly eliminated (>71% of the dose) through metabolic oxidation to its primary metabolite, 4-hydroxy FLU, exclusively by the P450 CYP29. As a result, FLU exhibits polymorph-dependent PK, which is affected by concomitant administration of CYP2C9 inhibitors such as fluconazole. Although FLU has been extensively studied and has been recommended as probe drug for CYP2C9 substrates, relatively few studies have been published regarding its PK/pharmacogenomic and clinical interactions [43–47].

The present PBPK/PD model leveraged data from multiple *in vitro* sources and *in vivo* human studies. Prior to model development, we performed a careful biopharmaceutic analysis, including formulation selection, biorelevant *in vitro* solubility, and dissolution experiments. Data analysis of the *in vitro* results enabled translation and extrapolation of the biopharmaceutic parameters to the *in vivo* luminal conditions, providing mechanistic insight into the oral absorption of the drug. The initial PBPK model was informed with allele-specific *in vitro* metabolism data to account for differences in the elimination, due to CYP2C9 genetic polymorphism, and successfully predicted (36 out of 38) observed concentration–time profiles and CYP2C9 genetic effects within a predefined twofold deviation boundary (Table 8). In both cases where MRD fell outside the twofold limit, the slowest dissolution rate, corresponding to 85% release only after 60 min, was used as the input profile and resulted in sub-optimal absorption and underprediction of C_{max} and AUC.

For further evaluation and enhanced prediction accuracy, we implemented a more stringent success measure consisting of a 25% deviation boundary. This predefined criterion is not meant to be equated to the bioequivalence acceptance limits (i.e., 80–125%), but rather is selected to be sufficiently conservative to prevent poor decision-making due to misclassified predictions. All individual model predictions for the pharmacokinetic parameters C_{max} , AUC_{inf} , and CL/F were within twofold, and 90%, 81%, and 74% of them, respectively, satisfied the 25% deviation criterion. The slight underprediction ($R_{pred/obs} = 0.76–0.78$) of C_{max} and AUC in the Jamali et al. study after oral administration of 100 mg was associated with the input of the slowest intestinal dissolution rate ($S_{DLM} = 0.0018$) [38]. By contrast, the C_{max} was overpredicted ($R_{pred/obs} = 1.36–1.39$) in CYP2C9 1*/3* individuals at 50 and 150 mg. Deviations from the 1.25-fold boundary in AUC ($R_{pred/obs} = 0.71–0.78$) and clearance ($R_{pred/obs} = 1.31–1.39$) were consistently predicted under all dissolution scenarios, except the slowest ($S_{DLM} = 0.0018$), when simulating the study by Patel et al. [4]. Nevertheless, it has to be noted that in most studies, the participants were not subjected to prior genotype screening, and only the mean plasma concentration–time profiles were reported.

Population simulations, after translation of *in vitro* release into *in vivo* dissolution rates, provided insight into the impact of absorption variables on FLU PK/PD. Interestingly, it was shown that differences between the fastest (85% dissolved in 2.5 min) and the slowest (85% dissolved in 60 min) *in vivo* dissolution rates ($S_{DLM} = 0.0018$ vs. $S_{DLM} = 0.125$) translated into a decrease in C_{max} of only approximately 20%, while t_{max} was prolonged by 30 min. These simulations indicate that *in vitro* dissolution rate might not be the most critical attribute for the *in vivo* performance. Instead, they suggest that the interplay between absorption and metabolism plays a key role, given also that flurbiprofen's half-life is rather short (3–7 h). Regardless of the shift in the regional absorption peak from mid-jejunum at the fastest dissolution rate to the ileum at the slowest dissolution rate, we predicted the absorption to be complete ($f_a > 0.93$). These (minor) differences in C_{max} and AUC_{inf} did not result in a similar degree of change in R_{max} and AUCE. In fact, they were mitigated to less than 7%, showing that *in vivo* dissolution rate has no or little effect on the degree and duration of analgesic effect. However, at the slowest dissolution rate, the TR_{max} was prolonged to 1h. These findings suggest that t_{max} might be not only a more sensitive metric in single-dose bioequivalence studies of FLU, but also more relevant for the onset of pain relief.

As a probe substrate of CYP2C9, FLU exhibits gene-dependent pharmacokinetics [47,83]. The PBPK model accurately predicted the impact of the three main CYP2C9 polymorphisms on the exposure of the drug in both Caucasian and Chinese healthy volunteers. Model predictions were within 1.25-fold for both AUC (0.91–1.12) and oral clearance (0.76–1.03), while C_{max} was only slightly overpredicted (up to 1.39-fold). These results further increased confidence in the validity of the allele-specific *in vitro* data and added to the overall model robustness. The observed decrease of about 27% and 40% in the clearance of CYP2C9 1*/2* and 1*/3* individuals, respectively, might need to be considered in terms of adjustments to the recommended dose of flurbiprofen. These findings are in agreement with a large genotype–phenotype correlation clinical study, in which the CYP2C9 genotype of 283 healthy subjects was correlated with the metabolic ratio of FLU, calculated from urine data, as the phenotypic metric [84]. In this study, the recommended dose for CYP2C9 1*/2* and 1*/3* subjects was found to be 84% and 60% of the dose administered to the wild type subjects, respectively. Nevertheless, in terms of pain relief, simulations did not show any differences in R_{max} and TR_{max} among polymorphic subjects. However, the return to 80% of the initial pain value was delayed by up to 7 h in CYP2C9*3 heterozygotes, implying a longer duration of action in those subjects. A similar behavior, but to a lesser extent (delay of up to 4.5 h), was also predicted for the CYP2C9 1*/2* subjects. In any case, potential flurbiprofen dose optimization in CYP2C9 polymorphic subjects should be carefully evaluated under consideration of the exposure–response and exposure–safety relationships.

The present PBPK analysis was extended to simultaneously investigate the effect of genetic polymorphism and perpetrator co-administration on FLU PK by predicting drug–drug and drug–gene interactions. The $R_{pred/obs}$ of DDI AUC, C_{max} , and CL/F ratios from 11 clinical studies with 200 and 400 mg fluconazole (inhibitor) and one with 600 mg rifampicin (inducer) co-administration ranged from 0.74 to 1.43 with GMFE values within 1.25-fold in 8, 9, and 10 out of 12 in total studies, respectively. Only one drug–drug–gene interaction study was available in the literature, in which flurbiprofen alone or together with 200 and 400 mg fluconazole was administered to CYP2C9 1*/1*, 1*/3*, and 3*/3* healthy volunteers [43]. Our model accurately described the plasma concentration–time profiles with and without the inhibitor in all polymorphic groups. On the basis of the *in silico* DDI studies, at a 400 mg dose of fluconazole, we would classify the interaction in 1*/1* (or assuming 1*/1*) subjects as weak/moderate with AUC ratio between 1.53 and 2.87. Interactions at a 200 mg dose of fluconazole and a 600 mg dose of rifampicin would be considered as weak, with AUC ratios of 1.51–1.94 and 0.63, respectively. The interaction for 1*/3* and 3*/3* subjects at 200 mg with AUC ratios 1.58 and 1.09, respectively, and at 400 mg fluconazole, with AUC ratios of 1.84 and 1.16, respectively, was predicted to be weak as well. All these simulated trials are in line with the results from the *in vivo* DDI studies. Interestingly, the flurbiprofen–fluconazole interaction was gene dose-dependent. Virtually no change in the apparent oral clearance occurring in 3*/3* subjects due to the already reduced CYP2C9 activity

was observed, and despite the very limited number of subjects ($n = 2$), this was also correctly predicted, indicating excellent model performance. From population simulations, a dose reduction of 34–38% in 1*/3* and 60–70% in 3*/3* subjects would be recommended. However, in the case of fluconazole administration, dose adjustments were required for 1*/1* and 1*/3*, but not for 3*/3* individuals.

In drug development and prior to phase II clinical studies, accumulated knowledge regarding the absorption, distribution, metabolism, and excretion attributes of an investigational compound is used for preliminary evaluation of its drug–drug interaction potential. Traditionally, significant exposure changes expected to result from co-medication or genetic polymorphism trigger implementation of dedicated clinical pharmacology studies. Unlike flurbiprofen, most drugs in industry’s contemporary pipelines undergo multiple clearance pathways, and thus exposure variations are expected with co-medication or genetic polymorphism in metabolizing enzymes and/or transporters. In such cases, the clinical trial strategy may not be time- and/or cost-effective and an alternative PBPK/PD modelling approach may be not only more practical, but in some cases indispensable if a wide array of complex drug–drug–gene interactions need to be assessed. The extent and appropriate design of the simulations highly depends on the intended use of the substrate in specific populations, the anticipated co-medications and genetic polymorphisms, the effect of pharmacokinetic changes in safety and efficacy of the drug (e.g., exposure-response relationships), and the design (cohorts, populations, inclusion/exclusion criteria) of prospective DDI or pharmacogenetic studies. In addition, if a drug is known to be subject to a major genetic polymorphism, the European Medicines Agency (EMA) recommends genotyping screening of subjects in exploratory bioavailability studies and all studies using parallel group design, even in crossover bioequivalence studies in case of safety or other pharmacokinetic concerns [85]. In this context, if a translational absorption-modeling framework is established, virtual bioequivalence might be a promising tool as part of the modeling and simulation strategy in both drug and generic drug development. Of course, concerns regarding the impact of genetic polymorphism on the PK/PD can be directly related to the frequency of polymorphic alleles in the population of interest. For example, the frequency of CYP2C9 wild type in Chinese populations is around 97–98%, whereas in Caucasians, approximately 35% of the overall population will have at least one of the CYP2C9*2 and/or CYP2C9*3, with an occurrence of 1*/2* and 1*/3* of up to 20% and 10%, respectively [11,86,87]. Thus, genotyping prior to a clinical study of a CYP2C9 substrate in Caucasians might be required, whereas it may be optional in Chinese populations.

5. Conclusions

This study highlights the usefulness of translational PBPK/PD modeling and simulation to mechanistically describe the absorption and predict the effect of formulation and CYP2C9 genetic polymorphism on the PK/PD of flurbiprofen. A detailed biopharmaceutic analysis, including appropriately designed biorelevant *in vitro* experiments of various flurbiprofen formulations, was performed initially, followed by *in vitro* data analysis and extrapolation to *in vivo* using a translational framework. Our comprehensive PBPK/PD analyses provided mechanistic insight into the impact of dissolution rate and genotype on the PK/PD. On the basis of these findings, we proposed clinically relevant exposure metric and potential dose adjustments. Furthermore, our PBPK model successfully predicted gene dose-dependent drug–drug interactions, highlighting the robustness of its performance. The present PBPK/PD model could be utilized in future biopharmaceutic applications, dose optimization justifications in healthy population with genetic variations, and PK extrapolations to patient or special populations such as rheumatoid arthritis patients and pediatrics.

Genetic variations and formulation *in vivo* performance appear to be major determinants of individual variability in drug efficacy and safety, representing a challenge in drug development. The translational PBPK/PD approach exemplified in this study attempts to bridge the gap between *in vitro*–*in silico*–*in vivo* and allows for accurate and robust clinical predictions tailored to target populations and genotypes, thus paving the way towards personalized medicine.

Supplementary Materials: The following are available online at <http://www.mdpi.com/1999-4923/12/11/1049/s1>, Table S1: Summary of main CYP2C9 genotype-based metabolic differences in the default inputs of the Simcyp North European Caucasian (NEurCaucasian) and Chinese healthy volunteer virtual populations. Table S2: Comparison of predicted and observed pharmacodynamic parameters (R_{max} , TR_{max} , and AUCE) values of flurbiprofen and calculation of predicted to observed ratio ($R_{pred/obs}$).

Author Contributions: Conceptualization, I.L.-K. and J.D.; methodology, I.L.-K. and J.D.; formal analysis, I.L.-K.; investigation, I.L.-K., J.D., R.C., M.J., and D.T.; writing—original draft preparation, I.L.-K.; writing—review and editing, I.L.-K., J.D., R.C., M.J., and D.T.; visualization, I.L.-K.; supervision, J.D. All authors have read and agreed to the published version of the manuscript.

Funding: This research was funded by the European Union’s Horizon 2020 Research and Innovation Program under grant agreement no. 674909 (PEARRL).

Acknowledgments: This work was supported by the European Union’s Horizon 2020 Research and Innovation Program under grant agreement no. 674909 (PEARRL).

Conflicts of Interest: The authors declare no conflict of interest.

References

1. Davies, N.M. Clinical pharmacokinetics of flurbiprofen and its enantiomers. *Clin. Pharm.* **1995**, *28*, 100–114. [[CrossRef](#)] [[PubMed](#)]
2. Dressman, J.B.; Berardi, R.R.; Elta, G.H.; Gray, T.M.; Montgomery, P.A.; Lau, H.S.; Pelekoudas, K.L.; Szpunar, G.J.; Wagner, J.G. Absorption of flurbiprofen in the fed and fasted states. *Pharm. Res.* **1992**, *9*, 901–907. [[CrossRef](#)] [[PubMed](#)]
3. Ozbay, L.; Unal, D.O.; Cakici, I.; Fenercioglu, A.; Erol, D. Clinical study on the bioequivalence of two tablet formulations of flurbiprofen. *Eur. J. Drug Metab. Pharm.* **2009**, *34*, 1–5. [[CrossRef](#)] [[PubMed](#)]
4. Patel, B.K.; Jackson, S.H.D.; Swift, C.G.; Hutt, A.J.; Jackson, S.H.D.; Swift, C.G.; Disposition, A.J.H. Disposition of flurbiprofen in man: Influence of stereochemistry and age. *Xenobiotica* **2003**, *33*, 1043–1057. [[CrossRef](#)]
5. Szpunar, G.J.; Albert, K.S.; Wagner, J.G. Pharmacokinetics of flurbiprofen in man. II. Plasma protein binding. *Res. Commun. Chem. Pathol. Pharmacol.* **1989**, *64*, 17–30.
6. Human Cytochrome P450 (CYP) Allele Nomenclature Committee. CYP2C9 Allele Nomenclature. Available online: <https://www.pharmvar.org/htdocs/archive/cyp2c9.htm> (accessed on 9 May 2020).
7. Yamazaki, H.; Inoue, K.; Chiba, K.; Ozawa, N.; Kawai, T.; Suzuki, Y.; Goldstein, J.A.; Guengerich, F.P.; Shimada, T. Comparative Studies on the Catalytic Roles of Cytochrome P450 2C9 and Its Cys-and Leu-Variants in the Oxidation of Warfarin, Flurbiprofen, and Diclofenac by Human Liver Microsomes. *Biochem. Pharmacol.* **1998**, *56*, 243–251. [[CrossRef](#)]
8. Van Booven, D.; Marsh, S.; McLeod, H.; Carrillo, M.W.; Sangkuhl, K.; Klein, T.E.; Altman, R.B. Cytochrome P450 2C9-CYP2C9. *Pharmacogenet. Genom.* **2010**, *20*, 277–281. [[CrossRef](#)]
9. Scott, S.A.; Khasawneh, R.; Peter, I.; Kornreich, R.; Desnick, R.J. Combined CYP2C9, VKORC1 and CYP4F2 frequencies among racial and ethnic groups. *Pharmacogenomics* **2010**, *11*, 781–791. [[CrossRef](#)]
10. Kirchheiner, J.; Brockmüller, J. Clinical consequences of cytochrome P450 2C9 polymorphisms. *Clin. Pharmacol. Ther.* **2005**, *77*, 1–16. [[CrossRef](#)]
11. Lee, C.R.; Goldstein, J.A.; Pieper, J.A. Cytochrome P450 2C9 polymorphisms: A comprehensive review of the in-vitro and human data. *Pharmacogenetics* **2002**, *12*, 251–263. [[CrossRef](#)]
12. Vieira, M.D.L.T.; Kim, M.J.; Apparaju, S.; Sinha, V.; Zineh, I.; Huang, S.M.; Zhao, P. PBPK model describes the effects of comedication and genetic polymorphism on systemic exposure of drugs that undergo multiple clearance pathways. *Clin. Pharmacol. Ther.* **2014**, *95*, 550–557. [[CrossRef](#)]
13. Jin, Y.; Borell, H.; Gardin, A.; Ufer, M.; Huth, F.; Camerisch, G. In vitro studies and in silico predictions of fluconazole and CYP2C9 genetic polymorphism impact on siponimod metabolism and pharmacokinetics. *Eur. J. Clin. Pharmacol.* **2018**, *74*, 455–464. [[CrossRef](#)]
14. Abend, A.; Heimbach, T.; Cohen, M.; Kesisoglou, F.; Pepin, X.; Suarez-Sharp, S. Dissolution and Translational Modeling Strategies Enabling Patient-Centric Drug Product Development: The M-CERSI Workshop Summary Report. *AAPS J.* **2018**, *20*, 60. [[CrossRef](#)] [[PubMed](#)]

15. Sager, J.E.; Yu, J.; Ragueneau-Majlessi, I.; Isoherranen, N. Minireview Physiologically Based Pharmacokinetic (PBPK) Modeling and Simulation Approaches: A Systematic Review of Published Models, Applications, and Model Verifications. *DRUG Metab. Dispos. Drug Metab. Dispos.* **2015**, *43*, 1823–1837. [[CrossRef](#)] [[PubMed](#)]
16. Zhao, P.; Rowland, M.; Huang, S.-M. Best practice in the use of physiologically based pharmacokinetic modeling and simulation to address clinical pharmacology regulatory questions. *Clin. Pharmacol. Ther.* **2012**, *92*, 17–20. [[CrossRef](#)]
17. Djebli, N.; Fabre, D.; Boulenc, X.; Fabre, G.; Sultan, E.; Hurbin, F. Physiologically Based Pharmacokinetic Modeling for Sequential Metabolism: Effect of CYP2C19 Genetic Polymorphism on Clopidogrel and Clopidogrel Active Metabolite Pharmacokinetics. *DRUG Metab. Dispos. Drug Metab. Dispos.* **2015**, *43*, 510–522. [[CrossRef](#)]
18. Storelli, F.; Desmeules, J.; Daali, Y. Physiologically-Based Pharmacokinetic Modeling for the Prediction of CYP2D6-Mediated Gene–Drug–Drug Interactions. *CPT Pharmacomet. Syst. Pharmacol.* **2019**, *8*, 567–576. [[CrossRef](#)]
19. Chen, Y.; Liu, L.; Nguyen, K.; Fretland, A.J. Utility of Intersystem Extrapolation Factors in Early Reaction Phenotyping and the Quantitative Extrapolation of Human Liver Microsomal Intrinsic Clearance Using Recombinant Cytochromes P450. *Drug Metab. Dispos.* **2011**, *39*, 373–382. [[CrossRef](#)]
20. Alqahtani, S.; Kaddoumi, A. Development of physiologically based pharmacokinetic/Pharmacodynamic model for Indomethacin disposition in pregnancy. *PLoS ONE* **2015**, *10*, e0139762. [[CrossRef](#)]
21. Riedmaier, A.E.; Lindley, D.J.; Hall, J.A.; Castleberry, S.; Slade, R.T.; Stuart, P.; Carr, R.A.; Borchardt, T.B.; Bow, D.A.J.; Nijssen, M. Mechanistic Physiologically Based Pharmacokinetic Modeling of the Dissolution and Food Effect of a Biopharmaceutics Classification System IV Compound-The Venetoclax Story. *J. Pharm. Sci.* **2018**, *107*, 495–502. [[CrossRef](#)]
22. Türk, D.; Hanke, N.; Wolf, S.; Frechen, S.; Eissing, T.; Wendl, T.; Schwab, M.; Lehr, T. Physiologically Based Pharmacokinetic Models for Prediction of Complex CYP2C8 and OATP1B1 (SLCO1B1) Drug–Drug–Gene Interactions: A Modeling Network of Gemfibrozil, Repaglinide, Pioglitazone, Rifampicin, Clarithromycin and Itraconazole. *Clin. Pharm.* **2019**, *58*, 1595–1607. [[CrossRef](#)]
23. Markopoulos, C.; Andreas, C.J.; Vertzoni, M.; Dressman, J.; Reppas, C. In-vitro simulation of luminal conditions for evaluation of performance of oral drug products: Choosing the appropriate test media. *Eur. J. Pharm. Biopharm.* **2015**, *93*, 173–182. [[CrossRef](#)] [[PubMed](#)]
24. Fuchs, A.; Leigh, M.; Kloefer, B.; Dressman, J.B. Advances in the design of fasted state simulating intestinal fluids: FaSSIF-V3. *Eur. J. Pharm. Biopharm.* **2015**, *94*, 229–240. [[CrossRef](#)]
25. Loisios-Konstantinidis, I.; Cristofolletti, R.; Fotaki, N.; Turner, D.B.; Dressman, J. Establishing virtual bioequivalence and clinically relevant specifications using in vitro biorelevant dissolution testing and physiologically-based population pharmacokinetic modeling. case example: Naproxen. *Eur. J. Pharm. Sci.* **2020**, *143*, 105170. [[CrossRef](#)]
26. Wang, J.; Flanagan, D.R. General solution for diffusion-controlled dissolution of spherical particles. 1. Theory. *J. Pharm. Sci.* **1999**, *88*, 731–738. [[CrossRef](#)]
27. Wang, J.; Flanagan, D.R. General solution for diffusion-controlled dissolution of spherical particles. 2. Evaluation of experimental data. *J. Pharm. Sci.* **2002**, *91*, 534–542. [[CrossRef](#)]
28. Mooney, K.G.; Mintun, M.A.; Himmelstein, K.J.; Stella, V.J. Dissolution kinetics of carboxylic acids I: Effect of pH under unbuffered conditions. *J. Pharm. Sci.* **1981**, *70*, 13–22. [[CrossRef](#)]
29. Mooney, K.G.; Mintun, M.A.; Himmelstein, K.J.; Stella, V.J. Dissolution Kinetics of Carboxylic Acids II: Effect of Buffers. *J. Pharm. Sci.* **1981**, *70*, 22–32. [[CrossRef](#)] [[PubMed](#)]
30. Mooney, K.G.; Rodriguez-gaxiola, M.; Mintun, M.; Himmelstein, K.J.; Stella, V.J. Dissolution Kinetics of Phenylbutazone. *J. Pharm. Sci.* **1981**, *70*, 1358–1365. [[CrossRef](#)]
31. Ozturk, S.S.; Palsson, B.O.; Dressman, J.B. Dissolution of Ionizable Drugs in Buffered and Unbuffered Solutions. *Pharm. Res.* **1988**, *5*, 272–282. [[CrossRef](#)]
32. Sheng, J.J.; McNamara, D.P.; Amidon, G.L. Toward an In Vivo dissolution methodology: A comparison of phosphate and bicarbonate buffers. *Mol. Pharm.* **2009**, *6*, 29–39. [[CrossRef](#)]

33. Serajuddin, A.T.M.; Jarowski, C. Effect of diffusion layer pH and solubility on the dissolution rate of pharmaceutical bases and their hydrochloride salts. I: Phenazopyridine. *J. Pharm. Sci.* **1985**, *74*, 142–147. [[CrossRef](#)]
34. Mei, C.; Li, B.; Yin, Q.; Jin, J.; Xiong, T.; He, W.; Gao, X.; Xu, R.; Zhou, P.; Zheng, H.; et al. Liquid chromatography-tandem mass spectrometry for the quantification of flurbiprofen in human plasma and its application in a study of bioequivalence. *J. Chromatogr. B Anal. Technol. Biomed. Life Sci.* **2015**, *993–994*, 69–74. [[CrossRef](#)]
35. Gonzalez-Younes, I.; Wagner, J.G.; Gaines, D.A.; Ferry, J.J.; Hageman, J.M. Absorption of flurbiprofen through human buccal mucosa. *J. Pharm. Sci.* **1991**, *80*, 820–823. [[CrossRef](#)]
36. Szpunar, G.J.; Albert, K.S.; Bole, G.G.; Dreyfus, J.N.; Lockwood, G.F.; Wagner, J.G. Pharmacokinetics of flurbiprofen in man. I. Area/dose relationships. *Biopharm. Drug Dispos.* **1987**, *8*, 273–283. [[CrossRef](#)] [[PubMed](#)]
37. Lee, Y.J.; Byeon, J.Y.; Kim, Y.H.; Kim, S.H.; Choi, C.I.; Bae, J.W.; Sohn, U.D.; Jang, C.G.; Lee, J.; Lee, S.Y. Effects of CYP2C9*1/*3 genotype on the pharmacokinetics of flurbiprofen in Korean subjects. *Arch. Pharm. Res.* **2015**, *38*, 1232–1237. [[CrossRef](#)]
38. Jamali, F.; Collins, D.S.; Berry, B.W.; Molder, S.; Cheung, R.; McColl, K.; Cheung, H. Comparative bioavailability of two flurbiprofen products: Stereospecific versus conventional approach. *Biopharm. Drug Dispos.* **1991**, *12*, 435–445. [[CrossRef](#)]
39. Suri, A.; Grundy, B.L.; Derendorf, H. Pharmacokinetics and pharmacodynamics of enantiomers of ibuprofen and flurbiprofen after oral administration. *Int. J. Clin. Pharmacol. Ther.* **1997**, *35*, 1–8.
40. Liu, Y.-M.; Liu, G.-Y.; Liu, Y.; Li, S.-J.; Jia, J.-Y.; Zhang, M.-Q.; Lu, C.; Zhang, Y.-M.; Li, X.-N.; Yu, C. Pharmacokinetic and Bioequivalence Comparison Between Orally Disintegrating and Conventional Tablet Formulations of Flurbiprofen: A Single-Dose, Randomized-Sequence, Open-Label, Two-Period Crossover Study in Healthy Chinese Male Volunteers. *Clin. Ther.* **2009**, *31*, 1787–1795. [[CrossRef](#)]
41. Lee, H.-I.; Choi, C.-I.; Byeon, J.-Y.; Lee, J.-E.; Park, S.-Y.; Kim, Y.-H.; Kim, S.-H.; Lee, Y.-J.; Jang, C.-G.; Lee, S.-Y. Simultaneous determination of flurbiprofen and its hydroxy metabolite in human plasma by liquid chromatography-tandem mass spectrometry for clinical application. *J. Chromatogr. B* **2014**, *971*, 58–63. [[CrossRef](#)]
42. Lee, C.R.; Pieper, J.A.; Frye, R.F.; Hinderliter, A.L.; Blaisdell, J.A.; Goldstein, J.A. Differences in flurbiprofen pharmacokinetics between CYP2C9*1/*1, *1/*2, and *1/*3 genotypes. *Eur. J. Clin. Pharmacol.* **2003**, *58*, 791–794. [[CrossRef](#)] [[PubMed](#)]
43. Kumar, V.; Brundage, R.; Oetting, W.S.; Leppik, I.E.; Tracy, T.S. Differential Genotype Dependent Inhibition of CYP2C9 in Humans. *Drug Metab. Dispos.* **2008**, *36*, 1242–1248. [[CrossRef](#)]
44. Hanley, M.J.; Masse, G.; Harmatz, J.S.; Court, M.H.; Greenblatt, D.J. Pomegranate juice and pomegranate extract do not impair oral clearance of flurbiprofen in human volunteers: Divergence from in vitro results. *Clin. Pharmacol. Ther.* **2012**, *92*, 651–657. [[CrossRef](#)]
45. Hanley, M.J.; Masse, G.; Harmatz, J.S.; Cancalon, P.F.; Dolnikowski, G.G.; Court, M.H.; Greenblatt, D.J. Effect of blueberry juice on clearance of buspirone and flurbiprofen in human volunteers. *Br. J. Clin. Pharmacol.* **2013**, *75*, 1041–1052. [[CrossRef](#)]
46. Greenblatt, D.J.; Von Moltke, L.L.; Perloff, E.S.; Luo, Y.; Harmatz, J.S.; Boston, M.A.Z. Interaction of flurbiprofen with cranberry juice, grape juice, tea, and fluconazole: In vitro and clinical studies. *Clin. Pharmacol. Ther.* **2006**, *450*, 125–133. [[CrossRef](#)]
47. Zgheib, N.K.; Frye, R.F.; Tracy, T.S.; Romkes, M.; Branch, R.A. Evaluation of flurbiprofen urinary ratios as in vivo indices for CYP2C9 activity. *Br. J. Clin. Pharmacol.* **2007**, *63*, 477–487. [[CrossRef](#)]
48. Daali, Y.; Samer, C.; Déglon, J.; Thomas, A.; Chabert, J.; Rebsamen, M.; Staub, C.; Dayer, P.; Desmeules, J. Oral flurbiprofen metabolic ratio assessment using a single-point dried blood spot. *Clin. Pharmacol. Ther.* **2012**, *91*, 489–496. [[CrossRef](#)]
49. U.S. Food and Drug Administration; A Center for Drug Evaluation and Research (CDER). *Physiologically Based Pharmacokinetic Analyses—Format and Content Guidance for Industry*; Food and Drug Administration: Silver Spring, MD, USA, 2018.
50. Kuepfer, L.; Niederalt, C.; Wendl, T.; Schlender, J.-F.; Willmann, S.; Lippert, J.; Block, M.; Eissing, T.; Teutonico, D. Applied Concepts in PBPK Modeling: How to Build a PBPK/PD Model. *CPT Pharmacomet. Syst. Pharmacol.* **2016**, *5*, 516–531. [[CrossRef](#)]

51. Ke, A.; Barter, Z.; Rowland-Yeo, K.; Almond, L. Towards a Best Practice Approach in PBPK Modeling: Case Example of Developing a Unified Efavirenz Model Accounting for Induction of CYPs 3A4 and 2B6. *CPT Pharmacomet. Syst. Pharmacol.* **2016**, *5*, 367–376. [[CrossRef](#)] [[PubMed](#)]
52. European Medicines Agency (EMA). *Committee for Medicinal Products for Human Use (CHMP) Guideline on the Reporting of Physiologically Based Pharmacokinetic (PBPK) Modelling and Simulation*; European Medicines Agency: London, UK, 2018.
53. Shebley, M.; Sandhu, P.; Emami Riedmaier, A.; Jamei, M.; Narayanan, R.; Patel, A.; Peters, S.A.; Reddy, V.P.; Zheng, M.; de Zwart, L.; et al. Physiologically Based Pharmacokinetic Model Qualification and Reporting Procedures for Regulatory Submissions: A Consortium Perspective. *Clin. Pharmacol. Ther.* **2018**, *104*, 88–110. [[CrossRef](#)] [[PubMed](#)]
54. Avdeef, A. pH-metric Solubility. 1. Solubility-pH Plots. Gibbs Buffer and pK, in Profiles from Bjerrum the Solid State. *Pharm. Pharmacol. Commun. Pharm. Pharmacol. Commun.* **1998**, *4*, 165–178. [[CrossRef](#)]
55. Czyski, A. Determination of the Lipophilicity of Ibuprofen, Naproxen, Ketoprofen, and Flurbiprofen with Thin-Layer Chromatography. *J. Chem.* **2019**, *2019*, 3407091. [[CrossRef](#)]
56. Kaiser, D.G.; Brooks, C.D.; Lomen, P.L. Pharmacokinetics of Flurbiprofen. *Am. J. Med.* **1986**, *80*, 10–15. [[CrossRef](#)]
57. Risdall, P.C.; Adams, S.S.; Crampton, E.L.; Marchant, B. The Disposition and Metabolism of Flurbiprofen in Several Species Including Man. *XENOBIOTICA* **1978**, *8*, 691–704. [[CrossRef](#)]
58. Aarons, L.; Khan, A.Z.; Grennan, D.M.; Alam-Siddiqi, M. The binding of flurbiprofen to plasma proteins. *J. Pharm. Pharmacol.* **1985**, *37*, 644–646. [[CrossRef](#)]
59. Lin, J.H.; Cocchetto, D.M.; Duggan, D.E. Protein-binding as a primary determinant of the clinical pharmacokinetic properties of nonsteroidal antiinflammatory drugs. *Clin. Pharm.* **1987**, *12*, 402–432. [[CrossRef](#)]
60. Yazdaniyan, M.; Briggs, K.; Jankovsky, C.; Hawi, A. The “High Solubility” Definition of the Current FDA Guidance on Biopharmaceutical Classification System May Be Too Strict for Acidic Drugs. *Pharm. Res.* **2004**, *21*, 293–299. [[CrossRef](#)]
61. Wang, L.; Bao, S.-H.; Pan, P.-P.; Xia, M.; Chen, M.-C.; Liang, B.-Q.; Dai, D.-P.; Cai, J.-P.; Hu, G.-X.; Xia, M.-M. Effect of CYP2C9 genetic polymorphism on the metabolism of flurbiprofen in vitro. *Drug Dev. Ind. Pharm.* **2015**, *41*, 1363–1367. [[CrossRef](#)]
62. Wang, H.; Yuan, L.; Zeng, S. Characterizing the effect of UDP-glucuronosyltransferase (UGT) 2B7 and UGT1A9 genetic polymorphisms on enantioselective glucuronidation of flurbiprofen. *Biochem. Pharmacol.* **2011**, *82*, 1757–1763. [[CrossRef](#)]
63. Jamei, M.; Turner, D.; Yang, J.; Neuhoff, S.; Polak, S.; Rostami-Hodjegan, A.; Tucker, G. Population-based mechanistic prediction of oral drug absorption. *AAPS J.* **2009**, *11*, 225–237. [[CrossRef](#)]
64. Darwich, A.S.; Neuhoff, S.; Jamei, M.; Rostami-Hodjegan, A. Interplay of Metabolism and Transport in Determining Oral Drug Absorption and Gut Wall Metabolism: A Simulation Assessment Using the “Advanced Dissolution, Absorption, Metabolism (ADAM)” Model. *Curr. Drug Metab.* **2010**, *11*, 716–729. [[CrossRef](#)]
65. Hens, B.; Brouwers, J.; Anneveld, B.; Corsetti, M.; Symillides, M.; Vertzoni, M.; Reppas, C.; Turner, D.B.; Augustijns, P. Gastrointestinal transfer: In vivo evaluation and implementation in in vitro and in silico predictive tools. *Eur. J. Pharm. Sci.* **2014**, *63*, 233–242. [[CrossRef](#)]
66. Psachoulas, D.; Vertzoni, M.; Goumas, K.; Kalioras, V.; Beato, S.; Butler, J.; Reppas, C. Precipitation in and Supersaturation of Contents of the Upper Small Intestine After Administration of Two Weak Bases to Fasted Adults. *Pharm. Res.* **2011**, *28*, 3145–3158. [[CrossRef](#)]
67. Cristofolletti, R.; Patel, N.; Dressman, J.B. Differences in Food Effects for 2 Weak Bases With Similar BCS Drug-Related Properties: What Is Happening in the Intestinal Lumen? *J. Pharm. Sci.* **2016**, *105*, 2712–2722. [[CrossRef](#)] [[PubMed](#)]
68. Paixão, P.; Bermejo, M.; Hens, B.; Tsume, Y.; Dickens, J.; Shedden, K.; Salehi, N.; Koenigsknecht, M.J.; Baker, J.R.; Hasler, W.L.; et al. Gastric emptying and intestinal appearance of nonabsorbable drugs phenol red and paromomycin in human subjects: A multi-compartment stomach approach. *Eur. J. Pharm. Biopharm.* **2018**, *129*, 162–174. [[CrossRef](#)]

69. Rodgers, T.; Rowland, M. Physiologically based pharmacokinetic modelling 2: Predicting the tissue distribution of acids, very weak bases, neutrals and zwitterions. *J. Pharm. Sci.* **2006**, *95*, 1238–1257. [[CrossRef](#)] [[PubMed](#)]
70. Crewe, H.K.; Barter, Z.E.; Rowland Yeo, K.; Rostami-Hodjegan, A. Are there differences in the catalytic activity per unit enzyme of recombinantly expressed and human liver microsomal cytochrome P450 2C9? A systematic investigation into inter-system extrapolation factors. *Biopharm. Drug Dispos.* **2011**, *32*, 303–318. [[CrossRef](#)]
71. Kuehl, G.E.; Lampe, J.W.; Potter, J.D.; Bigler, J. Glucuronidation of nonsteroidal antiinflammatory drugs Identifying the enzymes in human liver microsomes. *Drug Metab. Dispos.* **2005**, *33*, 1027–1035. [[CrossRef](#)] [[PubMed](#)]
72. Mano, Y.; Usui, T.; Kamimura, H. Predominant contribution of UDP-glucuronosyltransferase 2B7 in the glucuronidation of racemic flurbiprofen in the human liver. *Drug Metab. Dispos.* **2007**, *35*, 1182–1187. [[CrossRef](#)]
73. Nielsen, L.M.; Sverrisdóttir, E.; Stage, T.B.; Feddersen, S.; Brøsen, K.; Christrup, L.L.; Drewes, A.M.; Olesen, A.E. Lack of genetic association between OCT1, ABCB1, and UGT2B7 variants and morphine pharmacokinetics. *Eur. J. Pharm. Sci.* **2017**, *99*, 337–342. [[CrossRef](#)]
74. Ayuso, P.; Neary, M.; Chiong, J.; Owen, A. Meta-analysis of the effect of CYP2B6, CYP2A6, UGT2B7 and CAR polymorphisms on efavirenz plasma concentrations. *J. Antimicrob. Chemother.* **2019**, *74*, 3281–3290. [[CrossRef](#)]
75. Edgington, A.N.; Schmitt, W.; Willmann, S. Development and evaluation of a generic physiologically based pharmacokinetic model for children. *Clin. Pharm.* **2006**, *45*, 1013–1034. [[CrossRef](#)]
76. Poulin, P.; Theil, F.-P. Development of a novel method for predicting human volume of distribution at steady-state of basic drugs and comparative assessment with existing methods. *J. Pharm. Sci.* **2009**, *98*, 4941–4961. [[CrossRef](#)]
77. Obach, R.S.; Baxter, J.G.; Liston, T.E.; Silber, B.M.; Jones, B.C.; MacIntyre, F.; Rance, D.J.; Wastall, P. The prediction of human pharmacokinetic parameters from preclinical and in vitro metabolism data. *J. Pharmacol. Exp. Ther.* **1997**, *283*, 46–58. [[PubMed](#)]
78. Kim, Y.; Hatley, O.; Rhee, S.J.; Yi, S.; Lee, H.A.; Yoon, S.; Chung, J.Y.; Yu, K.S.; Lee, H. Development of a Korean-specific virtual population for physiologically based pharmacokinetic modelling and simulation. *Biopharm. Drug Dispos.* **2019**, *40*, 135–150. [[CrossRef](#)]
79. Myrand, S.P.; Sekiguchi, K.; Man, M.Z.; Lin, X.; Tzeng, R.Y.; Teng, C.H.; Hee, B.; Garrett, M.; Kikkawa, H.; Lin, C.Y.; et al. Pharmacokinetics/genotype associations for major cytochrome P450 enzymes in native and first- and third-generation Japanese populations: Comparison with Korean, Chinese, and Caucasian populations. *Clin. Pharmacol. Ther.* **2008**, *84*, 347–361. [[CrossRef](#)]
80. Yoon, Y.-R.; Shon, J.-H.; Kim, M.-K.; Lim, Y.-C.; Lee, H.-R.; Park, J.-Y.; Cha, I.-J.; Shin, J.-G. Frequency of cytochrome P450 2C9 mutant alleles in a Korean population. *Br. J. Clin. Pharmacol.* **2008**, *51*, 277–280. [[CrossRef](#)]
81. Avdeef, A.; Berger, C.M. pH-Metric Solubility. 2: Correlation Between the Acid-Base Titration and formulations for use in early animal bioavailability and toxicity studies. Later in development, solubility takes on a broader. *Pharm. Res.* **2000**, *17*, 85–89. [[CrossRef](#)]
82. Karow, A.R.; Bahrenburg, S.; Garidel, P. Buffer capacity of biologics—from buffer salts to buffering by antibodies. *Biotechnol. Prog.* **2013**, *29*, 480–492. [[CrossRef](#)]
83. Lee, C.B.; Pieper, J.A.; Frye, R.F.; Hinderliter, A.L.; Blaisdell, J.A.; Goldstein, J.A. Tolbutamide, flurbiprofen, and losartan as probes of CYP2C9 activity in humans. *J. Clin. Pharmacol.* **2003**, *43*, 84–91. [[CrossRef](#)]
84. Vogl, S.; Lutz, R.W.; Schönfelder, G.; Lutz, W.K. CYP2C9 genotype vs. metabolic phenotype for individual drug dosing—A correlation analysis using flurbiprofen as probe drug. *PLoS ONE* **2015**, *10*, e0120403. [[CrossRef](#)]
85. EMA Committee for Proprietary Medicinal Products (CPMP). *Note for Guidance on the Investigation of Bioavailability and Bioequivalence*; European Medicines Agency: London, UK, 2000.

86. Dai, D.P.; Xu, R.A.; Hu, L.M.; Wang, S.H.; Geng, P.W.; Yang, J.F.; Yang, L.P.; Qian, J.C.; Wang, Z.S.; Zhu, G.H.; et al. CYP2C9 polymorphism analysis in Han Chinese populations: Building the largest allele frequency database. *Pharm. J.* **2014**, *14*, 85–92. [[CrossRef](#)]
87. Scordo, M.G.; Akillu, E.; Yasar, U.; Dahl, M.-L.; Spina, E.; Ingelman-Sundberg, M. Genetic polymorphism of cytochrome P450 2C9 in a Caucasian and a black African population. *Br. J. Clin. Pharmacol.* **2001**, *52*, 447–450. [[CrossRef](#)]

Publisher’s Note: MDPI stays neutral with regard to jurisdictional claims in published maps and institutional affiliations.



© 2020 by the authors. Licensee MDPI, Basel, Switzerland. This article is an open access article distributed under the terms and conditions of the Creative Commons Attribution (CC BY) license (<http://creativecommons.org/licenses/by/4.0/>).

Physiologically Based Pharmacokinetic/Pharmacodynamic Modeling to Support Waivers of *In Vivo* Clinical Studies: Current Status, Challenges, and Opportunities

Ioannis Loios-Konstantinidis and Jennifer Dressman*



Cite This: *Mol. Pharmaceutics* 2021, 18, 1–17



Read Online

ACCESS |

Metrics & More

Article Recommendations

ABSTRACT: Physiologically based pharmacokinetic/pharmacodynamic (PBPK/PD) modeling has been extensively applied to quantitatively translate *in vitro* data, predict the *in vivo* performance, and ultimately support waivers of *in vivo* clinical studies. In the area of biopharmaceutics and within the context of model-informed drug discovery and development (MID3), there is a rapidly growing interest in applying verified and validated mechanistic PBPK models to waive *in vivo* clinical studies. However, the regulatory acceptance of PBPK analyses for biopharmaceutics and oral drug absorption applications, which is also referred to variously as “PBPK absorption modeling” [Zhang et al. *CPT: Pharmacometrics Syst. Pharmacol.* 2017, 6, 492], “physiologically based absorption modeling”, or “physiologically based biopharmaceutics modeling” (PBBM), remains rather low [Kesisoglou et al. *J. Pharm. Sci.* 2016, 105, 2723] [Heimbach et al. *AAPS J.* 2019, 21, 29]. Despite considerable progress in the understanding of gastrointestinal (GI) physiology, *in vitro* biopharmaceutic and *in silico* tools, PBPK models for oral absorption often suffer from an incomplete understanding of the physiology, overparameterization, and insufficient model validation and/or platform verification, all of which can represent limitations to their translatability and predictive performance. The complex interactions of drug substances and (bio)enabling formulations with the highly dynamic and heterogeneous environment of the GI tract in different age, ethnic, and genetic groups as well as disease states have not been yet fully elucidated, and they deserve further research. Along with advancements in the understanding of GI physiology and refinement of current or development of fully mechanistic *in silico* tools, we strongly believe that harmonization, interdisciplinary interaction, and enhancement of the translational link between *in vitro*, *in silico*, and *in vivo* will determine the future of PBBM. This Perspective provides an overview of the current status of PBBM, reflects on challenges and knowledge gaps, and discusses future opportunities around PBPK/PD models for oral absorption of small and large molecules to waive *in vivo* clinical studies

KEYWORDS: *physiologically based pharmacokinetic/pharmacodynamic modeling, oral absorption, pharmacometrics, biopharmaceutics, bioequivalence*

■ INTRODUCTION

Physiologically based pharmacokinetic/pharmacodynamic (PBPK/PD) modeling has become a well-established tool to support model-informed drug discovery and development as well as to support interactions with health authorities, including regulatory submissions. Even though the majority of applications involving PBPK modeling to inform regulatory decision-making is still centered around organ impairment, there is a rapidly growing interest in applying verified and validated PBPK models in the area of biopharmaceutics and oral drug absorption.^{4,5} For a long time, the pharmacometric as well as the modeling and simulation (M&S) community had overlooked oral drug absorption, and indeed it is still often described with an oversimplified first or zero-order process. More recently, due to the contribution of various initiatives from academic, industrial and regulatory bodies,^{6–8} oral absorption models have evolved to dynamic, semi- or fully mechanistic, state-of-the-art models, which can often account for the complex processes and interactions involved: starting with drug administration through to the arrival of the drug substance in the venous blood.

The term “PBPK analyses for biopharmaceutics and oral drug absorption applications”, which is also referred to variously as “PBPK absorption modeling”,¹ “physiologically based absorption modeling” or “physiologically based biopharmaceutics modeling” (PBBM), emphasizes the mechanistic character of the absorption model component.^{2,3,9} However, the emphasis on a mechanistic evaluation of absorption in no way compromises the importance of the distribution, metabolism, excretion, and interaction processes involved in PBPK models. The potential for using PBPK analyses for biopharmaceutics (or PBBM, as its shorthand) to waive *in vivo* bioequivalence studies is well recognized by pharmaceutical industries, regulatory agencies, and academic

Received: September 5, 2020

Revised: November 19, 2020

Accepted: November 24, 2020

Published: December 15, 2020



consortia alike.^{3,4,9} Within this framework, the emerging field of virtual bioequivalence (VBE) and clinical trial simulation offers multiple opportunities to apply modeling and simulation (M&S) approaches to inform, or even reduce, the number of clinical studies required and to streamline drug development by bringing safe and efficacious drugs faster to patients. Of course, this is of great importance not only for generic but also for new drug development since several bioavailability/bioequivalence (BA/BE) studies are often required in the process of bringing a drug candidate to market. Other applications of PBBM with the aim of a “waiver” include, but are not limited to, predicting the outcome of dedicated clinical pharmacology food effect studies and interactions with acid-reducing agents/proton pump inhibitors (ARA/PPI) that lead to alterations in drug absorption, as well as establishing clinically relevant drug product specifications (CRDPS). Furthermore, predictions of alterations in oral drug absorption due to physiological changes or disease in specific (e.g., pediatric, geriatric, achlorhydric) or patient (e.g., cancer, Crohn’s) populations are also of interest. However, the acceptance rate of PBPK modeling and simulation analyses in the context of biopharmaceutics and oral drug absorption applications for regulatory purposes currently remains rather low.^{5,10} Further progress toward the understanding of the interplay between GI physiology, formulation and drug properties as well as on the identifiability, parametrization, and validation of PBBM/PBPK models is required to increase confidence in their performance and thus their impact on regulatory decision-making.^{5,10}

In this context, the purpose of this position paper is to present an overview of the current status of PBPK modeling analyses for biopharmaceutics, identify challenges and knowledge gaps around modeling oral drug absorption, and discuss opportunities for PBPK/PD modeling in support of waivers of *in vivo* clinical studies.

■ CURRENT STATUS

BCS-Based Biowaivers, Clinically Relevant Drug Product Specifications, and Virtual Bioequivalence. *BCS-Based Biowaivers.* The BCS (Biopharmaceutics Classification System)-based biowaiver approach is intended to reduce the need for *in vivo* bioequivalence studies by providing an appropriate surrogate for *in vivo* bioequivalence, whereby *in vivo* bioequivalence studies may be exempted if appropriate *in vitro* data can be generated. BCS-based biowaivers are applicable only to orally administered immediate-release (IR) solid dosage forms or suspensions where the drug substance(s) is categorized as BCS class I or III and meets the predefined solubility, permeability, and dissolution criteria.^{11,12} Additional criteria are linearity of the pharmacokinetics of the drug within the context of the permeability assessment, negligible expectation of inactive ingredient effects on the oral bioavailability of the drug, and the absence of a narrow therapeutic index.^{11,12} Recently, the International Council for Harmonization of Technical Requirements for Pharmaceuticals for Human Use (ICH) drafted guidance on BCS-based biowaivers (M9), the final version of which has been adopted by the Committee of Human Medicinal Products (CHMP) of the European Medicines Agency (EMA) and came into effect at the end of July 2020.¹³ Although the current guidelines advocate that the BCS-based biowaiver principles may be applied to BE purposes other than those specified in their context provided there is a thorough scientific rationale, the potential use of PBPK

modeling to support BCS-based biowaiver applications is not explicitly stated.

The current BCS-biowaiver approach has been widely criticized for being overdiscriminating and overly strict, excluding opportunities not only for scientifically justified extensions to certain BCS class II compounds but also for drug substances which are in theory eligible for BCS-based biowaivers but failed to comply with criteria in the dissolution performance.^{14–20} Several publications have implemented PBBM approaches, including VBE, to investigate the variables limiting drug absorption, support possible BCS-based biowaiver extensions, and recommend specifications based on the *in vivo* performance.^{16,20–26} On the other hand, it has been suggested that products containing drugs belonging to BCS class I and III might exhibit a high risk of bioequivalence failure due to their intrinsic pharmacokinetic properties (e.g., if they have a high first-pass effect or short half-life) and that the eligibility of their products for biowaiver might need to be revised.²⁷ Further concerns have been raised, especially for products including BCS class III drugs, on the potential interactions of different excipients with gut transporters, which in turn could lead to increased risk for bioequivalence.^{28–32} On the whole, it seems that regulatory confidence in the performance of PBPK models for justification of biowaivers is still rather tentative.

Clinically Relevant Specifications. Developing and justifying dissolution specifications for product release can be a challenge for industry and regulatory agencies during the review of a new drug (NDA) and abbreviated new drug applications (ANDA) for new and generic drugs, respectively.³³ In the past, dissolution specifications were established based on batch consistency, but over the past decade or so, the emphasis has shifted toward linking *in vitro* dissolution specifications to *in vivo* performance. The traditional establishment of *in vitro-in vivo* correlations/reasons (IVIVC/R) is slowly being replaced by a PBPK-IVIVC/R framework, with the aim of defining a dissolution space within which all drug product batches would be expected to be bioequivalent to each other and/or to a reference batch. Using this approach, a mechanistic IVIVC/R becomes possible, meaning that the processes of *in vivo* dissolution, permeation (passive, transporter-mediated uptake/efflux), and gut wall metabolism can be isolated and distinguished, thus permitting the direct correlation of *in vitro* with *in vivo* dissolution. From an industrial perspective, PBPK to inform IVIVC/R and establish clinically relevant specifications is considered to be a routine tool, with several successful examples already published in the open literature.^{33–36} PBPK-IVIVC/R-specific challenges and opportunities have been discussed elsewhere.^{1,34,37} In the regulatory setting, PBPK modeling to define clinically relevant specifications has been successful in a wide range of applications, including drug substance particle size distribution, change of manufacturing site or process, post-approval specifications related to drug product shelf life, and polymorphic purities.^{4,21,33}

Virtual Bioequivalence. Numerous publications have highlighted the importance of mechanistic understanding between *in vitro*, *in silico*, and *in vivo* events, which should lead to confidence in prospective clinical trial simulation and waivers of *in vivo* relative BA/BE studies.^{3,17,20,24,26,38} In this context, the emerging field of VBE has been attracting the attention of stakeholders in academia, industry, and regulatory agencies. Although there is not yet any formal regulatory framework, the

FDA has been encouraging the use of VBE as a tool to justify dissolution specifications, product quality and to support the prediction of food effects, pH-dependent DDIs, and other biopharmaceutical applications. Interestingly, VBE approaches have already been adopted by the Office of Generic Drugs (OGD) within the FDA to investigate the risk associated with salt-to-base conversion in prasugrel products and the impact of isopropyl alcohol and slow dissolution on the *in vivo* performance of warfarin sodium tablets.^{25,39} Furthermore, case examples from both academia and industry have showcased the opportunities that VBE offers towards a better understanding of the critical attributes related to the product *in vivo* performance and elimination of unnecessary clinical studies.^{16,17,20,26,40–46} Nevertheless, one should be mindful of the challenges and limitations related to this relatively recent concept and the need to gain further confidence in prospective model performance by validating the results with BE studies in healthy and/or the relevant specific/patient populations.

Food Effects and pH-Dependent Drug–Drug Interactions. *Food Effects.* Assessment of the effect of food on the rate and extent of absorption is part of the development of an orally administered drug product. Often, meal effect studies are conducted early in drug development as part of the first-in-human studies and may be repeated later with the to-be-marketed formulation to inform the product label. According to US-FDA guidance for Industry, “Food-Effect Bioavailability and Bioequivalence Studies”, conducting a food effect bioavailability study is recommended for a drug candidate during the investigational new drug application (IND) period and for generic drug products as part of the ANDA. However, for ANDAs of immediate-release products, a waiver of the fed state bioequivalence study may be possible when the labeling of the reference listed drug states that the product should be taken only on an empty stomach.⁴⁷ By contrast, a food effect study is recommended for all modified-release (MR) products regardless of the classification of the drug substance according to the BCS. In the regulatory setting, for an NDA, the absence of a food effect on bioavailability is not established if the 90% confidence interval (CI) for the ratio of population geometric means between fed and fasted treatments, based on log-transformed data, is not contained within the equivalence limits of 80–125% for either AUC_{inf} (or AUC_{0-t} when appropriate) or C_{max} . When the 90% CI fails to meet the limits of 80–125%, the sponsor should provide specific recommendations on the clinical significance of the food effect based on what is known from the total clinical database about dose–response (exposure–response) and/or PK/PD relationships of the drug under study. The clinical relevance of any difference in T_{max} and lag time should also be indicated by the sponsor.⁴⁸ In order to anticipate, characterize, and/or mitigate a food effect, significant resources may need to be invested during clinical development. For that reason, PBPK models can be a useful tool to foster an understanding of the underlying food–drug interaction mechanisms, predict the clinical impact, extrapolate to various scenarios (e.g., formulation changes), and thus potentially be applied to waive fed state BE studies. Recently, Tistaert et al. summarized the industry’s perspective on the use of PBBM to predict food effects by presenting a sample of five successful case examples.⁴⁹ Within the industry, PBPK models for food effect predictions have been routinely implemented for internal decision-making and risk assessment, during first-in-human (FIH) to inform formulation development, the multiple-ascending dosing (MAD) regimen,

formulation modifications during late-stage clinical development, and life cycle management.⁴⁹ In 2018, a review from the FDA examined the predictive performance of PBPK models in 48 food effect cases, of which 39 were prospective predictions.⁵⁰ The examples were distributed among the BCS classes almost uniformly, with a slightly higher proportion of class I compounds (37%).⁵⁰ Successful prospective predictions, within 1.25-fold, were achieved for 59% and 49% of the predicted versus observed AUC and C_{max} food effect ratios (i.e., the AUC or C_{max} ratio in the fed versus the fasted state), respectively. Nonetheless, due to limited understanding of GI physiology under fed conditions, the variety of meals and possible food–drug interactions, and the commonly applied “top-down” optimization of critical parameters such as dissolution and precipitation rates, confidence in using PBPK modeling to prospectively predict food effects is still considered low.^{50,51} Interestingly, only 3% of the presented cases described a negative food effect, highlighting the importance of increasing our understanding of the mechanisms behind this type of interaction, especially for poorly soluble compounds.⁵⁰ Despite several successful examples and proposed workflows, it must be acknowledged that best practices in PBPK modeling for food effects have not yet been established, and significant improvement not only on the currently available *in silico* (e.g., PBPK platforms) but also on the *in vivo* (e.g., aspiration, MRI studies) and *in vitro* (e.g., fed state transfer models, permeability assays) tools is needed. Additionally, the importance of interactions of food components with intestinal enzymes and transporters leading to clinically significant alterations of exposure should be more fully explored. At present, data regarding such interactions are limited, and it is thus difficult to quantify their impact on PK using PBPK models.^{52–55} For a detailed review of the literature regarding the interactions of food components with drug-metabolizing enzymes and uptake or efflux transporters in the gut, we refer to Won et al.⁵⁶

Drug–Drug Interactions on Absorption. Similar to food effects, PBPK modeling for biopharmaceutics has been commonly applied to predict and describe pH-dependent DDIs mediated from coadministration of the drug and gastric acid-reducing agents (ARAs). The three main ARA classes on the market include antacids, histamine H2 receptor antagonists (H2RAs), and proton pump inhibitors (PPIs). Among patients across all fields of medicine, especially in oncology, ARAs are often used for the symptomatic relief of drug side effects and GI-related diseases. As a result of their frequent use, there is substantial potential for DDIs. Clinical data for several weakly basic compounds has shown reduced exposure (C_{max} and AUC) and, occasionally, prolonged T_{max} in subjects or patients with elevated gastric pH.⁵⁷ Currently, no specific regulatory framework is available.⁵⁷ To initiate work in this area, in 2018, the U.S. FDA posted a public docket titled “Framework for Assessing pH-Dependent Drug–Drug Interactions” to solicit information and encourage dialogue, with the aim of establishing guidelines for the assessment of pH-dependent DDIs.⁵⁸ Recently, in November 2020, the FDA distributed a draft guidance entitled: “Evaluation of Gastric pH-Dependent Drug Interactions With Acid-Reducing Agents: Study Design, Data Analysis, and Clinical Implications” for commenting purposes only.⁵⁹ Mitra et al. presented a cross-industry perspective with seven successful case examples of PBBM in the prediction of ARA effect on drug exposure.⁶⁰ The discussion was focused on the impact of ARA on the exposure

due to elevated gastric pH, especially for poorly soluble weakly basic drugs.⁶⁰ The authors suggested that waiving dedicated ARA clinical studies on a case-by-case scenario, when appropriately supported by PBPK modeling, clinical data, and appropriate biopharmaceutics experiments, would be a way forward. Although predicting the interaction of ARAs might be in some ways less complicated than forecasting food effects, for some ARAs, other mechanisms (e.g., chelation by antacids) might be involved along with the increase in gastric pH.⁵⁷ At this point, it is critical to identify biopredictive biopharmaceutics tools and use these to gain confidence in model performance and predictive accuracy of PBPK models regarding all ARA mechanisms, in order to establish best practices, that will allow for waivers of the respective clinical studies.⁵⁷ In any case, similar to food effects and postabsorptive DDIs, the clinical relevance of such interactions should be assessed by taking into account the dose–response relationships for both efficacy and safety.

■ KNOWLEDGE GAPS, CHALLENGES, AND LIMITATIONS

Oral intake is the preferred route of drug administration due to its noninvasive character and convenience for the patient. Oral drug absorption is affected by physiological variables including, but not limited to, pH, transit time and motility, bile and pancreatic secretions, food components, epithelial transport and gut wall metabolism. Thus, it is evident that drug substances/dosage forms encounter a highly dynamic and heterogeneous environment from the very first moment of their administration until reaching the systemic circulation. The complex interplay of physiological variables, dosage forms, and drug attributes ultimately defines the overall oral absorption and drug product *in vivo* performance. Despite significant advancements in the knowledge of GI physiology and progress on the predictive performance of *in vitro* and *in silico* models, a complete understanding is still lacking, and several questions around this dynamic interplay remain unanswered. Currently, knowledge gaps are identified in three main areas of interest: (a) understanding and characterization of GI physiology (*in vivo*), (b) translatability and predictive accuracy of biopharmaceutics tools (*in vitro-in vivo*) and (c) integration of parts a and b into *in silico* models and their predictive performance (*in vitro-in silico-in vivo*).

Gastrointestinal Physiology. The interaction of GI physiology with oral dosage forms under various conditions (healthy versus disease, fasted versus fed), GI regions, and populations remains, as yet, incompletely understood. Only limited data from aspiration and imaging studies are available even in the fasted state, which has been the most extensively studied.^{61–66} In addition, due to the experimental complexity of such trials, only a few different dosing conditions/sampling sites can be included in each study, and the sample size is usually small. This not only hampers appropriate statistical analysis but also limits the understanding of the underlying variability of physiological parameters and their distribution. Although it is well recognized that high interindividual variability (%CV > 100) is associated with several physiological variables in the GI tract, which are critical for oral dosage form performance (e.g., gastric emptying, intraluminal volumes), insight into within-subject (i.e., interoccasion) variability is very limited.⁶⁷

Furthermore, significant knowledge gaps have been identified in our understanding of *in vivo* dissolution and

precipitation in both the fasted and fed states, together with their variability. This is primarily because of limitations in directly accessing and measuring these parameters, the constantly changing volumes in the lumen, the complex hydrodynamics, and the high heterogeneity observed. It has been suggested that *in vivo* dissolution is governed by both reaction and diffusion at the molecular level.⁶⁸ In addition, the effect of microenvironment pH in the interface between the solid undissolved drug molecules and liquid *in vitro* is well-documented.^{69–72} However, the importance of surface pH *in vivo*, especially in a highly regulated and dynamic environment like the GI tract, remains unknown and practically impossible to quantify. Along the same lines, challenges and high variability have been identified with measuring the *in vivo* buffer capacity. Litou et al. have summarized values of pH and buffer capacity measured in human aspirates from the upper GI tract in healthy adults and investigated the impact of sample handling on the reported numbers.⁷³ This work discusses the vagaries of *in vivo* aspiration studies and the variability introduced by the sample handling protocols, as well as the analysis of the collected samples. Despite multiple efforts to characterize the contents of the GI tract from human aspiration studies, mainly in healthy adults, it has to be acknowledged that those represent “snapshots” of the GI lumen rather than capturing the whole dynamic nature of the physiological processes. Magnetic resonance imaging (MRI) studies have provided useful information on the gastric emptying, GI transit time, volumes, and motility in both fasted and fed states, suggesting the distribution of GI water in pockets and impact of gastric and gallbladder secretions, but again these are “snapshots”.^{74–78} Hydrodynamics, pressure, contraction forces and *in vivo* disintegration in the stomach have also been studied to some extent.⁷⁹ However, the impact of these parameters on the performance of oral dosage forms has not yet been fully elucidated.

Additionally, there are several, yet to be answered, questions associated with micelle-mediated solubilization and *in vivo* precipitation. Understanding of the relative contribution of bile and/or food components on the solubilization of drug substances, the partitioning between the micellar and aqueous phase and the biophysical interactions of drug molecules with the micellar structures is perceived as a promising area of research.^{80–87} At the same time, the mechanisms of *in vivo* supersaturation, precipitation, and redissolution and their interplay with drug permeation and transport deserve further investigation.^{62,88–91} Several bioenabling formulations have been developed to enhance oral bioavailability such as nanoparticles, self-emulsifying drug delivery systems, cyclodextrin complexes, solid dispersions, and lipid-based formulations.⁹² For instance, the effects of lipolysis on drug release from lipid-based formulations *in vivo* are unknown,^{93,94} while the penetration of the intestinal mucosa by nanoparticles,^{95,96} as well as the uptake of dendrimer-drug conjugates and their transepithelial transport, are still an area of speculation.⁹⁷

Food intake can have a major impact on oral absorption, and a better understanding of the mechanisms underlying food–drug interactions is crucial for food effect predictions. Administration of food affects the gastric motility, pH, bile secretion, the intestinal fluid composition and, therefore, drug solubilization and dosage form performance.^{63,74,75,98–101} Despite diligent research on the gastric secretions and emptying from the fed stomach,^{74,99,101,102} because of the heterogeneous nature of meals, it remains challenging to isolate

the emptying of drug/dosage form from that of water, chyme, or solid meal particles. The situation becomes even more complex considering mixing or grinding forces in the different parts of the stomach, viscosity, *in vivo* disintegration, osmolarity, and partitioning between aqueous and micellar phases. Although the lipidic content in food has been often associated with increased solubilization of poorly soluble lipophilic compounds, the dynamic interactions of drug molecules with the micellar structures that are built, or with other food components and chyme in the lumen, remain unclear. At the same time, micelle-mediated solubilization may not necessarily result in increased absorption and a positive food effect. Entrapment, sequestration, or chelation with the micellar structures has been reported *in vitro*, leading to the hypothesis that there may be a significant reduction of the fraction available for permeation across the apical enterocyte membrane.¹⁰³ A recent report on the clinical DDI of fenebrutinib with the strong CYP3A4 inhibitor, itraconazole, supports this hypothesis. In that study, itraconazole was administered as a cyclodextrin solution together with fenebrutinib, and the DDI was not as pronounced as expected.¹⁰⁴ It was subsequently shown *in vitro* that fenebrutinib is bound to the cyclodextrin and when this was taken into account in a retrospective PBPK analysis, it was possible to describe the observed effect.¹⁰⁴ In this context, further investigation on the type, extent, and most importantly, the kinetics of such interactions is imperative. Similarly, lipidic structures or ultrastructures formed after food intake have been shown to interact with lipid-based formulations.¹⁰⁵ However, despite several *in vitro* efforts,^{80,106,107} the *in vivo* mechanisms as well as the impact of lipid digestion on the supersaturation/precipitation, transport, and overall absorption have yet to be elucidated. In addition, the relative contribution and specific effects of food components (lipids, proteins, carbohydrates) need to be investigated further.¹⁰⁸ Other considerations include possible inhibitory effects on intestinal permeability, enzymes, or transporters (e.g., CYP3A4, OATP2B1, Pgp, BCRP), increased splanchnic blood flow, and gut microbiome interaction with micellar structures.^{56,85,109,110} Recent research has demonstrated the effect of several excipients and food additives on the inhibition of uptake and efflux transporters in the gut, especially of OAT12B1 and Pgp, *in vitro*, *in situ*, or in animal species.^{111–116} Other studies have shown that bacterial metabolism from gut microbiota could counterbalance this effect by metabolizing susceptible excipients to inactive metabolites.¹¹⁷ At the same time, some excipients have been found capable of enhancing drug permeation across the enterocyte apical membrane *in vitro*. The potential for these so-called absorption-modifying excipients to enable oral drug absorption has been recently reviewed by Dahlgren et al.¹¹⁸ The clinical relevance of such effect in humans has yet to be explored and may be a promising area of research in terms of assisting the understanding of formulation/food interactions in the gut at a molecular level. Further analysis of food-drug interactions can be found elsewhere.^{56,119,120}

Apart from the upper small intestine, which is usually the major site of absorption, increasing interest in the contribution of the lower parts of the GI tract, i.e., the ileum, cecum, and colon, on the overall drug absorption has been expressed. Recently, the physiological differences among the segments of the GI tract and their implications for oral drug absorption have been reviewed by Vertzoni et al.¹²¹ Studies have investigated the physiological dimensions, motility, fluid

composition, luminal transit, and flow in the distal ileum and colon of healthy volunteers as well as patients with inflammatory bowel disorders.^{122–126} Nevertheless, the abundance of transporters and bacterial metabolic enzymes and their activity in the ileum and colon, drug permeation and uptake processes, and the interaction of dosage forms with the colonic environment is not well explored.^{86,87,127–131} In general, quantifying drug permeation and uptake, and especially regional differences in these, have always been challenging.¹²¹

Three decades after the largest existing data set of human intestinal permeability was published, important knowledge gaps remain on this topic.¹³² The need for improved methods to assess human intestinal permeability, its regional differences, as well as the effect of physiological constituents (e.g., ultrastructures, colloids), food, and/or functional excipients, has consistently been stated.^{118,133–136} Quantification of the gut wall permeation (transcellular versus paracellular, passive versus active), metabolic pathways, and efflux/uptake transporters, as well as their interplay with physiological or formulation components, is lacking. Uptake and permeation in the colon, relative volume, and content of colonic fluids, especially when the colon is the site of drug action (e.g., in inflammatory bowel diseases, colonic cancer), are of particular interest.

Physiological alterations of the GI tract in some specific subject groups, e.g., pediatric, elderly and various patient populations, e.g., obese, colonic cancer, cirrhotic, ulcerative colitis, can affect oral drug absorption and thus safety and efficacy. In a recent comprehensive review, Stillhart et al.¹³⁷ summarized physiological implications in nondisease, GI-disease, and systemic disease populations. Briefly, further research is required to shed light on the altered physiology (and ontogeny) of the GI tract and dosage form interactions with physiological variables in pediatric, elderly, and obese populations, patients with celiac disease, ulcerative colitis or Crohn's disease, cirrhotic, diabetic, bariatric surgery, Parkinson's and nonalcoholic fatty liver disease patients. Very few reports on these matters are available in the literature.^{138–147} Similarly, the complete picture of the consequences of chronic administration of ARA/PPIs on GI physiology, oral absorption, and DDIs, especially in oncology patients, is also lacking.^{148,149} The same holds true for the availability of tools and current knowledge on food effects in specific populations.^{120,137} Effects of age, disease, race, or ethnicity in intestinal permeability and gut wall metabolism are only partly understood. In addition, reports have associated the decreased bioavailability of mizoribine in healthy Japanese subjects with polymorphisms on the concentrative nucleoside transporter 1 (*SLC28A1*).¹⁵⁰ Similar, salt intake in healthy Japanese subjects led to significantly higher bioavailability of mizoribine.¹⁵¹ Others have reported the effects on the bioavailability of digoxin *in vivo* due to a mutant allele (C3435T) at exon 26 of the *MDR1* gene.^{152,153} On the other hand, it was suggested that, for the transporters ABCB1, ABCG2, ABCC2, and ABCC3, the lack of variability in bioavailability and drug response may be attributed to polymorphisms in transporter genes, whereas transcriptional regulation or post-transcriptional modification seems to be more critical.¹⁵⁴ The impact of genetic polymorphism on OATPs-mediated uptake and/or BCRP-mediated efflux with implications for oral absorption has been documented as well.^{155–157} Therefore, the impact of genetic

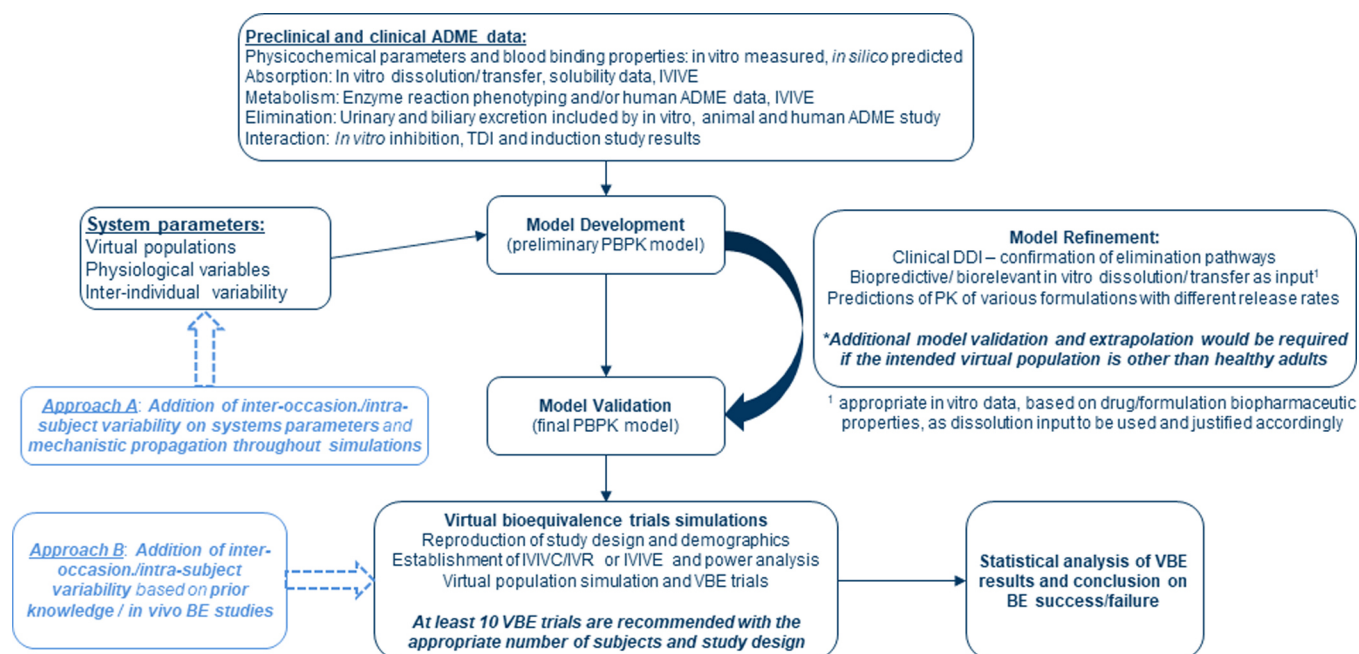


Figure 1. Proposed PBPK modeling workflow for establishment and assessment of virtual bioequivalence. Implementation of intrasubject or interoccasion variability can be implemented either as variability in system/physiological parameters and mechanistic propagation throughout simulations (Approach A) or based on prior knowledge from *in vivo* PK studies (Approach B).

polymorphisms and epigenetic factors such as diet deserves more intensive research efforts.^{158,159}

In Vitro Tools. It is evident that knowledge gaps in GI physiology directly impact the predictive performance and mechanistic insight provided by *in vitro* biopharmaceutic tools and *in silico* models. Despite the significant progress achieved in both *in vitro* and *in silico* biopredictive tools, which have enabled their widespread use for predicting *in vivo* performance, a broader and deeper understanding of GI physiology will lead to further improvements in current biopredictive biopharmaceutic tools and PBPK models, with the aim of making them fully mechanistic.

The translational link between *in vitro-in silico-in vivo* is not yet well established in several areas of PBPK modeling for biopharmaceutics. Regarding solubility and dissolution as input to PBPK models, it has been acknowledged that the relative contribution of surfactants in micelle-mediated solubilization and the specific interactions of drug molecule/dosage form with the micellar structure is only partly understood. Concerns around the appropriate input value for solubility when building PBPK models for bioenabling formulations like solid dispersions or nanoparticles have also been raised.¹⁶⁰ Limitations on the available *in vitro* and *in silico* dissolution models exist as well. *In vitro*, these are often related to buffer species (e.g., phosphate vs bicarbonate), buffer capacity, hydrodynamics, and biorelevance. On the other hand, current dissolution models are not considered fully mechanistic, and their applicability needs to be assessed on a case-by-case basis. For example, the Takano model using the *z*-factor can be appropriate for drugs/dosage forms, where the initial dissolution rate is critical but may be less appropriate for other drugs/dosage form combinations.^{16,161} Nevertheless, it has to be noted that such input (i.e., *z*-factor) is often obtained from *in vitro* dissolution in aqueous media that does not adequately reflect the luminal contents of the GI tract. Pepin et al. have proposed the use of fitted particle size distribution

(PSD) to simulate *in vivo* dissolution in cases where the absorption is dissolution limited.²¹ Others have recommended a stepwise *in vitro-in vivo* extrapolation of biopharmaceutic parameters approach as promising and more mechanistic.^{17,20,162,163} In any case, further research on establishing and validating the *in vitro-in vivo* link and development of more mechanistic dissolution models will be needed to further increase confidence in PBBM.

Even more challenging is the translation of *in vitro* to *in vivo* supersaturation/precipitation. Despite numerous *in vitro* precipitation models, which have been reviewed elsewhere,¹⁶⁴ mixed results from their use in *in silico* models have been reported.^{165,166} Since the drug may precipitate to a metastable form, characterization of both the precipitation profile and the precipitate (e.g., solid state, particle size) is highly advisable.⁴ Inclusion of an absorptive sink model is preferred by many researchers for supersaturation/precipitation measurement to better gauge the likelihood of precipitation *in vivo*, as well as to capture the dynamic concentration driving force for membrane transport.¹⁶⁷ Nevertheless, *in vitro* models often overpredict *in vivo* precipitation, and the interplay between supersaturation, precipitation, redissolution, and uptake *in vivo*, especially for enabling formulations, is not yet entirely understood.^{90,91,168,169} It seems that the golden mean between *in vitro* complexity, biorelevance, and model parametrization has yet to be found.

Moreover, the lack of mechanistic models which can link chemistry manufacturing and control (CMC) parameters as well as formulation properties with *in vitro* tests and *in vivo* performance has been highlighted as a major caveat of current PBPK models.^{4,33} It is intended that the relationship between *in vitro* dissolution and critical quality attributes (CQA) will be integrated within PBBM as part of the Quality by Design (QbD) paradigm.

PBPK Modeling Aspects. Improvements to the current PBPK platforms with regard to the above-mentioned

Table 1. Summary of Current Knowledge Gaps in Gastrointestinal Physiology, Challenges, and Future Opportunities for the Improvement of the PBPK Models' Performance for Biopharmaceutic Applications and Oral Drug Absorption

knowledge gaps	challenges	opportunities and future actions
characterization of GI contents in specific and patient populations	limitations in accessibility and visualization of GI lumen contents	additional aspiration and imaging studies in disease and specific populations and after administration of different types of formulations or drugs
regional differences of GI tract in specific and patient populations	availability of noninvasive and real-time imaging technologies	
quantification of <i>in vivo</i> disintegration, surface pH, and hydrodynamics and their relevance for oral absorption <i>in vivo</i>	experimental complexity	appropriate study design, including administration at multiple occasions, allowing adequate statistical analysis
identification and quantification of micelle–drug biophysical and molecular interactions	sample size ($n \leq 12$)	implementation of innovative analytical and imaging technologies
interactions of gut microbiota with excipients, micellar structures, and drugs <i>in vivo</i>	highly dynamic and heterogeneous environment	further investigation of technologies such as computed tomography, nuclear imaging, capsule endoscopy, molecular dynamics simulations, and synchrotron small-angle X-ray scattering
relevance of distal ileum and colon fluid composition and volume <i>in vivo</i> for oral drug absorption	highly variable environment	
effects of obesity, fatty liver and Parkinson's diseases, age, race and ethnicity, and diet on intestinal solubilization, permeation, and absorption	human aspirates represent "snapshots" of the GI lumen rather than capturing completely its dynamic nature	development of real time data analysis and visualization tools with possible integration into PBPK models
effect of <i>in vivo</i> lipolysis on drug release	translational link between <i>in vitro</i> , <i>in silico</i> , and <i>in vivo</i> is difficult to be established	
interplay of <i>in vivo</i> precipitation/redissolution and permeation		implementation of nonlinear dynamic systems techniques to model GI physiology and variability
micelle-mediated solubilization and interactions (entrapment) <i>in vivo</i>		nonlinear mixed effect modeling to explain GI population variability and improve clinical trial simulations
relevance of lysosomal trapping and lymphatic absorption <i>in vivo</i>		further investigation on GI tracers, markers and use of biomarkers to identify and quantify physiological processes or disease states
relevance and extent of colonic absorption		improved method to assess and quantify mechanisms of gut wall transport and impact of formulation/excipients on epithelial permeation
gut enzymes and transporters abundance/expression in healthy, disease, and specific populations		in-depth profiling of GI tract in specific and disease populations along with food-drug/enzymes/transporters and excipients-enzymes/transporters interactions
relevance of colonic permeation and absorption <i>in vivo</i>		PBPK modeling of potential mechanisms and delivery systems for oral administration of large molecules
effects of genetic polymorphisms on intestinal metabolism, transporter-mediated uptake and efflux		enhance collaboration between translational M&S, biopharmaceutics scientists, pharmacometricians, and clinicians
nanoparticle effects on drug permeation and interaction with the intestinal mucosa		enhance bottom-up PBPK predictability
effect of lipids and micelle-mediated transport on drug permeation		
quantification of the effects of food constituents and meal composition on GI physiology and oral drug absorption		
effects of meal composition on gastric motility, secretions, viscosity, hydrodynamics, and shear forces <i>in vivo</i>		
differentiation of water, chyme, and solid particle gastric emptying		
effect of meal, mixing and grinding forces, viscosity and osmolality on <i>in vivo</i> disintegration, and drug absorption		
characterization of micellar structures observed <i>in vivo</i> in the fed state under various meal compositions.		
effect of lipid structures or ultrastructured on lipid-based formulations		
GI contents characterization under various meal compositions and in specific or disease populations		
interaction of food components with gut enzymes and/or transporters		
effect of food on drug permeation		
quantification of intrasubject variability of GI physiology parameters		
identification and quantification of covariates among GI physiology parameters		
identification of subject-by-formulation interactions		
quantification of the impact of CQA/CMA on the <i>in vivo</i> release and drug absorption		

physiological considerations are anticipated to increase confidence in the predictive performance. Some of the main topics of interest are intestinal permeability and regional differences (e.g., extent of colonic absorption), active transport and gut wall metabolism, and the impact of functional excipients on oral uptake. For instance, best practices for the estimation of permeability from *in vitro/in situ* experiments have not been established. Even though mechanistic permeability, hydrodynamics, and dynamic bile salt models are implemented in some platforms, further verification of their performance will underscore their utility.^{170–172} Furthermore, only very limited data, mostly from very small sample sizes and fasted healthy adults, on intraindividual variability of physiological variables are available.^{67,81} As VBE is attracting more and more attention, it is crucial to better understand and implement both intersubject and within-subject variability as well as their distribution.^{20,45} Incorporation of within-subject variability in PBPK models can be achieved either empirically using prior knowledge (e.g., from previous BE studies) or mechanistically by adding it appropriately to the physiological parameters and propagating it throughout simulation at the population level (Figure 1).^{20,45} On the other hand, as earlier discussed, there is very little known about within-subject variability and the covariate relationships between the GI physiology parameters.⁶⁷ Arbitrary inclusion of such relationships might lead to false-negative predictions, whereas omitting it could have the opposite results. In this case, and especially for highly variable drugs, a risk assessment approach based on the “worst-case” scenario might be a way forward. In this context, there is an immediate need for properly designed *in vivo* studies, which will enable quantification of intrasubject variability and covariate analysis of the GI physiology variables. Inter- and intrasubject variability in the fed state, in specific or disease populations, as well as subject-by-formulation variability could be considered as uncharted waters at the moment, while the debate on best practices for clinical trials simulation, their sample size and the number of trials is ongoing.

Regarding predictions of food effects and ARA/PPI interactions, all physiological considerations should be taken into account. Currently, not all aspects of fed physiology can be captured in the *in silico* models due to the paucity of relevant *in vivo* data. These include interactions between food components (e.g., lipids, carbohydrates) and the drug substance/dosage form, interactions with enzymes and transporters, fed state precipitation models, intraluminal volumes and fluid composition arising from different meals in different populations (e.g., elderly), and the effects of complex colloid structures. The ability to simulate ARA/PPI interactions using PBPK modeling is more advanced, with the caveat that mechanisms other than elevated gastric pH, like chelation and ARA-induced metabolic or transporter DDIs, may also need to be considered and explicitly modeled. However, implementation of results from *in vitro* experiments using biorelevant media simulating hypo-/achlorhydric populations has proven beneficial.^{173–175}

Apart from physiological or translational challenges and limitations, we would like to stress the importance of ensuring structural and statistical identifiability in every PBPK modeling activity. Parameter estimation or optimization should be performed cautiously and needs to be well justified, as the risk of nonidentifiability is higher in extensively parametrized models like quantitative systems pharmacology (QSP) and PBPK, especially in the absence of intravenous data or when

the input data comes from several sources. Overparametrization or optimization of systems parameters without solid justification constitutes common malpractices as well. Last but not least, lack of transparency and publication bias toward positive results can be a limitation to confidence in PBPK model performance, and there should be more emphasis put on learning from negative results. Clearly listed assumptions, identifiability assessment, a detailed modeling and simulation analysis plan, and fully transparent models constitute the way forward to best practices in PBPK modeling.

■ OPPORTUNITIES AND FUTURE ACTIONS

Considering the increasing number of drug candidates exhibiting unfavorable and complex absorption properties in development, it is likely that efficient oral drug delivery will become even more challenging in the future. Past successes hold no guarantee for the future, as the number of drug candidates with challenging physicochemical and biopharmaceutical properties, such as high molecular weight, low aqueous solubility, stability, and/or permeability, has increased dramatically. In 2019, the US FDA granted marketing authorization of the first oral glucagon-like peptide 1, the first large molecule that has been approved for oral use.¹⁷⁶ This signifies a new era for oral absorption and offers plentiful opportunities for further *in vivo* research and computational tools. Increased effort and knowledge will be required to successfully respond to the contemporary challenges of oral drug development of not only small, but also of large, new molecules.

Multistakeholder, cross-continent research consortia such as the OrBiTo, PEARRL (www.pearrl.eu), UNGAP (www.cost.eu/actions/CA16206), and DDMore (www.ddmore.eu) projects,^{177,178} bringing together leading scientists in academia, industry, and regulatory agencies, have stimulated interdisciplinary dialogue, fostered interdisciplinary collaboration, and contributed to recent advances in oral biopharmaceutics and *in silico* tools. In order to best address the current knowledge gaps, exchange of knowledge and information is required to characterize and reduce uncertainty in physiological parameters as well as quantify and analyze the physiological variability to enhance bottom-up PBPK predictability and streamline oral drug development (Table 1). This clearly indicates the motivation for continued research, the extensive integration of knowledge, and increased interdisciplinary and intersectoral collaboration between biopharmaceutics, M&S and formulation scientists, statisticians and pharmacometricians, as well as gastroenterologists, clinicians, and engineers who will contribute to the refinement or development of mechanistic *in/ex vivo*, *in vitro*, and *in silico* models.

Regarding the above-mentioned challenges in the characterization of the GI tract, a major limiting factor remains the problematic accessibility or visualization of its contents. Several advanced, preferably noninvasive and real-time, imaging technologies have been adopted to overcome this hurdle, but further progress is still required. Magnetic resonance (MR), contrast-enhanced MR, computed tomography (CT) and nuclear imaging, capsule endoscopy, 3D endoscope imaging, high-resolution electrical mapping, and electrogastrogram have been used to visualize the gut lumen (patho)-physiology and gain insight into the *in vivo* behavior of drug/formulation in preclinical species, healthy humans, and patients.^{179–185} Furthermore, systematic exploration of the capabilities of molecular dynamics (MD) simulations, synchrotron small-

angle X-ray scattering, coherent anti-Stokes Raman spectroscopy, and surface plasmon resonance would promote understanding of membrane transport, drug-colloidal structures interactions, lipid imaging at the molecular level, drug or excipient release, disposition, and intracellular concentrations.^{83,84,186,187} Thus, a plethora of opportunities not only for GI imaging but also for the development of data analysis and *in silico* tools, which will be interacting or even be integrated into PBPK models, is foreseen.

Supporting these efforts, further integration of PBPK with pharmacometrics is more than essential. Nonlinear mixed effect (NLME) modeling would be helpful to analyze, defragment, and reproduce the primary sources of variability observed in the GI tract. Common stochastic (e.g., Monte Carlo simulation) or resampling (e.g., bootstrap) techniques and Bayesian approaches are considered beneficial to better understand the distribution of inter- and intrasubject variability as well as for a more accurate parameter estimation.^{188–195} As a result, this would accelerate advancements in the field of virtual bioequivalence and increase confidence by allowing more mechanistic and reliable simulations with fully incorporated population variability (Figure 1). At the same time, the integration of pharmacometrics and PBPK tools will improve clinical trial simulation and further optimize individualized and targeted treatment. Furthermore, the potential benefits from using GI markers or tracers and endogenous substrates to understand the gut or other (patho)-physiologies have been highlighted.^{196–200} Bile acids and their conjugates have been identified as promising biomarkers to assess liver injury, cholestasis, and in general, liver disease.^{199,201,202} Additionally, postprandial serum bile acids in humans might be used to indicate differences in absorptive patterns.²⁰³ Recently, the benefit of endogenous substrates such as coproporphyrin I and III, glycochenodeoxycholate sulfate, and chenodeoxycholate glucuronide to assess transporter drug–drug interactions, especially for OAT1B1/3, OAT1/3, and BCRP substrates, using PBPK modeling has been acknowledged and has sparked intensive research efforts.^{204–214} In this context, biomarker modeling, especially for in-patient populations, is another point where the interaction of pharmacometricians with biopharmaceutic scientists would be advantageous for developing more mechanistic applications of PBPK models. Similar, further exploration of the as yet scarcely studied intercorrelations of GI physiological parameters using covariate analysis is essential to accurately define individual GI physiologies within PBPK platforms.

The lack of *in vivo* human data with regard to interactions of food components/nutrients and excipients with enzymes, transporters, and in general with the intraluminal environment must be overcome by extensive research in order to improve knowledge about and enable incorporation of such interactions into *in silico* models. Limited information about the GI physiology in specific age groups (e.g., pediatric, elderly) and patient populations (e.g., cancer, cirrhotic) of different ethnic groups represents another limitation to the confidence in current PBPK models/platforms. Effects of different types of meals or enzymes (e.g., lipases) on formulation performance and drug absorption, transporters and metabolizing enzymes abundance and activity levels in patient populations, potential mechanisms for oral administration of large molecules, the impact of the gut microbiome or mucosal integrity in inflammatory bowel diseases, the ontogeny of the GI tract,

and physiological alterations due to dietary habits or obesity are only some of the opportunities to be explored in the arena of oral drug absorption. In this context, there is a clear need for further analytical assays, aspiration, and imaging studies, providing improved characterization and in-depth profiling of the GI tract, which, in turn, would enable the development and verification of mechanistic *in vitro* and *in silico* models. Until now, most studies of this type have been focused on healthy adults and have studied just a few drugs and mainly conventional formulations, hindering extrapolation to other populations, compounds and bioenabling formulations. Thus, standardization of methodologies and best practices in aspiration or imaging studies would foster these efforts. Further, imaging and omics data could help to quantify and provide mechanistic insight into the molecular interactions between drugs, excipients, food components and the intestinal membrane, enzymes/transporters, and microbiota *in vivo*.^{112,116}

At the same time, wherever possible, enhanced reproducibility and comparability of *in vivo*, *in vitro*, and *in silico* models are considered essential. The clinical relevance of formulation and food effects as well as ARA/PPI interactions encompasses not only the capturing changes in pharmacokinetics caused by the interactions but also the ramifications for safety and efficacy. Therefore, further linking PBPK models with a pharmacodynamic (PD) or toxicodynamic (TD) model is crucial for decision-making in clinical practice. A well-established exposure/response relationship is thus required to forecast the clinical outcome.

A major area of opportunity waiting to be exploited is the translation of CMC changes to clinical impact. The development of *in silico* tools to describe manufacturing processes and critical quality attributes (CQA) linked to *in vitro* tests, which will subsequently be connected with PBPK models, is of great interest. It is crucial to capture the effect of CQA changes on the *in vitro* and *in vivo* performance within the QbD and BioRAM paradigm so that confidence in PBPK predictions of drug quality and clinically relevant specifications will allow waivers of *in vivo* studies.²¹⁵

Furthermore, open-source tools, repositories (e.g., Open Systems Pharmacology suite, DDMore), and a common programming language/interface (e.g., Pharmacometric Markup Language) may improve transparency and interconnectivity on the application of current and future tools.^{177,216,217} A holistic approach, combining the understanding of the rate-limiting processes and their interplay to predict *in vivo* performance, is warranted. Regardless of the PBPK application, it will be up to pharmacometricians, M&S, and biopharmaceutics scientists working together to establish a thorough understanding of all underlying assumptions/limitations and mechanisms critical to the clinical outcome.


In conclusion, we believe that advancements in the understanding of GI physiology in different populations, ethnic groups, age groups, and disease states, development of fully mechanistic *in silico* tools, and interdisciplinary interaction, harmonization, and enforcement of the translational link between *in vitro*, *in silico*, and *in vivo* will shape the future of PBPK modeling for oral drug absorption. Foreseen is a scenario where state-of-the-art *in silico* models will confidently replace many *in vivo* clinical studies and allow for cost and time-effective, model-informed drug discovery, and development.

AUTHOR INFORMATION

Corresponding Author

Jennifer Dressman – Institute of Pharmaceutical Technology, Goethe University, Frankfurt am Main 60438, Germany; Fraunhofer Institute of Translational Pharmacology and Medicine (ITMP, Frankfurt am Main 60438, Germany; Email: dressman@em.uni-frankfurt.de

Author

Ioannis Loiosos-Konstantinidis – Institute of Pharmaceutical Technology, Goethe University, Frankfurt am Main 60438, Germany;  orcid.org/0000-0003-2586-3577

Complete contact information is available at: <https://pubs.acs.org/10.1021/acs.molpharmaceut.0c00903>

Notes

The authors declare no competing financial interest.

ACKNOWLEDGMENTS

This work was supported by the European Union's Horizon 2020 Research and Innovation Program under grant agreement no. 674909 (PEARRL).

REFERENCES

- (1) Zhang, X.; Duan, J.; Kesisoglou, F.; Novakovic, J.; Amidon, G.; Jamei, M.; Lukacova, V.; Eissing, T.; Tsakalozou, E.; Zhao, L.; Lionberger, R. Mechanistic Oral Absorption Modeling and Simulation for Formulation Development and Bioequivalence Evaluation: Report of an FDA Public Workshop. *CPT: Pharmacometrics Syst. Pharmacol.* **2017**, *6* (8), 492–495.
- (2) Kesisoglou, F.; Chung, J.; Van Asperen, J.; Heimbach, T. Physiologically Based Absorption Modeling to Impact Biopharmaceutics and Formulation Strategies in Drug Development-Industry Case Studies. *J. Pharm. Sci.* **2016**, *105*, 2723.
- (3) Heimbach, T.; Suarez-Sharp, S.; Kakhi, M.; Holmstock, N.; Olivares-Morales, A.; Pepin, X.; Sjögren, E.; Tsakalozou, E.; Seo, P.; Li, M.; Zhang, X.; Lin, H.-P.; Montague, T.; Mitra, A.; Morris, D.; Patel, N.; Kesisoglou, F. Dissolution and Translational Modeling Strategies Toward Establishing an In Vitro-In Vivo Link—a Workshop Summary Report. *AAPS J.* **2019**, *21* (2), 29.
- (4) Pepin, X. J.; Parrott, N.; Dressman, J.; Delvadia, P.; Mitra, A.; Zhang, X.; Babiskin, A.; Kolhatkar, V.; Suarez-Sharp, S. Current State and Future Expectations of Translational Modeling Strategies to Support Drug Product Development, Manufacturing Changes and Controls: A Workshop Summary Report. *J. Pharm. Sci.* **2020**.
- (5) Shebley, M.; Sandhu, P.; Emami Riedmaier, A.; Jamei, M.; Narayanan, R.; Patel, A.; Peters, S. A.; Reddy, V. P.; Zheng, M.; de Zwart, L.; Beneton, M.; Bouzom, F.; Chen, J.; Chen, Y.; Cleary, Y.; Collins, C.; Dickinson, G. L.; Djebli, N.; Einolf, H. J.; Gardner, I.; Huth, F.; Kazmi, F.; Khalil, F.; Lin, J.; Odinecs, A.; Patel, C.; Rong, H.; Schuck, E.; Sharma, P.; Wu, S.-P.; Xu, Y.; Yamazaki, S.; Yoshida, K.; Rowland, M. Physiologically Based Pharmacokinetic Model Qualification and Reporting Procedures for Regulatory Submissions: A Consortium Perspective. *Clin. Pharmacol. Ther.* **2018**, *104* (1), 88–110.
- (6) ORBITO | IMI Innovative Medicines Initiative <https://www.imi.europa.eu/projects-results/project-factsheets/orbito> (accessed Nov 8, 2020).
- (7) Pharmaceutical Education with Regulatory Links (PEARRL) IMI <https://www.pearrl.eu/> (accessed Nov 8, 2020).
- (8) Ungap cost action CA16205 <https://gbiomed.kuleuven.be/english/research/50000715/50000716/ungap> (accessed Nov 8, 2020).
- (9) U.S. Food and Drug Administration Center for Drug Evaluation and Research (CDER). Guidance for Industry The Use of Physiologically Based Pharmacokinetic Analyses — Biopharmaceutics Applications for Oral Drug Product Development, Manufacturing Changes, and Controls <https://www.fda.gov/media/142500/download> (accessed Oct 11, 2020).
- (10) Sager, J. E.; Yu, J.; Ragueneau-Majlessi, I.; Isoherranen, N. Physiologically Based Pharmacokinetic (PBPK) Modeling and Simulation Approaches: A Systematic Review of Published Models, Applications, and Model Verification. *Drug Metab. Dispos.* **2015**, *43* (11), 1823–1837.
- (11) U.S. Food and Drug Administration Center for Drug Evaluation and Research (CDER). Guidance for Industry Waiver of In Vivo Bioavailability and Bioequivalence Studies for Immediate-Release Solid Oral Dosage Forms Based on a Biopharmaceutics Classification System <https://www.fda.gov/media/70963/download> (accessed Nov 7, 2020).
- (12) European Medicines Agency Committee for Medicinal Products for Human use (CHMP). Guideline on the investigation of bioequivalence (revision 1) https://www.ema.europa.eu/en/documents/scientific-guideline/guideline-investigation-bioequivalence-rev1_en.pdf (accessed Nov 7, 2020).
- (13) Bransford, P.; Cook, J.; Gupta, M.; Haertter, S.; He, H.; Ju, R.; Kanodia, J.; Lennernäs, H.; Lindley, D.; Polli, J. E.; Wenning, L.; Wu, Y. ICH M9 Guideline in Development on Biopharmaceutics Classification System-Based Biowaivers: An Industrial Perspective from the IQ Consortium. *Mol. Pharmaceutics* **2020**, 361–372.
- (14) Loiosos-Konstantinidis, I.; Paraiso, R. L. M.; Fotaki, N.; McAllister, M.; Cristofolletti, R.; Dressman, J. Application of the Relationship between Pharmacokinetics and Pharmacodynamics in Drug Development and Therapeutic Equivalence: A PEARRL Review. *J. Pharm. Pharmacol.* **2019**, *71* (4), 699–723.
- (15) Yazdani, M.; Briggs, K.; Jankovsky, C.; Hawi, A. The “High Solubility” Definition of the Current FDA Guidance on Biopharmaceutical Classification System May Be Too Strict for Acidic Drugs. *Pharm. Res.* **2004**, *21* (2), 293–299.
- (16) Hofsä, M. A.; Dressman, J. Evaluation of Differences in Dosage Form Performance of Generics Using BCS-Based Biowavier Specifications and Biopharmaceutical Modeling - Case Examples Amoxicillin and Doxycycline. *J. Pharm. Sci.* **2020**, *109*, 2437.
- (17) Cristofolletti, R.; Dressman, J. B. Use of Physiologically Based Pharmacokinetic Models Coupled with Pharmacodynamic Models to Assess the Clinical Relevance of Current Bioequivalence Criteria for Generic Drug Products Containing Ibuprofen. *J. Pharm. Sci.* **2014**, *103* (10), 3263–3275.
- (18) Kovačević, I.; Parojčić, J.; Homšek, I.; Tubić-Grozdanis, M.; Langguth, P. Justification of Biowaiver for Carbamazepine, a Low Soluble High Permeable Compound, in Solid Dosage Forms Based on IVIVC and Gastrointestinal Simulation. *Mol. Pharmaceutics* **2009**, *6* (1), 40–47.
- (19) Cristofolletti, R.; Rowland, M.; Lesko, L. J.; Blume, H.; Rostami-Hodjegan, A.; Dressman, J. B. Past, Present, and Future of Bioequivalence: Improving Assessment and Extrapolation of Therapeutic Equivalence for Oral Drug Products. *J. Pharm. Sci.* **2018**, *107* (10), 2519–2530.
- (20) Loiosos-Konstantinidis, I.; Cristofolletti, R.; Fotaki, N.; Turner, D. B.; Dressman, J. Establishing Virtual Bioequivalence and Clinically Relevant Specifications Using In Vitro Biorelevant Dissolution Testing and Physiologically-Based Population Pharmacokinetic Modeling. Case Example: Naproxen. *Eur. J. Pharm. Sci.* **2020**, *143*, 105170.
- (21) Pepin, X. J. H.; Flanagan, T. R.; Holt, D. J.; Eidelman, A.; Treacy, D.; Rowlings, C. E. Justification of Drug Product Dissolution Rate and Drug Substance Particle Size Specifications Based on Absorption PBPK Modeling for Lesinurad Immediate Release Tablets. *Mol. Pharmaceutics* **2016**, *13*, 3256.
- (22) Pepin, X. J. H.; Sanderson, N. J.; Blanz, A.; Grover, S.; Ingallinera, T. G.; Mann, J. C. Bridging In Vitro Dissolution and In Vivo Exposure for Acalabrutinib. Part I. Mechanistic Modelling of Drug Product Dissolution to Derive a P-PSD for PBPK Model Input. *Eur. J. Pharm. Biopharm.* **2019**, *142*, 421–434.

- (23) Cristofolletti, R.; Dressman, J. B. Bridging the Gap Between In Vitro Dissolution and the Time Course of Ibuprofen-Mediating Pain Relief. *J. Pharm. Sci.* **2016**, *105* (12), 3658–3667.
- (24) Babiskin, A. H.; Zhang, X. Application of Physiologically Based Absorption Modeling for Amphetamine Salts Drug Products in Generic Drug Evaluation. *J. Pharm. Sci.* **2015**, *104* (9), 3170–3182.
- (25) Fan, J.; Zhang, X.; Zhao, L. Utility of Physiologically Based Pharmacokinetic Absorption Modeling to Predict the Impact of Salt-to-Base Conversion on Prasugrel HCl Product Bioequivalence in the Presence of Proton Pump Inhibitors. *AAPS J.* **2017**, *19* (5), 1479–1486.
- (26) Doki, K.; Darwich, A. S.; Patel, N.; Rostami-Hodjegan, A. Virtual Bioequivalence for Achlorhydric Subjects: The Use of PBPK Modelling to Assess the Formulation-Dependent Effect of Achlorhydria. *Eur. J. Pharm. Sci.* **2017**, *109*, 111–120.
- (27) Colón-Useche, S.; González-Álvarez, I.; Mangas-Sanjuan, V.; González-Álvarez, M.; Pastoriza, P.; Molina-Martínez, I.; Bermejo, M.; García-Arieta, A. Investigating the Discriminatory Power of BCS-Biowaiver in Vitro Methodology to Detect Bioavailability Differences between Immediate Release Products Containing a Class I Drug. *Mol. Pharmaceutics* **2015**, *12* (9), 3167–3174.
- (28) Ruiz-Picazo, A.; Lozoya-Agullo, I.; González-Álvarez, I.; Bermejo, M.; González-Álvarez, M. Effect of Excipients on Oral Absorption Process According to the Different Gastrointestinal Segments. *Expert Opin. Drug Delivery* **2020**, *0* (0), 1.
- (29) Chen, M. L.; Sadrieh, N.; Yu, L. Impact of Osmotically Active Excipients on Bioavailability and Bioequivalence of BCS Class III Drugs. *AAPS J.* **2013**, *15* (4), 1043–1050.
- (30) Al-Ali, A. A. A.; Nielsen, R. B.; Steffansen, B.; Holm, R.; Nielsen, C. U. Nonionic Surfactants Modulate the Transport Activity of ATP-Binding Cassette (ABC) Transporters and Solute Carriers (SLC): Relevance to Oral Drug Absorption. *Int. J. Pharm.* **2019**, *566* (May), 410–433.
- (31) Flanagan, T. Potential for Pharmaceutical Excipients to Impact Absorption: A Mechanistic Review for BCS Class 1 and 3 Drugs. *Eur. J. Pharm. Biopharm.* **2019**, *141* (May), 130–138.
- (32) García-Arieta, A. Interactions between Active Pharmaceutical Ingredients and Excipients Affecting Bioavailability: Impact on Bioequivalence. *Eur. J. Pharm. Sci.* **2014**, *65*, 89–97.
- (33) McAllister, M.; Flanagan, T.; Boon, K.; Pepin, X.; Tistaert, C.; Jamei, M.; Abend, A.; Kotzagiorgis, E.; Mackie, C. Developing Clinically Relevant Dissolution Specifications for Oral Drug Products—Industrial and Regulatory Perspectives. *Pharmaceutics* **2020**, *12* (1), 19.
- (34) Stillhart, C.; Pepin, X.; Tistaert, C.; Good, D.; Van Den Bergh, A.; Parrott, N.; Kesisoglou, F. PBPK Absorption Modeling: Establishing the In Vitro-In Vivo Link—Industry Perspective. *AAPS J.* **2019**, *21*, 1.
- (35) Lennernäs, H. Regional Intestinal Drug Permeation: Biopharmaceutics and Drug Development. *Eur. J. Pharm. Sci.* **2014**, *57* (1), 333–341.
- (36) Abend, A.; Heimbach, T.; Cohen, M.; Kesisoglou, F.; Pepin, X.; Suarez-Sharp, S. Dissolution and Translational Modeling Strategies Enabling Patient-Centric Drug Product Development: The M-CERSI Workshop Summary Report. *AAPS J.* **2018**, *20* (3), 1.
- (37) Stillhart, C.; Parrott, N. J.; Lindenberg, M.; Chalus, P.; Bentley, D.; Szepes, A. Characterising Drug Release from Immediate-Release Formulations of a Poorly Soluble Compound, Basmisanil, Through Absorption Modelling and Dissolution Testing. *AAPS J.* **2017**, *19* (3), 827–836.
- (38) Al-Tabakha, M. M.; Alomar, M. J. In Vitro Dissolution and in Silico Modeling Shortcuts in Bioequivalence Testing. *Pharmaceutics* **2020**, *12* (1), 45.
- (39) Zhang, X.; Wen, H.; Fan, J.; Vince, B.; Li, T.; Gao, W.; Kinjo, M.; Brown, J.; Sun, W.; Jiang, W.; Lionberger, R. Integrating In Vitro, Modeling, and In Vivo Approaches to Investigate Warfarin Bioequivalence. *CPT: Pharmacometrics Syst. Pharmacol.* **2017**, *6* (8), 523–531.
- (40) Ibarra, M.; Valiente, C.; Sopena, P.; Schiavo, A.; Lorier, M.; Vázquez, M.; Fagiolino, P. Integration of in Vitro Biorelevant Dissolution and in Silico PBPK Model of Carvedilol to Predict Bioequivalence of Oral Drug Products. *Eur. J. Pharm. Sci.* **2018**, *118*, 176–182.
- (41) Mitra, A.; Kesisoglou, F.; Dogterom, P. Application of Absorption Modeling to Predict Bioequivalence Outcome of Two Batches of Etoricoxib Tablets. *AAPS PharmSciTech* **2015**, *16* (1), 76–84.
- (42) Jereb, R.; Opara, J.; Legen, I.; Petek, B.; Grabnar-Peklar, D. In Vitro-In Vivo Relationship and Bioequivalence Prediction for Modified-Release Capsules Based on a PBPK Absorption Model. *AAPS PharmSciTech* **2020**, *21* (1), 1–11.
- (43) Rebeka, J.; Jerneja, O.; Igor, L.; Boštjan, P.; Aleksander, B.; Simon, Ž.; Albin, K. PBPK Absorption Modeling of Food Effect and Bioequivalence in Fed State for Two Formulations with Crystalline and Amorphous Forms of BCS 2 Class Drug in Generic Drug Development. *AAPS PharmSciTech* **2019**, *20* (2), 1–10.
- (44) Basu, S.; Yang, H.; Fang, L.; Gonzalez-Sales, M.; Zhao, L.; Trame, M. N.; Lesko, L.; Schmidt, S. Physiologically Based Pharmacokinetic Modeling to Evaluate Formulation Factors Influencing Bioequivalence of Metoprolol Extended-Release Products. *J. Clin. Pharmacol.* **2019**, *59* (9), 1252–1263.
- (45) Wedagedera, J.; Cain, T.; Pathak, S. M.; Jamei, M. *Virtual Bioequivalence Assessment of Two Tramadol Formulations Using the Advanced Dissolution Absorption and Metabolism (ADAM) Model via Simcyp R Package*; 2017.
- (46) Pathak, S. M.; Patel, N.; Wedagedera, J.; Turner, D. B.; Jamei, M.; Rostami-Hodjegan, A.; Limited, S. *Establishment of Virtual Bioequivalence Using Population-Based PBPK Modelling: Application to the Setting of Dissolution Limits*; 1997; Vol. 11.
- (47) U.S. Food and Drug Administration Center for Drug Evaluation and Research (CDER). Guidance for Industry Bioequivalence Studies with Pharmacokinetic Endpoints for Drugs Submitted Under an ANDA <https://www.fda.gov/media/87219/download> (accessed Nov 7, 2020).
- (48) U.S. Food and Drug Administration Center for Drug Evaluation and Research (CDER). Guidance for Industry Food-Effect Bioavailability and Fed Bioequivalence Studies <https://www.fda.gov/media/70945/download> (accessed Nov 7, 2020).
- (49) Tistaert, C.; Heimbach, T.; Xia, B.; Parrott, N.; Samant, T. S.; Kesisoglou, F. Food Effect Projections via Physiologically Based Pharmacokinetic Modeling: Predictive Case Studies. *J. Pharm. Sci.* **2019**, *108*, 592–602.
- (50) Li, M.; Zhao, P.; Pan, Y.; Wagner, C. Predictive Performance of Physiologically Based Pharmacokinetic Models for the Effect of Food on Oral Drug Absorption: Current Status. *CPT: Pharmacometrics Syst. Pharmacol.* **2018**, *7* (2), 82–89.
- (51) Jones, H. M.; Chen, Y.; Gibson, C.; Heimbach, T.; Parrott, N.; Peters, S. A.; Snoeys, J.; Upreti, V. V.; Zheng, M.; Hall, S. D. Physiologically Based Pharmacokinetic Modeling in Drug Discovery and Development: A Pharmaceutical Industry Perspective. *Clin. Pharmacol. Ther.* **2015**, *97*, 247–262.
- (52) Harris, R. Z.; Jang, G. R.; Tsunoda, S. Dietary Effects on Drug Metabolism and Transport. *Clin. Pharmacokinet.* **2003**, *42*, 1071–1088.
- (53) Dresser, G. K.; Kim, R. B.; Bailey, D. G. Effect of Grapefruit Juice Volume on the Reduction of Fexofenadine Bioavailability: Possible Role of Organic Anion Transporting Polypeptides*. *Clin. Pharmacol. Ther.* **2005**, *77* (3), 170–177.
- (54) Dresser, G. Fruit Juices Inhibit Organic Anion Transporting Polypeptide-Mediated Drug Uptake to Decrease the Oral Availability of Fexofenadine. *Clin. Pharmacol. Ther.* **2002**, *71* (1), 11–20.
- (55) Misaka, S.; Yatabe, J.; Müller, F.; Takano, K.; Kawabe, K.; Glaeser, H.; Yatabe, M. S.; Onoue, S.; Werba, J. P.; Watanabe, H.; Yamada, S.; Fromm, M. F.; Kimura, J. Green Tea Ingestion Greatly Reduces Plasma Concentrations of Nadolol in Healthy Subjects. *Clin. Pharmacol. Ther.* **2014**, *95* (4), 432–438.

- (56) Won, C. S.; Oberlies, N. H.; Paine, M. F. Mechanisms Underlying Food-Drug Interactions: Inhibition of Intestinal Metabolism and Transport. *Pharmacol. Ther.* **2012**, *136* (2), 186–201.
- (57) Lahner, E.; Annibale, B.; Delle Fave, G. Systematic Review: Impaired Drug Absorption Related to the Co-Administration of Antisecretory Therapy. *Aliment. Pharmacol. Ther.* **2009**, *29* (12), 1219–1229.
- (58) U.S. Food and Drug Administration. [Docket No. FDA-2018-N-1820], Framework for Assessing pH-Dependent Drug-Drug Interactions: Establishment of a Public Docket; Request for Comments <https://www.govinfo.gov/content/pkg/FR-2018-05-22/pdf/2018-10927.pdf> (accessed Aug 3, 2020).
- (59) U.S. Food and Drug Administration Center for Drug Evaluation and Research (CDER). *Guidance for Industry Evaluation of Gastric pH-Dependent Drug Interactions With Acid-Reducing Agents: Study Design, Data Analysis, and Clinical Implications*. 2020. <https://www.fda.gov/media/144026/download> (accessed 2020-12-01).
- (60) Mitra, A.; Parrott, N.; Miller, N.; Lloyd, R.; Tistaert, C.; Heimbach, T.; Ji, Y.; Kesisoglou, F. Prediction of PH-Dependent Drug-Drug Interactions for Basic Drugs Using Physiologically Based Biopharmaceutics Modeling: Industry Case Studies. *J. Pharm. Sci.* **2020**, *109* (3), 1380–1394.
- (61) Kalantzi, L.; Goumas, K.; Kalioras, V.; Abrahamsson, B.; Dressman, J. B.; Reppas, C. Characterization of the Human Upper Gastrointestinal Contents under Conditions Simulating Bioavailability/Bioequivalence Studies. *Pharm. Res.* **2006**, *23* (1), 165–176.
- (62) Petrakis, O.; Vertzoni, M.; Angelou, A.; Kesisoglou, F.; Bentz, K.; Goumas, K.; Reppas, C. Identification of Key Factors Affecting the Oral Absorption of Salts of Lipophilic Weak Acids: A Case Example. *J. Pharm. Pharmacol.* **2015**, *67* (1), 56–67.
- (63) Van Den Abeele, J.; Brouwers, J.; Mattheus, R.; Tack, J.; Augustijns, P. Gastrointestinal Behavior of Weakly Acidic BCS Class II Drugs in Man - Case Study of Diclofenac Potassium. *J. Pharm. Sci.* **2016**, *105* (2), 687–696.
- (64) Moreno de, M. P. la C.; Oth, M.; Deferme, S.; Lammert, F.; Tack, J.; Dressman, J.; Augustijns, P. Characterization of Fasted-State Human Intestinal Fluids Collected from Duodenum and Jejunum. *J. Pharm. Pharmacol.* **2006**, *58* (8), 1079–1089.
- (65) Sager, M.; Grimm, M.; Jedamzik, P.; Merdivan, S.; Kromrey, M. L.; Hasan, M.; Koziolok, M.; Tzvetkov, M. V.; Weitschies, W. Combined Application of MRI and the Salivary Tracer Technique to Determine the in Vivo Disintegration Time of Immediate Release Formulation Administered to Healthy, Fasted Subjects. *Mol. Pharmaceutics* **2019**, *16* (4), 1782–1786.
- (66) Schiller, C.; Fröhlich, C. P.; Giessmann, T.; Siegmund, W.; Mönnikes, H.; Hosten, N.; Weitschies, W. Intestinal Fluid Volumes and Transit of Dosage Forms as Assessed by Magnetic Resonance Imaging. *Aliment. Pharmacol. Ther.* **2005**, *22* (10), 971–979.
- (67) Grimm, M.; Koziolok, M.; Kühn, J. P.; Weitschies, W. Interindividual and Intraindividual Variability of Fasted State Gastric Fluid Volume and Gastric Emptying of Water. *Eur. J. Pharm. Biopharm.* **2018**, *127* (March), 309–317.
- (68) Macheras, P.; Iliadis, A.; Melagraki, G. A Reaction Limited in Vivo Dissolution Model for the Study of Drug Absorption: Towards a New Paradigm for the Biopharmaceutic Classification of Drugs. *Eur. J. Pharm. Sci.* **2018**, *117*, 98–106.
- (69) Mooney, K. G.; Mintun, M. A.; Himmelstein, K. J.; Stella, V. J. Dissolution Kinetics of Carboxylic Acids II: Effect of Buffers. *J. Pharm. Sci.* **1981**, *70* (1), 22–32.
- (70) Ozturk, S. S.; Dressman, J. B.; Palsson, B. O. On the Use of the Quasi-Equilibrium Assumption for Drug Dissolution. *Pharm. Res.* **1990**, *07*, 425–430.
- (71) Ozturk, S. S.; Palsson, B. O.; Dressman, J. B. Dissolution of Ionizable Drugs in Buffered and Unbuffered Solutions. *Pharm. Res.* **1988**, *5* (5).
- (72) Krieg, B. J.; Taghavi, S. M.; Amidon, G. L.; Amidon, G. E. In Vivo Predictive Dissolution: Comparing the Effect of Bicarbonate and Phosphate Buffer on the Dissolution of Weak Acids and Weak Bases. *J. Pharm. Sci.* **2015**, *104* (9), 2894–2904.
- (73) Litou, C.; Psachoulas, D.; Vertzoni, M.; Dressman, J.; Reppas, C. Measuring pH and Buffer Capacity in Fluids Aspirated from the Fasted Upper Gastrointestinal Tract of Healthy Adults. *Pharm. Res.* **2020**, *37* (3), 1–12.
- (74) Koziolok, M.; Grimm, M.; Garbacz, G.; Kühn, J.-P.; Weitschies, W. Intra-gastric Volume Changes after Intake of a High-Caloric, High-Fat Standard Breakfast in Healthy Human Subjects Investigated by MRI. *Mol. Pharmaceutics* **2014**, *11* (5), 1632–1639.
- (75) Schneider, F.; Grimm, M.; Koziolok, M.; Modeß, C.; Dokter, A.; Roustom, T.; Siegmund, W.; Weitschies, W. Resolving the Physiological Conditions in Bioavailability and Bioequivalence Studies: Comparison of Fasted and Fed State. *Eur. J. Pharm. Biopharm.* **2016**, *108*, 214–219.
- (76) Fruehauf, H.; Goetze, O.; Steingoetter, A.; Kwiatek, M.; Boesiger, P.; Thumshirn, M.; Schwizer, W.; Fried, M. Intersubject and Intrasubject Variability of Gastric Volumes in Response to Isocaloric Liquid Meals in Functional Dyspepsia and Health. *Neurogastroenterol. Motil.* **2007**, *19* (7), 553–561.
- (77) Kwiatek, M. A.; Menne, D.; Steingoetter, A.; Goetze, O.; Forras-Kaufman, Z.; Kaufman, E.; Fruehauf, H.; Boesiger, P.; Fried, M.; Schwizer, W.; Fox, M. R. Effect of Meal Vol. and Calorie Load on Postprandial Gastric Function and Emptying: Studies under Physiological Conditions by Combined Fiber-Optic Pressure Measurement and MRI. *Am. J. Physiol. - Gastrointest. Liver Physiol.* **2009**, *297* (5), G894.
- (78) Mudie, D. M.; Murray, K.; Hoad, C. L.; Pritchard, S. E.; Garnett, M. C.; Amidon, G. L.; Gowland, P. A.; Spiller, R. C.; Amidon, G. E.; Marciani, L. Quantification of Gastrointestinal Liquid Volumes and Distribution Following a 240 ML Dose of Water in the Fasted State. *Mol. Pharmaceutics* **2014**, *11* (9), 3039–3047.
- (79) Kwiatek, M. A.; Fox, M. R.; Steingoetter, A.; Menne, D.; Pal, A.; Fruehauf, H.; Kaufman, E.; Forras-Kaufman, Z.; Brasseur, J. G.; Goetze, O.; Hebbard, G. S.; Boesiger, P.; Thumshirn, M.; Fried, M.; Schwizer, W. Effects of Clonidine and Sumatriptan on Postprandial Gastric Vol. Response, Antral Contraction Waves and Emptying: An MRI Study. *Neurogastroenterol. Motil.* **2009**, *21* (9), 928.
- (80) Yeap, Y. Y.; Trevaskis, N. L.; Quach, T.; Tso, P.; Charman, W. N.; Porter, C. J. H. Intestinal Bile Secretion Promotes Drug Absorption from Lipid Colloidal Phases via Induction of Super-saturation. *Mol. Pharmaceutics* **2013**, *10* (5), 1874–1889.
- (81) Elvang, P. A.; Bohsen, M. S.; Stein, P. C.; Bauer-Brandl, A.; Riethorst, D.; Brouwers, J.; Augustijns, P.; Brandl, M. Co-Existing Colloidal Phases of Human Duodenal Aspirates: Intraindividual Fluctuations and Interindividual Variability in Relation to Molecular Composition. *J. Pharm. Biomed. Anal.* **2019**, *170*, 22–29.
- (82) Elvang, P. A.; Stein, P. C.; Bauer-Brandl, A.; Brandl, M. Characterization of Co-Existing Colloidal Structures in Fasted State Simulated Fluids FaSSiF: A Comparative Study Using AF4/MALLS, DLS and DOSY. *J. Pharm. Biomed. Anal.* **2017**, *145*, 531–536.
- (83) Phan, S.; Salentinig, S.; Hawley, A.; Boyd, B. J. How Relevant Are Assembled Equilibrium Samples in Understanding Structure Formation during Lipid Digestion? *Eur. J. Pharm. Biopharm.* **2015**, *96*, 117–124.
- (84) Rezhdo, O.; Di Maio, S.; Le, P.; Littrell, K. C.; Carrier, R. L.; Chen, S. H. Characterization of Colloidal Structures during Intestinal Lipolysis Using Small-Angle Neutron Scattering. *J. Colloid Interface Sci.* **2017**, *499*, 189–201.
- (85) Enright, E. F.; Griffin, B. T.; Gahan, C. G. M.; Joyce, S. A. Microbiome-Mediated Bile Acid Modification: Role in Intestinal Drug Absorption and Metabolism. *Pharmacol. Res.* **2018**, *133*, 170–186.
- (86) Müllertz, A.; Fatouros, D. G.; Smith, J. R.; Vertzoni, M.; Reppas, C. Insights into Intermediate Phases of Human Intestinal Fluids Visualized by Atomic Force Microscopy and Cryo-Transmission Electron Microscopy Ex Vivo. *Mol. Pharmaceutics* **2012**, *9* (2), 237–247.
- (87) Müllertz, A.; Reppas, C.; Psachoulas, D.; Vertzoni, M.; Fatouros, D. G. Structural Features of Colloidal Species in the Human Fasted Upper Small Intestine. *J. Pharm. Pharmacol.* **2015**, *67* (4), 486–492.

- (88) Hens, B.; Brouwers, J.; Corsetti, M.; Augustijns, P. Supersaturation and Precipitation of Posaconazole Upon Entry in the Upper Small Intestine in Humans. *J. Pharm. Sci.* **2016**, *105* (9), 2677–2684.
- (89) Rubbens, J.; Brouwers, J.; Tack, J.; Augustijns, P. Gastrointestinal Dissolution, Supersaturation and Precipitation of the Weak Base Indinavir in Healthy Volunteers. *Eur. J. Pharm. Biopharm.* **2016**, *109*, 122–129.
- (90) Psachoulas, D.; Vertzoni, M.; Goumas, K.; Kalioras, V.; Beato, S.; Butler, J.; Reppas, C. Precipitation in and Supersaturation of Contents of the Upper Small Intestine After Administration of Two Weak Bases to Fasted Adults. *Pharm. Res.* **2011**, *28* (12), 3145–3158.
- (91) Kourentas, A.; Vertzoni, M.; Symillides, M.; Goumas, K.; Gibbon, R.; Butler, J.; Reppas, C. Effectiveness of Supersaturation Promoting Excipients on Albendazole Concentrations in Upper Gastrointestinal Lumen of Fasted Healthy Adults. *Eur. J. Pharm. Sci.* **2016**, *91*, 11–19.
- (92) Williams, H. D.; Trevaskis, N. L.; Charman, S. A.; Shanker, R. M.; Charman, W. N.; Poutou, C. W.; Porter, C. J. H. Strategies to Address Low Drug Solubility in Discovery and Development. *Pharmacol. Rev.* **2013**, *65*, 315–499.
- (93) Carrière, F. Impact of Gastrointestinal Lipolysis on Oral Lipid-Based Formulations and Bioavailability of Lipophilic Drugs. *Biochimie* **2016**, *125*, 297–305.
- (94) Koehl, N. J.; Holm, R.; Kuentz, M.; Jannin, V.; Griffin, B. T. Exploring the Impact of Surfactant Type and Digestion: Highly Digestible Surfactants Improve Oral Bioavailability of Nilotinib. *Mol. Pharmaceutics* **2020**, *17* (9), 3202–3213.
- (95) Sugano, K. Possible Reduction of Effective Thickness of Intestinal Unstirred Water Layer by Particle Drifting Effect. *Int. J. Pharm.* **2010**, *387* (1–2), 103–109.
- (96) Li, H. L.; Zhao Bin, X.; Ma, Y. K.; Zhai, G. X.; Li, L. B.; Lou, H. X. Enhancement of Gastrointestinal Absorption of Quercetin by Solid Lipid Nanoparticles. *J. Controlled Release* **2009**, *133* (3), 238–244.
- (97) Sadekar, S.; Ghandehari, H. Transepithelial Transport and Toxicity of PAMAM Dendrimers: Implications for Oral Drug Delivery. *Adv. Drug Delivery Rev.* **2012**, *64*, 571–588.
- (98) Koziolok, M.; Schneider, F.; Grimm, M.; Mode, C.; Seekamp, A.; Roustom, T.; Siegmund, W.; Weitschies, W. Intragastric pH and Pressure Profiles after Intake of the High-Caloric, High-Fat Meal as Used for Food Effect Studies. *J. Controlled Release* **2015**, *220* (Pt A), 71–78.
- (99) Pentafragka, C.; Vertzoni, M.; Symillides, M.; Goumas, K.; Reppas, C. Disposition of Two Highly Permeable Drugs in the Upper Gastrointestinal Lumen of Healthy Adults after a Standard High-Calorie, High-Fat Meal. *Eur. J. Pharm. Sci.* **2020**, *149*, 105351.
- (100) Van Den Abeele, J.; Schilderink, R.; Schneider, F.; Mols, R.; Minekus, M.; Weitschies, W.; Brouwers, J.; Tack, J.; Augustijns, P. Gastrointestinal and Systemic Disposition of Diclofenac under Fasted and Fed State Conditions Supporting the Evaluation of in Vitro Predictive Tools. *Mol. Pharmaceutics* **2017**, *14*, 4220.
- (101) Rubbens, J.; Brouwers, J.; Tack, J.; Augustijns, P. Gastric and Duodenal Diclofenac Concentrations in Healthy Volunteers after Intake of the FDA Standard Meal: In Vivo Observations and in Vitro Explorations. *Mol. Pharmaceutics* **2019**, *16* (2), 573–582.
- (102) Goetze, O.; Treier, R.; Fox, M.; Steingoetter, A.; Fried, M.; Boesiger, P.; Schwizer, W. The Effect of Gastric Secretion on Gastric Physiology and Emptying in the Fasted and Fed State Assessed by Magnetic Resonance Imaging. *Neurogastroenterol. Motil.* **2009**, *21* (7), 725.
- (103) Hens, B.; Brouwers, J.; Corsetti, M.; Augustijns, P. Gastrointestinal Behavior of Nano- and Microsized Fenofibrate: In Vivo Evaluation in Man and in Vitro Simulation by Assessment of the Permeation Potential. *Eur. J. Pharm. Sci.* **2015**, *77*, 40–47.
- (104) Chen, Y.; Ma, F.; Jones, N. S.; Yoshida, K.; Chiang, P.; Durk, M. R.; Wright, M. R.; Jin, J. Y.; Chinn, L. W. Physiologically-Based Pharmacokinetic Model-Informed Drug Development for Fenebrutinib: Understanding Complex Drug-Drug Interactions. *CPT: Pharmacometrics Syst. Pharmacol.* **2020**, *9* (6), 332–341.
- (105) Mueller, E. A.; Kovarik, J. M.; van Bree, J. B.; Grevel, J.; Lückner, P. W.; Kutz, K. Influence of a Fat-Rich Meal on the Pharmacokinetics of a New Oral Formulation of Cyclosporine in a Crossover Comparison with the Market Formulation. *Pharm. Res.* **1994**, *11* (1), 151–155.
- (106) Yeap, Y. Y.; Trevaskis, N. L.; Porter, C. J. H. The Potential for Drug Supersaturation during Intestinal Processing of Lipid-Based Formulations May Be Enhanced for Basic Drugs. *Mol. Pharmaceutics* **2013**, *10* (7), 2601–2615.
- (107) Yeap, Y. Y.; Trevaskis, N. L.; Porter, C. J. H. Lipid Absorption Triggers Drug Supersaturation at the Intestinal Unstirred Water Layer and Promotes Drug Absorption from Mixed Micelles. *Pharm. Res.* **2013**, *30* (12), 3045–3058.
- (108) Mariani, L.; Cox, E. F.; Pritchard, S. E.; Major, G.; Hoad, C. L.; Mellows, M.; Hussein, M. O.; Costigan, C.; Fox, M.; Gowland, P. A.; Spiller, R. C. Additive Effects of Gastric Volumes and Macronutrient Composition on the Sensation of Postprandial Fullness in Humans. *Eur. J. Clin. Nutr.* **2015**, *69* (3), 380–384.
- (109) Nakanishi, T.; Tamai, I. Interaction of Drug or Food with Drug Transporters in Intestine and Liver. *Curr. Drug Metab.* **2015**, *16* (9), 753–764.
- (110) Enright, E. F.; Joyce, S. A.; Gahan, C. G. M.; Griffin, B. T. Impact of Gut Microbiota-Mediated Bile Acid Metabolism on the Solubilization Capacity of Bile Salt Micelles and Drug Solubility. *Mol. Pharmaceutics* **2017**, *14* (4), 1251–1263.
- (111) Ruiz-Picazo, A.; Gonzalez-Alvarez, M.; Gonzalez-Alvarez, I.; Bermejo, M. Effect of Common Excipients on Intestinal Drug Absorption in Wistar Rats. *Mol. Pharmaceutics* **2020**, *17* (7), 2310–2318.
- (112) Zou, L.; Ni, Z.; Tsakalozou, E.; Giacomini, K. M. Impact of Pharmaceutical Excipients on Oral Drug Absorption: A Focus on Intestinal Drug Transporters. *Clin. Pharmacol. Ther.* **2019**, *105* (2), 323–325.
- (113) Engel, A.; Oswald, S.; Siegmund, W.; Keiser, M. Pharmaceutical Excipients Influence the Function of Human Uptake Transporting Proteins. *Mol. Pharmaceutics* **2012**, *9* (9), 2577–2581.
- (114) Gurjar, R.; Chan, C. Y. S.; Curley, P.; Sharp, J.; Chiong, J.; Rannard, S.; Siccardi, M.; Owen, A. Inhibitory Effects of Commonly Used Excipients on P-Glycoprotein in Vitro. *Mol. Pharmaceutics* **2018**, *15* (11), 4835–4842.
- (115) Sjöstedt, N.; Deng, F.; Rauvala, O.; Tepponen, T.; Kidron, H. Interaction of Food Additives with Intestinal Efflux Transporters. *Mol. Pharmaceutics* **2017**, *14* (11), 3824–3833.
- (116) Pottel, J.; Armstrong, D.; Zou, L.; Fekete, A.; Huang, X. P.; Torosyan, H.; Bednarczyk, D.; Whitebread, S.; Bhatarai, B.; Liang, G.; Jin, H.; Ghaemi, S. N.; Slocum, S.; Lukacs, K. V.; Irwin, J. J.; Berg, E. L.; Giacomini, K. M.; Roth, B. L.; Shoichet, B. K.; Urban, L. The Activities of Drug Inactive Ingredients on Biological Targets. *Science* **2020**, *369* (6502), 403–413.
- (117) Zou, L.; Spanogiannopoulos, P.; Pieper, L. M.; Chien, H. C.; Cai, W.; Khuri, N.; Pottel, J.; Vora, B.; Ni, Z.; Tsakalozou, E.; Zhang, W.; Shoichet, B. K.; Giacomini, K. M.; Turnbaugh, P. J. Bacterial Metabolism Rescues the Inhibition of Intestinal Drug Absorption by Food and Drug Additives. *Proc. Natl. Acad. Sci. U. S. A.* **2020**, *117* (27), 16009–16018.
- (118) Dahlgren, D.; Sjöblom, M.; Lennernäs, H. Intestinal Absorption-Modifying Excipients: A Current Update on Preclinical in Vivo Evaluations. *Eur. J. Pharm. Biopharm.* **2019**, *142*, 411–420.
- (119) Pentafragka, C.; Symillides, M.; McAllister, M.; Dressman, J.; Vertzoni, M.; Reppas, C. The Impact of Food Intake on the Luminal Environment and Performance of Oral Drug Products with a View to in Vitro and in Silico Simulations: A PEARRL Review. *J. Pharm. Pharmacol.* **2019**, *71*, 557–580.
- (120) Koziolok, M.; Alcaro, S.; Augustijns, P.; Basit, A. W.; Grimm, M.; Hens, B.; Hoad, C. L.; Jedamzik, P.; Madla, C. M.; Maliepaard, M.; Mariani, L.; Maruca, A.; Parrott, N.; Pávek, P.; Porter, C. J. H.; Reppas, C.; van Riet-Nales, D.; Rubbens, J.; Stelova, M.; Trevaskis, N. L.; Valentová, K.; Vertzoni, M.; Čepo, D. V.; Corsetti, M. The Mechanisms of Pharmacokinetic Food-Drug Interactions - A

Perspective from the UNGAP Group. *Eur. J. Pharm. Sci.* **2019**, *134*, 31–59.

(121) Vertzoni, M.; Augustijns, P.; Grimm, M.; Koziolok, M.; Lemmens, G.; Parrott, N.; Pentafragka, C.; Reppas, C.; Rubbens, J.; Van Den Abeele, J.; Vanuytsel, T.; Weitschies, W.; Wilson, C. G. Impact of Regional Differences along the Gastrointestinal Tract of Healthy Adults on Oral Drug Absorption: An UNGAP Review. *Eur. J. Pharm. Sci.* **2019**, *134*, 153–175.

(122) Vertzoni, M.; Diakidou, A.; Chatziliadis, M.; Söderlind, E.; Abrahamsson, B.; Dressman, J. B.; Reppas, C. Biorelevant Media to Simulate Fluids in the Ascending Colon of Humans and Their Usefulness in Predicting Intracolonic Drug Solubility. *Pharm. Res.* **2010**, *27* (10), 2187–2196.

(123) Vertzoni, M.; Goumas, K.; Söderlind, E.; Abrahamsson, B.; Dressman, J. B.; Poulou, A.; Reppas, C. Characterization of the Ascending Colon Fluids in Ulcerative Colitis. *Pharm. Res.* **2010**, *27* (8), 1620–1626.

(124) Reppas, C.; Karatza, E.; Goumas, C.; Markopoulos, C.; Vertzoni, M. Characterization of Contents of Distal Ileum and Cecum to Which Drugs/Drug Products Are Exposed during Bioavailability/Bioequivalence Studies in Healthy Adults. *Pharm. Res.* **2015**, *32* (10), 3338–3349.

(125) Murray, K.; Hoad, C. L.; Mudie, D. M.; Wright, J.; Heissam, K.; Abreht, N.; Pritchard, S. E.; Al Atwah, S.; Gowland, P. A.; Garnett, M. C.; Amidon, G. E.; Spiller, R. C.; Amidon, G. L.; Marciani, L. Magnetic Resonance Imaging Quantification of Fasted State Colonic Liquid Pockets in Healthy Humans. *Mol. Pharmaceutics* **2017**, *14* (8), 2629–2638.

(126) Fadda, H. M.; Sousa, T.; Carlsson, A. S.; Abrahamsson, B.; Williams, J. G.; Kumar, D.; Basit, A. W. Drug Solubility in Luminal Fluids from Different Regions of the Small and Large Intestine of Humans. *Mol. Pharmaceutics* **2010**, *7* (5), 1527–1532.

(127) Drozdziak, M.; Gröer, C.; Penski, J.; Lapczuk, J.; Ostrowski, M.; Lai, Y.; Prasad, B.; Unadkat, J. D.; Siegmund, W.; Oswald, S. Protein Abundance of Clinically Relevant Multidrug Transporters along the Entire Length of the Human Intestine. *Mol. Pharmaceutics* **2014**, *11* (10), 3547–3555.

(128) Karatza, E.; Goumas, C.; Muenster, U.; Reppas, C.; Vertzoni, M. Ex Vivo Evaluation of Degradation Rates of Metronidazole and Olsalazine in Distal Ileum and in Cecum: The Impact of Prandial State. *Int. J. Pharm.* **2017**, *534* (1–2), 237–241.

(129) Diakidou, A.; Vertzoni, M.; Goumas, K.; Söderlind, E.; Abrahamsson, B.; Dressman, J.; Reppas, C. Characterization of the Contents of Ascending Colon to Which Drugs Are Exposed after Oral Administration to Healthy Adults. *Pharm. Res.* **2009**, *26* (9), 2141–2151.

(130) Müllertz, A.; Fatouros, D. G.; Vertzoni, M.; Reppas, C. Unravelling the Ultrastructure of Ascending Colon Fluids from Patients with Ulcerative Colitis by Cryogenic Transmission Electron Microscopy. *J. Pharm. Pharmacol.* **2013**, *65* (10), 1482–1487.

(131) Tran, T.; Fatouros, D. G.; Vertzoni, M.; Reppas, C.; Müllertz, A. Mapping the Intermediate Digestion Phases of Human Healthy Intestinal Contents from Distal Ileum and Caecum at Fasted and Fed State Conditions. *J. Pharm. Pharmacol.* **2017**, *69* (3), 265–273.

(132) Lennernas, H. Human Intestinal Permeability. *J. Pharm. Sci.* **1998**, *87* (4), 403–410.

(133) Dahlgren, D.; Roos, C.; Lundqvist, A.; Tannergren, C.; Sjöblom, M.; Sjögren, E.; Lennernas, H. Time-Dependent Effects on Small Intestinal Transport by Absorption-Modifying Excipients. *Eur. J. Pharm. Biopharm.* **2018**, *132*, 19–28.

(134) Chen, M. L.; Amidon, G. L.; Benet, L. Z.; Lennernas, H.; Yu, L. X. The BCS, BDDCS, and Regulatory Guidances. *Pharm. Res.* **2011**, *28* (7), 1774–1778.

(135) Olivares-Morales, A.; Lennernas, H.; Aarons, L.; Rostami-Hodjegan, A. Translating Human Effective Jejunal Intestinal Permeability to Surface-Dependent Intrinsic Permeability: A Pragmatic Method for a More Mechanistic Prediction of Regional Oral Drug Absorption. *AAPS J.* **2015**, *17* (5), 1177–1192.

(136) Dahlgren, D.; Cano-Cebrián, M. J.; Olander, T.; Hedeland, M.; Sjöblom, M.; Lennernas, H. Regional Intestinal Drug Permeability and Effects of Permeation Enhancers in Rat. *Pharmaceutics* **2020**, *12* (3), 242.

(137) Stillhart, C.; Vučićević, K.; Augustijns, P.; Basit, A. W.; Batchelor, H.; Flanagan, T. R.; Gesquiere, I.; Greupink, R.; Keszthelyi, D.; Koskinen, M.; Madla, C. M.; Matthys, C.; Miljuš, G.; Mooij, M. G.; Parrott, N.; Ungell, A. L.; de Wildt, S. N.; Orlu, M.; Klein, S.; Müllertz, A. Impact of Gastrointestinal Physiology on Drug Absorption in Special Populations—An UNGAP Review. *Eur. J. Pharm. Sci.* **2020**, *147*, 105280.

(138) Wang, P.; Zhang, Y.-J.; Li, Y.-R.; Liu, X.-M.; Lv, S.-Y.; Xia, X.-Y. A Correlation between Gastrointestinal Dysfunction and Cirrhosis Severity. *Medicine (Philadelphia, PA, U. S.)* **2018**, *97* (37), No. e12070.

(139) Kalaitzakis, E.; Simrén, M.; Abrahamsson, H.; Björnsson, E. Role of Gastric Sensorimotor Dysfunction in Gastrointestinal Symptoms and Energy Intake in Liver Cirrhosis. *Scand. J. Gastroenterol.* **2007**, *42* (2), 237–246.

(140) Fukui, H.; Wiest, R. Changes of Intestinal Functions in Liver Cirrhosis. *Inflamm. Intest. Dis.* **2016**, *1* (1), 24–40.

(141) Madrid, A. M.; Cumsille, F.; Defilippi, C. Altered Small Bowel Motility in Patients with Liver Cirrhosis Depends on Severity of Liver Disease. *Dig. Dis. Sci.* **1997**, *42* (4), 738–742.

(142) Gunnarsdottir, S. A.; Sadik, R.; Shev, S.; Simrén, M.; Sjövall, H.; Stotzer, P. O.; Abrahamsson, H.; Olsson, R.; Björnsson, E. S. Small Intestinal Motility Disturbances and Bacterial Overgrowth in Patients with Liver Cirrhosis and Portal Hypertension. *Am. J. Gastroenterol.* **2003**, *98* (6), 1362–1370.

(143) Abu-Shanab, A.; Quigley, E. M. M. The Role of the Gut Microbiota in Nonalcoholic Fatty Liver Disease. *Nat. Rev. Gastroenterol. Hepatol.* **2010**, *7*, 691–701.

(144) Effinger, A.; O'Driscoll, C. M.; McAllister, M.; Fotaki, N. Impact of Gastrointestinal Disease States on Oral Drug Absorption - Implications for Formulation Design - a PEARRL Review. *J. Pharm. Pharmacol.* **2019**, *71*, 674–698.

(145) Petroni, M. L. Review Article: Gall-Bladder Motor Function in Obesity. *Aliment. Pharmacol. Ther.* **2000**, *14*, 48–50.

(146) Cho, J.; Lee, Y. J.; Kim, Y. H.; Shin, C. M.; Kim, J. M.; Chang, W.; Park, J. H. Quantitative MRI Evaluation of Gastric Motility in Patients with Parkinson's Disease: Correlation of Dyspeptic Symptoms with Vol.etry and Motility Indices. *PLoS One* **2019**, *14* (5), e0216396.

(147) Smet De, J.; Van Bocxlaer, J.; Boussery, K. The Influence of Bypass Procedures and Other Anatomical Changes in the Gastrointestinal Tract on the Oral Bioavailability of Drugs. *J. Clin. Pharmacol.* **2013**, *53*, 361–376.

(148) Budha, N. R.; Frymoyer, A.; Smelick, G. S.; Jin, J. Y.; Yago, M. R.; Dresser, M. J.; Holden, S. N.; Benet, L. Z.; Ware, J. A. Drug Absorption Interactions between Oral Targeted Anticancer Agents and PPIs: Is PH-Dependent Solubility the Achilles Heel of Targeted Therapy. *Clin. Pharmacol. Ther.* **2012**, *92* (2), 203–213.

(149) Patel, D.; Bertz, Richard; Ren, Song; David Boulton, W.; Mats, Någård A Systematic Review of Gastric Acid-Reducing Agent-Mediated Drug-Drug Interactions with Orally Administered Medications. *Clin. Pharmacokinet.* **2020**, *59*, 447–462.

(150) Fukao, M.; Ishida, K.; Sakamoto, T.; Taguchi, M.; Matsukura, H.; Miyawaki, T.; Hashimoto, Y. Effect of Genetic Polymorphisms of SLC28A1, ABCG2, and ABCC4 on Bioavailability of Mizoribine in Healthy Japanese Males. *Drug Metab. Pharmacokinet.* **2011**, *26* (5), 538–543.

(151) Ishida, K.; Fukao, M.; Watanabe, H.; Taguchi, M.; Miyawaki, T.; Matsukura, H.; Uemura, O.; Zhang, Z.; Unadkat, J. D.; Hashimoto, Y. Effect of Salt Intake on Bioavailability of Mizoribine in Healthy Japanese Males. *Drug Metab. Pharmacokinet.* **2013**, *28* (1), 75–80.

(152) Sakaeda, T.; Nakamura, T.; Horinouchi, M.; Kakumoto, M.; Ohmoto, N.; Sakai, T.; Morita, Y.; Tamura, T.; Aoyama, N.; Hirai, M.; Kasuga, M.; Okumura, K. MDR1 Genotype-Related Pharmacokinetics

kinetics of Digoxin after Single Oral Administration in Healthy Japanese Subjects. *Pharm. Res.* **2001**, *18* (10), 1400–1404.

(153) Nakamura, T.; Sakaeda, T.; Horinouchi, M.; Tamura, T.; Aoyama, N.; Shirakawa, T.; Matsuo, M.; Kasuga, M.; Okumura, K. Effect of the Mutation (C3435T) at Exon 26 of the MDR1 Gene on Expression Level of MDR1 Messenger Ribonucleic Acid in Duodenal Enterocytes of Healthy Japanese Subjects. *Clin. Pharmacol. Ther.* **2002**, *71* (4), 297–303.

(154) Bruhn, O.; Cascorbi, I. Polymorphisms of the Drug Transporters ABCB1, ABCG2, ABCC2 and ABCC3 and Their Impact on Drug Bioavailability and Clinical Relevance. *Expert Opin. Drug Metab. Toxicol.* **2014**, *10* (10), 1337–1354.

(155) Shitara, Y.; Maeda, K.; Ikejiri, K.; Yoshida, K.; Horie, T.; Sugiyama, Y. Clinical Significance of Organic Anion Transporting Polypeptides (OATPs) in Drug Disposition: Their Roles in Hepatic Clearance and Intestinal Absorption. *Biopharm. Drug Dispos.* **2013**, *34*, 45–78.

(156) Tornio, A.; Vakkilainen, J.; Neuvonen, M.; Backman, J. T.; Neuvonen, P. J.; Niemi, M. SLCO1B1 Polymorphism Markedly Affects the Pharmacokinetics of Lovastatin Acid. *Pharmacogenet. Genomics* **2015**, *25* (8), 382–387.

(157) Ieiri, I.; Higuchi, S.; Sugiyama, Y. Genetic Polymorphisms of Uptake (OATP1B1, 1B3) and Efflux (MRP2, BCRP) Transporters: Implications for Inter-Individual Differences in the Pharmacokinetics and Pharmacodynamics of Statins and Other Clinically Relevant Drugs. *Expert Opin. Drug Metab. Toxicol.* **2009**, *5*, 703–729.

(158) Péter, S.; Navis, G.; de Borst, M. H.; von Schacky, C.; van Orten-Luiten, A. C. B.; Zhernakova, A.; Witkamp, R. F.; Janse, A.; Weber, P.; Bakker, S. J. L.; Eggersdorfer, M. Public Health Relevance of Drug-Nutrition Interactions. *Eur. J. Nutr.* **2017**, *56* (2), 23–36.

(159) Boullata, J. I. Drug and Nutrition Interactions: Not Just Food for Thought. *J. Clin. Pharm. Ther.* **2013**, *38* (4), 269–271.

(160) Purohit, H. S.; Trasi, N. S.; Sun, D. D.; Chow, E. C. Y.; Wen, H.; Zhang, X.; Gao, Y.; Taylor, L. S. Investigating the Impact of Drug Crystallinity in Amorphous Tacrolimus Capsules on Pharmacokinetics and Bioequivalence Using Discriminatory In Vitro Dissolution Testing and Physiologically Based Pharmacokinetic Modeling and Simulation. *J. Pharm. Sci.* **2018**, *107* (5), 1330–1341.

(161) Hofsäss, M. A.; Dressman, J. Suitability of the Z-Factor for Dissolution Simulation of Solid Oral Dosage Forms: Potential Pitfalls and Refinements. *J. Pharm. Sci.* **2020**, *109* (9), 2735.

(162) Pathak, S. M.; Schaefer, K. J.; Jamei, M.; Turner, D. B. Biopharmaceutic IVIVE—Mechanistic Modeling of Single- and Two-Phase In Vitro Experiments to Obtain Drug-Specific Parameters for Incorporation Into PBPK Models. *J. Pharm. Sci.* **2019**, *108* (4), 1604–1618.

(163) Arora, S.; Pansari, A.; Kilford, P.; Jamei, M.; Gardner, I.; Turner, D. B. Biopharmaceutic In Vitro In Vivo Extrapolation (IVIV_E) Informed Physiologically-Based Pharmacokinetic Model of Ritonavir Norvir® Tablet Absorption in Humans Under Fasted and Fed State Conditions. *Mol. Pharmaceutics* **2020**, *17*, 2329.

(164) O'Dwyer, P. J.; Litou, C.; Box, K. J.; Dressman, J. B.; Kostewicz, E. S.; Kuentz, M.; Reppas, C. In Vitro Methods to Assess Drug Precipitation in the Fasted Small Intestine - a PEARRL Review. *J. Pharm. Pharmacol.* **2019**, *71* (4), 536–556.

(165) Pathak, S. M.; Ruff, A.; Kostewicz, E. S.; Patel, N.; Turner, D. B.; Jamei, M. Model-Based Analysis of Biopharmaceutic Experiments to Improve Mechanistic Oral Absorption Modeling: An Integrated In Vitro In Vivo Extrapolation Perspective Using Ketoconazole as a Model Drug. *Mol. Pharmaceutics* **2017**, *14* (12), 4305–4320.

(166) Butler, J.; Hens, B.; Vertzoni, M.; Brouwers, J.; Berben, P.; Dressman, J.; Andreas, C. J.; Schaefer, K. J.; Mann, J.; McAllister, M.; Jamei, M.; Kostewicz, E.; Kesisoglou, F.; Langguth, P.; Minekus, M.; Müllertz, A.; Schilderink, R.; Koziolok, M.; Jedamzik, P.; Weitschies, W.; Reppas, C.; Augustijns, P. In Vitro Models for the Prediction of In Vivo Performance of Oral Dosage Forms: Recent Progress from Partnership through the IMI OrBiTo Collaboration. *Eur. J. Pharm. Biopharm.* **2019**, *136*, 70–83.

(167) Kourentas, A.; Vertzoni, M.; Barmapsalou, V.; Augustijns, P.; Beato, S.; Butler, J.; Holm, R.; Ouwerkerk, N.; Rosenberg, J.; Tajiri, T.; Tannergren, C.; Symillides, M.; Reppas, C. The BioGIT System: A Valuable In Vitro Tool to Assess the Impact of Dose and Formulation on Early Exposure to Low Solubility Drugs After Oral Administration. *AAPS J.* **2018**, *20* (4), 1.

(168) Carlert, S.; Lennernäs, H.; Abrahamsson, B. Evaluation of the Use of Classical Nucleation Theory for Predicting Intestinal Crystalline Precipitation of Two Weakly Basic BSC Class II Drugs. *Eur. J. Pharm. Sci.* **2014**, *53* (1), 17–27.

(169) Wagner, C.; Jantravid, E.; Kesisoglou, F.; Vertzoni, M.; Reppas, C.; B. Dressman, J. Predicting the Oral Absorption of a Poorly Soluble, Poorly Permeable Weak Base Using Biorelevant Dissolution and Transfer Model Tests Coupled with a Physiologically Based Pharmacokinetic Model. *Eur. J. Pharm. Biopharm.* **2012**, *82* (1), 127–138.

(170) Schütt, M.; Stamatoopoulos, K.; Simmons, M. J. H.; Batchelor, H. K.; Alexiadis, A. Modelling and Simulation of the Hydrodynamics and Mixing Profiles in the Human Proximal Colon Using Discrete Multiphysics. *Comput. Biol. Med.* **2020**, *121*, 103819.

(171) Stamatoopoulos, K.; Pathak, S. M.; Marciani, L.; Turner, D. B. Population-Based PBPK Model for the Prediction of Time-Variant Bile Salt Disposition within GI Luminal Fluids. *Mol. Pharmaceutics* **2020**, *17* (4), 1310–1323.

(172) Pade, D.; Jamei, M.; Rostami-Hodjegan, A.; Turner, D. B. Application of the Mech Peff Model to Predict Passive Effective Intestinal Permeability in the Different Regions of the Rodent Small Intestine and Colon. *Biopharm. Drug Dispos.* **2017**, *38* (2), 94–114.

(173) Litou, C.; Vertzoni, M.; Goumas, C.; Vasdekis, V.; Xu, W.; Kesisoglou, F.; Reppas, C. Characteristics of the Human Upper Gastrointestinal Contents in the Fasted State Under Hypo- and A-Chlorhydric Gastric Conditions Under Conditions of Typical Drug - Drug Interaction Studies. *Pharm. Res.* **2016**, *33* (6), 1399–1412.

(174) Segregur, D.; Flanagan, T.; Mann, J.; Moir, A.; Karlsson, E. M.; Hoch, M.; Carlile, D.; Sayah-Jeanne, S.; Dressman, J. Impact of Acid-Reducing Agents on Gastrointestinal Physiology and Design of Biorelevant Dissolution Tests to Reflect These Changes. *J. Pharm. Sci.* **2019**, *108*, 3461–3477.

(175) Kesisoglou, F.; Vertzoni, M.; Reppas, C. Physiologically Based Absorption Modeling of Salts of Weak Bases Based on Data in Hypochlorhydric and Achlorhydric Biorelevant Media. *AAPS PharmSciTech* **2018**, *19* (7), 2851–2858.

(176) Bucheit, J. D.; Pamulapati, L. G.; Carter, N.; Malloy, K.; Dixon, D. L.; Sisson, E. M. Oral Semaglutide: A Review of the First Oral Glucagon-Like Peptide 1 Receptor Agonist. *Diabetes Technol. Ther.* **2020**, *22*, 10–18.

(177) Swat, M. J.; Moodie, S.; Wimalaratne, S. M.; Kristensen, N. R.; Lavielle, M.; Mari, A.; Magni, P.; Smith, M. K.; Bizzotto, R.; Pasotti, L.; Mezzalana, E.; Comets, E.; Sarr, C.; Terranova, N.; Blaudez, E.; Chan, P.; Chard, J.; Chatel, K.; Chenel, M.; Edwards, D.; Franklin, C.; Giorgino, T.; Glont, M.; Girard, P.; Grenon, P.; Harling, K.; Hooker, A. C.; Kaye, R.; Keizer, R.; Kloft, C.; Kok, J. N.; Kokash, N.; Laibe, C.; Laveille, C.; Lestini, G.; Mentré, F.; Munafo, A.; Nordgren, R.; Nyberg, H. B.; Parra-Guillen, Z. P.; Plan, E.; Ribba, B.; Smith, G.; Trocóniz, I. F.; Yvon, F.; Milligan, P. A.; Harnisch, L.; Karlsson, M.; Hermjakob, H.; Le Novère, N. Pharmacometrics Markup Language (PharmML): Opening New Perspectives for Model Exchange in Drug Development. *CPT: Pharmacometrics Syst. Pharmacol.* **2015**, *4*, 316–319.

(178) Abrahamsson, B.; McAllister, M.; Augustijns, P.; Zane, P.; Butler, J.; Holm, R.; Langguth, P.; Lindahl, A.; Müllertz, A.; Pepin, X.; Rostami-Hodjegan, A.; Sjögren, E.; Berntsson, M.; Lennernäs, H. Six Years of Progress in the Oral Biopharmaceutics Area - A Summary from the IMI OrBiTo Project. *Eur. J. Pharm. Biopharm.* **2020**, *152*, 236–247.

(179) Saphier, S.; Rosner, A.; Brandeis, R.; Karton, Y. Gastro Intestinal Tracking and Gastric Emptying of Solid Dosage Forms in Rats Using X-Ray Imaging. *Int. J. Pharm.* **2010**, *388* (1–2), 190–195.

- (180) Gómez-Lado, N.; Seoane-Viaño, I.; Matiz, S.; Madla, C. M.; Yadav, V.; Aguiar, P.; Basit, A. W.; Goyanes, A. Gastrointestinal Tracking and Gastric Emptying of Coated Capsules in Rats with or without Sedation Using CT Imaging. *Pharmaceutics* **2020**, *12* (1), 81.
- (181) Lu, K. H.; Cao, J.; Oleson, S. T.; Powley, T. L.; Liu, Z. Contrast-Enhanced Magnetic Resonance Imaging of Gastric Emptying and Motility in Rats. *IEEE Trans. Biomed. Eng.* **2017**, *64* (11), 2546–2554.
- (182) Blaabjerg, L. I.; Fan, L.; Chen, X.; Sassene, P. J. The Use of Capsule Endoscopy to Determine Tablet Disintegration in Vivo. *Pharmaceutics* **2020**, *12* (6), 498.
- (183) Berry, R.; Miyagawa, T.; Paskaranandavivel, N.; Du, P.; Angeli, T. R.; Trew, M. L.; Windsor, J. A.; Imai, Y.; O'Grady, G.; Cheng, L. K. Functional Physiology of the Human Terminal Antrum Defined by High-resolution Electrical Mapping and Computational Modeling. *Am. J. Physiol. - Gastrointest. Liver Physiol.* **2016**, *311* (5), G895–G902.
- (184) Gharibans, A. A.; Kim, S.; Kunkel, D. C.; Coleman, T. P. High-Resolution Electrogastrogram: A Novel, Noninvasive Method for Determining Gastric Slow-Wave Direction and Speed. *IEEE Trans. Biomed. Eng.* **2017**, *64* (4), 807–815.
- (185) Yoshimoto, K.; Yamada, K.; Watabe, K.; Takeda, M.; Nishimura, T.; Kido, M.; Nagakura, T.; Takahashi, H.; Nishida, T.; Iijima, H.; Tsujii, M.; Takehara, T.; Ohno, Y. Gastric Contraction Imaging System Using a 3-D Endoscope. *IEEE J. Transl. Eng. Heal. Med.* **2014**, *2*, 1.
- (186) Potcoava, M. C.; Futia, G. L.; Aughenbaugh, J.; Schlaepfer, I. R.; Gibson, E. A. Raman and Coherent Anti-Stokes Raman Scattering Microscopy Studies of Changes in Lipid Content and Composition in Hormone-Treated Breast and Prostate Cancer Cells. *J. Biomed. Opt.* **2014**, *19* (11), 111605.
- (187) Viitala, T.; Granqvist, N.; Hallila, S.; Raviña, M.; Yliperttula, M. Elucidating the Signal Responses of Multi-Parametric Surface Plasmon Resonance Living Cell Sensing: A Comparison between Optical Modeling and Drug-MDCKII Cell Interaction Measurements. *PLoS One* **2013**, *8* (8), No. e72192.
- (188) Krauss, M.; Burghaus, R.; Lippert, J.; Niemi, M.; Neuvonen, P.; Schuppert, A.; Willmann, S.; Kuepfer, L.; Görlitz, L. Using Bayesian-PBPK Modeling for Assessment of Inter-Individual Variability and Subgroup Stratification. *Silico Pharmacol.* **2013**, *11* (1), 6.
- (189) Krauss, M.; Tappe, K.; Schuppert, A.; Kuepfer, L.; Goerlitz, L. Bayesian Population Physiologically-Based Pharmacokinetic (PBPK) Approach for a Physiologically Realistic Characterization of Interindividual Variability in Clinically Relevant Populations. *PLoS One* **2015**, *10* (10), 1–22.
- (190) Krauss, M.; Schuppert, A. Assessing Interindividual Variability by Bayesian-PBPK Modeling. *Drug Discovery Today: Dis. Models* **2016**, *22* (xx), 15–19.
- (191) Lang, J.; Vincent, L.; Chenel, M.; Ogungbenro, K.; Galetin, A. Simultaneous Ivabradine Parent-Metabolite PBPK/PD Modelling Using a Bayesian Estimation Method. *AAPS J.* **2020**, *22* (6), 1–16.
- (192) Tsiros, P.; Bois, F. Y.; Dokoumetzidis, A.; Tsiliki, G.; Sarimveis, H. Population Pharmacokinetic Reanalysis of a Diazepam PBPK Model: A Comparison of Stan and GNU MCSim. *J. Pharmacokinet. Pharmacodyn.* **2019**, *46* (2), 173–192.
- (193) Jamei, M. Recent Advances in Development and Application of Physiologically-Based Pharmacokinetic (PBPK) Models: A Transition from Academic Curiosity to Regulatory Acceptance. *Curr. Pharmacol. Reports* **2016**, *2* (3), 161–169.
- (194) Jamei, M. Where Do PBPK Models Stand in Pharmacometrics and Systems Pharmacology? *CPT: Pharmacometrics Syst. Pharmacol.* **2020**, *9*, No. 75.
- (195) Wendling, T.; Tsamandouras, N.; Dumitras, S.; Pigeolet, E.; Ogungbenro, K.; Aarons, L. Reduction of a Whole-Body Physiologically Based Pharmacokinetic Model to Stabilise the Bayesian Analysis of Clinical Data. *AAPS J.* **2016**, *18* (1), 196–209.
- (196) Sager, M.; Jedamzik, P.; Merdivan, S.; Grimm, M.; Schneider, F.; Kromrey, M. L.; Hasan, M.; Oswald, S.; Kühn, J.; Koziolok, M.; Weitschies, W. Low Dose Caffeine as a Salivary Tracer for the Determination of Gastric Water Emptying in Fed and Fasted State: A MRI Validation Study. *Eur. J. Pharm. Biopharm.* **2018**, *127*, 443–452.
- (197) Feldman, M.; Smith, H. J.; Simon, T. R. Gastric Emptying of Solid Radiopaque Markers: Studies in Healthy Subjects and Diabetic Patients. *Gastroenterology* **1984**, *87* (4), 895–902.
- (198) Parker, H. L.; Liu, D.; Curcic, J.; Ebert, M. O.; Schwizer, W.; Fried, M.; Steingoetter, A. Gastric and Postgastric Processing of ¹³C Markers Renders the ¹³C Breath Test an Inappropriate Measurement Method for the Gastric Emptying of Lipid Emulsions in Healthy Adults. *J. Nutr.* **2017**, *147* (7), 1258–1266.
- (199) Luo, L.; Aubrecht, J.; Li, D.; Warner, R. L.; Johnson, K. J.; Kenny, J.; Colangelo, J. L. Assessment of Serum Bile Acid Profiles as Biomarkers of Liver Injury and Liver Disease in Humans. *PLoS One* **2018**, *13* (3), e0193824.
- (200) Baier, V.; Cordes, H.; Thiel, C.; Castell, J. V.; Neumann, U. P.; Blank, L. M.; Kuepfer, L. A Physiology-Based Model of Human Bile Acid Metabolism for Predicting Bile Acid Tissue Levels After Drug Administration in Healthy Subjects and BRIC Type 2 Patients. *Front. Physiol.* **2019**, *10* (SEP), 1192.
- (201) Brock, W. J.; Beaudoin, J. J.; Slizgi, J. R.; Su, M.; Jia, W.; Roth, S. E.; Brouwer, K. L. R. Bile Acids as Potential Biomarkers to Assess Liver Impairment in Polycystic Kidney Disease. *Int. J. Toxicol.* **2018**, *37* (2), 144–154.
- (202) Li, M.; Liu, S.; Wang, M.; Hu, H.; Yin, J.; Liu, C.; Huang, Y. Gut Microbiota Dysbiosis Associated with Bile Acid Metabolism in Neonatal Cholestasis Disease. *Sci. Rep.* **2020**, *10* (1), 1–10.
- (203) Angelin, B.; Bjorkhem, I. Postprandial Serum Bile Acids in Healthy Man: Evidence for Differences in Absorptive Pattern between Individual Bile Acids. *Gut* **1977**, *18* (8), 606–609.
- (204) Asaumi, R.; Menzel, K.; Lee, W.; Nunoya ichi, K.; Imawaka, H.; Kusuhara, H.; Sugiyama, Y. Expanded Physiologically-Based Pharmacokinetic Model of Rifampicin for Predicting Interactions With Drugs and an Endogenous Biomarker via Complex Mechanisms Including Organic Anion Transporting Polypeptide 1B Induction. *CPT: Pharmacometrics Syst. Pharmacol.* **2019**, *8* (11), 845–857.
- (205) Shen, H.; Chen, W.; Drexler, D. M.; Mandlekar, S.; Holenarsipur, V. K.; Shields, E. E.; Langish, R.; Sidik, K.; Gan, J.; Humphreys, W. G.; Marathe, P.; Lai, Y. Comparative Evaluation of Plasma Bile Acids, Dehydroepiandrosterone Sulfate, Hexadecanedioate, and Tetradecanedioate with Coproporphyrins I and III as Markers of OATP Inhibition in Healthy Subjects. *Drug Metab. Dispos.* **2017**, *45* (8), 908–919.
- (206) Lai, Y.; Mandlekar, S.; Shen, H.; Holenarsipur, V. K.; Langish, R.; Rajanna, P.; Murugesan, S.; Gaud, N.; Selvam, S.; Date, O.; Cheng, Y.; Shipkova, P.; Dai, J.; Humphreys, W. G.; Marathe, P. Coproporphyrins in Plasma and Urine Can Be Appropriate Clinical Biomarkers to Recapitulate Drug-Drug Interactions Mediated by Organic Anion Transporting Polypeptide Inhibition. *J. Pharmacol. Exp. Ther.* **2016**, *358* (3), 397–404.
- (207) Yoshikado, T.; Toshimoto, K.; Maeda, K.; Kusuhara, H.; Kimoto, E.; Rodrigues, A. D.; Chiba, K.; Sugiyama, Y. PBPK Modeling of Coproporphyrin I as an Endogenous Biomarker for Drug Interactions Involving Inhibition of Hepatic OATP1B1 and OATP1B3. *CPT: Pharmacometrics Syst. Pharmacol.* **2018**, *7* (11), 739–747.
- (208) Mori, D.; Kimoto, E.; Rago, B.; Kondo, Y.; King-Ahmad, A.; Ramanathan, R.; Wood, L. S.; Johnson, J. G.; Le, V. H.; Vourvahis, M.; David Rodrigues, A.; Muto, C.; Furihata, K.; Sugiyama, Y.; Kusuhara, H. Dose-Dependent Inhibition of OATP1B by Rifampicin in Healthy Volunteers: Comprehensive Evaluation of Candidate Biomarkers and OATP1B Probe Drugs. *Clin. Pharmacol. Ther.* **2020**, *107* (4), 1004–1013.
- (209) Billington, S.; Shoner, S.; Lee, S.; Clark-Snustad, K.; Pennington, M.; Lewis, D.; Muzi, M.; Rene, S.; Lee, J.; Nguyen, T. B.; Kumar, V.; Ishida, K.; Chen, L.; Chu, X.; Lai, Y.; Salphati, L.; Hop, C. E. C. A.; Xiao, G.; Liao, M.; Unadkat, J. D. Positron Emission Tomography Imaging of [¹¹C]Rosuvastatin Hepatic Concentrations and Hepatobiliary Transport in Humans in the Absence and Presence of Cyclosporin A. *Clin. Pharmacol. Ther.* **2019**, *106* (5), 1056–1066.

(210) Mori, D.; Kashihara, Y.; Yoshikado, T.; Kimura, M.; Hirota, T.; Matsuki, S.; Maeda, K.; Irie, S.; Ieiri, I.; Sugiyama, Y.; Kusuhara, H. Effect of OATP1B1 Genotypes on Plasma Concentrations of Endogenous OATP1B1 Substrates and Drugs, and Their Association in Healthy Volunteers. *Drug Metab. Pharmacokinet.* **2019**, *34* (1), 78–86.

(211) Tsuruya, Y.; Kato, K.; Sano, Y.; Imamura, Y.; Maeda, K.; Kumagai, Y.; Sugiyama, Y.; Kusuhara, H. Investigation of Endogenous Compounds Applicable to Drug-Drug Interaction Studies Involving the Renal Organic Anion Transporters, OAT1 and OAT3, in Humans. *Drug Metab. Dispos.* **2016**, *44* (12), 1925–1933.

(212) Takehara, I.; Yoshikado, T.; Ishigame, K.; Mori, D.; Furihata ichi, K.; Watanabe, N.; Ando, O.; Maeda, K.; Sugiyama, Y.; Kusuhara, H. Comparative Study of the Dose-Dependence of OATP1B Inhibition by Rifampicin Using Probe Drugs and Endogenous Substrates in Healthy Volunteers. *Pharm. Res.* **2018**, *35* (7), 1–13.

(213) Takehara, I.; Terashima, H.; Nakayama, T.; Yoshikado, T.; Yoshida, M.; Furihata, K.; Watanabe, N.; Maeda, K.; Ando, O.; Sugiyama, Y.; Kusuhara, H. Investigation of Glycochenodeoxycholate Sulfate and Chenodeoxycholate Glucuronide as Surrogate Endogenous Probes for Drug Interaction Studies of OATP1B1 and OATP1B3 in Healthy Japanese Volunteers. *Pharm. Res.* **2017**, *34* (8), 1601–1614.

(214) Chu, X.; Liao, M.; Shen, H.; Yoshida, K.; Zur, A. A.; Arya, V.; Galetin, A.; Giacomini, K. M.; Hanna, I.; Kusuhara, H.; Lai, Y.; Rodrigues, D.; Sugiyama, Y.; Zamek-Gliszczynski, M. J.; Zhang, L. Clinical Probes and Endogenous Biomarkers as Substrates for Transporter Drug-Drug Interaction Evaluation: Perspectives From the International Transporter Consortium. *Clin. Pharmacol. Ther.* **2018**, *104* (5), 836–864.

(215) Selen, A.; Dickinson, P. A.; Müllertz, A.; Crison, J. R.; Mistry, H. B.; Cruañes, M. T.; Martinez, M. N.; Lennernäs, H.; Wigal, T. L.; Swinney, D. C.; Polli, J. E.; Serajuddin, A. T. M.; Cook, J. A.; Dressman, J. B. The Biopharmaceutics Risk Assessment Roadmap for Optimizing Clinical Drug Product Performance. *J. Pharm. Sci.* **2014**, *103* (11), 3377–3397.

(216) Lippert, J.; Burghaus, R.; Edginton, A.; Frechen, S.; Karlsson, M.; Kovar, A.; Lehr, T.; Milligan, P.; Nock, V.; Ramusovic, S.; Riggs, M.; Schaller, S.; Schlender, J.; Schmidt, S.; Sevestre, M.; Sjögren, E.; Solodenko, J.; Staab, A.; Teutonico, D. Open Systems Pharmacology Community—An Open Access, Open Source, Open Science Approach to Modeling and Simulation in Pharmaceutical Sciences. *CPT: Pharmacometrics Syst. Pharmacol.* **2019**, *8*, 878–882.

(217) Smith, M. K.; Moodie, S. L.; Bizzotto, R.; Blaudez, E.; Borella, E.; Carrara, L.; Chan, P.; Chenel, M.; Comets, E.; Gieschke, R.; Harling, K.; Harnisch, L.; Hartung, N.; Hooker, A. C.; Karlsson, M. O.; Kaye, R.; Kloft, C.; Kokash, N.; Lavielle, M.; Lestini, G.; Magni, P.; Mari, A.; Mentré, F.; Muselle, C.; Nordgren, R.; Nyberg, H. B.; Parra-Guillén, Z. P.; Pasotti, L.; Rode-Kristensen, N.; Sardu, M. L.; Smith, G. R.; Swat, M. J.; Terranova, N.; Yngman, G.; Yvon, F.; Holford, N. Model Description Language (MDL): A Standard for Modeling and Simulation. *CPT: Pharmacometrics Syst. Pharmacol.* **2017**, *6* (10), 647–650.

Appendix A4. Curriculum vitae

Appendix A5. Eidesstattliche Erklärung

ERKLÄRUNG

Ich erkläre hiermit, dass ich mich bisher keiner Doktorprüfung im Mathematisch-Naturwissenschaftlichen Bereich unterzogen habe.

Frankfurt am Main, den20.11.2021.....

Unterschrift



Versicherung

Ich erkläre hiermit, dass ich die vorgelegte Dissertation über

" Physiologically based population pharmacokinetic/
pharmacodynamic modeling and simulation approaches to
support waivers of in vivo clinical pharmacology studies "

selbständig angefertigt und mich anderer Hilfsmittel als der in ihr angegebenen nicht bedient habe, insbesondere, dass alle Entlehnungen aus anderen Schriften mit Angabe der betreffenden Schrift gekennzeichnet sind.

Ich versichere, die Grundsätze der guten wissenschaftlichen Praxis beachtet, und nicht die Hilfe einer kommerziellen Promotionsvermittlung in Anspruch genommen zu haben.

Frankfurt am Main, den20.11.2021.....

(Unterschrift)

